JAERI-M
86-080

NEANDC(J)120/U
INDC(JPN)106/L

PROCEEDINGS OF THE 1985 SEMINAR ON NUCLEAR DATA

June 1986

(Ed.) Tetsuo ASAMI and Motoharu MIZUMOTO

日本原子力研究所
Japan Atomic Energy Research Institute

JAERI-Mレポートは，日本原子力研究所が不定期に公刊している研究報告書です。
入手の問合わせは，日本原子力研究所技術情報部情報資料課（〒319－11茨城県那珂郡東海村）あて，お申しこしください。なお，このほかに財団法人原子力弘済会資料センター（〒319-11茨城県那珂郡東海村日本原子力研究所内）で複写による実費頒布をおこなっております。

JAERI-M reports are issued irregularly.
Inquiries about availability of the reports should be addressed to Information Division, Department of Technical Information, Japan Atomic Energy Research Institute, Tokai-mura, Naka-gun, Ibaraki-ken 319-11, Japan.

編集兼発行　日本原子力研究所
印　　刷　日立高速印刷株式会社

JAERI-M 86- 080

NEANDC(J)120/U
INDC(JPN)106/U

Proceedings of the 1985 Seminar on Nuclear Data

(Ed.) Tetsuo ASAMI and Motoharu MIZUMOTO

Japanese Nuclear Data Committee

Tokai Research Establishment, JAERI
Japan Atomic Energy Research Institute
Tokai-mura, Naka-gun, Ibaraki-ken

(Received May 2, 1986)

The 1985 Seminar on Nuclear Data was held on November 12 to 14, 1985 at Tokai Research Establishment of Japan Atomic Energy Research Institute. This is an annual meeting which have been held since 1978, with the support of Japanese Nuclear Data Committee. Four researchers from China and one from Indonesia participated in this seminar.

The seminar was divided into seven sessions including Poster session. The subjects are: (1) Nuclear data activities in each country, (2) Activities of JNDC Working Groups, (3) Topics, (4) Relation between absolute and relative measurements of nuclear data, (5) Nuclear data for fusion reactors, and (6) Problems on heavy nuclide nuclear data. Poster session was carried out with the title of "Neutron cross-section measurements and facilities in Japan". The Proceedings include the contributed papers presented in this seminar and the descriptions for Posters. The texts are reproduced directly from the Authors' manuscripts without re-typing.

Programme and Executive Committee.

S. Igarasi	(Chairman, JAERI)
M. Akiyama	(University of Tokyo)
T. Asami	(JAERI)
A. Hasegawa	(JAERI)
I. Kimura	(Kyoto University)
H. Matsunobu	(Sumitomo Atomic Energy Industries, Ltd.)
M. Mizumoto	(JAERI)
T. Nakagawa	(JAERI)

R. Nakasima (Hosei University)
M. Nakazawa (University of Tokyo)
I. Otake (I.S.L., Ltd.)
K. Sugiyama (Tohoku University)
T. Yoshida (NAIG Co., Ltd.)

Keywords: Nuclear Data, Measurement, Neutron Cross Section, Facility, Heavy Nuclide, JNDC, Fusion Reactors

１９８５年核データ研究会報告書

日本原子力研究所東海研究所シグマ研究委員会
（編）　浅見哲夫・水本元治

（１９８６年５月２日受理）

１９８５年核データ研究会は，１９８５年（昭和60年）11月12日～14日に日本原子力研究所の東海研究所において開催された。この研究会は１９７８年以来毎年，シグマ研究委員会の下で開催されている恒例のものであるが，今回はとくに，中国から４名，インドネシアから１名の研究者の参加をえて国際的な雰囲気の中で催された。

研究会では，次のテーマが採り挙げられた。(1)　各国の核データ活動，(2)　シグマ研究委員会のワーキング・グループの活動，(3)　核データのトピックス，(4)　核データの絶対測定と相対測定の関係，(5)　核融合炉用核データ，(6)　重い核のデータ。この他にポスターセッションとして「日本国内における中性子断面積の測定ならびに装置」のテーマが採り挙げられた。

この報告書には，これらの発表論文およびポスター発表の内容が収録してある。各報文は，著者の原稿に手を加えることなくそのまま直接に写真印刷を行った。

プログラム・実行委員会委員

五十嵐信一（委員長・日本原子力研究所）
秋山　雅胤（東京大学原子力工学研究施設）
浅見　哲夫（日本原子力研究所）
大竹　　巌（㈱アイ・エス・エル）
木村　逸郎（京都大学原子炉実験所）
椙山　一典（東北大学）
中川　庸雄（日本原子力研究所）
中沢　正治（東京大学原子力工学研究施設）
中嶋　龍三（法政大学）
長谷川　明（日本原子力研究所）
松延　廣幸（住友原子力工業㈱）
水本　元治（日本原子力研究所）
吉田　　正（日本原子力事業㈱）

東海研究所：〒３１９－１１　茨城県那珂郡東海村白方字白根２－４

CONTENTS

POSTER SESSION

1. OPENING SESSION

1.1 Opening and Welcome Address

N. Shikazono
Japan Atomic Energy Institute

Good afternoon (ladies and) gentlemen. It is a great pleasure for me to open the meeting on nuclear data, today. This meeting, as you know, used to be an internal meeting of JNDC, that is Japan Nuclear Data Committee. The first meeting was held in 1978. Since then, we have been continuing to hold this meeting once a year. Topics were mainly selected from the domestic activities in the nuclear data field: measurements, evaluations, and applications of the nuclear data.

It is needless to say that for the nuclear data activity, the international collaboration is the most important. Exchange of data and information, and collaborations have to be made. A single country alone cannot do much works, of course.

Unfortunately, Japan is isolated geographically from Europe or the United States. The geographic situations of People's Republic of China, Indonesia and any other Asian countries are in the same situation. We know that we have to make much effort to do the international collaboration.

Of course Japan joins to IAEA and OECD/NEA DATA BANK, but we have some disadvantages for the collaboration works with western countries because of the geographic isolation. Japan is far from most of the western countries. You need typically a 15 hours flight, a big time difference which is quite uncomfortable, and a large cost as well.

So, it should be nice to establish the collaborative relationship between countries within the asian area, just as the western countries do among their neibouring countries. We will certainly have much advantages if we can proceed the international collaboration between the neibouring asian countries extensively. You can depart from your country in the morning, and you can discuss with your collaborator in the afternoon. If you are in hurry, you can even go back home in the evening within a day.

Last year, we have tried to extend this meeting from the domestic meeting to the inter-regional one in the Asia-Pacific region. We asked several countries for joining the meeting. The response was rather good, but unfortunately no outside countries could attend the meeting eventually, although we had four contributed papers, one from Australia and three from People's Republic of China.

This year, we are very happy to have the guests here from People's Republic of China and Indonesia. We would like to welcome all the guests. Now, let me introduce Dr. Wang Da-hai, could you stand up please?, Dr. Cai Shaohui, Dr. shen Jian, and Dr. Wang Yaoquing, from People's Republic of China. And Dr. Lasijo from Indonesia. Thank you, please sit down.

We are going to have an opportunity of learning about activities of People's Republic of China and Indonesia in this meeting very soon.

This is the first meeting to involve the members of other countries. We would like to keep this situation and continue the inter-regional meeting also next year, and in the future we hope more guests coming from different countries. We should make effort to do so.

What's more, we are going to have a big international conference on Nuclear Data here in Japan in 1988. We expect more than 300 people will participate the conference coming from all over the world. This is the first big international conference on Nuclear Data which will be held in Japan or Asian area, so, the Japanese scientists as well as the asian scientists are supposed to contribute significantly to the conference.

We have still three years to go until the big event in 1988, but three years are not long enough to do much work. There must be many ways to contribute to the conference. For example, it could be a good way to choose some specified subjects, and have concentration and collaboration regarding to the limited number of subjects. Anyway, I hope discussions in this meeting will be helpful for considering this matter.

Another thing I'd like to mention is the fundamental question, that is, where to go and what to do for the nuclear data activity in the

future, which has been repeatedly argued and discussed so far among the JNDC members. It is of course impossible to give a definite answer for that question immediately, and we may have several kinds of answers. For some people, it may be quite clear, for some other people, it may be not. Anyway, I think, the important thing is that we should keep it in mind all the time and keep effort to find out what the best solution is. I hope the discussions in this meeting will also be helpful and fruitful to give some idea for this problem. Thank you.

1.2 Progress on Nuclear Data Work at IAE

Wang Da-Hai

Institute of Atomic Energy
P.O. Box 275, Beijing, China

Nuclear data program is one of the main research in IAE. Some progress of it are presented focusing the discussion on the nuclear data evaluation and measurement work.

1. The Nuclear Data Evaluation

The recent activities of nuclear data in IAE were reported in last seminar on nuclear data at JAERI(1). This article makes some complement to that.

As mentioned before, the Chinese Nuclear Data Center (CNDC) was founded at IAE in 1975. Now CNDC consists of four groups:

Experimental Nuclear Data Evaluation,
Nuclear Theory and Nuclear Data Calculation,
Multigroup Constant Generation and Integral Testing,
Nuclear Data Library.

The CNDC is engaged in Nuclear Data Compilation and Evaluation, as well as the organization and coordination on the co-operation network in China. The main co-operators are:

Beijing University,
Qinghua University,
Fudan University,
Sichuan University,
Jilin University,
Nankai University,
Institute of Nuclear Research in Shanghai,
Southwest Institute of Nuclear Reactor Engineering,

Southwest Physics Institute,
Beijing Normal University,
Institute of Applied Physics and Computational Mathematics(in Beijing).

The CNDC organized some working groups, such as:
Charged particle Nuclear Reaction Data,
Fission Yield,
Nuclear Structure and Decay Data,
Neutron Resonance Parameter and level Density,
Transactinium Isotope Nuclear Data,
Neutron Nuclear Data Evaluation for General Purpose,
γ Production Data,
Benchmark Testing of CENDL-1,
Group Constant for Reactor,
Theoretical Calculation of Medium Heavy and Fissionable Nuclei.

After several years of hard work done by all network members, the first version of CENDL-1 has been finished in this year. It is in ENDF/B-1V format and stored on magnetic tapes. It includes 36 nuclei or element. They are: H, D, T, He-3, He-4, Li-6, Li-7, Be-9, B-10, B-11, N, O, F-19, Na-24, Mg, Al-27, Si. V. Cr, Fe, Ni, Cu, Zn, Zr, Nb, Mo, Sn, Hg, Ta, W, Au, Pb, U-235, U-238, Pu-239, Pu-240, which are an important for general purposes such as fission and fusion reactor and other applications. The work for CENDL-2 has been started. It will be a new version of CENDL-1 and will contain all files and the nuclei contained will be extended to about 50 nuclei.

Up to now, the evaluation of nuclear structure and decay data on mass chain A=51, 54 and 56 nuclei have been finished. According to the agreement with Dr. S. Pearlstein (the Director of NNDC), the mass chain A=170 and 172 are being evaluated.

According to the contract of the cooperation research program between IAEA and IAE, the neutron data evaluation and calculation for actinide nuclides are being carried out. The Am-241 neutron data evaluation has been finished (2). The

optical model was used to calculate the total cross section, the shape-elastic scattering cross section and angular distribution. The Hauser- Feshbach statistical theory with width fluctuation correction was used to calculate the reaction cross section and secondary neutron energy spectra and angular distribution (the incident neutron energy range is 0.001 to 3 Mev). The evaporation model including the pre-equilibrium statiatical theory based on exition model was used to calculate the cross section and secondary neutron energy spectra of each openned channels (the incident neutron energy range is from 3 to 20 Mev). As a example, comparisons of (n,γ), (n, f) channels theoretical calculated cross sections to the experiments are given in Fig. 1 and 2. It is shown by those figures that the theoretical calculated results agree with experiments satisfactorily. The evaluated cross section of all channels is shown in fig. 3.

Since the capture process of Am-241 plays an important role in the determing of the Cm-242 and Cm-244 yield. My colleagues have paid more attention to the capture cross section evaluation and the isomeric branching evaluation. After considering the several integral testing results, which are larger than the calculated ones by 10%, a value of thermal capture cross section has been recommented to 632b. Then the measurement result of Weston et al. has been renomalized to this value and the resonance parameters have correspondingly been adjusted. All of them should be 5-7% higher than the recommended before. It also points out that the discrepancy existing between the monoenergetic and integral branching ratio results remain to be solved. But it favors to recommend the integral results.

To complement the energy regions and reaction channels, in which the experimental data are not available, successful nuclear model theories have been adopted to calculate the data as mentioned before. In this year, a unified code for calculating the medium heavy nucleus has been developed. The multi-particle emission process and pre-equilibrium emission process were considered in the evaporation model.

The part direct interaction was taken into account in the calculation of the low level inelastic scattering. The agreement of the calculation with experiment has been improved on a series of nuclei.

The systematics studies on the exitation functions of (n,2n) and (n,x) (x=p,d, ,t,He-3) reactions have been carried out and finished recently (3). The purpose of this work is to attempt to establish the systematics of the behaviours of (n,2n) and (n,x) excitation function based on a body of new measurements up to 25 Mev. Based on the constant temperature evaporation model taking into account the pre-equilibrium contribution formulas containing two parameters have been obtained.These formulas reproduce the measured (n,2n),(n,p),and (n,α) data satisfactory,showing in figures 4,5,and 6,and more accurate prediction than before for the unmeasured data would be expected.

Multigroup constant processing code RQCR for thermal neutron reactor and KQCS for fast neutron reactor were reported in last seminar at JAERI. In this year,an interface code LEK which is used to link ENDF/B-1V format with code KQCS was developed. LEK makes it possible for CNDC to generate multigroup constants from evaluated nuclear data file in ENDF/B-1V format.

In order to test CENDL ,some codes such as GYSNF, DSNF, NDP,TDBDC,PETRC,FEONAN have been developed.GYSNF is an anisotropic scattering code of Carlson SN method and DSNF is a discrete ordinate SN code. NDP and TDBDC is one and two dimentional diffusion program respectively. PETRC is two dimentional diffusion perturbation program. They can be used to calculate integral quantities for fast benchmark assemblies. FEONAN is used to calculate the uncollided transmitted spectra and to test the total cross section for Fe,O,Na and N in CENDL.

2. Nuclear data measurements

Nuclear data measurements have been carried out since early 1960's in China. Now,several accelerators and neutron

generators for nuclear data measurements are in operation. They are:

1) AVF cyclotron (Ep=3-15Mev),2.5 MV Van de Graaff accelerator,500 KV Cockcroft-Walton generator,at IAE.

2) 400 KV Cockcroft-Walton generator,at Qinhua University,Beijing.

3) 600 KV Cockcroft-Walton generator with post helix accelerator,at Beijing Normal University.

4) AVF cyclotron (Ep=3-30Mev),400 KV neutron generator, at Institute of Nuclear Research,Shanghai.

5) 2.5 MV Van de Graaff accelerator,at Fudan University.

6) cyclotron (Ed=12 Mev),2.5 MV Van de Graaff accelerator,400 KV Cockcroft-Walton generator,at Sichan University.

Some new facilities are being installed or tested in China. They are:

1) HI-13 Tandem accelerator,at IAE.

2) 4MV Van de Graaff accelerator,6 MV Tandem accelerator,at Institute of Nuclear Research,Shanghai.

3) 4.5 MV Van de Graaff accelerator, 6 MV Tandem accelerator, at Beijing University.

Nuclear data measurements are mainly carried out at IAE. Some experimental results obtained recently at IAE are presented as follows:

1) Fission cross section

The absolute fission cross section of Np-237 was measured (4) in the energy range 4.0-5.5 Mev using a recoil proton semiconductor detector telescope and fission ionization chamber place back-to-back system. The correction factors were considered carefully. The error is 2.5 %. The results shown in Fig. 7 are higher than the evaluation data of ENDF/B-V.

2) Fission yield

Some mass chain yields and cumulative yields for the 5,8.3 and 14 Mev neutron induced fission of U-238 are measured by using of radiochemical techniques followed by γor ß counting and Ge(Li) -ray spectrum method.(5)(6)(7).

The absolute measurement of fission rate is carried out by a double ionization chamber containing two thin, standardized deposits of U-238. The target is attached to double ionization chamber. The results are shown in Fig.8 and 9. As reported by others previously, a fine structure is observed at the mass number of 134 in neutron energy of 14.9 Mev. Some mass chains are measured for the first time.

3) Elastic scattering cross section

The elastic scattering angular distribution of D(n,n) has been measured by means of time-of-flight method on 8.6 Mev of neutron energy at cyclotron. The Deuterate gas cell was used as neutron source. The deuterate scintillation detector (ϕ 22X30 mm) was used as the scatterer, as well as the zero time signal for time-of-flight. Liquid scintillation ST-451 was used as neutron detector. The PSD was used for n-γ identification. The flight path is 2.15 m and time resolution is 2.5 ns. The n-p scattering cross section was used for the nomalization. The time of flight spectrum from deuterate scintillator is shown in Fig.10. The elastic scattering angular distribution of D(n,n) obtained is shown in Fig.11. The comparision of our experimental data with P-D shift calculated result and Faddeev equation calculated result is shown in Fig.12. It is found that the experimental data is a little more higher than those calculation at small angle region. The evaluation data ENDF/B-IV is little lower than experimental data data(to see Fig.11).

4) Double differential cross section

The double differential cross section of U-238 has been measured by means of associated particle time-of-flight method at 14.2 Mev neutron energy. The metal sample of U-238 is Φ_{out}30 x Φ_{in}10X30 mm in size. The flight path is 3 M and time resolution is 1 ns. As an example, the time spectra at θ =35° is shown in Fig. 13. The results are being analyzed.

5) threshold reaction cross section

The (n,2n) and (n,particle) cross sections are of importance for various application purposes, such as in fusion reactor research and dosimetry. Consequently, some threshold reaction

cross sections of a series nuclei have been measured by use of activation method .Some experimental results obtained recently are described as examples.

$^{58}Ni(n,2n)^{57}Ni$: Our result is shown in Fig.14. It agrees with Pau Win's value. After comparision of evaluation for this reaction,our recommended curve is similar with the possible trend assumed by Vlasov in 1976.

$^{181}Ta(n,2n)^{180m}Ta$: It is recommended that a medium curve would be reasonable .If the same decay data is used for different results,the agreement between them becomes better. The comparision is shown in Fig.15.

$^{54}Fe(n,\alpha)^{51}Cr$: the result is shown in Fig. 16.

$^{51}V(n,\alpha)^{48}Sc$: the result is shown in Fig.17. The recent results from different laboratories have a good agreement.

6) Neutron fluence measurements

The accurate measurements of fast neutron fluence and neutron source emission rate are of importance for absolute cross section measurement. Some methods for that,such as hydrogen proportional counter,recoil telescope,associated particle method and standard long counter have been developed. We joined the international intercomparison of neutron fluence (at 144, 565 Kev and 14 Mev) and neutron source emission rate,which was organized by IAEA through NPL.The results are shown in Fig. 18,19,20,21. It points out that our results are satisfatory.

Reference

(1) JAERI-M,85-835
(2) Gu Fuhua,private communication.
(3) Zhang Jin,Zhao Zhixiang et al. to be published.
(4) Wu JinXia et al. Chin. Jour. of Nucl. Phys.6(1984)369.
(5) Yield Group, Nucl. Chem. and RadioChem. 6(1984)183.
(6) Li Ze et al. Chin.Jour. of Nucl.Phys. 7(1985)97.
(7) Liu CongGui et al. Chin.Jour. of Nucl.Phys. 7(1985)235.

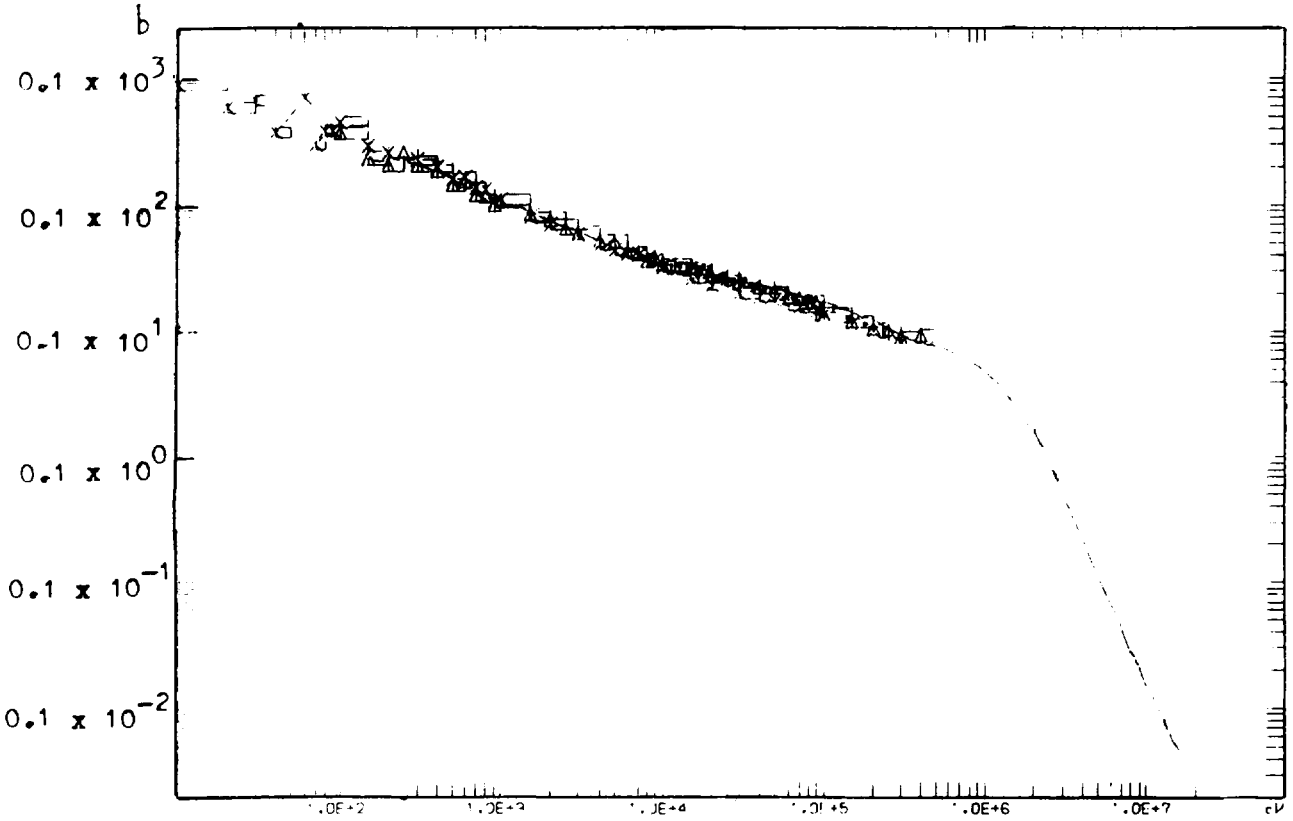

Fig. 1 Radiative Capture Cross Section of ^{241}Am

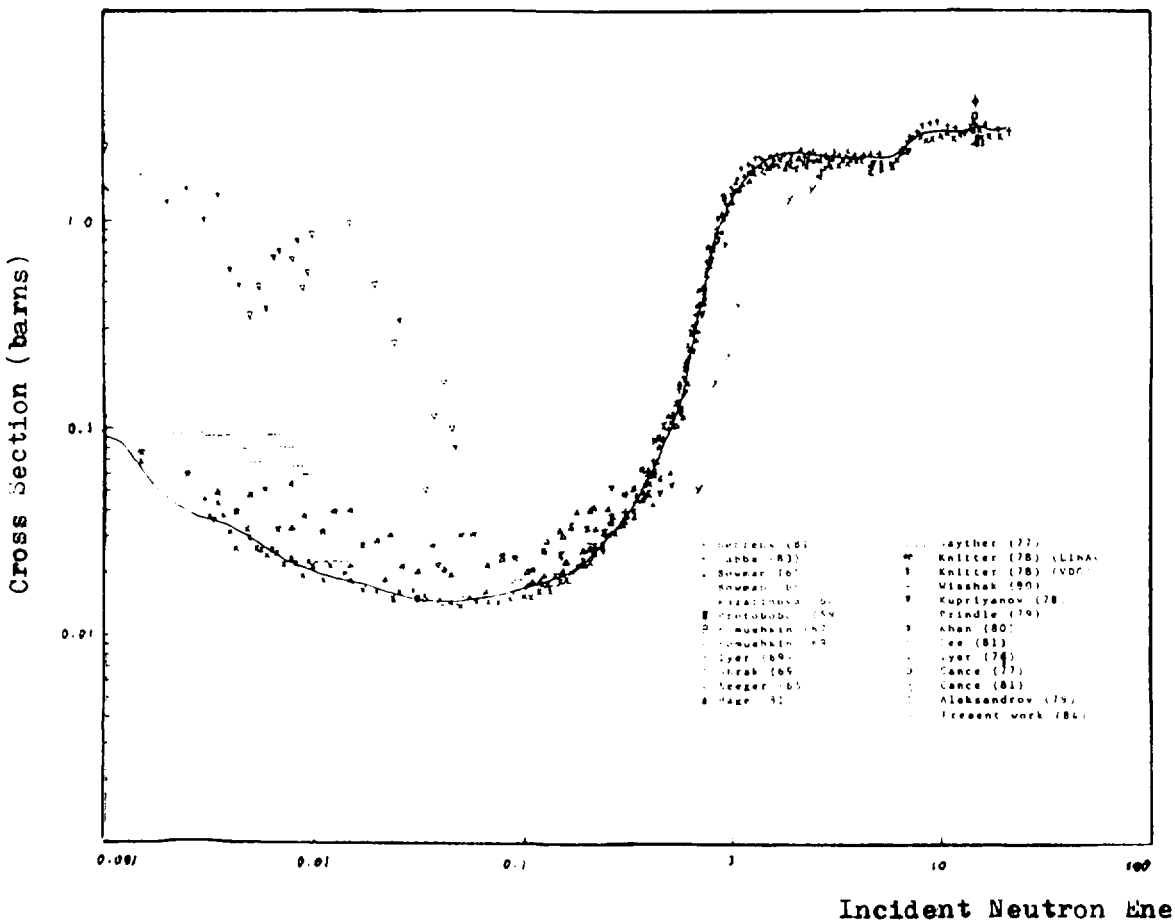

Fig. 2 Fission Cross Section of ^{241}Am

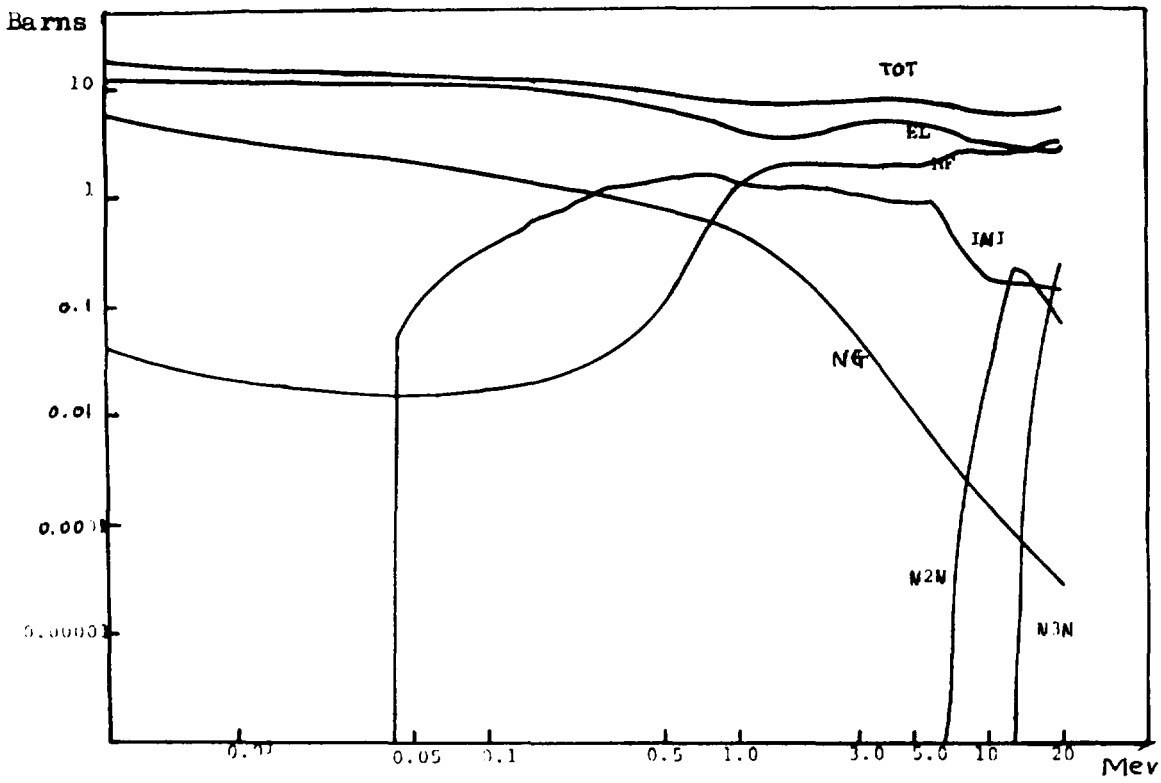

Fig. 3 Calculated cross sections of
Various reaction channels

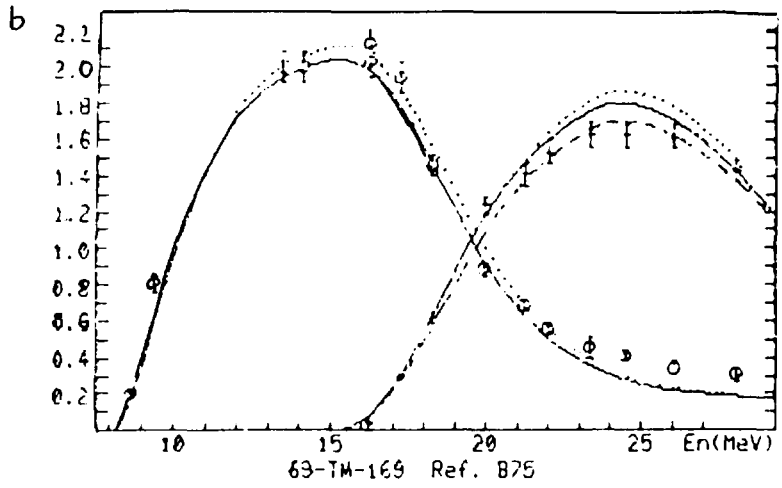

Fig. 4 Calculations with parameters from:
... (n,2n fitting; --- (n,3n fitting; —— systematics.

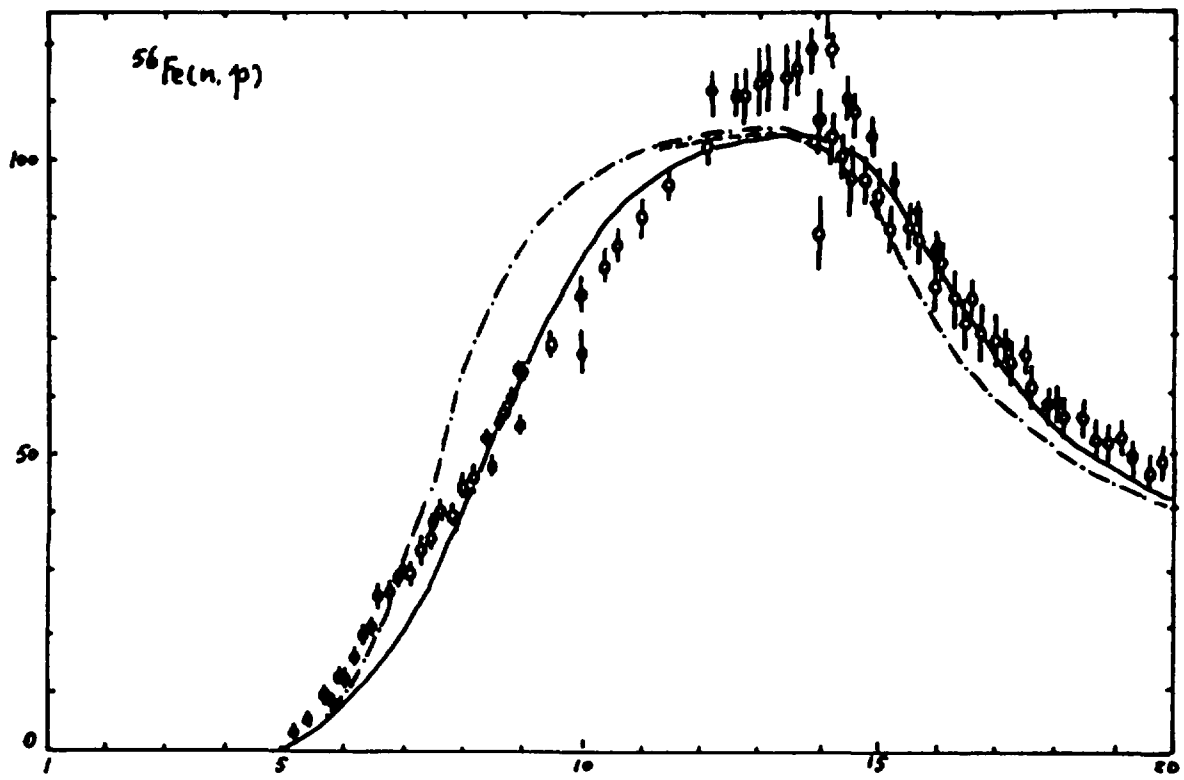

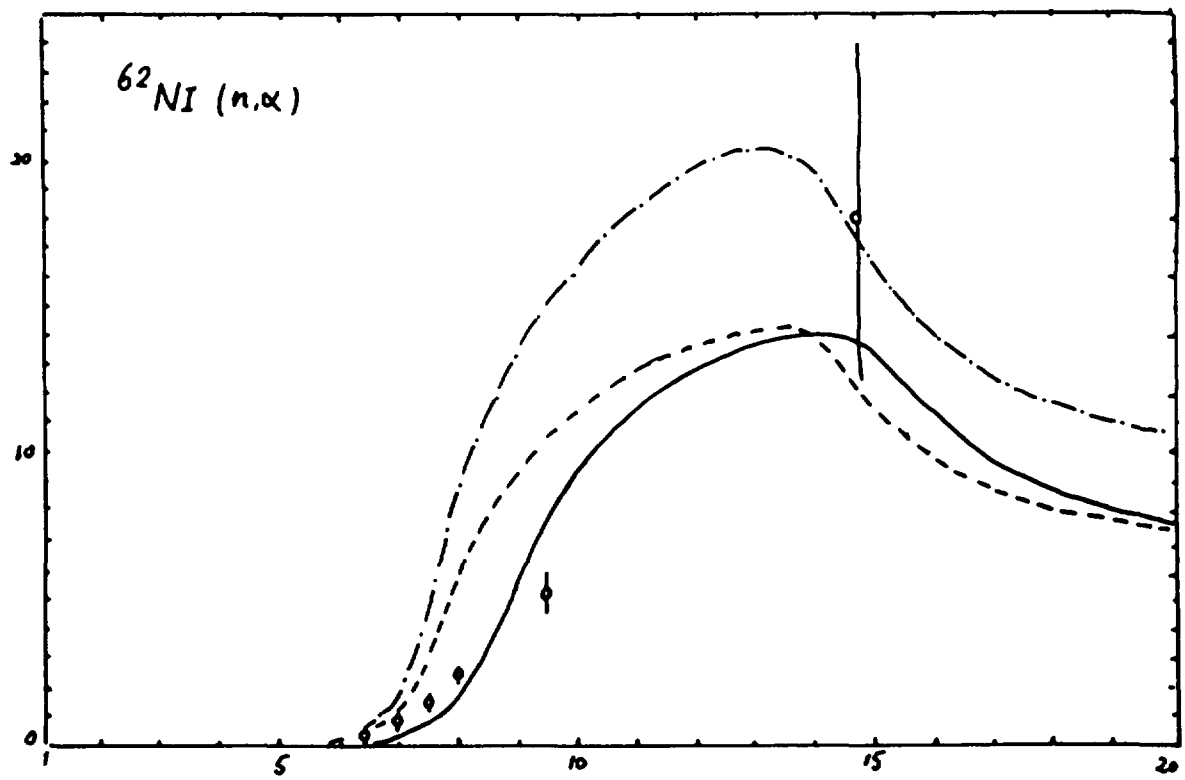

Fig. 5 and Fig. 6 ; ——— Fitting Curve

- - - Single Parameter Calculation

-·-·- Two Parameter Calculation

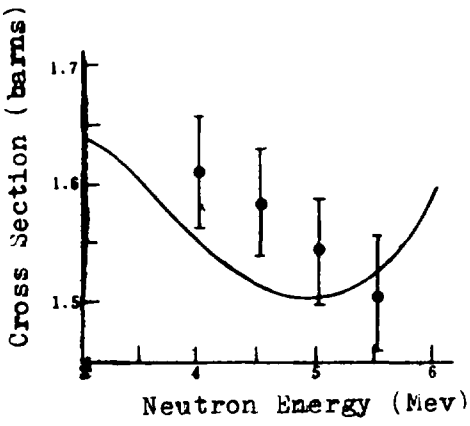

Fig. 7 ^{237}Np Fission Cross

- ● Present Work
- – ENDF/B-V

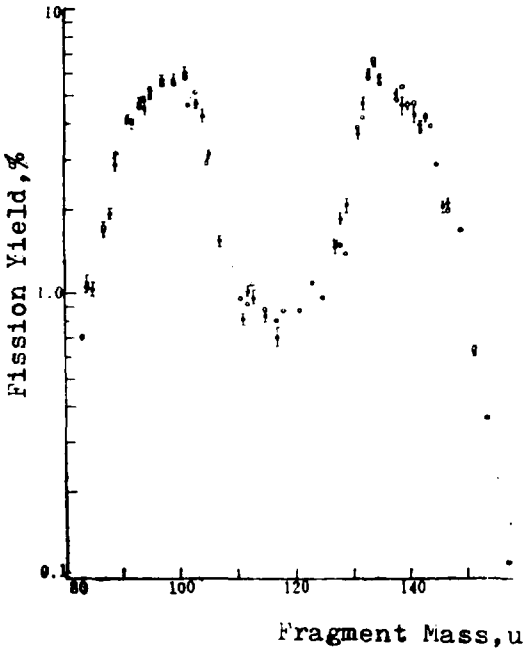

Fig. 8 14.9 Mev Neutron-Induced ^{238}U Fission Yield

- ● Present Work
- o D.E.Adams et al.

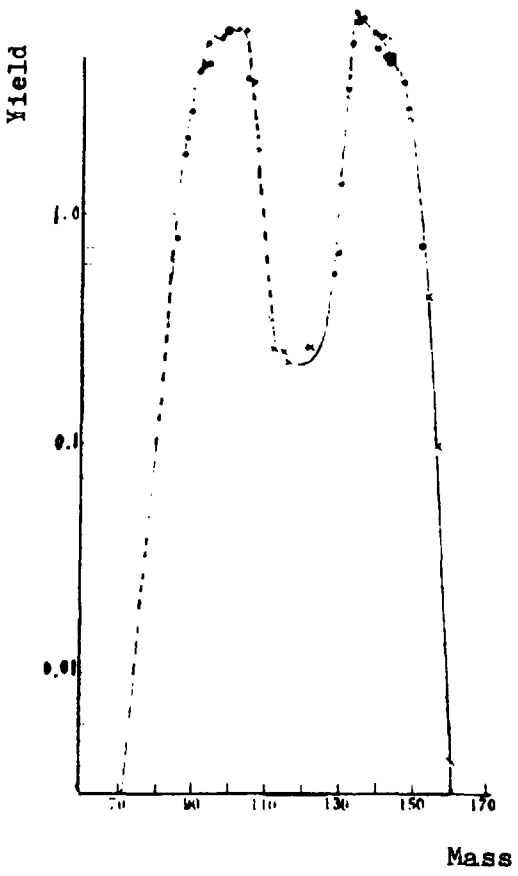

Fig. 9 8.3 Mev Neutron Induced Fission Yield of ^{238}U

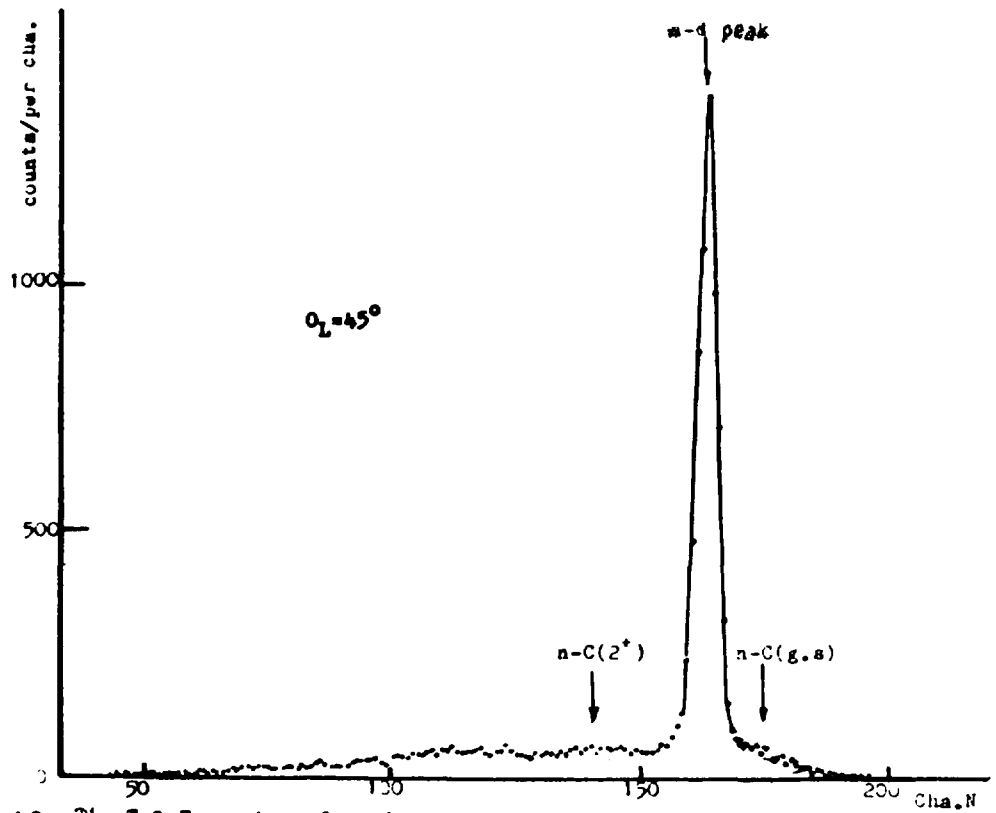

Fig. 10 The T.O.F spectrum from deuterate scintillation scatterer En=8.6 MeV
The threshold of scattering detector was about 10 KeV, T_{ch}=0.71 ns

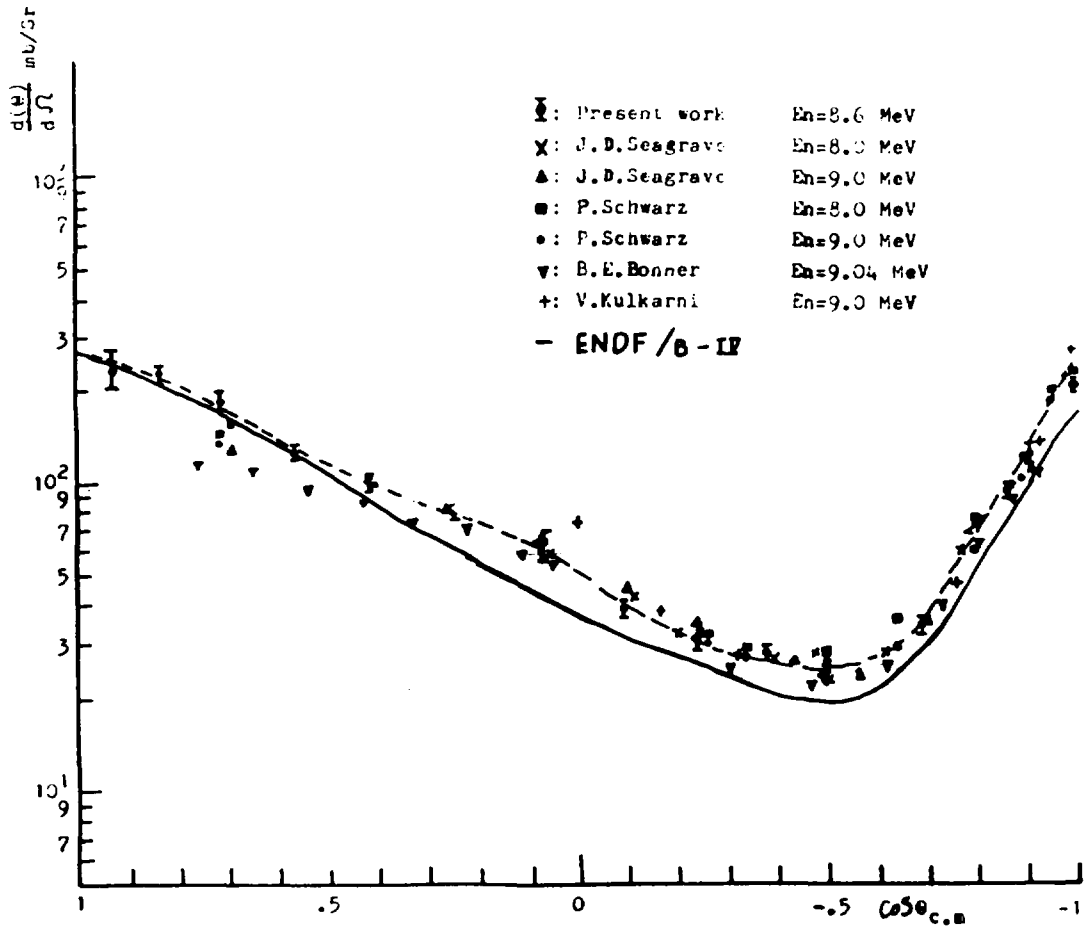

Fig. 11 The elastic scattering angular distribution from deuterium

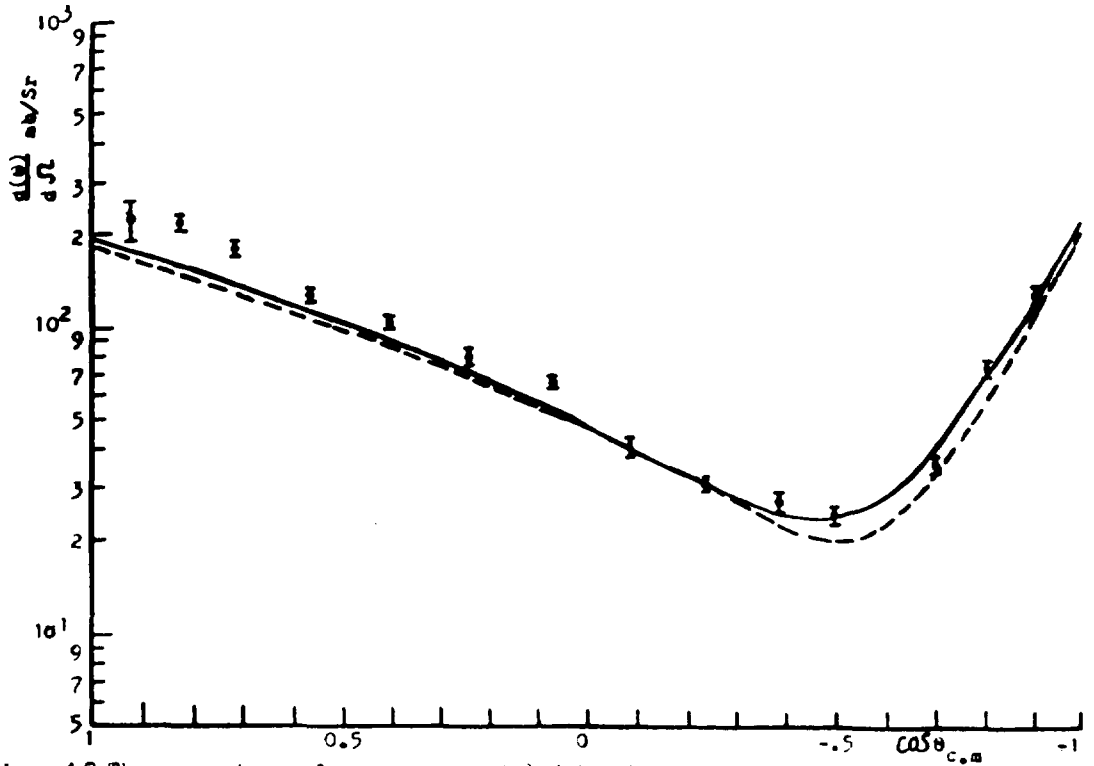

Fig. 12 The comparison of our experimental data with calculated results of theor.
I our experimental data En=8.6MeV. —— P-d phase shift calculated result
En=3.5 MeV. ---- Faddeev Equation calculated result

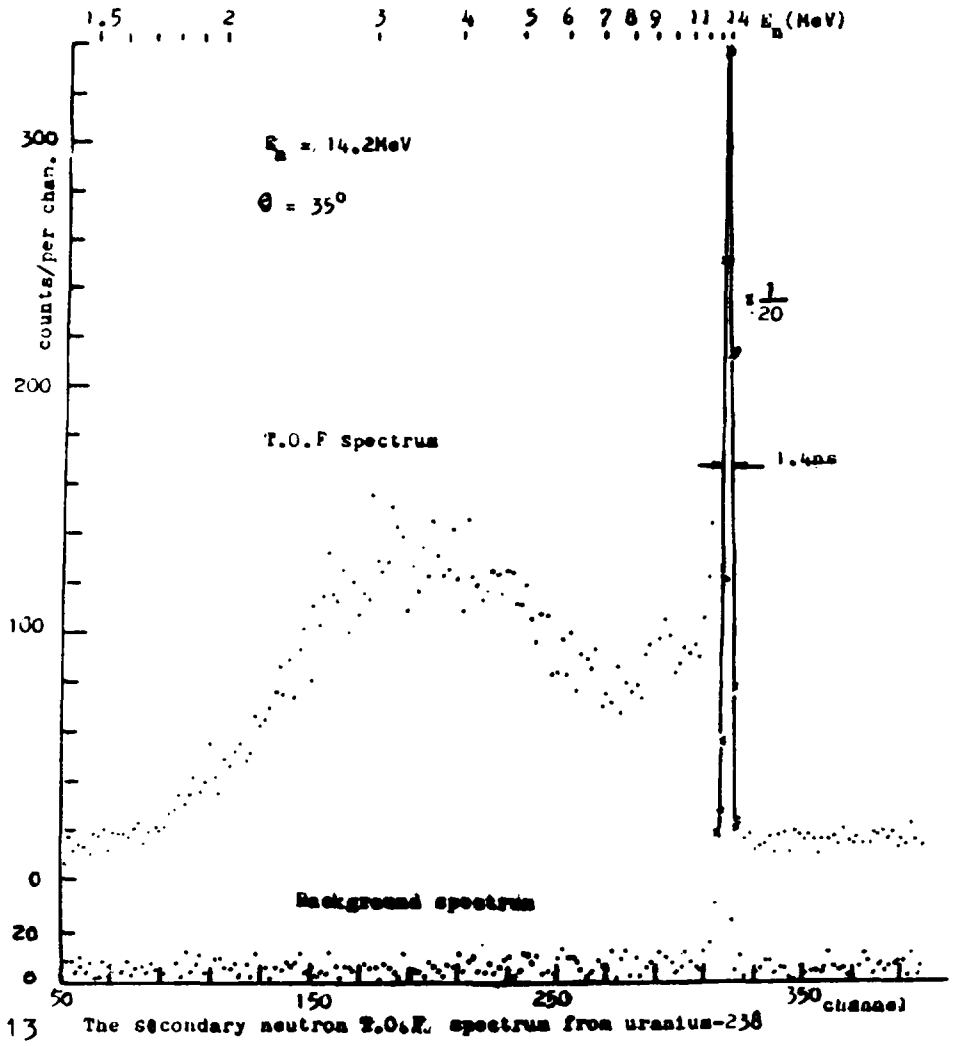

Fig. 13 The secondary neutron T.O.F. spectrum from uranium-238

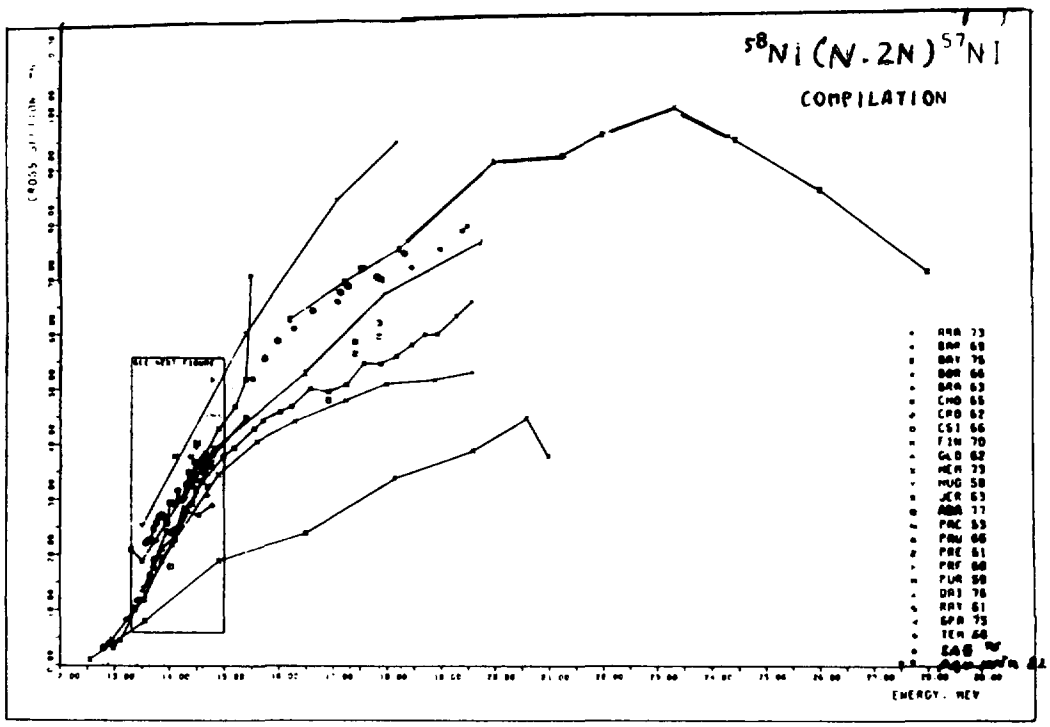

Fig.14 Compilation of data for $^{58}Ni(n,2n)^{57}Ni$ reaction cross section

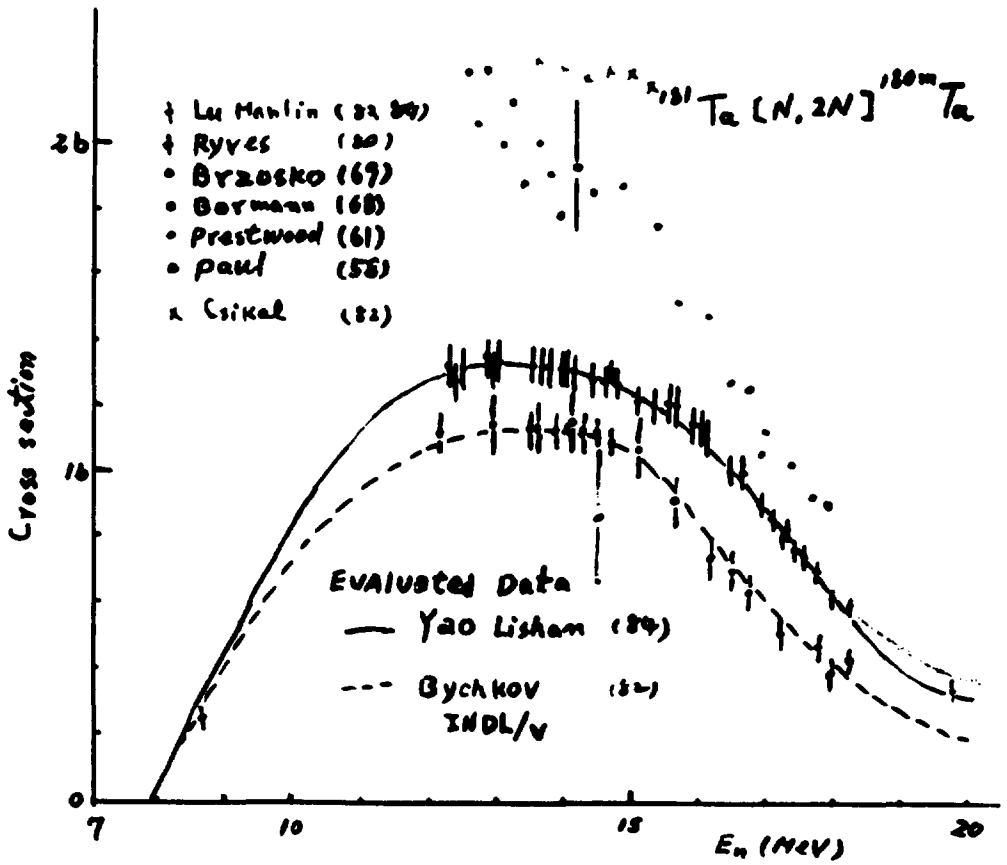

Fig.15 $^{181}Ta(n,2n)^{180m}Ta$

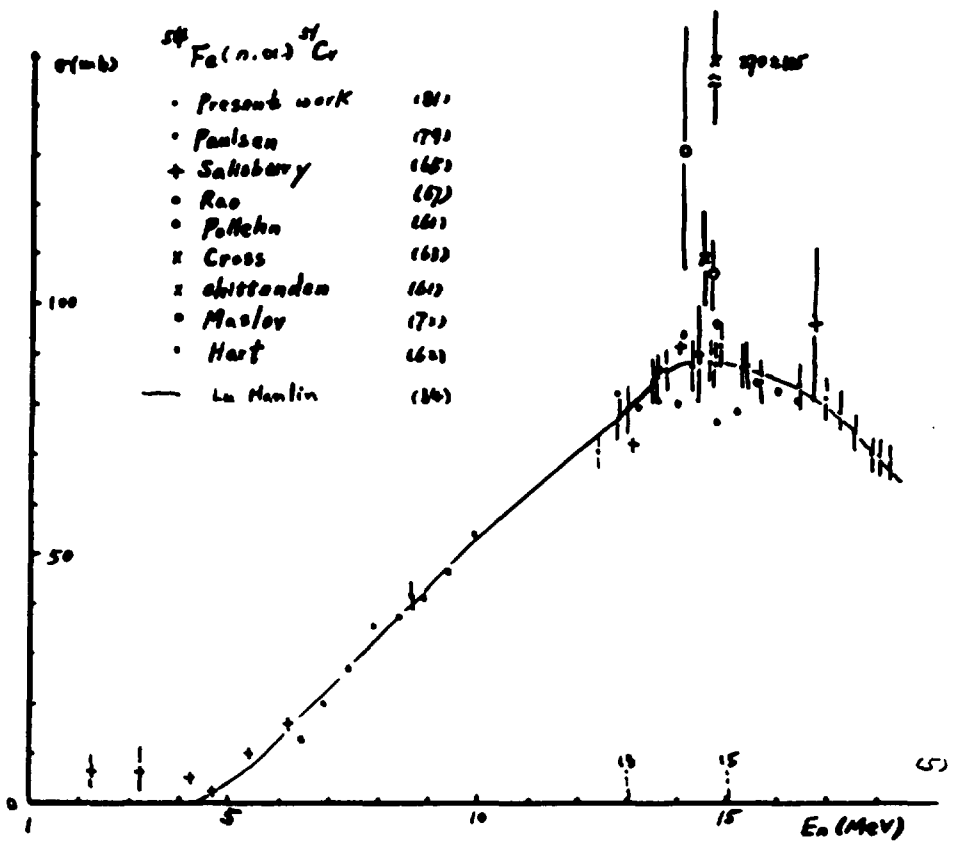

Fig.16 $^{54}Fe(n,\alpha)^{51}Cr$

Fig.17 $^{51}V(n,\alpha)^{48}Sc$

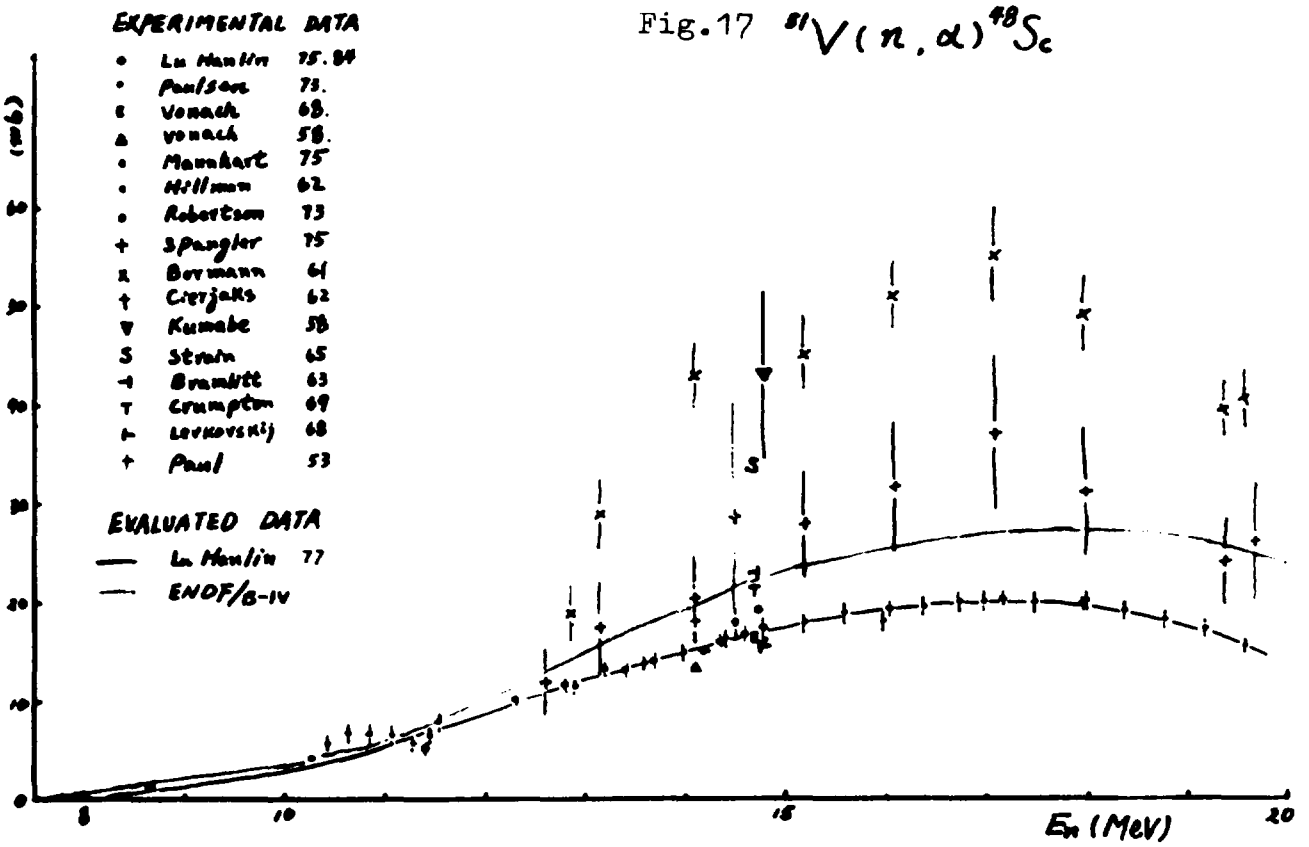

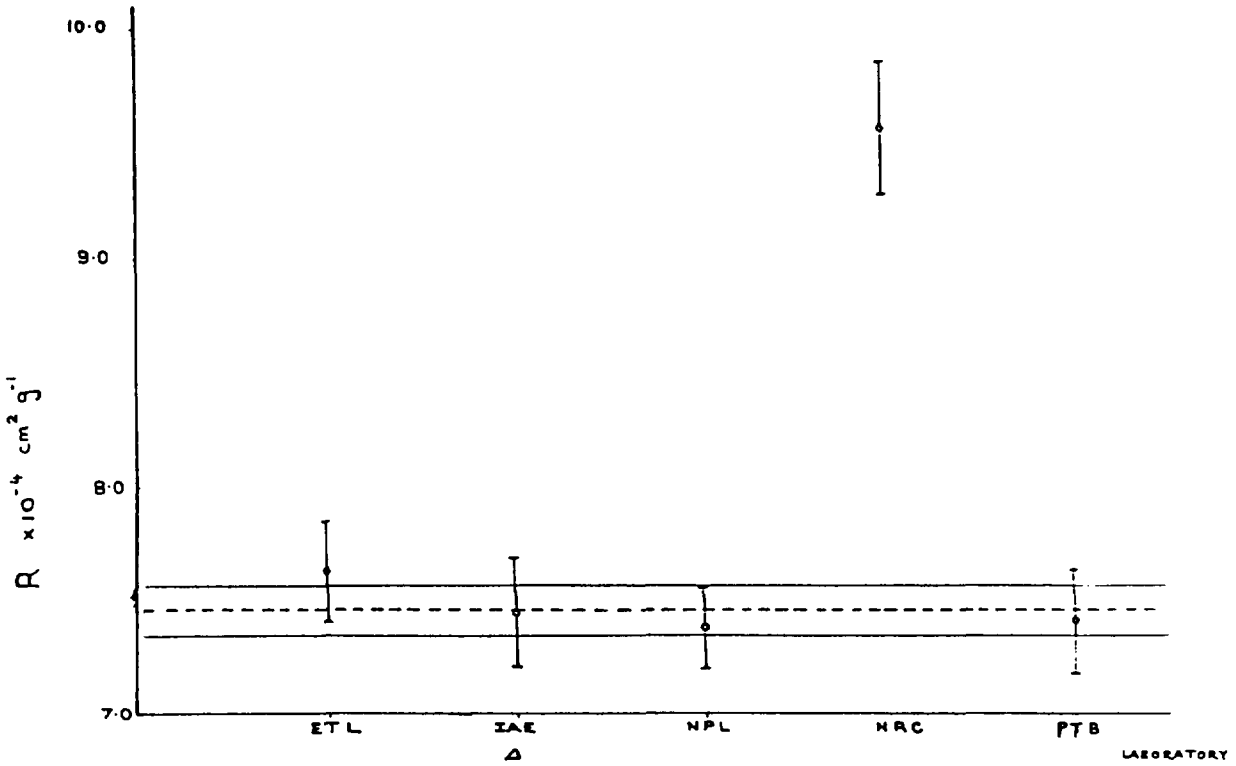

Fig.18 International fluence-rate intercomparison for neutron energy 144 Kev

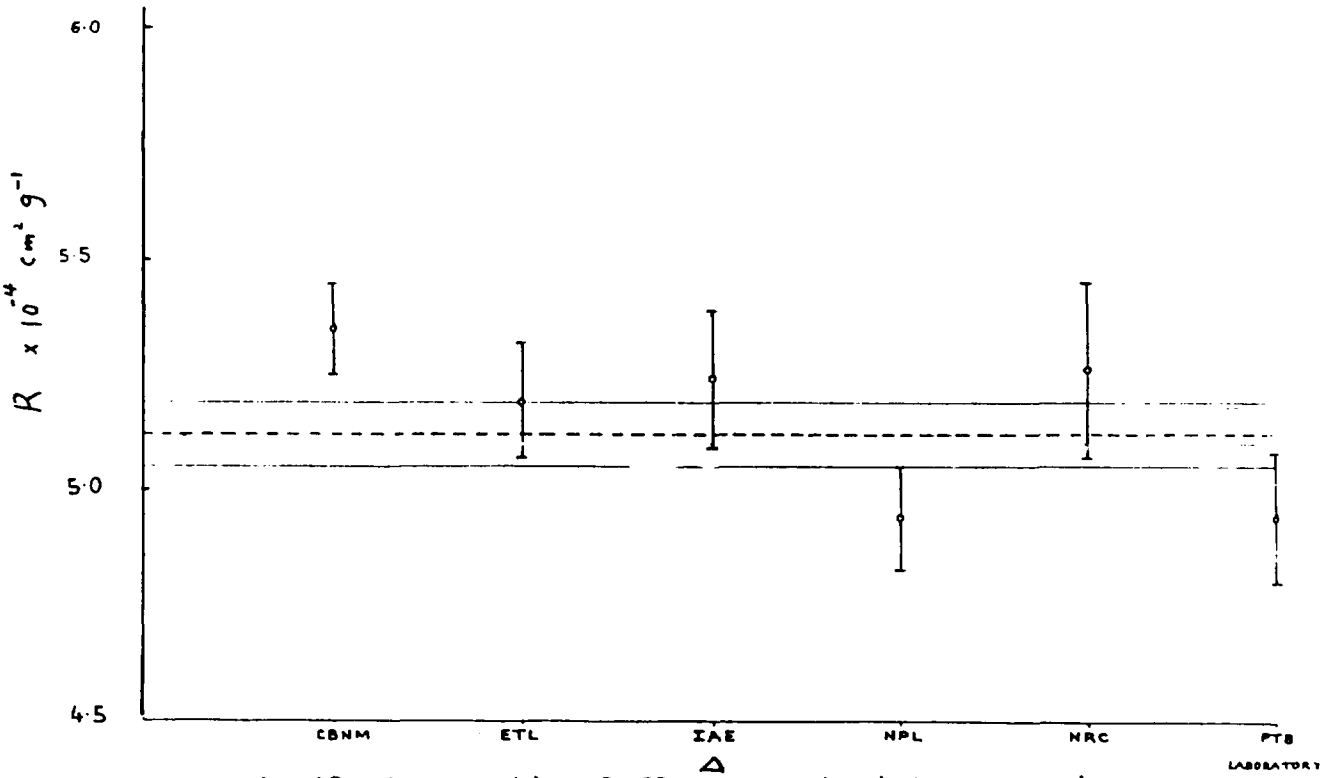

Fig.19 International fluence-rate intercomparison for neutron energy 565 Kev

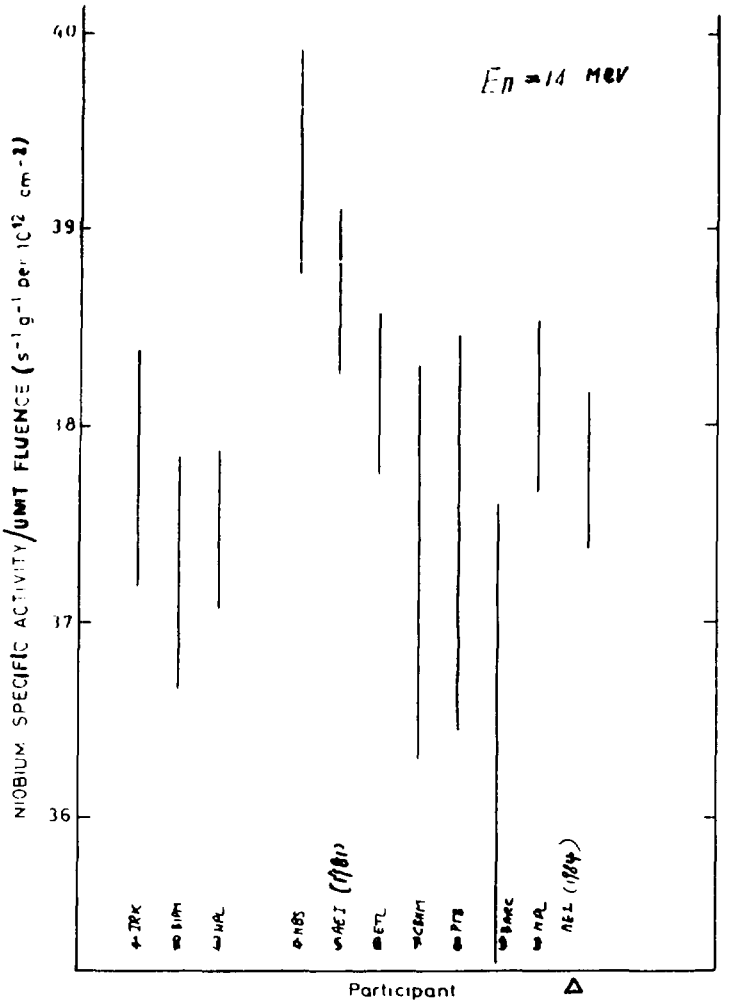

Fig.20 NIOBIUM ACTIVATION INTERCOMPARISON 1981

Fig.21 Data normalised to standard cross sections and corrections

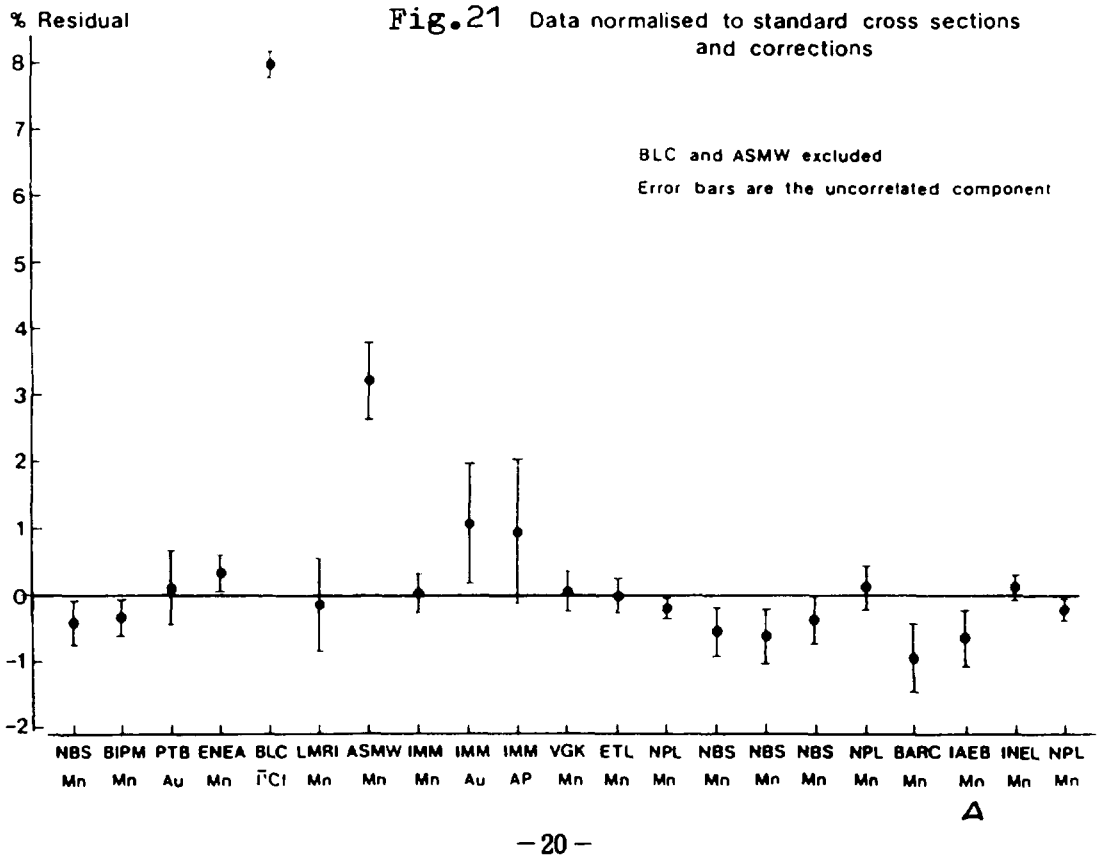

1.3 SOME NUCLEAR ACTIVITIES IN INDONESIA

R.S. L A S I J O

RESEARCH CENTRE FOR NUCLEAR TECHNIQUES

BANDUNG, INDONESIA

A b s t r a c t

Historical and constitutional background of BATAN and its activities are presented. Several experimental facilities possibly relevant to nuclear data activities are also discussed.

I N T R O D U C T I O N

Interest in nuclear field in Indonesia was organized for the first time in 1954, when the Committee for the Investigation of Radioactivity was formed. In 1958 this Committee was transformed to the Institute of Atomic Energy, and subsequently, in 1964, it was changed to the National Atomic Energy Agency. The establishment of a reactor Centre in Bandung, in 1965, was the milestone of starting the experimental and other nuclear activities in Indonesia.

NATIONAL ATOMIC ENERGY AGENCY (BATAN).

According to the Law No. 31, 1964, the assignment of BATAN is stated as follows :

> " To carry out, to regulate and supervise researches and utilizations of the atomic energy in Indonesia, for the sake of the safety, health and welfare of the people of Indonesia ".

This law confirms the status of BATAN as the sole body to be rensponsible for all activities involving atomic (nuclear) energy in Indonesia.

The function of BATAN is then derived into three fields of activities :

1. Manpower development, with the objective of widespreading knowledge in the uses of atomic energy, upgrading radiation workers, and calling for the people participation in the atomic energy development programs, and is subdivided into two sectors.

   a. Sector of education and training is to organize courses and trainings in nuclear science and technology, for internal BATAN's personnels as well as for other participants from outside BATAN.

   b. Sector of applications is to train and direct bodies outside BATAN to obtain knowledge and technical skill in radioisotope applications, especially for researches in agriculture, medicine, geological survey and industry.

2. Technical development, with the objective of the advancement of nuclear science and technology, and is subdivided into three sectors.

   a. Research and development sector.
      - isotope and radiation applications
      - fuel element and reactor technology
      - nuclear instrumentation and radiation protection
      - basic research in physics, chemistry and biology

- radioactive waste management.

b. Exploration , evaluation, exploitation and processing of nuclear materials.

c. Radioisotope production and fuel element fabrication.

3. Supervision, with the objective of creating lawful conditions in the uses of atomic energy, and is divided into three sectors.
~~three reactors~~.

a. Making laws and regulations for the uses of atomic energy.

b. Licencing and issuing minimum requirements for atomic installations and workers.

c. Inspection and supervision for atomic installations, workers, and environmental protection against radiations.

In the framework of the above activities the organization of BATAN is then structured as in Figure 1.
BATAN is chaired by a Director General, who is responsible to the Atomic Energy Council, which is chaired by the President of the Republic of Indonesia.

The Director General is assisted by two Deputies, subordinating several bureaus and centres. Assistants to the Director General are also a Secretariat and a Centre for Education and Training.

The new centre, UPT - PPIN, is also directly under the Director General, is located at Serpong, near Jakarta, and, according to plan , will be about twice the size of the whole present BATAN. , The new 30 MW Multipurpose reactor will be installed at this centre. Hence to successfully establish the new centre, most of the funds and forces of BATAN are now concentrated to its development.

SOME FACILITIES OF INTEREST

In the following discussion it is worthwhile to show several facilities , which are available or will be available, and are possibly relevant to nuclear data activities.

1. TRIGA MARK II Reactor with its irradiation facilities at PPTN Bandung, as shown in Figure 2 :

- Neutron diffracto-meter at tangential beam hole is currently used for crystal structure and magnetic studies.

- Beryllium detector neutron spectrometer at radial piercing beam hole, was earlier used for inelastic experi-

ments,but recently it was slightly modified and used for texture study.

- Twin neutron diffractometers at radial beam hole. One will be used for structure study and the other for texture study. Due to lack of fund the installation is delayed.

- Gamma spectrometer at thermal column beam hole will be used for thermal neutron radioactive capture study. The same situation as twin diffractometers, the installation is also delayed.

2. Tunzini Sames neutron generator at PAIR, Pasar Jumat, Jakarta. This machine was used for activation experiments, but at present is out of order. Attempt to repair the machine is still unsuccessful due to lack of spareparts and fund. We do hope the situation is getting more favourable in the near future. When the machine is successfully restored we plan to use it for fast neutron nuclear data measurements.

3. Multipurpose reactor, MPR-30, with its irradiation facilities, at Serpong, near Jakarta. The reactor is under construction and is expected to start operation in 1987. Small angle neutron scattering spectrometer is being designed with possibly cold neutron source, in cooperation with the Government of the Federal Republic of Germany. The beam hole lay-out and tentative experimental design is shown in Figure 3 and 4. The small angle neutron scattering facility is furnished with neutron guide system, and will be used for studies in solid state and materials science.

   A neutron diffractometer is also expected to be installed, in cooperation with the Government of Japan (JAERI).

4. At the some center, at Serpong there will also be installed a fixed energy cyclotron, with the following specifications.

Particle	Energy (Mev)	Current(uA) Interior	Exterior
proton	26	200	60
deuteron	15	300	100
He-3	38	135	60
He-4	30	90	40

The cyclotron will primarily be used for radioisotope production, but proposal for other uses is still possible.

5. Computing facilities.
   At PPTN Bandung there are available a minicomputer PDP-11/34A of 112 kiloword capacity and several microcomputers. At BATAN's Head Office in Jakarta an IBM Computer of 1 Megabyte capacity and several microcomputers are also available. At Serpong (UPT-PPIN) there will be about three VAX computers of total capacity exceed 10 Megabyte.

NUCLEAR DATA GROUP

The importance of nuclear data in several activities like the calculations of core design and analyses, shielding problems, etcetera and the growth of activities in several nuclear science and technology, nuclear data group may contribute a very important role in the future nuclear energy development in Indonesia.
Cooperation with more advanced institutes like JAERI in nuclear data activities is very important and very helpful in establishing the group in Indonesia.

----------(kh)----------

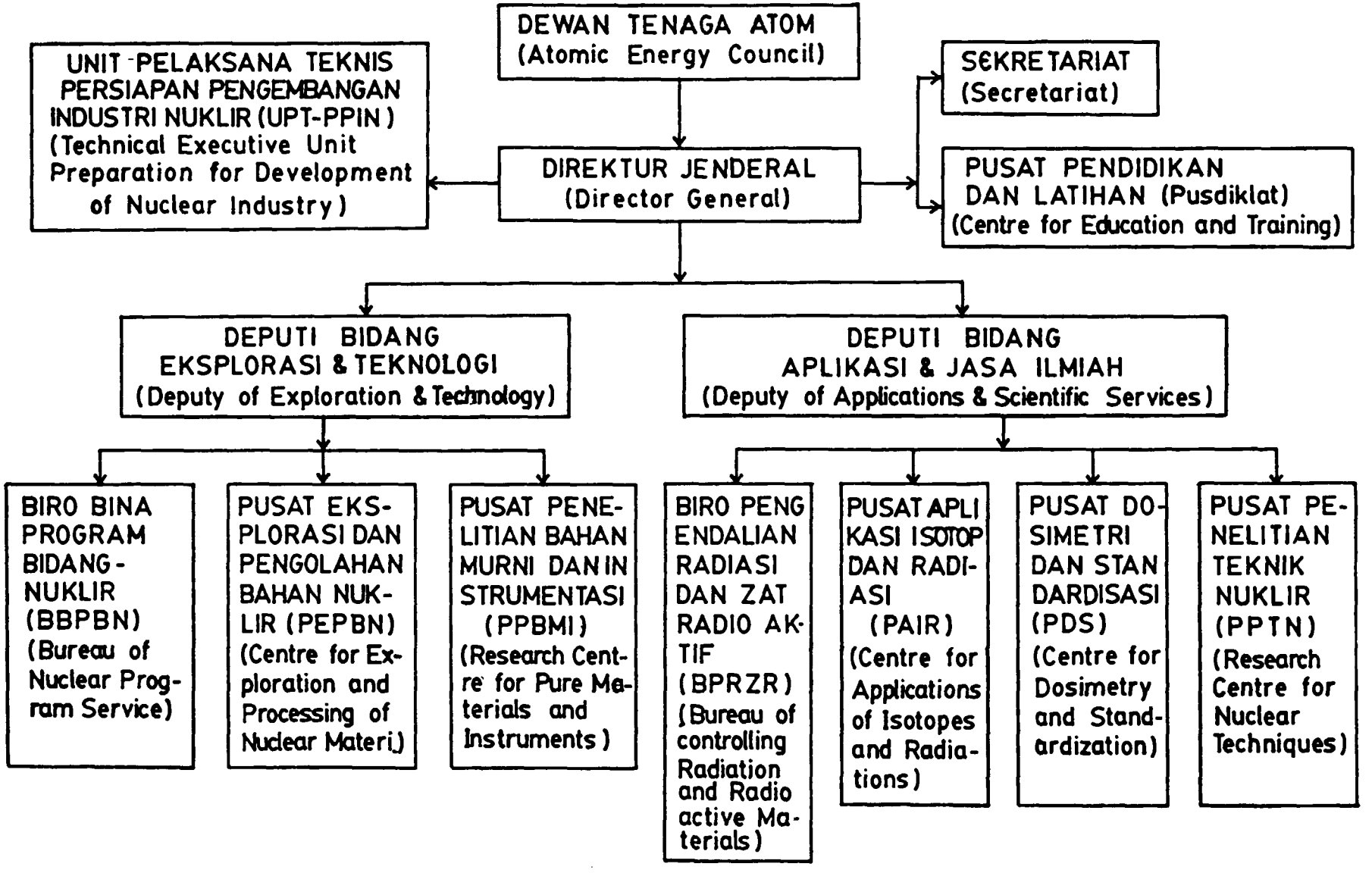

Fig. 1 ORGANIGRAM BADAN TENAGA ATOM NASIONAL (BATAN)
(National Atomit Energy Agency)

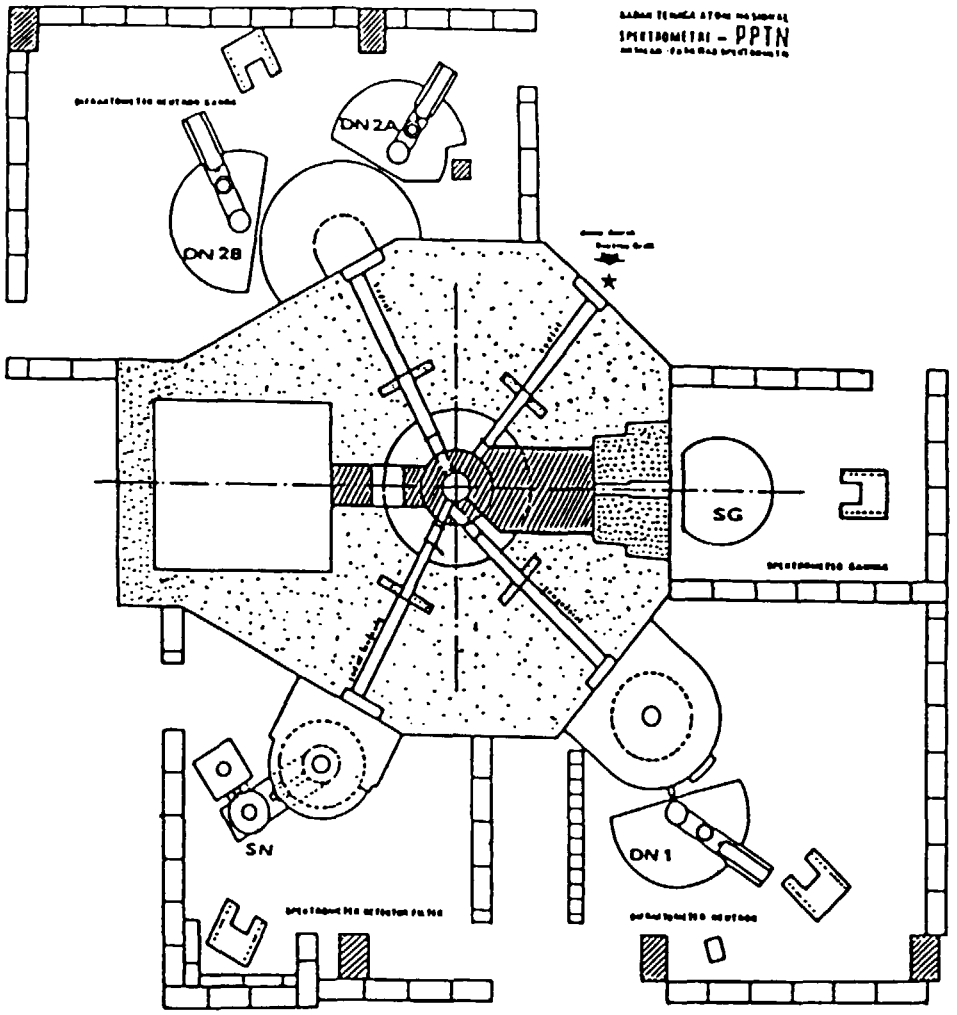

Fig.2 Lay-out of 1 MW TRIGA Mark II Reactor and instrumentations.

DN1 = Neutron Diffractometer
Detectors : BF_3, He-3.
Resolution: 45' at 2θ = 16.30°
60' at 2θ = 40.26°
75' at 2θ = 68.58°
Made : Home made.

SN = Neutron Spectrometer
Detectors : BF_3, He-3 (for texture studies)
Inverted Filter Beryllium (for inelastic scatterings)
Resolution: (for texture)
50' at 2θ = 19.80°
64' at 2θ = 31.50°
76' at 2θ = 40.80°
Made : Arms, by BARC, India.
Other parts, home made.

DN2A & DN2B = Twin Neutron Diffractometer
Detectors : BF_3, He-3.
Resolution: Expected to be the same as DN1.
Made : home made (still under construction)

SG = In Beam Gamma Ray Spectrometer
Detectors : NaI(Tl), HPGermanium.
Resolution: NaI(Tl) 315 keV at 1.33 MeV
HPGe 2.5 keV at 1.33 MeV
Made : Home made (still under construction)

X-Ray Spectrometer (situated in other room)
Detector : NaI(Tl).
Resolution: 12' at 2θ = 38.50° (Cu-Kα)
10' at 2θ = 82.50° (Cu-$K\alpha_1$)
18' at 2θ = 137.50° (Cu-$K\alpha_1$)
Made : Shimatzu, Japan.

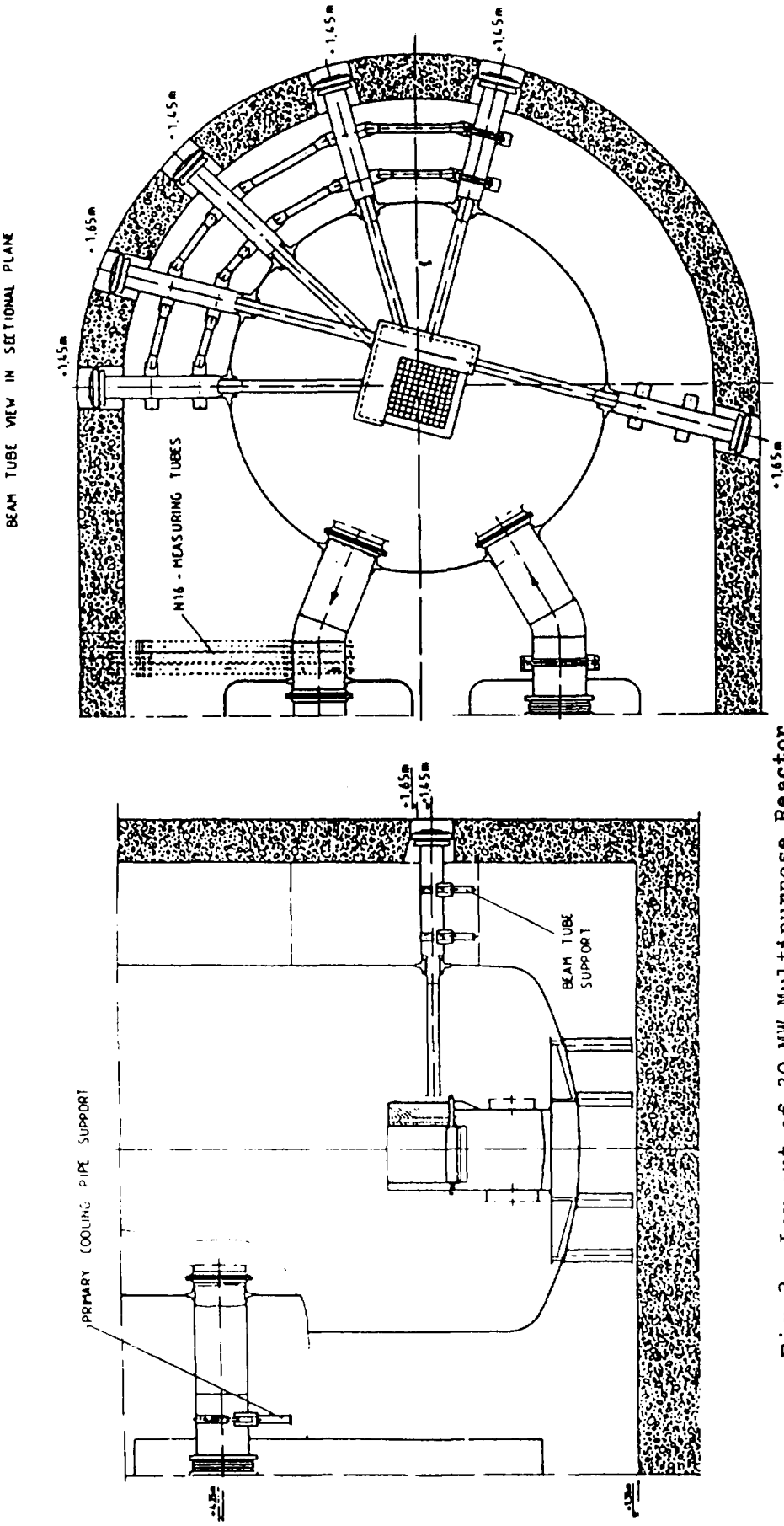

Fig.3 Lay-out of 30 MW Multipurpose Reactor with irradiation facilities.

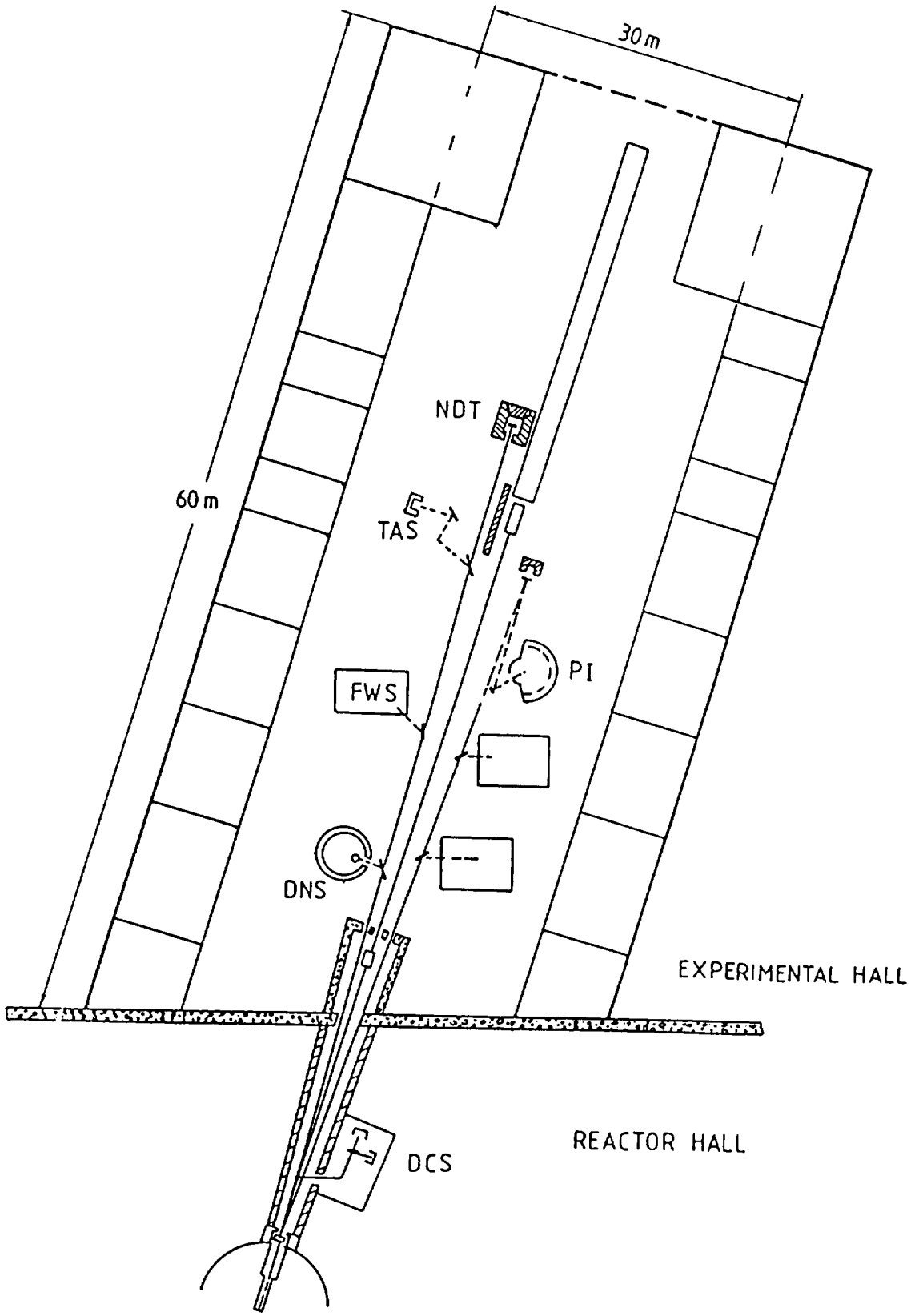

Fig.4 Sketch of the neutron-guide hall with neutron guides and instrumentations

2. ACTIVITIES OF JNDC WORKING GROUPS

2.1 Fission-Product Cross Section Evaluation, Integral Tests and Adjustment Based on Integral Data

Fission-Product Nuclear Data Working Group
Japanese Nuclear Data Committee

T. Watanabe (KHI), S. Iijima, M. Kawai (NAIG), M. Sasaki (MAPI)
T. Nakagawa, Y. Nakajima, Y. Kikuchi, H. Nishimura (JAERI),
T. Nishigori (Osaka U.), H. Matsunobu (SAI), H. Zukeran (Hitachi ERL)

Abstract

Recent activities made by Fission-Product Nuclear Data Working Group in JNDC were briefed. This review consists of following three parts.

1. The JENDL-2 fission product data file was recently completed (Ref. 1) which contains neutron cross sections for 100 nuclides from Kr to Tb. The evaluation was made by using the latest data of capture cross sections and resonance parameters. The optical model parameters and level density parameters were re-evaluated. The results of the previous integral tests using the data of the STEK sample reactivity and CFRMF sample activation were also reflected on the evaluations. Details are reported in Ref. (2 $\sim$ 4).

2. The integral test of JENDL-2 fission-product cross sections is now in progress using the EBR-II sample irradiation data and the STEK and CFRMF data. The 70 group constants were generated by MINX code with the self-shielding factor tables. The values of the normal and adjoint fluxes and their uncertainties necessary for 70 group evaluation were obtained by spline fitting interpolation using the value of Ref. (14).

3. The adjustment of evaluated cross sections based on the integral data is also in progress using the Bayesian least-square method. The data adjustment will be made especially to (1) the nuclides which only integral data are available (e.g., Xe-131, 132, 134, Pm-147, Eu-152, 154) and to (2) those which the differential and integral data are mutually inconsistent (e.g., Tc-99, Ag-109, Eu-151, 153). The cross section covariances are generated by the "strength function model" taking into account of the statistical model uncertainty (Ref. 5). The uncertainties of neutron spectra and adjoint spectra were also taken into account as the "method uncertainties". Interium results of integral test and adjustment are presented and discussed.

The near-future scope of the work and the plan for JENDL-3 are briefly described.

1. Introduction

The objective of this presentation is to give a brief review of the recent activities made by JNDC FPND WG. The review consists of three parts as follows:

The first part is the evaluation of JENDL-2 fission products data file. This work was recently completed.

As the evaluation methods were already published (Ref. 1 ∿ 3), only summary will be given here to explain the characteristics of JENDL-2 FP file.

The second part presents the interium results of the integral test of JENDL-2 FP. EBR-II experiments were analysed together with the STEK and the CFRMF experiment which had once been analysed in the previous JENDL-1 FP integral test (Ref. 6 ∿ 9).

The third part is the adjustment of the cross section values using the integral test results. In order to quantitatively reflect the integral test results adjustments based on Bayesian principle (Ref. 10) were applied especially to the nuclides which belongs to the following two categories;

(1) those for which only integral data are available,
(2) those for which the differential and integral data are mutually inconsistent.

Near future scope of the work and the future plan for JENDL-3 are briefly described.

2. Evaluation of JENDL-2 Fission Products Data File

The main aspects of JENDL-2 FP data file and the characteristics of the evaluation method are shown in Table 1 and 2.

In the energy region from 10^{-5} eV to the upper boundary of the resolved resonance region, the parameters in the multilevel Breit-Wigner formula were sought and obtained in order to make the formula well agree with the measured cross section data. Negative energy resonance levels were introduced here to improve the agreement of the formula with the measured values of the 2,200 m/s cross section and the resonance integral. The status of the resolved resonance region evaluation are shown in Table 3.

Up to 100 keV, unresolved resonance description by strength function models (ASREP; Ref. 11) was adopted to represent the measured cross sections or evaluated ones.

Above 100 kev, the optical models and statistical theory calculations (CASTHY; Ref. 12) were used. The optical model parameters were evaluated using the SPRT method.

The level density parameters for the Gilbert-Cameron formula were completely re-evaluated using the recently published Dobs and level scheme data (Ref. 13).

The smooth capture cross sections were fitted to the recently measured data. Where no measurement data were available, systematics or the previous integral test results were used. These data status are shown in Table 3. We can see that the JENDL-2 FP file owes greatly to ORELA measurements.

For the secondary neutron energy distribution of the continuum inelastic scattering process, the evapolation models were applied.

3. Results of Integral Test of JENDL-2 FP

Integral tests are in progress using STEK, CFRMF and EBR-II (Ref. 6 ∿ 8) experiments. The summaries of these experiments are shown in Table 4.

In the STEK experiment, the reactivities were measured by pile oscillation method, and relative values (ρ/ρ_o) normalized to the fission rate of 1g U-235 which is multiplied by the worth of Cf-252 and is presented in the following formula.

$$\frac{\rho}{\rho_o} = \frac{M_{235}}{M_s} \frac{\sum_i \phi_i \left(\sum_k \sigma_{cik} A_k\right) \phi_i^* + \sum_{ij} \phi_i \left(\sum_k \sigma_{sk}(i \to j) A_k\right) (\phi_j^* - \phi_i^*)}{\sum_i \sigma_{fi}^{235} \phi_i \sum_j X_j^{252} \phi_j^*}$$

Here

ϕ_i	;	i-th group neutron flux in sample position
ϕ_i^*	;	i-th group adjoint flux in sample position
σ_{cik}	;	i-th group capture cross section for k-th nuclide
$\sigma_{sk}(i \to J)$	;	k-th nuclide scattering cross section from group i to j
σ_f^{235}	;	i-th group fission cross section for U-235
X_j^{252}	;	i-th group Cf-252 spontaneous fission spectrum
A_k	;	k-th nuclide atomic abundances in the sample

For normal and adjoint flux (ϕ, ϕ^*), σ_f^{235}, and X^{252}, the evaluated values given in Ref. (14) were adopted in this test. Interpolation was made from those reported values to obtain the data for the JFS-3 70 group structure using 3rd order B spline method (BINTFX).

The flux in STEX sample position is shown in Fig. 1 for example. Group constants σ_c and σ_s were prepared by using MINX program from the JENDL-2 FP file assuming 1/E spectrum.

For C, Al, Cl original JFS-3 library was used in the present analysis. To make macroscopic cross section of sample, resonance shielding in the finite sample was taken into account.

In the latest integral data of the CFRMF experiment, which differs from the preliminarily published ones, the average activation cross sections were reported.

Treatment of the flux and resonance shielding are same as in the STEK analysis.

In the EBR-II experiment, infinite dilution capture cross sections were measured in 6 spectrum fields, and the flux are processed with the same method as that of STEK analysis.

The program system used in these integral tests are shown in Fig. 2. The main analysis program is FPSSR.

Although only interium results have been obtained until now, C/E values are shown in Table 5. Brief discussions and comparisons with the results of JENDL-1, JEF-1, and ENDF/B-V for important FP nuclides for FBR are as follows.

Rh-103

In the STEK experiment C/E values distribute from 0.74 to 2.12, and compared to JENDL-1 for STEK-1000, the C/E value become worse from 0.96 to 1.09. As the C/E value for STEK-1000 using JEF-1 is reported to be 0.99 a detailed examination will be necessary to this nuclide.

Ru-101

In the STEK experiment, C/E values are between 0.98 and 1.18, and compared to JENDL-1 and JEF-1 better agreement is obtained.

Tc-99

For STEK-1000, JENDL-2 and JEF-1 give C/E value as 0.94 and 0.95 respectively, while for CFRMF 1.23 and 1.2. Using ENDF/B-V (Ref. 16), C/E is 1.15. So inconsistency is seen between the integral data. JENDL-2 gives better C/E than JENDL-1.

Cs-133

C/E value for CFRMF is 0.91, and JEF-1 and ENDF/B-V give 1.02 and 0.95 respectively. For STEK-1000 JEF-1 and JENDL-2 gives 1.01 and 0.81. So the capture cross section obtained in JENDL-2 seem to be slightly small and detailed examination is necessary.

Pd-106

C/E value are between 1.19 and 1.33, and largely differed in the inverse direction compared with the JENDL-1 results. As JEF-1 gives consistent results, re-examination seems necessary.

Sm-149

In EBR-II data, JENDL-2 gives C/E values more than 10% better than ENDF/B-V. In STEK-1000, JENDL-2 gives agreement of almost same order with that of JEF-1.

Ag-109

For the CFRMF experiment JENDL-2, ENDF/B-V and JEF-1 gives C/E as 0.67, 0.86 and 0.9 respectively. So detailed examination is necessary.

Compared to the results of JENDL-1, JENDL-2 FP file gives the number of nuclides which gives better C/E is 25, the number of nuclides which gives worse C/E is 10.

So it may be considered that better consistency is obtained in JENDL-2 FP.

As these results are of intrium nature, detailed investigations for following items are necessary.

(1) Effects of spatial flux shielding of strong absorber nuclides; e.g., Rh-103, Ag-109, and Tc-99. These nuclides show very large C/E values for STEK-4000 data because of its soft spectrum.

(2) Reasons for large diversion of C/E in weak absorbers.

To almost all weak absorber, C-E for ρ/ρ_0 show discrepancies in same direction, and the largest discrepancies are obserbed in STEK-500 where scattering component have the largest contribution (Fig. 2).

The possible reasons may be

a. the effects of capture cross sections
b. the inelastic scattering cross sections
c. effects of added nuclides such as O, AL, etc.
d. inaccuracy of adjoint flux

Seeing from the status of differential data, uniform shift of capture cross sections for such large numbers of nuclides are unjustifiable. In JENDL-1 integral test of O showed large discrepancy in which scattering component contributes mostly and cross section is regarded to be accurate. So effects of b. to d. should be examined in future.

4. Adjustment of the Cross Section by the Integral Test Results

Test adjustments are in progress for the nuclides which only integral data are available (Xe-131, 132, 134, Pm-147, Eu-152, 154) and those which shows mutual inconsistency between the data (Tc-99, Ag-109, Eu-151, 153). The basic theorem is based on Bayesian principle (Ref. 10). Cross section covariances are generated using strength function models taking into account of the statistical model uncertainty (Ref. 5). Uncertainty of normal and adjoint flux was also taken into account as "method uncertainty". The formula is fundamentally as follows, and the flow diagram of the program are shown in Fig. 2.

$$T' = T + MG^{+}W(R^{e} - R^{c}(T)) \qquad W = \frac{1}{V^{m} + V^{e} + GMG^{+}}$$

$$R^{c}(T') = R^{c}(T) + G(T' - T) = R^{c}(T) + GMG^{+}W(R^{e} - R^{c}(T))$$

$$M' = M - MG^{+}WGM$$

$$V^{c}(T') = (V^{e} + V^{m})W[GMG^{+} + V^{m}W(V^{e} + V^{m})]$$

Here

- T ; cross section to be adjusted
- M ; covariance matrix for T
- G ; sensitivity coefficient of T for integral data R
- R ; vector of integral data
- V ; covariance matrix of integral data R

The upper suffices stand for as follows.

- $+$; transposed matrix
- $'$; adjusted quantity
- m ; method uncertainty
- c ; calculated quantity

As this work is in progress now, only preliminary results are obtained and shown in Table 6 and Fig. 4.

From these results it is evident that cross sections are improved for nuclides which have no differential data, however, discrepancy remained for nuclide which have small uncertainty in differential cross sections such as Ag-109.

Although the adjustment has been made only to one integral data, results seems to be promising.

Extensive adjustment work using multi-integral data are going to be carried out in near future.

5. Near Future Plan

Including the detailed analysis explained above, JNDC FPND WG have made following near future plan and the scope of JENDL-3.

(1) Extensive integral test and adjustment
(2) Preparation of pseudo FP cross sections to apply to FBR (work started)
(3) Evaluation of JENDL-3 FP data file
    (a) Extension to about 180 nuclides
    (b) Feedback from the integral tests
    (c) Inclusion of (n, 2n), (n, Xp), and (n, X) reaction using simplified calculational models
    (d) Evaluation of covariance matrix

6. Acknowledgement

The authors would like to thank to members of JAERI Nuclear Data Center for their support to file evaluation and to Dr. M. Nakagawa for the support in our preparing of group constants and analysis programs in JFS-3 group structure.

References

1. JENDL-2 Fission Products Cross Section File edited by T. Nakagawa
2. 1984 Nuclear Data Seminar, JAERI-M85-035, p.371 (1985)
3. Aoki, T. et al., Evaluation of FP cross sections for JENDL-2, a paper presented to poster session of Int. Conf. on Nuclear Data for Basic and Applied Science, Santa Fe, May 1985
4. JNDC FP Nuclear Data Working Group, Evaluation of Fission Products Cross Sections for JENDL JAERI-M84-182, p.31 (1984)
5. Gruppelaar, H., IAEA-110, Vol. II p.61 (1976)
6. Anderl, R.A., EGG-PHYS-5182 (1980)
7. Veenema, J.V. et al., ECN-10 (1976)
8. Harker, Y.D. et al., NEANDC(E)-209"L" (1979)
9. Iijima, S. et al., NEANDC(E)-209"L" p.317 (1979)
10. Dragt, J.B. et al., Nucl. Sci. and Eng. 62,117 (1976)
11. Kikuchi, Y., ASREP Manual
12. Igarasi, S., CASTHY Manual
13. Gilbert, A. and Cameron, A.G.B., Can. J. Phys. 43,1446 (1965)
14. Dekkar, J.W.M. et al., ECN-35 (1978)
15. Gruppelaar, H. et al., Integral test of fission product cross section Nucl. Data for Basic and Applied Science, Santa Fe, May 1985
16. Anderl, R.A., EGG-PHYS-5406 (1981)

Table 1 Main Aspects of JENDL-2 FP Data File

Number of nuclides	: 100	Z = 36 (Kr) - 65 (Tb) except Sn and most of Te.
		: 99.6% of total FP poisoning in FBR. 195% of ^{239}Pu fission yield.
Energy range	: 10^{-5} eV - 20 MeV	
Reactions	: Total, capture, elastic and Inelastic scattering. Some threshold reactions for Nb and Mo isotopes.	

Table 2 Characteristics of Evaluation Method

(1) Adoption of new resonance and capture data up to July, 1984.

(2) Complete re-evaluation of resonance parameters.

(3) Feedback from integral test results on JENDL-1 and -1.5 files.

(4) Thermal cross sections adjusted by introducing the negative resonance.

(5) Unresolved resonance description up to 100 KeV by the "strength function model" (ASREP code).

(6) Optical model and statistical theory calculation at high energy (CASTHY code). New parameterology for optical model parameters and level density parameters. Re-evaluation of level scheme data. Gamma-ray strength function adjusted to capture data.

(7) Full use of parameter data base system, JOBSETTER (CASTHY).

Table 3 Status of Evaluated Resolved Resonance Levels and Capture Cross Section to be fitted in Optical Model Calculation

S: Systematics

Nuclide	Upper boundary of resonance region (eV)	No.	Formula	Recent σ_c measurement	S_γ adjustment
Kr-83	272.0	3	MLBW	-	OLD
84	2480.0	3	MLBW	-	OLD
85	no resonances		-	-	S
86	no resonances		-	-	S
Rb-85	8468.0	117	MLBW	-	OLD
87	12460.0	28	MLBW	-	OLD
Sr-86	37120.0	75	MLBW	ORL	ORL
87	14080.0	115	MLBW	ORL	ORL
88	300000.0	13	MLBW	ORL	ORL
90	no resonances		-	-	S
Y-89	48000.0	49	MLBW	ORL, BRC	ORL
Zr-90	171000.0	30	MLBW	ORL	ORL
91	15500.0	35	MLBW	ORL	ORL
92	71000.0	15	MLBW	ORL	ORL
93	300.0	1	MLBW	-	S, Integral test
94	53500.0	18	MLBW	ORL	ORL
95	no resonances		-	-	S
96	45000.0	9	MLBW	-	S
Nb-93	7000.0	139	MLBW	ORL, TIT	ORL
Mo-92	50000.0	19	MLBW	ORL	ORL
94	20000.0	13	MLBW	ORL	ORL
95	2000.0	21	MLBW	ORL	ORL
Mo-96	19000.0	15	MLBW	ORL	ORL
97	1800.0	23	MLBW	ORL	ORL
98	32000.0	30	MLBW	ORL	ORL
100	26000.0	33	MLBW	ORL	ORL
Tc-99	4219.0	142	MLBW	ORL	ORL
Ru-100	11890.0	72	MLBW	ORL	ORL
101	720.0	44	MLBW	ORL	ORL
102	13400.0	98	MLBW	ORL	ORL
103	no resonances		-	-	S
104	11120.0	52	MLBW	ORL	ORL
106	no resonances		-	-	S
Rh-103	3580.0	164	MLBW	ORL, BRC, ANL	ORL
Pd-104	279.0	1	SLBW	ORL	ORL
105	2048.5	199	MLBW	ORL	ORL
106	423.0	1	SLBW	ORL	ORL
107	3500.0	138	MLBW	ORL	ORL
108	9000.0	140	MLBW	ORL	ORL
110	8000.0	107	LMBW	ORL	ORL

Nuclide	Upper boundary of resonance region (eV)	No.	Formula	Recent σ_c measurement	S_γ adjustment
Ag-107	7009.5	289	MLBW	ORL, JAE	JAERI
109	7095.5	289	MLBW	ORL, JAE	JAERI
Cd-110	7000.0	52	MLBW	ORL	ORL
111	1800.0	110	MLBW	ORL	ORL
112	7000.0	68	MLBW	ORL	ORL
113	2000.0	37	MLBW	ORL	ORL
114	8000.0	39	MLBW	ORL	ORL
116	9000.0	22	MLBW	ORL	ORL
In-115	2000.0	206	MLBW	TIT, BNL	TIT
Sb-121	2000.0	146	MLBW	-	OLD Natural, IT
123	2500.0	95	MLBW	-	OLD Natural, IT
124	no resonances		-	-	S
Te-128	21420.0	20	MLBW	-	OLD
I-127	4252.0	356	MLBW	TIT	TIT
129	3391.0	127	MLBW	ORL	ORL
Xe-131	2250.0	41	MLBW	(ORL)	S
132	4400.0	6	MLBW	-	KFK
133	no resonances		-	-	S
134	2500.0	2	MLBW	-	KFK
135	190.0	1	SLBW	-	S
136	no resonances		-	(ORL)	S
Cs-133	5975.0	318	MLBW	ORL, KTO	KTO (TIT)
135	88.0	2	MLBW	-	S
137	1590.0	2	MLBW	-	S
Ba-134	10575.0	22	MLBW	ORL	ORL
135	5960.0	149	MLBW	ORL	ORL
136	34490.0	16	MLBW	ORL	ORL
137	11885.0	33	MLBW	ORL	ORL
138	100000.0	28	MLBW	ORL	ORL
La-139	25862.0	102	MLBW	ORL	ORL
Ce-140	200000.0	50	MLBW	ORL, BRC	ORL
142	3560.0	6	MLBW	KFK	S
144	no resonances		-	-	S
Pr-141	13226.0	120	MLBW	ORL	ORL
Nd-142	26000.0	27	MLBW	ORL, FEI	ORL
143	5000.0	113	MLBW	ORL, JAE	JAERI
144	12000.0	36	MLBW	ORL, FEI	ORL
145	4000.0	184	MLBW	ORL, JAE	JAERI
146	10000.0	44	MLBW	ORL, JAE, FEI	JAERI
148	8000.0	68	MLBW	ORL, JAE, FEI	JAERI
150	13690.0	79	MLBW	FEI	FEI
Pm-147	102.0	44	MLBW	-	S

Nuclide	Upper boundary of resonance region (eV)	No.	Formula	Recent σ_c measurement	S_γ adjustment
Sm-147	1809.0	213	MLBW	JAE, FEI	JAERI
148	no resonances		-	FEI	FEI
149	423.9	158	MLBW	JAE, FEI, RPI	JAERI, FEI
150	1538.0	23	MLBW	FEI	FEI
151	246.1	121	MLBW	-	S
152	5029.0	92	MLBW	FEI	FEI
154	4654.0	36	MLBW	FEI	FEI
Eu-151	98.2	92	MLBW	JAE, FEI, ORL, HAR	ORL
152	6.55	14	MLBW	-	S
153	97.2	73	MLBW	JAE, FEI, ORL, HAR	ORL
154	26.2	20	MLBW	-	S
155	29.7	8	MLBW	-	S
Gd-155	181.8	98	MLBW	JAE, BRC	JAERI
156	2214.0	90	MLBW	BRC, FEI	FEI
157	303.7	60	MLBW	JAE, BRC	JAERI
158	6580.0	95	MLBW	BRC, FEI	FEI
160	4224.0	45	MLBW	BRC, FEI	FEI
Tb-159	1188.0	228	MLBW	ORL, JAE	JAERI

Statistics in resonance formula

No	11
MLBW	86
SLBW	3

Simbols and statistics in S_γ adjustment

ORL	47	:	Measured at ORELA
JAERI	11	:	Measured at JAERI
S	22	:	Evaluated from Systematics
Others	9		
TIT	3	:	Measured at TIT
FEI	8	:	Measured at FEI
OLD		:	Published before 1970

In the CASTHY calculations, S_γ were adjusted to those data.

Table 4 Characteristics of Integral Test Data

	CFRMF	EBR-II	STEK
Method of measurement	Activation	Irradiation	Oscillator
Measured nuclides	27	9	56
Quantity of measurement	Average $\sigma_{act.}$	Average σ_c	ρ/ρ_o
Measured fields	1	6	5
Position	Core center	Core center and reflector	Core center
Group No. of flux	73	47	26
Group No. of covariance of flux	26	Only standard deviation	Only standard deviation

Table 6 Results of Preliminary Adjustment of Cross Section by Integral Test

	R^{exp}	$\sqrt{V^{exp}}/R^{exp}$	C/E	$\sqrt{V^{cal}}/R^{cal}$	$\sqrt{V^{cal}+V^{m}+V^{exp}}/R^{cal}$	C'/E	$\sqrt{V^{cal}}/R^{cal}$	x^2
		(%)		(%)	(%)		(%)	
^{132}Xe CFRMF	4.39^{-2}	7.7	1.29	19.5	21.0	1.02	5.7	1.21
^{147}Pm CFRMF	6.41^{-1}	13.0	1.12	10.5	16.4	1.07	8.2	0.48
^{152}Eu EBR-II								
core 51	3.61	11.2	0.64	16.8	24.3	0.81	12.2	5.32
core 52	10.09	16.1	0.90	14.6	23.3	0.94	11.5	0.22
^{154}Eu EBR-II								
core 51	2.66	9.6	0.70	15.6	23.1	0.87	10.3	4.31
core 52	8.39	15.1	0.84	13.9	22.9	0.90	11.2	0.69
^{109}Ag CFRMF	3.18^{-1}	9.7	0.69	5.6	–	0.72	5.2	9.48

Table 5 Interium Results of Integral Test

Nuclide	Library	CFRMF	STEK		Nuclide	Library	CFRMF	STEK	
				STEK-1000					STEK-1000
Rb-87	JENDL-2	1.43 (10)			Mo-98	JENDL-2	1.16 (6)	0.83∿10.20	4.11
	JENDL-1					JENDL-1	1.24	0.99∿10.80	4.47
Zr-90	JENDL-2		0.46 ∿ 0.87	6.69	Mo-100	JENDL-2	1.03 (17)	0.80 ∿ 3.19	3.07
	JENDL-1		0.40 ∿ 0.81	0.62		JENDL-1	0.89	0.88 ∿ 2.55	2.19
Zr-91	JENDL-2		0.00 ∿ 1.46	0.00067	Tc-99	JENDL-2	1.23 (15)	0.83 ∿ 1.03	0.94
	JENDL-1		0.22 ∿ 1.35	0.32		JENDL-1	1.21	0.68 ∿ 0.96	0.86
Zr-92	JENDL-2		0.35 ∿ 1.18	0.68	Ru-101	JENDL-2		0.98 ∿ 1.18	0.98
	JENDL-1		0.38 ∿ 1.08	0.62		JENDL-1		0.91 ∿ 1.18	0.91
Zr-93	JENDL-2		0.13 ∿ 8.87	0.16	Ru-102	JENDL-2	1.01 (7)	0.87 ∿ 2.09	1.21
	JENDL-1		0.29 ∿ 9.06	0.29		JENDL-1	1.58	1.15 ∿ 3.72	1.90
Zr-96	JENDL-2		0.16 ∿ 1.38	0.68	Ru-104	JENDL-2	0.95 (6)	0.79 ∿ 1.25	1.25
	JENDL-1		0.00 ∿ 0.48	0.48		JENDL-1	1.17	0.91 ∿ 1.42	1.42
Nb-93	JENDL-2		1.05 ∿ 1.24	1.10	Rh-103	JENDL-2		0.74 ∿ 2.12	1.09
	JENDL-1		0.98 ∿ 1.24	1.06		JENDL-1		0.62 ∿ 1.67	0.96
Mo-92	JENDL-2		0.90 ∿ 3.05	1.77	Pd-104	JENDL-2		1.02 ∿ 2.87	2.01
	JENDL-1		0.82 ∿ 2.68	1.62		JENDL-1		0.84 ∿ 2.33	1.61
Mo-94	JENDL-2		0.85 ∿10.00	6.16	Pd-105	JENDL-2		0.94 ∿ 1.07	1.01
	JENDL-1		0.66 ∿ 8.71	5.01		JENDL-1		0.77 ∿ 0.90	0.81
Mo-95	JENDL-2		0.98 ∿ 1.16	1.16	Pd-106	JENDL-2		1.19 ∿ 1.33	1.33
	JENDL-1		0.91 ∿ 1.11	1.09		JENDL-1		0.73 ∿ 0.80	0.80
Mo-96	JENDL-2		0.83 ∿ 5.01	2.92	Pd-107	JENDL-2		0.93 ∿ 1.07	1.02
	JENDL-1		0.76 ∿ 2.83	2.28		JENDL-1		0.75 ∿ 0.87	0.82
Mo-97	JENDL-2		0.97 ∿ 1.22	1.08	Pd-108	JENDL-2	0.99 (7)	1.05 ∿ 1.91	1.91
	JENDL-1		0.95 ∿ 1.20	1.06		JENDL-1	0.82	1.10 ∿ 1.90	1.90

Nuclide	Library	CFRMF	STEK		Nuclide	Library	CFRMF	STEK	
				STEK-1000					STEK-1000
Pd-110	JENDL-2		0.74 ∿ 5.02	0.74	Xe-134	JENDL-2	1.38 (7)		
	JENDL-1		0.43 ∿ 3.53	0.43		JENDL-1	1.65		
Ag-107	JENDL-2	0.87 (19)			Cs-133	JENDL-2	0.91 (7)	0.59 ∿ 1.03	0.81
	JENDL-1	0.99				JENDL-1	1.01	0.62 ∿ 0.95	0.79
Ag-109	JENDL-2	0.67 (10)	0.63 ∿ 1.27	0.79	Cs-135	JENDL-2		0.72 ∿ 1.06	0.87
	JENDL-1	1.03	0.78 ∿ 1.37	1.00		JENDL-1		0.74 ∿ 1.05	0.90
Cd-111	JENDL-2		0.77 ∿ 1.16	0.81	Cs-137	JENDL-2	0.13 (25)		
	JENDL-1					JENDL-1			
In-115	JENDL-2		0.92 ∿ 2.59		La-139	JENDL-2	1.02 (5)	0.52 ∿ 1.27	0.65
	JENDL-1					JENDL-1	1.21	0.55 ∿ 4.66	0.91
Sb-121	JENDL-2	0.89 (8)			Ce-140	JENDL-2	(7)	0.70 ∿ 0.93	0.74
	ENDF-B4	1.11				JENDL-1	27.2	0.57 ∿ 0.62	0.57
Sb-123	JENDL-2	1.02 (7)							
	ENDF/B-4	1.09							
Te-128	JENDL-2								
	JENDL-1								
I-127	JENDL-2	1.07 (10)							
	JENDL-1	1.23	0.67 ∿ 1.09	0.88					
I-129	JENDL-2	1.16 (7)							
	JENDL-1	1.49	1.26 ∿ 1.58	1.27					
Xe-131	JENDL-2		1.02 ∿ 1.20	1.18					
	JENDL-1		1.04 ∿ 1.29	1.21					
Xe-132	JENDL-2	1.29 (8)							
	JENDL-1	1.11							

Nuclide	Library	CFRMF	STEK		EBR-II		Nuclide	Library	CFRMF	STEK		EBR-II	
				STEK-1000	Core	Reflector					STEK-1000	Core	Reflector
Ce-142	JENDL-2	0.86 (7)	0.49 ∿ 0.82	0.49			Sm-149	JENDL-2		1.00 ∿ 2.19	1.07	0.88 (6)	1.01 (14)
	JENDL-1	2.05	0.44 ∿ 0.58	0.44				JENDL-1		0.84 ∿ 1.36	0.91		
Pr-141	JENDL-2	0.85 (15)	0.48 ∿ 1.99	1.10			Sm-150	JENDL-2		0.80 ∿ 1.20	0.95		
	JENDL-1	0.92	0.76 ∿ 1.37	0.98				JENDL-1		0.86 ∿ 1.42	1.05		
Nd-142	JENDL-2		0.04 ∿14.60	0.06			Sm-151	JENDL-2		0.79 ∿ 1.25	1.04		
	JENDL-1		0.02 ∿13.50	0.02				JENDL-1		0.81 ∿ 1.30	1.02		
Nd-143	JENDL-2		0.87 ∿ 1.56	1.24	0.85 (6)	0.86 (14)	Sm-152	JENDL-2	1.00 (6)	0.59 ∿ 1.46	0.85		
	JENDL-1		0.83 ∿ 1.53	1.16				JENDL-1	1.19	0.67 ∿ 1.75	0.98		
Nd-144	JENDL-2		0.25 ∿ 1.72	0.25	0.76 (6)	0.75 (14)	Sm-154	JENDL-2	(5)	0.51 ∿ 1.35	0.84		
	JENDL-1		0.36 ∿ 6.45	0.37				JENDL-1	0.12	0.60 ∿ 1.42	0.88		
Nd-145	JENDL-2		0.76 ∿ 1.50	0.90	0.83 (6)	0.80 (14)	Eu-151	JENDL-2	0.83 (6)	0.76 ∿ 1.37	0.87	0.68 (8)	0.70 (15)
	JENDL-1		0.47 ∿ 0.94	0.65				JENDL-1	0.87	0.78 ∿ 1.25	0.89		
Nd-146	JENDL-2	1.23 (7)	0.24 ∿ 2.40	0.24			Eu-152	JENDL-2				0.64 (11)	0.90 (16)
	JENDL-1	1.00	0.01 ∿ 1.80	-0.06				JENDL-1					
Nd-148	JENDL-2	1.10 (14)	0.25 ∿ 5.42	5.42			Eu-153	JENDL-2	0.91 (7)	0.84 ∿ 1.10	0.9	0.83 (7)	0.87 (14)
	JENDL-1	1.49	0.91 ∿ 9.55	9.55				JENDL-1	0.96	0.86 ∿ 1.06	0.9		
Nd-150	JENDL-2	1.35 (12)	0.24 ∿ 2.06	1.29			Eu-154	JENDL-2				0.70 (10)	0.84 (15)
	JENDL-1	1.84	0.46 ∿ 4.36	2.56				JENDL-1					
Pm-147	JENDL-2	1.10 (13)	0.89 ∿ 1.03	0.91			Gd-156	JENDL-2		0.75 ∿ 1.48	0.80		
	JENDL-1	1.13	0.89 ∿ 1.00	0.90				JENDL-1					
Sm-147	JENDL-2		0.82 ∿ 1.24	1.02	0.84 (6)	1.01 (13)	Gd-157	JENDL-2		0.75 ∿ 3.57	0.75		
	JENDL-1		0.82 ∿ 1.28	1.02				JENDL-1					
Sm-148	JENDL-2		0.73 ∿12.90	1.10			Tb-159	JENDL-2		0.94 ∿ 1.01	0.94		
	JENDL-1		0.85 ∿18.70	1.44				JENDL-1					

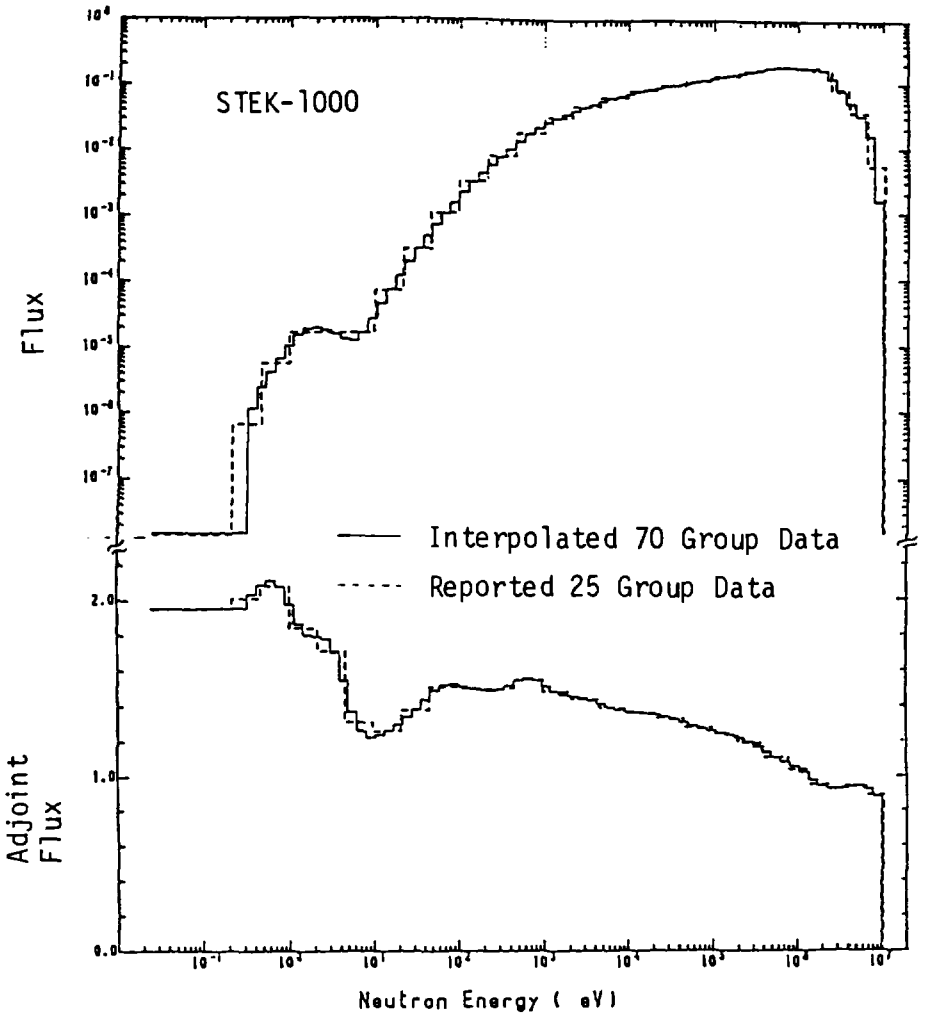

Fig. 1 Example of Flux Used in Integral Test

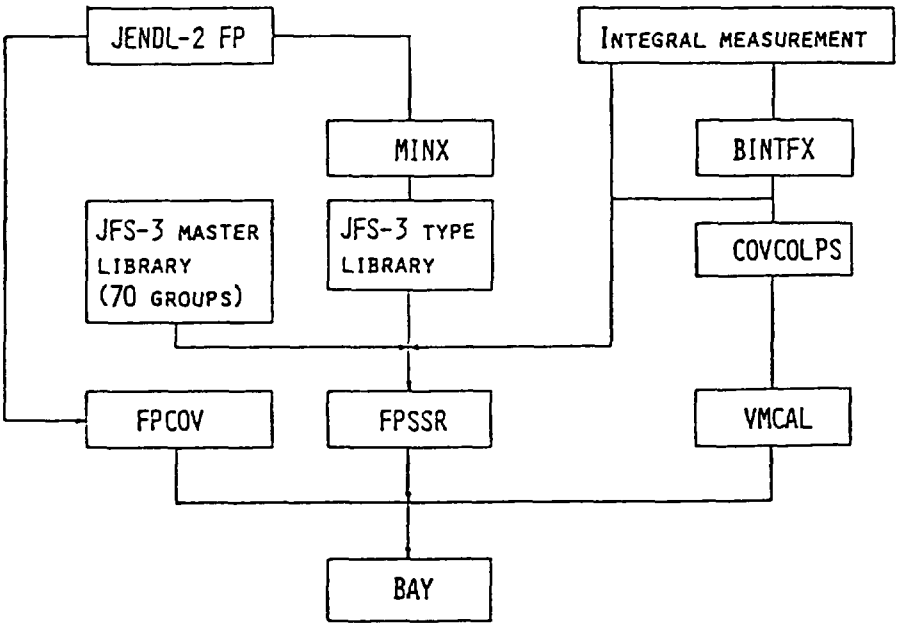

Fig. 2 Flow Diagram of Integral Test and Adjustment

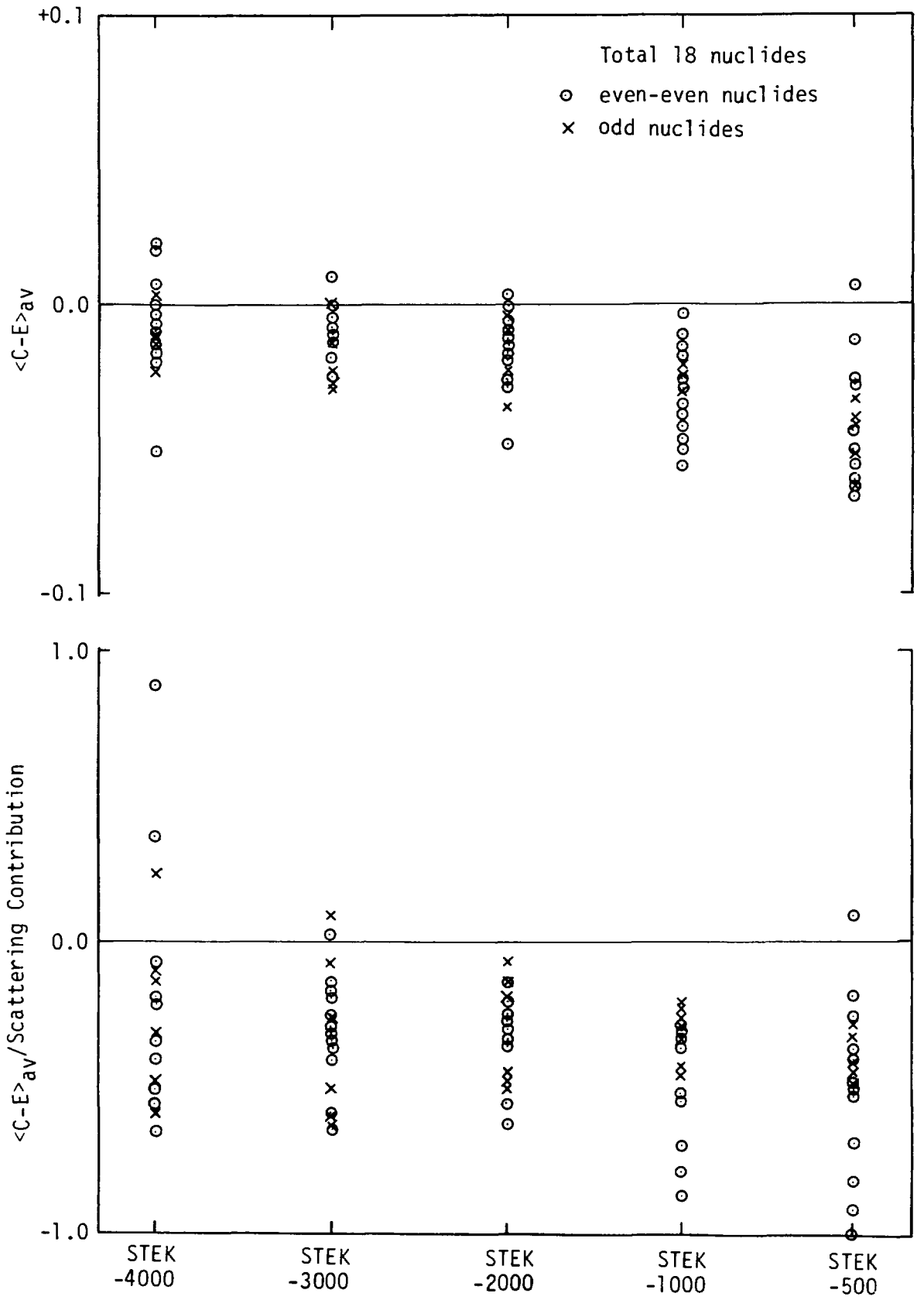

Fig. 3 $\langle C-E \rangle_{av}$ and $\langle C-E \rangle_{av}$/Scattering Contribution in Integral Test of STEK experiment for weak absorber

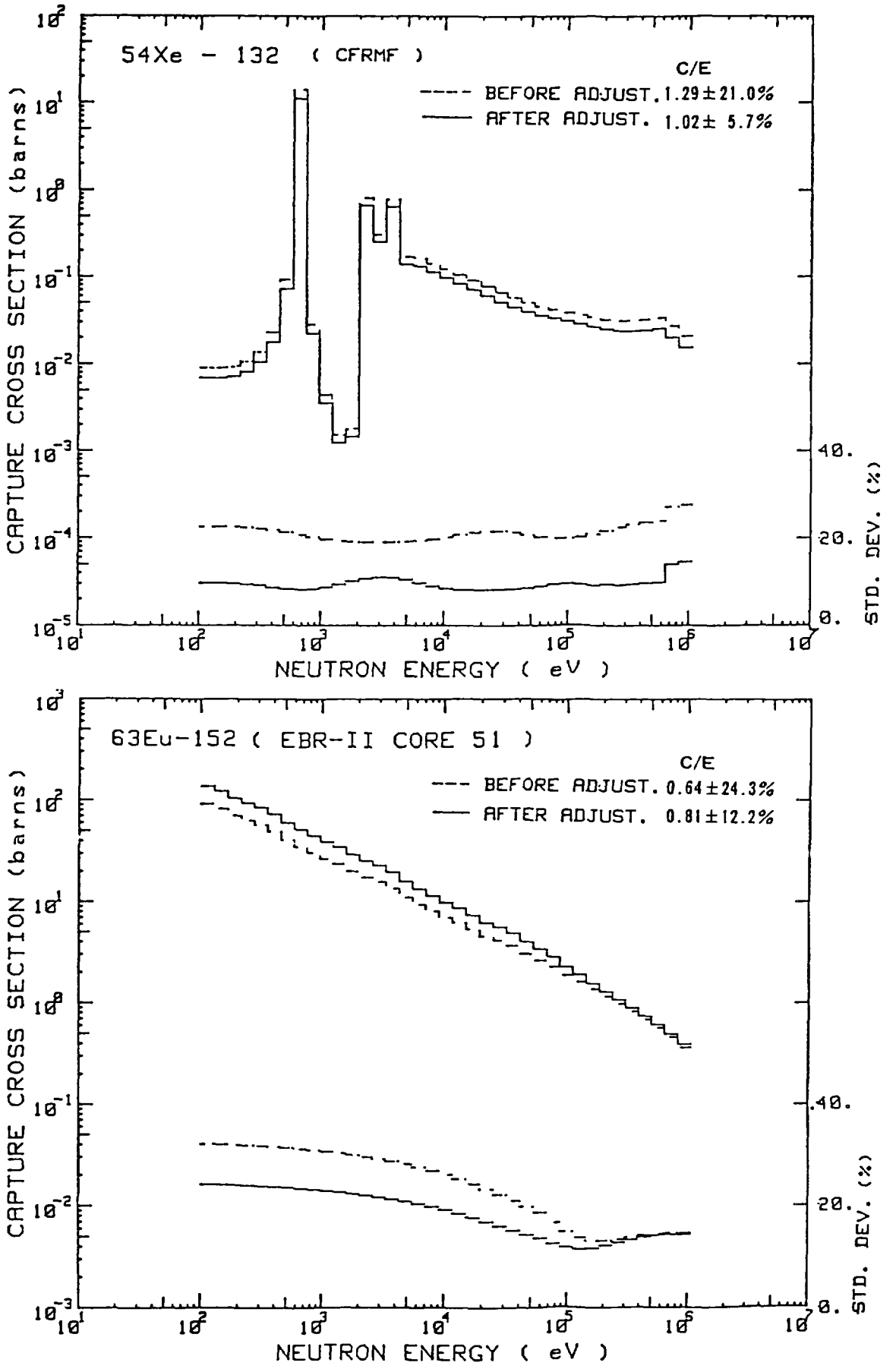

Fig. 4 Cross Section Change between before and after Adjustment for Xe-131 and Eu-152

2.2 Evaluation of Threshold Reaction Data

Sub-working Group on Nuclear Data for Gas Production
Japanese Nuclear Data Commitee

(presented by T. Sugi (JAERI))

Abstract

In the present working group, we investigate and prepare the experimental data systematics, the calculational methods and the theoretical model parameters which are common to the evaluation of structural materials cross sections. The activities made in our working group are briefly reviewed.

1. Introduction

The JENDL-2 is recognized as unsatisfactory concerning the threshold reaction cross sections and gamma-ray production data for structural materials. Revisions and implementations are to be made in JENDL-3. The aim of the present working group is to investigate and prepare
(1) the experimental data systematics,
(2) the calculational methods, and
(3) the theoretical model parameters.
These are common to the evaluation of structural materials cross sections.

In this paper we review the activity of our working group and related topics.

2. Systematics of 14 MeV Cross Sections

The following are the systematic trends of charged particle emission cross sections for 23 isotopes of Ti(Z = 22) to Cu(Z = 29).

Fig. 1 shows the plot of experimental (n,p) cross sections at 14 MeV vs. neutron excess parameter (N-Z)/A. The cross section value tends to decrease as the neutron excess parameter increases. Kumabe and Fukuda[1] proposed the following empirical formula of (n,p) corss section at 14 MeV.

$$\sigma_{n,p}(14\ \text{MeV}) = 21.8\ A \exp[-34(N-Z)/A]\ [\text{barn}].$$

The solid and dashed lines show the cross section values for Ti and Ni given by this farmula and THRESH-2[2] code, respectively. In THRESH-2 calculation we used the parameter values built in the code.

We can see that the systematics by Kumabe and Fukuda reproduces the experimental data well. The systematics for (n,p) cross sections used in THRESH-2 code is clearly inappropriate.

(n,α) cross sections

Fig. 2 shows the plot of experimental (n,α) cross sections at 14 MeV vs. neutron excess parameter. Also in this case, the cross section value tends to decrease as the neutron excess parameter increases, and the systematics by Kumabe and Fukuda reproduces the experimental data well. The same argument as (n,p) cross section applies to the THRESH-2 built-in parameters.

(n,d) and (n,t) cross section

Table 1 and 2 show the experimental (n,d) and (n,t) cross section data together with the systematics by Oaim[3] and the calculated value by THRESH-2. The THRESH-2 calculation overestimates the cross section values, because of very large charged particle cross section built in the code.

3. Level Density Parameters

The composite level density parameters of Gilbert-Cameron type were newly determined for nuclides in structural material region. The coefficient of spin cut-off parameter was taken as 0.146 instead of 0.0888. The energy dependence of spin cut-off parameter for constant temperature region was assumed as linear in excitation energy as proposed by Gruppelaar.[4]

The level density parameters were obtained from the s-wave resonance level spacing data and the low-lying level scheme data. When the s-wave resonance data not available, the a-parameter was determined either by interpolation or by the fit to low-lying level scheme.

Two methods were adopted to determine the parameters of constant temperature formula. One is the conventional total observable level density fit,[5] and the other is the spin-selection method to take account of missing of low-lying levels of high spin by the observation.[6]

Fig. 3 shows the example of application of spin-selection method to Co-60 levels. The lower straight line (slightly curved due to the energy dependence of spin cut-off parameter) is the spin-selected fit. The upper line is the total level cumulation predicted from the spin-selected level density. The gap between the upper line and the upper staircase plot indicates the missing of high spin levels.

Fig. 4 and 5 show respectively the a- and T- parameter values determined by the total observable level density fit. It is seen that apart from the shell closing effect and the odd-even effect, the relation $a \sim A/7$ holds approximately, in contrast to the frequently used relation $a \sim A/8$. Also, T-parameter may by approximated by $T \sim 65/A$.

4. Inverse Cross Sections

We calculated the inverse cross sections and the transmission coefficients of the (n,p), (n,α), (n,d), (n,t) and (n,^{3}He) reactions for nuclides in structural material region by ELISE-3.[7] The used optical model parameters are shown in Table 3.

Fig. 6 shows the inverse cross sections for ^{65}Cu(n,X) reactions. In Fig. 7 the inverse cross sections calculated by different optical model parameters are compared. For the (n,p) reaction, Menet and Perey are compared, and for the (n,α) reaction, Huizenga-Igo and Lemos are compared.

We use these inverse cross section for the pre-equilibrium and the equilibrium calculations.

5. Calculation with GNASH

The computer code GNASH[13] consists of the multi-step Hauser-Feshbach calculation combined with a pre-equiliblium calculation and a direct reaction correction by input. The excitation functions and the particle emission spectra were calculated for ^{59}Co, ^{58}Ni, ^{60}Ni, ^{63}Cu, ^{65}Cu. Some modifications were made in these calculations.[14]

Input parameters

For example in Cu case, the imput parameters used are as follows:

Optical Model Parameters:
- n: Hetrik et al.[15]
- p: Perey(8A)
- α: Lemos[10]

Level Density Parameters:
determined by the spin selection method

γ-ray Strength Function:
Brink-Axel type, El giant resonance E_G = 18 MeV, Γ_G = 6 MeV, normalization constant $2\pi\Gamma_\gamma/D_0$, where D_0 is recalculated from a-value, Γ_γ is either assumed or adjusted to fit the measured neutron capture cross section in keV region.

Pre-equilibrium Process:
Kalbach parameter: F2 = K/100 = 1.0
the single particle level density parameter: $g = (6/\pi^2)a$
For α-particle emission process, the pick up process component is reduced by a factor of 1/2.

Direct Reaction Correction:
For inelastic scattering process, the direct reaction is considered by inputing the result of Hetrick's DWBA calculation.[15]

Results

The calculated results for Cu are shown in Fig. 8 to Fig. 11.

In Fig. 8, the calculated neutron emission spectrum is compared with the experimental data of Hermsdorf et al.[16], together with

spectral components. The calculation agrees well with the experimental data.

In Fig. 9, the calculated proton- and α-emission spectrum is compared with the experimental data.[17] A good agreement is also obtained.

Fig. 10 and Fig. 11 shows the (n,2n) and the (n,α) corss section curves, respectively. In the (n,α) case, the agreement with old experimental data of Paulsen[18] is not good, however, recent data of Winkler[19] are in better agreement with the present calculation.

6. The Development of PEGASUS Code

A simplified approach for the cross section calculation was made at first using THRESH-2[2]. The results were, however, unsatisfactory especially for charged particle emission reactions. Therefore, a more physical code PEGASUS was developed. It stands for Pre-equilibrium and Equilibrium calculation of GAS production cross section Using Systematics and the main feature of it is as follows:

The Calculational Method

(1) The closed from exciton model pre-equilibrium theory, and the evapration theory are used.
(2) The cluster formation factor method of Iwamoto-Harada-Sato[20] was adopted for the pre-equilibrium emission of cluster charged particles.
(3) The competition of γ-ray emission with particle emission is taken into account in the second stage evapration process.
(4) The angular distribution can be calculated by the method as used in PREANG[21] code.

Input Data and Parameters

(1) Q-value (atomic mass table)
(2) the inverse cross sections $\sigma_{inv}(\varepsilon)$
(3) Kalbach constant $|M|^2 = K/(A^3 E_c)$
(4) the cluster formation factor F_{lm} and its normalization constant γ
(5) the level density parameters

Calculational Results

The examples of PEGASUS calculation are shown in Fig. 12 to Fig. 15. In the cases of ^{56}Fe(n,p) and ^{54}Fe(n,α), the agreement with the experimental data is good. On the contrary, in the case of ^{51}V(n,p) and ^{51}V(n,α), the agreement is no good. For these case, the adjustment of input parameter is necessary.

7. Concluding Remarks

Now we get following results.

(1) The systematics of 14 MeV (n,p) and (n,α) corss sections Kumabe and Fukuda[1] reproduces the available experimental data fairly well.

(2) The level density parameters of Gilbert-Cameron type were determined systematically for nuclides in structural materials region. The relations a ~ A/7 and T ~ 65/A holds approximatelly.

(3) The inverse reaction cross section is strongly influenced by optical model parameters. Thus the selection of optical model parameters is important in the cross section calculations.

(4) The detailed calculation with GNASH code[13] was made for Co, Ni and Cu isotopes. Good results were obtained for cross sections and particle emission spectra by proper selection of optical model parameters and adjustment of the other parameter values.

(5) A simplified approach by THRESH-2 code[2] was unsatisfactory. Therefore we are developing a more physical code PEGASUS which uses exciton model pre-equilibrium theory and the evaporation theory.

References

(1) Kumabe, I., Fukuda, K., NEANDC(J)-65U (1978), p.45
(2) Pearlstein, S., Program THRESH-2, Argonne Code Center (1975)
(3) Qaim, S.M., Proc. Int. Conf. on Neutron Physics and Nuclear Data for Reactors and other Applied Purposes, Harwell (1978), p.1088.
(4) Grupperaar, H., ECN-13 (1977)
(5) Iijima, S., Yoshida, T., Aoki, T., Watanabe, T., Sasaki, M., Journal of Nuclear Science and Technology, 20, 10 (1984)
(6) Yamamuro, N., Int. Conf. on Nuclear Data for Basic and Applied Science, Santa Fe, Session JB29 (1985)
(7) Igarashi, S., JAERI-1224 (1972)
(8) Menet, J.J.H., et al., Phys. Rev. C4, 1114 (1971)
(8A) Perey, F.G., Phys. Rev. 131, 745 (1963)
(9) Huizenga, J.R. and Igo, G., Nucl. Phys. 29, 462 (1962)
(10) Lemos, O.F., ORSAY serie A, No. 136 (1972)
(11) Lohr, J.M., Haeberli, W., Nucl. Phys. A232, 381 (1974)
(12) Bechetti, F.D. Jr., Greenlees, G.W., Polarization Phonomena in Nuclear Reactions, p.682, The univ. of Wisconsin Press (1971)
(13) Young, P.G. and Arthur, E.D., LA-6947 (1978)
(14) Kawai, M., JAERI-M 085-035, p.205 (1985) Yamamuro, N., priv. communication
(15) Hetrick, D.H., Fu, C.Y., Larson, P.C., ORNL/TM-9083 (1984)
(16) Hermsdorf, D., et al., Zfk-277 (1974)
(17) Grimes, S.M., Haight, R.C., Nucl. Phys. 84, 177 (1966)
(18) Paulsen, A., et al., Nukleonik, 10, 91 (1967)
(19) Winkler, G., et al., Nucl. Sci. Eng. 76, 30 (1980)
(20) Sato, K., Iwamoto, A., Harada, K., Phys. Rev. C28, 1527 (1983)
(21) Akkermans, J.M., Grupperaar, H., ECN-60 (1979)
(22) Grimes, S.M., et al., Nucl. Sci. Eng. 62, 187 (1977)
(23) Grimes, S.M., et al., BNL-NCS-50681, p.297 (1977)
(24) Grimes, S.M., Haight, R.C., Phys. Rev. C19, 2127 (1979)
(25) Qaim, S.M., Stöcklin, G., Nucl. Phys. A257, 233 (1976)
(26) Perey, C.M. and Prey, F.G., Atomic Data and Nuclear Data Tables 17, 1 (1976)

Table 1 (n,d) cross section values at 15 MeV
(unit: [mb])

reaction	experiment	(ref.)	systematics by Qaim[3]	calc. by THRESH-2
^{46}Ti (n,d) ^{45}Sc	9±4	(22)	27.5	106
^{48}Ti (n,d) ^{47}Sc	7±3	(22)	7.4	38.7
^{51}V (n,d) ^{50}Ti	7	(23)	4.8	56.5
^{50}Cr (n,d) ^{49}V	12±4	(24)	33.6	169
^{52}Cr (n,d) ^{51}V	8±3	(24)	9.9	58.3
^{54}Fe (n,d) ^{53}Mn	10±4	(24)	41.6	214
^{56}Fe (n,d) ^{55}Mn	8±3	(24)	12.9	62.5
^{58}Ni (n,d) ^{57}Co	14±6	(24)	47.0	278
^{60}Ni (n,d) ^{59}Co	11±4	(24)	16.3	70.4
^{63}Cu (n,d) ^{62}Ni	9±4	(24)	11.1	87.7
^{65}Cu (n,d) ^{64}Ni	10±4	(24)	4.4	58.2

Table 2 (n,t) cross section values at 14.6 MeV
(unit: [μb])

reaction	experiment	(ref.)	systematics by Qaim[3]	calc. by THRESH-2
^{46}Ti (n,t) ^{44m}Sc	< 20	(25)		
^{46}Ti (n,t) ^{44g}Sc	115±35	(25)	61	1.07×10^{4}
^{56}Fe (n,t) ^{54}Mn	45±12	(25)	52	7.84×10^{3}
^{58}Ni (n,t) ^{56}Co	92±27	(25)	76	3.44×10^{4}
^{60}Ni (n,t) ^{58}Co	61±20	(25)	56	7.65×10^{3}

Table 3 The optical model parameters used for inverse cross section calculations
(unit: [MeV], [fm], notation: same as Perey's compilation [ref. (26)])

particle (ref.)	real	imaginary	spin-orbit	Coulomb
proton (8)	$V = 49.9 - 0.22E + 26.4(N-Z)/A + 0.4(Z/A^{1/3})$, $r_0 = 1.16$, $a_0 = 0.75$	$W = 1.2 + 0.09E$ $W_D = 4.2 - 0.05E + 15.5(N-Z)/A$, $r_W = r_D = 1.37$, $a_W = a_D = 0.74 + 0.008E + 1.0(N-Z)/A$	$V_{SO} = 6.04$, $r_{SO} = 1.064$, $a_{SO} = 0.78$	$r_C = 1.25$
proton (8A)	$V = 53.3 - 0.55E + 27(N-Z)/A + 0.4(Z/A^{1/3})$, $r_0 = 1.25$, $a_0 = 0.65$	$W_D = 13.5 \pm 2.0$, $r_D = 1.25$, $a_D = 0.47$	$V_{SO} = 7.5$, $r_{SO} = 1.25$, $a_{SO} = 0.47$	$r_C = 1.25$
alpha (9)	$V = 50$, $r_0 = 1.17 + 1.77A^{-1/3}$, $a_0 = 0.576$	$W =$ (interpolation from table), $r_W = 1.17 \quad 1.77A^{-1/3}$, $a_W = 0.576$		$r_C = 1.17$
alpha (10)	$V = 193 - 0.15E$, $r_0 = 1.37$, $a_0 = 0.56$	$W = 21 + 0.25E$, $r_W = 1.37$, $a_W = 0.56$		$r_C = 1.4$
deutron (11)	$V = 91.13 + 2.2(Z/A^{1/3})$, $r_0 = 1.05$, $a_0 = 0.86$	$W_D = 218/A^{2/3}$, $r_D = 1.43$, $a_D = 0.50 + 0.013\ A^{2/3}$	$V_{SO} = 7.0$, $r_{SO} = 0.75$, $a_{SO} = 0.5$	$r_C = 1.3$
triton (12)	$V = 165.0 - 0.17E - 6.4(N-Z)/A$, $r_0 = 1.20$, $a_0 = 0.72$	$W = 46.0 - 0.33E - 110(N-Z)/A$, $r_W = 1.40$, $a_W = 0.84$	$V_{SO} = 2.5$, $r_{SO} = 1.20$, $a_{SO} = 0.72$	$r_C = 1.30$
He-3 (12)	$V = 151.9 - 0.17E + 50(N-Z)/A$, $r_0 = 1.20$, $a_0 = 0.72$	$W = 41.7 - 0.33E + 44(N-Z)/A$, $r_W = 1.40$, $a_W = 0.88$	$V_{SO} = 2.5$, $r_{SO} = 1.20$, $a_{SO} = 0.72$	$r_C = 1.30$

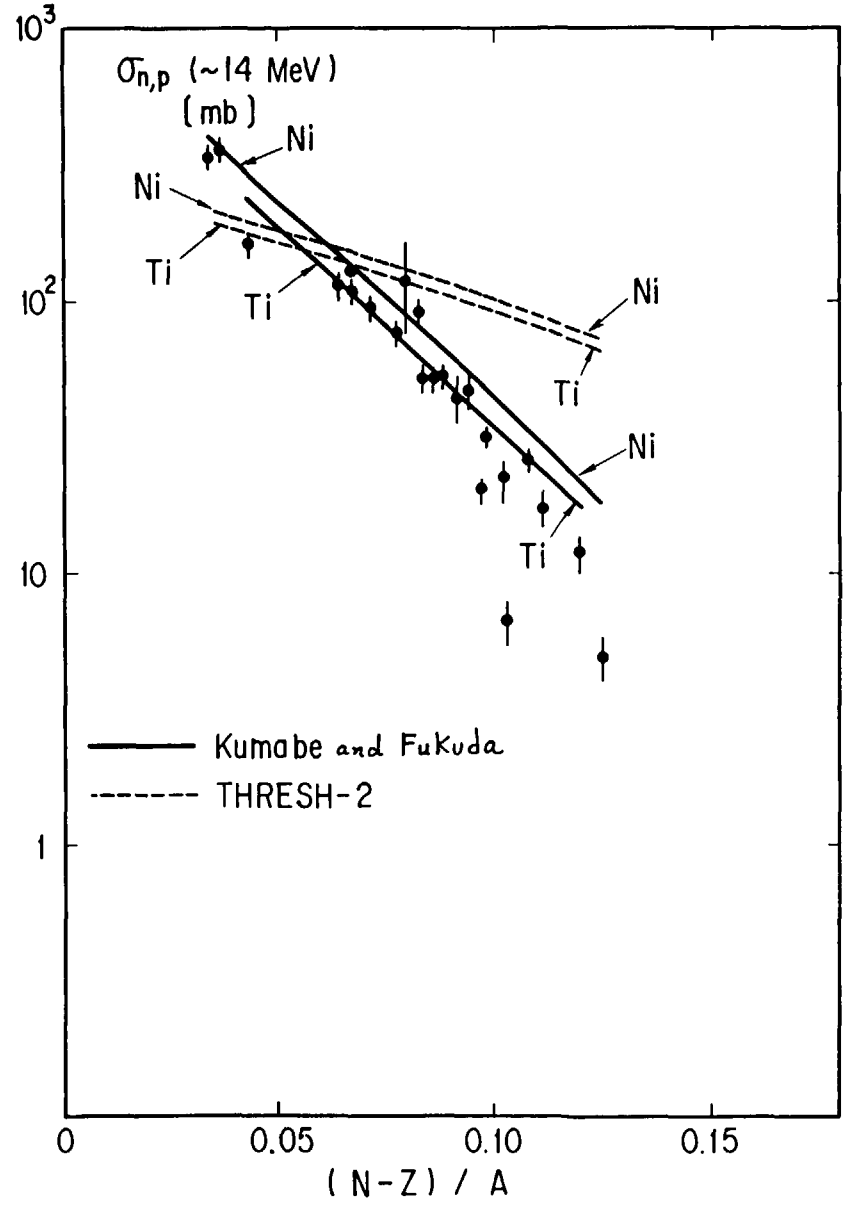

Fig. 1 The experimental (n, p) cross sections at 14MeV vs. neutron excess parameter (N − Z)/A

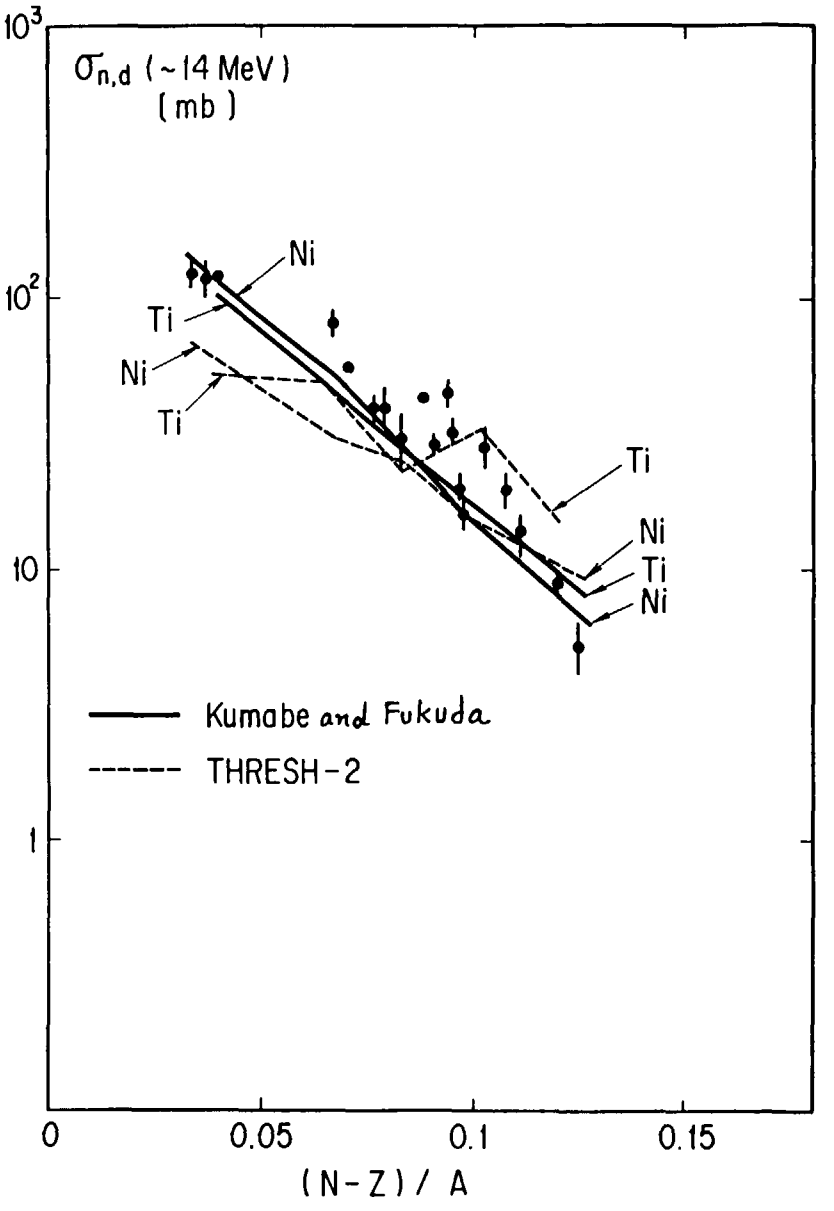

Fig. 2 The experimental (n, α) cross sections at 14MeV vs. neutron excess parameter (N − Z)/A

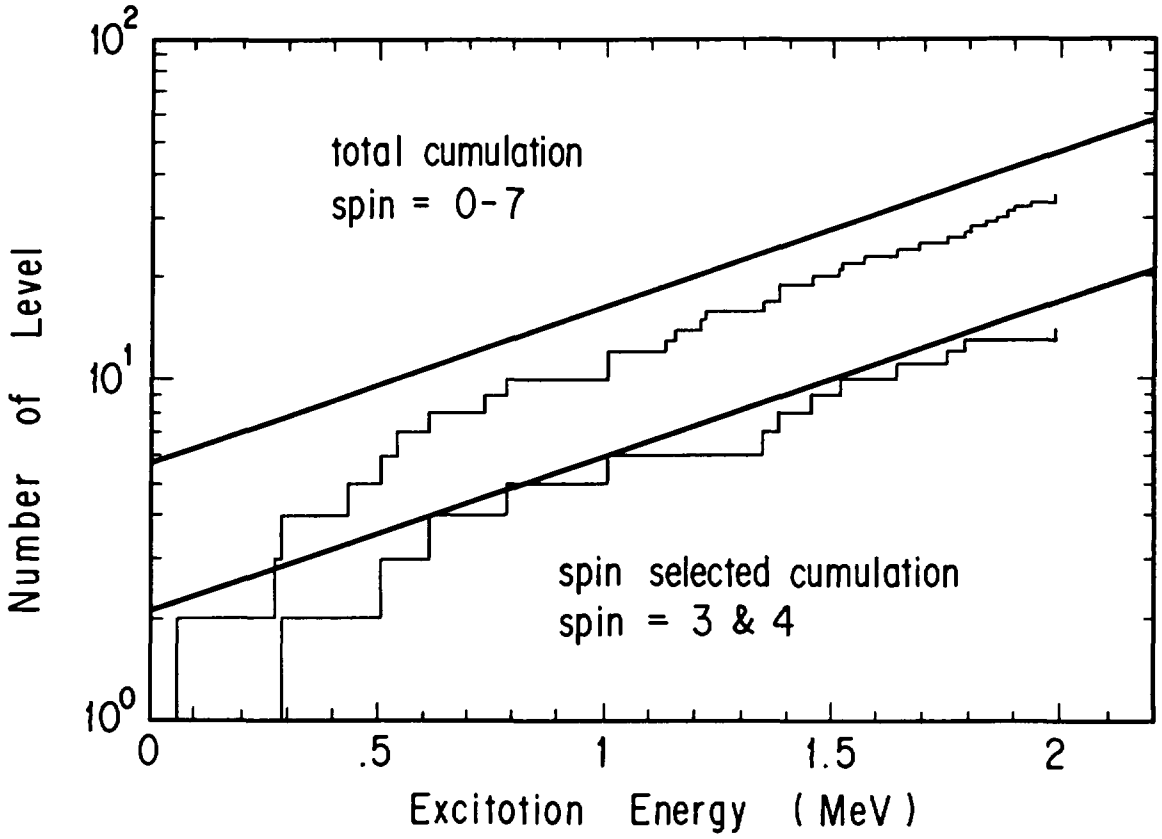

Fig. 3 The application of spin−selection method to ^{60}Co levels

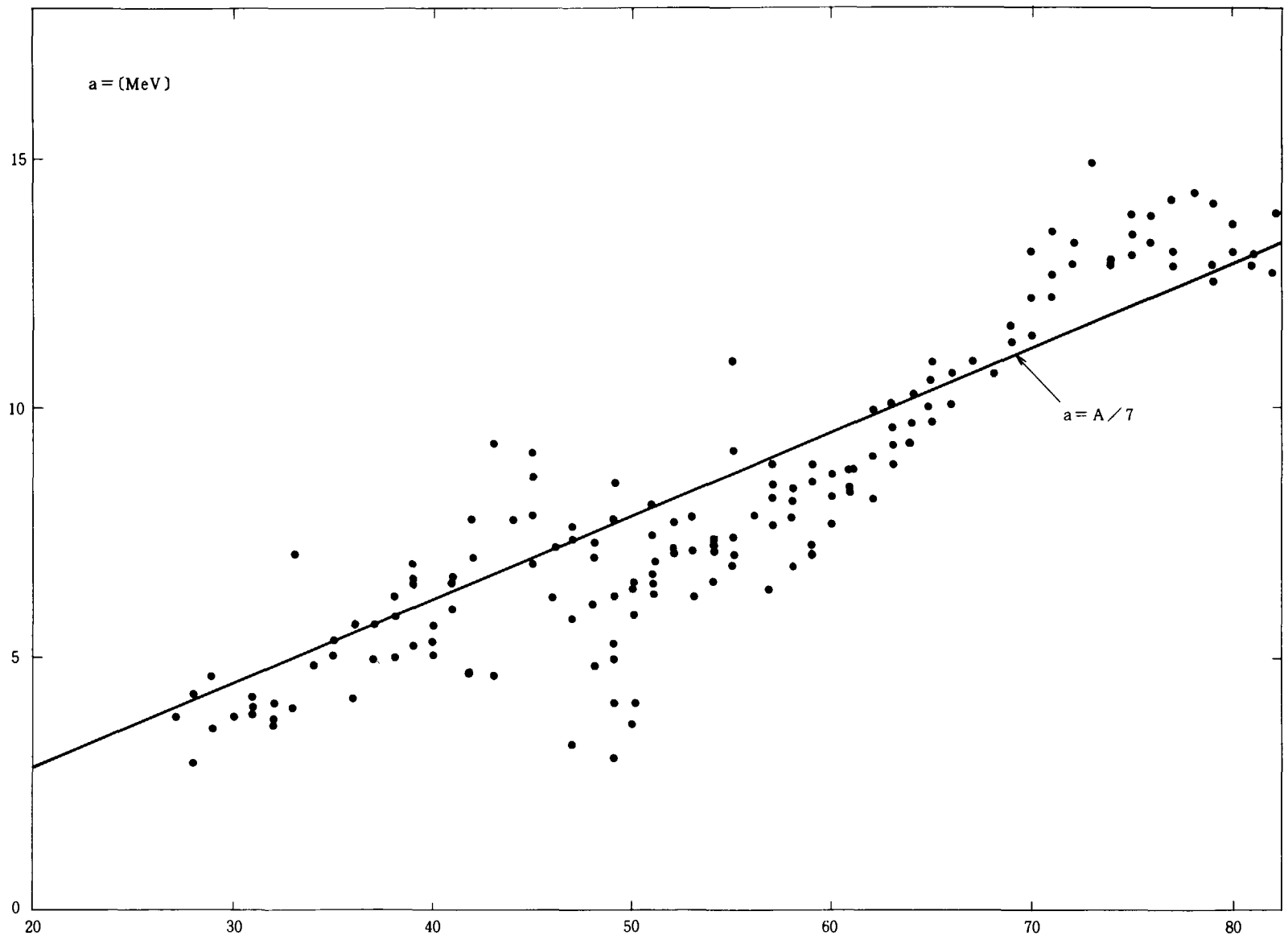

Fig. 4 a－parameter values

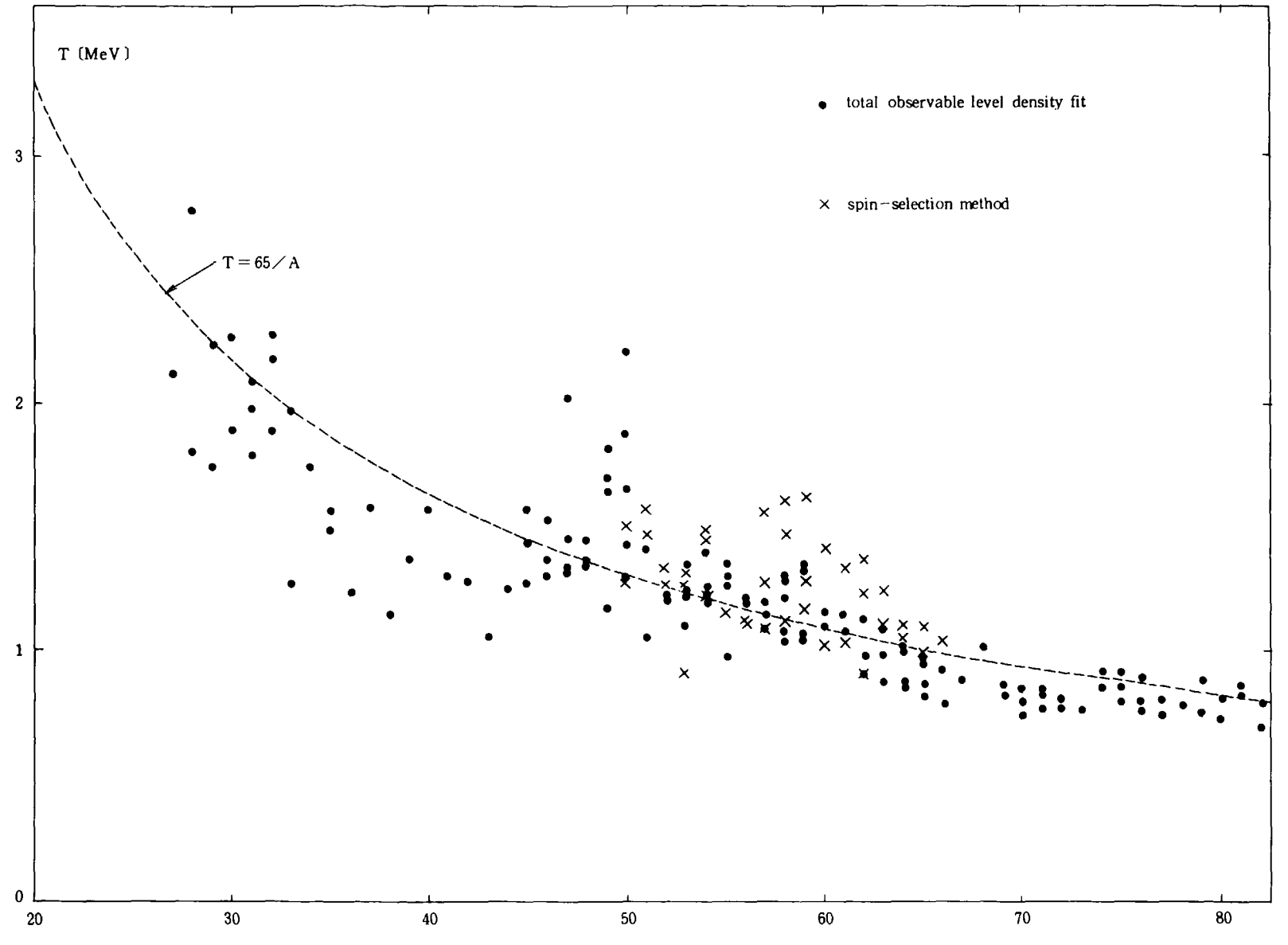

Fig. 5 T-parameter values

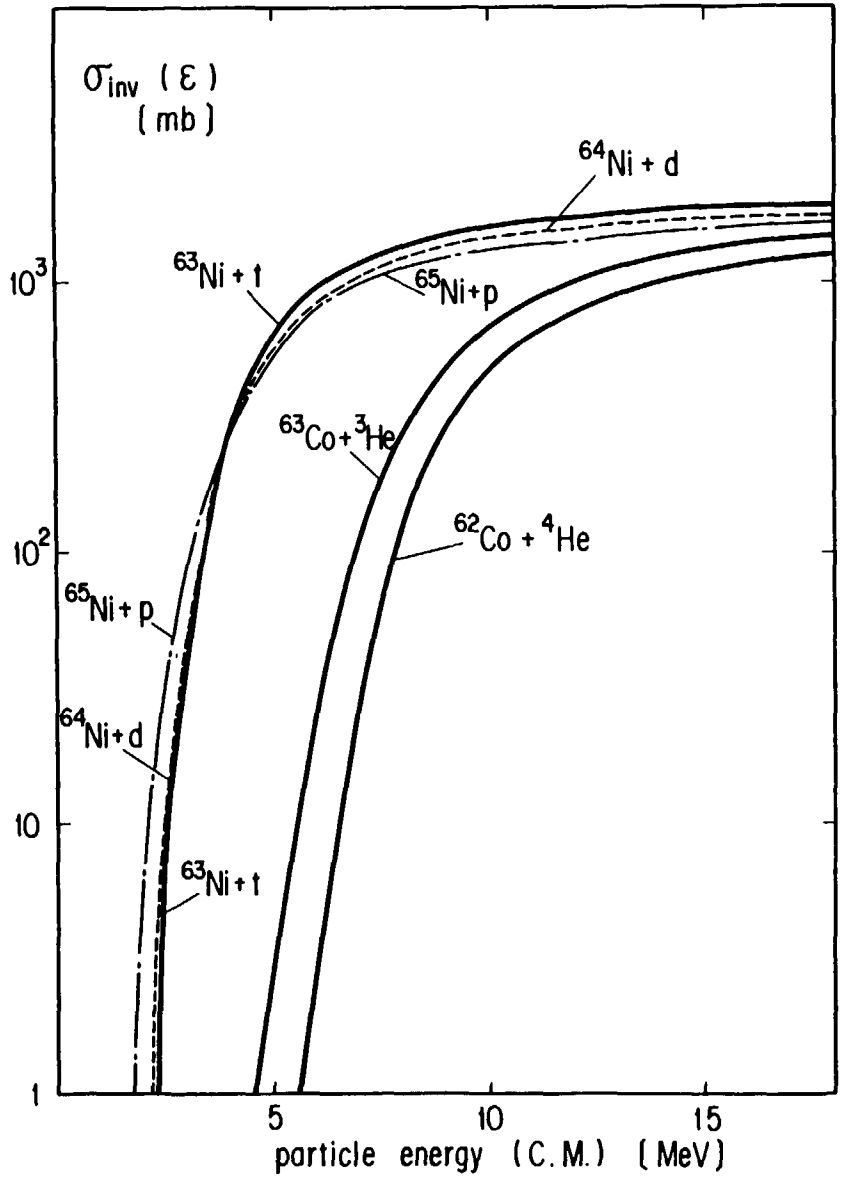

Fig. 6 The inverse cross sections for ^{65}Cu (n, X) reactions

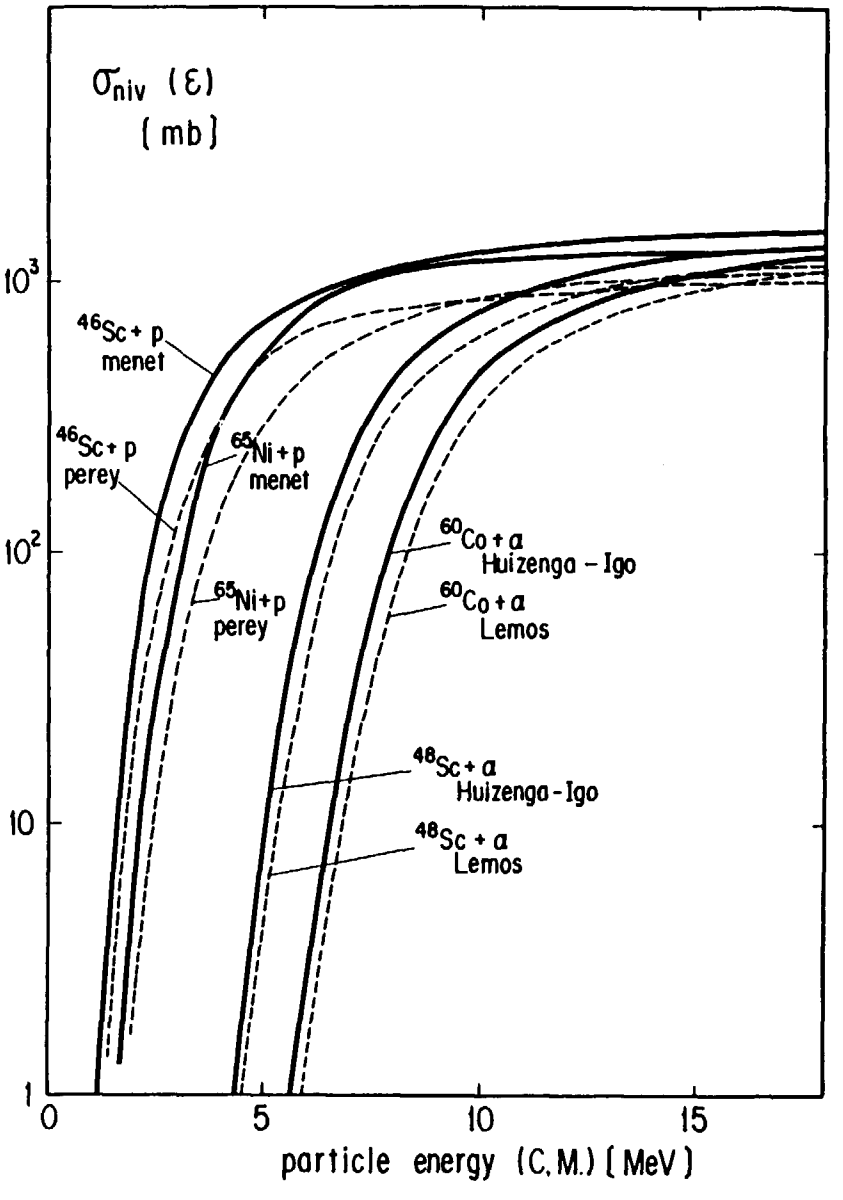

Fig. 7 The inverse cross sections calculated with different optical model parameters

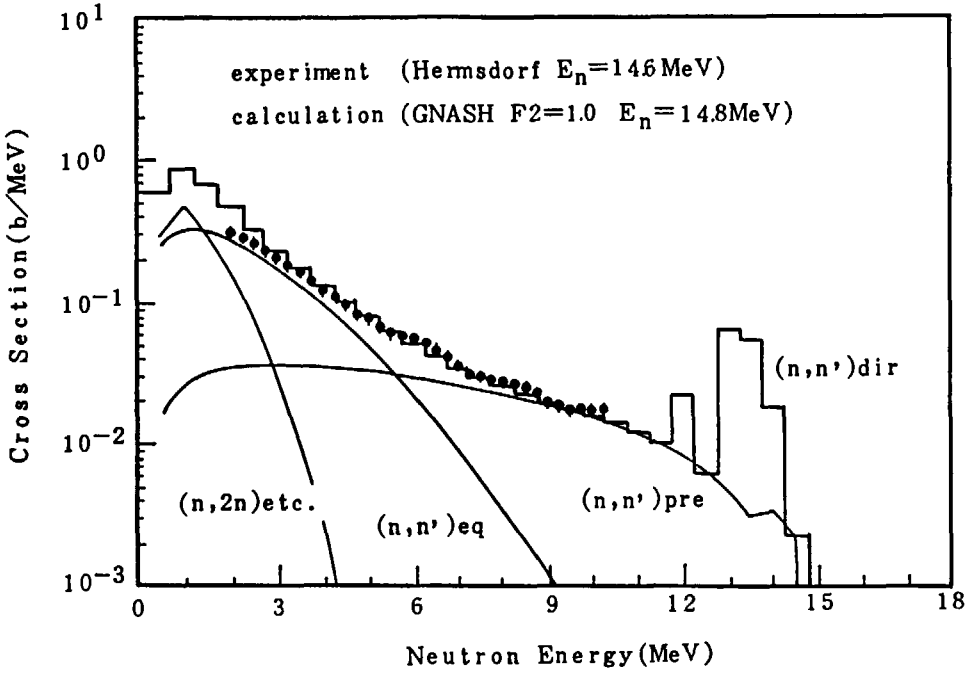

Fig. 8 The neutron emission spectrum of Cu-neutron reactions calculated by GNASH code

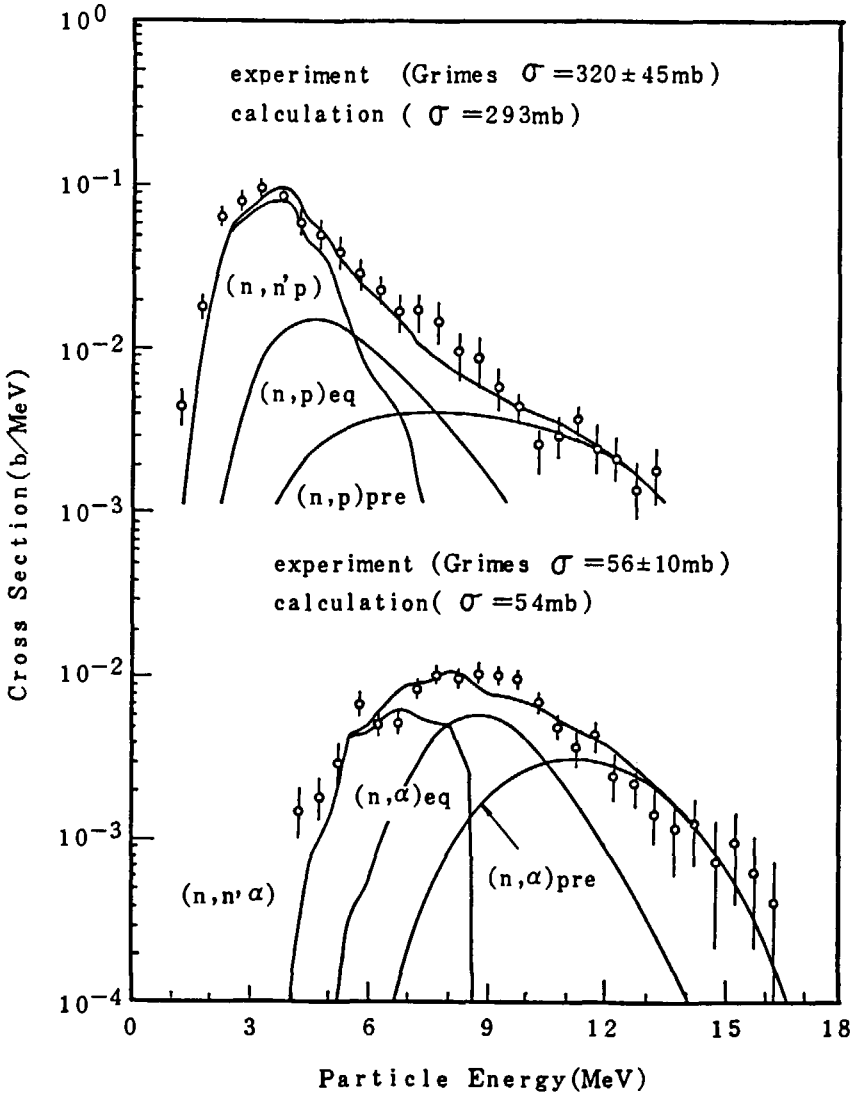

Fig. 9 The proton- and α-emission spectrum of Cu-neutron reactions calculated by GNASH code

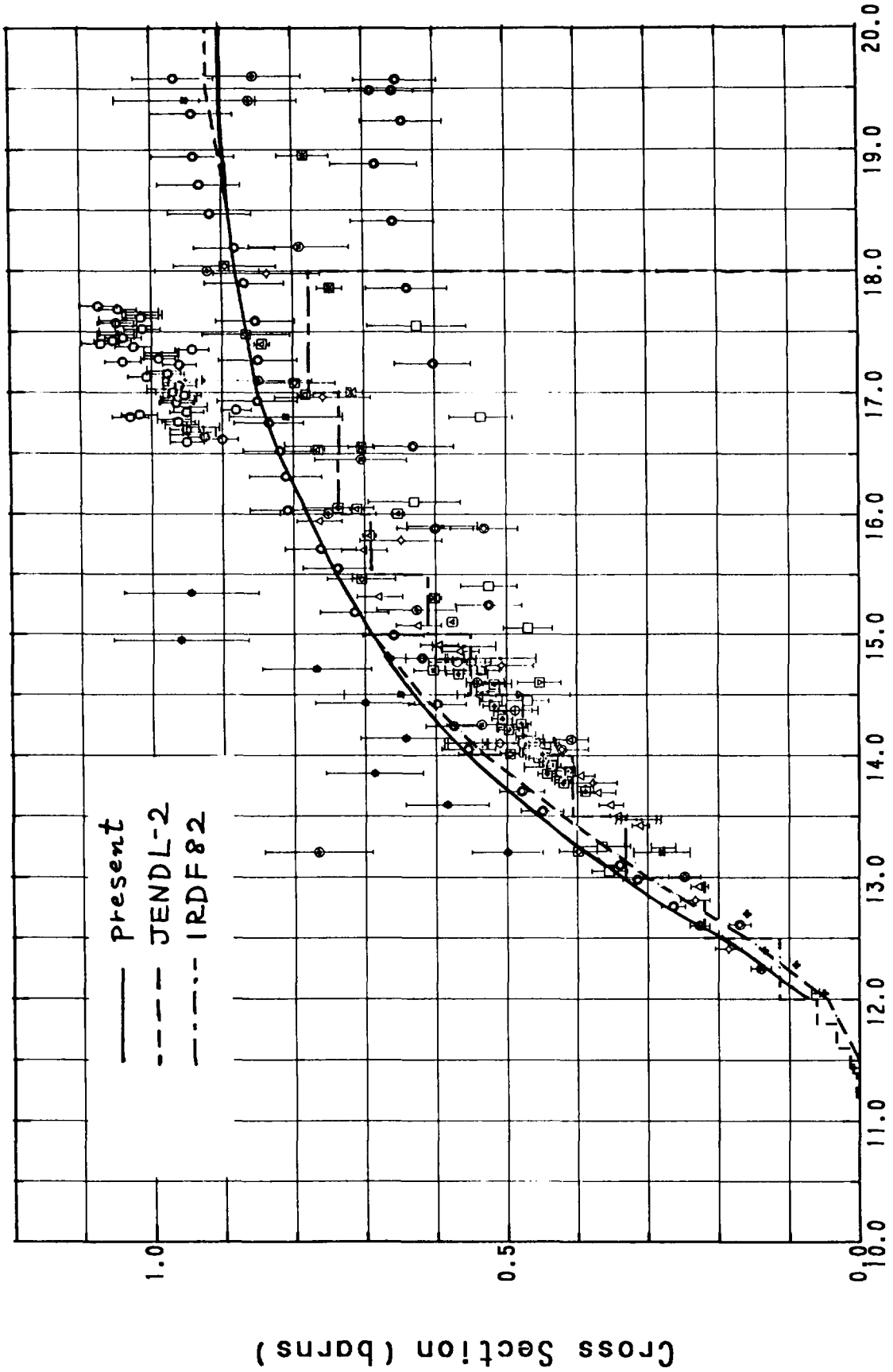

Fig.10 The cross section for ^{63}Cu (n, 2n) reaction calculated by GNASH code

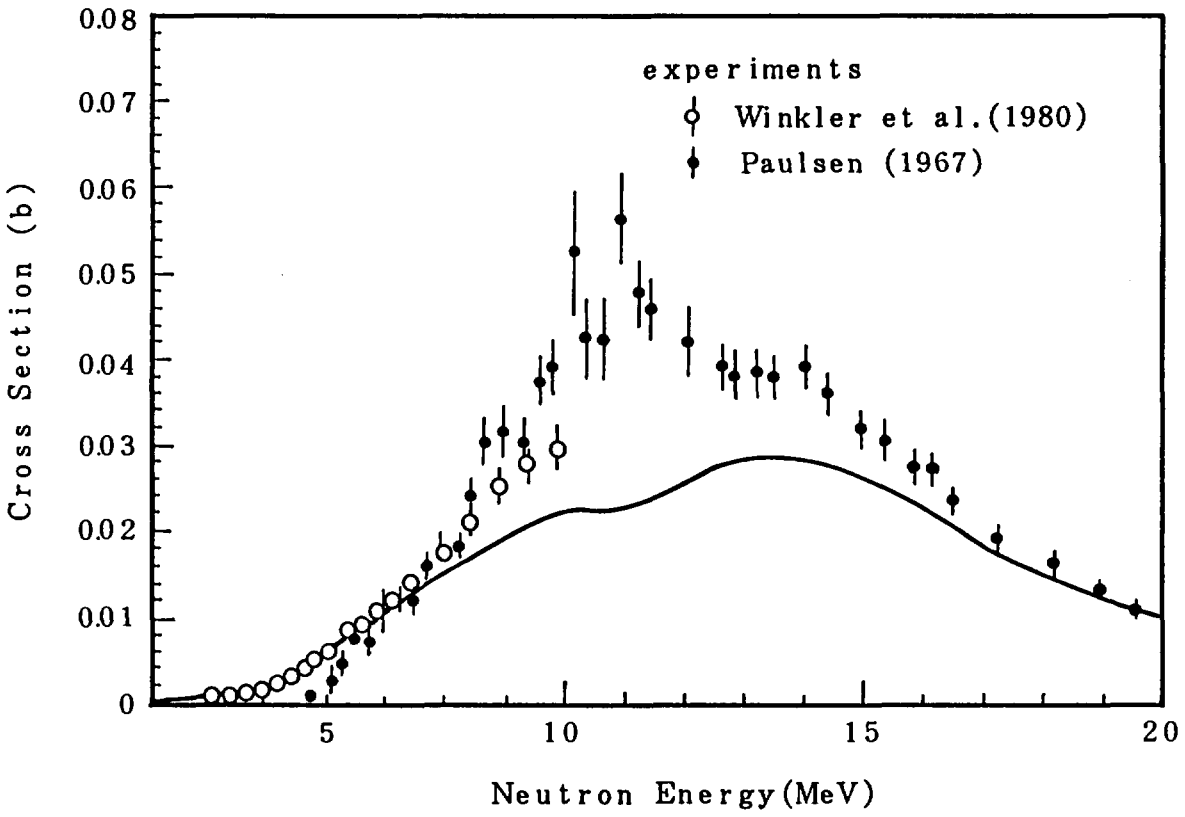

Fig. 11 The cross section for ^{63}Cu (n, α) reaction calculated by GNASH code

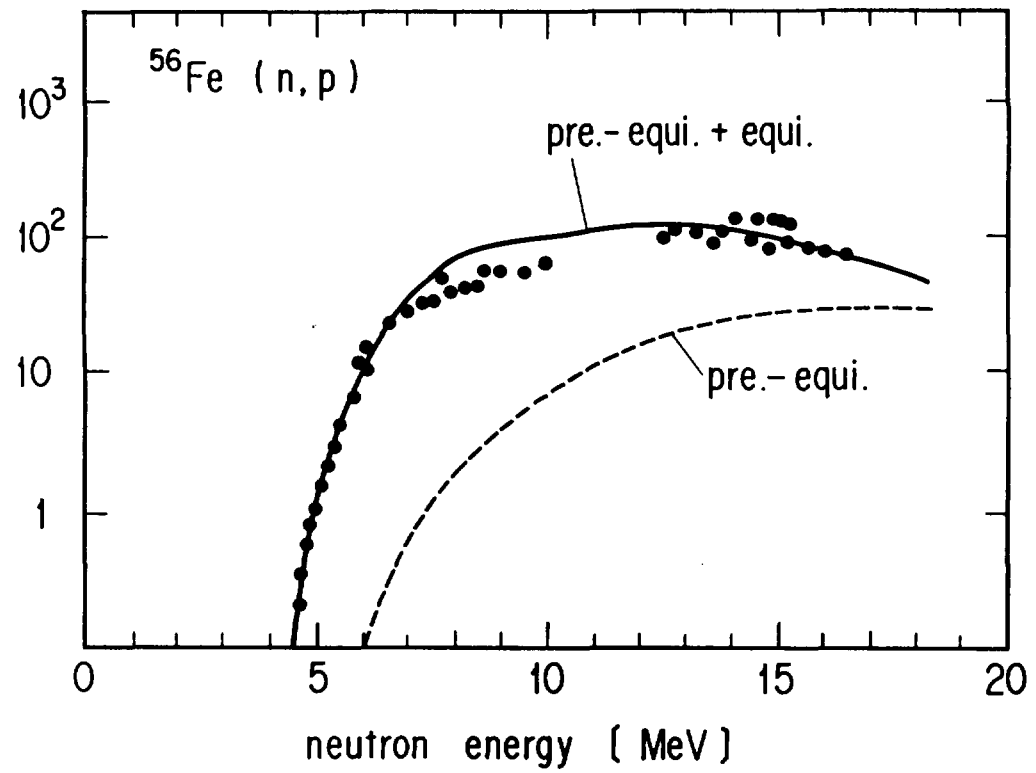

Fig. 12 The cross section for ^{56}Fe (n, p) reaction calculated by PEGASUS code

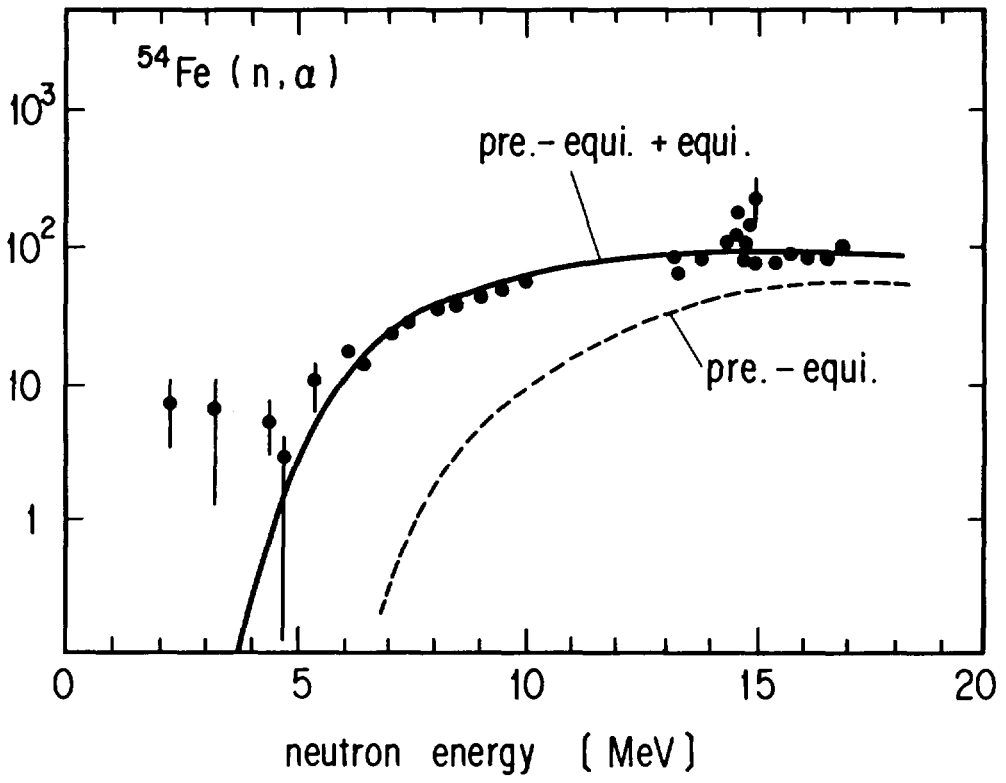

Fig. 13 The cross section for ^{54}Fe (n, α) reaction calculated by PEGASUS code

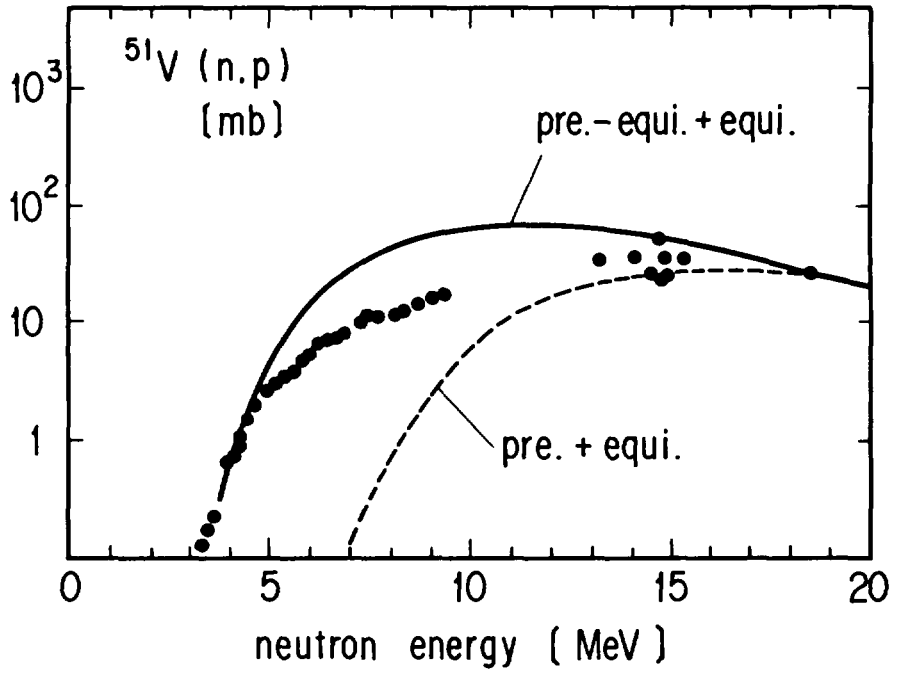

Fig. 14 The cross section for ^{51}V (n, p) reaction calculated by PEGASUS code

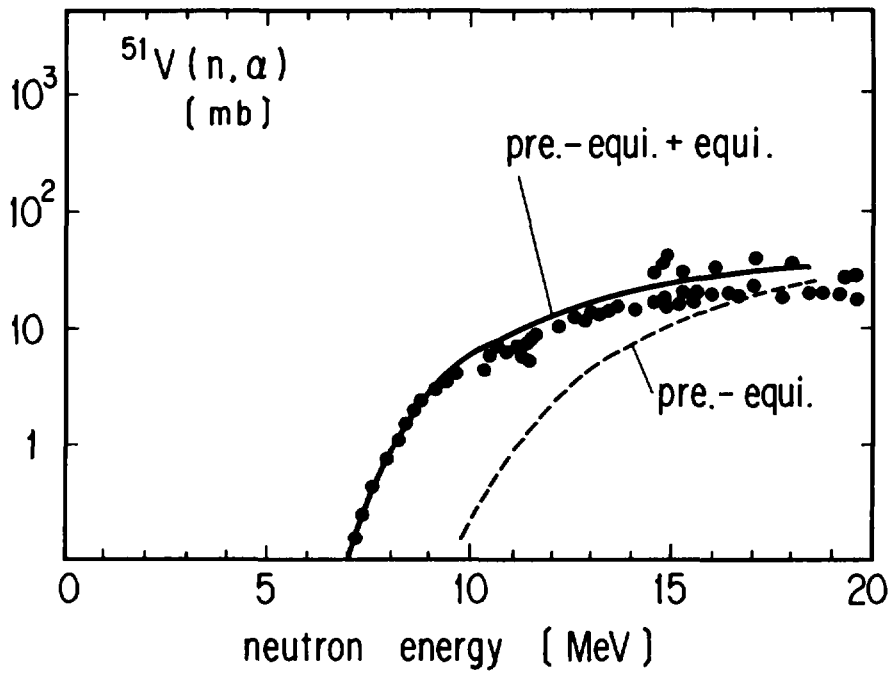

Fig.15 The cross section for $^{51}V(n, \alpha)$ reaction calculated by PEGASUS code

2.3 Problems of Decay Heat Calculations

J. Katakura

Japan Atomic Energy Research Institute

Tokai-mura, Naka-gun, Ibaraki-ken

In the decay heat calculations, average decay energies($\bar{E}_\beta$ and $\bar{E}_\gamma$) of fission-product nuclides play an important role. For nuclides with no experimental informations or insufficient decay schemes, it is needed to estimate the decay energies by theoretical model. To adopt the theoretically estimated decay energies, careful examination of decay schemes is required for the nuclides with experimental data.

Besides the average decay energies, gamma-ray spectra from aggregate fission-product nuclides are needed to improve the qualities of the decay data. The estimation of the gamma-ray spectra of the nuclides with no experimental decay schemes was carried out on the same basis as the average decay-energy estimation and was applied to calculations of the gamma-ray spectra from the aggregate fission-product nuclides. The good agreement was obtained between the measured spectra and the calculated ones by using the estimated spectra.

1. Introduction

In the decay heat calculations, many nuclear data, such as fission yield, half-life or decay constant, decay energy and so on, are needed. In these data, the decay energy is very important, especially, at short cooling times after fissions. At the short cooling times, short-lived fission-product nuclides with large Q_β contribute to the decay heat, but the decay data of these nuclides are often insufficient for the decay heat application. In usual β-γ experiments, high energy gamma rays are sometimes unobserved because of the decreasing ''observation efficiency'' with the gamma-ray energy.[1] Therefore, higher levels fed by beta decay are not recognized or strength of the beta branches to the higher levels is underestimated. This fact leads to the enhanced beta strength to the lower

levels, that is, high energy beta rays are enhanced. So the average beta energy($\bar{E}_\beta$) is overestimated and the average gamma decay energy($\bar{E}_\gamma$) is underestimated. This situation is known to be "Pandemonium Effect"[2]. In order to avoid the effect, the Working Group on Decay Heat Evaluation of the Japanese Nuclear Data Committee estimated the decay energies($\bar{E}_\beta$ and $\bar{E}_\gamma$) theoretically for nuclides with large Q_β values or no experimantal informations[3]. And fairly good agreement was obtained between the calculations and the measurements for the decay heats of important fissioning nuclides. However, slight discrepancies still remained[4]. To diminish the discrepancies, reexamination has been performed[5].

Besides the decay energy, gamma-ray spectra are needed to check the decay energy and to improve their quality. The estimation of gamma-ray spectra of nuclides with no experimental spectra was performed and was applied to the spectrum calculation of aggregate fission-product nuclides[6].

In this report, the reexamination of the decay data to diminish the discrepancies is described and the estimation of gamma-ray spectra is also given. In chapter 2, the previous adoption of the theoretically estimated decay energy is given. The reexamination of the decay energy is described in chapter 3. The calculation of the gamma-ray spectra from the aggregate fission-product nuclides is presented in chapter 4.

2. Previous adoption of theoretically estimated decay energy

The first version of nuclear data library of fission-product nuclides was compiled and released in 1983 by the Working Group on Decay Heat Evaluation of the Japanese Nuclear Data Committee[7]. In this library, the theoretically estimated decay energies($\bar{E}_\beta$ and $\bar{E}_\gamma$) are adopted for some nuclides. The estimation was carried out by "gross theory" of beta decay. The nuclides for which the theoretical estimation was adopted are classified into following three categories.

I : Nuclide of which half-life and decay scheme are known but of which Q_β value is larger than 5 MeV.

II : Nuclide of which half-life is measured but of which decay scheme is not known.

III: nuclide of which half-life and decay scheme are not known.

It is essential point to adopt the theoretically estimated decay energy for the nuclides in the first category. As the decay schemes of these nuclides are measured, the decay energies of the nuclides can be obtained from the decay schemes. These nuclides, however, have large Q_β values. Then, the "Pandemonium Effect" may appear in their decay schemes.

Figure 1 shows the comparison between the measured decay heat and the calculated ones before and after the adoption of the estimated decay energy for the nuclides in the first category. The upper part shows beta-ray component from ^{235}U fissions by thermal neutrons and the lower part it's gamma-ray component. The curve A is the calculation before the adoption, that is, the calculation based on only the experimental decay energies. This curve shows the overestimation of the beta-ray component and the underestimation of the gamma-ray component. The curve B is the calculation after the replacement of decay energies by the theoretically estimated values. This curve shows good agreement with the measurement. The agreement is also obtained in the case of ^{239}Pu fissions by thermal neutrons as shown in Fig. 2. The curve JNDC is the calculation with the estimated decay energies for the nuclides with large Q_β. The results have better agreement in both beta-ray and gamma-ray components than the results using another library, such as ENDF/B-IV, B-V and so on. The gamma-ray component, however, shows slight discrepancies at about one thousand seconds after fissions.

3. Reexamination of decay energy

The reexamination of decay data of all experimentally identified nuclides was carried out irrespective of their Q_β values to diminish the remained discrepancies[5]. In the reexanimation process, an attention was payed on the ratio of obserbed highest level energy(E_L) to Q_β, that is, E_L/Q_β and the number of levels fed by the beta decay(N_L). The decay scheme with larger E_L/Q_β and N_L is more preferable. But it is a matter of course that the values of log ft and the trend of level density in the daughter nucleus was also taken into account. In this way, the decay energies were changed from the estimated values to the experimental ones and vice versa for some nuclides. Besides these nuclides, the decay energies of some other nuclides were changed by the recalculation or the adoption of newly measured

data. As the result, the decay energies of total about 150 nuclides were changed. The calculated decay heat and it's C/E after the reexamination are shown in Fig. 3. The results before the reexamination are also shown. This figure shows the gamma-ray component of the decay heat from ^{239}Pu fissions by fast neutrons. The curves of JNDC FILE and JNDC FILE(1.5V) are the results of previous calculations. The curve of MOD. JNDC FILE is the result of the calculation after the reexamination. In the previous calculations, the maximum disagreement between the calculation and the measurement is about 15%. In the calculation after the reexamination, it becomes about 5%. The beta-ray component is shown in Fig.4. The calculation after the reexamination also diminishes the discrepancy. As seen in these cases, careful examination of decay scheme is needed for the adoption of the theoretically estimated decay energy.

4. Gamma-ray spectrum calculation

In the decay heat calculation, only the average decay energies are used explicitly and the spectra is not explicitly appeared. To check the reliability of the decay data and to improve their quality, the spectrum data are needed because the spectrum data are base of the derivation of the decay energies. However, the same problem as in the decay heat calculation appeares. Namely, the spectrum data of short-lived nuclides with large Q_β are unmeasured or insufficient. The calculated gamma-ray spectra from aggregate fission-product nuclides are shown in Figs.5 and 6 with the measured spectra. These spectra are normalized to be decay heat by summing up the all data point. In these calculations, only the nuclides having the experimentally measured gamma-ray spectra are considered. So the difference between the calculation and the measurement is due to the contribution of nuclides with no experimental spectra or insufficient spectra. Figure 5 shows the spectrum at 500.0 seconds after ^{235}U fissions by thermal neutrons. The agreement between the calculation and the measurement is fairly good in this case. This good agreement indicates that the nuclides contributing to the spectrum at this cooling time have sufficient spectrum data. Figure 6 shows the spectrum at 2.7 seconds after ^{235}U fissions by thermal neutrons. In this case, large disagreement is seen between the calculation and the measurement. At short cooling time, the nuclides with no experimental data or insufficient spectrum data largely contribute to the aggregate spectrum. To complement the gap between the measurement and the calculation, the

estimation of gamma-ray spectrum was performed for the nuclides with no experimental spectra[6]. In this estimation, the gross theory of beta decay and a cascade gamma-ray transition model was used.

A schematic illustration of gamma-ray cascade process following beta decay is shown in Fig. 7. Initial level population density of daughter nucleus b(E) is obtained by the beta strength function based on the gross theory. The gamma-ray emission process is treated with a cascade gamma-transition model in which all levels in the daughter nucleus are treated as continuous. Then the level population g(E') at the energy E' caused by the beta feeding and the gamma de-excitation of the higher levels is written as,

$$g(E') = \int_{E'}^{E_{max}} (b(E'') + g(E''))(E'' - E')^3 S_\gamma(E''-E')\rho(E')dE''$$

where $S_\gamma(E''-E')$ and $\rho(E')$ are Brink-Axel type gamma-ray strength function[8] and Gibert-Cameron type level density[9], respectively. In this expression, only the E1-type gamma transition is taken into account. This equation can be solved in a numerical manner starting from E_{max}, which is equal to Q_β, towards the lower energy, successively. The intensity of the gamma-ray $I(E_\gamma)$ is represented as follows.

$$I(E_\gamma) = \int_0^{E_{max}} dE' \int_{E'}^{E_{max}} dE'' \delta(E''-E'-E_\gamma)(b(E'') + g(E''))(E''-E')^3 \times S_\gamma(E''-E')\rho(E')$$

In this manner, the typical spectra of fission-product nuclides were prepared. They were classified by atomic mass, Q_β value and odd-evenness of proton or neutron numbers. For the atomic mass, the numbers of light and heavy mass peaks of the fission yield were selected. Namely, 95 and 96 werte selected for the light mass peak and 139 and 140 for the heavy mass peak. The Q_β values were taken to be 5, 7, 9 and 11 MeV. And then, even-even, even-odd, odd-even and odd-odd nuclides were considered. So total 32 spectra were prepared. For applying these estimated spectra to the summation calculation, an appropriate spectrum of a nuclide was selected in the categories and was applied with renormalization constant which is equal to the average gamma decay energy. This renormalization ensures the absolute value of the calculated spectrum.

The calculated spectra from the aggregate fission-product nuclides are

shown in Figs. 8 and 9 comparing the measured spectra. Figure 8 shows the gamma-ray spectrum at 2.7 seconds after ^{235}U fissions by thermal neutrons. The solid curve is a calculation after the adoption of the estimated spectra for nuclides with no experimental spectra. The dashed curve is a calculation before the adoption. The gap between the measurement and the calculation is complemented well. Some discrepancies, however, still remain in the regions of about 4.5 MeV and beyond 6 MeV. As all levels in the daughter nucleus are treated as continuos in the estimation, the detailed structures of the gamma rays are not reproduced. Figure 9 shows the gamma-ray spectrum at 2.7 seconds after ^{239}Pu fissions by thermal neutrons. The notations are the same as in Fig. 8. The disagreement between the measurement and the calculation improves fairly well, too. But some discrepancies are also seen. Apart from these discrepancies, the gap between the measurement and the calculation is complemented by the introduction of the estimated spectra for the nuclides with no experimental spectra. This fact provides a support for the present estimation in it's adequacy.

5. Conclusion

In the calculations of the decay heat and the gamma-ray spectra from the aggregate fission-product nuclides, it is essential point to estimate the decay energies and the gamma-ray spectra of the nuclides with no experimental informations or insufficient data. Especialy for the nuclides with experimental data, careful examination is needed to decide whether the data are sufficient or insufficient. In the present report, the reexamination of the decay data was given and good improvement of the decay heat calculation was obtained. And also the estimation of gamma-ray spectrum was given on the same basis as in the estimation of the decay energy. By introducing the estimated spectra, the gap between the measurement and the calculation was complemented well. So the evaluations of the decay heat and the spectrum from the aggregate fission-product nuclides can be carried out consistently.

Acknowledgements

The author thanks to the member of the Working Group on Decay Heat Evaluation of the Japanese Nuclear Data Committee.

References

1). Hardy, J. C. et al., Phys. Lett. 71B, 307 (1977)

2). Workshop on microscopic beta and gamma data, in NEANDC speciallists meeting on yields and decay data of fission product nuclides, BNL 51778 (1983)

3). Yoshida, T. and Nakasima, R., J. Nucl. Sci. 18, 393 (1981)

4). Katakura, J. et al, JAERI-M 84-117 (1984)

5). Katakura, J. and Nakasima, R., to be submitted

6). Yoshida, T. and Katakura, J., Nucl. Sci. Eng. to be published

7). Tasaka, K. et al., JAERI 1287 (1983)

8). Brink, D. M., Doctoral Thesis, Oxford University (1966)
Axel, P., Phys. Rev. 126, 671 (1962)

9). Gilbert, A. and Cameron, A. G. W., Can. J. Phys. 43, 1446 (1965)

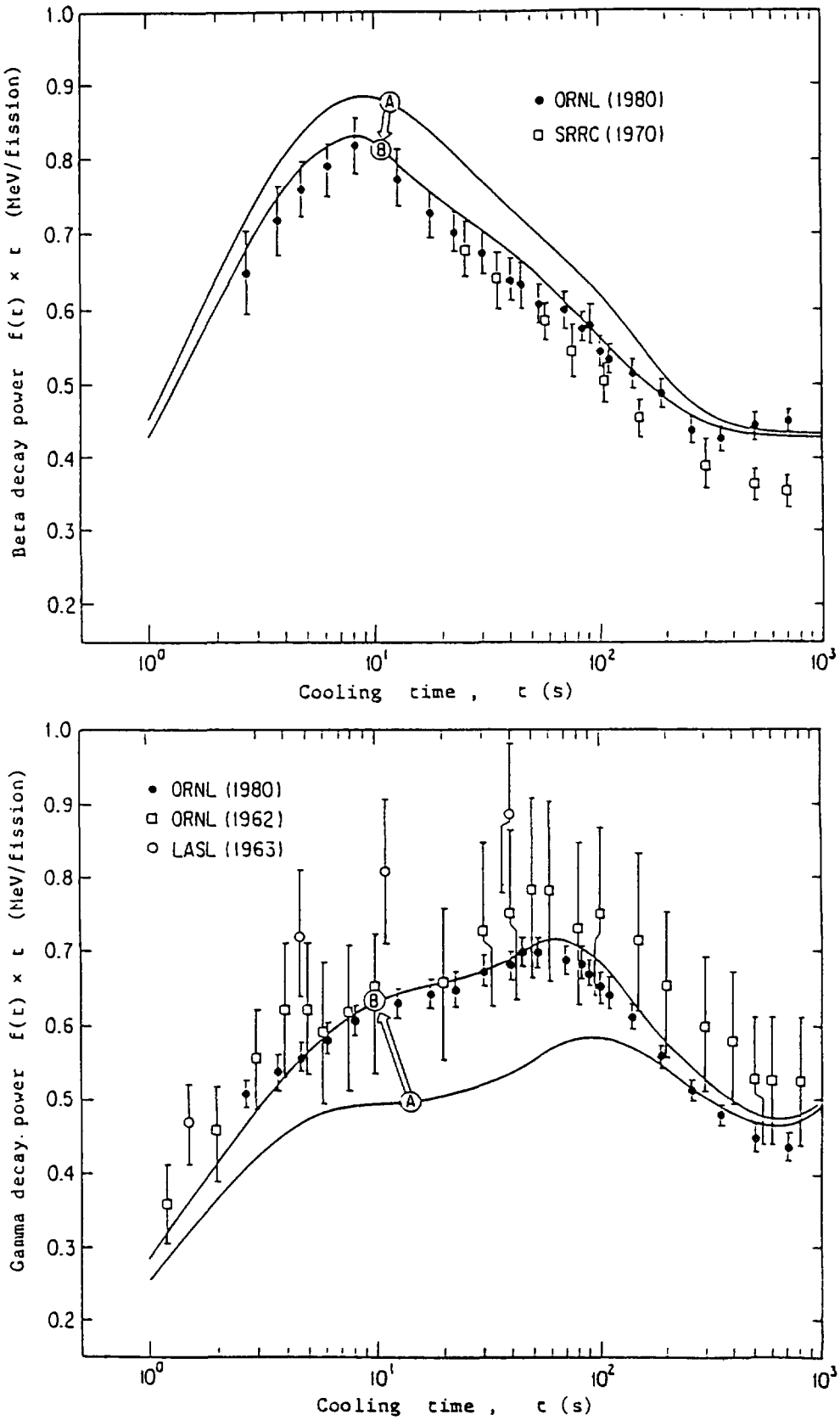

Fig. 1 Effect of using theoretical decay energy on the calculated decay heat of ^{235}U fissions.
The curve A is the calculation based on only experimental decay energy. The curve B is the calculation after the adoption of the theoretical estimated values. (Ref. 7))

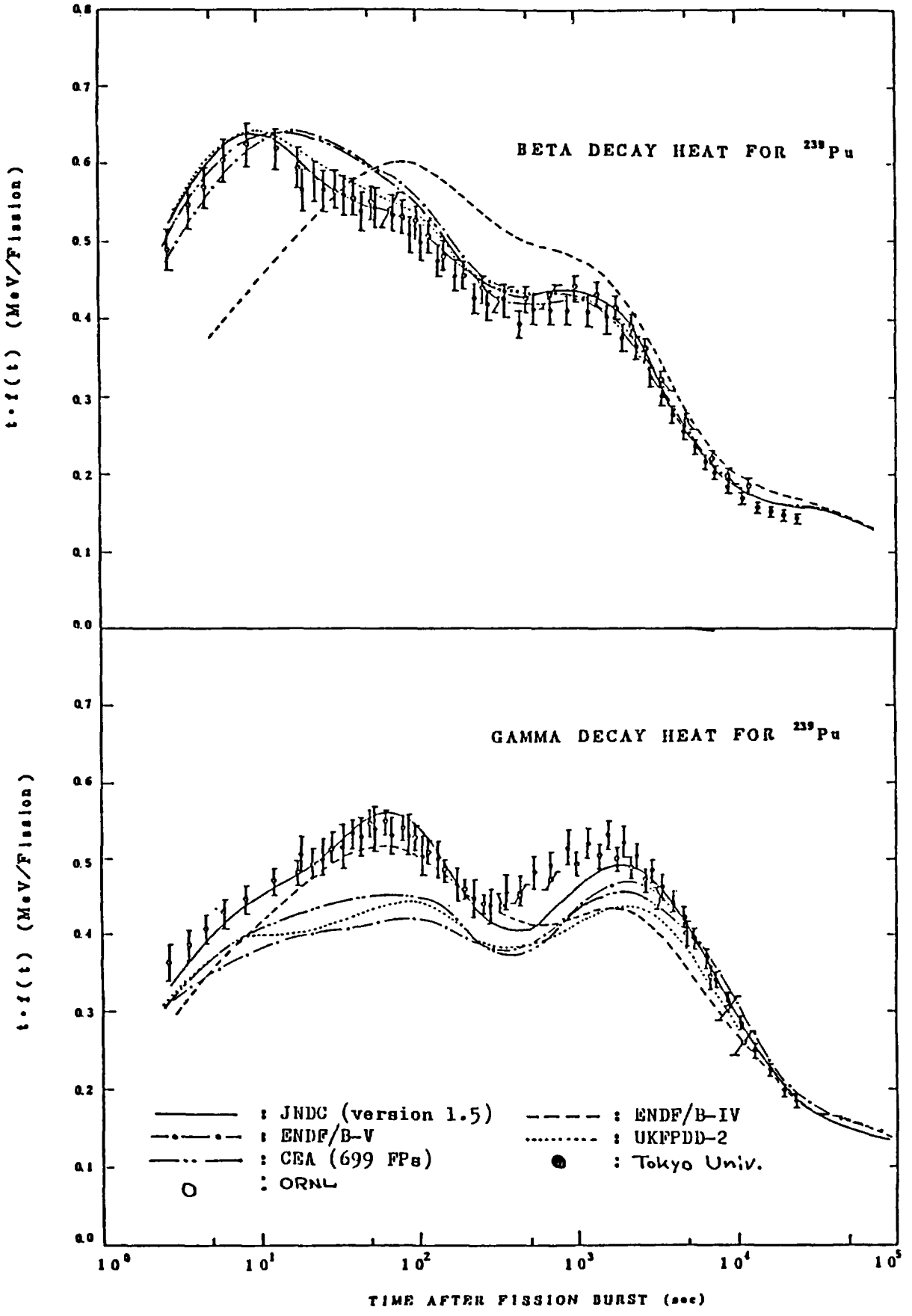

Fig. 2 ^{239}Pu decay heat after a fission burst.

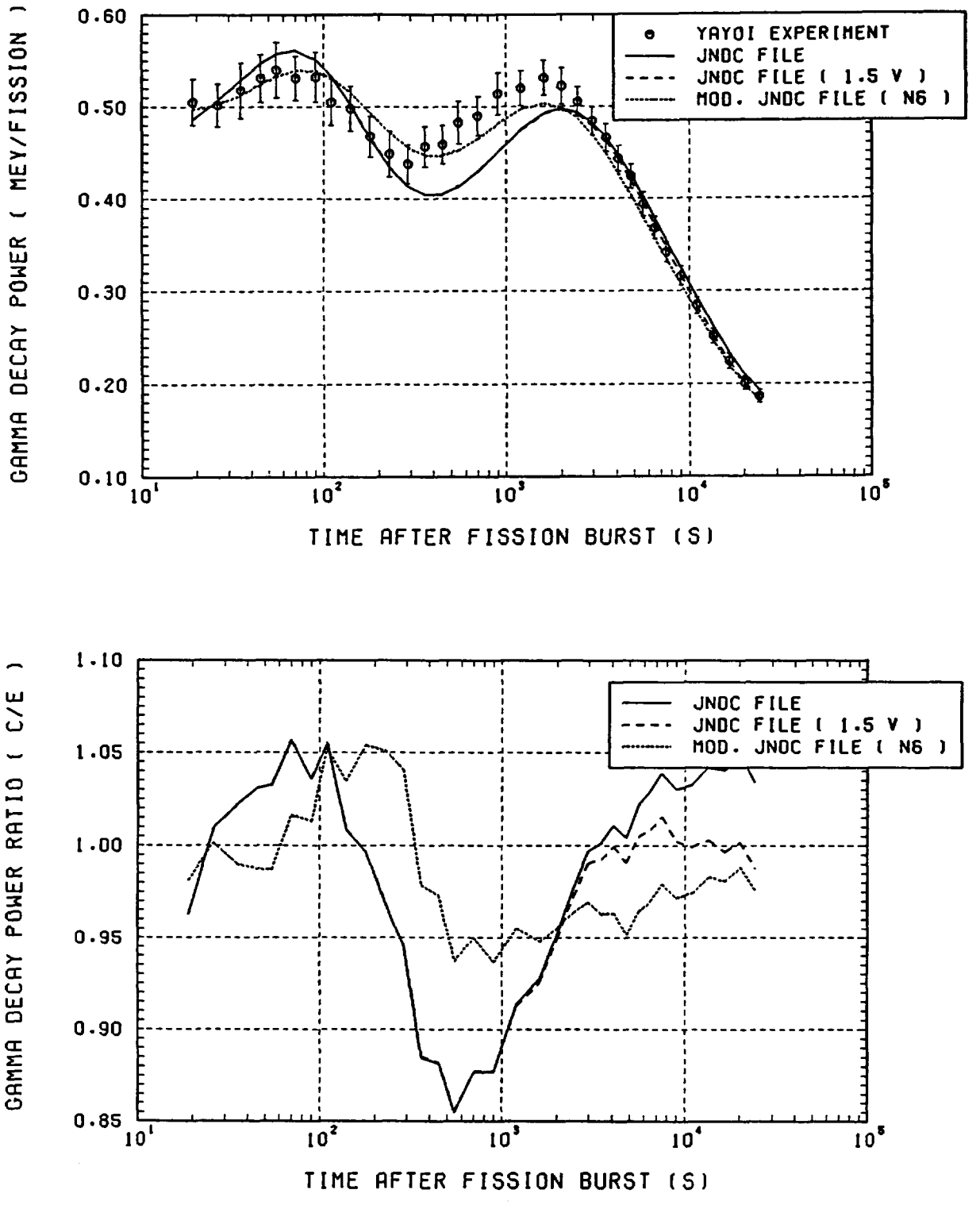

Fig. 3 Gamma-ray component of ^{239}Pu fissions by fast neutrons. The curve MOD. JNDC FILE (N6) is the result after the reexamination of the decay data. The curves of JNDC FILE and JNDC FILE (1.5V) are the results before the reexamination.

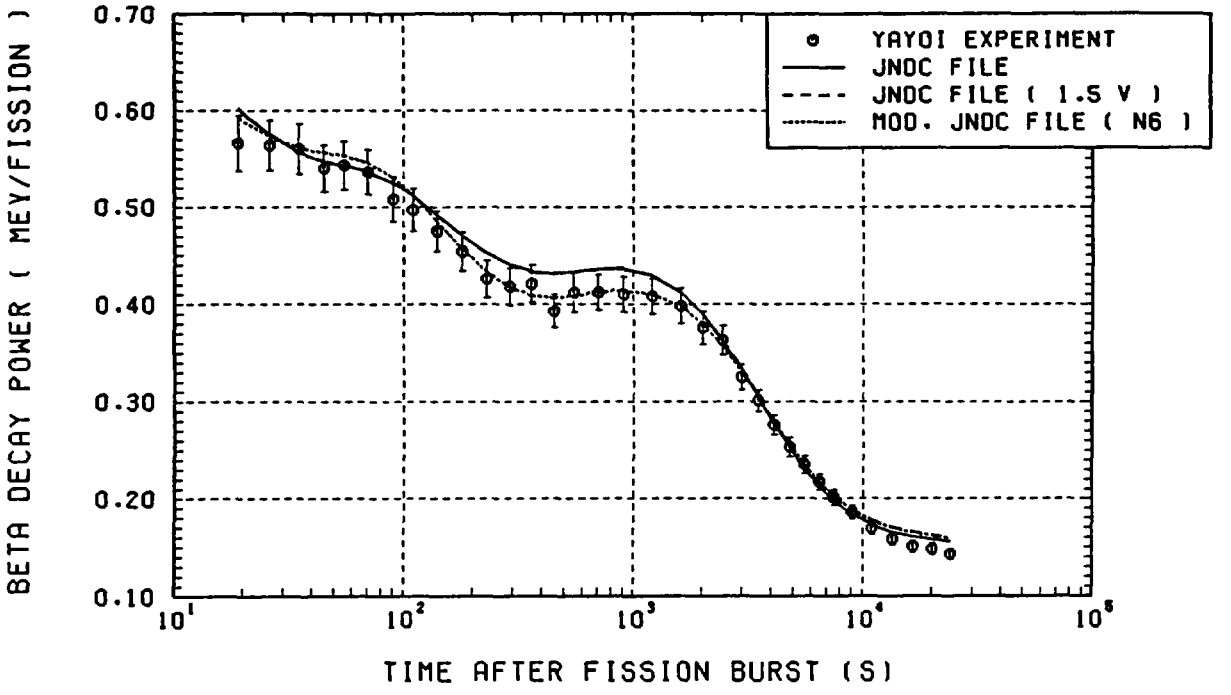

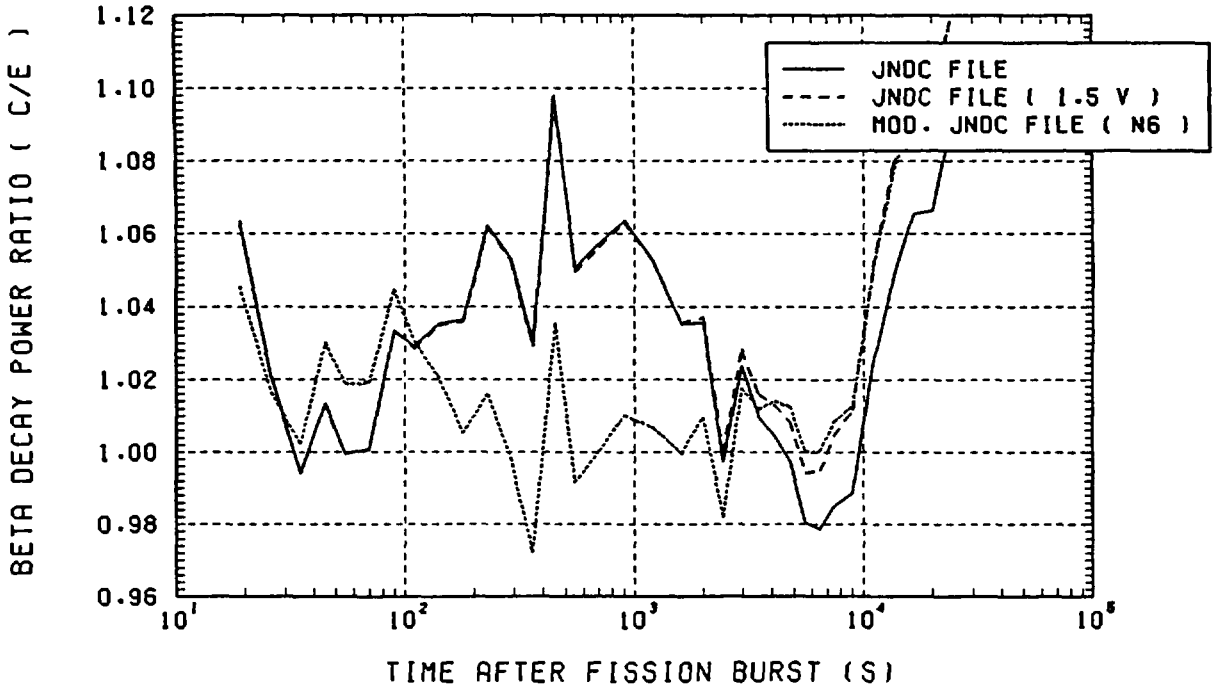

Fig. 4 Beta-ray component of ^{239}Pu fissions by fast neutrons. The curve MOD. JNDC FILE (N6) is the result after the reexamination of the decay data. The curves of JNDC FILE and JNDC FILE (1.5V) are the results before the reexamination.

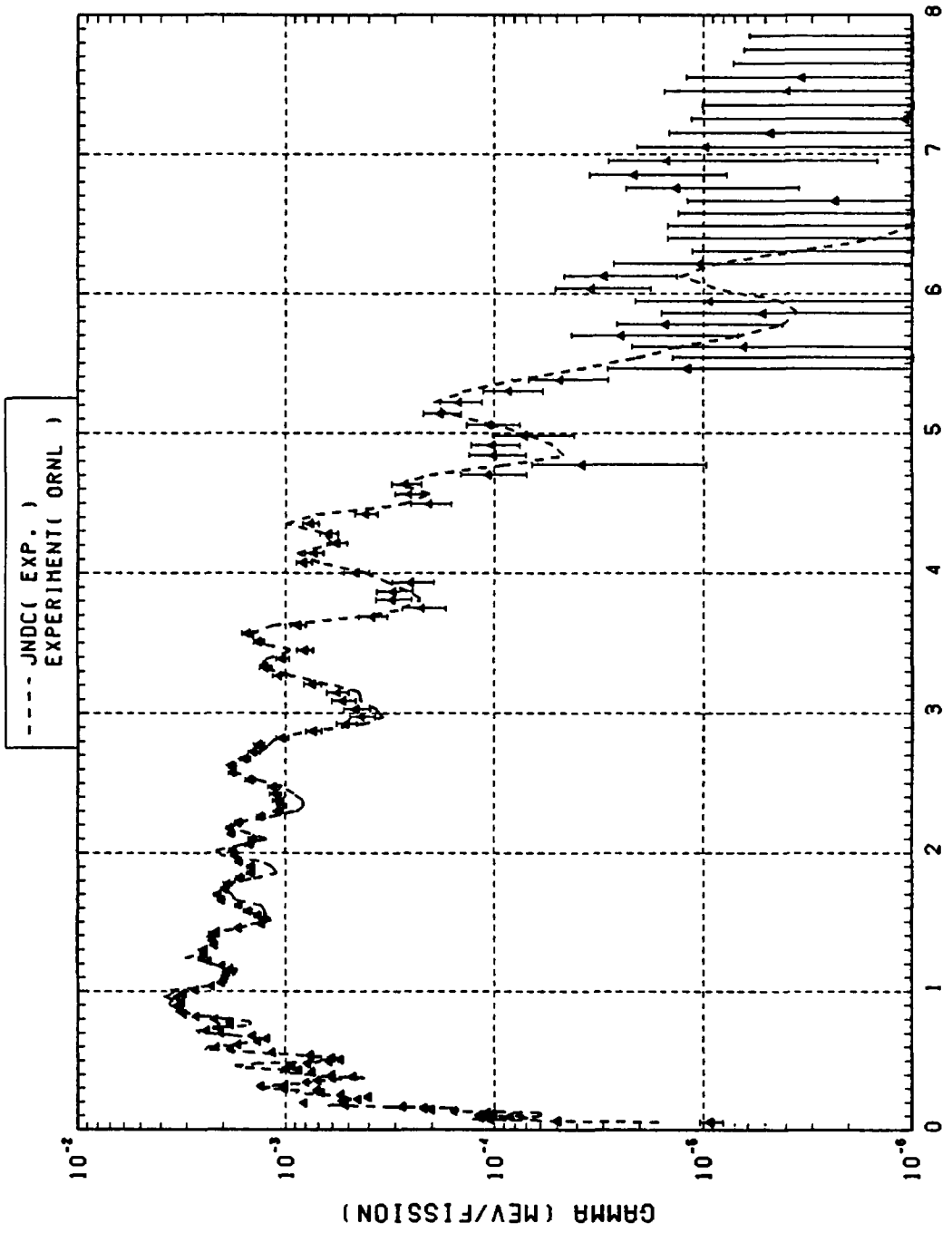

Fig. 5 Aggregate gamma-ray spectrum at 500.0 seconds after ^{235}U fissions.
The calculation is based on only experimental spectrum data.

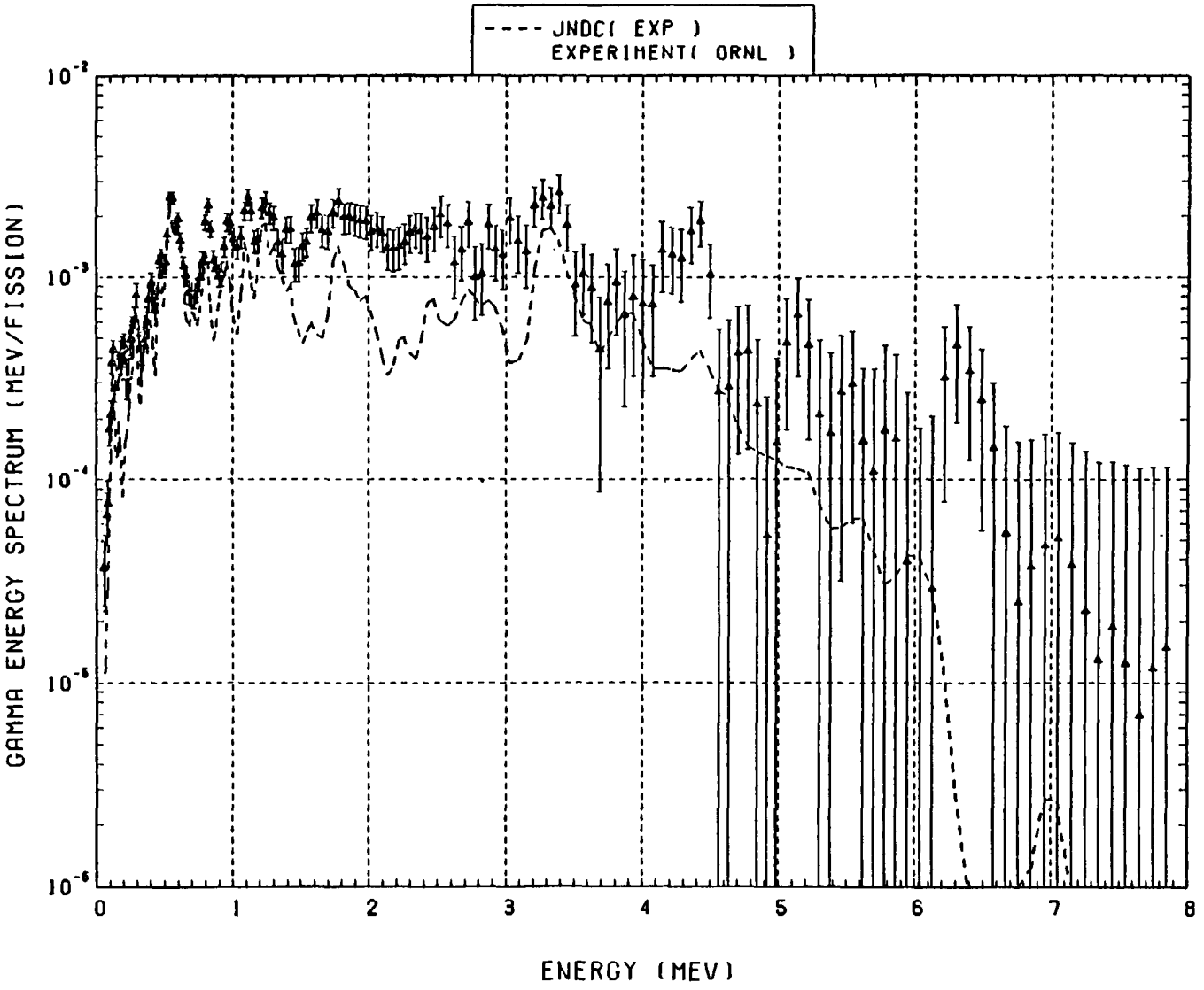

Fig. 6 Aggregate gamma-ray spectrum at 2.7 seconds after ^{235}U fissions.

The calculation is based on only experimental spectrum data.

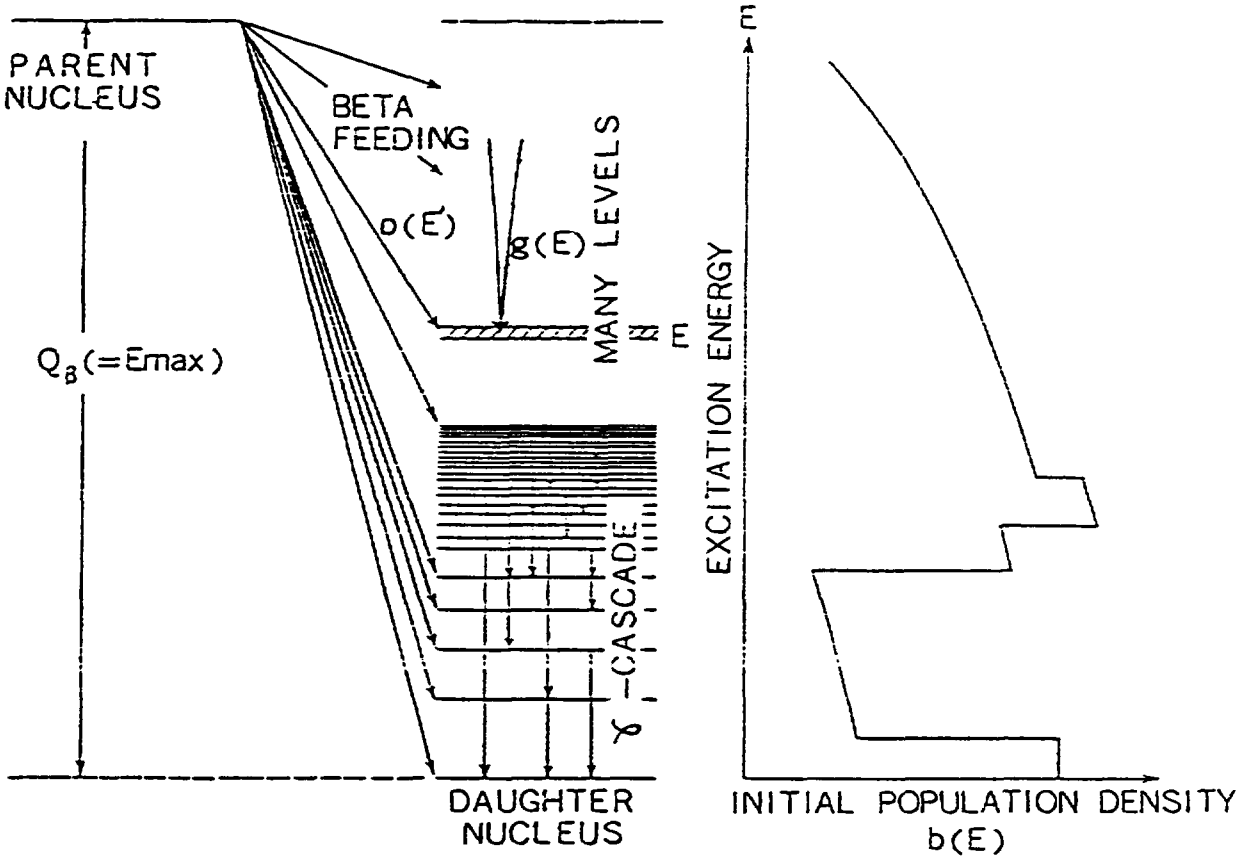

Fig. 7 A schematic illustration of delayed-gamma-ray cascade process.
(Ref. 6))

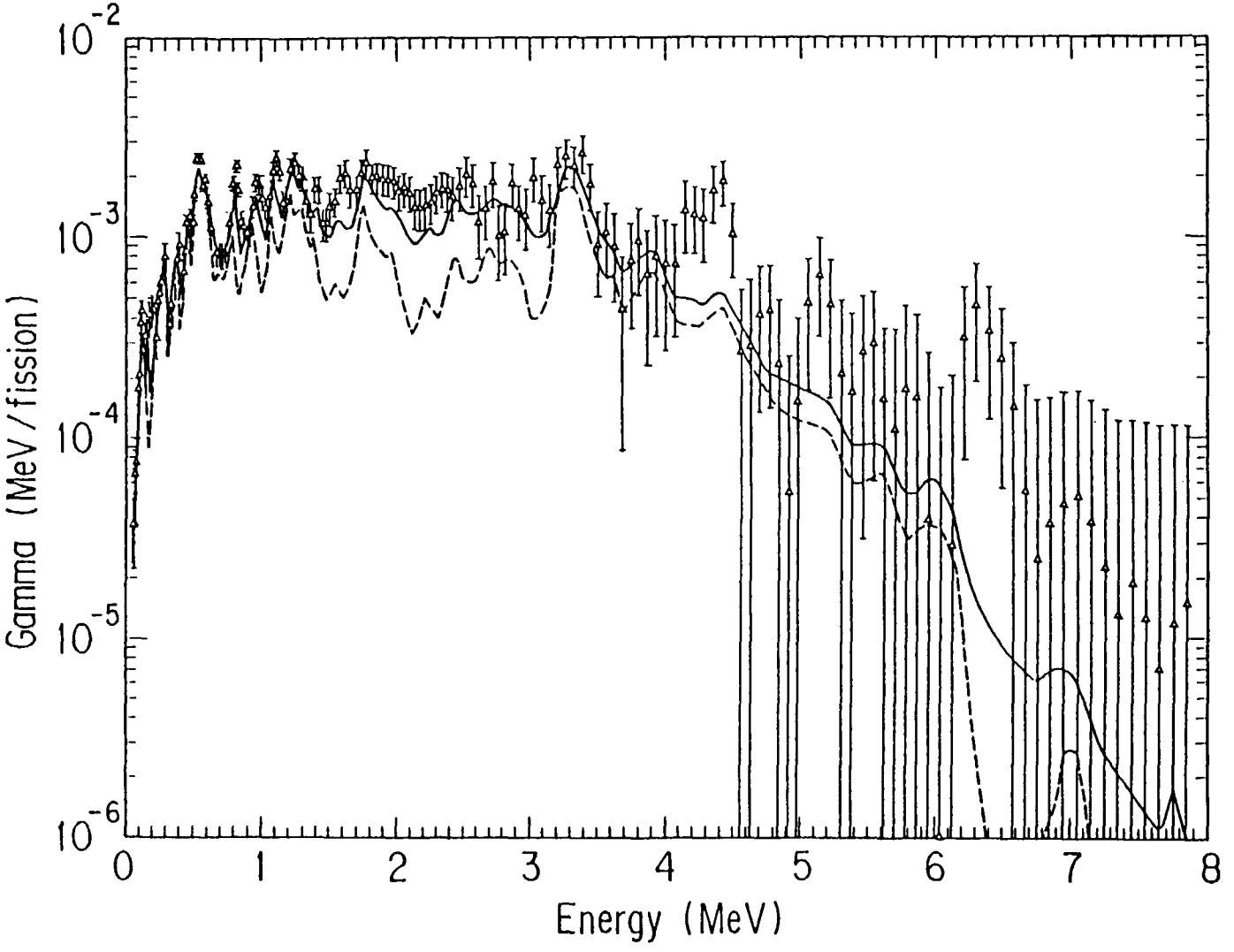

Fig. 8 Effect of estimated spectra on aggregate gamma-ray spectrum at 2.7 seconds after ^{235}U fissions by thermal neutrons. The solid curve is a calculation using the estimated spectra. The dashed curve is a calculation using only the experimental spectra. The measured data is taken from ORNL/NUREG-39 (1978).

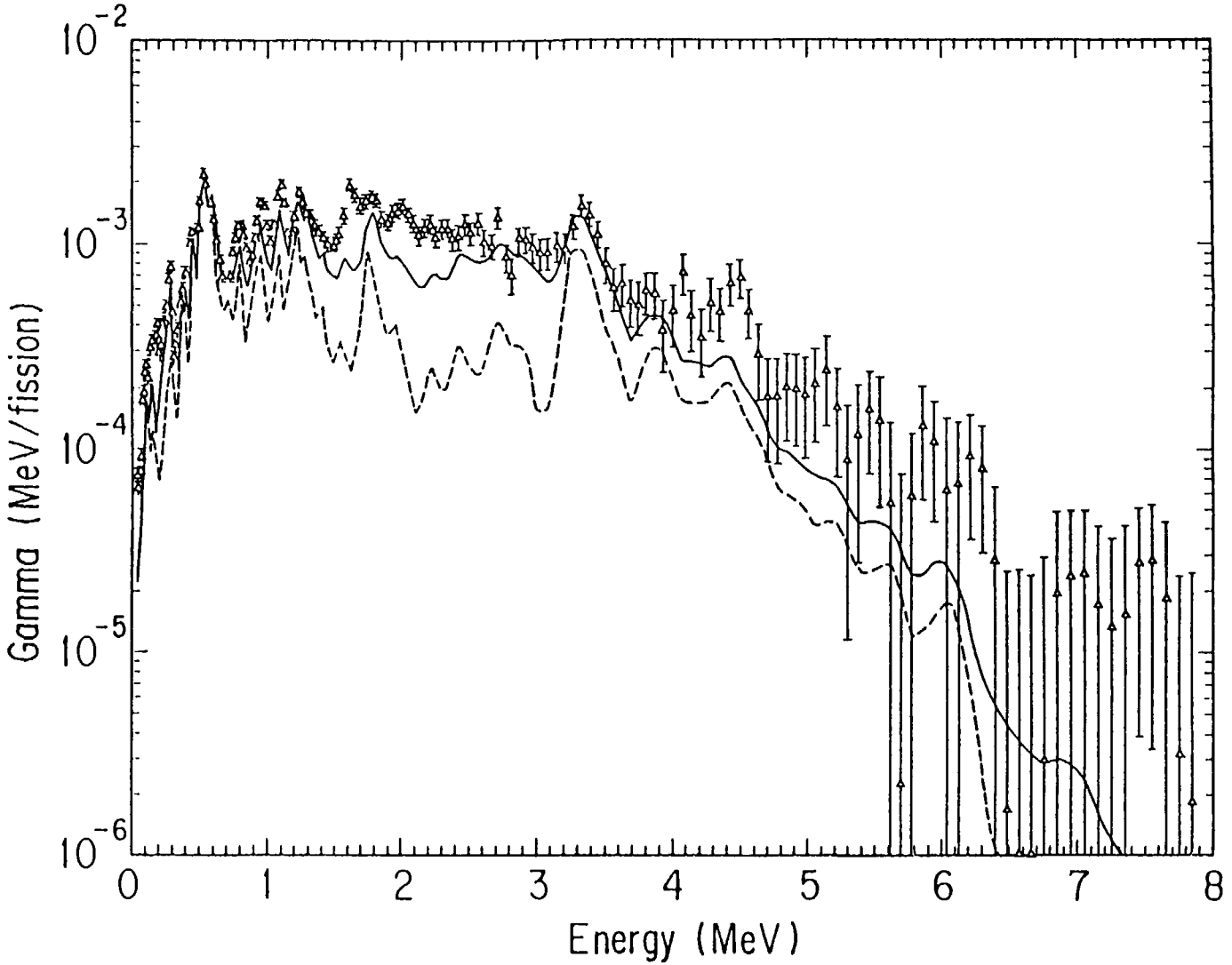

Fig. 9 Effect of estimated spectra on aggregate gamma-ray spectrum at 2.7 seconds after ^{239}Pu fissions by thermal neutrons. The solid curve is a calculation using the estimated spectra. The dashed curve is a calculation using only the experimental spectra. The measured data is taken from ORNL/NUREG-66 (1980).

3. TOPICS

3.1 P_n values of ^{94}Rb and ^{95}Rb measured by a β-γ spectroscopic method

K. OKANO, Y. KAWASE and Y. FUNAKOSHI*

Research Reactor Institute, Kyoto University, Kumatori-cho,
Sennan-gun, Osaka 590-04, Japan

Abstract—The delayed neutron emission probabilities(P_n values) of ^{94}Rb and ^{95}Rb have been measured as (9.73±0.62)% and (8.60±0.57)%, respectively, by a β-γ spectroscopic method utilizing the on-line isotope separator KUR-ISOL. This method can be usefully applied if a pure isotopic and mass-separated ion beam is available and the absolute emission probabilities per decay of main γ rays emitted from relevant nuclides are well established.

INTRODUCTION

The delayed neutron emission probabilities(P_n) are important quantities for reactor design, as these are used to predict the effective delayed neutron fraction(β_{eff}) and the effective delayed neutron decay constant(λ_{eff}). Although the P_n values of fission-product nuclides have been measured at several laboratories using on-line isotope separators and neutron detectors, the discrepancies between the reported values are generally considerable. In the course of our nuclear spectroscopic investigations, it was recognized that the Pn value can be determined fairly precisely utilizing a pure isotopic and mass-separated beam from ISOL and a high resolution Ge(Li) γ-ray detector, if the absolute emission probabilities per decay of main γ rays emitted from relevant nuclides are well established. To examine the applicability of this method, the P_n values of ^{94}Rb and ^{95}Rb have been measured using He-jet type KUR-ISOL(Okano et al., 1981). The procedure and the results obtained are presented. Preliminary results of the present work have been reported previously(Okano et al., 1983,1984).

EXPERIMENTAL PROCEDURE AND RESULTS

The P_n value of ^{94}Rb was determined utilizing a pure ^{94}Rb beam from KUR-ISOL. The contamination of ^{93}Rb or ^{94}Sr ion beam at the mass 94 was measured and found to be less than 0.05%, as the surface ionization ion source coupled with a He-jet system was operated at the temperature below 1500°C(Kawase et al., 1985). The ion beam was collected for period T_i on

*Present address:National Laboratory for High Energy Physics, Oho-machi, Tsukuba-gun, Ibaraki-ken 305, Japan.

an aluminized Mylar tape at the beam collecting port of the ISOL. Then the activity was cooled for T_c and was measured by a coaxial Ge(Li) detector for T_m at a well-shielded measuring port 20cm below the collecting port. The measurements were automatically and cyclically performed until enough counts were accumulated. The dead time loss of the pulse-height analyzer was kept less than 1% to reduce correction. One of the γ-ray spectra thus measured at mass 94 is shown in Fig.1.

The number of ^{93}Sr nuclei produced by the delayed neutron emission was determined by measuring the peak counts C_n of the 590.2keV γ ray following the decay of ^{93}Sr. The number of ^{94}Sr nuclei survived was determined by measuring the peak counts C_1 of the 1427.7keV γ ray following the decay of ^{94}Sr. As the half-life of ^{94}Rb is very short(2.7s) compared with the cooling time T_c(≳30s), the peak counts C_n and C_1 can be expressed as

$$C_n = n_0 b_n \varepsilon_n P_n \lambda_0 (1 - e^{-\lambda_n T_m}) \, e^{-\lambda_n T_c} \frac{(1 - e^{-\lambda_n T_i})}{\lambda_n(\lambda_0 - \lambda_n)} \qquad (1)$$

and

$$C_1 = n_0 b_1 \varepsilon_1 (1 - P_n) \lambda_0 (1 - e^{-\lambda_1 T_m}) \, e^{-\lambda_1 T_c} \frac{(1 - e^{-\lambda_1 T_i})}{\lambda_1(\lambda_0 - \lambda_1)}, \qquad (2)$$

respectively, where n_0 is the number of incident ^{94}Rb nuclei per second, b_n and b_1 are the absolute γ-ray emission probabilities per decay, ε_n and ε_1 are the photopeak detection efficiencies of the Ge(Li) detector, the subscripts n and 1 referring to the 590.2 and 1427.7keV γ rays, respectively, and λ_0, λ_n, and λ_1 are the decay constants of ^{94}Rb, ^{93}Sr and ^{94}Sr, respectively. The value of b_n is taken from the most recent and accurate decay scheme determined by Bischof and Talbert(1977), while b_1 was determined to be 0.945±0.010 by us(Funakoshi et al., 1984). The values of λ_n and λ_1 are also derived from the half-lives of ^{93}Sr and ^{94}Sr recently determined by us as 7.41±0.04min and 75.3±0.2s, respectively(Okano et al., 1986). The values of the parameters used are summarized in Table 1. The averaged value of the two measurements listed is (9.73±0.62)%. It should be noted that this value has to be revised if more precise nuclear parameters are known in future.

In the case of the measurements on ^{95}Rb, the number of ^{94}Sr nuclei produced by the delayed neutron emission was determined by measuring the 1427.7keV γ ray mentioned before and the number of ^{95}Sr nuclei survived was determined by measuring the 756.7keV γ ray following the decay of 64.0d ^{95}Zr, as the emission probability of this γ ray per decay is well established(Debertin et al., 1975, Hopke and Meyer, 1976, Lederer and Shirley, 1978).

The measurements were performed collecting the ^{95}Rb ion beam continuously for 10 hours and measuring the yield of the 1427.7keV γ ray on line at the collecting port. After 2 days of cooling period, the yield of the 756.7keV γ ray was measured for 15 days, in just the same geometry as the on-line measurements. Unfortunately, a small amount of mixture of ^{94}Rb ion beam at mass 95 was unavoidable in this measurement. This effect was corrected for by using the yield of the 836.9keV γ ray which originates from the delayed neutron emission leading to the excited states of ^{94}Sr as well as from the β^- decay of ^{94}Rb. The peak counts of the 1427.7, 756.7 and 836.9keV γ rays expressed as C_n, C_l and C_c, respectively, are then given as

$$C_n = n_0 b_n \varepsilon_n P_n + n_c b_n \varepsilon_n, \tag{3}$$

$$C_l = n_0 b_l \varepsilon_l (1 - P_n)\ K(T_i, T_c, T_m) \tag{4}$$

and

$$C_c = n_c b_c \varepsilon_c + n_0 \varepsilon_c P_{n\ exc}, \tag{5}$$

where n_0 is the number of incident ^{95}Rb nuclei per second, the quantities with suffixes n, l and c refer to the 1427.7, 756.7 and 836.9keV γ rays, respectively, K is the decay correction factor for the 756.7keV γ ray and $P_{n\ exc}$ is the delayed neutron emission probability to the excited states of ^{94}Sr leading to the emission of the 836.9keV γ ray.

The difference of the measurable quantities, $C_n - C_c(b_n\varepsilon_n/b_c\varepsilon_c) \equiv C_n'$, is then equal to $n_0 b_n \varepsilon_n P_n (1-(R/b_c))$ with $R \equiv P_{n\ exc}/P_n$. P_n is then expressed as

$$P_n = \left[1 + \frac{C_l b_n \varepsilon_n}{C_n' b_l \varepsilon_l} \cdot \frac{(1 - (R/b_c))}{K(T_i, T_c, T_m)} \right]^{-1} \tag{6}$$

The values of measured quantities and nuclear parameters are as shown in Table 2 and one gets $P_n = (8.60 \pm 0.57)\%$ for ^{95}Rb.

CONCLUSION

Present results obtained for ^{94}Rb and ^{95}Rb are in good agreement with those obtained by using LOHENGRIN(Asghar et al., 1975) and OSTIS(Ristori et al., 1979) at Grenoble, as can be seen from Table 3. Present results are, however, somewhat smaller than those obtained by OSIRIS(Lund et al., 1980), and some disagreements are also noted with the results obtained by SOLIS (Engler and Ne'eman,1981). The results of some earlier works or the works done by an ion counting technique(Amarel et al., 1969, Roeckl et al., 1974, Reeder et al., 1977) deviate from these. It seems to be verified by the present measurement that the fairly accurate P_n value can be obtained by a

β-γ spectroscopic method utilizing a pure ion beam from ISOL, if the absolute γ-ray emission probabilities per decay of relevant nuclides are well established. As the discrepancy between the reported P_n value is still large, it seems worth while to examine them by a completely different method as reported here in future.

REFERENCES

Amarel I. et al.(1969) J. Inorg. Nucl. Chem. 31, 577.
Asghar M. et al.(1975) Nucl. Phys. A247, 359.
Bischof C. J. and Talbert, Jr. W. L.(1977) Phys. Rev. C15, 1047.
Debertin K. et al.(1975) Ann. Nucl. Energy 2, 37.
Engler G. and Ne´eman E.(1981) Nucl. Phys. A367, 29.
Funakoshi Y. et al.(1984) Nucl. Phys. A431, 461.
Funakoshi Y. et al. unpublished results.
Hoff P. (1981) Nucl. Phys. A359, 9.
Hopke P. K. and Meyer R. A.(1976) Phys. Rev. C13, 434.
Jung G. (1980) Ph. D. thesis, Giessen Univ.(unpublished).
Kawase Y. et al.(1985) Nucl. Instrum. Meth. 241, 305.
Kratz K.-L. et al.(1981) Proc. of the 4th Int. Conf. on nuclei far from stability, CERN 81-09, 317.
Lund E. et al.(1980) Z. Phys. A294, 233.
Okano K. et al.(1981) Nucl. Instrum. Meth. 186, 115.
Okano K. et al.(1983) Annu. Rep. Res. Reactor Inst. Kyoto Univ. 16, 47.
Okano K. et al.(1984) Annu. Rep. Res. Reactor Inst. Kyoto Univ. 17, 110.
Okano K. et al.(1986) to be published.
Reeder P. L. et al.(1977) Phys. Rev. C15, 2108.
Ristori C. et al.(1979) Z. Phys. A290, 311.
Roeckl E. et al.(1974) Nucl. Phys. A222, 621.

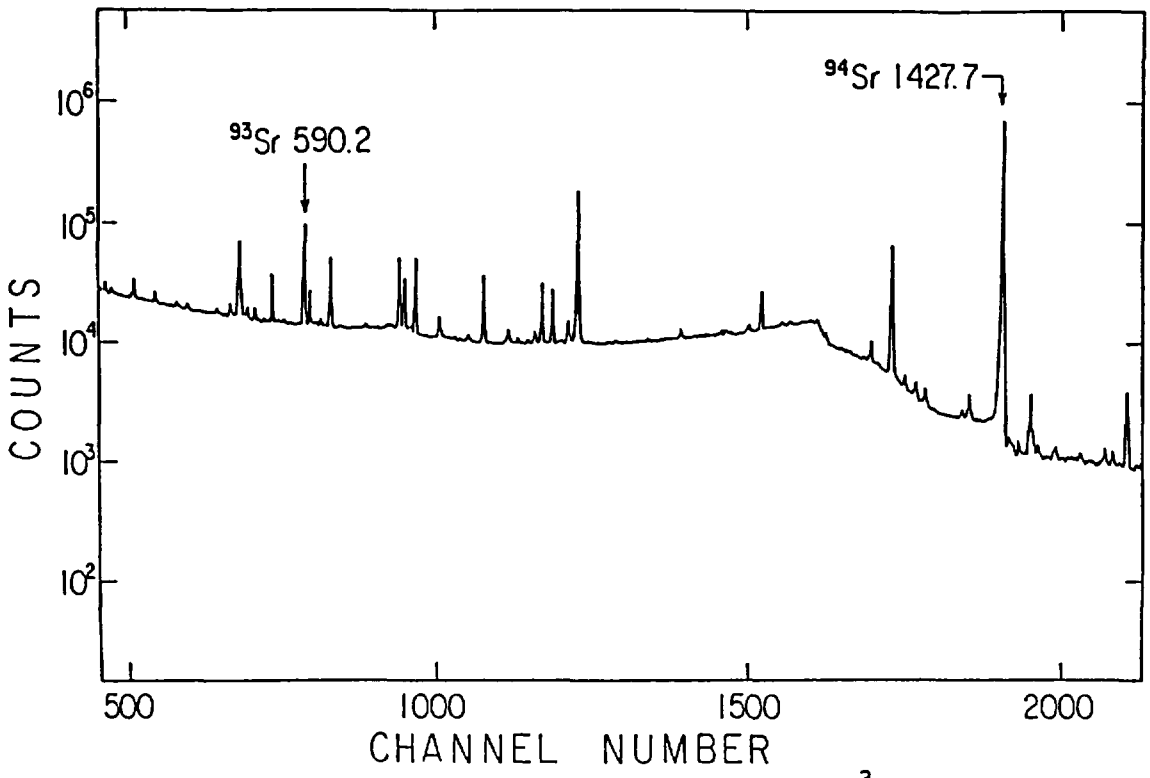

Fig. 1 γ-ray spectrum measured at mass 94 with a 142cm^3 Ge(Li) detector.

Table 1 Parameters used in the evaluation of eqs. (1) and (2). Measurement I and measurement II were performed with a 142cm^3 and a 58cm^3 Ge(Li) detector, respectively.

Parameter	Adopted value		Reference
	Measurement I	Measurement II	
C_1/C_n	10.40±0.84	10.18±0.51	
b_1	0.945±0.010	0.945±0.010	Funakoshi et al. (1984)
b_n	0.665±0.029	0.665±0.029	Bischof et al. (1977)
$\varepsilon_1/\varepsilon_n$	0.494±0.025	0.417±0.013	
λ_0	0.2548±0.0010 s^{-1}	0.2548±0.0010 s^{-1}	
λ_1	0.009205±0.000025 s^{-1}	0.009205±0.000025 s^{-1}	Okano et al. (1986)
λ_n	0.001559±0.000009 s^{-1}	0.001559±0.000009 s^{-1}	Okano et al. (1986)
T_i	75.00 s	75.00 s	
T_c	107.00 s	30.00 s	
T_m	75.00 s	222.00 s	
Results	P_n=(9.60±1.00)%	P_n=(9.80±0.71)%	

Table 2 Parameters used in the evaluation of eq. (6).

Parameter	Adopted value	Reference
C_1/C'_n	2.211±0.117	
b_1	0.547±0.007	Debertin et al.(1975) Hopke et al. (1976) Lederer et al.(1978)
b_n	0.945±0.010	Funakoshi et al.(1984)
b_c	0.972±0.003	Jung(1980) Funakoshi et al. (unpublished results)
$\varepsilon_1/\varepsilon_n$	1.634±0.049	
$\varepsilon_n/\varepsilon_c$	0.659±0.020	
R	0.3325±0.0070	Hoff(1981) Kratz et al.(1981)
K(10.0h,41.82h, 356.28h)	0.1447±0.0002	
Result	P_n=(8.60±0.57)%	

Table 3 Reported P_n values of ^{94}Rb and ^{95}Rb.

P_n(%)		ISOL	Reference
^{94}Rb	^{95}Rb		
9.6 ± 0.8	8.4 ± 0.5	LOHENGRIN	Asghar et al.(1975)
9.7 ± 0.5	8.6 ± 0.5	OSTIS	Ristori et al.(1979)
10.1 ± 0.6	8.9 ± 0.6	OSIRIS	Lund et al.(1980)
11.1 ± 0.9	8.2 ± 0.8	SOLIS	Engler et al.(1981)
9.73± 0.62	8.60± 0.57	KUR-ISOL	Present results

3.2 THE SENSITIVITY THEORY FOR INERTIAL CONFINEMENT PELLET FUSION SYSTEM

CAI SHAOHUI
(CNDC., & Inst. of Appl. Phys. and Comput. Mathes.)

ZHANG YUQUAN
(Inst. of Appl. Phys. and Comput. Mathes.)

ABSTRACT

A sensitivity theory for inertial confinement pellet fusion systems is developed based on a physical model similar to that embodied in the laser fusion code MEDUSA. The theory presented here can be an efficient tool for estimating the effects of many alternations in the data field. Our result is different from Greenspan's work in 1980.

I. INTRODUCTION

The sensitivity analysis theory for linear problems in fission reactor physics and shielding has been proved to be a very useful tool both for scoping studies and for sensitivity and uncertainty analysis [1]. These successes have created considerable interest in extending such approaches to sensitivity analysis of inherently non-linear problems in other areas, such as reactor thermal-hydraulic problem [2],[3], reactor burn-up problem [4],[5] and reactor safety problem [6]. The necessary and sufficient conditions underlying the development of sensitivity theory for non-linear systems have subsequently been established by Cacuci [7].

A sensitivity theory in the inertial confinement pellet fusion problem was first presented by Greenspan [8]. In his paper, however, the difference between the Eulerian representation and

Lagrangean representation of the equations of fluid motion has not been noticed. The final formulas derived by him look doubtful. In this paper, we intend to derive the sensitivity theory for inertial confinement pellet fusion system in Lagrangean representation as simple as possible. Only five dependent variables are used to describe the physical properties of the plasma medium : the positon $\vec{R}$, density ρ, velocity $\vec{u}$, ion temperature T_i and electron temperature T_e. The equations used to describe the time evolution of these variables as a function of space consist of: the velocity equation, the continuity equation, the momentum equation, and the energy equations for ions and electrons. The main assumptions that have been made and the model of pellet fusion system are summarized in Sec. II. In Sec. III we derive a set of coupled linear equations for the derivatives of the state functions ($\vec{R}$, ρ, $\vec{u}$, T_i and T_e) with respect to input data. The derivation of the appropriate adjoint system and the expression of sensitivities in terms of adjoint functions are presented in Sec. IV; and a brief discussion of the theorectical results are given in Sec. V.

II. PELLET FUSION MODEL

The system to be study here is a spherical fusion pellet which is irradiated by an intense laser, electron or ion beams. The physical model used for deriving the sensitivity theory is similar to (and slightly simpler than) that embodied in the laser fusion code MEDUSA [9] We make the following assumptions in the interest of simplicity:

1. The plasma is assumed to consist of a charge-neutral mix-

ture of electrons (e) and of ions and atoms which are collectively reffered to as ions' (i). Charge neutrality requires that electrons and ions have the same macroscopic velocity (i.e. fluid velocity) u.

2. Neither the ionization nor the finite range of the charge reaction products is taken into account, so that the number of electrons in each Lagrangean fluid element remains invariant.

3. The plasma is completely transparent to neutron and photon, and therefore we need not consider their interaction between plasma.

4. The burn-up of the pellet fusion is so low that the composition of the pellet can be assumed to be constant during the whole time; and also the loss of mass and the change in momentum due to the leakage of neutrons. can be neglected.

Taking the usual notations with Lagrangean coordinates (m, t), we use the following equations to describe the pellet behavior:

$$\frac{DR}{Dt} = u, \tag{1}$$

$$\rho R^2 \frac{\partial R}{\partial m} = 1, \tag{2}$$

$$\frac{Du}{Dt} = -R^2 \frac{\partial}{\partial m} (P_i + P_e + q), \tag{3}$$

$$\rho c_{vi} \frac{DT_i}{Dt} = \frac{1}{\rho}[T_i (\frac{\partial P_i}{\partial T_i})_\rho + q] \frac{D\rho}{Dt} + \rho S_i, \tag{4}$$

$$\rho c_{ve} \frac{DT_e}{Dt} = \frac{1}{\rho} T_e (\frac{\partial P_e}{\partial T_e})_\rho \frac{D\rho}{Dt} + \rho S_e, \tag{5}$$

where m, the Lagrangean coordinate, is given by

$$m = \int_0^R \rho(R', t_0) R'^2 dR',$$

here t_0 is an initial time. $\frac{D}{Dt}$ denotes the time derivative with respect to a point moving along with the fluid. It is related to $\frac{\partial}{\partial t}$, the time derivative with respect to a fixed point of space by

$$\frac{D}{Dt} = \frac{\partial}{\partial t} + u\frac{\partial}{\partial R};$$

$$q = l^2 \rho \left(\frac{\partial u}{\partial m}\right)^2 St\left(-\frac{\partial u}{\partial m}\right) \tag{6}$$

is the artificial pseudo-viscous pressure[§], where l is a constant having the dimensions of a length [10], and

$$St(x) = \begin{cases} 0 & x < 0 \\ 1 & x \geq 0 \end{cases}$$

is the unit step function. The source terms in Eqs. (4) and (5) consist of several contributions, i.e.,

$$S_i = H_i - K + Y_i, \tag{7}$$

$$S_e = H_e + K + Y_e + J + X, \tag{8}$$

where

$$H_x = \frac{\partial}{\partial m} R^4 \kappa_x \rho \frac{\partial T_x}{\partial m}, \qquad x = i, e \tag{9}$$

is the flow of heat due to thermal conduction;

$$K = C_K \rho (T_i - T_e) T_e^{-3/2} \tag{10}$$

is the rate of exchange of energy between ions and electrons;

$$Y_x = \sum_{k,l} C_{kl}^x \rho^2 \langle \overline{\sigma v (T_i)} \rangle_{kl} \tag{11}$$

is the rate of thermolnuclear energy deposited directly in the ions (x=i) and electrons (e) of the plasma, due to the summed contributions from all possible fusion reations (expressed by

---

§ The artificial pseudo-viscous pressure was introduced by von Neumann and Richtmyer[10] in order to get rid of the discontinuous solution of the equations of fluid dynamics whenever shock presented.

the kl combinations):

$$J = -C_J \rho \, T_e^{1/2} \tag{12}$$

is the rate of bremsstrahlung energy emission, and X is the rate of absorption of laser (or other beam) energy.

For convenience, let us rewrite the source terms S_x as

$$S_i = H_i + Q_i, \tag{7'}$$

$$S_e = H_e + Q_e + X, \tag{8'}$$

where

$$Q_i = -K + Y_i = Q_i(\rho, T_i, T_e, a_{Qi}), \tag{13}$$

$$Q_e = K + Y_e + J = Q_e(\rho, T_i, T_e, a_{Qe}); \tag{14}$$

$$K_x = K_x(\rho, T_x, a_{K_x}) \tag{15}$$

is the thermal conductivity;

$$c_{vx} = c_{vx}(\rho, T_x, a_{\varepsilon x}) = \left(\frac{\partial \varepsilon_x}{\partial T_x}\right)_\rho \tag{16}$$

is the specific heat capacity;

$$p_x = p_x(\rho, T_x, a_{p_x}) \tag{17}$$

is the pressure function; and

$$T_x \left(\frac{\partial p_x}{\partial T_x}\right)_\rho = p_x - \rho^2 \left(\frac{\partial \varepsilon_x}{\partial \rho}\right)_{T_x} \tag{18}$$

is the thermodynamic relation, and ε_x is the specific internal energy. The coefficients a's appeared in Eqs. (13) through (17) are the sum of all physical parameters which appeared in Q, K_x, ε_x and p_x respectively.

Note that this model does not consider the details of the beam-pellet interaction and assumes that the beam energy deposition profile X is given. In order to describe ion-beam fusion problems one ought to add an external energy source term to the ion temperature equation, expressing the rate of absorption of the beam energy (as a function of position and time) by the ions.

The initial and boundary conditions for Eqs. (1) through (5) are as follows:

1. Initial values:

$R(m, t_0)$, $\rho(m, t_0)$, $u(m, t_0)$, $T_x(m, t_0)$ are given. (19)

2. Central boundary conditions:

$$R(0, t) = u(0, t) = \left(R^2 \frac{\partial T_x}{\partial m}\right)_{m=0} = 0, \tag{20}$$

3. Outer boundary conditions:

$$\sum_x P_x(m_J, t) + q_J(m_J, t) = T_x(m_J, t) = 0, \tag{21}$$

where $m_J = \int_0^{R_J} \rho(R, t)\, R^2 dR$, R_J is the radius of the outer boundary of the system at the initial time t_0.

4. Interface conditions: R, u, $\sum_x P_x + q$, T_x and $K_x \rho \frac{\partial T_x}{\partial m}$ are continuous functions of m at a physical interface. (22)

For the sensitivity analysis, it is assumed that the physical problem described by Eqs. (1) through (5) and Eqs. (19) through (22) admits a unique solution $\mathcal{U}(\mathcal{X})$, where $\mathcal{X} = [m, t]^T$ is the phase space position vector, $\mathcal{U}(\mathcal{X}) = [R(m, t), \rho(m, t), u(m, t), T_i(m, t), T_e(m, t)]^T$ is the distribution function vector or the so-called state vector; and the superscript T denotes a transposed vector.

Suppose we are interested in an integral performance parameter or response P, defined as an explicit functional of the state vector $\mathcal{U}$ and the vector $\mathcal{A} = [a_1, a_2, \ldots, a_H]$ of input data:

$$P = P[\mathcal{U}, \mathcal{A}] = \int F[\mathcal{U}(\mathcal{X}), \mathcal{A}(\mathcal{X}), \mathcal{X}]\, d\mathcal{X}, \tag{23}$$

where

$$\int \ldots d\mathcal{X} = 4\pi \int_{t_0}^{t_f} dt \int_0^{m_J} \ldots dm,$$

and F is an explicit function of $\mathcal{U}$, $\mathcal{A}$ and $\mathcal{X}$. For example, if we are interested in the total fusion energy yield during the pellet implosion, then this parameter can be written as

$$4\pi \int dt \int dm \sum_{k,\ell} C_{k\ell} \rho \langle \overline{\sigma v} \rangle_{k\ell}.$$

The goal of sensitivity theory is to determine the change in P due to changes $\delta\mathcal{A} = [\delta a_1, \delta a_2, \ldots, \delta a_M]^T$ in the vector $\mathcal{A}$ of input data. To second order in δa_h, this equivalent to determining

$$\delta P = \sum_{h=1}^{M} \frac{dP}{da_h} \delta a_h .$$

To this end, the sensitivity derivatives dP/da_h need to be evaluated. These quantities can be used not only to estimate changes in P due to changes in a_h, but also to rank the relative importance of input data and to calculate uncertainties in P due to uncertainties in the input data [1]

To derive the sensitivity derivatives dP/da_h, we simply differentiate P with respect to a_h, noting that P is an explicit functional of a_h and the state vector $\mathcal{U}(\mathcal{X})$, and that $\mathcal{U}(\mathcal{X})$ is an implicit function of a_h. Differentiating Eq. (23), we get

$$\frac{dP}{da_h} = \frac{\partial P}{\partial a_h} + \int F'_{\mathcal{U}} \frac{d\mathcal{U}}{da_h} d\mathcal{X} , \tag{24}$$

where

$$\frac{\partial P}{\partial a_h} = 4\pi \int dt \int dm \frac{\partial F}{\partial a_h} = \langle F'_{a_h} \rangle \tag{25}$$

is the direct effect of a_h on P, while

$$\int F'_{\mathcal{U}} \frac{d\mathcal{U}}{da_h} d\mathcal{X} = 4\pi \int dt \int dm \left[\frac{\partial F}{\partial R}\frac{dR}{da_h} + \frac{\partial F}{\partial \rho}\frac{d\rho}{da_h} + \frac{\partial F}{\partial u}\frac{du}{da_h} + \frac{\partial F}{\partial T_i}\frac{dT_i}{da_h} + \frac{\partial F}{\partial T_e}\frac{dT_e}{da_h} \right]$$

$$= \langle F'_{\mathcal{U}}, \frac{d\mathcal{U}}{da_h} \rangle \tag{26}$$

is the indirect effect term representing the implicit dependence of P on a_h through the state vector $\mathcal{U}$, and $\langle \ , \ \rangle$ denotes integration over the phase space: $\langle \ , \ \rangle = 4\pi \int dt \int dm$.

Since F is an explicit function $\mathcal{U}$ and $\mathcal{A}$, $F'_{\mathcal{U}}$ and F'_{a_h} are analytic functions obtained by simple differentiation of F. The

direct effect can be obtained by (numerical) integration. In order to evaluate the indirect effect, the vector

$$\psi_h = [\frac{dR}{da_h},\ \frac{d\rho}{da_h},\ \frac{du}{da_h},\ \frac{dT_i}{da_h},\ \frac{dT_e}{da_h}]^T = [\psi_{Rh},\ \psi_{\rho h},\ \psi_{uh},\ \psi_{Tih},\ \psi_{Teh}]^T \quad (27)$$

must be determined.

III. THE GOVERNING EQUATIONS FOR THE DERIVATIVES OF STATE VECTOR WITH RESPECT TO INPUT DATA

Differentiating Eqs. (1) through (5) with respect to a_h implicitly, one gets the following equations for ψ_h[§]:

(For convenience, we will omitt the subscript 'h' below)

$$\frac{D}{Dt}\psi_R - \psi_u = S_R, \quad (28)$$

$$(\frac{2}{R}+\rho R^2\frac{\partial}{\partial m})\psi_R+\frac{1}{\rho}\psi_\rho = S_\rho, \quad (29)$$

$$\frac{2\alpha_1}{R}\psi_R+R^2\frac{\partial}{\partial m}(\alpha_2\psi_\rho)+[\frac{D}{Dt}+R^2\frac{\partial}{\partial m}(\alpha_3\frac{\partial}{\partial m}\circ)]\psi_u+$$

$$+R^2\frac{\partial}{\partial m}(\alpha_4\psi_{T_i})+R^2\frac{\partial}{\partial m}(\alpha_5\psi_{Te})=S_u, \quad (30)$$

$$-4\rho\frac{\partial}{\partial m}(\beta_1 R\psi_R)+\{-\beta_2\frac{D}{Dt}-\rho\frac{\partial}{\partial m}[(\beta_3+\beta_5)R^2\circ]+\beta_4\}\psi_\rho -$$

$$-\alpha_3\frac{D\ln\rho}{Dt}\frac{\partial}{\partial m}\psi_u+\{\beta_6\frac{D}{Dt}-\rho\frac{\partial}{\partial m}(\beta_7 R^2\circ)+\beta_8-\rho\frac{\partial}{\partial m}(R^4\kappa_i\rho\frac{\partial}{\partial m}\circ)\}\psi_{T_i}+$$

$$+\beta_9\psi_{Te}=S_{T_i}, \quad (31)$$

---

§ By differentiating Eq. (6) and making use of the properties of the unit step function $St(x)$ and Dirac δ-function, we get:

$$\frac{d}{dx}St(x) = \delta(x),$$

$$x\,\delta(-x) = -x\,\delta(x) = 0,$$

then the derivative of φ with respect to input data a_h is obtained as $\frac{d\varphi}{da_h} = \frac{\varphi}{\rho}\frac{d\rho}{da_h}+2\ell^2\rho(\frac{\partial u}{\partial m})St(-\frac{\partial u}{\partial m})\frac{\partial}{\partial m}\frac{du}{da_h} = \frac{\varphi}{\rho}\psi_{\rho h}+\alpha_3\frac{\partial}{\partial m}\psi_{uh}$.

$$-4\rho\frac{\partial}{\partial m}(\gamma_1 R\psi_R)+\{-\gamma_2\frac{D}{Dt}-\rho\frac{\partial}{\partial m}[(\gamma_3+\gamma_5)R^2\circ]+\gamma_4\}\psi_\rho+\gamma_9\psi_{Ti}+$$
$$+\{\gamma_6\frac{D}{Dt}-\rho\frac{\partial}{\partial m}(\gamma_7 R^2\circ)+\gamma_8-\rho\frac{\partial}{\partial m}(R^4\kappa_e\rho\frac{\partial}{\partial m}\circ)\}\psi_{Te}=S_{Te}, \quad (32)$$

where

$$\alpha_1=R^2\frac{\partial}{\partial m}(p_i+p_e+q), \quad (33) \qquad \alpha_2=\frac{\partial(p_i+p_e)}{\partial\rho}+\frac{q}{\rho}, \quad (34)$$

$$\alpha_3=2l^2\rho(\frac{\partial u}{\partial m})St(-\frac{\partial u}{\partial m}), \quad (35) \qquad \alpha_4=\frac{\partial p_i}{\partial T_i}, \quad (36)$$

$$\alpha_5=\frac{\partial p_e}{\partial T_e}, \quad (37) \qquad \beta_1=\rho R^2\kappa_i\frac{\partial T_i}{\partial m}, \quad (38)$$

$$\beta_2=\frac{1}{\rho}(T_i\frac{\partial p_i}{\partial T_i}+q), \quad (39) \qquad \beta_3=\beta_1\frac{\partial\ln\kappa_i}{\partial\rho}, \quad (40)$$

$$\beta_4=(c_{vi}+\rho\frac{\partial c_{vi}}{\partial\rho})\frac{DT_i}{Dt}+\frac{1}{\rho}\frac{D\rho}{Dt}(\frac{T_i}{\rho}\frac{\partial p_i}{\partial T_i}-T_i\frac{\partial^2 p_i}{\partial\rho\partial T_i})-\rho\frac{\partial Q_i}{\partial\rho}-$$
$$-Q_i-\frac{\partial}{\partial m}(\beta_1 R^2), \quad (41)$$

$$\beta_5=\frac{\beta_1}{\rho}, \quad (42) \qquad \beta_6=\rho c_{vi}, \quad (43) \qquad \beta_7=\beta_1\frac{\partial\ln\kappa_i}{\partial T_i}, \quad (44)$$

$$\beta_8=\rho\frac{DT_i}{Dt}\frac{\partial c_{vi}}{\partial T_i}-\frac{1}{\rho}\frac{D\rho}{Dt}(\frac{\partial p_i}{\partial T_i}+T_i\frac{\partial^2 p_i}{\partial T_i^2})-\rho\frac{\partial Q_i}{\partial T_i}, \quad (45)$$

$$\beta_9=-\rho\frac{\partial Q_i}{\partial T_e}, \quad (46) \qquad \gamma_1=\rho R^2\kappa_e\frac{\partial T_e}{\partial m}, \quad (47)$$

$$\gamma_2=\frac{T_e}{\rho}\frac{\partial p_e}{\partial T_e}, \quad (48) \qquad \gamma_3=\gamma_1\frac{\partial\ln\kappa_e}{\partial\rho}, \quad (49)$$

$$\gamma_4=(c_{ve}+\rho\frac{\partial c_{ve}}{\partial\rho})\frac{DT_e}{Dt}+\frac{1}{\rho}\frac{D\rho}{Dt}(\frac{T_e}{\rho}\frac{\partial p_e}{\partial T_e}-T_e\frac{\partial^2 p_e}{\partial\rho\partial T_e})-$$
$$-\rho\frac{\partial Q_e}{\partial\rho}-Q_e-\frac{\partial}{\partial m}(\gamma_1 R^2)-X, \quad (50)$$

$$\gamma_5=\frac{\gamma_1}{\rho}, \quad (51) \qquad \gamma_6=\rho c_{ve}, \quad (52) \qquad \gamma_7=\gamma_1\frac{\partial\ln\kappa_e}{\partial T_e}, \quad (53)$$

$$\gamma_8=\rho\frac{DT_e}{Dt}\frac{\partial c_{ve}}{\partial T_e}-\frac{1}{\rho}\frac{D\rho}{Dt}(\frac{\partial p_e}{\partial T_e}+T_e\frac{\partial^2 p_e}{\partial T_e^2})-\rho\frac{\partial Q_e}{\partial T_e}, \quad (54)$$

$$\gamma_9=-\rho\frac{\partial Q_e}{\partial T_e}; \quad (55)$$

and

$$S_R=0, \quad (56)$$

$$S_\rho=0, \quad (57)$$

$$S_u = -R^2 \frac{\partial}{\partial m}\left[\frac{\partial P_i}{\partial a} + \frac{\partial P_e}{\partial a}\right], \tag{58}$$

$$S_{Ti} = -\rho \frac{DT_i}{Dt}\frac{\partial C_{vi}}{\partial a} + \frac{T_i}{\rho}\frac{D\rho}{Dt}\frac{\partial^2 P_i}{\partial a \partial T_i} + \rho \frac{\partial}{\partial m}\left(R^2 \beta_1 \frac{\partial \ln \kappa_i}{\partial a}\right) + \rho \frac{\partial Q_i}{\partial a}, \tag{59}$$

$$S_{Te} = -\rho \frac{DT_e}{Dt}\frac{\partial C_{ve}}{\partial a} + \frac{T_e}{\rho}\frac{D\rho}{Dt}\frac{\partial^2 P_e}{\partial a \partial T_e} + \rho \frac{\partial}{\partial m}\left(R^2 \gamma_1 \frac{\partial \ln \kappa_e}{\partial a}\right) + \rho \frac{\partial Q_e}{\partial a} + \rho \frac{\partial X}{\partial a}, \tag{60}$$

The intial and boundary conditions for Ψ can be deduced from Eqs. (19) through (22). The results are:

1. Initial values:

$$\Psi_R(m, t_0) = \Psi_\rho(m, t_0) = \Psi_u(m, t_0) = \Psi_{T_x}(m, t_0) = 0. \tag{61}$$

2. Central boundary conditions:

$$\Psi_R(0, t) = \Psi_u(0, t) = \left(R^2 \frac{\partial}{\partial m}\Psi_{T_x}\right)_{m=0} = 0. \tag{62}$$

3. Outer boundary conditions:

$$\left[\frac{d(P_i + P_e + q)}{da}\right]_{m_J} \equiv \left(\alpha_2 \Psi_\rho + \alpha_3 \frac{\partial}{\partial m}\Psi_u + \alpha_4 \Psi_{Ti} + \alpha_5 \Psi_{Te} + \sum_x \frac{\partial P_x}{\partial a}\right)_{m_J} = 0,$$

and $$\Psi_{T_x}(m_J, t) = 0. \tag{63}$$

4. Interface conditions:

$$\Psi_R,\ \Psi_u,\ \frac{d(P_i + P_e + q)}{da} = \alpha_2 \Psi_\rho + \alpha_3 \frac{\partial}{\partial m}\Psi_u + \alpha_4 \Psi_{Ti} + \alpha_5 \Psi_{Te} + \sum_x \frac{\partial P_x}{\partial a},\ \Psi_{T_x},$$

$$\frac{d}{da}\left[\rho R^2 \kappa_i \frac{\partial T_i}{\partial m}\right] \equiv \frac{2\beta_1}{R}\Psi_R + (\beta_3 + \beta_5)\Psi_\rho + \beta_7 \Psi_{Ti} + \rho R^2 \kappa_i \frac{\partial \Psi_{Ti}}{\partial m} + \beta_1 \frac{\partial \ln \kappa_i}{\partial a},$$

and $$\frac{d}{da}\left[\rho R^2 \kappa_e \frac{\partial T_e}{\partial m}\right] \equiv \frac{2\gamma_1}{R}\Psi_R + (\gamma_3 + \gamma_5)\Psi_\rho + \gamma_7 \Psi_{Te} + \rho R^2 \kappa_e \frac{\partial \Psi_{Te}}{\partial m} + \gamma_1 \frac{\partial \ln \kappa_e}{\partial a}$$

are continuous functions of m at a physical interface. (64)

For convenience, let us express Eqs. (28) through (32) in a compact operator's notation as

$$\mathcal{L}\Psi = \mathcal{S}. \tag{65}$$

where

$$\mathcal{S} = [S_R,\ S_\rho,\ S_u,\ S_{Ti},\ S_{Te}]^T. \tag{66}$$

Notice that all the parameters appeared in the operator $\mathcal{L}$

and the source term $\mathcal{S}$ are dependent on the state vector $\mathcal{U}$ and are not dependent on Ψ . Hence Eqs. (65) is linear for Ψ. To solve such equation, the original Eqs. (1) through (5) must be solved first for a specific problem to set up the parameters in the linearized equation (65). After Ψ has been determined dP/da can be evaluated.

It is important to also note that Eq. (65) is independent of the particular response P being studied, and P appears explicity only in the defining expression for dP/da. Eq. (65), however, does depend explicity on da through the source term. Consequently, from the standpoint of computational costs, the calculation method described above is advantageous to employ only if, in the problem under consideration, the number of different responses of interest exceeds the number of input data. However, the pellet fusion problem as well as a large number of problems of practical interest are characterized by very large data bases and comparatively few responses. In such situation, it is not economical to employ such equation to study all derivatives of a given response with respect to the input data. Hence it is clearly desirable to devise an alternative procedure to evaluate the sensitivity, to avoid the necessity of **repeatedly** solving Eq. (65).

IV. THE ADJOINT EQUATIONS

Notice the linearized equations (28) through (32) only have source terms that depend on da, and since their solution is really needed only to evaluate the indirect effect $\langle F'_a, \Psi \rangle$, it is far simpler to define a set of adjoint equations independent

of da to solve this same problem. The adjoint operators for Eqs. (28) through (32) are easily derived, and what remains to be done in the derivation is to identify appropriate source terms and boundary and final conditions for these new equations.

Using the definition of an adjoint operator,

$$\langle \mathcal{L}^*\psi^*, \psi \rangle = \langle \psi^*, \mathcal{L}\psi \rangle + BT[\psi^*, \psi]. \tag{67}$$

Here the vector ψ^* belongs to the domain of $\mathcal{L}^*$, and $BT[\psi^*, \psi]$ is the boundary term which represents the bilinear term of ψ and ψ^* evaluated on the appropriate boundary in phase space.

The operator $\mathcal{L}^*$ is then explicitely determined by following the inner products as prescribed in Eq. (67) followed by appropriate manipulations (e.g., integration by parts), so as to transfer the operations on ψ to operations on ψ^*. The spelled-out form of the equations adjoint to Eqs. (28) through (32) is found to be:

$$-\frac{DR^*}{Dt} - R^2\frac{\partial \rho p^*}{\partial m} + 2\frac{\alpha_1 u^*}{R} + 4R\left[\beta_1\frac{\partial}{\partial m}(\rho T_i^*) + \gamma_1\frac{\partial}{\partial m}(\rho T_e^*)\right] = S_R^*, \tag{68}$$

$$\frac{\rho^*}{\rho} - \alpha_2\frac{\partial}{\partial m}R^2 u^* + \left[\frac{D}{Dt}(\beta_{2\circ}) + R^2(\beta_3+\beta_5)\frac{\partial}{\partial m}(\rho_\circ) + \beta_4\right]T_i^* +$$

$$+\left[\frac{D}{Dt}(\gamma_{2\circ}) + R^2(\gamma_3+\gamma_5)\frac{\partial}{\partial m}(\rho_\circ) + \gamma_4\right]T_e^* = S_p^*, \tag{69}$$

$$-R^* - \frac{Du^*}{Dt} + \frac{\partial}{\partial m}q^* = S_u^*, \tag{70}$$

$$-\alpha_4\frac{\partial}{\partial m}(R^2 u^*) + \left\{-\frac{D}{Dt}(\beta_{6\circ}) + R^2\beta_7\frac{\partial}{\partial m}(\rho_\circ) + \beta_8 - \frac{\partial}{\partial m}\left[R^4\kappa_i\rho\frac{\partial}{\partial m}(\rho_\circ)\right]\right\}T_i^* +$$

$$+\gamma_9 T_e^* = S_{T_i}^*, \tag{71}$$

and

$$-\alpha_5\frac{\partial}{\partial m}(R^2 u^*) + \beta_9 T_i^* + \left\{-\frac{D}{Dt}(\gamma_{6\circ}) + R^2\gamma_7\frac{\partial}{\partial m}(\rho_\circ) + \gamma_8 - \frac{\partial}{\partial m}\left[R^4\kappa_e\rho\frac{\partial}{\partial m}(\rho_\circ)\right]\right\}T_e^* =$$

$$= S_{T_e}^*, \tag{72}$$

where

$$q^* = \alpha_3 \left(\frac{\partial}{\partial m} R^2 u^* + \frac{D \ln \rho}{D t} T_i^* \right), \tag{73}$$

can be treated as an adjoint term to q [see Eq. (6)].

Moreover we obtain the following expression for the boundary term:

$$\begin{aligned} BT[\psi^*, \psi] = -4\pi \int_0^{m_J} dm \Big[& R^* \psi_R - (\beta_2 T_i^* + \gamma_2 T_e^*) \psi_\rho + u^* \psi_u + \beta_6 T_i^* \psi_{T_i} + \gamma_6 T_e^* \psi_{T_e} \Big]_{t_0}^{t_f} - \\ -4\pi \sum_{j=1}^{J} \int_{t_0}^{t_f} dt \Big[& R^2 \left(\rho \rho^* - \frac{2\beta_1}{R} \rho T_i^* - \frac{2\gamma_1}{R} \rho T_e^* \right) \psi_R + R^2 u^* \left(\alpha_2 \psi_\rho + \alpha_3 \frac{\partial}{\partial m} \psi_u + \alpha_4 \psi_{T_i} + \alpha_5 \psi_{T_e} \right) - \\ & - R^2 \rho T_i^* \left(\frac{2\beta_1}{R} \psi_R + \beta_3 \psi_\rho + \beta_5 \psi_\rho + \beta_7 \psi_{T_i} + R^2 \kappa_i \rho \frac{\partial}{\partial m} \psi_{T_i} \right) - \\ & - R^2 \rho T_e^* \left(\frac{2\gamma_1}{R} \psi_R + \gamma_3 \psi_\rho + \gamma_5 \psi_\rho + \gamma_7 \psi_{T_e} + R^2 \kappa_e \rho \frac{\partial}{\partial m} \psi_{T_e} \right) + \\ & + R^4 \kappa_i \rho \frac{\partial \rho T_i^*}{\partial m} \psi_{T_i} + R^4 \kappa_e \rho \frac{\partial \rho T_e^*}{\partial m} \psi_{T_e} - q^* \psi_u \Big]_{m_{j-1}}^{m_j} . \end{aligned} \tag{74}$$

Since an adjoint equation that is independent of da is desired, boundary and final conditions as well as the adjoint sources must be chosen to eliminate any terms in the boundary term $BT[\psi^*, \psi]$ that contain unknown values of ψ. Using the known boundary and initial conditions for ψ [see Eqs. (61) through (64)], the following conditions can be shown to satisfy the desired criteria:

1. Final values:

$$R^*(m, t_f) = u^*(m, t_f) = T_x^*(m, t_f) = 0. \tag{75}$$

2. Central boundary conditions:

$$u^*(0, t) = \left[R^2 \frac{\partial}{\partial m} (\rho T_x^*) \right]_{m=0} = 0. \tag{76}$$

3. Outer boundary conditions:

$$\rho^*(m_J, t) = T_x^*(m_J, t) = q^*(m_J, t) = 0. \tag{77}$$

4. Interface conditions:

$\rho\rho^*$, u^*, ρT_x^*, $\kappa_x \rho \frac{\partial \rho T_x^*}{\partial m}$ and q^* are continuous functions of m at a physical interface. (78)

The selection of the adjoint boundary conditions reduces $BT[\psi^*, \psi]$ to $\hat{B}T[\psi^*, \psi]$, where $\hat{B}T[\psi^*, \psi]$ contains only known values of ψ evaluated on the boundary in phase space:

$$\hat{B}T[\psi^*, \psi] = 4\pi \sum_{j=1}^{J+1} \int_{t_0}^{t_f} R_j^2 [-u_j^* \Delta(\sum_x \frac{\partial P_x}{\partial a})_j + (\beta_i \rho T_i^*)_j \Delta(\frac{\partial \ln \kappa_i}{\partial a})_j + (\gamma_i \rho T_e^*)_j \Delta(\frac{\partial \ln \kappa_e}{\partial a})_j] dt + 4\pi \int_{t_0}^{t_f} R_J^2 u_J^* (\sum_x \frac{\partial P_x}{\partial a})_J \, dt. \quad (79)$$

where

$$\Delta(\sum_x \frac{\partial P_x}{\partial a})_j \equiv (\sum_x \frac{\partial P_x}{\partial a})_{m_j^+} - (\sum_x \frac{\partial P_x}{\partial a})_{m_j^-},$$

and

$$\Delta(\frac{\partial \ln \kappa_x}{\partial a})_j \equiv (\frac{\partial \ln \kappa_x}{\partial a})_{m_j^+} - (\frac{\partial \ln \kappa_x}{\partial a})_{m_j^-}.$$

Let us rewrite Eqs. (68) through (72) in operator's notation as

$$\mathcal{L}^* \psi^* = \mathcal{S}^*. \quad (80)$$

By substituting Eqs. (80) and (65), it can be seen that Eq. (67) is equivalent to

$$\langle \mathcal{S}^*, \psi \rangle = \langle \psi^*, \mathcal{S} \rangle + \hat{B}T[\psi^*, \psi]. \quad (81)$$

Comparing Eq. (81) to Eq. (26), it is clear that choosing

$$\mathcal{S}^* = F'_u = [\frac{\partial F}{\partial R}, \frac{\partial F}{\partial \rho}, \frac{\partial F}{\partial u}, \frac{\partial F}{\partial T_i}, \frac{\partial F}{\partial T_e}], \quad (82)$$

the left side of Eq. (81) becomes identical to indirect effect. Thus if ψ^* satisfies the adjoint equation:

$$\mathcal{L}^* \psi^* = F'_u, \quad (83)$$

subject to the boundary conditions expressed in Eqs. (75) through (78), then we have

$$\frac{dP}{da} = \langle F'_a \rangle + \langle \psi^*, \mathcal{S} \rangle + BT[\psi^*, \psi] =$$

$$= 4\pi \int dt \int dm \frac{\partial F}{\partial a} + 4\pi \int dt \int dm \left[u^* S_u + T_i^* S_i + T_e^* S_e \right] +$$

$$+ \hat{B}\Gamma \left\langle \psi^*, \psi \right\rangle . \qquad (84)$$

These last two equations are the final products of the sensitivity theory based on the used of adjoint functions for pellet fusion problems. A single original and a single adjoint problem solution is all that is need to evaluate all the derivaties of a given response with respect to a large number of input data. The adjoint equations derived are independent of da, and da appears explicitly only through the direct effect and the source terms in Eq. (84). The adjoint equations, however, do depend explicitly on the particular response being studied through the source vector in Eq. (83). Therefore this sensitivity analysis methodology is very efficient and convenient to use for scoping studies of pellet fusion design.

V. DICUSSION

The sensitivity theory in terms of adjoint functions for pellet fusion system was presented. The adjoint equations of hydrodynamics derived above are different from Greenspan's work in the following two aspects:

1. To the velocity equation [see Eq. (1)] of the fundamental equations there corresponds an R^*-equation [see Eq. (68)].
2. Since the conservation of mass is satisfied automatically in Lagrangean representation [see Eq. (2)], **Equation (69)** does not contain the time derivative of ρ^* correspondingly.

The form of the adjoint equations and their boundary and

final conditions are much similar to those of the original hydrodynamic equations [Eqs.(1) through (5)] This indicates that the computational effort required for the solution of the adjoint equations is comparable to that required for the solution of the original equations. Moreover, the adjoint equations are linear in $\psi^* = [R_i^*, \rho^*, u^*, T_i^*, T_e^*]^T$. These probably make them easier to be solved than the original equations.

More of a problem is the fact that the adjoint problem requires the solution of the original equations to determine its input data base. This means that essentially the whole original problem solution path, including the whole time evolution of the physical quantities of plasma as a function of space must be first solved and saved for an adjoint calculation. This will be a very large bookkeeping problem for the pellet fusion problems. The practicability of the sensitivity analysis for the pellet fussion system is still a yet unfinished research task.

REFERENCES

[1]. C. R. Weisbin, et.al., Nucl. Sci. Eng., 66, 307 (1978).
[2]. E. M. Oblow, Nucl. Sci. Eng., 68, 322 (1978).
[3]. D. G. Cacuci, Nucl. Sci. Eng., 75, 88 (1980).
[4]. M. L. Williams, Nucl. Sci. Eng., 70, 20 (1979).
[5]. E. Greenspan et. al., Nucl. Sci. Eng., 73, 210 (1980).
[6]. D. G. Cacuci, Nucl. Sci. Eng., 83, 112 (1983).
[7]. D. G. Cacuci, J. Math. Phys., 22, 2794 (1981).
[8]. E. Greenspan, Nucl. Sci. Eng., 74, 185 (1980).
[9]. J. P. Christiansen et. al., Comput. Phys. Commun., 7, 271 (1974).
[10]. R. D. Richtmyer and K. W. Morton, Difference Methods for Initial-Value Problems, Interscince, New York, (1967), p.313.

4. RELATION BETWEEN ABSOLUTE AND RELATIVE MEASUREMENTS OF NUCLEAR DATA

4.1 Monoenergetic Neutron Fluence Standards

Taichi MICHIKAWA
Electrotechnical Laboratory
1-1-4 Umezono, Sakura-mura, Niihari-gun, Ibaraki-ken

Some topics on the standardization of monoenergetic fast neutron fluence are discussed taking account of the relationship between neutron fluence standards and nuclear standard data. Neutron fluence standards at energies of 144- and 565-keV, and that at nearly 14MeV energy region are concentrated in this paper. At 144- and 565-keV, non-linear energy response of proton-recoil proportional counter is discussed based on the energy dependence of $\bar{W}$-value of recoil-protons in gas. Preliminary results of international intercomparison for 144- and 565-keV neutron fluence using $^{115}In(n,\gamma)^{116m}In$ reaction are reviewed briefly. At 14~15 MeV of neutrons, the associated α-particle method is used as the primary standards for neutron fluence determination; the interference effect of $^{3}He(d,p)^{4}He$ reaction following β-decay of tritium in the target to the associated α countings is discussed. Proton-recoil telescope also plays a role of primary standards of monoenergetic neutron fluence above ~2.5MeV, and in this paper both non-parallel incidence effect of neutrons and multiple-scattering effect of recoil-protons in radiator are described for the determinations of absolute telescope efficiency by Monte Carlo method.

1. Introduction

Primary monoenergetic neutron fluence standards are generally established with using the proton-recoil type detectors, except in the case of associated α-particle counting method, and therefore total and/or differential neutron elastic scattering cross-sections for hydrogen are basic standard data for primary neutron fluence. In this paper we concentrate on standardization of monoenergetic neutron fluences at 144- and 565-keV, and that at nearly 14MeV energy region. At 144- and 565-keV, proton-recoil proportional counters filled with H_2 or CH_4 gas are the primary standard devices for determination of neutron fluences, and non-linear energy response of proton-recoil proportional counter is discussed based on the energy-dependence of $\bar{W}$-value of recoil-protons in gas, as a topics. Correction factors for absolute efficiency in the proportional

counter due to the above effect were estimated to be 1.018 and 1.010 at neutron energies of 144- and 565-keV, respectively, by Monte Carlo calculation. Then, preliminary results of international intercomparison for 144- and 565-keV neutron fluence using $^{115}In(n,\gamma)^{116m}In$ reaction are reviewed briefly. It must be pointed out that the correction for target-scattering effect of neutrons is important for neutron capture cross-section measurements of nuclei having large cross-sections in lower neutron energy region; the ratio of $^{115}In(n,\gamma)$ capture cross-sections at 144keV to that at 565keV has a discrepancy of 10% between measured value and ENDF/B-V file at the present stage.

At 14~15 MeV of neutrons, the associated α-particle method is used as the primary standards for neutron fluence determination; the interference effect of $^{3}He(d,p)^{4}He$ reaction following β-decay of tritium in the target to the associated α-particle counting in $T(d,n)^{4}He$ reaction is discussed. Contribution of ^{3}He+d α-particles to the associated α-counting was measured, as an example, to be increasing by 0.25% per year after target preparation at incident deuteron energy of 0.26MeV for typical TiT thickness of 0.4~0.5mg·cm^{-2}. Proton-recoil telescope also plays a role of primary standards of monoenergetic neutron fluence above ~2.5MeV, and in this paper both non-parallel incidence effect of neutron beam and multiple scattering effect of recoil-protons in radiator are discussed at neutron energy of 14MeV for the determination of absolute telescope efficiency by Monte Carlo method. For the standardization of monoenergetic 14~20MeV neutron field, differential elastic scattering cross-section of H(n,n), especially $\sigma_{n\text{-}p}(180^{\circ})$, should be evaluated more accurately than at the present status.

2. Relationship between Neutron Fluence Standards and Nuclear Standard Data

Primary monoenergetic neutron fluence standards are generally established with using proton-recoil proportional counters at lower neutron energies and proton-recoil telescope at higher neutron energies except in the case of associated particle counting technique. Therefore, as shown in Fig.1, total and/or differential neutron elastic scattering cross-sections for hydrogen are the basic standard data for primary neutron fluence standards. Nuclear reaction cross-sections such as $^{6}Li(n,t)\alpha$, $^{10}B(n,\alpha)^{7}Li$, $^{27}Al(n,\alpha)^{24}Na$, $^{197}Au(n,\gamma)^{198}Au$, $^{235}U(n,f)$ and $^{238}U(n,f)$ are recommended as the standard reference data by IAEA/NDC,[1] and are usually measured absolutely using the standard neutron fluence field. Other neutron cross-section data are usually obtained by relative measurements with using these standard reference data.

3. Some Remarks on Absolute Neutron Fluence Determination with Proton-Recoil Proportional Counter

The cylindrical type proportional counters filled with H_2 or CH_4 gas are used for the determination of monoenergetic neutron fluences below ~1.2MeV in the Electrotechnical Laboratory. Each proportional counter has the sensitive volume of 50mmϕ × 152mm and gas pressure of 98.6kPa. Table 1 shows the uncertainties associated with the absolute fluence determinations using the proportional counter at neutron energies of 144- and 565-keV. It is more difficult to determine the absolute neutron fluence at lower neutron energies due to disturbance caused by the electronic noise and γ-rays background, and to the non-linear response of protons caused by the energy-dependence of $\overline{W}$-value of protons in H_2 or CH_4 gas. Uncertainty of n-p total scattering cross-sections does not occupy the main parts of total uncertainties. The uncertainties associated with the estimations of total numbers of hydrogen nuclei and recoil-protons in the sensitive volume are rather large compared with the uncertainty of n-p scattering cross-sections. Overall uncertainties for absolute fluence determination are ±1.6 ~2.3% at neutron energy region above ~100keV at the present state of metrology.

Among some problems in the measuring techniques with proton-recoil proportional counters, non-linearity effects of proton response in gas due to energy-dependence of $\overline{W}$-value of protons in gas are discussed below. Usually total numbers of recoil-protons produced in the sensitive volume of the counter are obtained from the total counts above a half of a maximum pulse height, multiplied by the ratio of total area A to the area B above half-maximum which is obtained from Monte-Carlo calculation, as shown in Fig.2(a), in order to avoid the spurious counts due to electronic noise and γ-rays background. Solid curve in Fig.2(a) shows the recoil-proton pulse height distribution when $\overline{W}$-values of protons are asssumed to be energy-independent, and on the other hand, typical pulse height distribution when $\overline{W}$-values are energy-dependent becomes as shown by dotted curve in Fig.2(a) because $\overline{W}$-values of protons tend to increase as the proton energy decreases. When we assumed as energy-dependence of $\overline{W}$-value to be represented by $\overline{W}(E)=W_0/(1-0.58/\sqrt{E})$ for CH_4 [2] where W_0 is $\overline{W}$-value at higher proton energy region and E is proton energy in unit of keV, the correction factors for ratio A/B were obtained from Monte Carlo calculation for our CH_4 filled proportional counter as shown in Fig.2(b); correction factors become larger as neutron energies become lower and their values are 1.018 and 1.010 at neutron enrgies of 144- and 565-keV respectively.

4. International Intercomparison Experiments for 144- and 565-keV Neutron Fluence Using $^{115}In(n,\gamma)^{116m}In$ Reaction

The purpose of international intercomparison is to confirm the accuracy of absolute determinations of monoenergetic neutron fluence between different standards laboratories. The second international intercomparison is now progressing at five neutron energies under the auspices of CCEMRI/CIPM* Section III, and as a branch, international comparison experiments were performed for 144 - and 565-keV neutron fluences using the transfer method of $^{115}In(n,\gamma)^{116m}In$ reaction coordinated by Dr. T.B.Ryves of National Physical Laboratory (Britain) in 1982-84.[3] The six national standards laboratories that took part in this intercomparison were Central Bureau for Nuclear Measurements (CBNM) in Geel, Electrotechnical Laboratory (ETL) in Tsukuba, Institute of Atomic Energy (IAE) in Beijing, National Physical Laboratory (NPL) in Teddington, National Research Council (NRC) in Ottawa and Physikalish-Technische Bundesanstalt (PTB) in Braunschweig.

Quantity to be measured in this intercomparison was K expressed as the ratio as follows;

$$K = \frac{\text{Saturated specific } \beta\text{-activity of } ^{116m}In}{\text{Absolute neutron fluence-rate}} \quad (cm^2 \cdot g^{-1})$$

Standard indium foils (25.4mmϕ × 0.05mmt) were circulated sequentially to each participating laboratory together with a small $4\pi\beta$ gas-flow proportional counter, a preamplifier and a ^{60}Co check source for normalizing the sensitivity of $4\pi\beta$ counter. Simultaneous irradiations of two indium foils for two hours were performed at distances of 8~20cm from neutron producing target, in order to correct for the room-scattered neutrons by fitting to the inverse-squares law. The contribution of room-scattered background to the In foil activities was 10% and 13% respectively for neutron energies of 144- and 565-keV at distance of 10cm from target in the ETL irradiation room (room size:11×11×11m). Corrections for target-scattered neutrons on the In foil activities were performed independently at each participating laboratory, but finally normalized by Ryves, coordinator, with common Monte Carlo code for different geometries of target holders used at different laboratories. Preliminary results of this international intercomparison analyzed by Ryves are shown in Fig. 3 (a) and (b) for 144- and 565-keV neutron fluences. Since the In foil transfer technique itself is considered to introduce random uncertainties of only 1~2% in this intercomparison, the results shown in Fig.3 represent the present status of the art

* Comité Consultatif pour les Etalons de Mesure des Rayonnements Ionisants /Comité International des Poids et Mesures

for monoenergetic neutron fluence determinations in the national standards laboratories. Since the results are based on only a provisional document prepared by Ryves and are under review among the members of CCEMRI/CIPM Section Ⅲ, the notations of A,B,C etc. are used instead of the name of each laboratory in Fig.3.

At 144keV, the value of laboratory D is ~30% higher than ones of other laboratories, and there might be any troubles in the fluence determination at the laboratory D. Hatched area shows the weighted mean among the participating laboratories excluding D. The result at 144keV is excellent with the spread of 3.4% (between A and C) excluding D, although the absolute fluence determination and In foil calibration (specific β-activity per unit neutron fluence-rate) are much more difficult at 144keV than at 565keV. At 565keV, which is usually considered to be an easy energy at which to make measurements, there is a large spread of 8.3% between F and C or E. There are clearly two-groups; one is the higher group of four laboratories, and another is the lower group of two laboratories. There may be any problems in the fluence determination at any one of two groups.

5. Remarks on the Ratio of $^{115}In(n,\gamma)^{116m}In$ Capture Cross-Section at 144keV to That at 565keV

The quantity which was measured at each participating laboratory in the intercomparison described in Sect.4 was K i.e. saturated specific β-activity of ^{116m}In per unit neutron fluence-rate, and therefore this quantity is proportional to $^{115}In(n,\gamma)^{116m}In$ capture cross-section. In this section, some remarks will be described on the ratios of $^{115}In(n,\gamma)$ capture cross-sections at 144keV to that at 565keV between the measured value and ENDF/B-V data. As mentioned in Sect.4, the target-scattered effect of neutrons is important in the In foil calibrations since the target-scattered neutrons, with energy of one order lower than the direct neutron energies of 144- and 565-keV, significantly activate the In foil having large cross-sections at lower neutron energies. In our case, correction factors for target-scattering on the In foil activities were estimated to be 0.922 and 0.980 at direct neutron energies of 144- and 565-keV, respectively, from the numerical calculations based on the differential elastic scattering cross-sections for materials of target backing and holder.

Table 2 shows the comparison between measured and ENDF/B-V values on the ratio R(144/565 keV) of $^{115}In(n,\gamma)$ capture cross-sections at 144keV to that at 565keV. The measured values in this table were obtained in the intercomparison experiments at NPL[4] and ETL mentioned in Sect.4. It is evident that there is at present a 10% discrepancy of ratio R(144/565 keV) between measured and ENDF/B-V

data values. The reasons of the discrepancy are either the ENDF/B-V data file for $^{115}In(n,\gamma)$ reaction is not correct or there is an unknown problem associated with the measuring techniques. Although this is one of the urgent problems to be solved, it is concluded that the corrections for target-scattered eff ect are important for the neutron cross-section measurements below a few hundred keV where many cross-sections are increasing rapidly as the neutron energy decreases.

6. Interference Effect of $^{3}He(d,p)^{4}He$ Reaction on the Associated α Countings in $T(d,n)^{4}He$ Reaction

Associated α-paticle counting method (APM) is the primary standards for 14~15MeV neutron fluence determination and its overall uncertainty can be obtained up to $\pm 1.0\%$ at the present state of art. Among some problems in the APM, interference effect of $^{3}He(d,p)^{4}He$ reaction on the associated α countings in $T(d,n)^{4}He$ reaction will be described below. ^{3}He nuclei are accumulating in tritium (TiT) target following β-decay of ^{3}H with half-life of 12.33y and the amount of ^{3}He in TiT target increases by ~5% per year. Alpha paticles produced from $^{3}He(d,p)^{4}He$ reaction have neighboring energy to α-particles from $T(d,n)^{4}He$ reaction and therefore α-paticles from both reactions can not be distinguished each other in APM, except in the cases where Time-Correlation or Time-of-Flight methods are used. In order to estimate the fractions of contributions of ^{3}He+d α particles to APM, a CsI scintillation detector with a $1\mu m$ thick aluminum window was used to measure the fluences of high energy ^{3}He+d protons in free air emitting through target backing (copper) at an angle of 0^{0} to the incident deuteron beam. The measured energy dispersion of high energy protons transmitted through a 0.25mm thick Cu backing was ~5% and ~2% at incident deuteron energies of 0.26- and 3.3-MeV, respectively. Table 3 represents the experimental result of contributions of ^{3}He+d α-particles to the associated α-particle countings in $T(d,n)^{4}He$ reaction. The results shown in Table 3 were obtained with just two years old TiT target with thickness of 0.4~0.5 $mg\cdot cm^{-2}$ and therefore it is concluded that contributions of $^{3}He(d,p)^{4}He$ reaction to the associated α countings in $T(d,n)^{4}He$ reaction are 0.25- and 0.49- percents per year at incident deuteron energies of 0.26- and 0.30-MeV, respectively, for typical TiT thickness of 0.4~0.5$mg\cdot cm^{-2}$. As seen in Table 3, the fact of fraction of contributions $\Phi p/\Phi n$ being ~5% per year in higher deuteron energy region proves that the ^{3}He atoms are steadily accumulating by ~5% per year following β-decay of ^{3}H, taking account of the shapes of cross-sections for both $^{3}He(d,p)^{4}He$ and $T(d,n)^{4}He$ reactions.

7. Some Remarks on Estimating the Absolute Efficiency of Proton-Recoil Telescope

Proton-recoil telescope plays a role of the primary standard device for determining the neutron fluences in high neutron energy region above ~2.5MeV. Table 4 represents the uncertainties associated with neutron fluence determination at 14.6MeV using the proton-recoil telescope. As seen in table 4, uncertainties of differential elastic scattering cross-sections of neutrons for hydrogen are main parts in the overall uncertainties of ±1.9%. Dimensions of the ETL telescope based on Los Alamos type have the distance of 62.5mm between polyethylene radiator and CsI(Tl) scintillator and the diameters of radiator and detector of 25mm. Absolute telescope efficiencies were obtained by the Monte Carlo method for various neutron energies and distances from a point source.[6] Among some problems in the telescope techniques, two kinds of corrections for telescope efficiency will be described below. One of them is the correction factor for telescope efficiency due to non-parallel incidence of neutrons from a point neutron source. Figure 4 gives the above correction factors as a function of distances between source and radiator ; the correction factors become larger as the distance decreases. Another correction factor is one due to multiple-scatterings of recoil-protons in radiator as shown in Fig. 5 where the thicknesses of radiators are 0.028mm and 0.309mm for neutron energies of 2.5- and 14.6-MeV respectively.

8. Conclusion

In this paper we concentrated on the monoenergetic neutron fluence standards at energies of 144- and 565-keV and that at nearly 14MeV energy region. First, since the recoil-proton type detectors play a role of the primary standards for neutron fluence metrology, differential elastic scattering cross-sectios for H(n,n) should be evaluated more accurately than at the present status in neutron energy region above ~10MeV. Secondly the corrections for the effects of secondary neutrons produced in the target backing or holder are important for the neutron cross-section measurements for materials having large cross-sections in lower neutron energy region ; elastically scattered neutrons from target backing in the neutron field below a few hundred keV or secondary neutrons produced by Cu(n,n') and Cu(n,2n) reactions in the backing in the 14MeV field bring about significant errors in the cross-section measurements at these neutron energy range. This is besides one of the conclusions obtained from the results of the second international intercomparison for monoenergetic fast neutron fluences organized under the auspices of CCEMRI/CIPM Section Ⅲ.

Many thanks are given to Mr.T.Kinoshita, Drs.K.Kudo, N.Kobayashi, Y.Hino and other Van de Graaff staffs for their cooperations to this work.

References

1) IAEA-TECDOC-335
"Nuclear Standard Reference Data", IAEA, Vienna, 1985
2) ICRU Report 31
"Average Energy Required to Produce an Ion Pair", P.18, USA, May 1979
3) T.B.Ryves
: "International fluence-rate Intercomparison for 144 and 565keV neutrons" (draft), October 1985.
4) J.B.Hunt
: NPL Report RS(INT) 81, September 1985
5) M.Mizumoto
: private communication
6) N.Kobayashi, T.Kinoshita and T.Michikawa
: Nucl. Instr. Methods in Phys. Res. A242 (1985) 164.

Table 1 Uncertainties associated with the absolute neutron fluence determinations using the proton-recoil proportional counter.

	144keV	565keV
sensitive volume	±1.0%	±1.0%
gas pressure, temperature	±0.5	±0.5
correction for non-linearity of proton response in gas	±0.6	±0.4
fitting with Monte Carlo spectrum	±1.7	±0.5
in- and out- scatter corrections of incident neutrons caused by detector wall	±0.7	±0.7
n-p total scattering cross-section	±0.5	±0.5
statistics	±0.1	±0.1
TOTAL $(\sum_i \sigma_i^2)^{\frac{1}{2}}$	±2.3%	±1.6%

Table 2 Comparison between measured and ENDF/B-V data values for the ratio of $^{115}In(n,\gamma)\ ^{116m}In$ capture cross-sections at 144keV to that at 565keV : R(144/565keV)

	National Physical Lab 4)	Electrotechnical Lab
Target backing	0.25 t×44.5φ Ag	0.33 t×38φ Ta and cooling fin
Value uncorrected for target-scattering	1.516±0.049	1.540±0.052
Value corrected for target-scattering	1.468±0.060	1.449±0.062
Ratio of ENDF/B-V	1.6011 5)	

Table 3 Experimental results of contributions of ^{3}He+d α-particles to associated α-particle countings in T(d,n)^{4}He reaction.

TiT target used is two years old and has typical TiT thickness of 0.4～0.5mg・cm^{-2}.

Incident deuteron energy (MeV)	d+^{3}He proton fluence ϕp (p・sr^{-1} at 0°)	d+T neutron fluence ϕn (n・sr^{-1} at 0°)	Percentage of contribution ϕp/ ϕn(%)
0.26	2.92×10^{7}	5.81×10^{8}	0.50
0.30	5.65×10^{7}	5.79×10^{8}	0.98
0.33	1.07×10^{8}	5.79×10^{8}	1.84
0.59	3.20×10^{8}	2.99×10^{8}	10.7
1.18	3.41×10^{8}	2.90×10^{8}	11.8
1.87	2.83×10^{8}	2.65×10^{8}	10.7
2.56	1.90×10^{8}	1.87×10^{8}	10.1

Date of certification for ^{3}H target used : 1983.1.6. by Amersham

Date of experiments : December 1984 ~ January 1985

Table 4 Uncertainties associated with the absolute neutron fluence determinations for 14.6MeV using the proton-recoil telescope.

Origin	Uncertainties (%)
Statistical	±0.2
Background subtraction	±0.5
n-p total elastic cross section	±0.8
n-p cross section anisotropy	±1.0
Radiator composition	±0.7
Target-to-telescope distance	±0.3
Internal telescope geometry	±0.9
Neutron energy	±0.2
Correction for neutron attenuation in Al window of telescope	±0.2
Overall (r s s)	±1.9

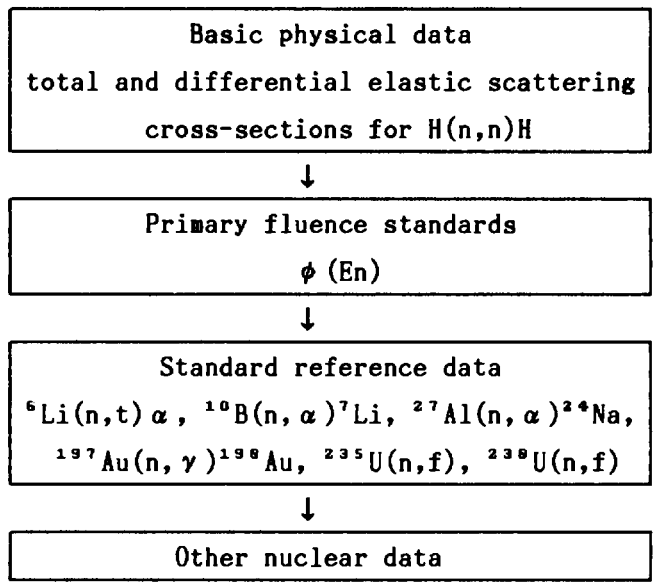

Fig. 1 Schematics on the relationship between neutron fluence standards and nuclear standard data

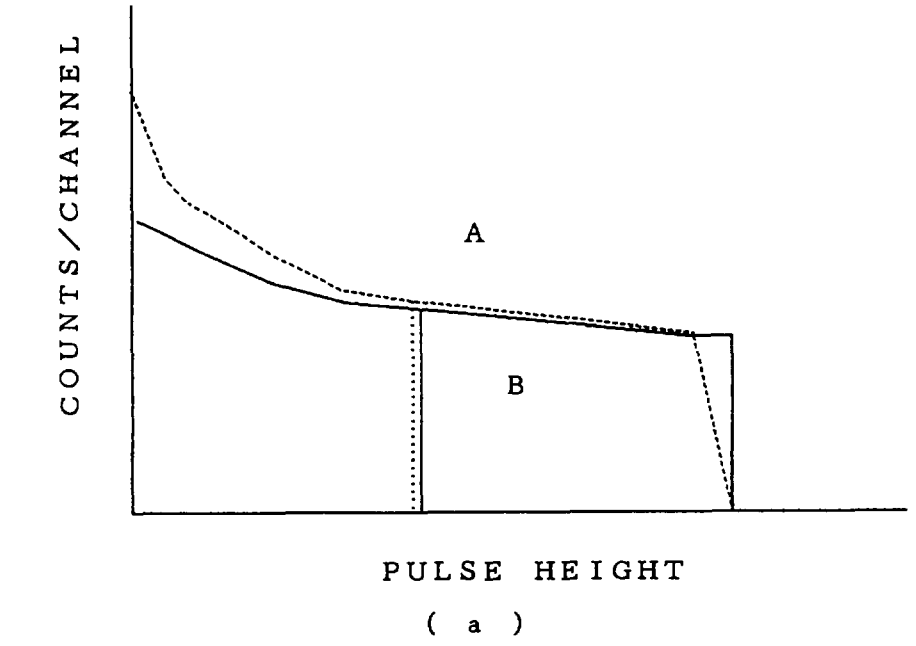

(a)

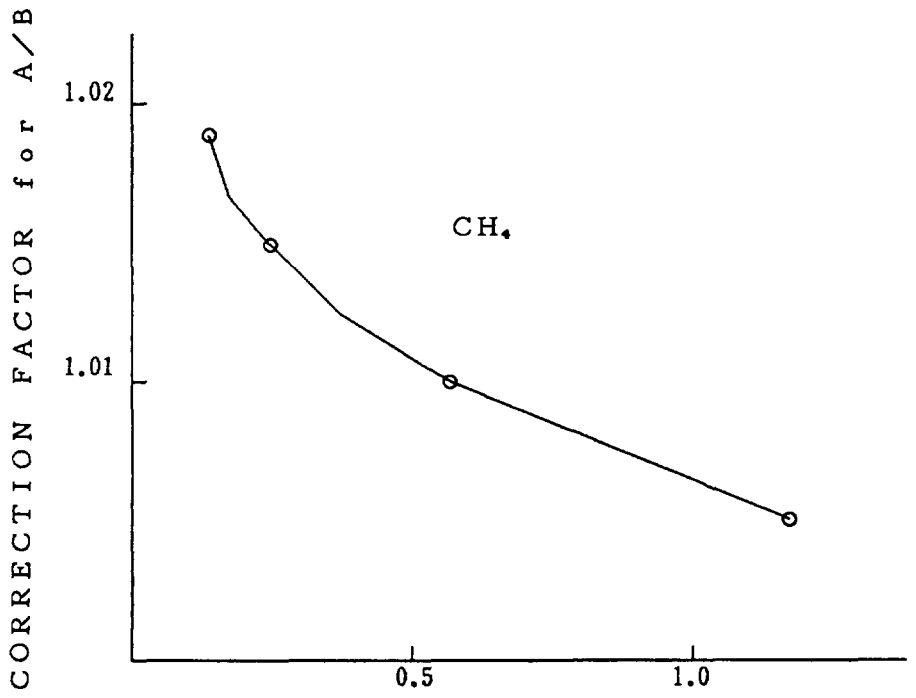

(b)

Fig. 2 (a) Typical pulse height distributions of recoil-protons in the gas proportional counter

Solid curve corresponds to the case assumed that W-value is independent on proton energy. Dotted line corresponds to the case where W-value depends on proton energy. "A" shows total area and "B" is area above a half of a maximum pulse height.

(b) Correction factors for the ratio A/B versus neutron energies for ETL proportional counter filled with CH_4 gas, given by Monte Carlo calculation.

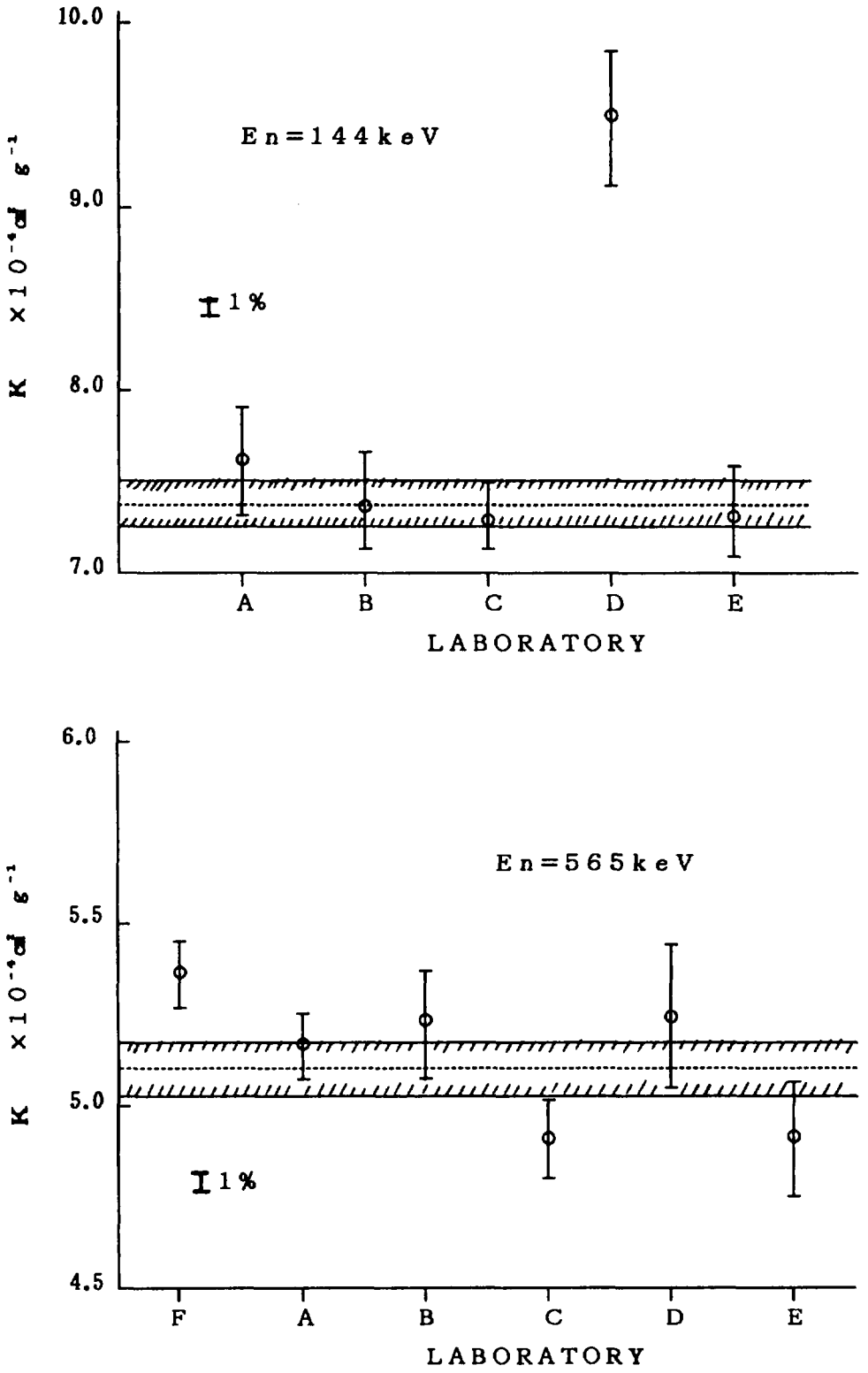

Fig. 3 Preliminary results of internationl intercomparison for 144- and 565-keV neutron fluences using $^{115}In(n,\gamma)\ ^{116m}In$ reaction reported by Ryves[3)]

Notations of A, B, C etc. are used instead of the names of participating laboraories.

Hatched area shows the weighted mean among the participating laboratories excluding laboratory D at 144keV.

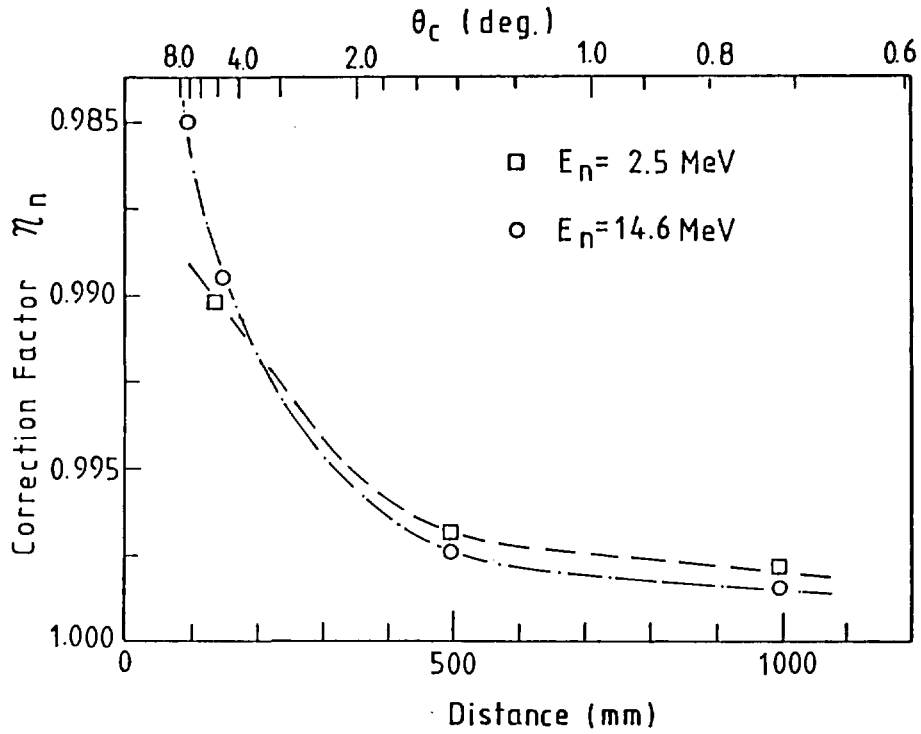

Fig. 4 Correction factors for telescope efficiency due to non-parallel incidences of neutrons as a function of distance between point source and radiator, given by Monte Carlo calculation [6]

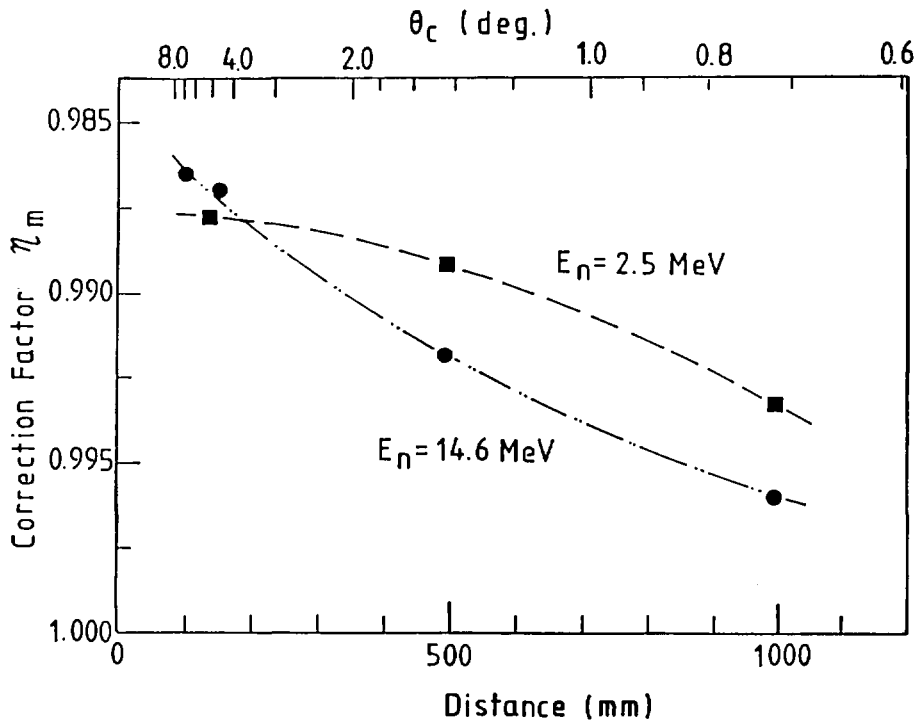

Fig. 5 Correction factors for telescope efficiency due to multiple-scatterings of recoil-protons in radiator as a function of distance between point source and radiator, given by Monte Carlo calculation.[6]
Radiator thicknesses used are 0.028mm and 0.309mm for neutron energies of 2.5- and 14.6-MeV repectively.

4.2 Comments on D-T Neutron Energy Determination

M. Nakazawa*, T. Iguchi**, H. Eguchi**

* Nuclear Engineering Research Laboratory, Univ. of Tokyo

Tokai-mura, Naka-gun, Ibaraki-ken

** Department of Nuclear Engineering, Univ. of Tokyo

7-3-1, Hongo, Bunkyo-ku, Tokyo

A practical technique for the average energy determination of D-T neutron sources is presented here, which is based on the activation-rate ratio data between $^{90}Zr(n,2n)^{89}Zr$ and $^{93}Nb(n,2n)^{92m}Nb$, and its applicability has been shown in the neutron energy measurements of D-T neutron generators of JAERI-FNS, OKTAVIAN and RTNS-II. Another comment is presented on the average neutron energy decreasing effect in the front region of the tritium target, which can be explained as the finite size effect of the deuteron beam at the tritium target.

1. Introduction

The determination of neutron energy is important as well as the measurements of neutron fluence in the neutron source characterization works for the neutron cross section measurements and neutronics benchmark experiments. Here are made two comments on these neutron energy determinations of D-T neutron generators, which produce so called 14 MeV neutrons basing on the T(d,n)He reactions by bombarding the deuteron beam with the tritium target.

The first comment is the development of a practical technique for the average energy determination of D-T neutron source using the activation-rate ratio method between the two reactions of $^{90}Zr(n,2n)^{89}Zr$ and $^{93}Nb(n,2n)^{92m}Nb$, which have been well applied to the dosimetry work of D-T neutron generators of JAERI-FNS, OKTAVIAN(Osaka Univ.) and RTNS-II (Lawrence Livermore National Laboratory).

The second comment is the neutron energy decreasing effect

in the front region of the tritium target, which can be attributed to the finite size effect of the deuteron beam at the tritium target. Actually the average neutron energy of the RTNS-II neutron generator has been found 14.4 MeV at 2 mm point from the tritium target assembly surface, while it has been 14.9 MeV at 30 cm in the forward direction.

2. A new technique of Zr/Nb activation ratio method

The activation cross-section curves of $^{90}Zr(n,2n)^{89}Zr$ and $^{93}Nb(n,2n)^{92m}Nb$ reactions are shown in Fig. 1, where it is found that the former reaction is linearly proportional to the neutron energy, while the latter is almost flat in this energy region. And it is easy to understand the activation rate ratio method of these two reactions as the D-T neutron energy determination technique, and the calibration curve of this ratio data to the neutron energy is summarized in Fig. 2, where our new data obtained in the Japanese standard neutron field of ETL are included.

Another feature of this Zr/Nb activation ratio method is the similarity of their gamma-ray energy values from ^{89}Zr(half life 78.43h, $E\gamma$ = 909 keV) and ^{92m}Nb(half life 243.6h, $E\gamma$ = 935 keV), which will make a great reduction of the uncertainty of counting efficiency values of Germanium gamma-ray spectro meter. The similarity of the half life will also serve to reduce the uncertainty of the experimental clock and the neutron irradiation history.

Using this new technique, the neutron energy determinations have been done in several D-T neutron generators of Univ. of Tokyo, JAERI-FNS, OKTAVIAN(Osaka Univ.) and RTNS-II (LLNL), that are shown in Fig. 3 and 4. Simple conclusions can be obtained from these results that the neutron energy of the forward direction is ranging between 14.8 and 14.9 MeV in those all generators independently on their accelerating voltages. This property is thought common feature for the 14 MeV neutron generator with the thick tritium target.

3. Neutron energy decreasing effect near the tritium target surface

Practical neutron energy of D-T neutron source is ranging between 14.9 MeV and 14.1 MeV depending on the neutron emmission angles from 0° to 90°, when the thick tritium target is applied, which is just one conclusion obtained in the previous section.

This neutron energy has been found to be decreased when the irradiation point is near the tritium target surface due to the finite size effect of neutron emission point on the tritium target due to the finiteness of deuteron beam.

In order to estimate this neutron energy decreasing effect in the RTNS-II , the detail mapping measurements near the target surface has been made using ^{93}Nb(n,2n) activation dosimeters, and those mapping data have been analyzed under the assumption that the neutron emission distribution on the tritium target is gaussian form. Typical data are shown in Fig. 5 where the standard deviation σ of this gaussian function is best selected as 8.0 mm.

Using these values, the neutron energy spectra at several distances from the tritium target are shown in Fig. 6, where it is clearly found the neutron energy spectrum is shifted to the lower energy region when going near to the tritium target. The average energy values along Z axis are ploted in Fig. 7.

From these results it can be said that the neutron energy decreasing effect of D-T neutron source is found in 10 cm or nearer regions from the tritium target, when the deuteron beam diameter is about 1 inch.

4. Conclusion

A new practical technique of the D-T neutron energy determination using the Zr/Nb activation-ratio has been successfully applied to several neutron generators and it is very interesting that the common feature of the neutron energy values around the D-T neutron generator have been made clear very generally.

A little special phenomena, named as the neutron energy

decreasing effect near the tritium target, have been found in the RTNS-II dosimetry work, that is important for the heavy neutron irradiation experiments using the close point to the tritium target to get more neutron fluences.

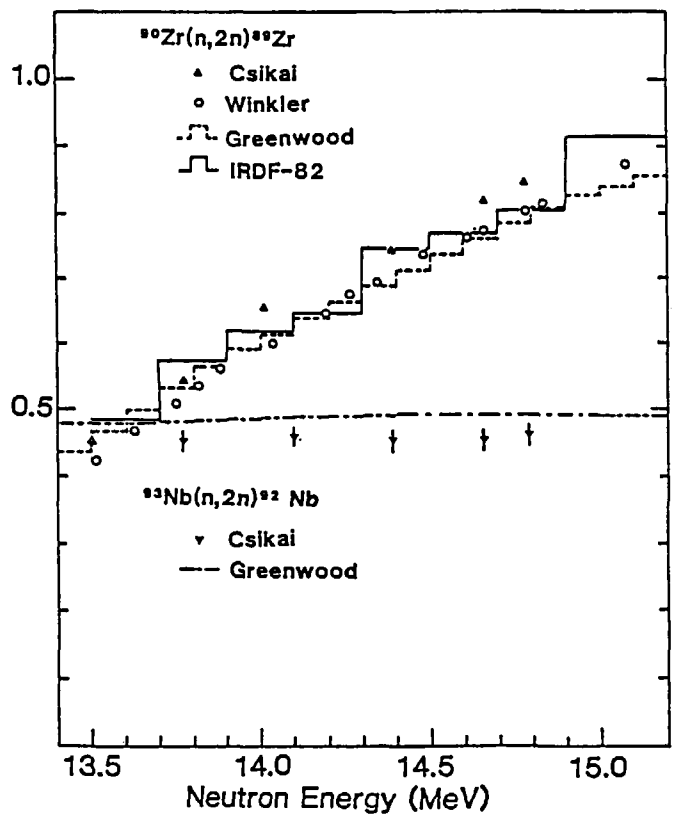

Fig.1 Reaction Cross-Sections of $^{90}Zr(n,2n)$ ^{89}Zr and $^{93}Nb(n,2n)$ ^{92m}Nb

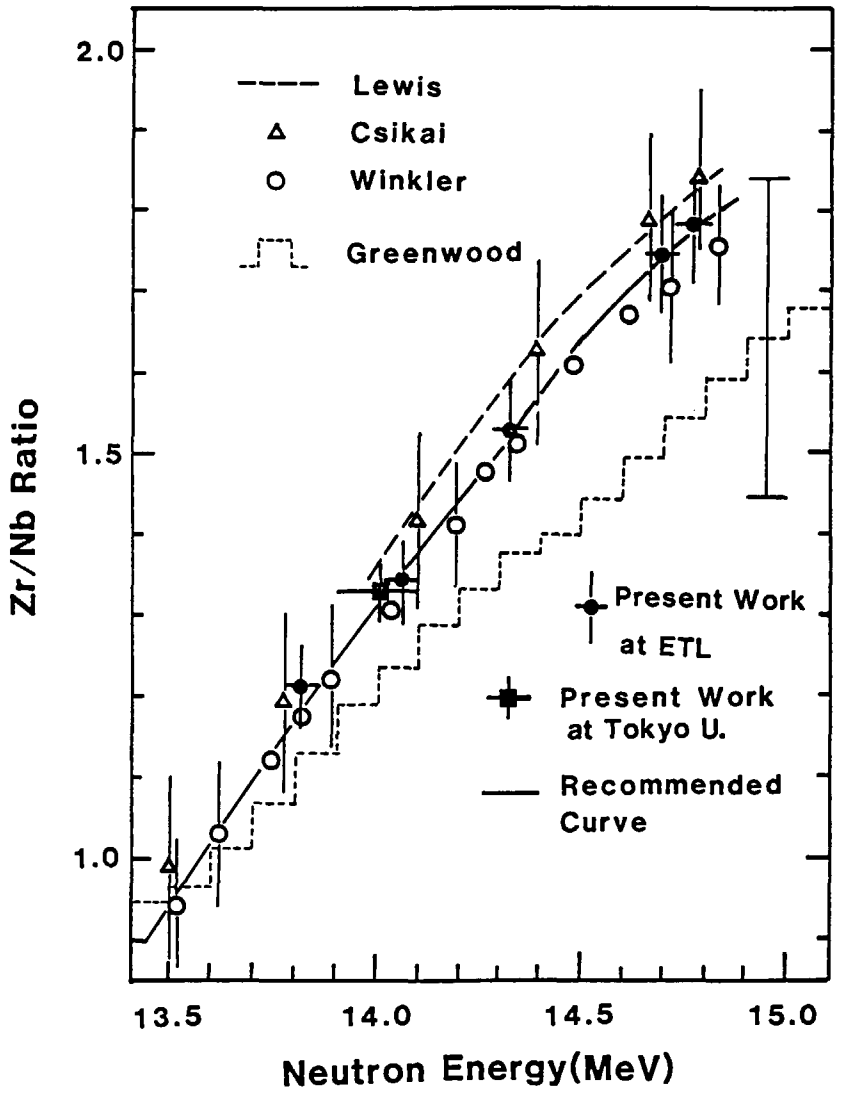

Fig.2 Calibration Curve of Zr/Nb Activation Ratio to Neutron Energy

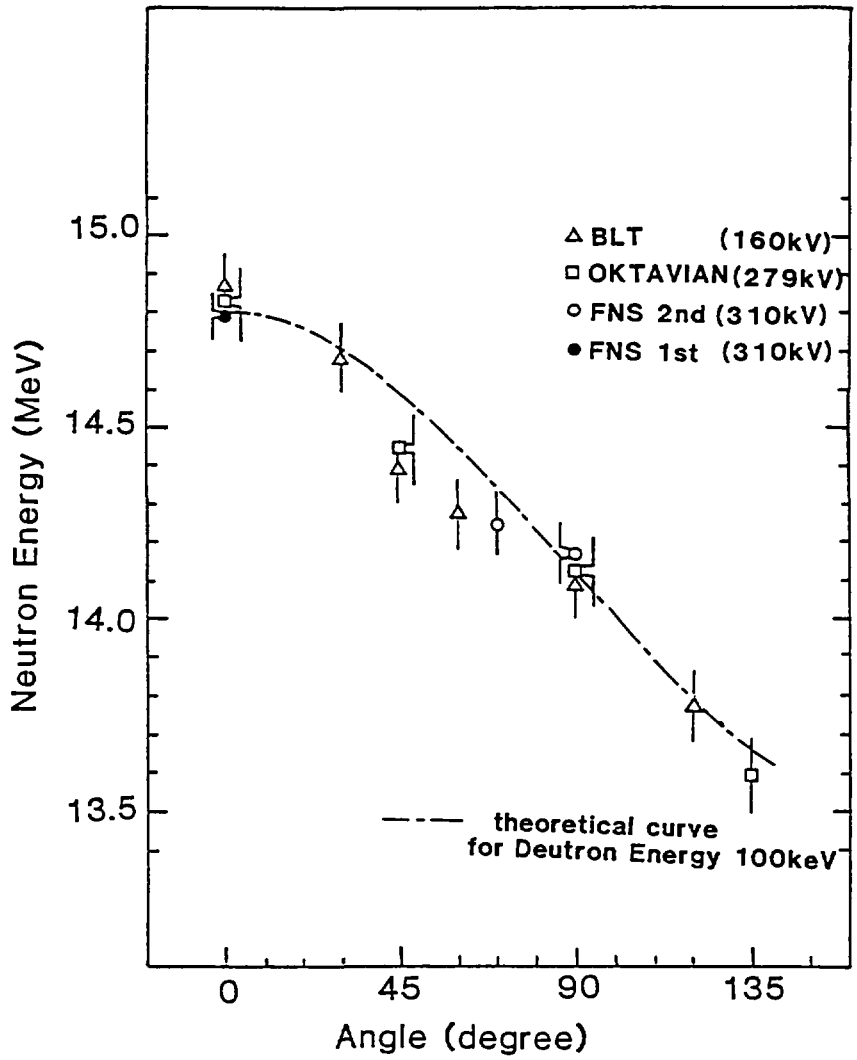

Fig.3 D-T Neutron Source Energy of Each Emission Angles, Measured by Zr/Nb Method

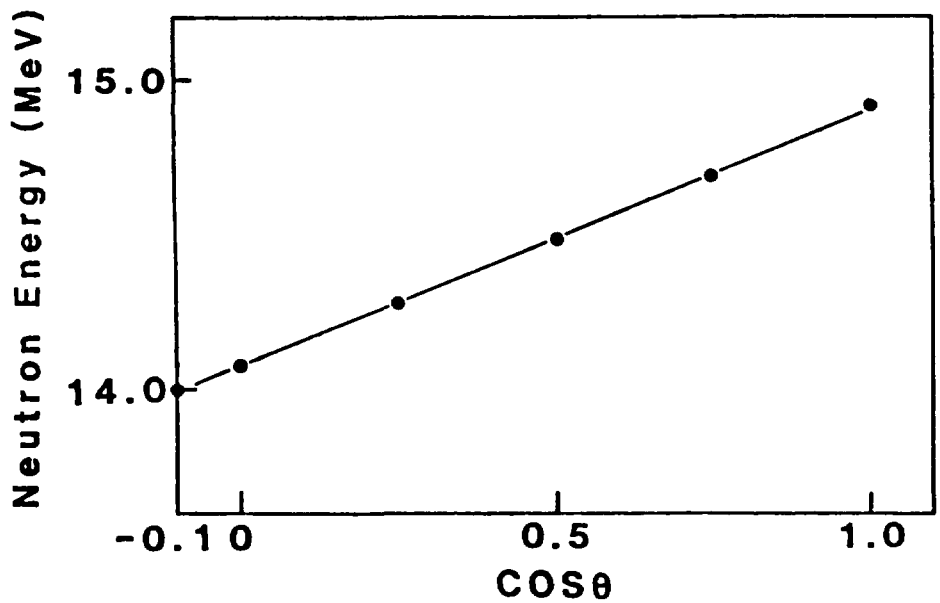

Fig.4 RTNS-II Neutron Source Energy of Each Emission Angle θ, Measured by Zr/Nb Method

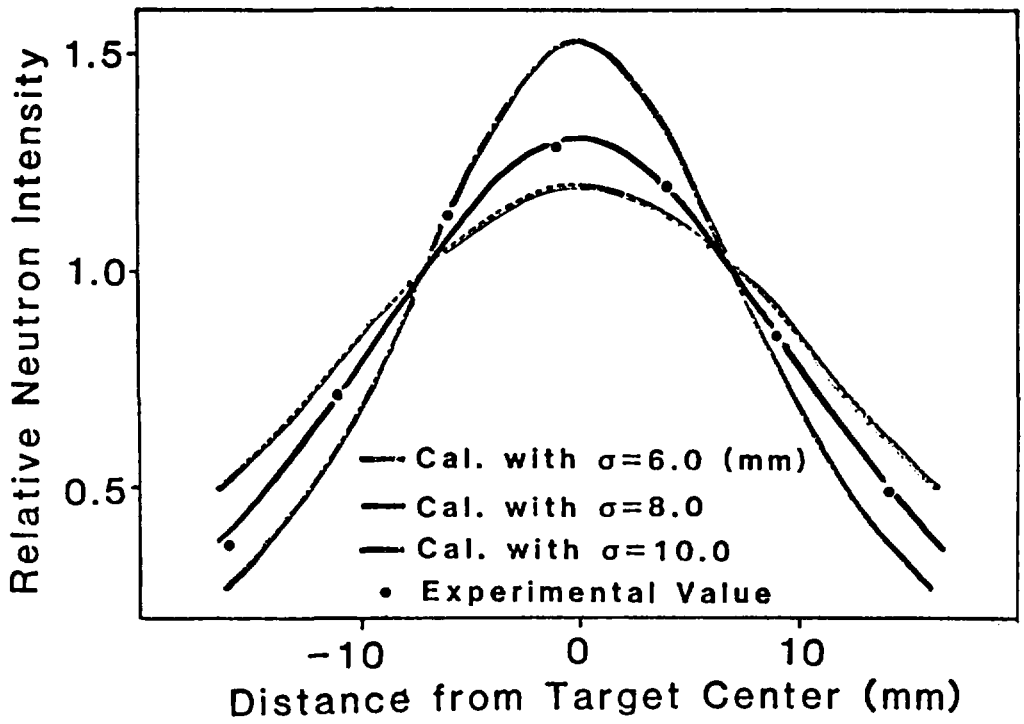

Fig.5 Comparisons of Neutron Flux Profile at 2 mm from Target between Measurement and Calculations

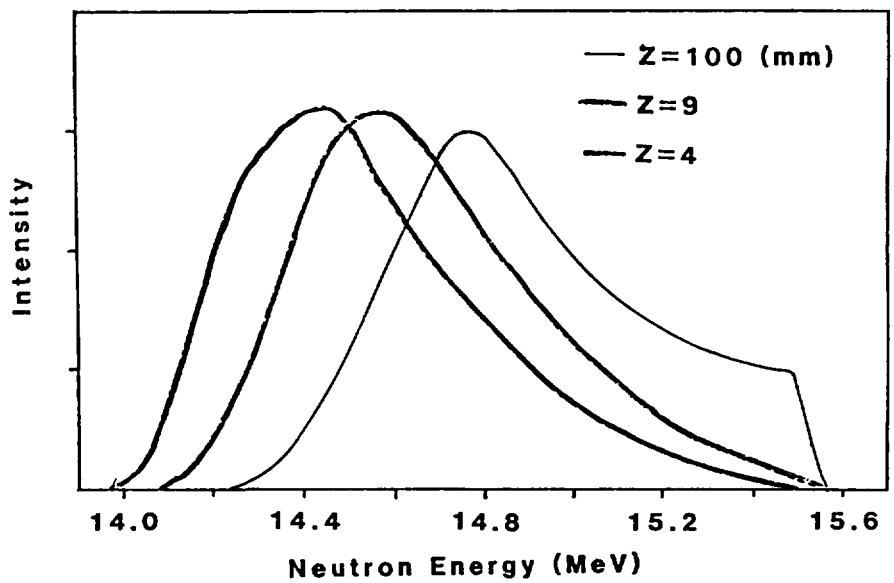

Fig.6 Forward Neutron Spectra of D-T Neutron Source at Each Distance Z from Target in RTNS-II

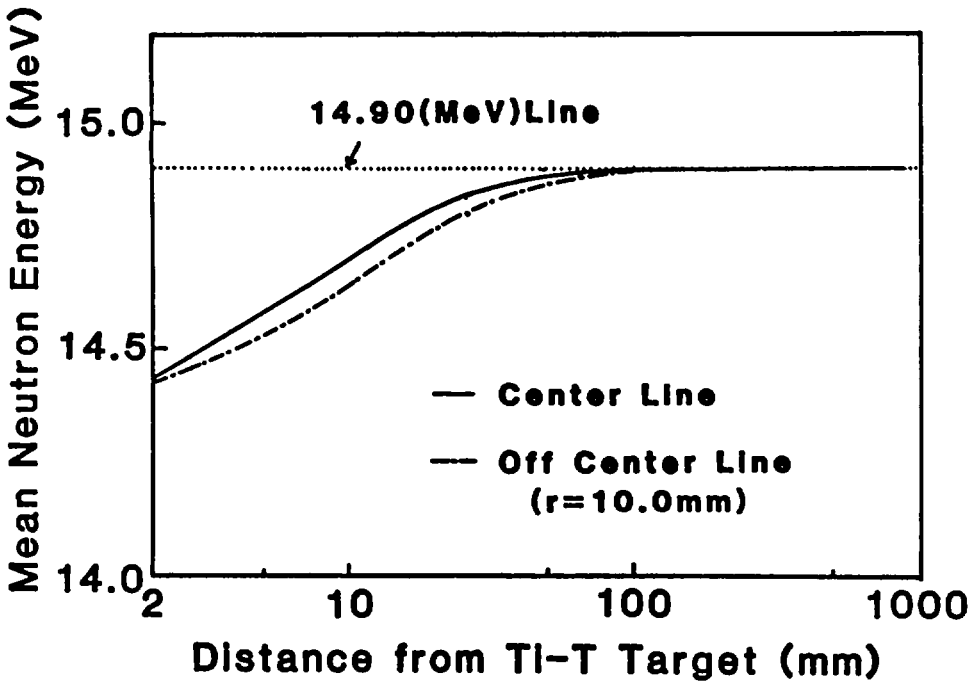

Fig.7 Neutron Energy Decreasing Effect in Near Target positions in RTNS-II

4.3 Standard cross section for neutron capture measurements (in the keV region)

Motoharu Mizumoto
Japan Atomic Energy Research Institute
Tokai-mura, Naka-gun, Ibaraki-ken

The cross sections of the $^{6}Li(n,\alpha)$, $^{10}B(n,\alpha)$ and $^{10}B(n,\alpha\gamma)$ reaction have been used as the standards for the keV capture cross section measurements. Large Q values of these reactions can be used in neutron detection and the cross sections are accurately known. Many data are available from the past experiments and the detailed evaluations have been carried out for the existing evaluated files. However, there are still some deficiencies in these data, especially for the ^{10}B + n reaction in the neutron energy range above 100 keV. In this report, the recent status for these standards will be discussed and the method, using these standards to calculate the efficiencies of ^{6}Li-glass and ^{10}B-NaI detector will be presented

1. Introduction

The incident neutron flux has to be determined in most cases for the analysis of capture yields and reduction of the cross section data. If the flux measurement is made relative to the standard cross section, the absolute neutron intensity can be easily obtained.

For standards to be used, the cross section values should be large and smooth. The standard cross sections for the keV capture measurements include several reactions as shown in Table 1. The H(n,n)H is considered to be most accurately known at the present. But, because this reaction is used to detect recoil energies transferred to protons, the neutron detection becomes difficult in the neutron energy below a few hundred keV. The $^{197}Au(n,\gamma)$ and $^{235}U(n,f)$ cross sections are also recommended as the standards in the keV region. The gold

has good physical properties, the sample is easy to prepare and its capture cross section is well established. By replacing the capture sample to be measured with the gold sample, capture measurements can be made using the same detector and electronics. But the resonance structure of gold in the cross section makes it difficult as the standard below 200 keV. The same resonance structure is observed in the case of the ^{235}U fission cross section. Therefore, in this paper, we will be concerned only about the ^{6}Li + n and ^{10}B + n reaction.

The ^{6}Li + n and ^{10}B + n data have been extensively discussed by many authors[1-4]. The comprehensive review by A.D. Carlson[2] described the characteristics and the present status of the standard data. W.P. Poenitz wrote a critical review[4] about the experimental data of the ^{6}Li + n and ^{10}B + n and made the recommendations for the ENDF/B-6 evaluation. Present paper is very much obliged to these previous review papers. We will discuss the status of the ^{6}Li + n cross section and ^{10}B + n cross section in the section 2 and section 3, respectively, particularly paying attention to the comparison of the JENDL to other evaluations and experimental data. In the section 4, we will give some example for calculating the detector efficiencies of ^{6}Li-glass and ^{10}B-NaI detector which are used for the capture experiments at the JAERI linac facility.

2. The status of $^{6}Li(n,\alpha)$ cross section

The $^{6}Li(n,t)^{4}He$ has a large Q value of 4.78 MeV which makes it easy to detect the emitted charged particles. The cross section has a nice 1/v energy dependence up to 20 keV. But this reaction has also some disadvantages: a large p-wave resonance at around 240 keV of which shape is difficult to determine, the unisotropic angular distribution of the emitted particles, and the high gamma-ray sensitivities. This reaction has been used for scintillation detectors, surface barrier detectors and ionization chambers. The glass

scintillation detectors with cerium activation become very popular for the neutron time-of-flight spectroscopy, because this detector has the relatively fast time response and large area that can be easily fabricated.

The existing experimental data, which are stored in the NESTOR-2 data file are shown in Fig. 1 together with the evaluation of JENDL-3PR2[5] and ENDF/B-5[6]. The experimental data taken after 1970 are given in the figure from 1 keV to 2 MeV. Some of the old data do not agree well in the shoulder of the p-wave resonance. The several new data taken after 1980 are not included in this figure. Overall agreement between the data below 100 keV is sufficiently good as the standard.

The references and some informations of these experiments are listed in Table 2. The complete reference list may be found in the previous review papers. The second column shows the neutron sources used and the third column give the method to determine the absolute neutron flux. The experiments using the manganese sulphate bath and the gray detector are considered to be absolute measurements. The other experiments are based on other standard cross sections such as the hydrogen scattering and ^{235}U fission cross sections. The last column gives the sample shape or detection methods. Almost all measurements were carried out using the ^{6}Li-glass.

In recent years, many measurements of the $^{235}U(n,f)$ cross section have been made relative to the $^{6}Li(n,\alpha)$ cross sections. Experimental results of the ratios of these two cross section values are shown in Fig. 2. This figure is reproduced from the Poenitz review paper[4]. Remarkably good agreement is obtained (see Reference 2 in detail). At the present, this ratio is one of the best known quantities between thermal and 1 MeV region.

Fig. 3 shows the ratios of the experimental values and the ENDF/B-5 to JENDL-3PR2 from 1 keV to 2 MeV. Since some of the old data are included and the discrepancies of the resonance energies for the 240 keV p-wave level are not taken

into account, the large differences between the data and evaluations are observed. The values of the ENDF/B-5 are lower than JENDL-3PR2 by about 1 % even in the low energy region. In the higher energy region above 100 keV, this difference increases by as much as 15 %. In the JENDL evaluation, the (n,α) cross section was calculated with the R-matrix theory below 1 MeV using the data by Macklin et al.[7], together with the total cross section by Smith et al.[8], and elastic cross section by Knitter et al.[9]. The calculated thermal cross sections is 940.33 barn while those of the ENDF/B-5 and ENDF/B-6 evaluations are 936 barn[2] and 935.9 barn[4], respectively. This may cause some significant effect to the calculation of the fusion reactor neutronics.

3. The status of the ^{10}B(n,α) and ^{10}B(n,$\alpha\gamma$) cross sections

The ^{10}B(n,α) cross section is the sum of the cross sections for the reactions ^{10}B(n,α_0)^{7}Li and ^{10}B(n,α_1)^{7}Li. These reactions have Q values of 2.792 and 2.314 MeV, respectively. The values of the ^{10}B(n,α) thermal cross section was measured very accurately in several experiments. The smooth and 1/v behavior of the ^{10}B(n,α) reaction continues up to the 50 keV, where the contributions from several resonances at 250, 350 and 510 keV become significant.

The ^{10}B(n,α) reaction has been used for proportional counters, ionization chambers and solid state detectors. Especially, the BF_3 proportional counter has been widely used for slow neutron detection. The combination of a BF_3 counter and a cylindrical moderator has been used as the flat response detector. The gamma-rays of 478 keV emitted from the ^{10}B(n,$\alpha\gamma$) reaction can be easily detected with gamma-ray detector such as NaI and Ge detectors. This geometry independent detection system is conveniently used for many neutron experiments.

The existing experimental data of the ^{10}B(n,α) cross section from the NESTOR2 file are shown in Fig. 4, together with the evaluations of JENDL-2[10] and the ENDF/B-5. As

pointed out by the previous review papers, few experimental results for these reactions have been obtained in the last several years. The references and some information for $^{10}B(n,\alpha)$ and $^{10}B(n,\alpha\gamma)$ are given in Tables 3 and 4, respectively. In some experiments, flat response detectors such as a long counter and a graphite sphere detector were used to determine the absolute neutron flux, the other experiments are based on other standards such as hydrogen scattering and $^{6}Li(n,\alpha)$ cross sections. The experiments made by Macklin[11] used the inverse reaction of $^{7}Li(\alpha,n)^{10}B$ to calculate the $^{10}B(n,\alpha)$ cross section. As the sample or the counter, the BF_3 and ^{10}B thin film were used to detect charge particles with the solid state detectors.

Fig. 6 reproduced from the paper by Poenitz[4] indicated the tremendous discrepancies between the experimental values and the evaluation above 200 keV for the $^{10}B(n,\alpha)$ cross section. Recent data differ by as much as 40 % from ENDF/B-5. According to the INDC/NEANDC Nuclear Standard File[12], this value is considered to be standard from thermal up to 200 keV.

Figs. 7 and 8 show the ratios of the experimental values and ENDF/B-5 to JENDL-2[10] for the $^{10}B(n,\alpha)$ and the $^{10}B(n,\alpha\gamma)$, respectively. The value of the ENDF/B-5 for $^{10}B(n,\alpha)$ reaction is higher than JENDL-2 by about 1 % in the low energy region below 100 keV. On the other hand, the value of ENDF/B-5 for $^{10}B(n,\alpha\gamma)$ is in good agreement with JENDL-2. The data of JENDL-2 are based on the measured values of Sowerby et al.[13] below 235 keV, and above that energy, the recommended value of ENDF/B-4 was adopted. The thermal cross section in the JENDL-2 file 3836 barn is in good agreement with those from ENDF/b-5 (3836.6 barn) and ENDF/B-6 (3838 barn).

4. Methods for calculation of detector efficiencies of ^{6}Li-glass and ^{10}B-NaI detector

The Monte Carlo program was developed to calculate the relative efficiencies of the flux detector for capture cross section measurements in the JAERI linac. The computer program

is called ELIS[14]. The detectors are a 11.1 cm diameter x 0.635 cm thick ^{6}Li-glass, which was supplied from Nuclear Enterprise Co., and the ^{10}B-NaI, which used the 0.058 atoms /barn metallic boron powder enriched to 93 %. The calculation is based on the standard cross section in the evaluated files of JENDL-2 for ^{6}Li(n,α) cross section and ENDF/B-5 for ^{10}B(n, $\alpha\gamma$) cross sections. The calculation also takes into account the multiple scattering effects due to the other scintillator constituents such as ^{7}Li, O and Si, and ^{11}B. Table 5 shows the nuclear contents for both detector systems and the photomultiplier window. Fig. 8 gives the calculated macroscopic total cross sections for various constituents. Fig. 9 shows the macroscopic cross sections for the ^{6}Li(n,α) reaction and the summed total cross section of the ^{6}Li-glass scintillator. The calculation of resonance shapes is based on the multi-level Breit-Wigner formula using the resonance parameters in BNL-325.

The relative efficiencies of the ^{6}Li-glass scintillator and ^{10}B-NaI are shown in Fig. 10. The peaks due to the scattering from Al, Si and O are observed in the efficiency curve for ^{6}Li-glass. Neutron flux shapes measured with two detectors systems are compared in Fig. 11. The structures observed in the spectra are due to the beam filters such as Na to normalize background , Pb to reduce gamma-flash and BN (Boron nitride) to absorb overlap neutrons. Although the spectrum shapes around 300 keV are quite different due to inadequacy of the multiple scattering calculation for the 240 keV resonance of ^{6}Li(n,α) reaction. Overall agreement is satisfactory within 2 - 3 % below 100 keV region.

5. Summary

As to the present status of these standard reactions, ^{6}Li + n and ^{10}B + n, the situation below 100 keV is reasonably well. The estimated uncertainties of the ENDF/B-5 are 1 % or less below 30 keV and increase to 2 % at 100 keV for the ^{6}Li(n, α) cross section, and 0.8 % and 0.7 % below 100 keV for the

$^{10}B(n,\alpha)$ and $^{10}B(n,\alpha\gamma)$ cross section, respectively. However, efforts are still needed to establish more accurate standards above 100 keV region.

In the ENDF/B-6 file[15], standard cross sections will be based on the simultaneous evaluations with the comprehensive R-matrix analysis, coupling all the experimental data such as total, elastic, (n,α), $(n,\alpha\gamma)$ and so on. Their analysis also combines other many standard cross sections from the H(n,n)H, ^{197}Au capture and ^{235}U fission as well as ^{6}Li + n and ^{10}B + n, taking into account the variance-covariance matrix information.

In the past, it seems that the standard cross sections in the JENDL evaluations have sometimes relied on the ENDF evaluations. Since to produce the accurate standard data files is extremely important, it is clear that much efforts have to be made for the JENDL-3 evaluations.

References

1. H. Derrien and L. Edvardson, Proc. Conf. on Neutron Standard and Applications. NBS Pub. 493. 14 (1977)
2. A.D. Carlson, Progress in Nuclear Energy. vol. 13. No. 2/3, 79 (1984)
3. P.G. Young and L. Stewart, Progress in Nuclear Energy, vol. 13, no. 2/3, 193 (1984)
4. W.P. Poenitz, Proc. of Advisory Group Meeting on Nuclear Standards Reference Data, 112 (1984)
5. K. Shibata, JAERI-M 84-194 (1984)
6. G.M. Hale et al., ENDF-201 (1979)
7. R.L. Macklin, R.W. Ingle and J. Halperin, N.S.E. 71, 205 (1984)
8. A.B. Smith et al., ANL/NDM-29 (1977)
9. H.-H, Knitter et al., EUR 5726e (1977)
10. T. Nakagawa(ed.), JAERI-M 84-103 (1984)
11. R.L. Macklin and J.H. Gibbons, Phys. Rev. 165 (1968) 1147
12. Nuclear Data Standards for Nuclear Measurements, 1982 INDC/NEANDC Nuclear Standards File, Technical Reports Series, No 227
13. M.G. Sowerby et al., AWRE-6316 (1973)
14. M. Sugimoto and M. Mizumoto, JAERI-M 82-193 (1982)
15. A.D. Carlson, W.P. Poenitz, G.M. Hale and R.W. Peelle, Proc. of Advisory Group Meeting on Nuclear Standards Reference Data, 77 (1984)

Table 1 Standard cross section for neutron capture measurements

Reaction	Energy range	Detection method
H(n,n)H	1 keV - 20 MeV	Recoil proton
$^{6}Li(n,t)^{4}He$	Thermal - 100 keV	Scintillation (glass), Surface barrier detector and ionization chamber
$^{10}B(n,\alpha)^{7}Li$	Thermal - 200 keV	Ionization chamber, surface barrier detector or scintillators
$^{10}B(n,\alpha_0+\alpha_1)^{7}Li$	Thermal - 200 keV	478 keV γ ray emission
$^{197}Au(n,\gamma)^{198}Au$ (In and Ta)	0.2 MeV - 3.5 MeV	Prompt γ ray detection and activation
$^{235}U(n,f)$	0.1 MeV - 20 MeV	Fission chamber

Table 2 Recent $^{6}Li(n,t)^{4}He$ measurements

Reference	Source	Flux determination	Sample or detector
Fort (1972)	Van de Graaff	Mn bath	glass
Poenitz (1974)	dynamitron	Gray detector	glass
Friensenhahn(1974)	linac	H(n,n)H	ionization chamber
Gayther (1977)	linac	$^{235}U(n,f)$	glass
Lamaze (1978)	linac	H(n,n)H	glass
Renner (1978)	linac	Thick plastic	glass
Macklin (1979)	linac	$^{235}U(n,f)$	glass
Engdahl (1981)	(γ,n)	Mn bath	^{6}LiF foil
Corvi (1983)	linac	$^{235}U(n,f)$	glass
Weston (1983)	linac	$^{235}U(n,f)$	glass

Table 3 Recent $^{10}B(n,\alpha)^{7}Li$ measurements

Reference	Source	Flux determination	Sample or detector
Davis (1961)	Van de Graaff	long counter	BF_3
Cox (1966)	Van de Graaff	spherical shell transm.	BF_3
Macklin (1968)	Van de Graaff	graphite sphere	$^{6}Li(\alpha,n)^{10}B$
Bogart (1969)	Van de Graaff	long counter	BF_3
Sowerby (1970)	linac	$^{6}Li(n,\alpha)$	BF^3
Friesenhahn (1974)	linac	H(n,n)H	^{10}B film
Sealock (1976)	Van de Graaff		^{10}B film

Table 4 Recent $^{10}B(n,\alpha\gamma)^{7}Li$ measurements

Reference	Source	Flux determination	Sample or Detector
Davis (1961)	Van de Graaff	long counter	BF_3
Macklin (1968)	Van de Graaff	graphite sphere	$^{7}Li(\alpha,n)^{10}B$
Nellis (1970)	Van de Graaff	long counter	^{10}B cylinder
Coates (1974)	linac	^{10}B vaseline detector	$^{10}B_2O_3$disk
Friesenhahn (1974)	linac	H(n,n)H	^{10}B disk
Sealock (1976)	Van de Graaff		^{10}B
Schrack (1978)	linac	H(n,n)H	^{10}B disk
Viesti (1979)	Van de Graaff	$T(p,n)^{3}He$	$^{10}B_4C$

Table 5 Nuclear contents of ^{6}Li-glass scintillator, a photomultiplier window and a ^{10}B sample.

Nuclei	^{6}Li-glass Scintillator (atoms/b)	Photomultipier window (atoms/b)	^{10}B sample (atoms/b)
^{6}Li	0.0171	-	-
^{7}Li	0.0007	-	-
^{16}O	0.0467	0.0456	-
^{24}Mg	0.0014	-	-
^{27}Al	0.0053	0.0006	-
^{28}Si	0.0140	0.0182	-
^{140}Ce	0.0003	-	-
^{10}B	-	0.0010	0.0581
^{11}B	-	0.0040	0.0048
^{23}Na	-	0.0017	-

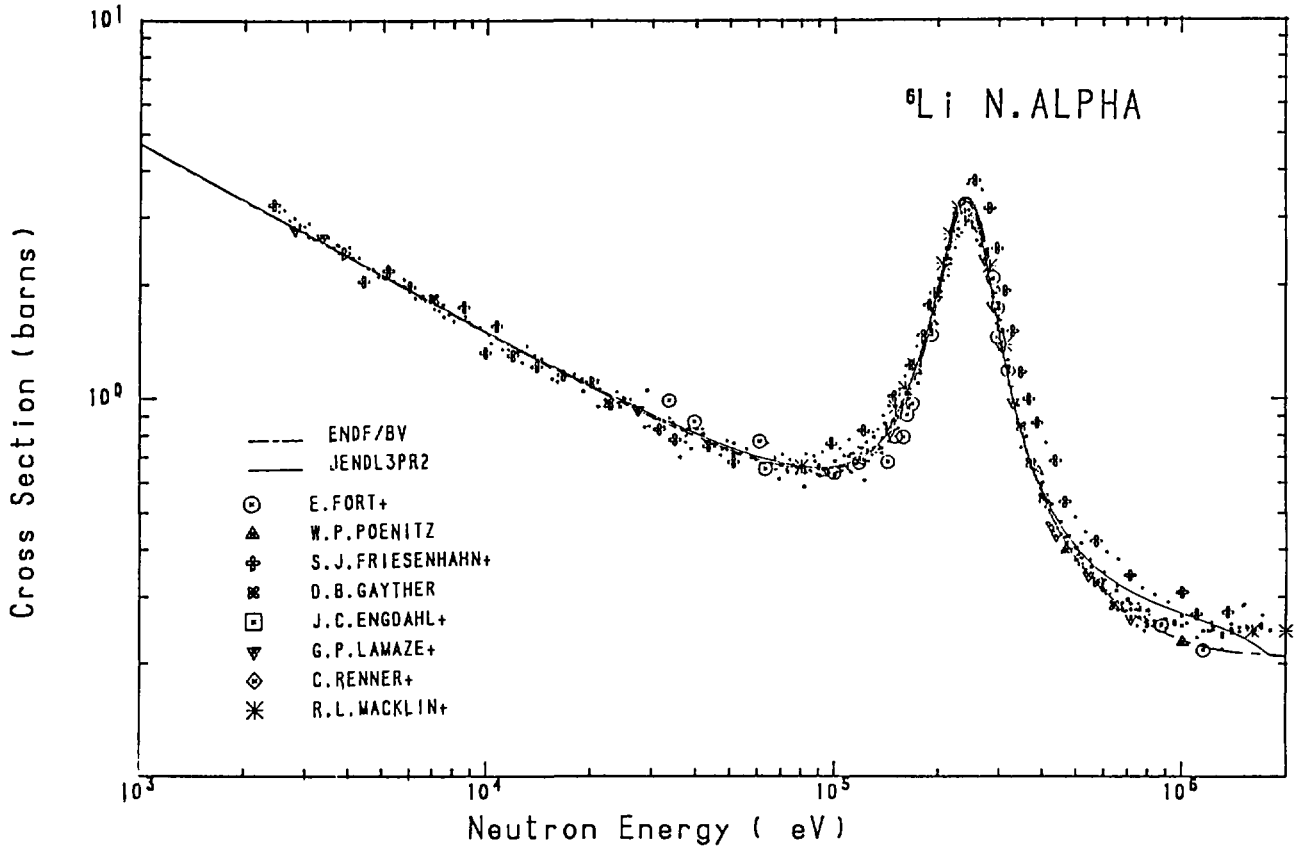

Fig. 1 Comparison of the ^{6}Li(n,α) cross section.

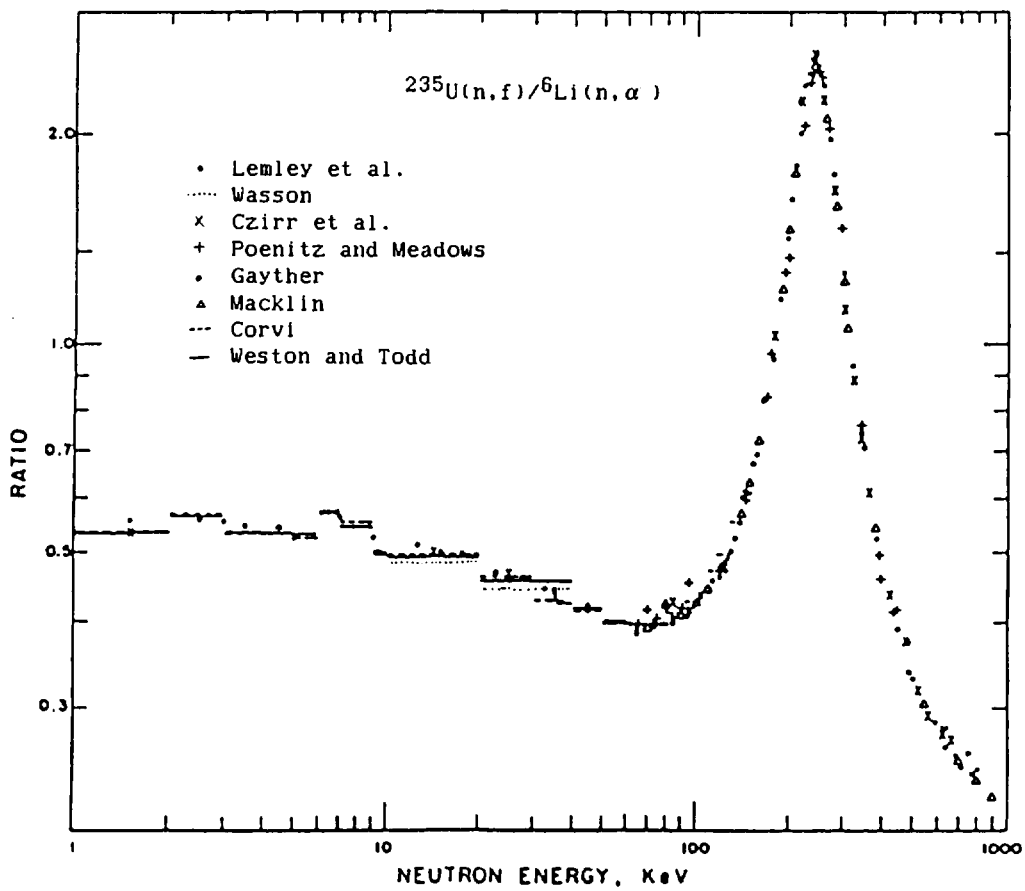

Fig. 2 Comparison of the shape measurements of the ^{6}Li(n,α) /^{235}U(n,f) ratio (Ref. 4)

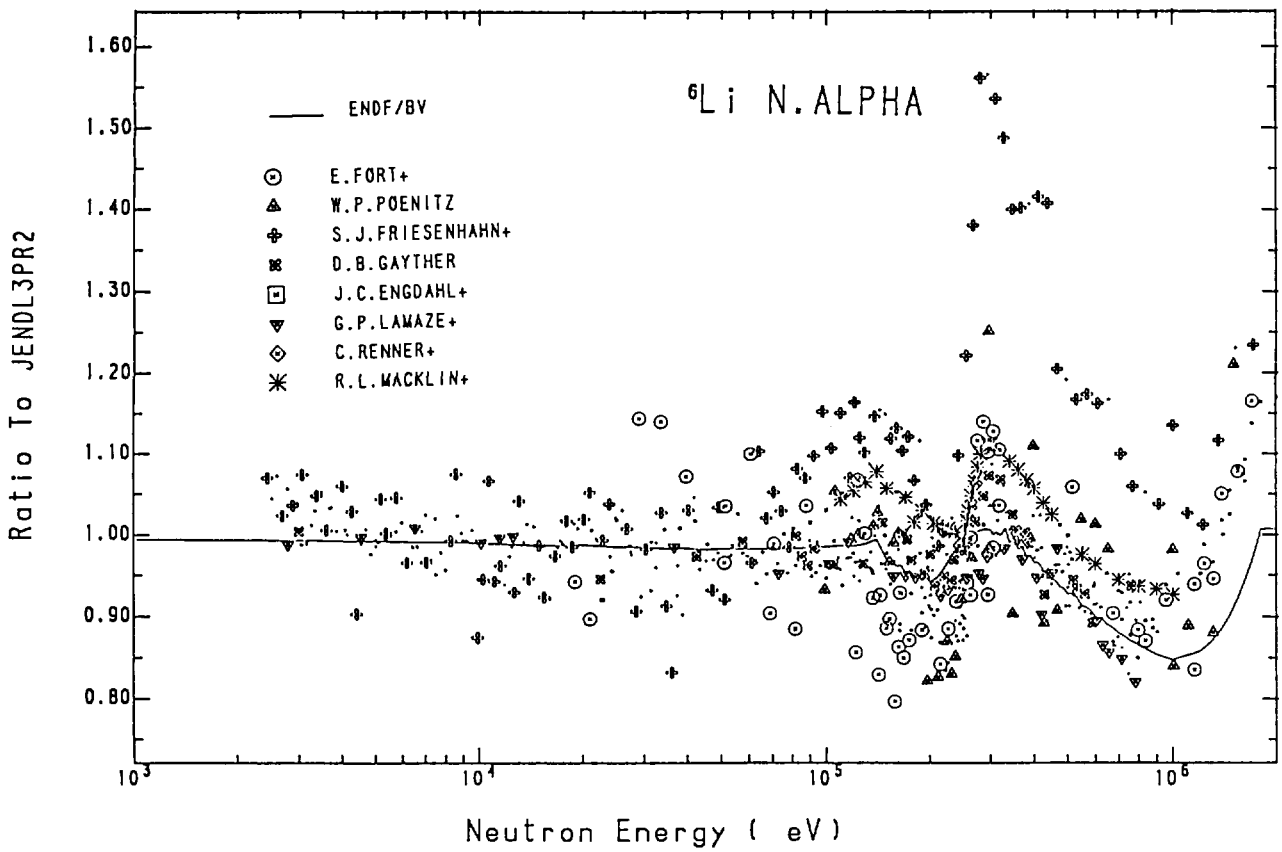

Fig. 3 Ratios of experimental data and ENDF/B-5 to JENDL-3PR2 for the ^{6}Li(n,α) cross section.

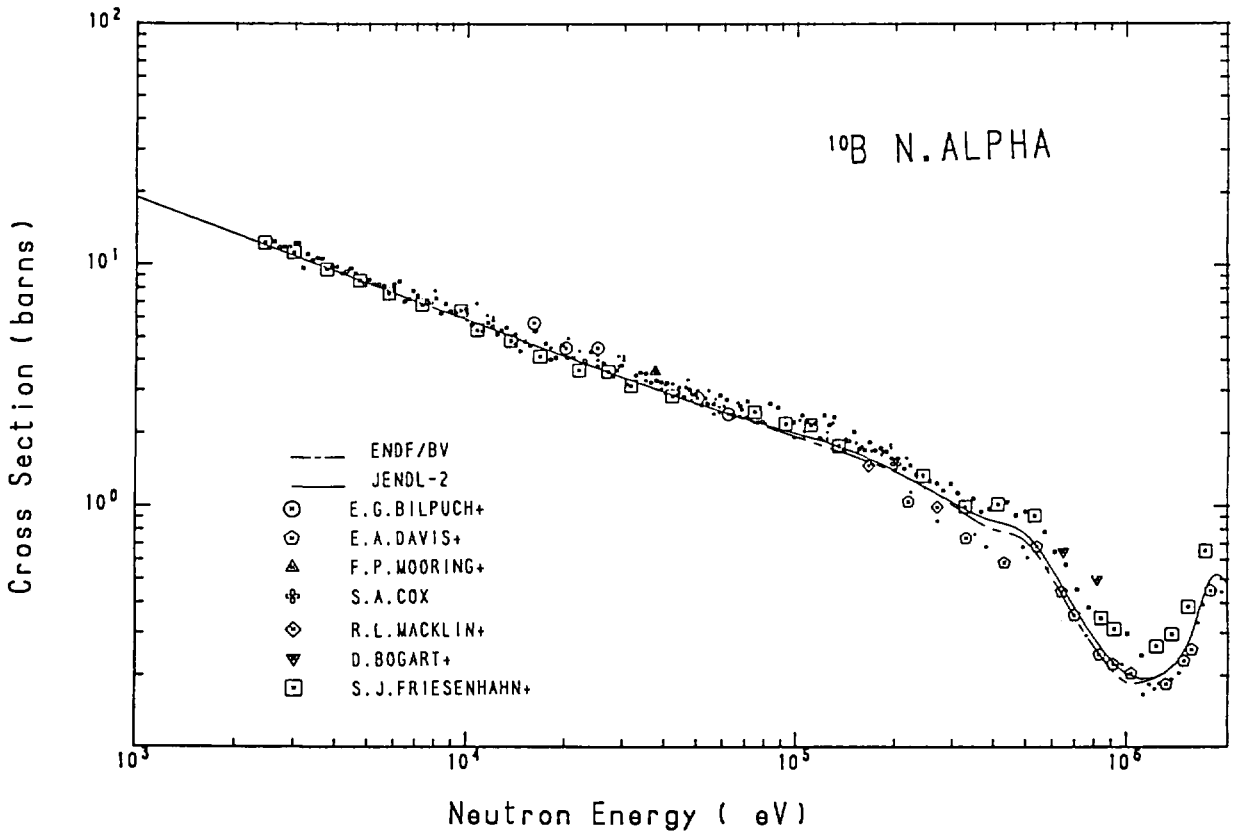

Fig. 4 Comparison of the ^{10}B(n,α) cross section.

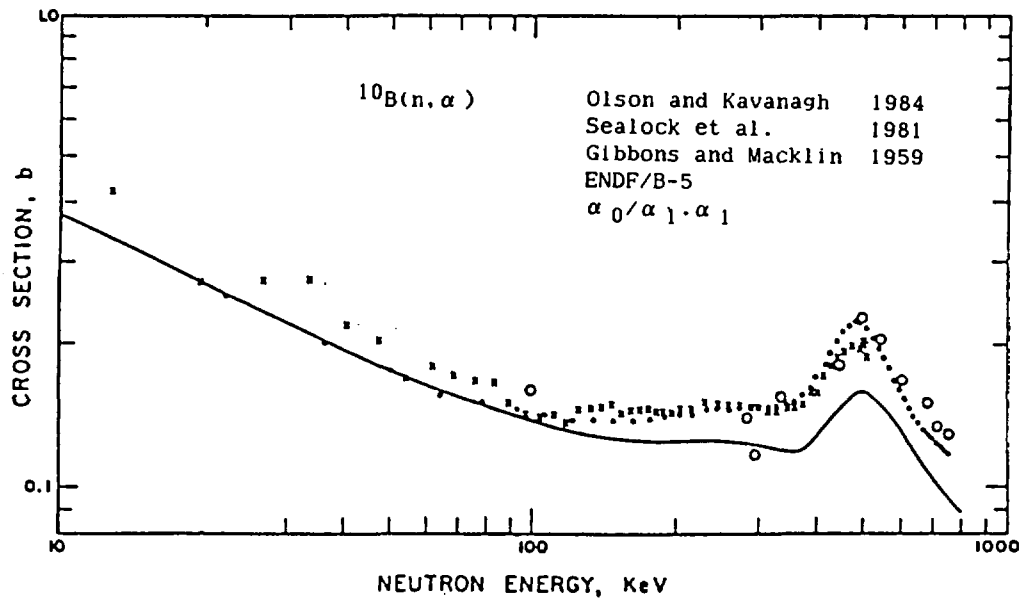

Fig. 5 Comparison of absolute measurements of the $^{10}B(n,\alpha)$ cross section. (Ref.4)

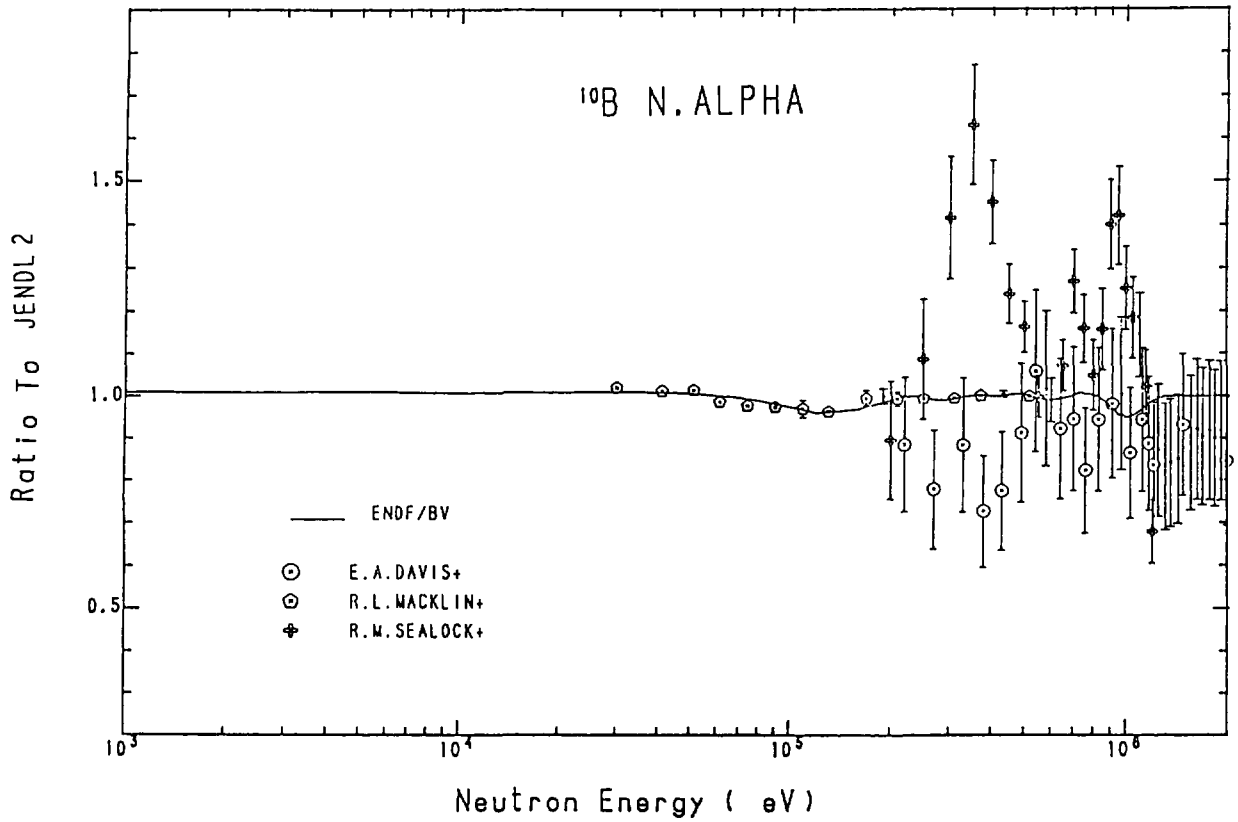

Fig. 6 Ratios of experimental data and ENDF/B-5 to JENDL-3PR2 for the $^{10}B(n,\alpha)$ cross section.

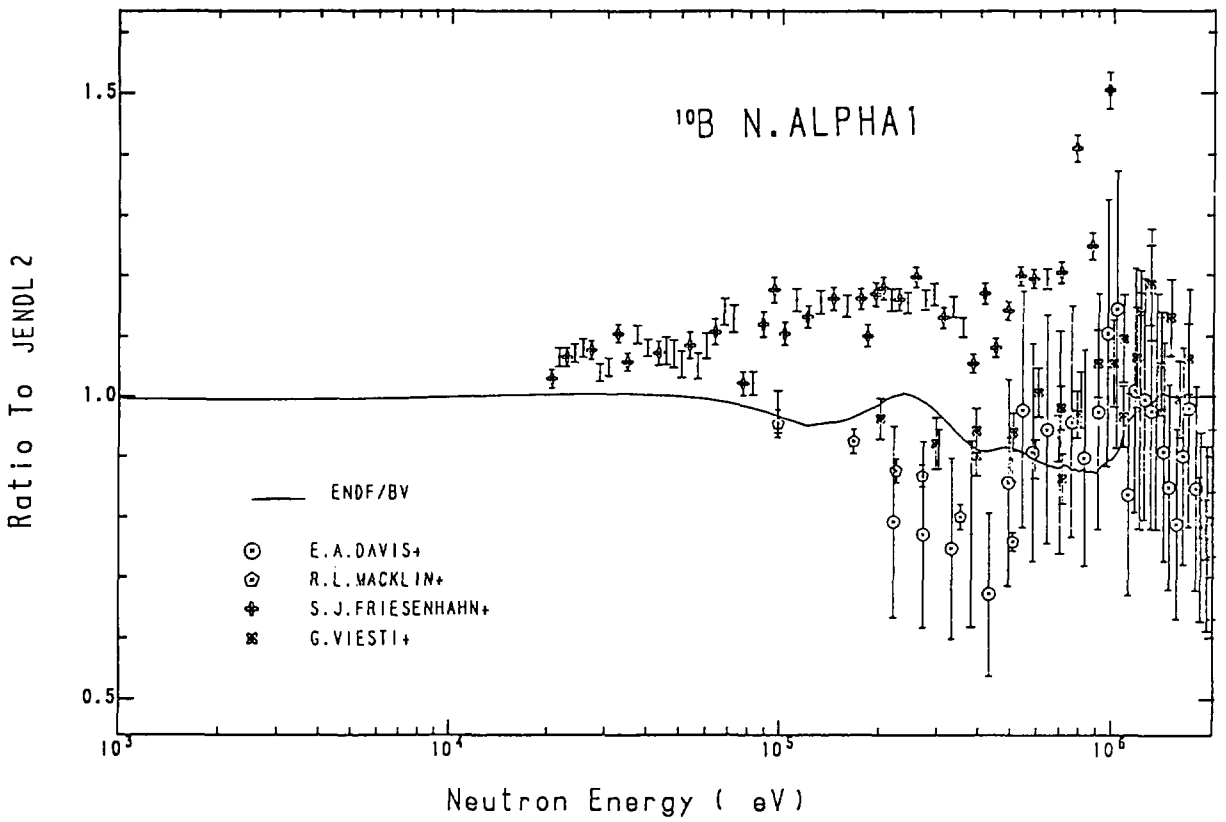

Fig. 7 Ratios of experimental data and ENDF/B-5 to JENDL-3PR2 for the $^{10}B(n,\alpha\gamma)$ cross section.

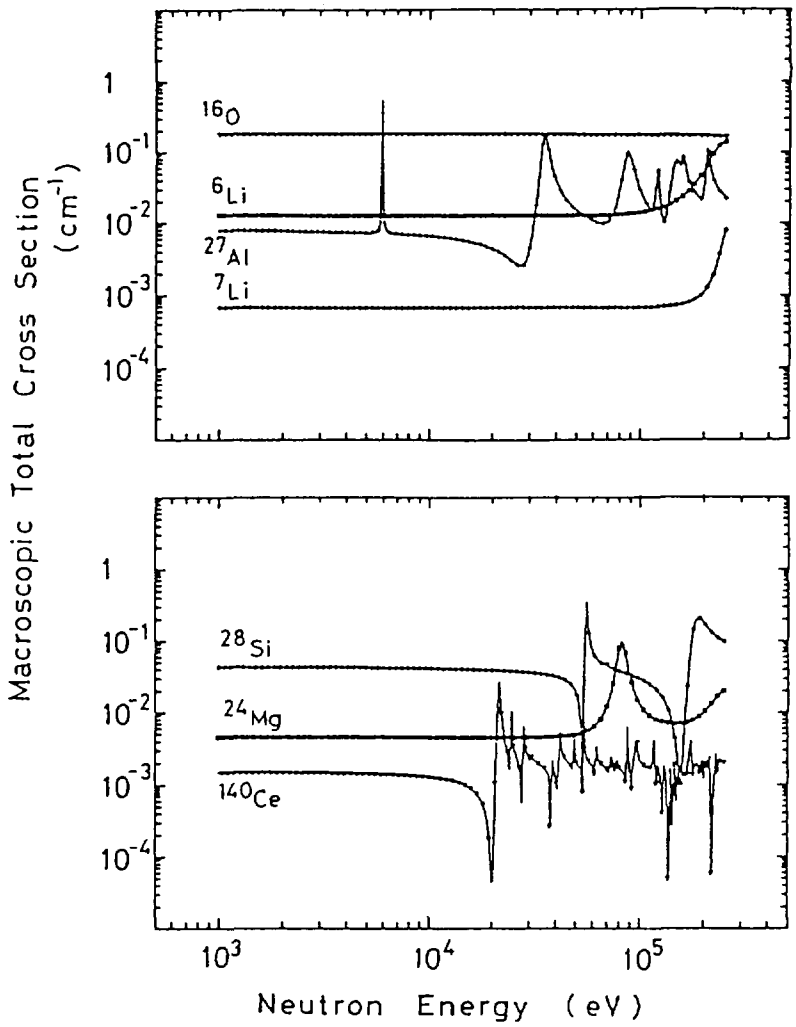

Fig. 8 The calculated macroscopic cross sections for the $^{6}Li(n,\alpha)$ reaction and constituents of the Li-glass scintillator.

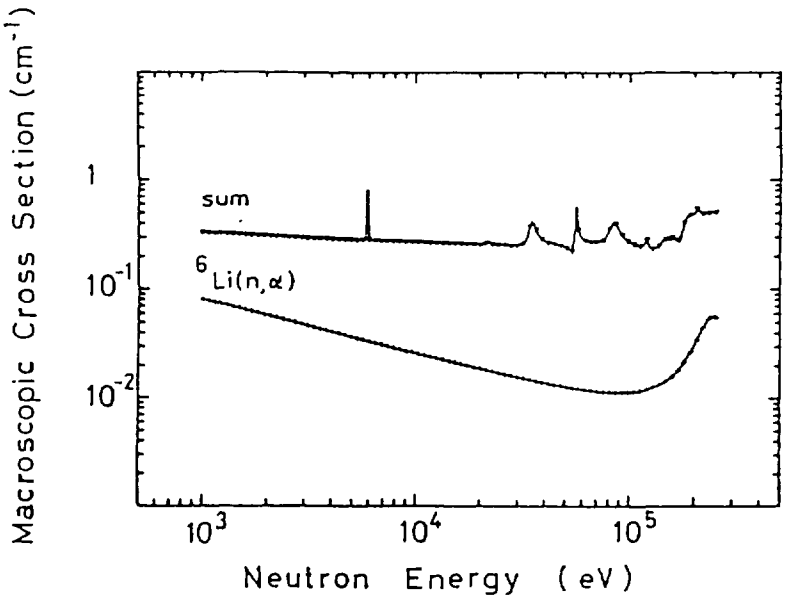

Fig. 9 The calculated summed cross section and $^{6}Li(n,\alpha)$ cross section.

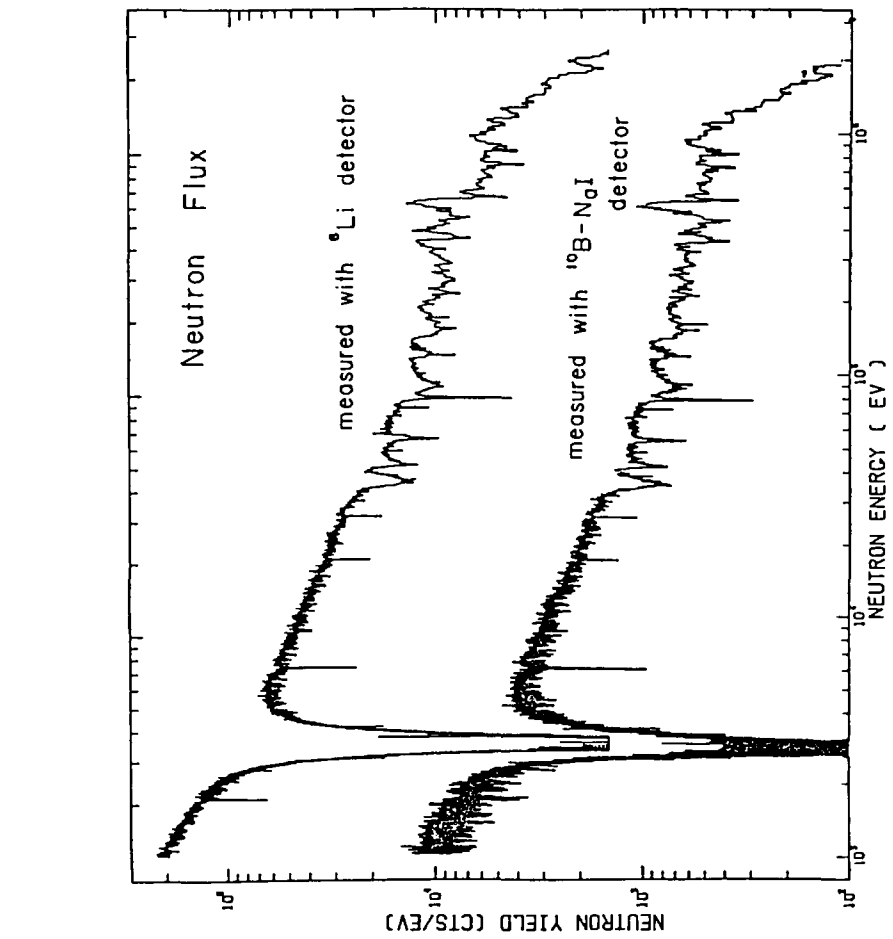

Fig. 11
Neutron flux shapes deduced by the calculated detector efficiencies of ^{6}Li-glass and ^{10}B-NaI. The structure observed in the figures are due to the beam filters such as Na, Al and Pb.

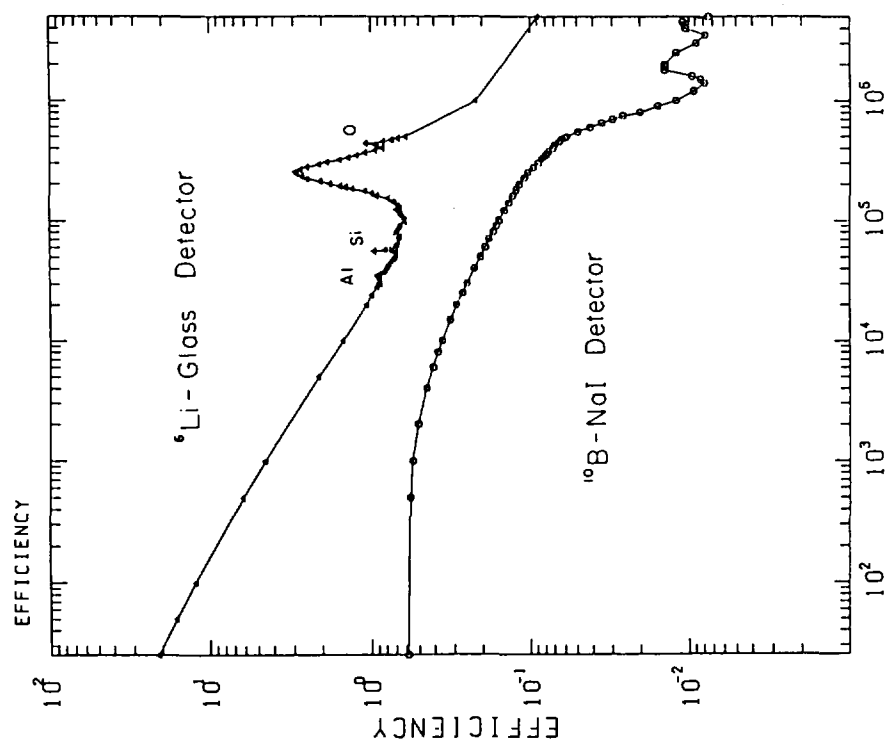

Fig. 10
Relative efficiencies of ^{6}Li-glass and ^{10}B-NaI detectors.

4.4 Difficulties in the Absolute Measurement of Fission Cross Sections

Naohiro Hirakawa
Tohoku University, Sendai, Miyagi

Difficulties when we plan to make an absolute fission cross section measurement with the present facility will be explained.

First, the status of the fission foils now used in the experiment are compared with those in the foreign laboratories and the necessity to develop a technique to fabricate thicker foil on a thin backing is stressed. Then, the techniques which can be used when we had enough quantities of samples are discussed. The reviewed techniques are : Poenitz's associated activity method, Time correlated associate particle method (TCAPM) of Wasson's, TCAPM of Arlt's, Reference to n-p scattering cross section of Barton's and the Black neutron detector of Wasson's. Last, the absolute measurement carried out for ^{238}U, ^{232}Th and ^{237}Np fission cross sections around 14MeV with the foil activation method is presented.

1. Introduction

We have measured fast neutron fission cross sections of actinoid elements relative to ^{235}U with the 4.5MeV Dynamitron Accelerator. In this case, the accuracy of the measured cross section is governed by the accuracy of ^{235}U fission cross section. Therefore, the evaluation people ask us to make the absolute measurement of ^{235}U. Here, I would like to explain why we are hesitating the absolute measurement.

To make an absolute measurement, it is necessary to make the following measurement and corrections.

(1) the measurement of the number of fissions,
(2) the assay of the amount of fissile materials,
(3) the measurement of the incident neutron flux,
(4) corrections.

Item (1), (2) and many of the (4) are also necessary in the relative measurement, but for the absolute measurement of ^{235}U fission cross section, special attention and technical development are necessary.

Table 1 shows the present uncertainties in the ^{235}U fission cross sections[1]. Therefore, the absolute measurement should be carried out within

3% in accuracy. Fig.1 shows the construction of the fission chamber which we are now using. Fission samples are placed at the center of the stainless steel case of 0.5mm thick. The fission deposit is electroplated on a platinum plate of 0.3 or 0.4mm thick. Its diameter is 25mm. Table 2 shows the fission foils we have used in the experiment. Generally, the thickness is about 100μg/cm^2 and the total amount is about 500μg. With these foils, we usually need several hours to obtain 10^4 counts at the position 5-7 cm apart from the target. But in the absolute measurement, the distance between the target and the sample, beam spot size at the target are restricted, and in the case of electrostatic machine, the neutron characteristics might change with time because of the target depletion, machine time cannot be extended too long. So if we want to attain the statistical error well within 1%, the thickness of the deposit should be substantially thicker, or we have to use the multi-plate fission chamber. Table 3 shows the characteristics of the fission foils used in the absolute fission measurement in the foreign laboratories. They are thicker or multi-plate chambers. Also, their backings are generally very thin, and since the attenuation between the sample deposit and the detector to measure the neutron flux should be corrected in the absolute measurement, this is very important. Since we do not have the experience in making thick homogeneous deposit on a thin backing, if we try to make tha absolute measurement, it is necessary to develope the technique.

Table 4 shows the corrections and associated uncertainties reported by Arlt[2]. Their corrections for the fragment absoption and the associated uncertainty is rather large. In our case of 100μg/cm^2 of fission foil, this correction is about 0.5% and the uncertainty is about 0.2%. Also the correction in the item extrapolation to pulse height zero should be smaller. So we have to make some trade off between the statistics and these corrections before making the experiment.

2. Assay of the Amount of Fissile Materials

The comparison of the assay with different techniques has been carried out in many laboratories and it is said that with the α counting method, it is possible to obtain the uncertainty of 0.3%[1]. However, as in the case in Table 4[2], the uncertainty of 0.93% is reported. However, in our foil which has been used until recently, the ^{235}U enrichment was about 93%, and it contained about 1% of ^{234}U. In this case, 96% of the α rays are emitted from ^{234}U and it was impossible to rely on α assay.

Therfore, we determined the assay with the thermal neutron irradiation at the D_2O thermal column of the Kyoto University Research Reactor. In this case, the uncertainty is governed by the thermal neutron cross section of ^{197}Au and ^{235}U, weight of Au foil, the estimation of the neutron flux attenu ation as well as the uncertainties of the extrapolation to zere pulse height and the self absorption. And the overall uncertainty was 1.6%. Thus this foil is inappropriate to make the absolute measurement. Recently, we obtained the sample of 99,9% enrichment and it contained only 0.03% of ^{234}U. In this case, 56% of α rays are from ^{235}U and it is possible to make the assay with less than 1% in uncertainty. However, the total amount now we have is 2mg and to make the absolute measurement, it is necessary to obtain more sample.

3. Determination of Incident Neutron Flux

If we had enough sample materials and necessary techniques in making the sample deposit, what difficulties exist in making the absolute fission measurement? There are following techniques for the measurement of incident neutron flux.

(1) Associated activity
(2) Time correlated associated particle method (TCAPM)
(3) Relative to H(n,p) cross section
(4) Black neutron detector method
(5) Bath technique.

3.1 Associated Activity

This method was applied by Poenitz[3]. He made spherical counters which sorround the vanadium target. Neutrons are produced by $^{51}V(p,n)^{51}Cr$ reaction. The quantity of the produced number of neutrons was obtained by measuring the γ activity of ^{51}Cr with a NaI detector. The efficiency of the detector was calibrated with the specially prepared standard ^{51}Cr source. His fission foils were thin but the large coated area of $180cm^2$ compensating the thinness(Fig.2). If we try to follow his experiment, the fabrication of the spherical chamber of wall thickness of 0.25 or 0.5mm is rather demanding. Also the calibration of the detector is not easy. Considering his corrections by the scattered neutrons and room return background are relatively large, it looks difficult to make the experiment within the required accuracy.

3.2 Time Correlated Associated Particle Method

Now the time correlated associated particle method becomes main method for the absolute measurement since this method directly determines the incoming neutron flux[4,5]. Fig.3 shows the experiment carried out by Wasson for 14.1 MeV neutrons. In TCAPM, the neutron flux is directly determined by measureing the number of α particles emitted to the opposite cone to the neutrons. To determine the cone precisely, the beam was limited to 3mm in diameter with the aperture. Since the neutrons corresponding to the counted α particles should pass the sample deposit, the sample deposit should be larger than the neutron flux cone and the deposit should be homogeneous. The fission cross section is basically given by Eq. (1),

$$\sigma = Y_{\alpha,f} / Y_{\alpha}.n \qquad (1)$$

where $Y_{\alpha,f}$: net coincidence count,

Y_{α} : net α yield,

n : areal density of ^{235}U given in unit of atoms/barn.

Since the n in the denominator is areal density, they measured the homogeneiety of the foil with the thermal neutron flux from a reactor of 1mm in diameter. Also, they determined the mass of the sample deposit by the thermal neutron irradiation with the reference ^{235}U foil and it was determined with the uncertainty of 0.3%. This is out of the reach of our present situation.

It is reported that their count rate of α rays was 2×10^4/s and the coincidence rate was 300 counts/h with 2 layers of foils with 500μg/cm^2 in areal density. They reported, to obtain the 0.9% of statistical error, they made 28 runs of 3-4 hours for each run. During the experiment, the tritium in the target was depleted and the neutron cone was changed. To avoid this, they had to change the target 10 times during the experiment. If it is necessary to exchange the target so often, it is quite a work because the exchange of the tritium target should be carried out in the hood outside of the target room according to the regulation of radiation protection. Also we do not have the experience for TCAPM and the technique must be developed. But if we make 100 hours of experiment with the count rate of 2×10^4 cps, the total count of the α detector reaches 10^{10} counts which exceeds the limit of radiation damage to the charged particle of a semi-conductor detector and the special attention may be necessary. The corrections and their uncertainties of their experiment are shown in Table 5.

If the handling of tritium target were difficult, the experiment with $D(d,n)^3He$ reaction can be considered. And this was carried out by the group

of Technical University of Dresden and Khlopin Radium Institute[2,6]. The set up of their experiment is shown in Fig.4. The radius of the vacuum chamber was about 40cm. The beam spot size was 3mm in diameter. In their experiment, background from D-d reaction other than the target, pile up of scattered deuterons and α particles caused by $^{12}C(d,n)$ reaction are significant, therfore, they used 2 semi-conductor detectors as the telescope and utilized the particle identification circuit. The fission chamber was a multi-plate type. The target was $(CD_2)_n$ foil and it was rotated with 2-4Hz. Therefore, the experimental arrangement was quite elaborate. And if we try to make this kind of experiment, a lot of developmental work will be required.

3.3 Reference to n-p Scattering Cross Section

As for the experiment which uses n-p scattering cross section as the reference, the proton recoil proportional counter or the counter telescope technique are usually employed[7,8,9]. But there is the novel method of Barton[10] which free from many of the corrections. They constructed a vacuum chamber shown in Fig.5. A ^{235}U foil and a polyethylene film were placed back to back 10cm from the target. In front of the ^{235}U foil, a semi-conductor detector was placed and it detected nearly 90% of the fission fragments. For the side of the polyethylene film, a Si proton detector was placed at the back of a platinum aperture 10 cm from the samples, and it detected only protons emitted to 0° to the incoming neutron beam.

Then the cross section ratio σ_{nf}/σ_{np} is given by Eq.(2),

$$\frac{\sigma_{nf}}{\sigma_{np}} = \frac{C_F N_p \Omega_p}{C_p N_U \Omega_F} \qquad (2)$$

N_p is given by measuring the weight of the polyethylene film, then, if we could evaluate $\Omega_p/N_U\Omega_F$, σ_{nf}/σ_{np} is determined. To obtain $\Omega_p/N_U\Omega_F$, they irradiated the equipment in a thermal column with exchanging the polyethylene film into the reference ^{235}U film. Since the fission fragments detected by the proton detector are those emitted 0° to the neutron beam, and these fission fragments are not stopped in the sample deposit, the ratio of the count rates of the two detectors is given by Eq.(3),

$$R = \frac{2N_s\Omega_p}{N_U\Omega_F} \qquad (3)$$

where N_s is the number of atoms in the reference ^{235}U foil. Then, $\Omega_p/N_U\Omega_F$ is determined and we could know the cross section ratio.

Although the corrections for the anisotropic emission of fission fragment

for the anisotropy of the recoil protons and the neutron inscatter are necessary in this experiment, the anisotropic effects are relatively small especially at low energy. Actually they obtained the fission cross sections between 1 and 6 MeV with the systematic uncertainties between 0.1 and 1.2%. If we try to make this experiment, it is necessary to obtain the standard ^{235}U foil, a homogeneous polyehtylene film and to make the calibration at a thermal column, but the high accuracy is expected compared with other techniques with relatively smaller effort.

3.4 Black Neutron Detector

Black Neutron Detector (BND) is mainly used in the Linac TOF experiment. Recently, Wasson reported the experiment carried out with Van de Graaff[11]. The neutron producing reaction was $^{7}Li(p,n)^{7}Be$. Fig.6 shows the experimental geometry used in their experiment. The efficiency of the BND was calculated with Monte Carlo technique and it was confirmed by TCAPM. The Monte Carlo result was considered to be correct to $\pm$1%. The most remarkable thing of the experiment was the fission chamber which was composed of 10 layers of 18cm x 10cm square fission foils. It is reported that if the Li target were irradiated for 12 hours with the average beam current of 3.5μA, the neutron energy changes due to the target depletion, therefore, it was necessary to restrict the experimental time of one run to about 10 hours. The count rate of the fission chamber is reported to be about 500 events/h with such a big fission chamber. Also there are relatively many corrections and uncertainties. Although we have the experience to construct a BND[12], to make the experiment, the improvement of the BND is necessary, but considering the counting statistics and the corrections and the amount of the fission sample, this is not an attractive experiment for us.

3.5 Bath Technique

This method was once used by Poenitz[3] as vanadium bath. The set up of the experiment was similar to the BND method but the neutron is detected with the γ activity of 1.4 MeV which is emitted from ^{52}V produced by $^{51}V(n,\gamma)^{52}V$ reaction in the vanadium sulfate solution placed at the position of BND. The number of neutrons entered into the solution was determined by the comparison of the ^{52}V activity with those produced when a standard ^{252}Cf source was placed in the solution. It is reported that the count rate was too low and it took 2 days for the experiment. In anyway this experiment looks unattractive so long as the efficiency of BND cannot be determined with high accuracy.

4. Absolute Measurement for 14 MeV Neutrons

As we have stated above, it is quite difficult to make the experiment within 2% of uncertainty. But, for certain nuclides and energy ranges, we are not required such a high accuracy and it is worthwhile to make the simpler and less demanding experiment. Therefore, we made the absolute fission cross section measurement of ^{232}Th, ^{237}Np and ^{238}U with the foil activation method around 14 MeV[13].

Fission foils and the assay of the amount of the fission samples are the same as those we stated before. The neutron source was T(d,n)^{4}He reaction. The measurement was carried out for the angles of 0°, 70° and 150° to the incoming deuteron beam axis, and the incident neutron energies were 13.49 $\pm$0.08, 14.35$\pm$0.10 and 15.01$\pm$0.10 MeV, respectively. For this energy region, the activity ratio of ^{90}Zr(n,2n)^{89}Zr and ^{93}Nb(n,2n)^{92m}Nb reaction is very sensitive to neutron energy, and the neutron energies were estimated with this ratio.

The experimental set up is shown in Fig.7. We have also used the counter telescope, but the counter telescope in our laboratory is still in developing stage and was not used as the neutron flux monitor. The construction of the fission chamber is shown in Fig.8. This is almost the same as the one which was shown before, but between the two fission foils placed were Au,Ni and Al foils (each 25mm in diameter and 0.2mm thick).

The detector was irradiated for 6-8 hours with DC beam at 10-12 cm from the neutron producing target. We always made 2 experimental runs by exchanging the position of the foils 180° to the center of the detector. By taking the geometrical average of the results of the 2 experimental runs, the corrections of the fission fragments anisotropy, neutron attenuation in the backing and the difference in the foil positions are almost cancel out.

After the irradiation, the activities of ^{24}Na and ^{57}Ni which are produced by ^{27}Al(n,α)^{24}Na and ^{58}Ni(n,2n)^{57}Ni reactions were measured with a pure Ge detector. Then using the cross section of ^{27}Al(n,α)^{24}Na reaction for the energies determined by the ^{89}Zr/^{92m}Nb activity ratio, the neutron flux was determined. The efficiency of the Ge detector was calibrated with the commercial standard γ source and ^{198}Au source calibrated with the 4$\pi\beta$-γ equipment.

Table 6 shows the corrections and associated errors of the present experiment. In our case, due to the thin foils, the corrections of the extrapolation to zero pulse height and the fission fragment loss were considerably small. We took 50% of the corrections as the uncertainties rather arbitrary.

However, the error of the Ge detector efficiency is quite large and this occupies most of the error. Therefore, to improve the present method, it is essential to obtain the reliable standard γ source. Table 7 shows the final results of the present experiment.

5. Acknowledgment

The author wish to express his thanks to Dr. K.Kanda of Tohoku University for his critical review of the manuscript.

References:

1) Sowerby, M.G. and Patrick, B.H.: Proc. Advisory Group Meeting on Nuclear Standard Reference Data: IAEA-TECDOC-335,(Geel,1984) p.135
2) Arlt, R. et al.: ibid p.174
3) Poenitz, W.P.: Nucl. Sci. Eng. 53,370(1974)
4) Wasson, O.A., Carlson, A.D. and Duvall, K.C.: Nucl. Sci. Eng. 68,197 (1978)
5) Cance, M. and Grenier, G.: Nucl. Sci. Eng. 68,197(1978)
6) Arlt, R. et al.: Proc. Conf. on Neutron Cross Sections and Technology, Knoxville (NBS 594) p.990
7) Yuan, H.: Proc. Advisory Group Meeting on Nuclear Reference Data (Geel 1984) p.167
8) Czirr, J.B. and Sidhu, G.S.: Nucl. Sci. Eng. 57,18(1975)
9) Cance, M. and Grenier, G.: CEA-N-2194 (1984)
10) Barton, D.M. et al.: Nucl. Sci. Eng. 60,369 (1976)
11) Wasson, O.A., Meier, M.M. and Duvall, K.C. Nucl. Sci. Eng. 81,196(1982)
12) Sasagawa, M. et al.:NETU 38,53 (1981) (Department of Nuclear Engineering, (Tohoku University)
13) Yoshida, K.: Master Thesis, Department of Nuclear Engineering Tohoku University(1984), In Japanese

Table 1
Uncertainties in $^{235}U(n,f)$
Cross Section[1]

E_n (MeV)	$\frac{\Delta\sigma_{nf}}{\sigma_{nf}}$ (%)
0.1	2-3
1.0	2-3
3.0	2-3
5.0	3-4
8.0	3-4
13	4
14	1.0
15	2
20	6

Table 2 Fission Foils Used at Tohoku University

Nuclide	Atomic %	Areal Density(μg/cm²)	Total Mass(μg)
U-235B	92.649	103.9	510
U-235C	99.9	90.2	443
U-238	99.97	92.6	455
U-233	99.47	115.5	567
U-234	99.07	117.9	579
U-236	88.97	89.9	441
Th-232	100	148.2	727
Np-237	100	18.76	92.1
Am-243	99.66	17.12	87.0
Pu-239	96.75	8.43	41.4

Table 3 Reported Fission Foil Characteristics Used in ^{235}U Absolute Fission Measurement

Experimenter	Areal Density (μg/cm²)	Total Mass (mg)	Backing(mmt)	Method
Poenitz[1]	400	8	Mo (0.13)	
	500	10	Mo (0.13)	
	400	7.811	vyns	BND
	55	10.23	Ag (0.25)	Associated
	75	13.91	Ag (0.25)	Activity
	60	11.24	Ag (0.50)	
	100	0.3856	SUS(0.13)	BND
	400	4.4		
Wasson[4]	520	2.012	Ti(0.006)	TCAPM
Cance & Grenier[5]	103.5	2.93	vyns+Al(40μg/cm²)	
Arlt('79)[6]	256.1		Ni-Cr(0.1)	
Arlt('84)[2]	1773.1		Ni-Cr(0.1)	
	(~400x3)			
	(~250x2)			
Czirr & Sidhu[8]	100x10	160	Al(7mg/cm²)	n-p scattering
Barton[10]	600(0.6μm)	1.9	SUS(0.003)	
Wasson[11]	100x10	170.9	Al(0.025)	BND

Table 4
An Example of Error Contributions and Their Uncertainties[2]

	Corrections	Error Contributions
Fissile layers		
--Areal density		0.93%
--Inhomogeneity		0.72%
Fission chamber efficiency		
--Extrapolation to pulse height zero	1.18%	0.26%
--Fragment absrrption	2.00%	0.85%
Counting coincidences		
--Statistics		1.26%
--Random coincidences	1.40%	0.17%
AP counting		
--Background	2.32%	0.67%
Neutron cone		
--Neutron scattering	0.25%	0.40%
--Effective fission foil thickness due to the cone aperture	0.05%	0.05%

Table 5
Values, Corrections and Uncertainties of Wasson's 14.1MeV TCAPM[4)]

Quantity	Value	Uncertainty in Cross Section Attributable to Uncertainty in Column 2 (%)
$Y(\alpha,f)/Y\alpha$	515.9×10^{-8}	0.9
Neutrons scattered from beam	2.6%	0.3
Fission fragment absorption	3.3%	0.8
Fission spectrum loss	1.5%	0.3
Neutron beam shape and deposit uniformity	1.0017	0.3
Fission in other isotopes	0.1%	---
Reference mass	1546.1 μg ^{235}U	0.1
Reference areal density	500.8 μg/cm^2	0.2
Thermal neutron scattering from platinum backing of reference deposit	2.0%	0.4
^{235}U areal density	1042 μg/cm^2	0.3
Cross section	2.080 b	1.5

Note: The value of each quantity is listed in column 2 and the one standard deviation uncertainty in the cross section resulting from the uncertainty in the quantity is given in column 3.

Table 6 Corrections and Errors in ^{238}U, ^{232}Th and ^{237}Np Fission Cross Section Measurement

Origin	^{238}U		^{232}Th		^{237}Np	
	Corrections	Errors	Corrections	Errors	Corrections	Errors
No. of fissions		0.6-0.8		0.9-1.1		0.8-1.0
---Statistics		0.5-0.7		0.1-0.9		0.7-0.9
---Extrapolation to zero pulse height	0.2-0.6	0.1-0.3	0.5-0.8	0.3-0.4	0.4-0.6	0.2-0.3
---Fission fragment loss	0.4	0.2	0.1	0.4	0.1	0.1
α assay		0.6		1.2		0.7
---Statistics		0.4		0.5		0.3
---Counter geometry		0.3		0.3		0.3
---Relative α activity		0.1		0.1		---
---Half life		0.1		0.5		0.5
Neutron flux		3.7-3.8		3.7-3.8		3.7-3.8
---Statistics		0.7-1.0		0.7-1.0		0.7-1.0
---Ge detector efficiency		3.4		3.4		3.4
---Al foil weight		0.5		0.5		0.5
---$^{27}Al(n,\alpha)^{24}Na$ reaction X-section		1.0		1.0		1.0
---^{24}Na half life		0.3		0.3		0.3
Overall		3.8-3.9		4.0-4.2		3.9-4.1

Table 7 Results of ^{238}U, ^{232}Th and ^{237}Np Fission Cross Section Measurement (barn)

Neutron Energy (MeV)	^{238}U	^{232}Th	^{237}Np
13.49±0.08	1.096±0.043	0.311±0.013	2.265±0.092
14.35±0.10	1.167±0.045	0.351±0.015	2.197±0.089
15.01±0.10	1.208±0.046	0.375±0.015	2.236±0.087

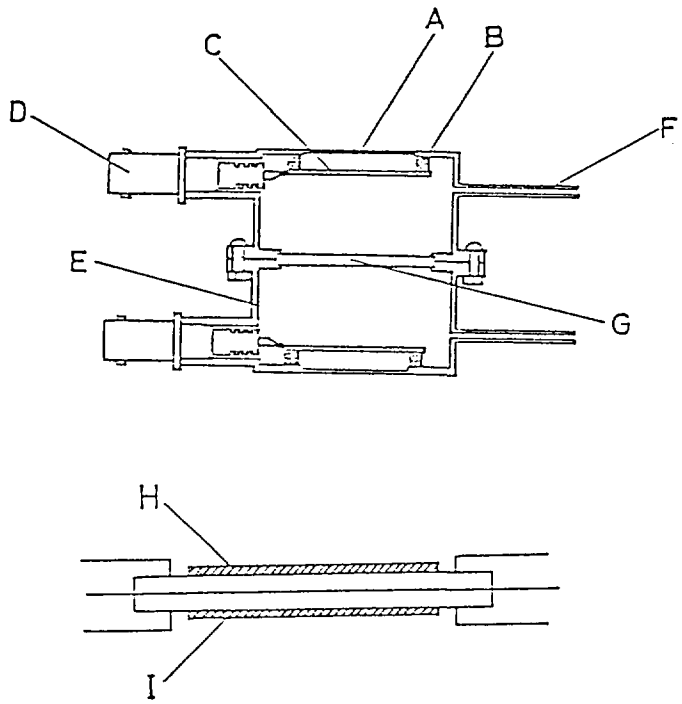

A stainless steel window (0.5 mm-t)
B electric insulator (ceramics)
C collector electrode (stainless steel,0.5 mm-t)
D HV connector
E stainless steel wall (1 mm-t)
F gas flow pipe
G fission samples
H U-235 sample
I X sample

Fig.1 Construction of fission chamber used at Tohoku University

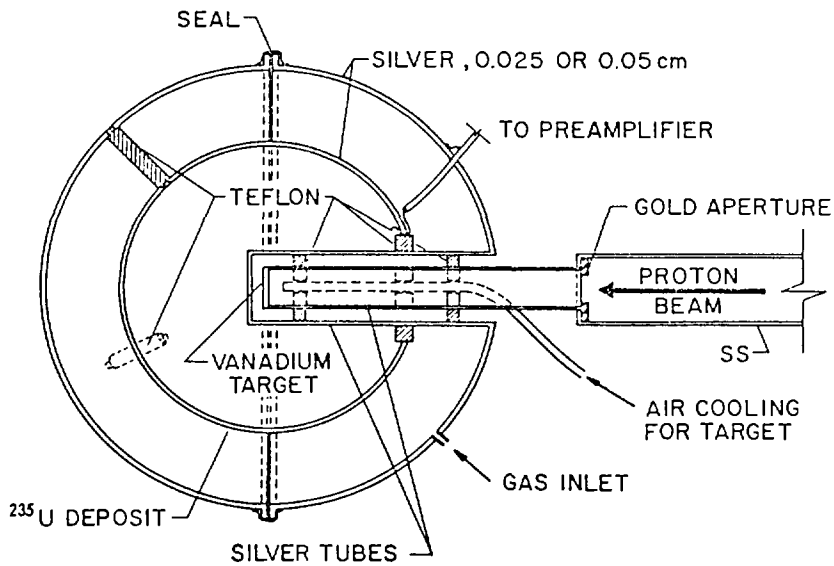

Fig.2 Poenitz's spherical counter for associated activity measurement[3].

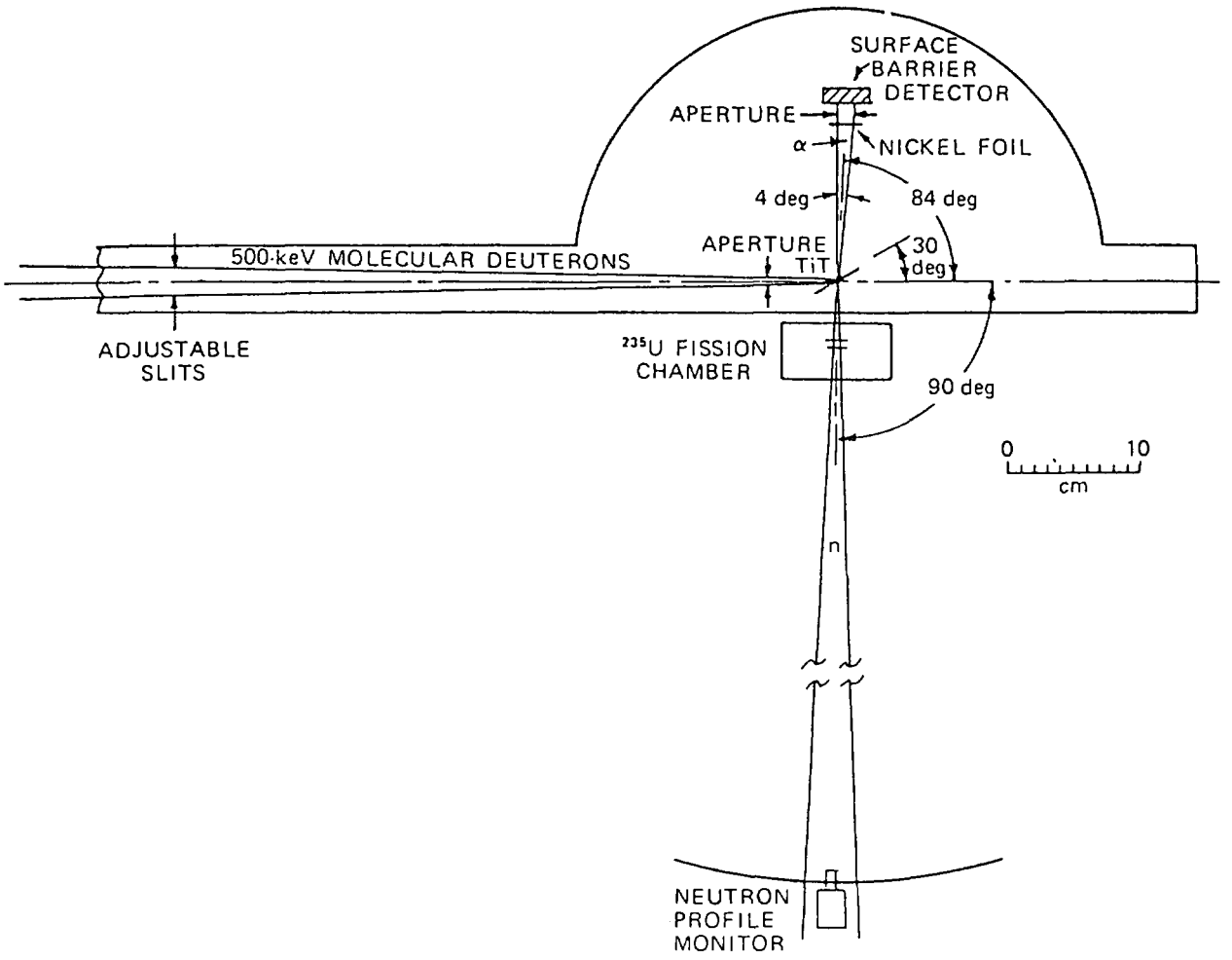

Fig.3 Experimental geometry used by Wasson for 14.1MeV neutron TCAPM[4)]

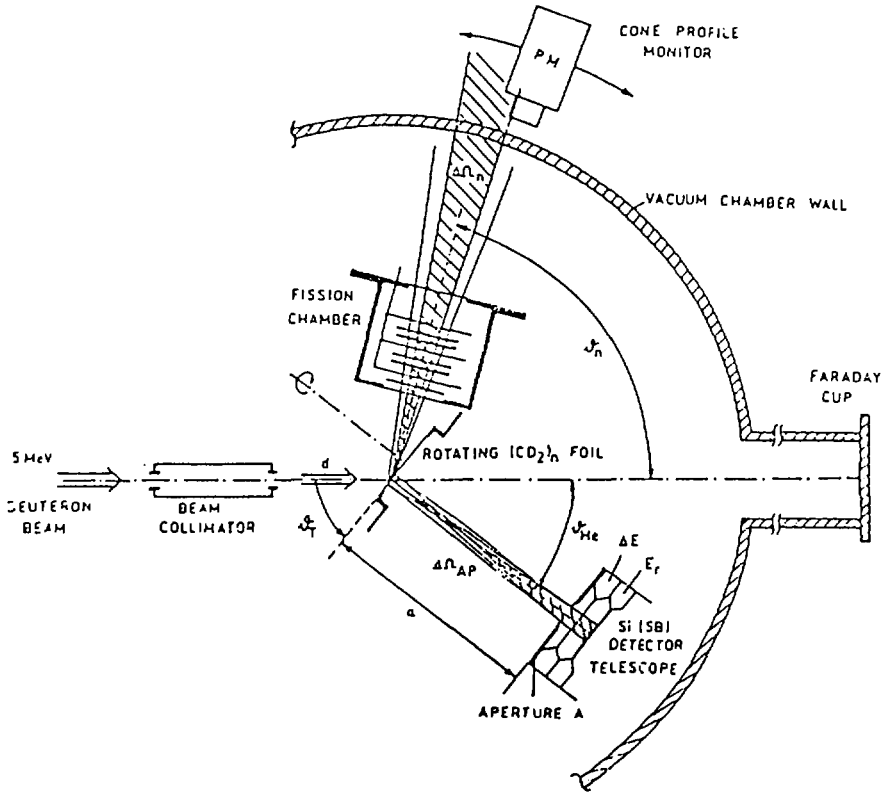

Fig.4 Experimental geometry used by Arlt for D-d neutrons[2)]

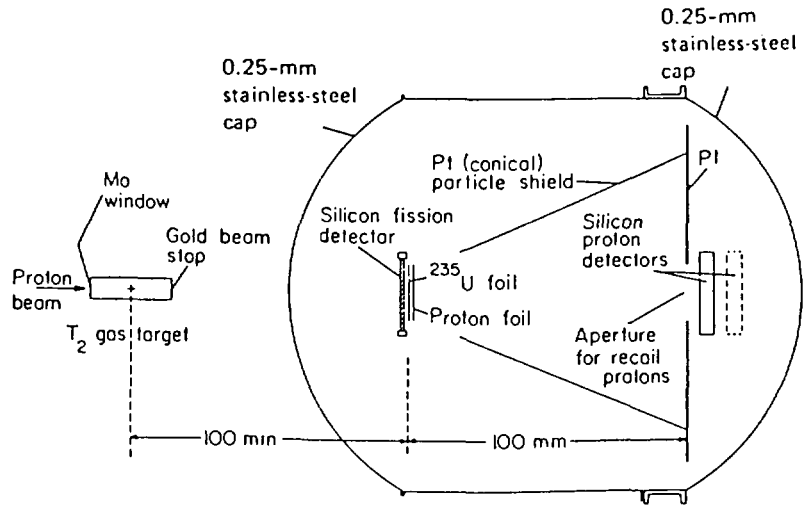

Fig.5 Experimental geometry used by Barton for reference to n-p scattering[10)]

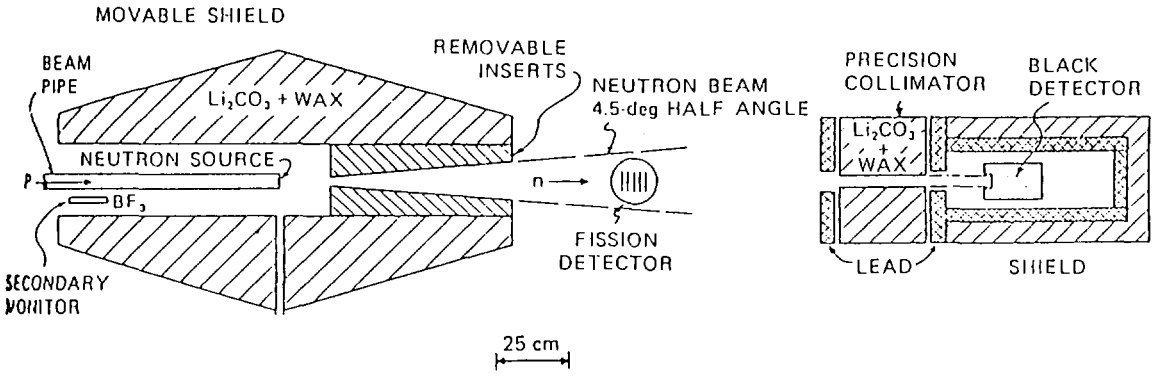

Fig.6 Experimental geometry used by Wasson for BND TOF method[11)]

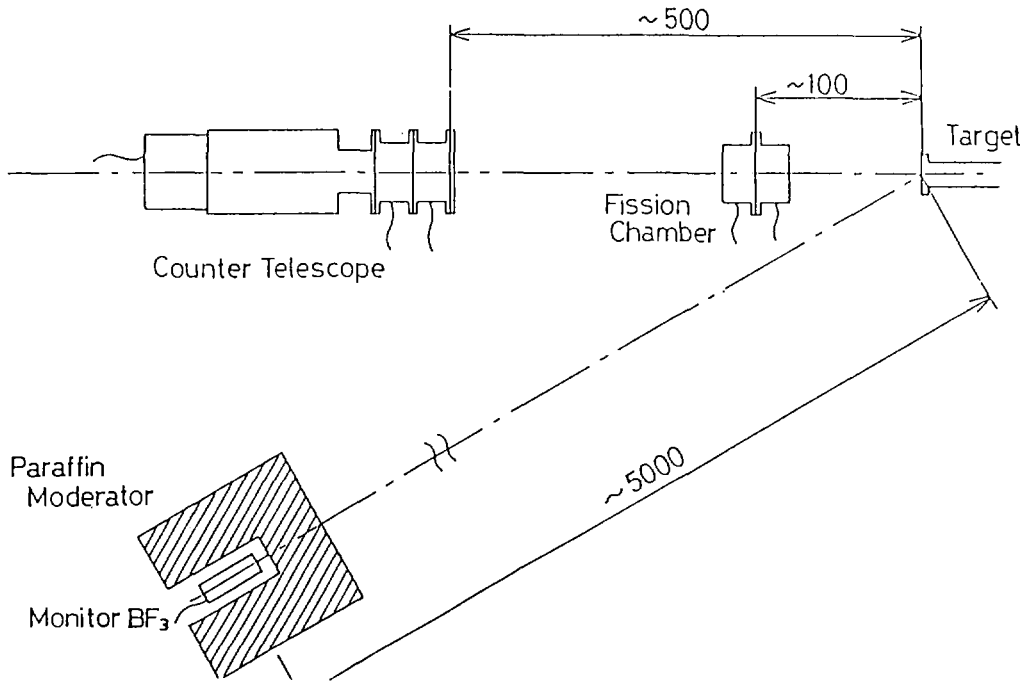

Fig.7 Experimental geometry used for 14MeV absolute measurement at Tohoku University

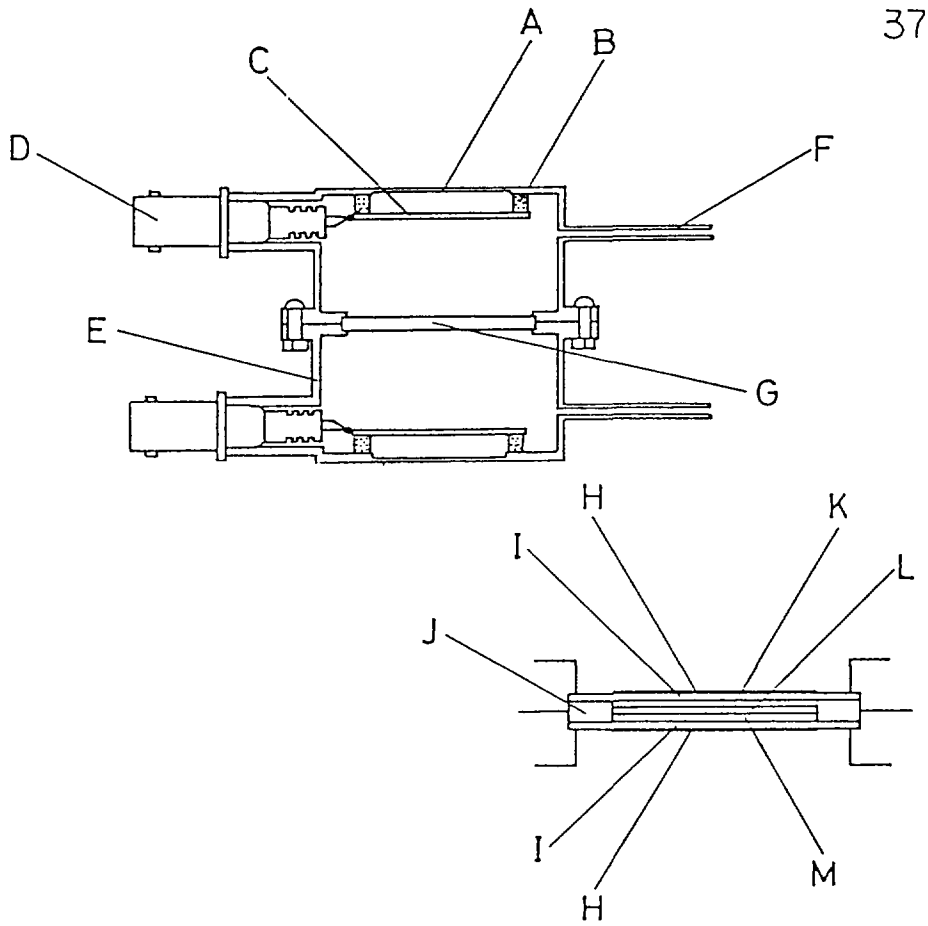

A stainless steel window (0.5 mm-t)
B electric insulator (ceramics)
C collector electrode (stainless steel, 0.5 mm-t)
D HV connector
E stainless steel wall (1 mm-t)
F gas flow pipe
G fission samples and activation detectors

H fission sample (25 mm-ϕ)
I Pt backing (36 mm-ϕ, 0.3/0.4 mm-t)
J activation detectors supporter (stainless steel)
K Au foil (25 mm-ϕ, 0.2 mm-t)
L Ni foil (25 mm-ϕ, 0.2 mm-t)
M Al foil (25 mm-ϕ, 0.2 mm-t)

Fig. 8 Construction of fission chamber used for 14MeV absolute measurement

4.5 Problems on Gamma-Ray Emission Rate in Cross-section Measurements

Toshio Katoh, Kiyoshi Kawade and Hiroshi Yamamoto
Department of Nuclear Engineering
Nagoya University
Furo-cho, Chikusa-ku, Nagoya

Abstract

The coincidence sum effect, the accuracy of detection efficiency, and the distance dependence of detection efficiency for the measurement of gamma-ray intensity are discussed in this paper. Comments on the data of values of absolute emission rates of gamma-rays are also presented.

1. Introduction

Measurements of fast(∿ 14 MeV) neutron activation cross-sections of fusion reactor materials have been made by measuring gamma-ray intensities from induced active nuclei. In these measurements, following problems must be taken into account to obtain accurate values of cross-sections.

(1) Coincidence sum effect in the measurement of gamma-ray spectra.

This effect will be important in case of measurements at short source-to-detector distance (specially for weak activity).

(2) Accuracy of detector efficiency of gamma-ray by the detector.

(3) Method to obtain the detection efficiency for the short source-to-detector distance.

(4) Accuracy of reference data of absolute emission rates of gamma-rays.

The decay scheme must be investigated.

Results of experimental study of these problems are presented in this paper.

2. Measurements of activation cross-sections

The procedures of the measurements of activation cross-sections are as follows.

(1) Fast neutron irradiation of samples to be measured.

(2) Measurements of gamma-ray intensities from induced active nuclei.

(3) Analysis of measured gamma-ray spectra.

From the obtained gamma-ray spectra, integral peak counts of principal gamma-rays of the induced active nuclei are obtained. By using the detection efficiency(ε), the gamma-ray intensity is obtained. The yield of activity and the cross-section(σ) are calculated from the gamma-ray intensity by using the absolute emission rate(η) of that gamma-ray. The relation between these factors is as the following formula(1).

$$C = \frac{\eta\varepsilon N\sigma}{\lambda}(1 - e^{-\lambda t_1}) \cdot e^{-\lambda t_2} \cdot (1 - e^{-\lambda t_3})\phi \qquad (1)$$

where C is the total number of counts under the photopeak,
η the number of γ-quanta per disintegration,
ε detection efficiency of the Ge(Li) detector,
σ the cross-section under study,
λ decay constant of the induced nuclei,
N the number of atoms of the target sample,
ϕ neutron flux at the sample,
t_1 irradiation time,
t_2 cooling time,
t_3 measuring time.

All the factors included in the formula(1) make effects on the final results of the cross-section. Among these factors, three factors, C, ε and η will be discussed in this paper.

3. Coincidence sum effect

Usually, the gamma-ray measurements are made at about 10 cm or more of distance between the gamma source and the

detector. However, in case of weak activities due to a small cross-section or a long life-time(small decay constant), the sample must be placed at a short distance position such as 5 cm or less to the surface of the detector. In this case, if the decaying nucleus emits two gamma-rays in cascade, there is some probability of detecting both successive gamma-rays in the detector simultaneously. At this moment, the detector generates one pulse signal for sum(or total) energy of both gamma-rays as the results of this coincidence phenomena, and the signal is registered at the sum energy position in the measured spectrum. Then, the original peak counts are reduced by the amount due to this effect.

We investigated this effect by using a source of ^{24}Na, which emits two gamma-rays in cascade, and that of ^{65}Zn, which emits only one gamma-ray. The ratio of peak counts of gamma-rays of ^{24}Na and ^{65}Zn as a function of distance is shown in Fig. 1. At the distance of 5 cm, the reduction of peak count of ^{24}Na due to the sum effect is seen and about 4 percent. At the distance larger than 10 cm, the effect becomes negligible. Then, it is necessary to consider this effect when the gamma-ray measurements of activity with many gamma-rays are made at a shorter distance than 10 cm. (Note : the angular correlation of the successive two gamma-rays must be taken into account, and then this effect should be investigated for each case).

4. Detection efficiency

The detection efficiency of the detector is usually obtained by measuring standard gamma-rays as is shown in Table 1. For the practical use of the efficiency, it is necessary to deduce an emipirical formula of efficiency or an efficiency curve from measured points of efficiency. We investigated the detail of the efficiency data as is shown in Fig. 2 by the $\varepsilon \times E_\gamma$ plot[1]. An empirical curve is also shown in the figure by a solid line which can be fitted by the empirical formula(2) by the SALS(Statistical Analysis with Least Squares Fitting, by Nakagawa and

Koyanagi) code.

$$\varepsilon = A_1\exp(-A_2E_\gamma) + A_3\exp(-A_4E_\gamma) + A_5\exp(-A_6E_\gamma) + A_7\exp(-A_8E_\gamma) + A_9 \quad (2)$$

The Fig. 3 shows the differences between the estimated values from the formula(2) and the experimental values. The figure shows the formula(2) is reliable with the accuracy within 2 percent.

5. Correction for the detection efficiency at a short distance

The multi-gammaray emitter such as ^{152}Eu and others as shown in Table 1 cannot be used to make an efficiency curve for the measurement at a short source-to-detector distance, since the coincidence sum effect is also caused in the measurements of these sources. Someone uses the detection efficiency curve at a long distance only by correcting the x^{-2} dependence for the distance(X). This method can be applied only for a thin detector. Practically, the detector has a finite size, and then the situation of detection at a short distance is different from the detection at a long distance[2].

We investigated the distance dependence of the efficiency curve and proposed[2] a formula(3) with a correction factor $D(x, E_\gamma)$, which depends on energy and distance.

$$\varepsilon_f(x, E_\gamma) = D(x, E_\gamma)\cdot\varepsilon_f(X, E_\gamma) \quad (3)$$

where $\varepsilon_f(X, E_\gamma)$ is a detection efficiency obtained at a distant position(X) by using standard sources.

The properties of $D(x, E_\gamma)$ are studied by using single gamma-ray emitters in Table 2.

The Fig.4 shows the distance dependence of each gamma-ray. The Fig. 5 shows the relation of $D^{-\frac{1}{2}}$ values and the distance(x). This figure shows that the relations are linear ones, but the lines do not intersect the horizontal

axis at 0 cm. However, if an effective depth(x_0) of interaction of gamma-ray and detector materials is considered, the D is proportional to $(x + x_0)^{-2}$. The x_0 is a function of gamma-ray energy. Finally we obtained the formula(4) for the correction factor D.

$$D(x, E_\gamma) = \left\{\frac{X + x_0}{x + x_0}\right\}^2 \cdot (1 - B(x, E_\gamma)) \qquad (4)$$

where x_0 is a function of energy expressed as

$$x_0 = a_1 - a_2\exp(-a_3 E_\gamma) - a_4\exp(a_5 E_\gamma)$$

and $B(x, E_\gamma)$ is a small correction term for the deviation of gamma-ray beam from the parallel beam.

6. Absolute emission rate

The gamma-ray intensities per disintegration(absolute emission rate) is necessary to obtain the yield of induced active nuclei from the measured gamma-ray intensities.

In most cases, the relative gamma-ray intensities are well known, but the beta branching ratios are not so well. Then, if there is a beta transition to the ground state of the daughter nucleus, the absolute intensities of gamma-rays become inaccurate. If no beta transition to the ground state is confirmed, the other beta branches can be estimated from the gamma-ray intensity balance of each level. If the measured gamma-ray has a high multipolarity, a large internal conversion coefficient must be considered. The probability of electron capture should be estimated for the positron and electron capture decay.

References

(1) Yoshizawa, Y., Iwata, Y., Kaku, T., Katoh, T., Ruan, J-Z., Kojima, T., Kawada, Y.: Nucl. Instr. Methods 174 pp 109-131 (1980)

(2) Kawade, K., Ezuka, M., Yamamoto, H., Sugioka, K., Katoh, T.: Nucl. Instr. Methods 190 pp 101-106 (1981)

Table 1 Standard sources for the measurement of detector efficiency

NUCLIDE	Energy(keV)
^{133}Ba	79.623, 80.997, 276.407, 302.859, 356.014, 383.859
^{134}Cs	563.27, 569.30, 604.68, 759.78, 801.86, 1038.53, 1167.89, 1365.17
^{137}Cs	661.660
^{54}Mn	834.843
^{60}Co	1173.238, 1332.501
^{152}Eu	121.7824, 244.6989, 295.939, 344.2811, 367.788, 411.117, 443.990, 586.294, 688.678, 778.925, 867.388, 1085.914, 1089.700, 1112.05, 1212.950, 1299.124, 1408.011

Table 2 Single gamma-ray emitting sources used for the present experiment

NUCLIDE	E_γ(keV)	Half-life
^{241}Am	59.54	433 y
^{170}Tm	84.25	128.6 d
^{141}Ce	145.44	32.55 d
^{114m}In	190.24	49.51 d
^{51}Cr	320.08	27.70 d
^{198}Au	411.80	2.696 d
^{137}Cs	661.66	30.17 y
^{54}Mn	834.85	312.2 d
^{65}Zn	1115.52	244.0 d

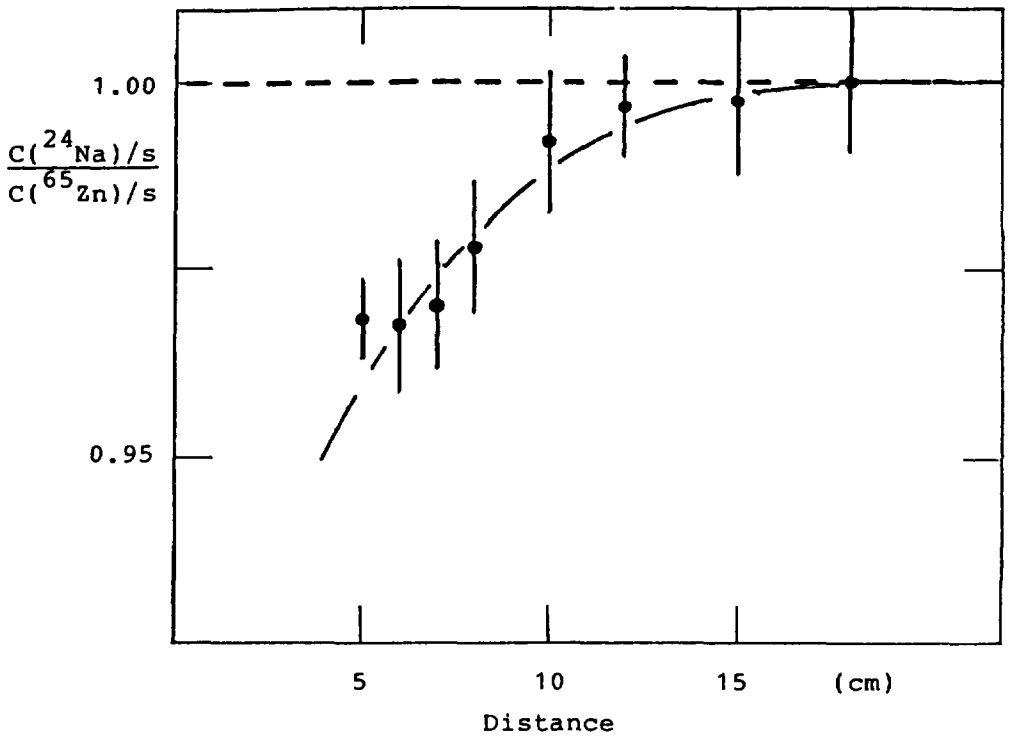

Fig. 1 The ratio of peak counts of gamma-rays of ^{24}Na and ^{65}Zn as a function of distance

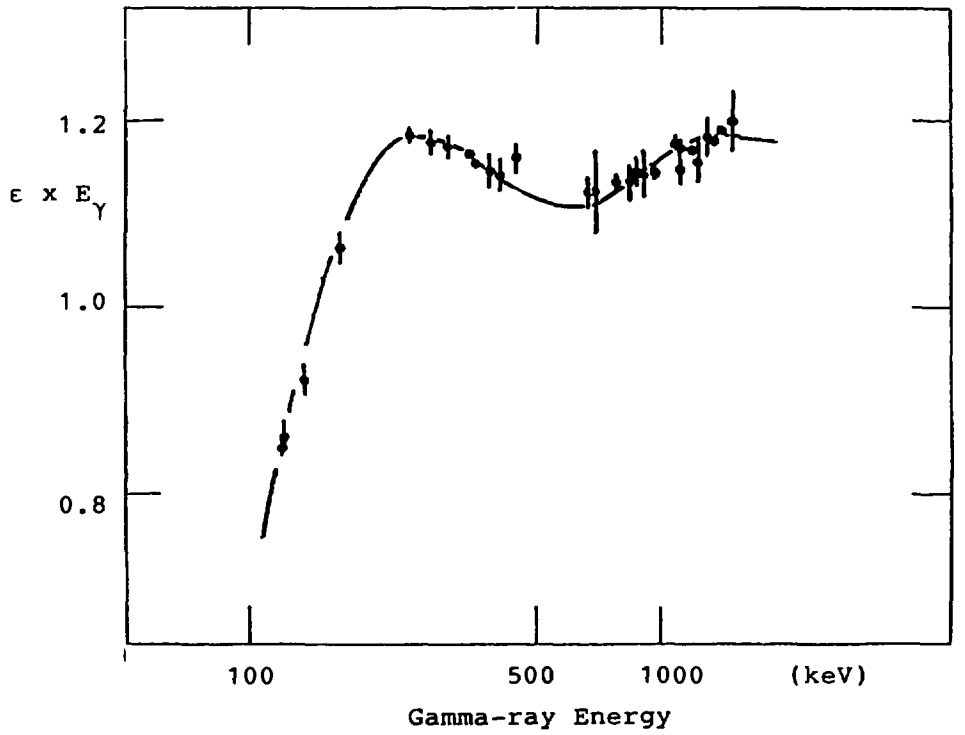

Fig. 2 The ε(efficiency) x E_γ plot

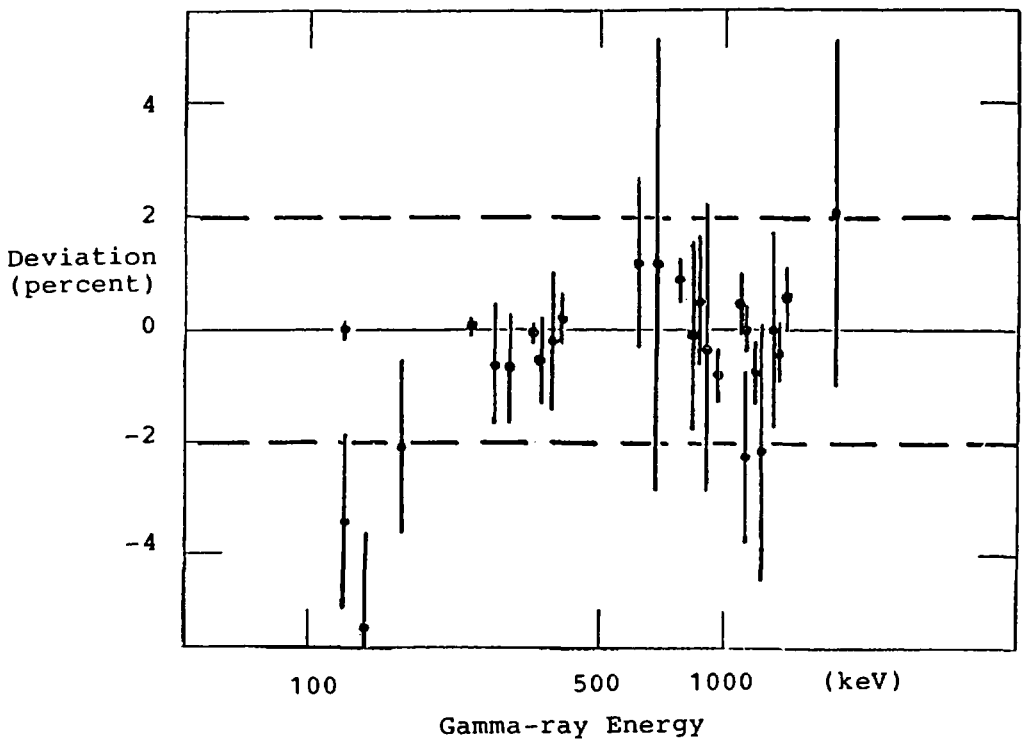

Fig. 3 The difference between the estimated values and the experimental values of detection efficiency

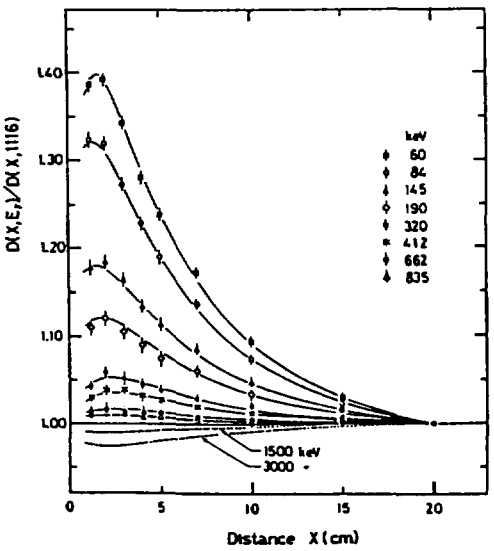

Fig. 4
Distance dependence of the correction factors, $D(x, E_\gamma)$

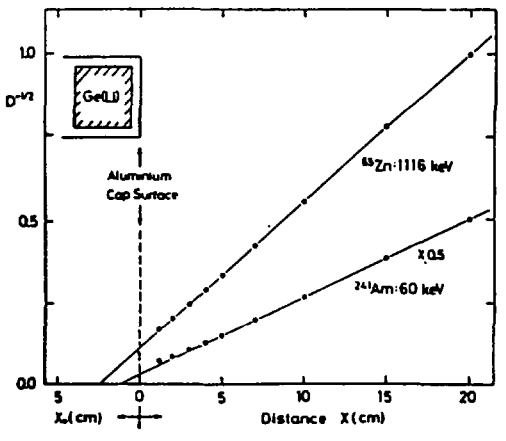

Fig. 5
The values of $D(x, E_\gamma)^{-\frac{1}{2}}$ for the source-to-detector distance

5. NUCLEAR DATA FOR FUSION REACTORS

5.1 Status of the Nuclear Data for Fusion Reactors

Yukinori KANDA

Department of Energy Conversion Engineering,
Kyushu University,
Kasuga, Fukuoka 816, Japan

Nuclear data demanded in a program of fusion reactor development are fusion reaction data of charged particles, neutron nuclear data, and decay data of radioactive nuclides. In this work, status of the neutron data for activation and gas production cross sections are intensively presented because they are important data in studies on selecting structural materials of fusion reactions.

Data of gas production cross section are increasing especially at 14 MeV although available data are insufficient for estimation of the number of gas atoms in neutron-irradiated sample. A great number of activation cross sections for candidate materials is needed in studies on fusion reactor development. Accurate data for reactions which produce the long life nuclides are scarce to study radioactive waste management. Model calculation to produce the data which are not available in experiments has been improved and can be useful for evaluation of the nuclear data for fusion reactors.

1. Introduction

There is difficulty to review the nuclear data for fusion reactors because the concept of fusion reactors is fluid. It is unknown at present what type of reactors is to be a power reactor in future and what kinds of materials are used in the reactor. Therefore, selection of the elements or nuclides to be used in fusion reactors is troublesome at this time. There are only candidate materials or elements which should be studied. A large amount of nuclear data for these materials must be actually prepared for studying the candidate materials for fusion reactor development.

The present review is restricted to the nuclear data for magnetic confinement and D-T fusion reactors.

Components and auxiliaries of the fusion reactor are list up taking account of rather materials than functions. They are shown in Table 1. In the periodic table shown as Table 2, the elements of the materials are marked with the capital letters defined in Table 1. It can be found that major elements are locally distributed.

Table 3 represents what kinds of nuclear data are demanded for fusion reactor development. In this work, status of the neutron data for activation and gas production cross sections listed as fifth and sixth rows in Table 3 are intensively reviewed because they are important data in studies on selecting structural materials of fusion reactors.

2. Gas production cross section

The most important parameters of neutron radiation damage in

the materials used for a first wall and structure are displacement per atom, called dpa, and He production rate.

The dpa can not be experimentally measured but calculated with assumption on physical processes. Regarding the nuclear data, not only the cross sections of whole scattering and reactions but also angular distributions and energy spectra of the emitted particle are used in this calculation. Generally speaking, the cross section data on the neutron scattering are abundant but on the charged-particle-emitted reactions scarce. These situation can be actually found in statistical figures of the number of experiments. Major residual nuclei of the charged-particle-emitted reaction cross sections which have been measured are radioactive. Their cross sections can be measured by an activation method. Available experiments on angular distribution and energy spectra of emitted particle are not so much not only for charged-particle but also neutron emission.

The reaction (n,n'p) and (n,d) have the same residual nucleous. They can not be discriminated by the activation method. The (n,d) can be measured by detecting of deuterons emitted from samples or by measuring deuterium accumulated in samples. These are common technique to the measurements of the gas production cross sections. Recently, sophisticated experimental methods have been developed and the measurements are increasing even though gradually.

Fig.1 shows α-particle spectrum from 316 SS bombarded by 11 MeV neutrons recently measured with a charged-particle TOF spectrometer at Ohio University[1]. This is the energy spectrum integrated over whole solid angle. The spectrum of emitted

protons was also measured in the same experiment. Energy variation of the He and H production cross section for 316 SS is shown in Fig.2. They have been measured by Grimes et al.[1]. The angular distribution and energy spectrum of the charged particles can be measured by such spectrometer experiments. However, many experiments can not be expected since the experiments are possible in extremely limited laboratories and consume a long measuring time. The experiments have another difficulty that a statistical error is so large that they are not suitable to measure an integrated cross section.

With respect to this point, a He accumulation method is useful. Helium production cross sections can be directly measured by this method in which He atoms produced by (n,xα) reactions and accumulated in the sample are measured after neutron irradiation.

The (n,xα) cross sections measured at 14 MeV are given in ref.2) comparing both the results obtained with He-accumulation method by Farrar's group of Rockwell International and the data of the magnetic spectrometer experiments by Haight and Grimes at Livermore. They are most of the data for (n,xα) which have ever been measured. The cross sections of deuterium and tritium productions have been measured with gas accumulation methods by Qaim's group[3] at Jülich.

The available data for gas production cross section are recently increasing but they are in the limited range of neutron energy. Nuclear reaction model calculation have to be used to interpolate or extrapolate the experiments of cross sections and emitted particle spectra in order to evaluate the nuclear data

applicable to fusion reactor development. The most of the model calculation utilized in the present time are based on the Hauser-Feshbach and pre-compound models. Fundamental requirement in these works is determination of proper parameters including in the formulae of the model. Many calculations have been in the world and have achieved useful success.

3. Activation Cross Section

Nuclear reactions needed for studies on induced radio activities in fusion reactors have been compiled from three recent works[4,5,6] on calculation for conceptual design of the reactors. It contains 168 reactions for 85 isotopes of 31 elements.

Table 4[5] shows the reactions of V, Cr, Fe and Ni which are typical elements in the candidate materials of fusion reactors. The residual nuclides of short half-life, approximately minutes to hours, are important in accidents of fusion reactors. The medium half-live nuclides, about days, are important for maintenance operations of reactors. Very long half-life nuclides are important in waste management. Among four elements, V and Cr have not very long half-life residual nuclides but Fe and Ni have. Fig.3[4] shows the decay characteristics of these elements. This is post shutdown radioactivity for the elements following exposure at the first-wall region to a wall loading of 1.5 MW/m^2 for 2 years. The activities of V and Cr decay faster than those of Fe and Ni depending half-lives of the nuclides.

Sources of the evaluated cross sections used in the HEDL activation library is presented in Mann's report[5], one of the

reference of Table 4. Table 5 is a part of his table including from V to Ni. Abreviation are shown in the table. Where cross sections are not available, mainly above 20 MeV, results from the modified THRESH-2 code are used to evaluate them. Of about 2400 reactions needed to treat the more important fusion materials, only 63% have cross-section values in this library and only 18% have values from evaluated libraries. It seems that the HEDL activation library needs the cross sections in the neutron energy region by 40 on 50 MeV, since it has been prepared primarily to calculate activities induced in FMIT. Therefore, great parts of cross sections are not available lack in the evaluated libraries.

A point to noticed in Mann's study is presentation of high ^{3}H production rate in structural materials. The data of ^{3}H production cross section are very scarce. Qaim's data[3,7] on ^{3}H production cross section shown in Fig.4 is very unique.

Examples of the cross sections for Fe comparing experiments and evaluations are presented in Fig.5[8]. It can be found that several data available but they are discrepant. The evaluated lines run reasonably against experiments. In D-T fusion reactors neutron flux of 14 MeV is very high at the first wall. The cross sections of its materials near 14 MeV should be carefully measured and evaluated.

Experiments for $^{54}Fe(n,\gamma)$ cross section near 14 MeV is not available as seen in Fig.5. This is not so important for the nuclear data of fast reactors but for the fusion reactor highly important. In the case of $^{59}Co(n,\gamma)$ in Fig.6[8] the residual nuclide of this reaction is ^{60}Co whose half-life is 5 years. There is a few experiments. Two evaluations seem to have a

different principle. For radiative capture, reaction rate induced by a softer part of neutron spectrum is large even at the first wall. Contribution from 14 MeV neutrons are lowered relatively. In the reaction of threshold energy near 14 MeV, however, the problem is highly important. It appears in $^{27}Al(n,2n)^{26}Al$.

Fig.7[9] shows new data of the cross sections producing long life state of ^{26}Al measured by Smither and Greenwood[10] and Sasao[11] and the lines of JENDL-2 and ENDF/B-V. The dotted line is 14 MeV neutron spectrum for 1 keV plasma temperature. The experimental data represent that selection of Al as the reactor material is preferable and potentiality of Al as a low activation material is raised.

4. Conclusions

Gas production and activation cross sections are key nuclear data for selection of fusion reactor materials.

Experiments of He-production cross section are increasing especially at 14 MeV. The energy range is expanding to other range even though step by step. This tendency is similar to the other gas-production reactions.

A great number of activation cross sections is needed in studies of selection of the fusion reactor materials. High accurate data for the reactions which produce long life nuclides are demanded especially at 14 MeV.

Reproducibility of experiments by model calculation has been improved. Experiments and model calculations should be used complementarilly to evaluate the nuclear data for fusion

reactors.

References

1) M. Ahmad et al., Nucl. Sci. Eng., 90, 311 (1985)

2) D. W. Kneff et al., J. Nucl. Mater., 103/104, 1451 (1981)

3) S. M. Qaim et al., Proc. Int. Conf. on Nuclear Data for Basic and Applied Science, Santa Fe, New Mexico, 13 to 17 May , 1985 (In press)

4) R. W. Conn et al., Fusion Technol., 5, 291 (1984)

5) F. M. Mann, Fusion Technol., 6, 273 (1984)

6) E. T. Chen, Fusion Technol., 8, 1423 (1985)

7) R. Wölfle et al., Nucl. Sci. Eng., 91, 162 (1985)

8) T. Asami, Private communication

9) K. Kanmada and H. Kakihana, J. Atomic Energy Sov. Japan, 27, 183 (1985) (In Japanese)

10) R. K. Smither and L. R. Greenwood, J. Nucl. Mater., 122/123, 1071 (1984)

11) M. Sasao, IPPJ-DT-115 (1985) Seminar at Insti. Plasma. Phys., Nagoya Univ.

Table 1 Components and Auxiliaries of Fusion Reactor

1.	Fuel (Plasma)	F
2.	First wall	W
3.	Tritium breeder (material)	T
4.	Structure	S
5.	Coolant	C
6.	Neutron multiplier	N
7.	Rflector	R
8.	Shield	L
9.	Magnet	M
10.	Electrical insulator	I
11.	Dosimeter	D
12.	Fusion-Fission hybrid	H

Table 3 Nuclear Data Need for Fusion Reactor

1. Charged particle reaction
2. Neutron emission data
3. Gamma-ray emission data
4. Tritium production cross section
5. Activation cross section
6. Gas production cross section
7. Data for radiation damage calculation
8. Data of energy diposition
9. Cross section of neutron dosimeter
10. Decay data of radiative nuclides

Table 2 Periodic Table of the Elements with materials for fusion reactor.

Period	Ia	IIa	IIIa	IVa	Va	VIa	VIIa	VIII	Ib	IIb	IIIb	IVb	Vb	VIb	VIIb	0
1	T F C L 1H															C 2He
2	T W C 3Li	C N R 4Be									S W L 5B	S W RL 6C	S W C 7N	TW C RL 8O D I	C 9F	10Ne
3	C 11Na	W 12Mg D I		Transition Elements							S TW R M 13Al D I	S TW 14Si D	S 15P D	S 16S	17Cl D	18Ar
4	C 19K D	20Ca L I	21Sc I	S W M 22Ti D	S W M 23V	S W R 24Cr	S 25Mn	S W RL 26Fe D	S 27Co D	S W R 28Ni D	W M 31Ga	W 32Ge	33As	34Se	35Br	36Kr
5	37Rb D	W 38Sr	W 39Y I	S TW R 40Zr D	S W M 41Nb D	S W N 42Mo	43Tc	44Ru	45RH D	46Pd	47Ag	48Cd	49In D	50Sn M	51Sb	52Te	53I	54Xe
6	55Cs	56Ba	57La	72Hf	S L 73Ta	S W L 74W	75Re	76Os	77Ir	78Pt	79Au D	80Hg D	81Tl	T C N 82L Pb I	W 83Bi	84Po	85At	86Rn
7	87Fr	88Ra	89Ac													

F: Fuel C: Coolant M: Magnet
W: First Wall N: Neutron Multiplier I: Electrical Insulator
T: ^{3}H breeding material R: Reflector D: Dosimeter
S: Structure L: Shield H: Fusion-Fission Hybrid

Lanthanides (Rare Earths)	58Ce	59Pr	60Nd	61Pm	62Sm	63Eu	W 64Gd	65Tb	66Dy	67Ho	68Er	69Tm	70Yb	71Lu
Actinides	H 90Th	91Pa	H 92U D	93Np D	H 94Pu	95Am	96Cm	97Bk	98Cf	99Es	100Fm	101Md	102No	103Lw

Table 4 An expample of the activation library.

HEDL Activation Library (February 1983)

Isotope	*n,n**	*n,2n*	*n,3n*	*n,na*	*n,np*	*n,nd*	*n,nt*	*n,nh*	*n,4n*	*n,g*	*n,p*	*n,d*	*n,t*	*n,h*	*n,a*	*n,2p*
^{50}V	X	TA	T	TA, Y	TA	T	T	T	•	A	TA	T	T	T	TA	T
^{51}V	X	TE	T	TE	TE	T	T	T	•	E	TE	TE	TE	T	TE	T
^{50}Cr	X	TE	T	TE	TA	T	T	T	•	A	TA	T	T	T	TE	T
^{52}Cr	X	TE	T	TE	TE	T	T	T	•	•	TA	T	T	T	TE	T
^{53}Cr	X	TE	T	TE	TA	T	T	T	•	•	TA	T	T	T	TE	T
^{54}Cr	X	TE	TE	T	TA	T	T	T	•	A	TA	T	T	T	TE	T
^{53}Mn	X	•, •	•	•	•	•	•	•	•	•	•	•	•	•	•	•
^{55}Mn	X	TE	TE	TE	TE	T	T	T	•, •	E	TE	TE	•	TE	TE	T
^{54}Fe	X	L, [h]Y	L, •	L	L	TH, •	TH	T	X	E	L	L	TH, •	T	L	T
^{55}Fe	X	•	•, Y	•	•	•	•, •	•	•, •	•	•	•	•	•	•	•
^{56}Fe	X	L	L	L	L	TH	TH	T	L, Y	•	L	T	TH	T	L	T
^{57}Fe	X	T	TA	T	TA	T	T	T	•	•	TA	T	T	T	T	T
^{58}Fe	X	T	T	T	TA	T	T	T	•	E	TA	T	T	T	TA	T
^{59}Co	X	TA, TA	T	TA	TA	T	T	T	•	EA, EA	TE	TE	TE	TE	TE	T
^{60}Co	•	•	•	•	•	•	•	•	•	•	•	•	•	•	•	•
^{58}Ni	X	TE	T	T	TA	TH	TH	T	•	E	TA, TA	T	TH	T	TE	T
^{59}Ni	X	T	T	T	T, •	T	T	T	•	E	TE	T, •	T	T	TE	T
^{60}Ni	X	TE	T	T	T	T, •	T	T	•	•	TA, TA	T	T, •	T	T	T
^{61}Ni	X	T	T	T	TA, TA	T	T, •	T	•	•	TA	T	T	T	T	T
^{62}Ni	X	T	T	T	TA	T	T, •	T	•	E	TA, TA	T	T	T	TE	T
^{63}Ni	•	•	•	•	•	•	•	•	•	•	•	•	•	•	•	•
^{64}Ni	X	TA	T	TA	TA	T	T, •	T	•	A	TA	T	T	T	TA	•

After Mann (1984)

X: Not allowed
A: ACTL-78
*: None
E: ENDF/B-V
T: Thresh
Y: IT decay only half-lige<1m
H: HEDL
L: LANL

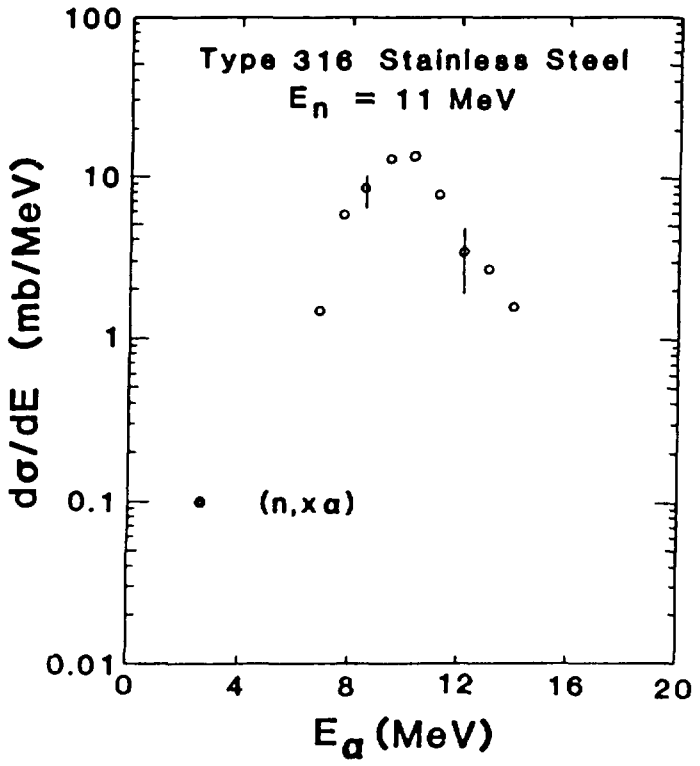

Fig.1 Angle-integrated cross sections for the (n,xα) reactions from 11-MeV neutron bombardment of Type 316 stainless steel, after ref.1).

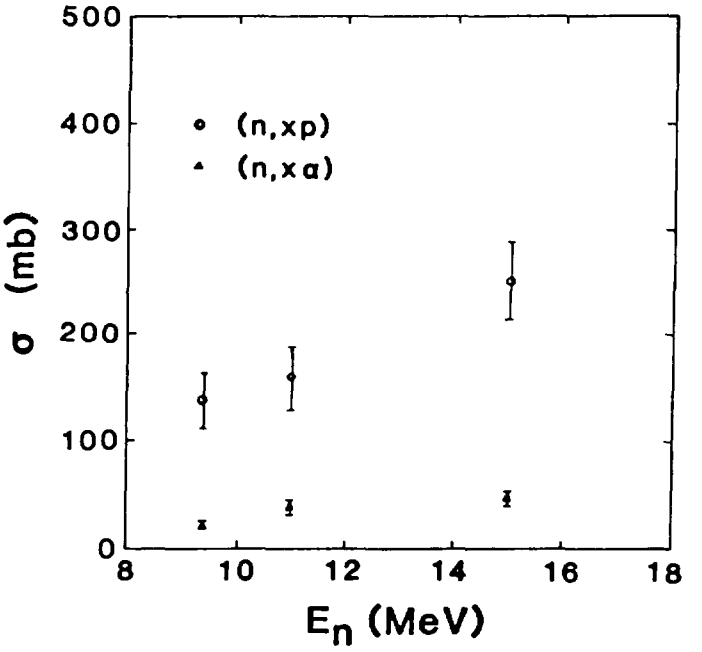

Fig.2 Neutron bomarding energy dependence of total (n,xp) and (n,xα) cross sections for Type 316 stainless steel. Data points are indicated by ○ for protons and by ▲ for alpha particles, after ref.1).

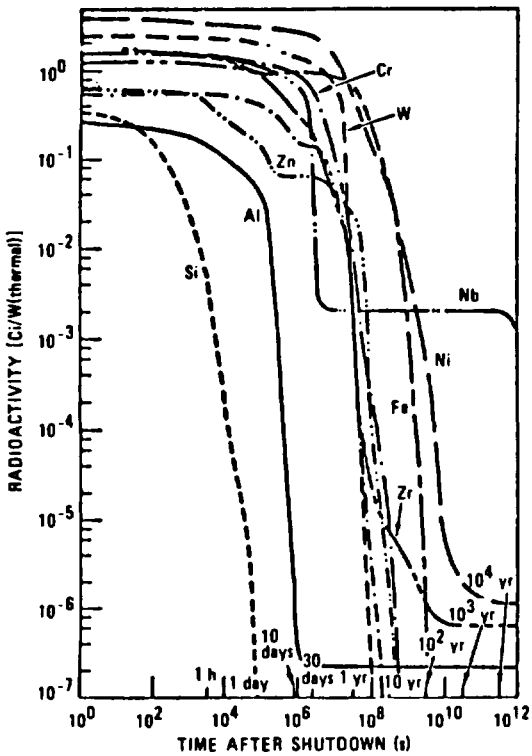

Fig.3 Postshutdown radioactivity for various emements following exposure at the first-wall region to an wall loading of 1.5 MW/m for 2 yr, ref.4).

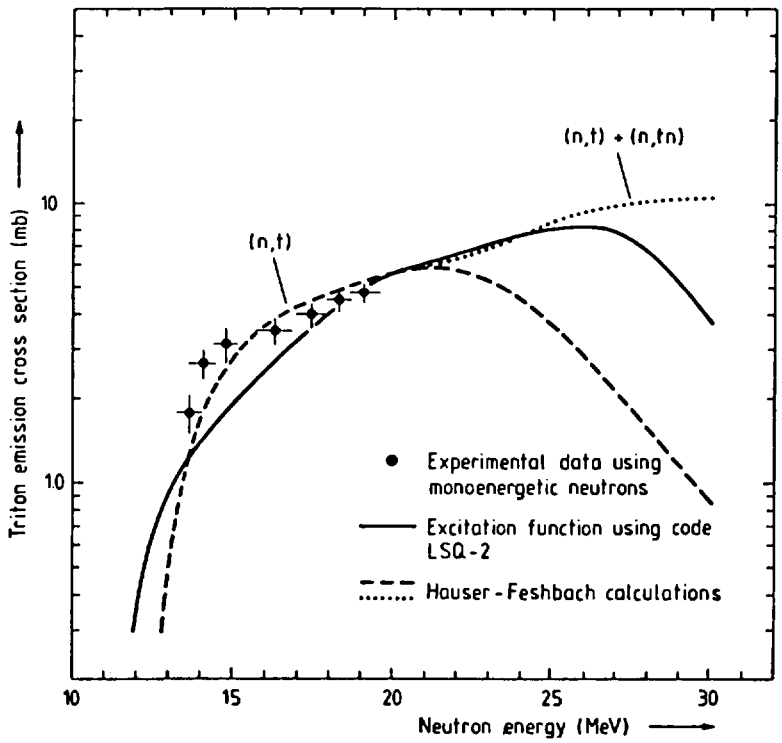

Fig.4 Excitation function of the [(n,t) +(n,tn)] reaction on ^{27}Al, after ref.3,7).

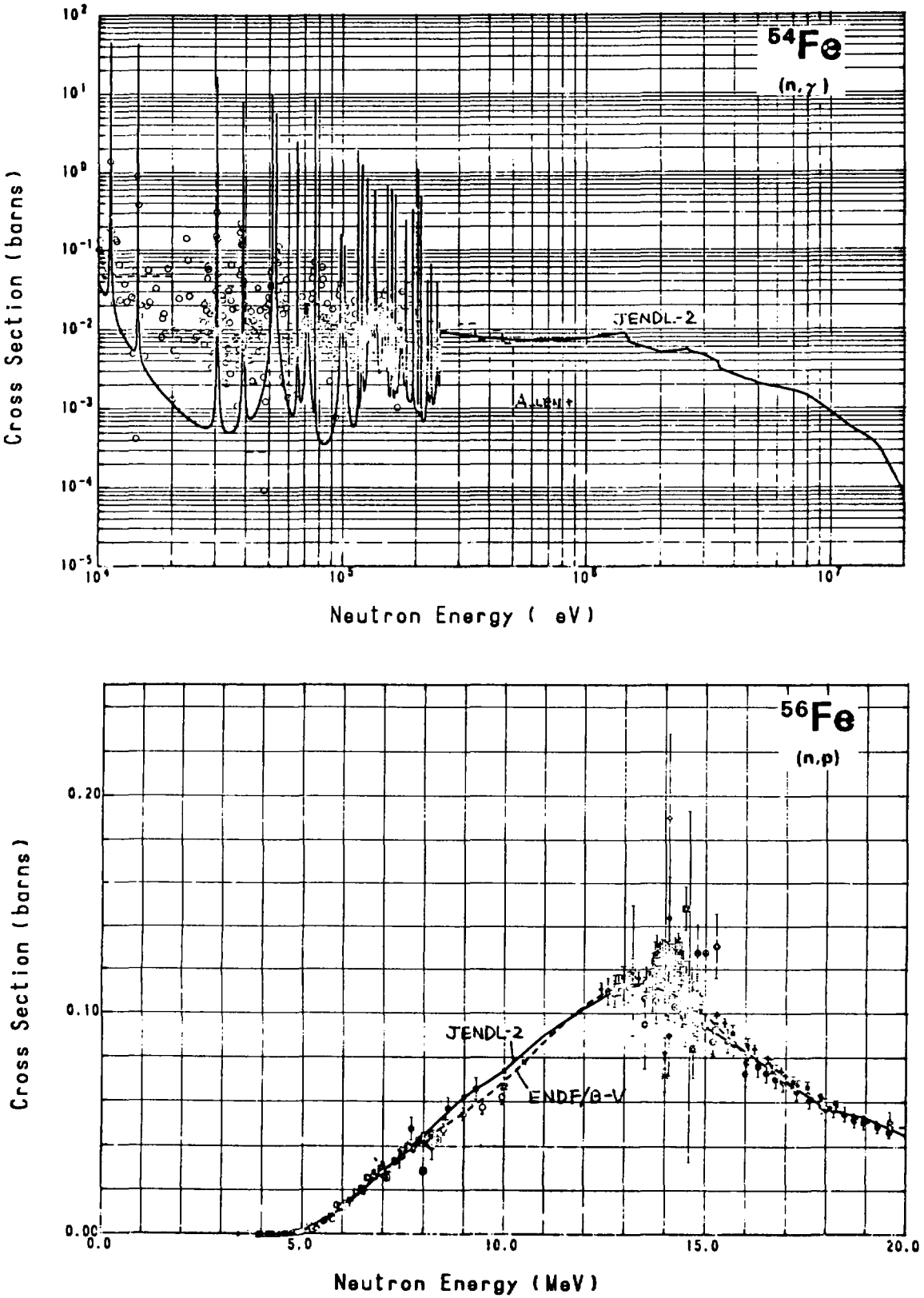

Fig.5 Exsample of the Cross Sections for Fe, ref.8).

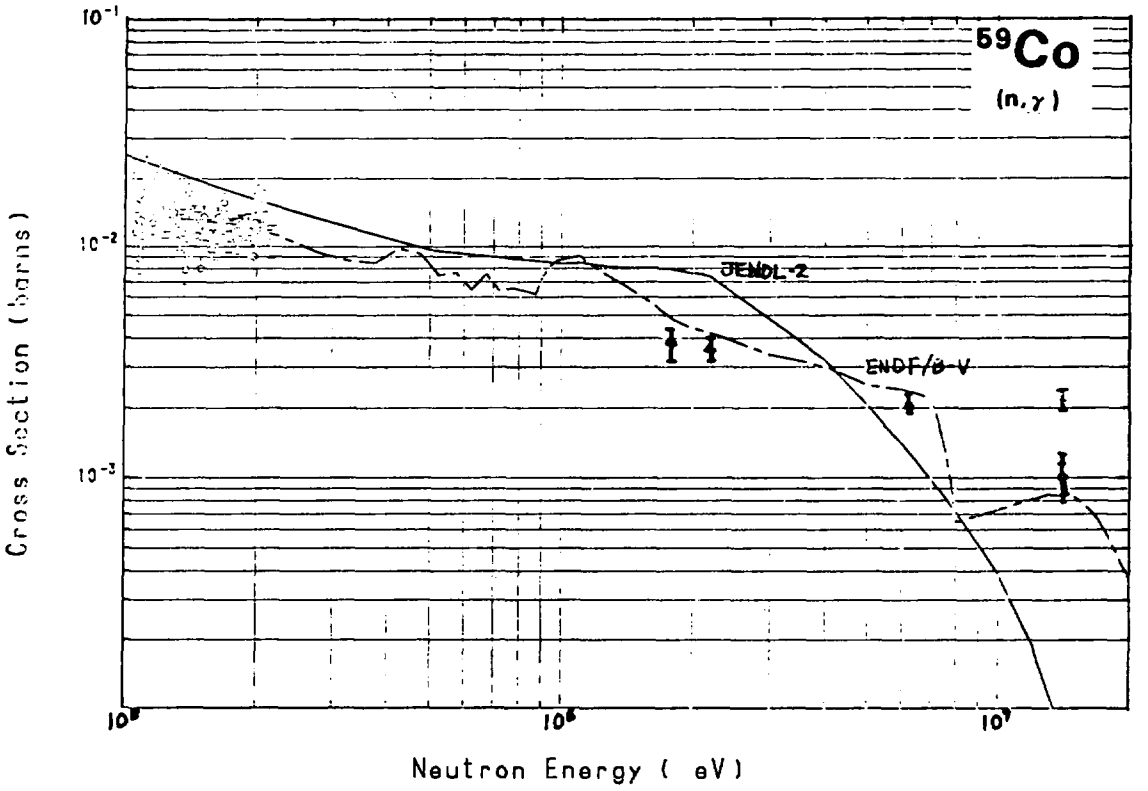

Fig.6 Comparison between experiments and evaluations of the cross section for $^{59}Co(n,\gamma)$, ref.8).

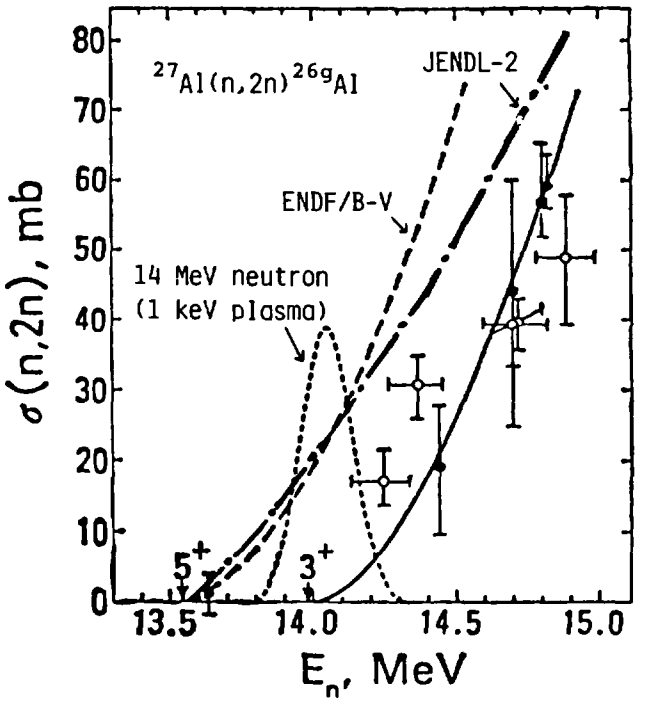

Fig.7 $^{27}Al(n,2n)^{26}Al$ reaction cross section. The figure except the curves of JENDL-2 and ENDF/B-V is quoted from ref.9). The solid circles are in ref.10) and the open circles in ref.11).

5.2 Nuclear Data and Integral Neutronics Experiments for Fusion Reactors

Tomoo Nakamura
Fusion Reactor Physics Laboratory
Department of Reactor Engineering
Japan Atomic Energy Research Institute
Tokai-mura, Naka-gun, Ibaraki-ken 319-11

The experimental activities concerned with the nuclear data at FNS are grouped into two types: a) the measurement of differential cross sections around 14 MeV for constituent nuclides of a fusion reactor and b) the examination of nuclear data by means of integral experiments and their analyses. The recent results are briefly reviewed.

1. Introduction

In the design of fusion reactor blankets and other components surrounding the plasma region, many basic quantities concerned are derived from nuclear calculation, for examples, tritium production, heat energy deposition and radiation dose.[1,2] Accordingly, the nuclear data used in the calculation are the most fundamental data base. The neutron cross sections available at present, however, are not always accurate enough to meet the design requirements in D-T fusion reactor.[3] Much more experimental efforts are needed for the acquisition and validation of the nuclear data in the neutron energy range above that of fast fission reactor.

The FNS is a high intensity 14 MeV neutron source facility installed exclusively for the research on fusion reactor physics and nuclear engineering.[4] The nuclear data studies at the FNS are categorized into two groups. The first is direct measurement of differential cross sections for neutrons around 14 MeV. The second is indirect means of integral experiment; experimental values obtained are compared with the calculational ones to examine the accuracies of the nuclear data used in the calculation in integral means.

In this paper, a brief review is given for the recent activities in the FNS group.

2. Cross section measurement

An experimental program is in progress to measure activation cross sections of various nuclides used in a fusion reactor by making most use of excellent neutron production capability of FNS. Coverage of about 200 different nuclear reactions are planned in a systematic way with unified experimental conditions for the neutron energy range from 13.5 to 15.0 MeV.

The measurement is performed either at 0° beam line or at 80° one depending on the experimental conditions, the source strength being typically about 3×10^{12} n/s and 2×10^{11}, respectively. The sample foils are placed around the target spot at the angles of 0° - 130° to the incident deuteron beam. Each foil is sandwiched by monitor foils, Al or Nb, to determine the neutron fluence during the irradiation at each position. After irradiation, gamma-ray spectra are measured by Ge detectors. The reaction rate is deduced from the measured gamma-ray counts and the decay data with necessary corrections. The accuracy of the data obtained are estimated typically to be within ± 6%. As is shown in Fig.1, the mean neutron energy in the reaction is determined from the emitted neutron spectra calculated by Monte Carlo code and the corresponding cross section curve; the Monte Carlo calculation takes the reaction kinematics and the structure of the target assembly into account in detail.

a) Cross sections of (n,2n) reactions were measured for ^{58}Ni, ^{59}Co, ^{90}Zr, ^{93}Nb and ^{197}Au. Threshold energies are 12.5, 10.8, 12.0, 9.3 and 8.5 MeV, respectively.[5] These reactions are important for the neutron dosimetry around the energy of D-T peak in a fusion reactor; it is also useful in fusion neutronics experiment as spetrum indices Por the direct component from the target. The cross section were obtained relative to that of ^{27}Al(n,a)^{24}Na as the reference cross section (Fig. 2), of which the uncertainty was assigned to be ± 3%. Some of the results are given in Figs. 3 - 5 together with previously evaluated and/or measured data. The summary of this series is given in Table 1.

Cross section data revised by the present results were applied in the calculation to predict the reaction rates of the foils of the same kind in the integral experiment. The reaction rate ratios of the calculation to experiment that was derived from the unfolded spectrum

obtained with multi-foil method were improved considerably by this revision as is shown in Fig. 6, indicating the validity of the set of new data.

b) A series of measurements on cross sections of activation reaction have being conducted for molibdenum and calcium just in the same way as was described above.[6] These are important elements in structural material and shielding material, respectively. Sometimes same radioactive nuclides are produced by different reactions like (n,p) and (n,np) for isotopes of the same element. Separated isotopes were used to obtain the individual contribution for main constituents of these elements. In these series niobium foils were employed as the monitor of the neutron fluence. Examples of the results are shown in Figs. 7 and 8.

3. Integral experiments

Integral experiments occupy major portion of FNS activities. If the choice of the experimental system is appropriate, the neutron field formed inside or leaking from a large-sized system covers the neutron energy region of interest in the fusion reactor research, starting from the neutron energy of D-T reaction. Two types of integral experiments are conducted on systems of simple composition and simple geometry: a) measurement of angle-dependent leakage spectra from a slab by TOF method, b) measurement of neutron spectrum and reaction rate distributions in a right cylinder.

a) Leakage spectrum measurements by TOF method have been carried out on graphite, lithium and lithium oxide slab assemblies of different thicknesses in different angles.[7,8,9] The neutrons emerging from well-defined measuring area of the rear surface of the assembly are detected by an NE213 liquid scintillation counter located about 7m away on a rotating table as is shown in Fig. 9. The flight time spectrum is converted to the angular neutron flux taking the detector efficiency into account. Experimental parameters of this series are summarized in Table 2.

The results obtained are used as benchmark data to examine the nuclear data and/or transport calculation methods used in the

analysis. Some examples of the results are shown in Figs. 10 and 11; the calculation were performed by DOT 3.5 transport code with nuclear data JENDL-3PR1, -3PR2, ENDF/B-1V or-V. It is observed that JENDL-3PR2 gives better agreement in general. Close examination of the comparison over the whole set of experimental results can provide excellent integral check of the nuclear data file, of which the work is in progress.

b) Integral experiments of another type have been conducted on three different assemblies: lithium oxide, graphite and their combination.[10] The dimension of each assembly was 63 cm in equivalent diameter and 61 cm in height. The neutron source was set on the central axis of the cylinder and 20 cm away from its front end. For the two-regioned assembly, front two-thirds was Li_2O and the rest was graphite. Reaction rate distributions were measured along the central axis on tritium production reactions and other reactions for spectral indices. The comparison of the calculated values and the experimental ones of the reaction rates provides the measure of integral accuracy of the the analysis. Some of the results obtained so far are shown in Figs. 12 - 14. It is an objective of this series to unfold the uncertainties due to the nuclear data of the medium. The other parameters affecting the calculated values, however, need be evaluated before final results are drawn out. A survey work for this was conducted on processing codes, group structures and spectrum weighting functions along with nuclear data files.[11] Figure 15 shows the case of weighting function for the Li2O-C assembly as an example. The results of the survey calculation is summarized in table 3.

4. Concluding remarks

Both differential and integral experiments are being conducted intensively at FNS to examine the accuracy of evaluated nuclear data or to provide data for the evaluation systematically, putting emphasis on JENDL-3PR file. As for differential experiment, cross sections of high threshold (n,2n) and other activation reactions were measured for 13.5 - 15.0 MeV neutron energy in good accuracies. The revised cross section based on the present experiment gave better and consistent results when applied to the comparison of reaction rates in integral

experiments.

In integral experiments, a set of data were obtained on the angle-dependent flux spectra from a slab assembly by TOF method. It provides effective means to examine the nuclear data of the medium as was demonstrated here. As for the integral experiments on reaction rates, overall accuracy of the calculational prediction are checked by means of the ratios of calculated to measured values for three different assemblies. Efforts are being continued in assigning the effects due to other factors in order to unfold the uncertainty due only to the nuclear data used in the analyses.

References

1) "International Tokamak Reactor - Phase II", International Atomic Energy Agency, Vienna (1983)
2) JAERI Fusion Reactor System Laboratory: "Conceptual Design of Blanket Structures for Fusion Experimental Reactor (FER) JAERI-M 83- 216 (in Japanese) (1983)
3) M. Abdou: Int. Conf on Nuclear Data for Science and Technology Anterp, Belgium, Sep. 6 - 10, 1982
4) T. Nakamura: Poster session, present meeting
5) Y. Ikeda et al.: Int. Conf. on Nuclear Data for Basic and Applied Science, Santa Fe, New Mexico, USA, May 13 - 17, 1985
6) Y. Ikeda et al.: p. 109, JAERI-M 85-116 (1985)
7) Y. Oyama and H. Maekawa: JAERI-M 83-195 (1983)
8) Y. Oyama et al.: JAERI-M 85-031 (1985)
9) S. Yamaguchi et al.: p.132, JAERI-M 85-116 (1985)
10) H. Maekawa: Proc. of Specialists' Meeting on Nuclear Data for Fusion Neutronics, Tokai, Jul. 23 - 25, 1985
11) Y. Oyama et al.: Private communication

Table 1 The Summary of the Results for High Threshold (n,2n) Ractions

Summary of results

1. $^{58}Ni(n,2n)$: higher than ENDF/B-V (> 14.5 MeV)
   lower than ENDF/B-V (< 14.0 MeV)
   agree with Winkler's data
2. $^{59}Co(n,2n)$: lower than ENDF/B-V
   agree with JENDL-2
3. $^{90}Zr(n,2n)$: agree with IRDF-82, Winkler's data
4. $^{93}Nb(n,2n)$: agree with Nethaway's data
   lower than ANL/FPP/TM-115(Greenwood)
5. $^{197}Au(n,2n)$: agree with ANL/FPP/TM-115(")

Table 2 Measurement of angle-dependent leakage spectrum.

- Time-of-flight method
- Thickness:
  -- 5, 20, and 40 cm for Li_2O and C slab assemblies
  -- 10 and 30 cm for lithium-metal slab assemblies
- Angle: 0, 12.2, 24.9, 41.8 and 66.8 deg
- Energy: 0.5 ~ 16 MeV for Li_2O and C slabs
  0.05 ~ 16 MeV for lithium-metal slabs

Table 3 Sensitivity of the Reaction Rate of the Choice in the Parameters

Parameter	Sensitive Energy Range	Sensitivity
Processing Code	Whole	2 -3 %
Group Structure	High and Low Ends	5 - 10 %
Weighting Function	Low	20 - 30 %
Cross Section File	Whole	10 %

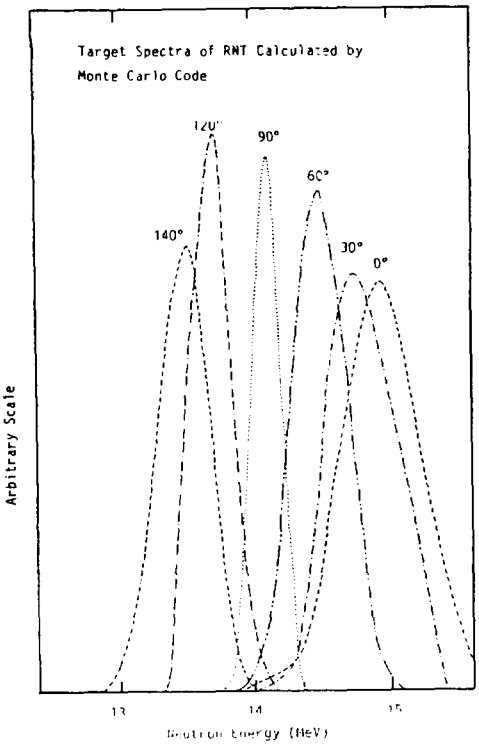

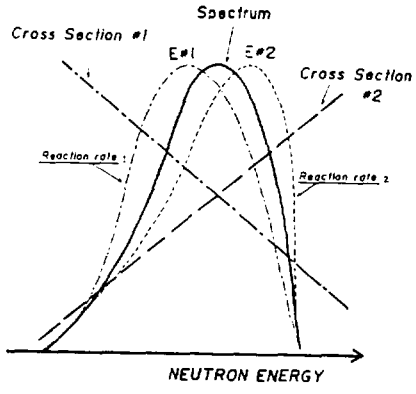

Fig. 1 Effective Reaction Energy

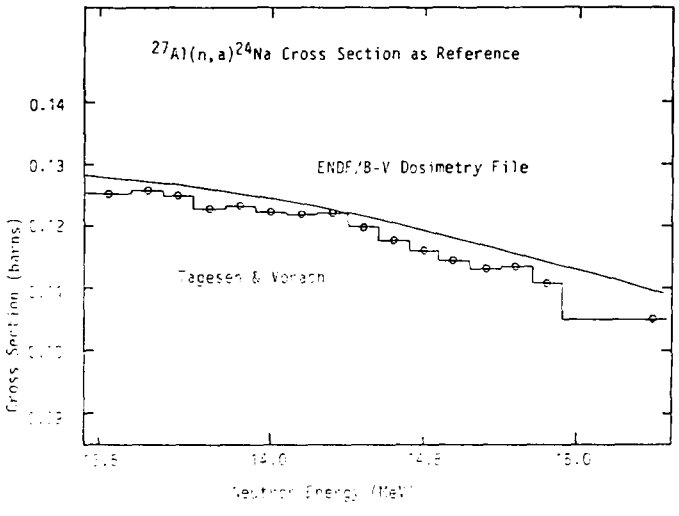

Fig. 2 Reference Cross Section

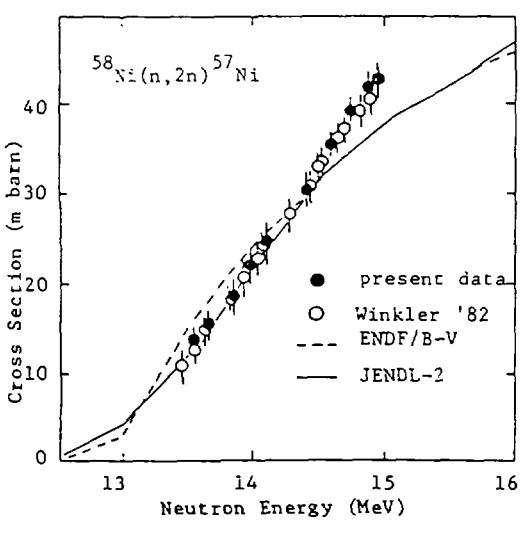

Fig. 3 Cross section of $^{58}Ni(n,2n)$

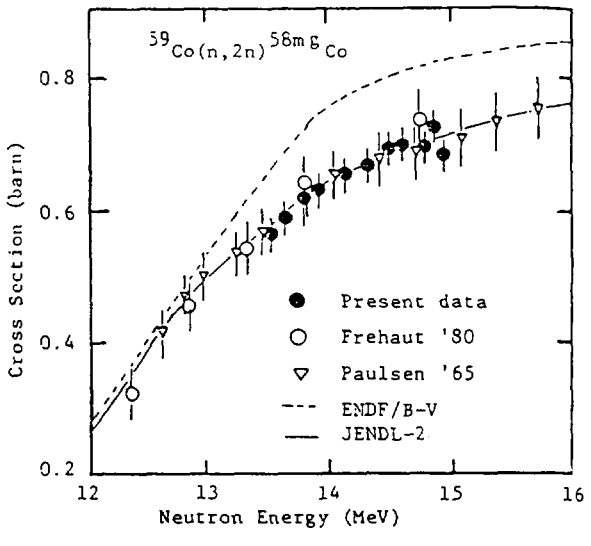

Fig. 4 Cross section of $^{59}Co(n,2n)$

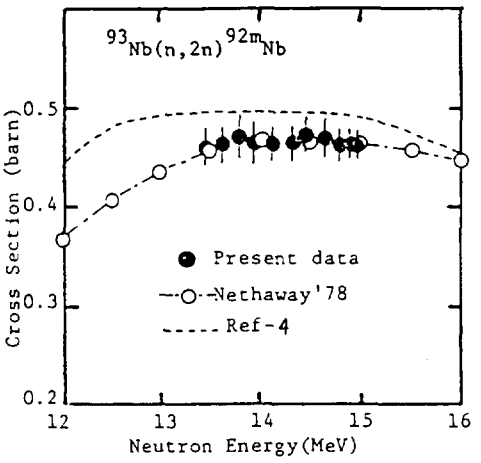

Fig. 5 Cross Section of ^{93}Nb(n,2n)

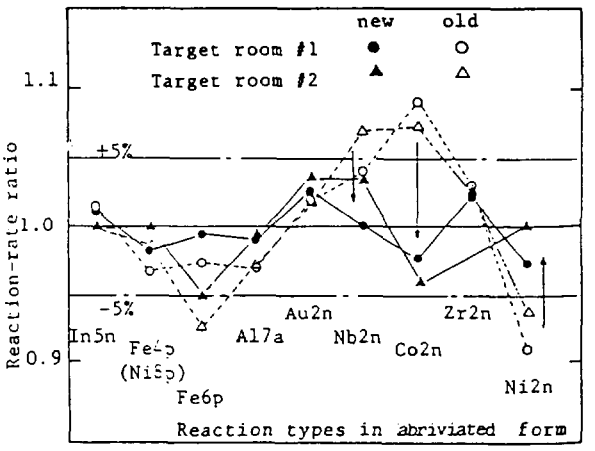

Fig. 6 Reaction-rate ratios of the calculation by unfolded spectra to the measurements

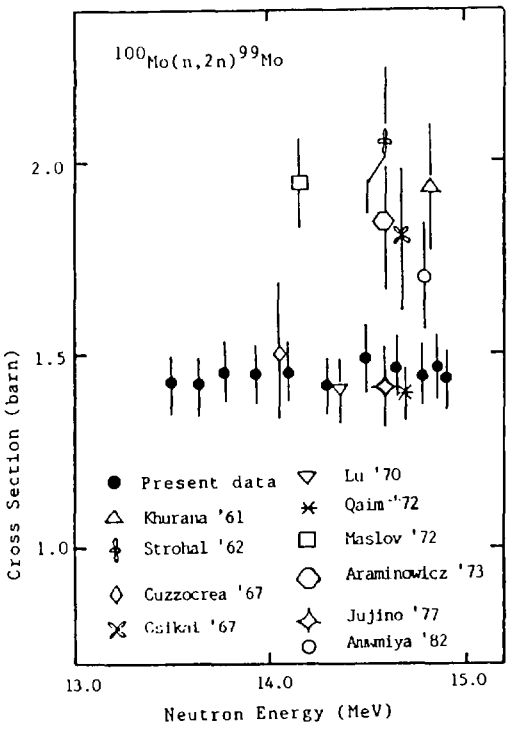

Fig. 7 Cross section of ^{100}Mo(n,2n)

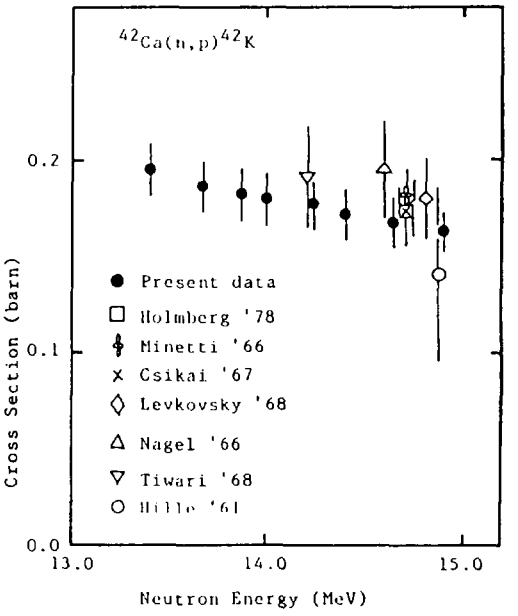

Fig. 8 Cross Section of ^{42}Ca(n,p)

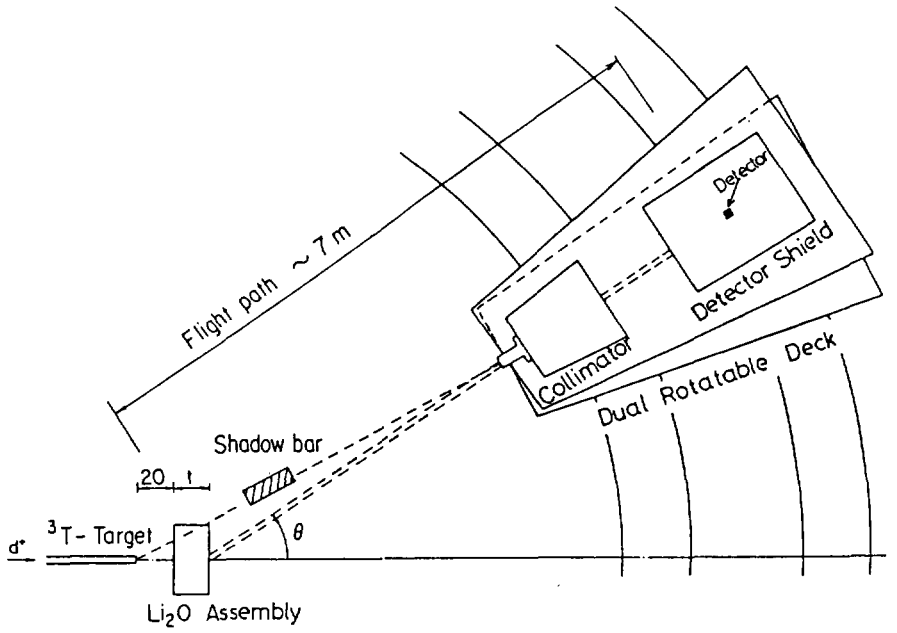

Fig. 9 Experimental Arrangement for Leakage Spectrum by TOF Method

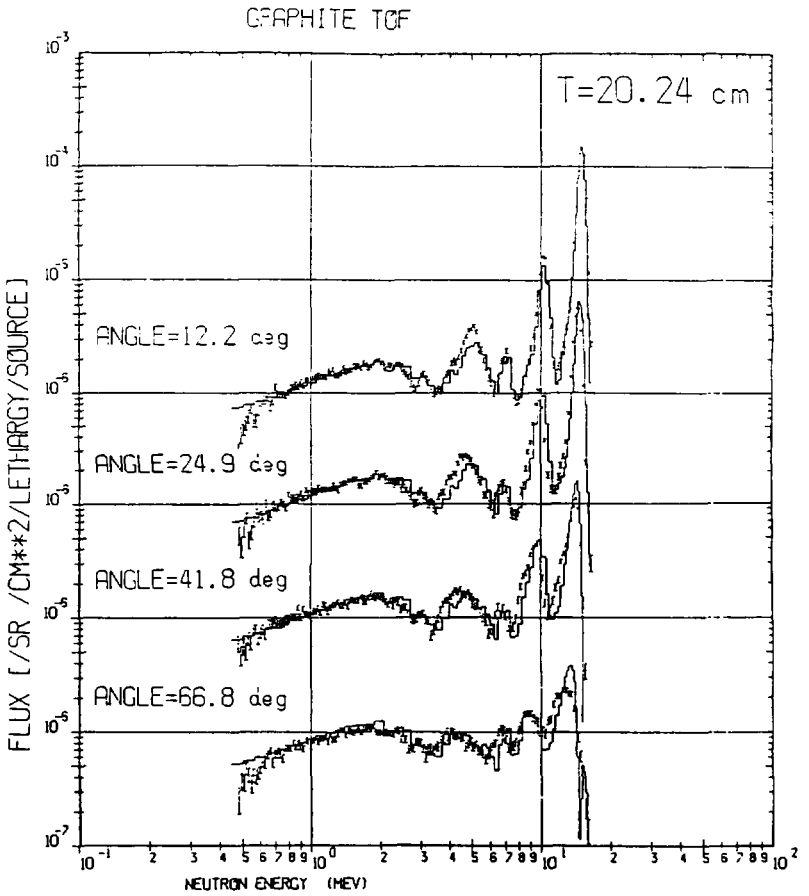

Fig. 10 Angle-dependence of leakage spectra from the20.24 cm thick Graphite Slab

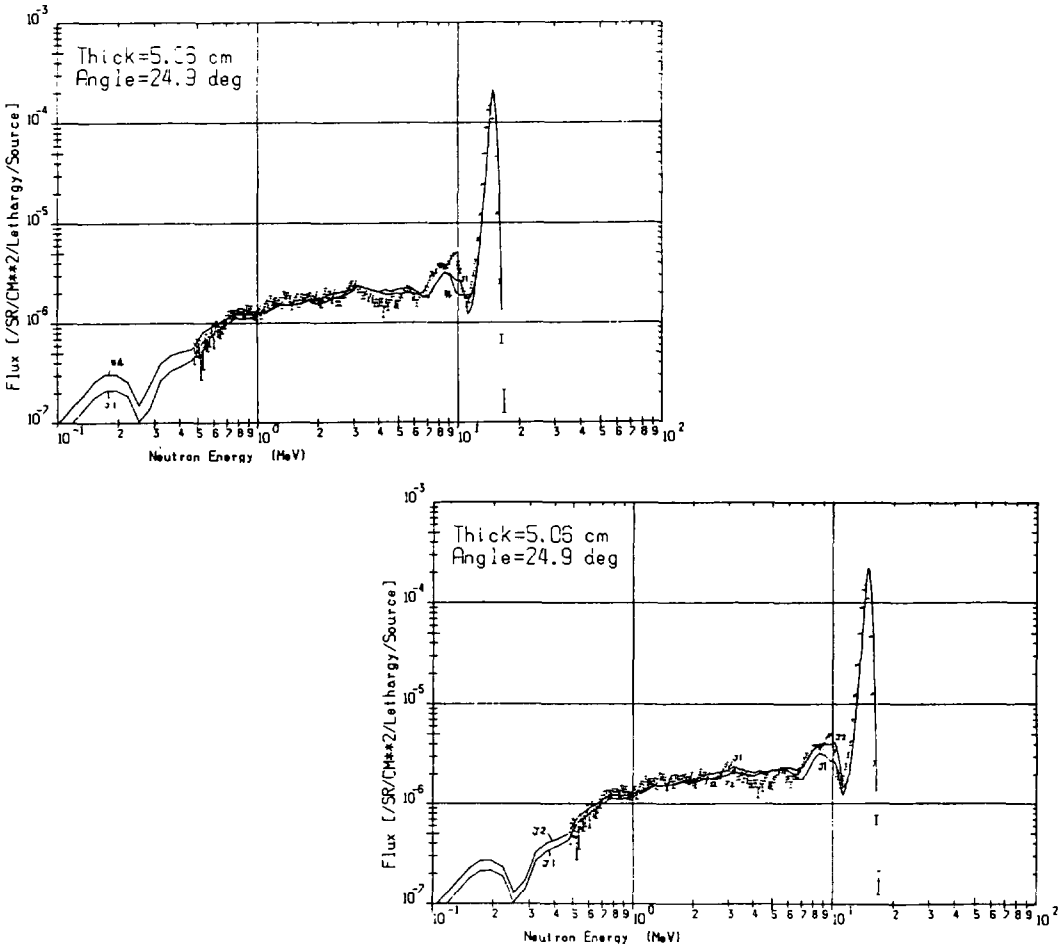

Fig. 11 Measured and Calculated Leakage Spectra from the 5.06 cm thick Slab

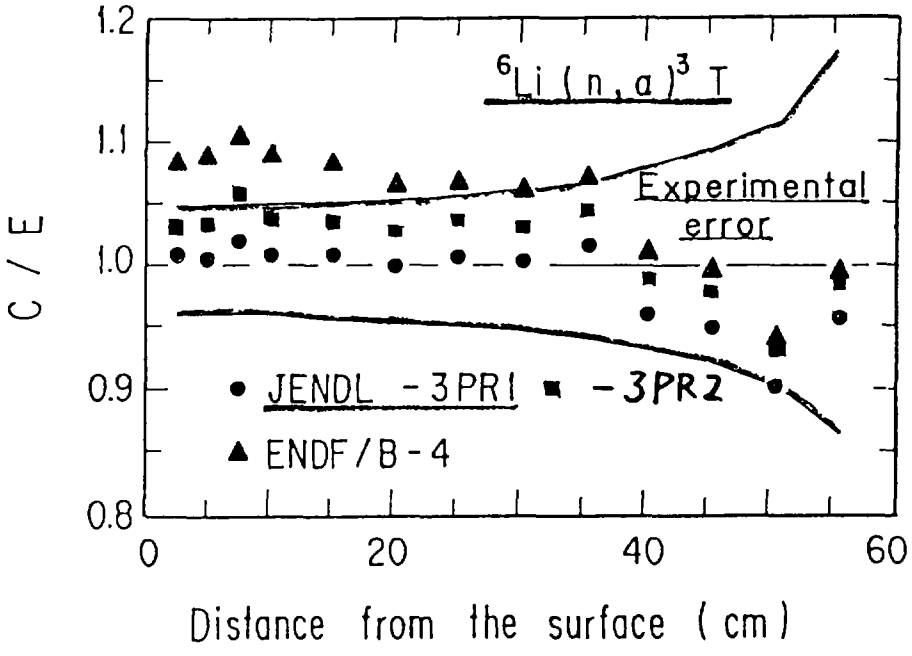

Fig. 12 Comparison of C/E values for tritium production rate of ^{6}Li in the Li_2O assembly.

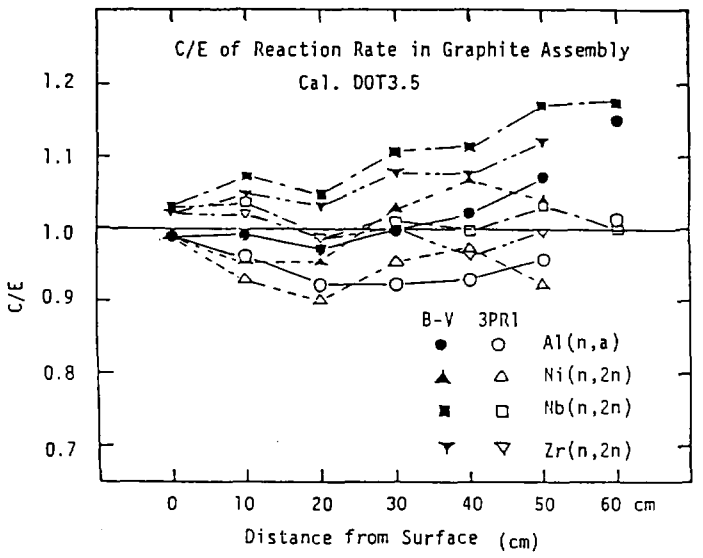

Fig. 13 The C/E Values of Reaction Rates for High Threshold Energy in Graphite Assembly

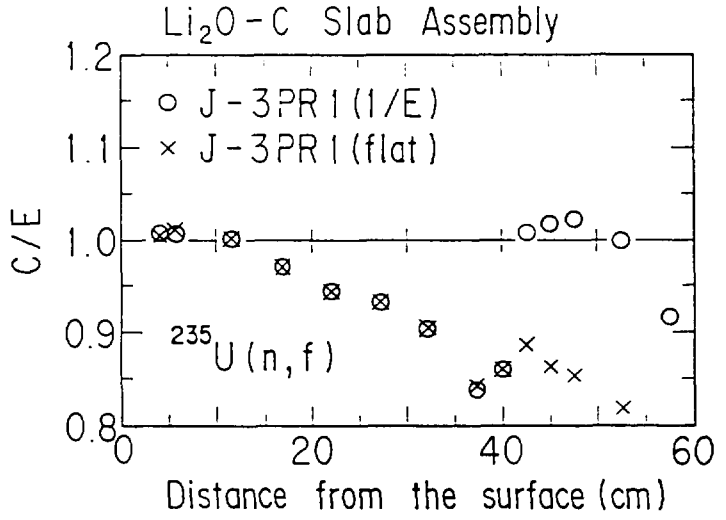

Fig. 14 Comparison of C/E Values for $^{235}U(n,f)$ Rate in the Li_2O Assembly

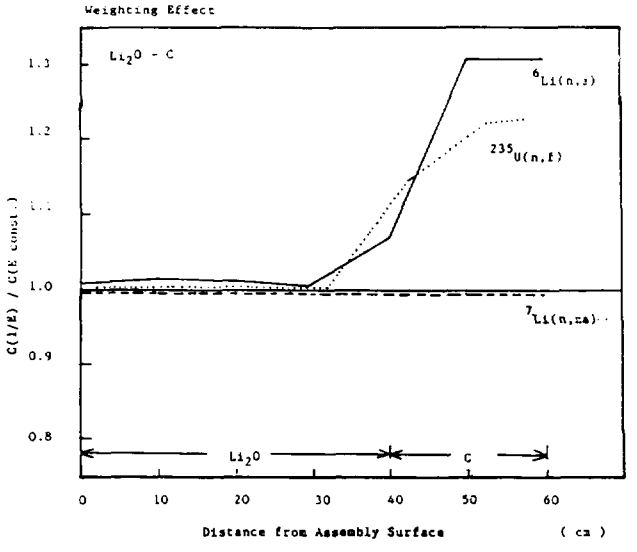

Fig. 15 Comparison of the Effect of Weighting Function for Cross Section Set in Survey Calculation

5.3 Nuclear Data for Fusion Blanket Neutronics

Akito Takahashi

Department of Nuclear Engineering
Osaka University
Yamadaoka 2-1, Suita, Osaka, Japan

Major problems in nuclear data are pointed out by summarizing results of recent integral experiments, especially from a tritium breeding point of view. Concerning the problems, latest studies on nuclear data for lithium, carbon and lead are introduced. Discussions are given for tritium production cross sections, (n,2n) cross sections and differential neutron emission cross sections at 14 MeV. Conclusions are recommendations for future reevaluations.

1. Summary of recent integral experiments

In last few years, integral experiments on fusion blanket neutronics have been done intensively in Japan, and somewhat in other countries. A key issue in these works can be found in calculational predicabilities of tritium breeding ratios in "fast" and "thermal" blankets. Discrepancies between experimental and calculational tritium-production-rates (TPR) or tritium-breeding-ratios (TBR) should be often fed back to problems of nuclear data adopted in calculations. Problems have been pointed out in tritum production cross sections and secondary neutron data of breeders (lithium or lithium-compounds) and reflectors (graphite, et al.) for fast blankets, and in (n,2n) cross sections and secondary neutron data of neutron multipliers (beryllium, lead, et al.) for thermal blankets.

At the OKTAVIAN facility of Osaka University, integral experiments and their analyses have been carried out for spherical asseblies of lithium metal[1-4], slabs of lithium metal[5] and lead spheres[6,7]. At the FNS facility of JAERI, works have been done for pseudo-spherical assemblies of Li_2O[8,9], slabs of Li_2O[10] and pseudo-cylindrical assemblies of Li_2O with beryllium layer[11]. At the RTNS-I facility of LLNL, neutron multiplication experiment was carried out for beryllium spheres[12].

A review paper on the works at OKTAVIAN[13] has been given already at the last Santa-Fe Conference, and the works at FNS are reviewed by Dr. Nakamura

in this seminar[14]. The analysis of the LLNL Be-sphere experiment has not thoroughly been done[12]. Therefore, we repeat here briefly the results and conclusions stated in our previous review[13]; For the 120 cm diam Li sphere experiment, very good agreements between experimental and calculational TPR are seen with $^{6}Li(n,t)$ reactions, while significant overestimation by the calculation using ENDF/B-IV and good agreement by the calculation using JENDL-3PR1 with respect to $^{7}Li(n,n't)$ reactions. For the 40 cm thick lithium slab with 20 cm graphite reflector, however, there are found discrepancies between experimental and calculational TPR in both of $^{6}Li(n,t)$ and $^{7}Li(n,n't)$ reactions. For the neutron multiplication experiments with lead spheres, calculations by using the ENDF/B-IV or V data underestimate significantly multiplication factors and give much softer leakage spectra than experiments. From these results, we can deduce some comments as follows;

a) TBR in a pure lithium blanket can be predicted within few % uncertainty by transport calculations using the JENDL-3PR1 data.
b) Discrepancies between experiment and calculation are considerably large for reflected blankets and neutron-multipliers.
c) Improvements on nuclear data of blanket materials should be stressed for secondary neutron emission data, e. g., DDX (double differential neutron emission cross sections) and (n,2n) cross sections.

After the Santa-Fe Conference on May 1985, some progresses are seen on re-analysis of intergral experiments, new measurements of DDX data and the latest evaluation JENDL-3PR2. Concerning the three comments above mentioned, latest works at OKTAVIAN are introduced in the following to show the present status of nuclear data for lithium, carbon and lead.

2. Lithium breeder

Tritium production rates in a 30 cm thick natural lithium slab with 20 cm thick graphite reflector have been measured[5] by using the rotating target neutron source of OKTAVIAN[15]. The experimental arrangement is shown in Fig.1, where incident 14 MeV neutron fluence on the Li slab surface is monitored by Nb foils and $^{6}Li_2CO_3$ and $^{7}Li_2CO_3$ pellets set up in 1 cm gaps between slabs are irradiated. Obtained tritium production rates for both of $^{6}Li(n,t)$ and $^{7}Li(n,n't)$ reaction are compared with calculations by a 1-d transport code NITRAN associating a special transverse leakage correction, as shown in Table-1. Calculations are done for three cases; by using a) ENDF/B-IV, b) JENDL-3PR1 and c) JENDL-3PR2. In the same table, TBR valu-

es obtained by integrating TPR over the lithium region are shown. For TBR, very good agreements are obtained in all of T_6, T_7 and T_t, in the case we used the latest JENDL-3PR2 data, while considerable disagreements with the JENDL-3PR1 results and much larger disagreements with the ENDF/B-IV. For TPR, as can be seen more clearly in Fig.2-a & 2-b, scattering of C/E values by the JENDL-3PR2 calculation is completely within experimental errors, while deviations of C/E values by the ENDF/B-IV calculation from 1.0 having experimental error bands are significant. As can be noticed from Table-1, TPR values by the JENDL-3PR1 calculation are deviated from experimental ones, especially in the vicinity of the breeder-reflector interface, i. e., at 32 cm. Since tritium production cross sections were not changed in the reevaluation from JENDL-3PR1 to JENDL-3PR2, the improvement above seen is coming from the change of secondary neutron data, e. g., energy- and angle-distribution data of lithium isotopes. As seen in Fig.2-a, C/E values in the graphite region tell us that the improvement of carbon nuclear data from ENDF/B-IV to JENDL-3PR2 is considerably effective.

The results of these recent integral experiments are quite consistent with some of reaction cross sections and DDX measurements undertaken recently. Let us see here the status of lithium data in JENDL-3PR2 by comparing with recent experimental data and evaluations, limiting for ^{7}Li(n,n't) cross sections and DDX around 14 MeV. In Fig.3 are shown ^{7}Li(n,n't) cross sections for 4 evaluations, compared with recent experimental values. Overestimation in ENDF/B-IV is now clear, and other three evaluations by Young[16], Goel[17] in KfK and JENDL-3PR2[18] go delicately through experimental data by Liskien[19], Maekawa in JAERI and Takahashi[5], although JENDL-3PR2 draws the lowest curve. An evaluation between Goel and JENDL-3PR2 looks nice. In Fig.4 are shown DDX data for natural lithium, comparing with the experiment[4] at OKTAVIAN and the ENDF/B-IV data. The JENDL-3PR2 data show drastic change from the ENDF/B-IV data and reproduce very well the experiment.

It can be said that nuclear data for lithium are about to become satisfactory by the JENDL-3PR2 evaluation, as far as the application to blanket neutronics is concerned.

3. Carbon reflector

Let us see the status of evaluated data by comparing with the latest DDX data[15] at 14.1 MeV incident energy. Although the detail of the experiment will be published elsewhere, a brief outline of the experiment is

shown in the poster session of this seminar[15]. In Fig.5-a & 5-b are shown typical experimental data in comparison with two evaluations, ENDF/B-V and JENDL-3PR2. Experimental data are available for 16 angle-points from 15 to 160 deg, and angle-integrated emission spectrum is obtained from these data as shown in Fig.6, where comparison is made with ENDF/B-V and JENDL-3PR2. The overall feature of the spectrum is well reproduced by both evaluations, but there are seen delicate differences in local energy regions. These delicate differences should be eliminated so far as the TBR predicability within few % uncertainty is claimed[20].

In order to see the status on differential cross sections of partial reaction channels, angle-differential cross sections are deduced from DDX data to be compared with two evaluations and the Baba's data[21], as shown in Figs. 7 & 8. For elastic scattering, agreement is good as a whole, but there are delicate deviations in more backward angles than about 50 deg; These deviations are corresponding to the difference in the 11-13 MeV range of Fig.6. The deviation in foreward angles is obvious for the 4.43 MeV state inelastic scattering; both evaluations give milder angular distributions and smaller cross sections (see Table-2), and this is reflected in the 8-10 MeV range of Fig.6. For the 7.65 MeV state inelastic scattering, our present data are significantly lower than the Baba's data and JENDL-3PR2. The reaction cross section of $^{12}C(n,n'3\alpha)$ is the sum of cross sections of the 7.65 MeV state, 9.64 MeV state and continuum inelastic scattering. In Fig.9 is given the present datum in comparison with the two evaluations and other experiments (see also Table-2). The present datum is significantly smaller than those of the two evaluations and Baba's, but much larger than the value by Haight in LLNL who measured α-particles.

Partial cross sections are summarized in Table-2, together with the results of lead. We can claim that delicate improvements are necessary for carbon nuclear data for fusion blanket neutronics applications.

4. Lead multiplier

In the same way with the case of carbon, we shall see the latest DDX data[15] by comparing with the evaluated data, and by deducing the (n,2n) cross section, too. In Fig.10-a & 10-b are shown typical DDX data in comparison with the ENDF/B-IV data (JENDL-3PR data are not available at the moment). Experimental data are available for 15 angle points from 20 to 160 deg, and the angle-integrated emission spectrum is obtained as shown in

Fig.11. The ENDF/B-IV data clearly underestimate the experimental in the energy region less than about 6 MeV where are emitted (n,2n) neutrons predominantly. Partial differential cross sections are shown in Fig.12. In addition to the slight angular dependence, differential emission cross sections of (n,2n) reaction by experiment are significantly larger than isotropic cross sections given in ENDF/B-IV. For the elastic scattering, experimental data are much smaller in more backward angles than 100 deg, compared with the ENDF/B-IV data. The two visible collective states, i.e., 2.6 and 4.3 MeV states, of inelastic scattering are fairly well evaluated in ENDF/B-IV. However, angular-dependence in the "continuum" region is ignored in ENDF/B-IV.

Partial cross section values at 14.1 MeV are summarized in Table-2. The result for the most important cross section, namely (n,2n), by this experiment is larger by 16 % than that of ENDF/B-IV*, and still higher than ENDF/B-V and other experiments (especially the recent datum by Iwasaki[22]). The present result is however very consistent with our previous result[13] (old exp. in Fig.13), and also consistent with the integral multiplication experiment[7].

5. Conclusions

Major problems in nuclear data for fusion blanket neutronics have been discussed only for limited cases concerning tritium breeding. As a conclusion, we can state the recommendations shown in Table-3 for future re-evaluation works on lithium, carbon and lead.

Of course, this kind of study should be extended to other elements important for the candidates of breeder compounds, first wall, structural materials, shield, etc..

Acknowledgment: The author would like to acknowledge Messrs. E. Ichimura, H. Sugimoto and N. Ishigaki for their assistances in experiments at OKTAVIAN. The appreciation is also due to the operation crew of OKTAVIAN.

---

* At the oral presentation, much higher value was shown. However, fatal error in data prosessing was found later.

References

1) K. Sugiyama, K. Kanda, S. Iwasaki, M. Nakazawa, H. Hashikura, T. Iguchi, H. Sekimoto, S. Itoh, K. Sumita, A. Takahashi and J. Yamamoto : Proc. 13th Symp. Fusion Technol., Sept. 1984, Varese Italy, Vol.2, 1375-1381, Pergamon Press (1984)
2) K. Sugiyama, K. Kanda, S. Iwasaki, N. Nakazawa, H. Hashikura, T. Iguchi, H. Sekimoto, S. Itoh, K. Sumita, A. Takahashi and J. Yamamoto : Proc. 6th ANS Topical Meet. Technology for Fusion Energy, March 1985, San Francisco USA, Fusion Technol., 8[1], Parts 2(A) & 2(B), 1491-1496 (1985)
3) T. Iguchi, M. Nakazawa, H. Hashikura, J. Yamamoto, A. Takahashi, K. Sumita, K. Sugiyama, K. Kanda, S. Itagaki, S. Itoh and Y. Hino : Proc. Conf. Nucl. Data for Basic and Applied Science, May 1985, Santa Fe USA, Radiation Effects (to be published)
4) J. Yamamoto, A. Takahashi, K. Kanda, S. Itoh, K. Yugami, K. Sugiyama and K. Sumita : "Measurements and Analysis of Leakage Neutron Spectra from Lithium Spheres with 14 MeV Neutrons", ibid., Radiation Effects (to be published)
5) A. Takahashi, Y. Yanagi, S. Kohno, N. Ishigaki, J. Yamamoto and K. Sumita : Proc. 13th Symp. Fusion Technol., Sept. 1984, Varese Italy, Vol.2, 1235-1241, Pergamon Press (1984)
6) A. Takahashi, J. Yamamoto, T. Murakami, K. Oshima, H. Oda, K. Fujimoto and K. Sumita : Proc. 12th Symp. Fusion Technol., Sept. 1982, Juelich FRG, Vol.1, 687-692, Pergamon Press (1982)
7) Y. Yanagi and A. Takahashi : OKTAVIAN Rep. A-8402, Osaka Univ. (1984)
8) H. Maekawa, K. Tsuda, T. Iguchi, Y. Ikeda, Y. Oyama, T. Fukumoto, Y. Seki and T. Nakamura : JAERI-M 83-196 (1983)
9) H. Maekawa, M. Nakagawa, Y. Ikeda, Y. Oyama, S. Yamaguchi, K. Tsuda, T. Fukumoto, A. Hasegawa, T. Mori, Y. Seki and T. Nakamura : "Integral Test of JENDL-3PR1 through Benchmark Experiments on Li_2O Slab Assemblies", Proc. Conf. Nucl. Data for Basic and Applied Science, May 1985, Santa Fe USA, Radiation Effects (to be published)
10) Y. Oyama and H. Maekawa : JAERI-M 83-195 (1983)
11) T. Nakamura, et al. : Trans. 1985 Fall Meet. AESJ, C40, pp.170 (1985)
12) C. Wong, et al. : "Measurements and Calculations of the Leakage Multiplication from Hollow Beryllium Sphere", Proc. 6th ANS Topical Meet. Technol. for Fusion Energy, March 1985, San Francisco USA, Fusion Tech., 8[1], (1985)

13) A. Takahashi : "Integral Measurements and Analysis of Nuclear Data Pertaining to Fusion Reactors", Proc. Conf. Nucl. Data for Basic and Applied Science, May 1985, Santa Fe USA, Radiation Effects (to be publ.)
14) T. Nakamura : "Nuclear Data and Integral Neutronics Experiments for Fusion Reactors", Proc. JNDC 1985 Seminar on Nucl. Data, Nov. 1985, Tokai Japan (to be publ. in JAERI-M); this seminar
15) A. Takahashi, E. Ichimura, H. Sugimoto and T. Katoh : "The OKTAVIAN neutron TOF and Irradiation Facility", ibid.; this seminar
16) P. G. Young : Trans. Am. Nucl. Soc., 39, 272 (1981)
17) B. Goel : Private communication
18) S. Chiba : Private communication
19) H, Liskien, et al. : Proc. Conf. Nucl. Data Sci. Tech., Antwerp 1982, p. 349, D. Reidel Publ. (1984)
20) M. A. Abdou, et al. : ANL/FPP/TM-177 (1983)
21) M. Baba, M. Ono, N. Yabuta, T. Kikuti and N. Hirakawa : "Scattering of 14.1 MeV Neutrons from B-10, B-11, C, N, O, F, and Si", Proc. Conf. Nucl. Data Basic Appl. Sci., May 1985, Santa Fe USA, Radiation Effects (to be published)
22) S. Iwasaki, H. Tamura, T. Inoue, T. Tamura, J. Koyama and K. Sugiyama : "Measurement and Analysis of Neutron Emission Spectra for Pb(n,Xn) Reaction between 14 and 20 MeV", ibid.

Table 1 : Tritium production rates and TBR in a 30 cm Li slab with a 20 cm graphite reflector

Reaction	*Axial Dis.(cm)	Reaction Rate				
		Exp.	err(%)	Cal. by NITRAN ENDF/B-Ⅳ	JENDL-3RP1	JENDL-3PR2
$^{7}Li(n,n'\alpha)T$	0.0	1.466E-2	5.7	1.6868E-2	1.4071E-2	1.4006E-2
	10.5	9.630E-3	5.9	1.1102E-2	9.4177E-3	9.7867E-3
	21.5	5.549E-3	6.5	6.1021E-3	5.2581E-3	5.6292E-3
	32.5	3.159E-3	7.8	3.3833E-3	2.9952E-3	3.2399E-3
	37.0	2.197E-3	8.2	2.3854E-3	2.1310E-3	2.3228E-3
	42.0	1.579E-3	9.9	1.6154E-3	1.4428E-3	1.5840E-3
	47.0	9.364E-4	12.4	1.0660E-3	9.5720E-4	1.0556E-3
	52.0	6.599E-4	18.3	6.4468E-4	5.7531E-4	6.2920E-4
	T_7	0.246	6.4	0.2797	0.2382	0.2473
$^{6}Li(n,\alpha)T$	0.0	6.617E-3	5.5	7.0813E-3	6.9136E-3	6.4844E-3
	10.5	4.294E-3	5.6	4.0206E-3	6.9597E-3	4.2900E-3
	21.5	4.448E-3	5.6	4.1262E-3	4.1131E-3	4.4854E-3
	32.5	4.788E-2	7.0	3.7874E-2	3.7074E-2	4.5236E-2
	37.0	1.070E-1	9.0	8.8507E-2	8.4058E-2	1.0333E-1
	42.0	1.170E-1	9.0	1.0923E-1	1.0221E-1	1.2500E-1
	47.0	9.668E-2	9.0	8.7120E-2	8.0942E-2	9.6968E-2
	52.0	2.658E-2	9.0	3.0149E-2	2.8144E-2	2.6828E-2
	T_6	0.148	5.6	0.1354	0.1342	0.1461
	Tt	0.394	6.2	0.4151	0.3723	0.3934

* Lithium region:0~32cm Graphite region:32~52cm

Table 2 : Partial cross sections at 14.1 MeV for carbon (upper) and lead (lower)

Partial cross sections for Carbon

	EXPERIMENT		JENDL3-PR2	ENDF/B-V
	σ(mb)	error	σ (mb)	σ (mb)
elastic	955	32	794	795
Q=-4.44 MeV	221	7	183	186
Q=-7.65 MeV	8.4	5.0	19.5	12.9
Q=-9.64 MeV	67.3	5.4	78.0	63.4
continuum	136	9	163	163
(n, n' 3α)	209	12	261	239

Partial cross sections for Lead

	EXPERIMENT		ENDF/B-IV
	σ(mb)	error	σ (mb)
elastic	---	--	2809
Q=-2.6 MeV	79	6	63.9
Q=-4.3 MeV	84	6	52.3
continuum	190	6	223
(n, 2n)	2492	75	2145

Table 3 : Recommendations for future reevaluation of nuclear data on lithium, carbon and lead

Lithium	ENDF/B-IV	JENDL-3PR2
	unsatisfied	satisfied
Carbon	**ENDF/B-V**	**JENDL-3PR2**
	unsatisfied	unsatisfied
elastic	SIG, AD	SIG, AD
4.43 MeV state	SIG, AD	SIG, AD
7.65 MeV state	AD	SIG, AD
9.64 MeV state	AD	AD
(n,n'3α)	SIG, AD, ED	SIG, AD, ED
Lead	**ENDF/B-IV**	
	unsatisfied	
elastic	AD	
2.6 MeV state	AD	
4.3 MeV state	SIG, AD	
inel. cont.	AD, ED	
(n,2n)	SIG, AD, ED	

SIG ; partial reaction cross section

AD ; angular distribution, ED ; energy distribution

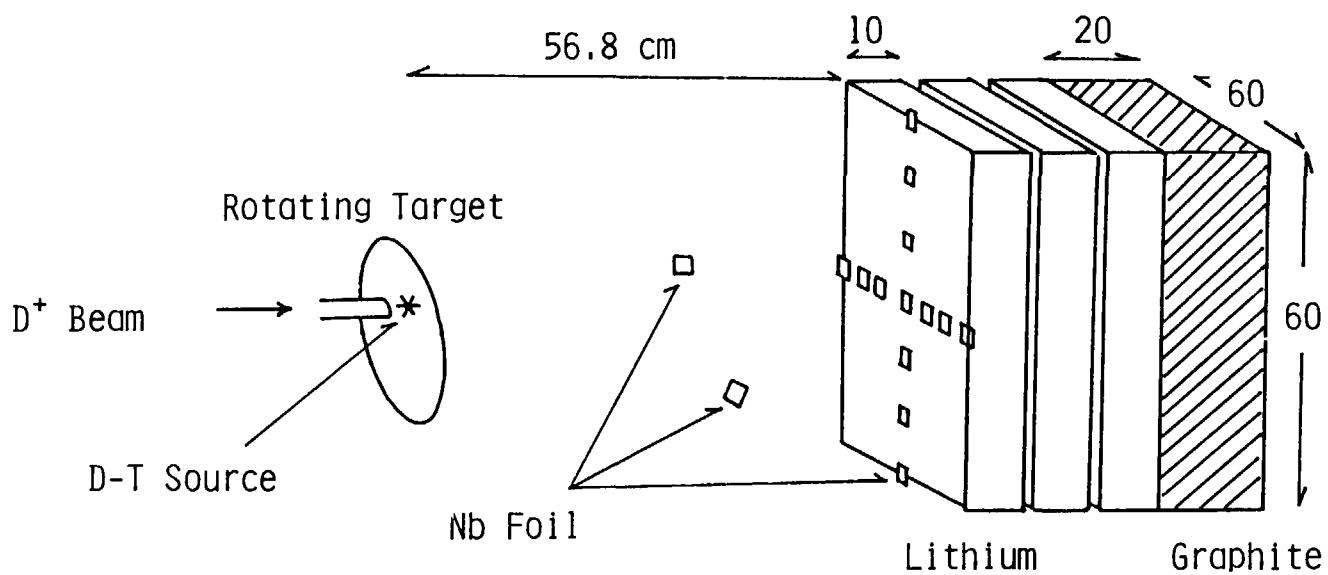

Fig.1 Experimental arrangement of TPR measurement in a 30 cm Li slab with graphite reflector

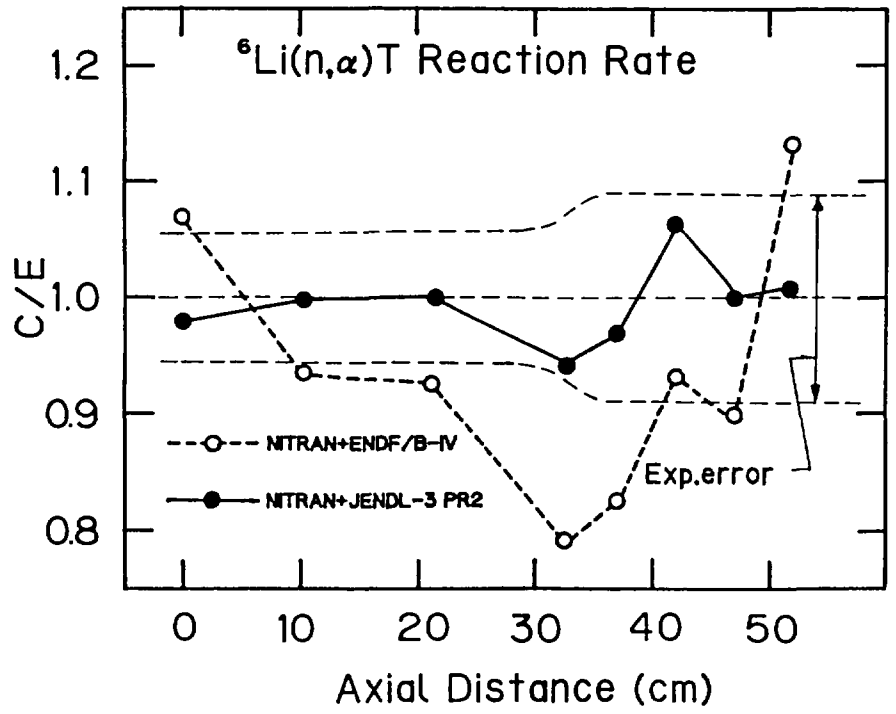

Fig.2-a C/E values of ^{6}Li(n,t) reaction rates in a 30 cm Li slab with graphite reflector

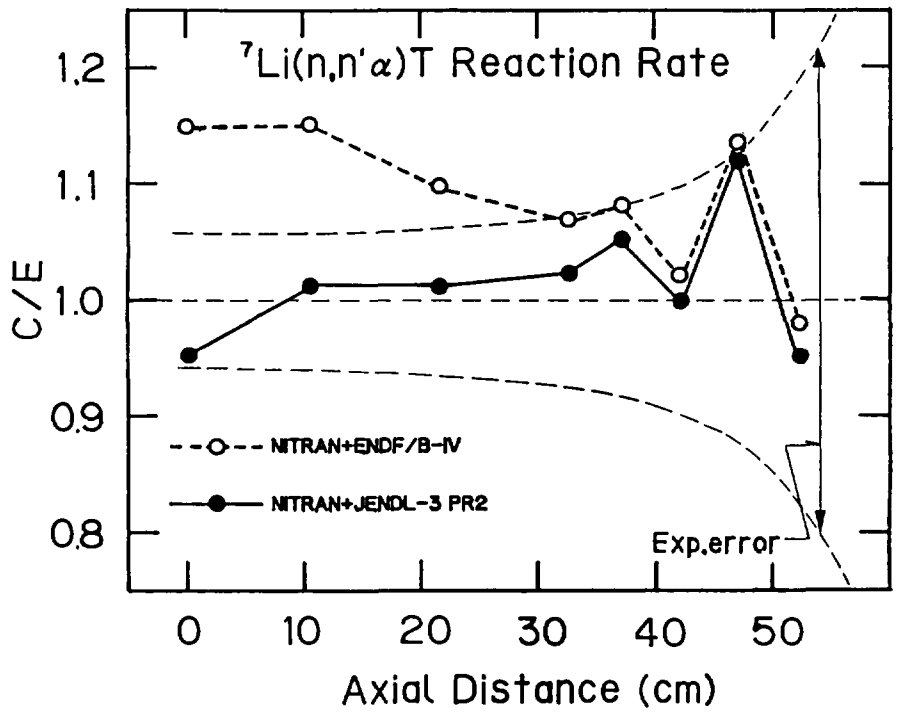

Fig.2-b C/E values of ^{7}Li(n,n't) reaction rates in a 30 cm Li slab with graphite reflector

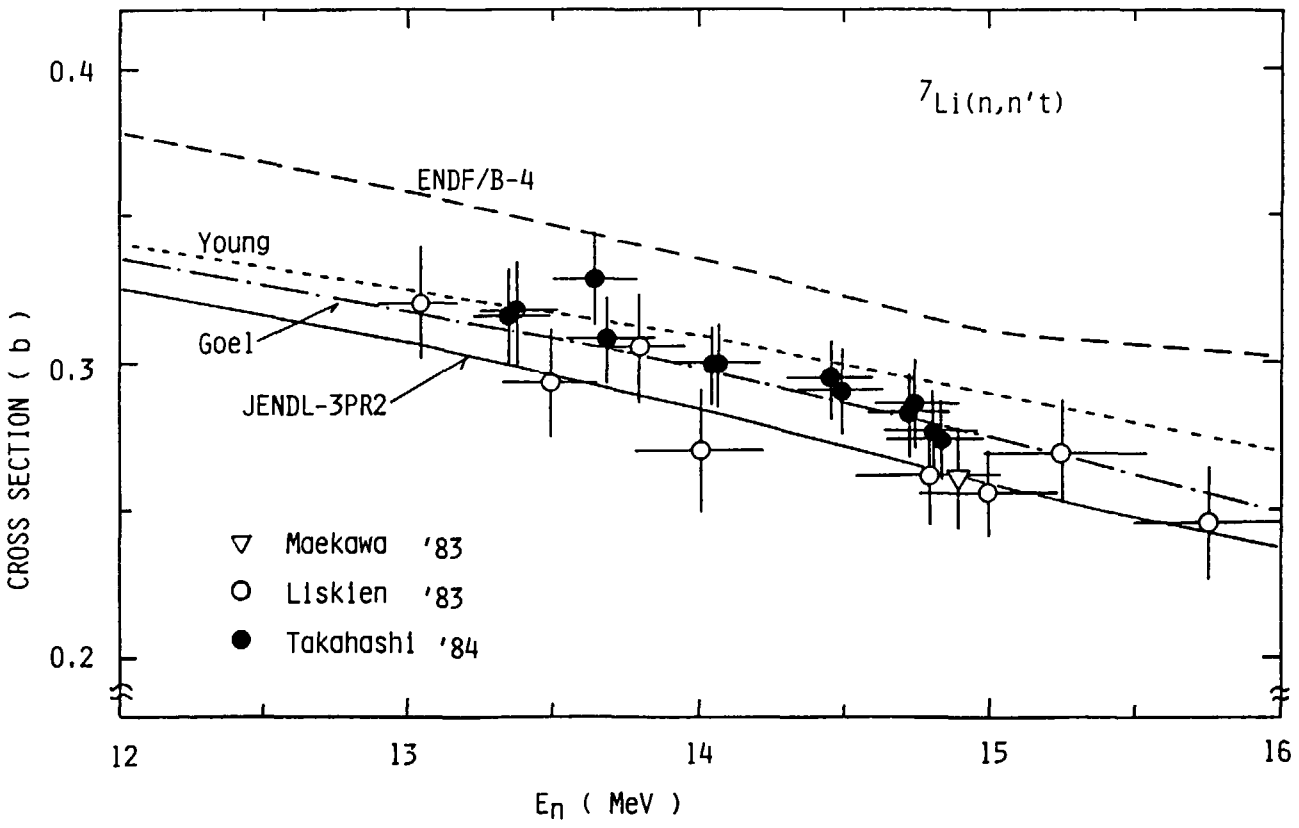

Fig.3 ^{7}Li(n,n't) cross sections around 14 MeV

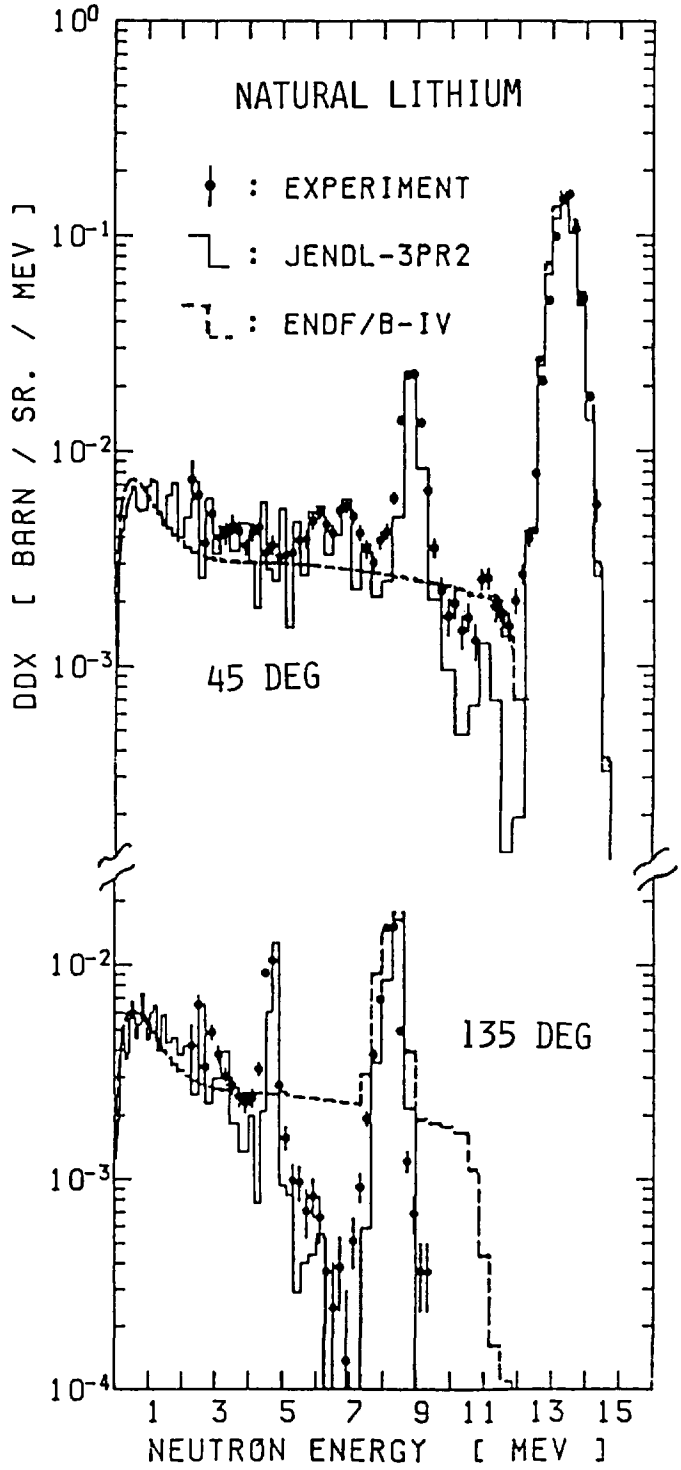

Fig.4 DDX data for natural lithium

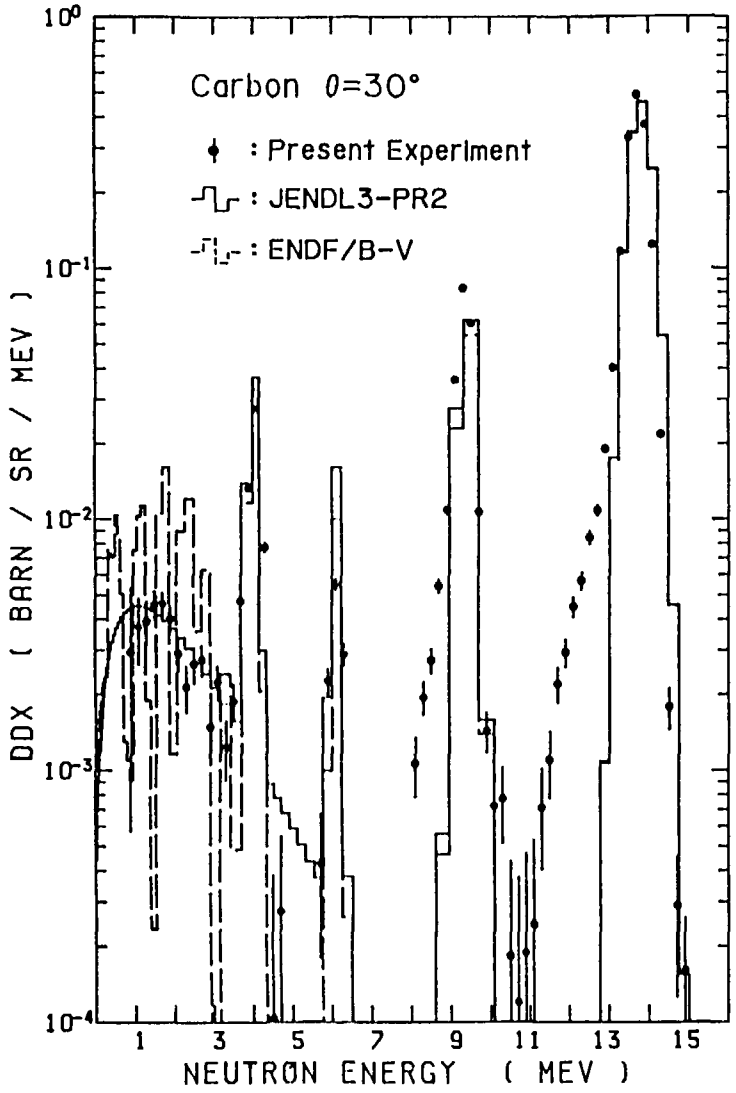

Fig.5-a
DDX data of carbon at 14.1 MeV incident neutron energy, for 30 deg (Lab. angle)

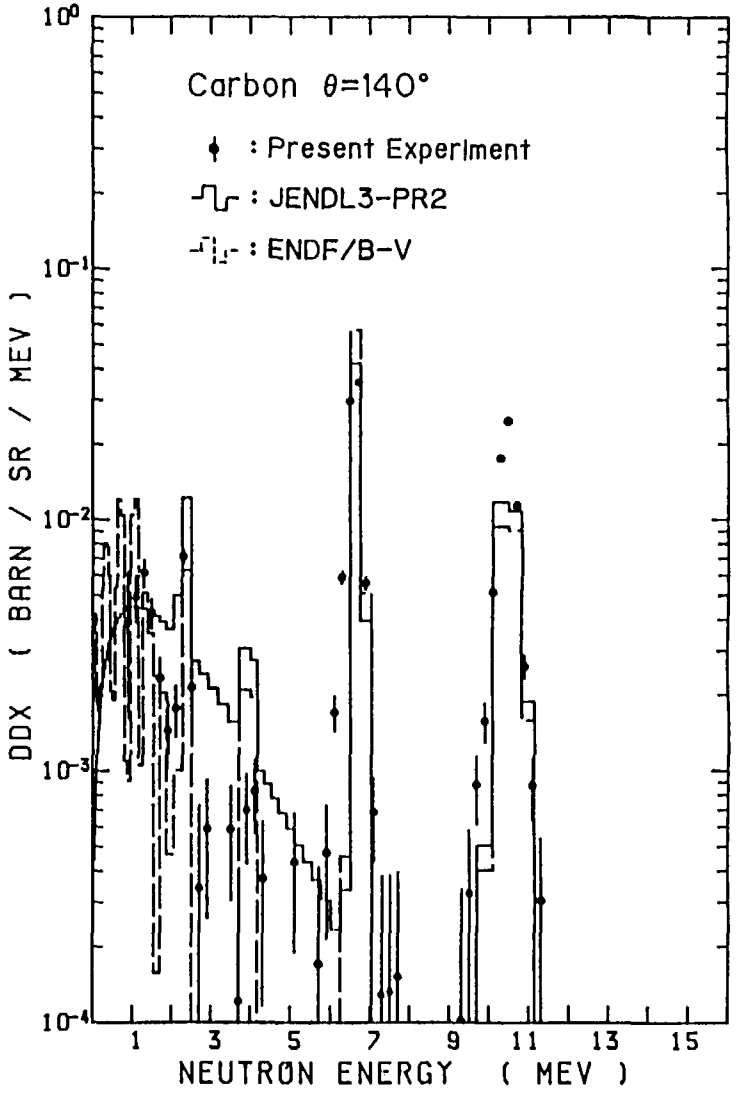

Fig.5-b
DDX data of carbon at 14.1 MeV incident neutron energy, for 140 deg (Lab. angle)

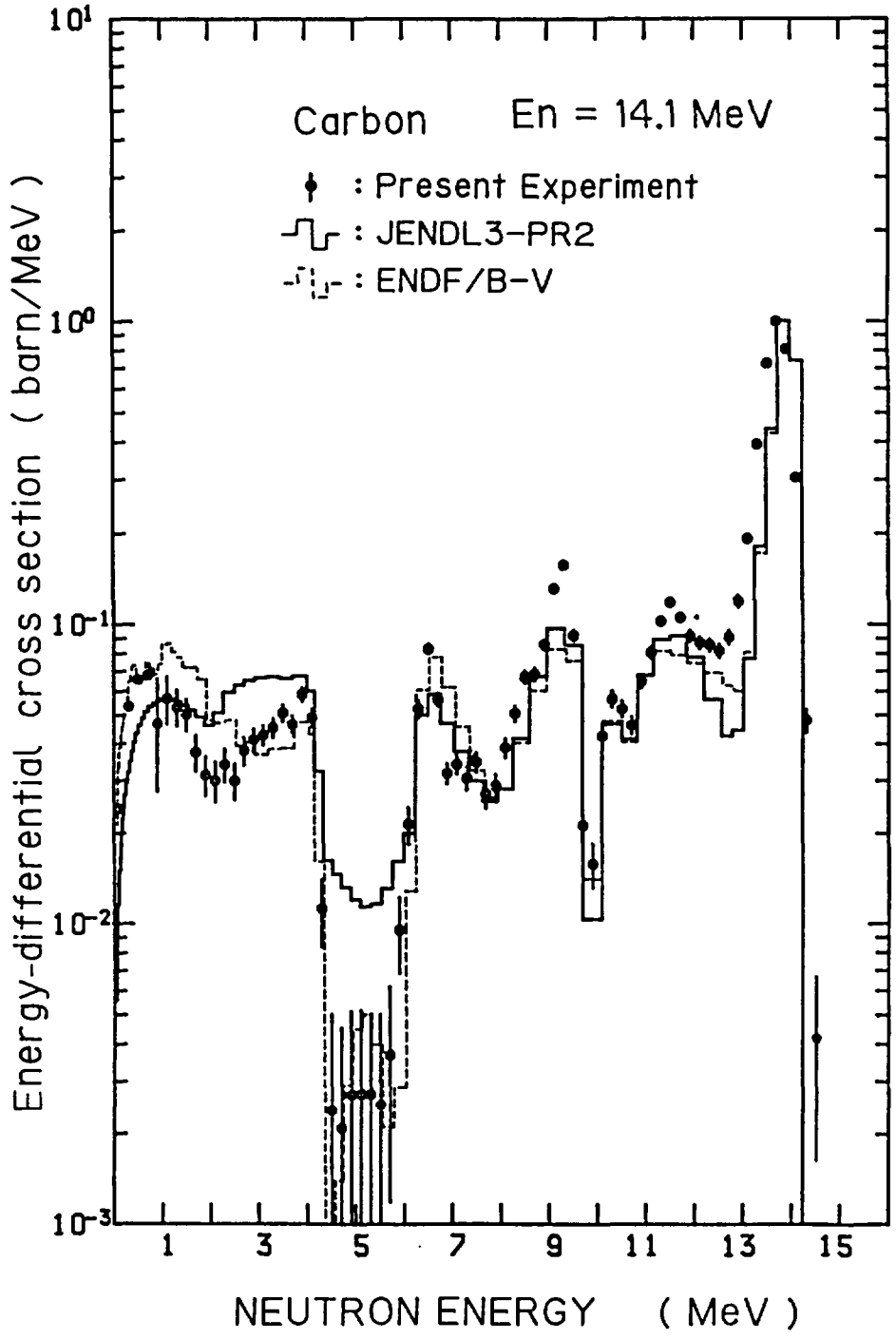

Fig.6 Angle-integrated neutron emission spectrum of carbon, at E_n=14.1 MeV

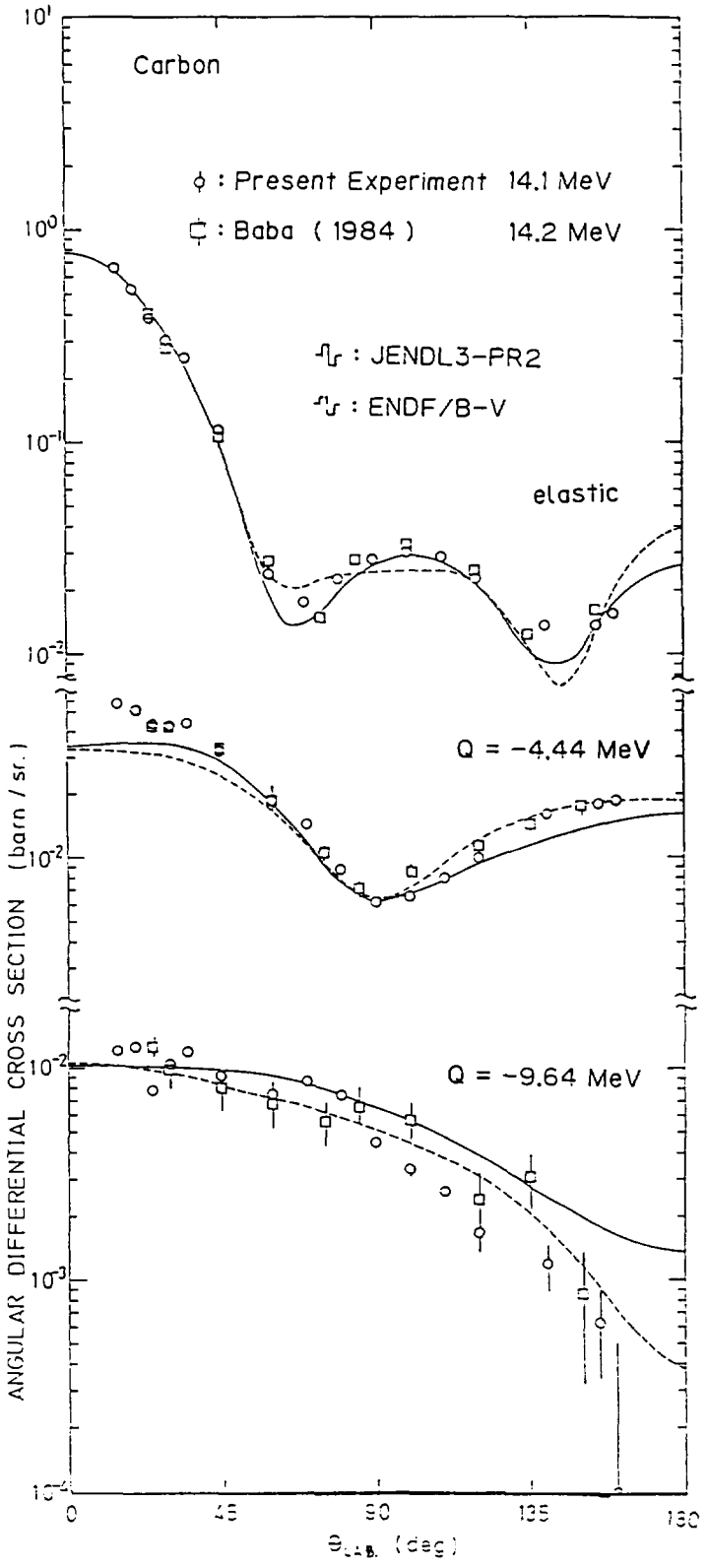

Fig.7 Partial differential cross sections of carbon at E_n=14.1 MeV, for elastic, 4.44 and 9.64 MeV state

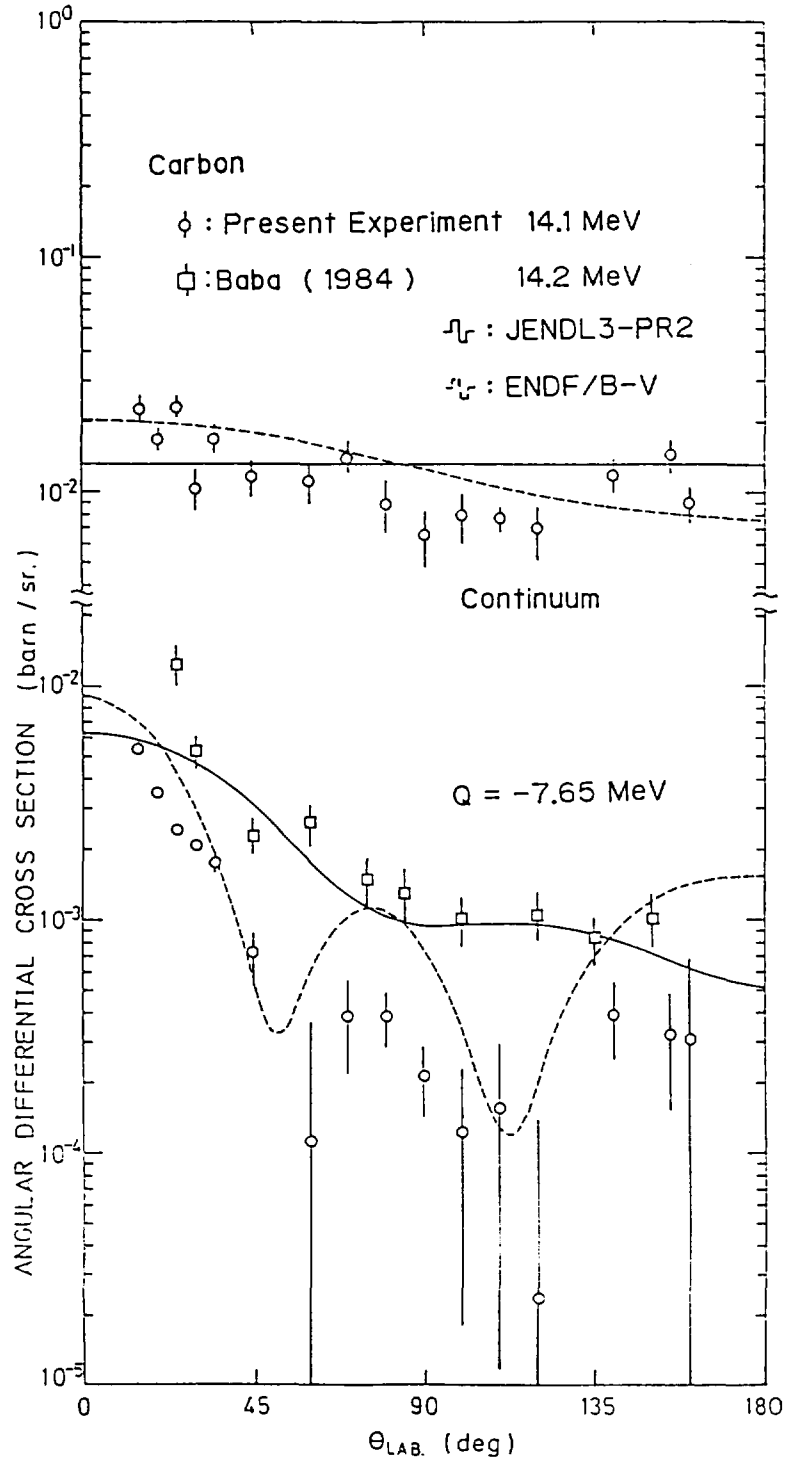

Fig.8 Partial differential cross sections of carbon at E_n=14.1 MeV, for continuum and 7.65 MeV state

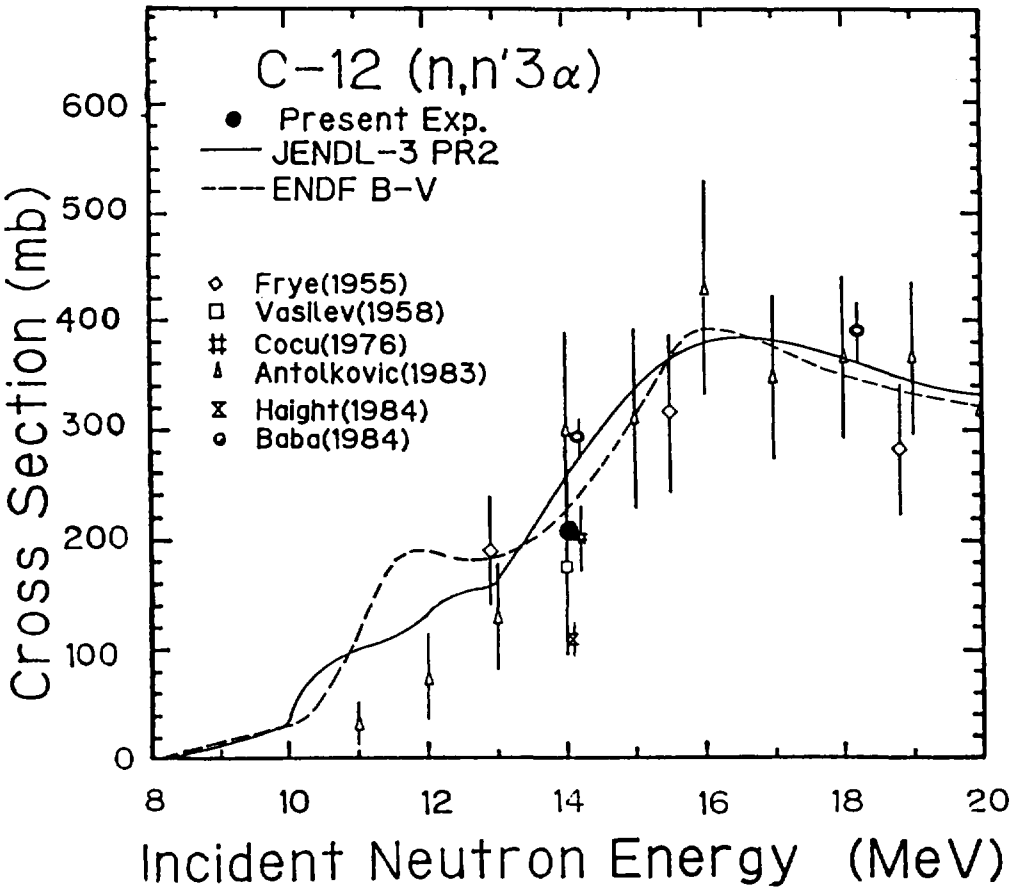

Fig.9 C(n,n'3α) cross sections

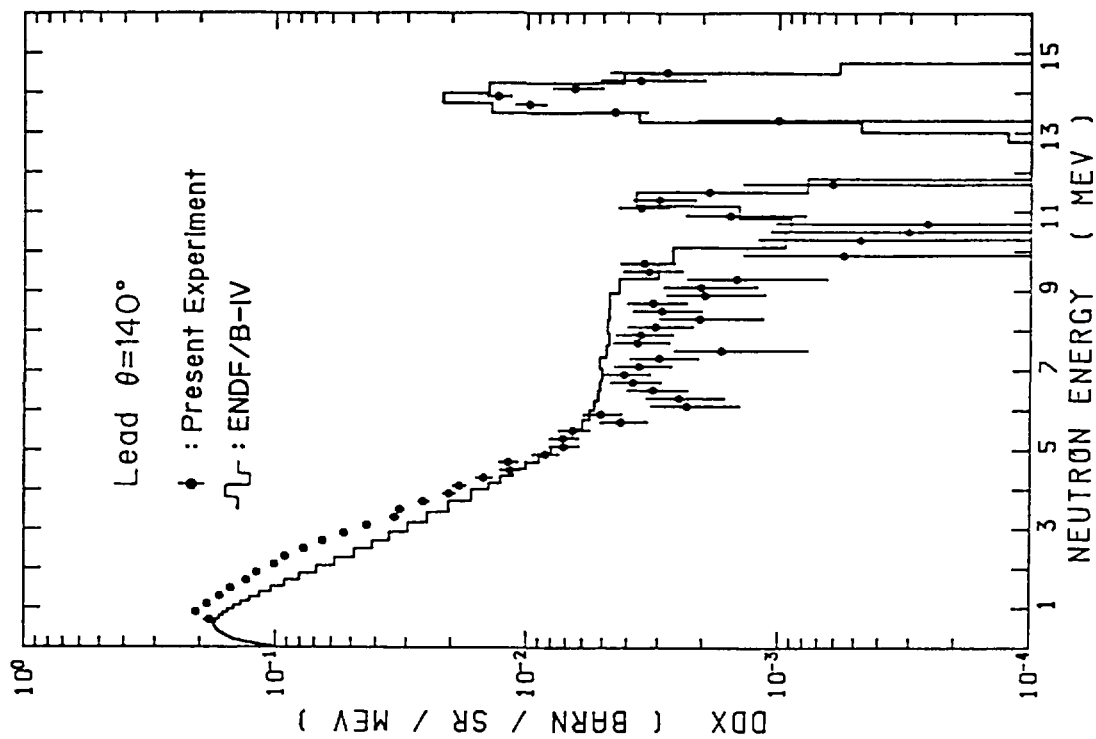

Fig.10-b DDX data of lead at E_n=14.1 MeV, for 140 deg (Lab. angle)

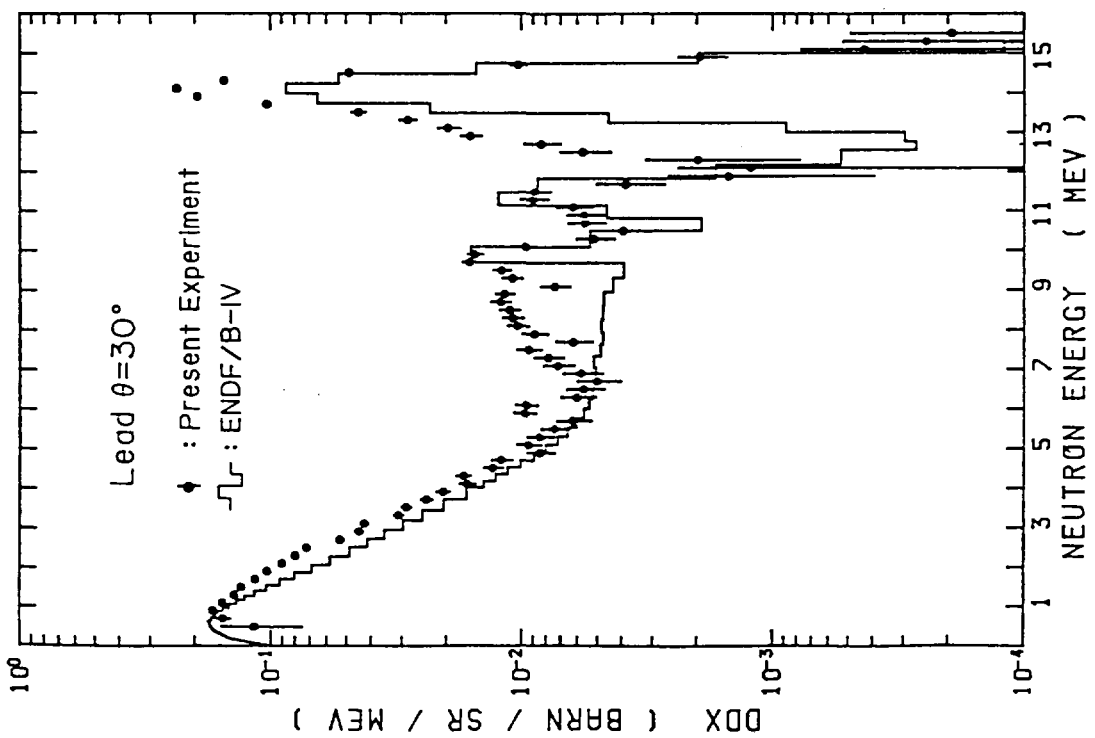

Fig.10-a DDX data of lead at E_n=14.1 MeV, for 30 deg (Lab. angle)

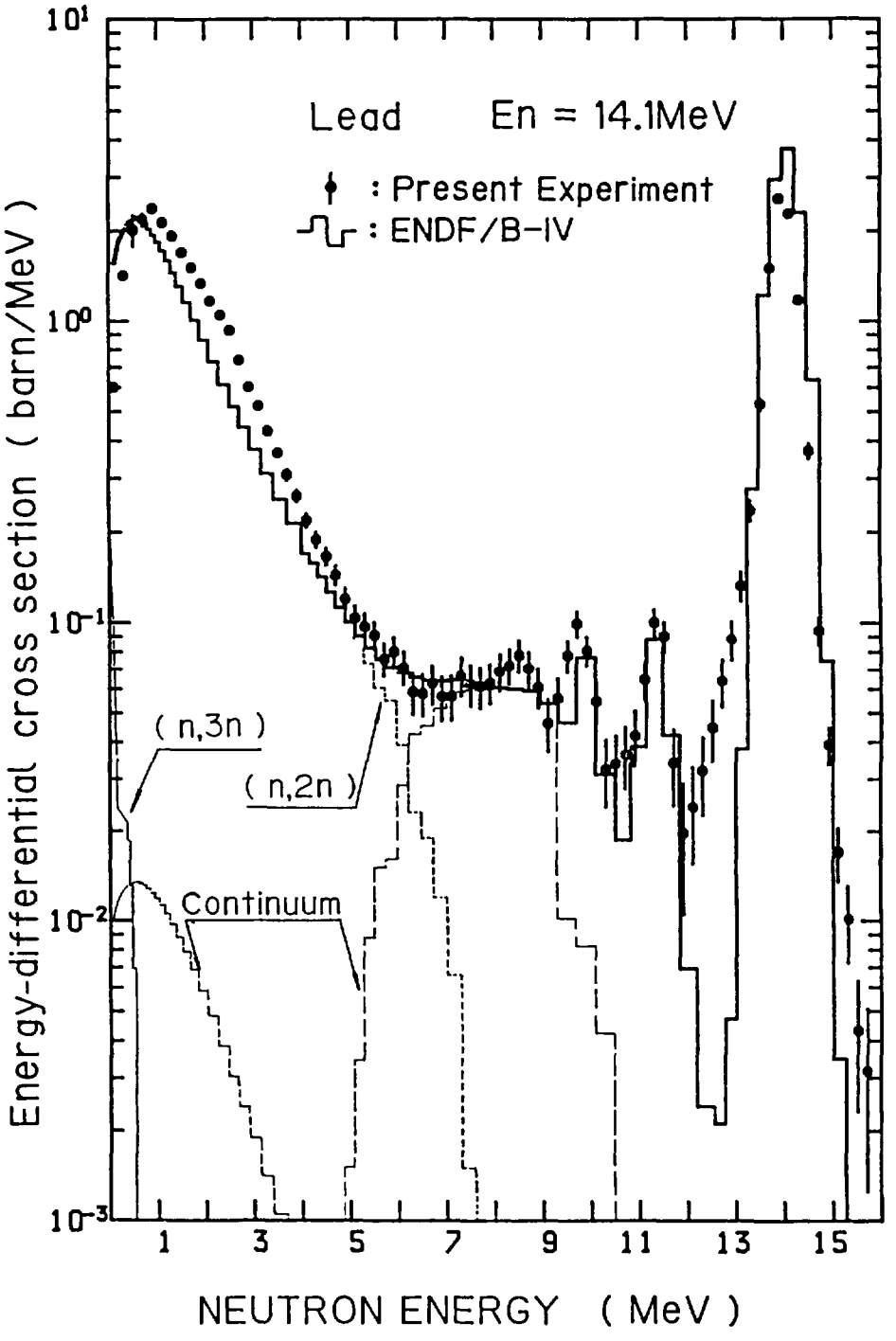

Fig.11 Angle-integrated neutron emission spectrum of lead, at E_n=14.1 MeV

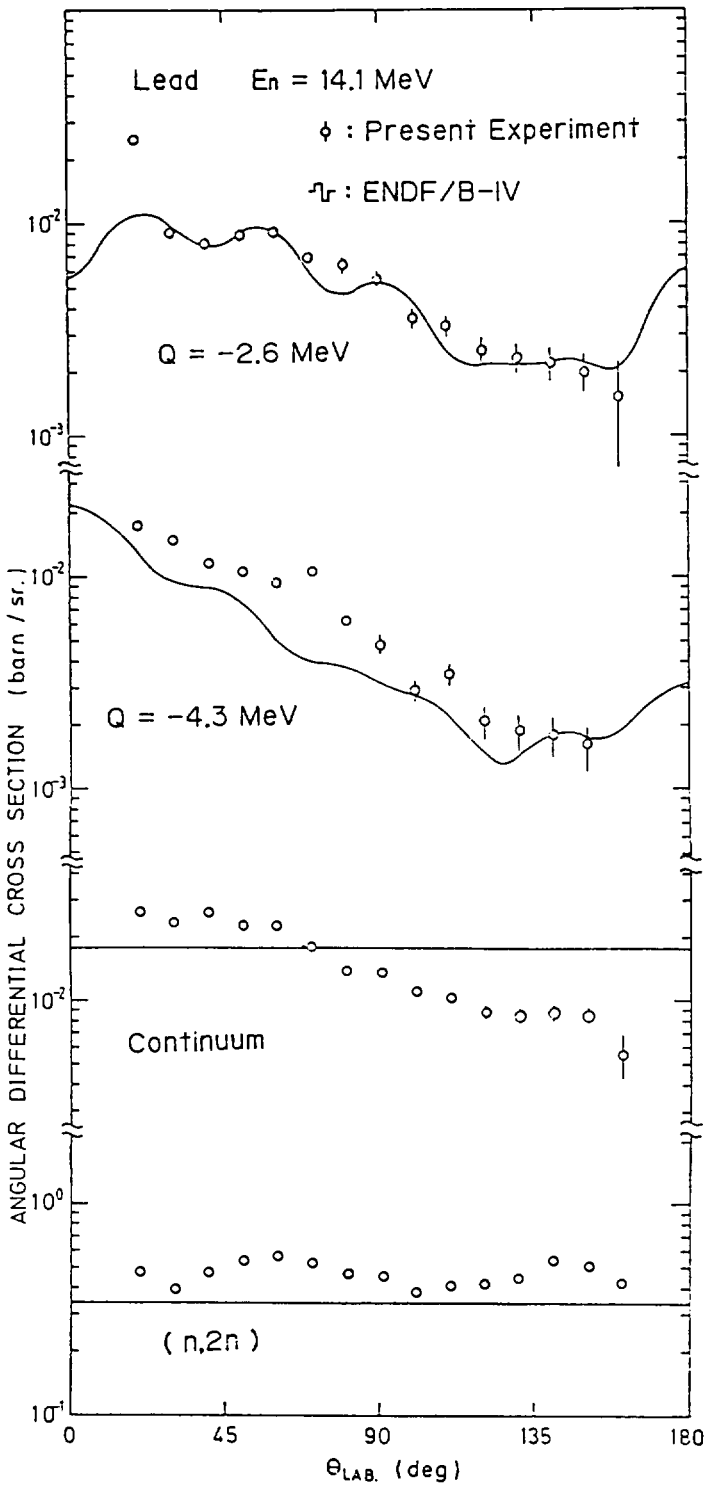

Fig.12 Partial differential cross sections of lead, at E_n=14.1 MeV

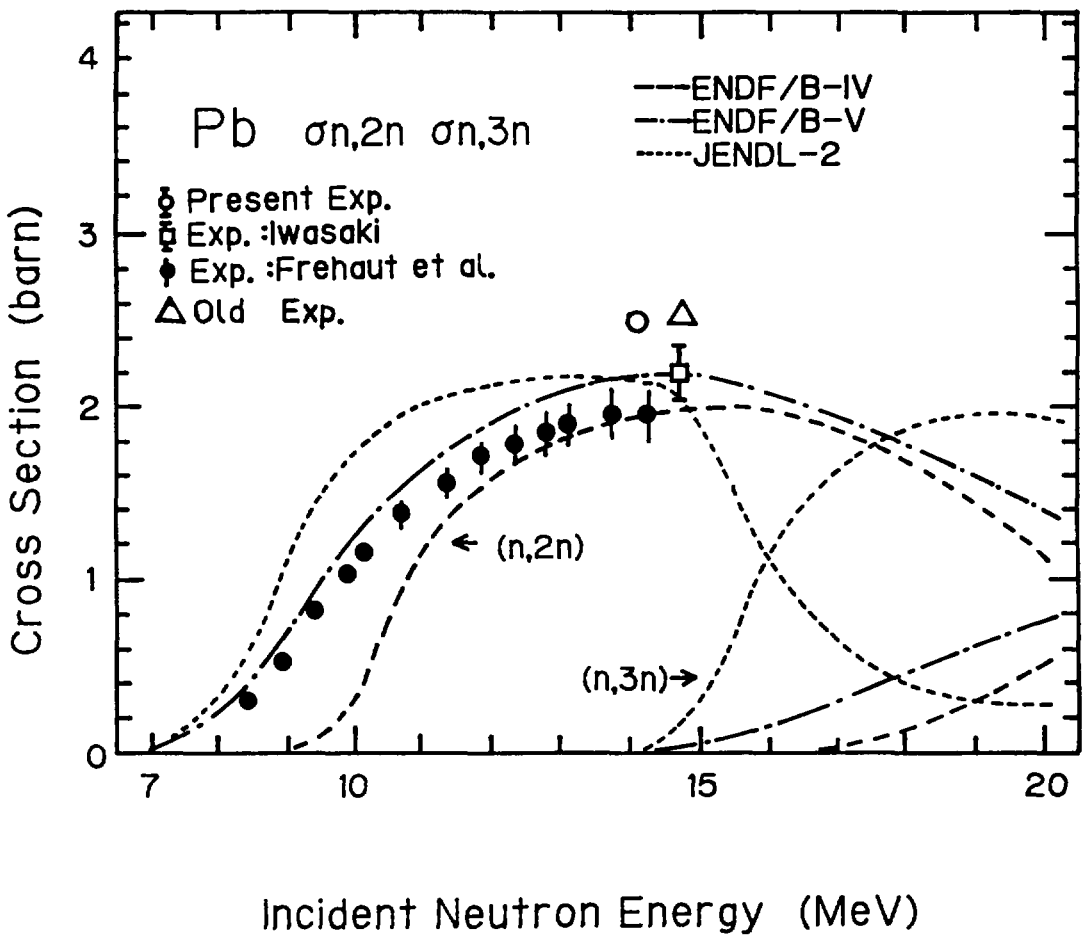

Fig.13 Pb(n,2n) cross sections

6. PROBLEMS ON HEAVY NUCLIDE NUCLEAR DATA

6.1 Nuclear Data Evaluation for Heavy Nuclides

Tsuneo Nakagawa
Japan Atomic Energy Research Institute
Tokai-mura, Naka-gun, Ibaraki-ken

The simultaneous evaluation for the fission cross section of ^{235}U, ^{238}U, ^{239}Pu, ^{240}Pu and ^{241}Pu, and the capture cross sections of ^{197}Au and ^{238}U was performed by the JNDC Subworking Group on Heavy Nuclide Data. The evaluated data was obtained in the energy range from 50 keV to 20 MeV by means of the generalized least-squares method and the B-spline functions. The presently obtained fission cross sections of ^{235}U and ^{239}Pu are a few percent smaller than the JENDL-2 data in the energy range below 1 MeV.

1. Introduction

Evaluation work of neutron nuclear data of the following 20 heavy nuclides for JENDL-3 is being made by the JNDC Subworking Group on Heavy Nuclide Data*).

^{228}Th, ^{230}Th, ^{232}Th, ^{233}Th, ^{234}Th, ^{231}Pa, ^{233}Pa, ^{232}U, ^{233}U, ^{234}U, ^{235}U, ^{236}U, ^{238}U, ^{237}Np, ^{236}Pu, ^{238}Pu, ^{239}Pu, ^{240}Pu, ^{241}Pu, ^{242}Pu.

Among the data of these nuclides, the fission cross sections of ^{235}U, ^{238}U, ^{239}Pu, ^{240}Pu and ^{241}Pu and the capture cross section of ^{238}U have been evaluated with the simultaneous evaluation method. The capture cross section of ^{197}Au was also taken into account because some of the fission and capture cross sections of ^{238}U were measured as the ratios to the ^{197}Au capture cross section.

Ratio measurements among cross sections are needed in order to perform the simultaneous evaluation. In the present evaluation, the following seven kinds of ratio data were taken into consideration.

---

*) Member of this subworking group

T. Asami, T. Houjuyama, Y. Kanda, M. Kawai, Y. Kikuchi, H. Matsunobu, T. Murata, Y. Nakajima, T. Nakagawa(subworking group leader), T. Osawa, M. Sasaki, T. Yoshida, T. Watanabe and A. Zukeran

$^{238}U(n,f)/^{235}U(n,f)$, $^{239}Pu(n,f)/^{235}U(n,f)$, $^{240}Pu(n,f)/^{235}U(n,f)$, $^{241}Pu(n,f)/^{235}U(n,f)$, $^{197}Au(n,\gamma)/^{238}U(n,f)$, $^{238}U(n,\gamma)/^{197}Au(n,\gamma)$, and $^{238}U(n,\gamma)/^{235}U(n,f)$.

The present evaluation was performed in the neutron energy range from 50 keV to 20 MeV. In this talk, the method of the our simultaneous evaluation is explained and the preliminary results are shown in graphs.

2. Method of Simultaneous Evaluation

The computer program for the simultaneous evaluation was developed by Uenohara and Kanda[1] of Kyushu University. This program is based on the generalized least-squares method and applies the B-spline functions as fitting functions.

1) Fitting function

The normalized B-spline functions are calculated from the following recurrence formula.

$$N_{r,j}(x) = \frac{x - \xi_j}{\xi_{j+r-1} - \xi_j} N_{r-1,j}(x) + \frac{\xi_{j+r} - x}{\xi_{j+r} - \xi_{j+1}} N_{r-1,j+1}(x), \quad (1)$$

$$N_{1,j}(x) = \begin{cases} 1 & \xi_j \leq x \leq \xi_{j+1}, \\ 0 & \text{for others.} \end{cases} \quad (2)$$

The $N_{r,j}(x)$ stands for the (r-1)st order normalized B-spline function in the jth interval from the node ξ_j to the next node ξ_{j+1}. Figure 1 shows the firstorder and second order (quadratic) normalized B-spline functions. The first order normalized B-spline function given in the upper part of Fig. 1 is called 'roof-function'. In the present work, we tried first the first order B-spline function. However, finally, the second order B-spline function was adopted in order to obtain smooth curves.

In the Uenohara's program, logarithms of cross sections are represented with the normalized B-spline functions.

$$\ell n\{\sigma_x(E)\} = \sum_j \theta_j N_{r,j}(x) \quad (3)$$

Then, ratio data of cross sections can be linearized as follows;

$$\ell n\{\sigma_x(E)/\sigma_Y(E)\} = \sum_j \theta_j N_{r,j}(x) - \sum_k \theta_k N_{r,k}(x) \quad (4)$$

2) Covariance matrices of experimental data

Covariance matrices of experimental data are needed in order to perform the generalized least-squares fitting. We adopted the following method of estimation of the covariance matrices recommended by the JNDC Subworking Group on Evaluation of Experimental Method[2,3].

If the cross section $\sigma(E)$ has partial errors due to uncertainty of parameter P_k, the true value of $\sigma(E)$ can be written as follows;

$$\sigma(E) = \sigma^0(E) + \sum_k \frac{\partial\sigma}{\partial P_k}\Delta P_k(E), \tag{5}$$

where $\sigma^0(E)$ is a measured cross section. Then, covariance between $\sigma(E_i)$ and $\sigma(E_j)$ is approximately estimated as

$$\mathrm{cov}(\sigma(E_i),\sigma(E_j)) \simeq \sum_k R^k_{ij}\Delta\sigma_k(E_i)\Delta\sigma_k(E_j), \tag{6}$$

where $\Delta\sigma_k(E_i)$ and $\Delta\sigma_k(E_j)$ are partial errors due to the uncertainty of the k-th parameter,

$$\Delta\sigma_k(E) \equiv \sqrt{\left\langle\left(\frac{\partial\sigma}{\partial P_k}\right)^2\right\rangle}\cdot\Delta P_k(E), \tag{7}$$

and R^k_{ij} is a correlation coefficient of the k-th partial errors between two energy points of E_i and E_j. In the present evaluation, since the correlation coefficient R^k_{ij} was assumed to be energy-independent, it can be written as R^k. Correlation among different partial errors were also assumed to be zero. Sometimes, measurements were done by using the same facility. In such cases, correlation seems to exist between such experiments. However, such correlation among different experiments was ignored. We also ignored correlations among data on different quantities, even in the case where they were measured by the same authors.

In the present evaluation, correlation coefficients R^k were roughly assumed as shown in Table 1. They were classified into three groups; strong correlation, medium correlation and weak or no correlation, and they were assumed to have values of 1.0, 0.5 and 0.0, respectively.

3. Results

Evaluators of the present work are

^{235}U -------- H. Matsunobu (Sumitomo Atomic Energy Industries),

^{238}U -------- Y. Kanda (Kyushu University),

^{239}Pu -------- M. Kawai (NAIG),

^{240}Pu -------- T. Murata (NAIG),
^{241}Pu -------- Y. Kikuchi (JAERI),
^{197}Au -------- Y. Nakajima (JAERI).

They selected experimental data from various literature and investigated their partial errors. The selected experimental data consist of about 75 sets, and 3400 energy points. Almost all of them were measured after 1970.

The experimental data were compiled in a special format and their covariance matrices were calculated from Eq. 6. Then, those data were gathered to Uenohara and Kanda at Kyushu University who did the calculation of the generalized least-squares fitting. After the calculation, the results were sent to JAERI so as to make graphs of comparison with experimental data and other evaluated data.

The discussion on the results was made at the meeting with related members. This procedure was repleated a few times. Then, the results shown in Figs. 2 to 12 have been obtained.

^{235}U fission cross section

Figure 2 shows the fission cross sections of ^{235}U in the energy range from 50 keV to 20 MeV. In comparison with JENDL-2 (dashed curve), the present result (solid curve) is low in the energy range below 1 MeV, almost the same between 1 and 10 MeV, and high above 10 MeV.

Figure 3 shows the ratios of the present evaluation and ENDF/B-V to JENDL-2. It is seen that the present result is lower by 2 or 3% than JENDL-2. ENDF/B-V[4] has the same tendency as the present result.

^{238}U fission cross section

The ratio data of the ^{238}U to ^{235}U fission cross sections are given in Fig. 4. The present result of the ratio seems to have been determined from the measurements by Behrens et al.[5] and Difillipo et al.[6] because of their small quoted errors. JENDL-2 also follows these two measurements. In Figs. 5 and 6, shown are the absolute measurements of ^{238}U fission cross section and ratio ones which are converted to cross sections by multiplying the presently evaluated ^{235}U fission cross section.

^{239}Pu fission cross section

Large discrepancies between JENDL-2 and the present result are found in the ^{239}Pu fission cross section as shown in Fig. 7 in which only cross-section measurements are given. In particular, differences are large in the energy range below 1 MeV.

Figure 8 shows the ratio data to the ^{235}U fission cross section. The differences between JENDL-2 and the present result are found also in this figure. The present result seems to be much faithful to experimental data than JENDL-2 except for the energy range above 10 MeV where the present result is larger than experimental values.

The ^{239}Pu fission cross section of JENDL-2 was evaluated by Kawai[7]. His preliminary evaluation for JENDL-2 was smaller than the present JENDL-2. However, such small cross section caused few percent smaller k_{eff} values of FBR benchmark cores. Therefore he did re-evaluation by adopting the large ratio data as shown in Fig. 8. On the other hand, for the ^{235}U fission cross section, larger values than the present result were also adopted by Matsunobu[7]. As a result, the large values were given for the ^{239}Pu fission cross section of JENDL-2.

Figure 9 compares the present result, ENDF/B-V and JENDL-2 by taking ratio to JENDL-2. The present result is about 5% smaller than JENDL-2 below 1 MeV. ENDF/B-V is also smaller than JENDL-2.

^{240}Pu fission cross section

The ^{240}Pu fission cross section is shown in Fig. 10 together with derived cross sections from ratio measurements. The present result reproduces well the experimental data in the whole energy range.

^{241}Pu fission cross section

Figure 11 shows the ^{241}Pu fission cross section. Cross-section measurements are data of Szabo[8,9] and Carlson et al.[10]. Others are derived cross sections from the ratio measurements. Discrepancies between JENDL-2 and the present result are relatively large.

The capture cross sections of ^{197}Au and ^{238}U capture cross sections were also shown in the seminar. However, they are neglected in this proceedings because they are too preliminary.

4. Conclusion

In the present simultaneous evaluation, we used the several kinds of ratio data to the ^{235}U fission cross section. Such ratio data can be converted into the ^{235}U fission cross section by applying the presently evaluated cross sections. Figure 12 shows the ^{235}U fission cross sections together with such derived ones. It is seen that the present result represents well the experimental data. The discrepancies around 10 MeV in Fig. 2 disappear in this figure.

By showing graphs, the results of the simultaneous evaluation done by the JNDC subworking group on heavy nuclide were explained. For convenience sake, the present result was named SEND-1 (Simultaneously Evaluated Nuclear Data, version 1). Benchmark test of SEND-1 was done by Takeda et al. and explained in this seminar[11].

References

1) Uenohara, Y. and Kanda, Y.: "Simultaneous Evaluation of Neutron Cross Section and Their Covariances for Some Reaction of Heavy Nuclei", Proc. International Conf. on Nuclear Data for Science and Technology, 1982 Antweep, 639 (1983).

2) Murata, T.: "Estimation of Covariance Matrix on the Experimental Data for Nuclear Data Evaluation", JAERI-M 85-035, 131 (1985).

3) Nakajima, Y.: "Measurements of Neutron Capture Cross Section", JAERI-M 84-010, 15 (1984) [in Japanese].

4) Edited by Kinsey, R.: "ENDF/B Summary Documentation", BNL-NCS-17541 (ENDF-201), 3rd Edition (ENDF/B-V) (1979).

5) Behrens, J.W. and Carlson, G.W.: Nucl. Sci. Eng., 63, 250 (1977).

6) Difilippo, F.C., Perez, R.B., de Saussure, G., Olsen, D.K. and Ingle, R.W.: Nucl. Sci. Eng., 68, 43 (1978).

7) Matsunobu, H., Kanda, Y., Kawai, M., Murata, T. and Kikuchi, Y.: "Simultaneous Evaluation of the Nuclear Data for Heavy Nuclides", Proc. International Conf. on Nuclear Cross Sections for Technology, 1979 Knoxville, 715 (1980).

8) Szabo, I., Filippi, G., Huet, J.L., Leroy, J.L. and Marquette, J.P.: "New Absolute Measurement of the Neutron-Induced Fission Cross Sections of ^{235}U, ^{239}Pu and ^{241}Pu from 17 keV to 1 MeV", Neutron Standards and Flux Normalization, AEC Symposium Series 23, 1970 ANL, 257 (1971).

9) Szabo, I., Leroy, J.L. and Marquette, J.P.: "Absolute Measurement of Fission Cross Section of ^{235}U, ^{239}Pu and ^{241}Pu between 10 keV and 2.6 MeV", Proc. Conf. on Neutron Phys., 1973 Kiev, 27 (1973).

10) Carlson, G.W., Behrens, J.W. and Czirr, J.B.: Nucl. Sci. Eng., 63, 149 (1977).

11) Takeda, T., Nishigori, T., Aoyama, T. and Suzuki, T.: "Integral Test for Heavy Nuclides", presented at this seminar.

Table 1 Correlation factors of partial errors

partial error	Correlation factor (R^k)
Sample thickness	1.0
Standard cross section	1.0
Detector efficiency	0.5
Time dependent background	0.0
Time independent background	0.5
Background (α pile-up, spontaneous fission, etc.)	1.0
Multiple scattering	0.5
Geometrical factors	1.0
Neutron flux	0.5
Absorption correction of neutron flux	1.0
Impurity	1.0
Extrapolation of discrimination	1.0
ν_p	1.0
Dead time	1.0
Time shift	1.0
Absorption correction of fission fragments	1.0
Normalization	1.0

1st order B-spline function

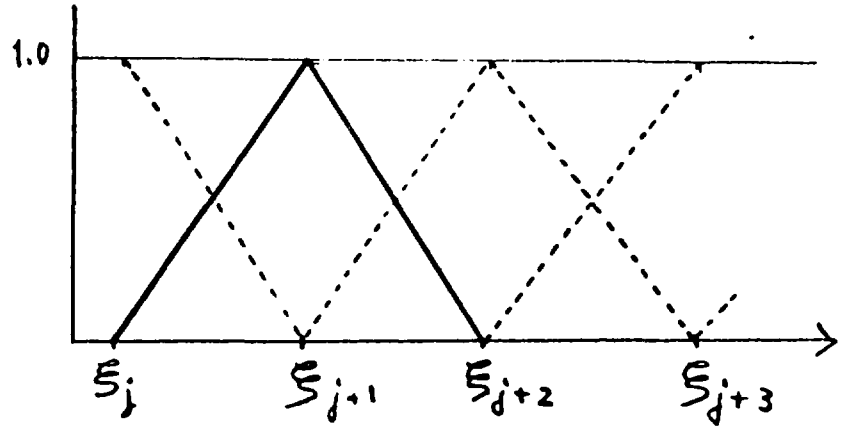

2nd order B-spline function

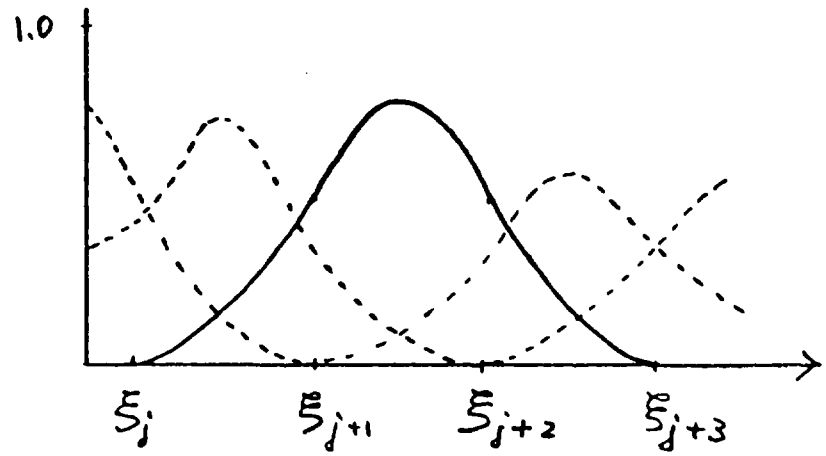

Fig. 1 Normalized B-spline functions.

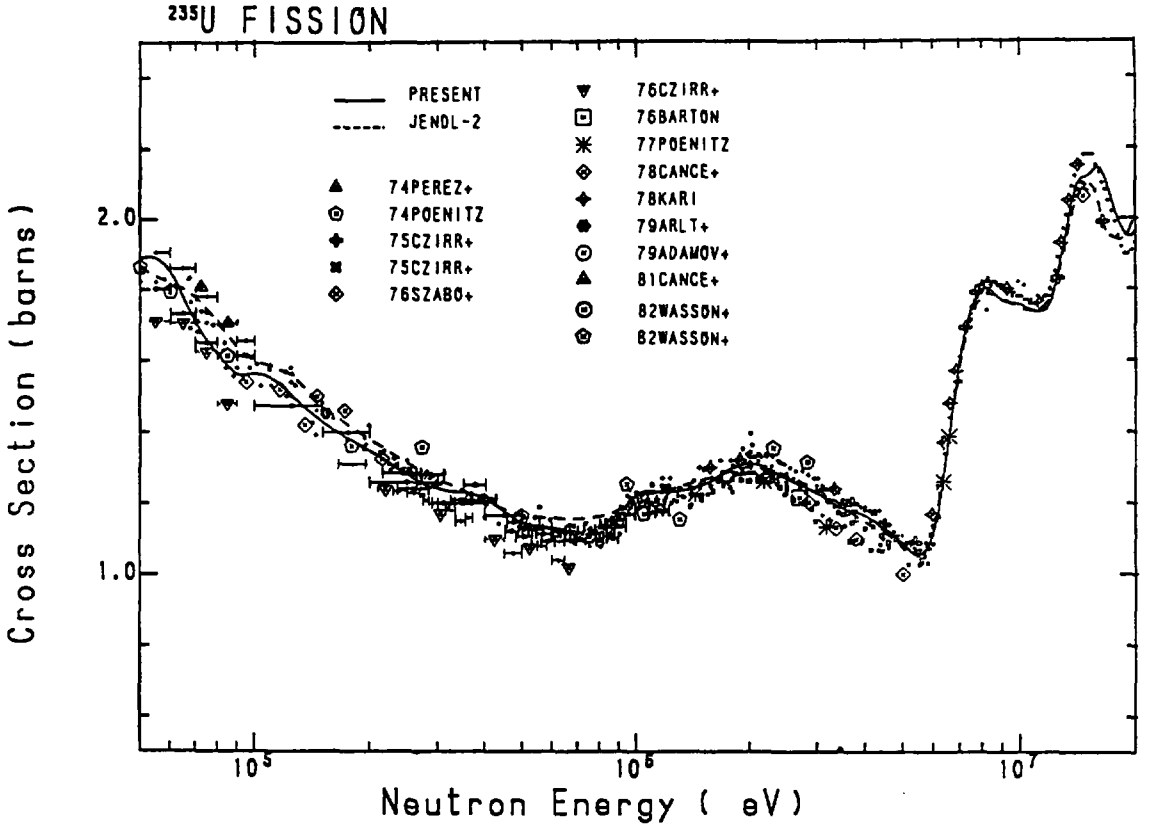

Fig. 2 ^{235}U fission cross section.

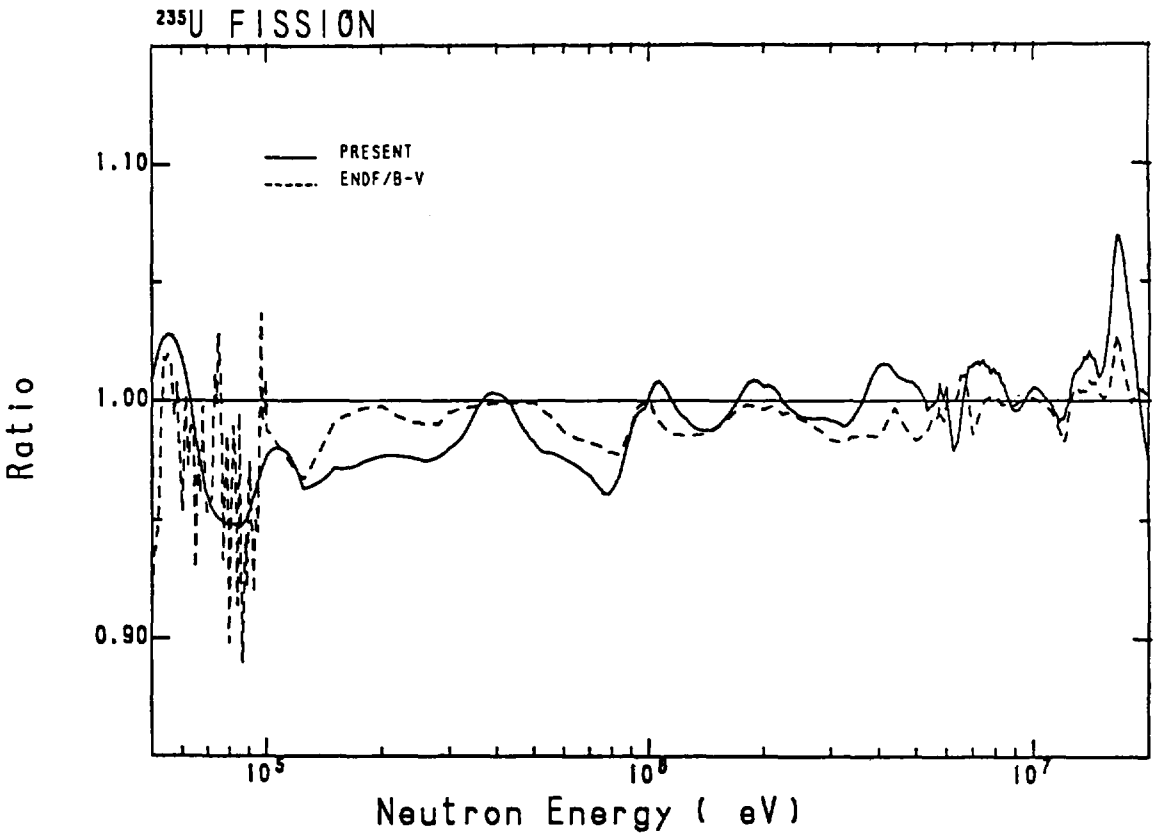

Fig. 3 Comparison of ^{235}U fission cross sections
Ratios to the ^{235}U fission cross section of JENDL-2 are shown.
The present result is smaller than JENDL-2 below 1 MeV.

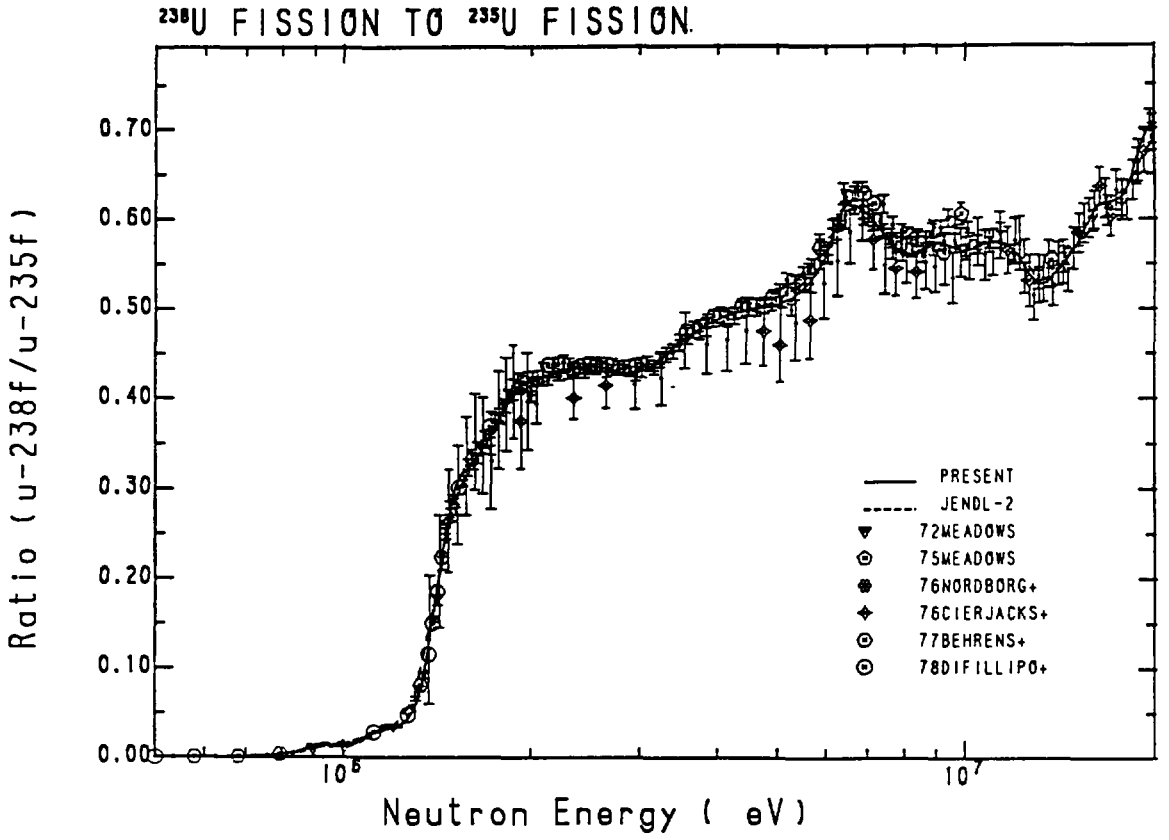

Fig. 4 Ratio data of ^{238}U to ^{235}U fission cross sections.

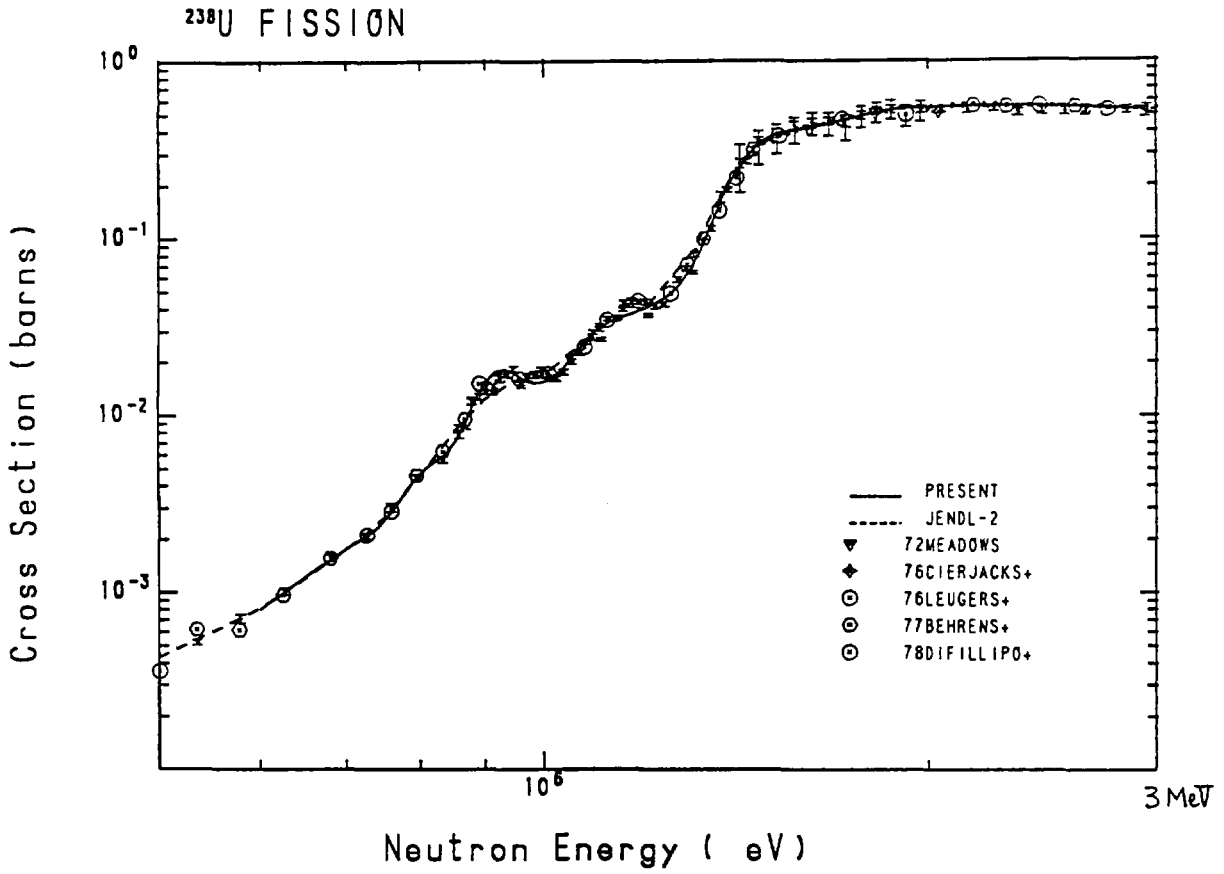

Fig. 5 ^{238}U fission cross section below 3 MeV.

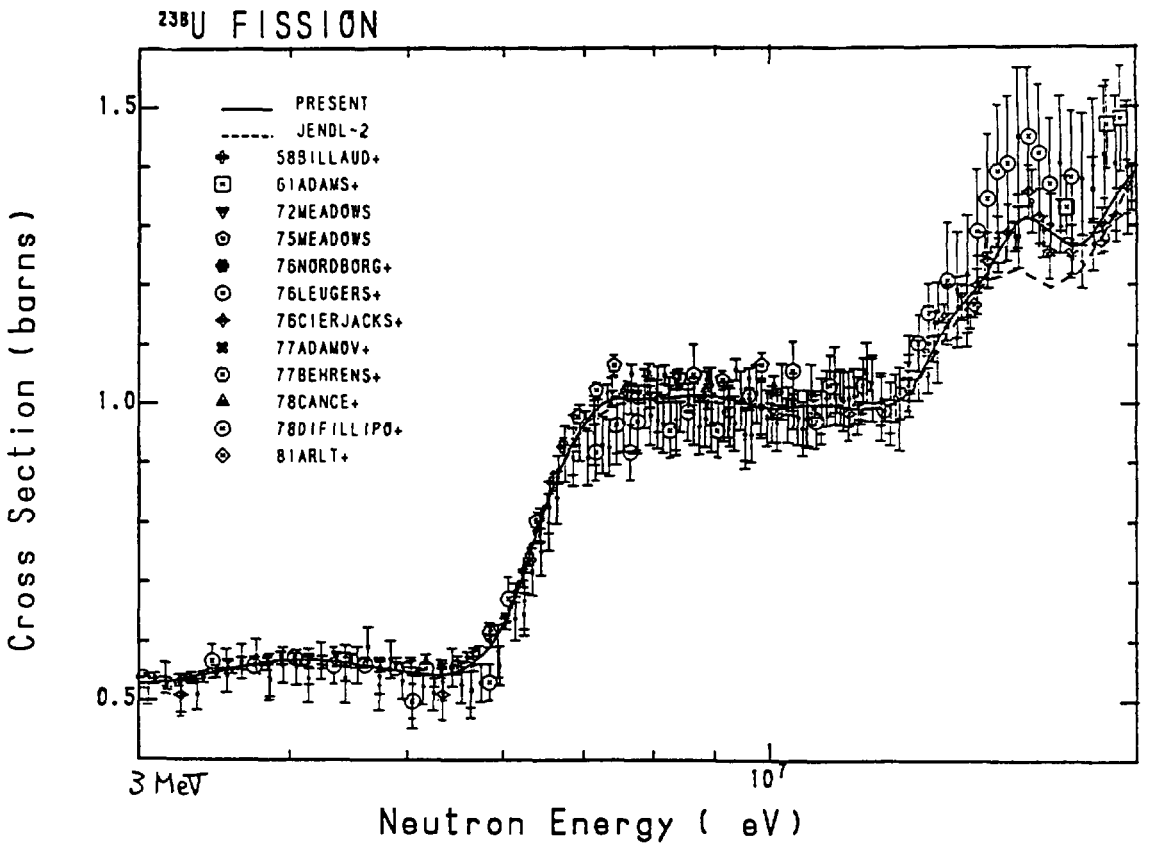

Fig. 6 ^{238}U fission cross section above 3 MeV.

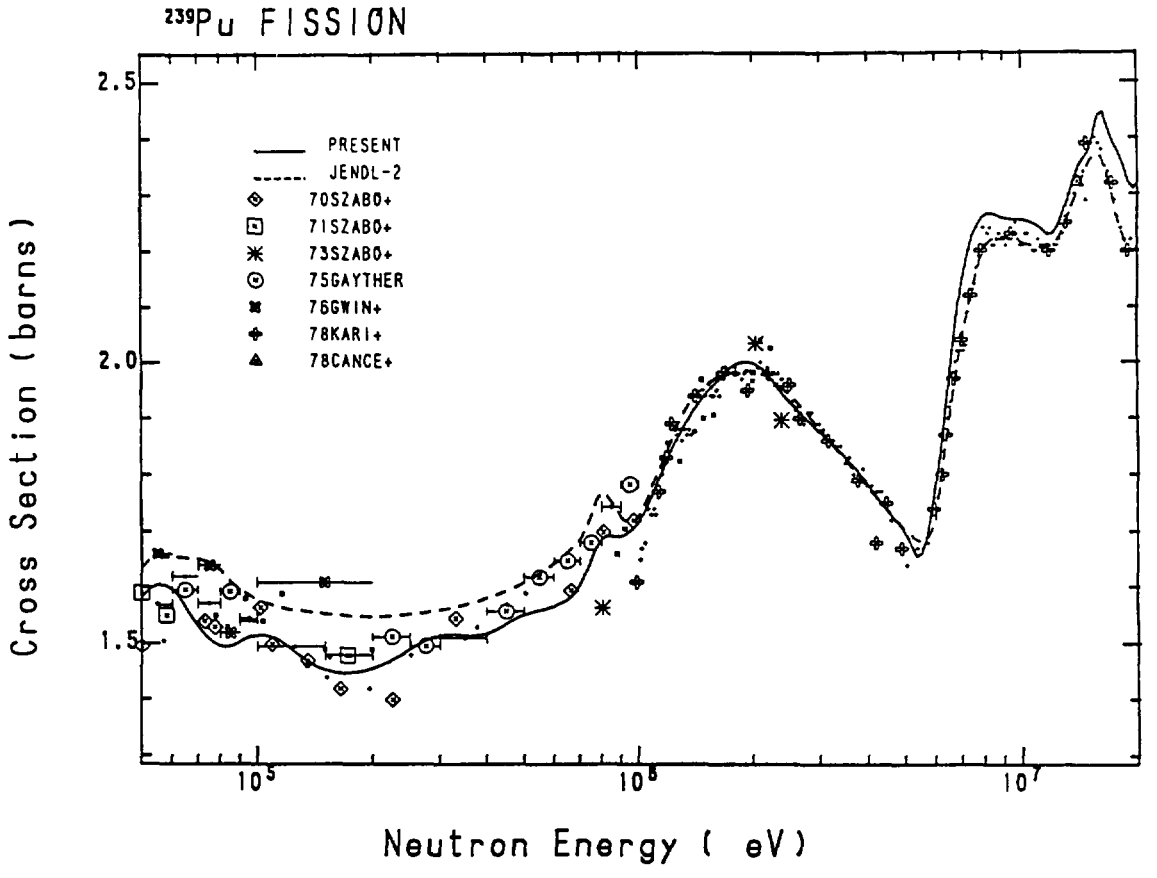

Fig. 7 ^{239}Pu fission cross section.

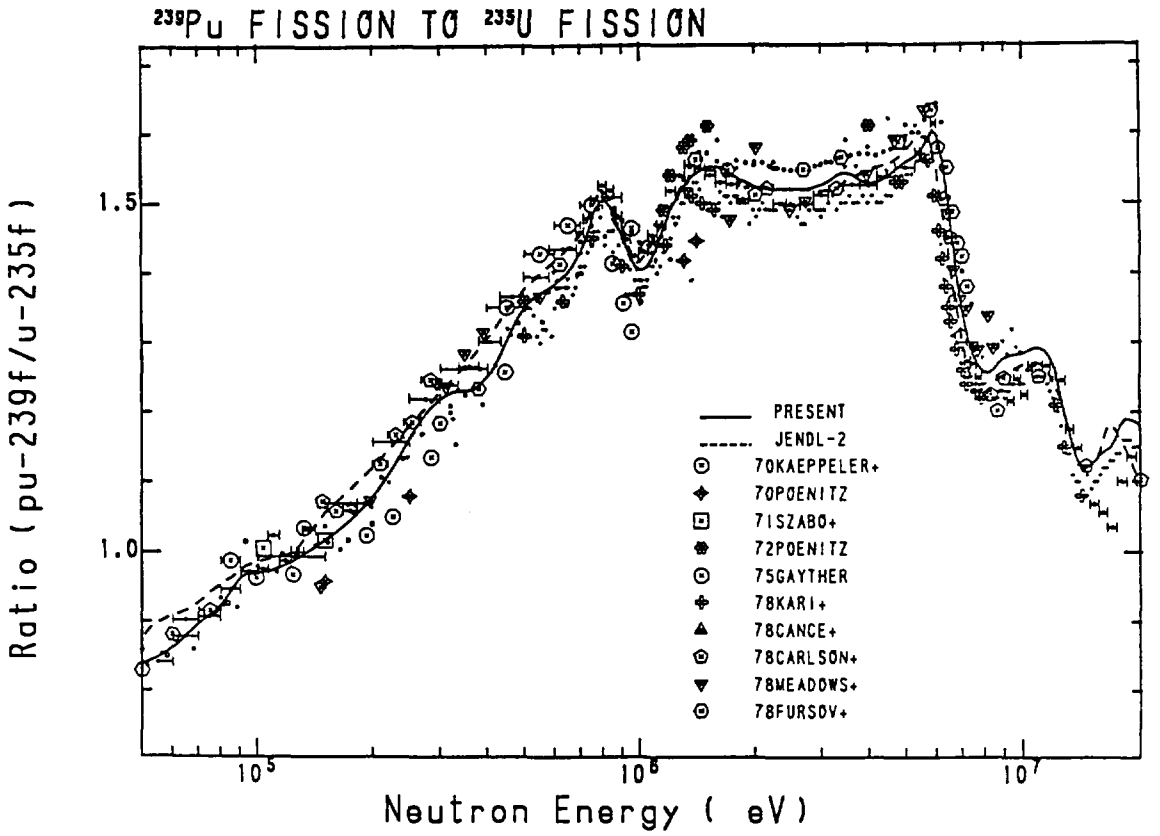

Fig. 8 Ratio data of ^{239}Pu to ^{235}U fission cross sections.

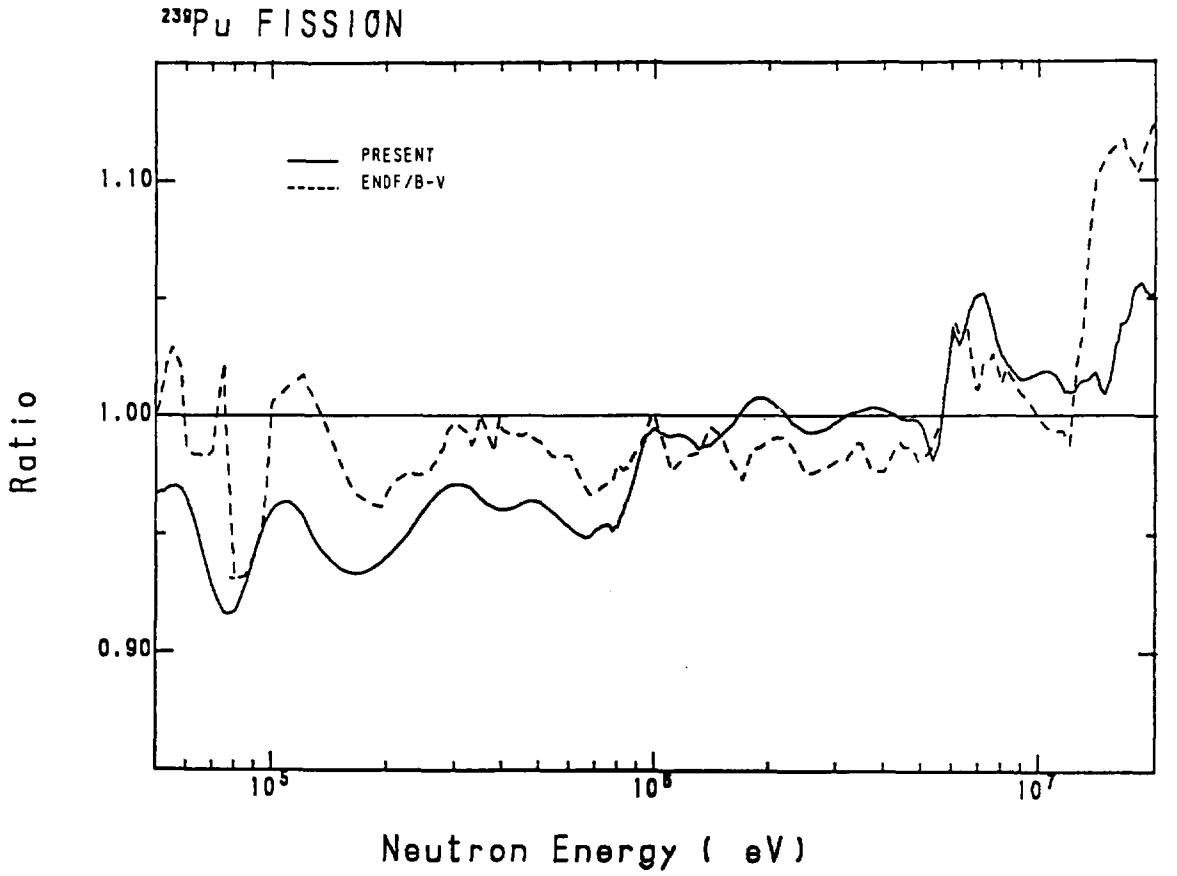

Fig. 9 Comparison of ^{239}Pu fission cross section.

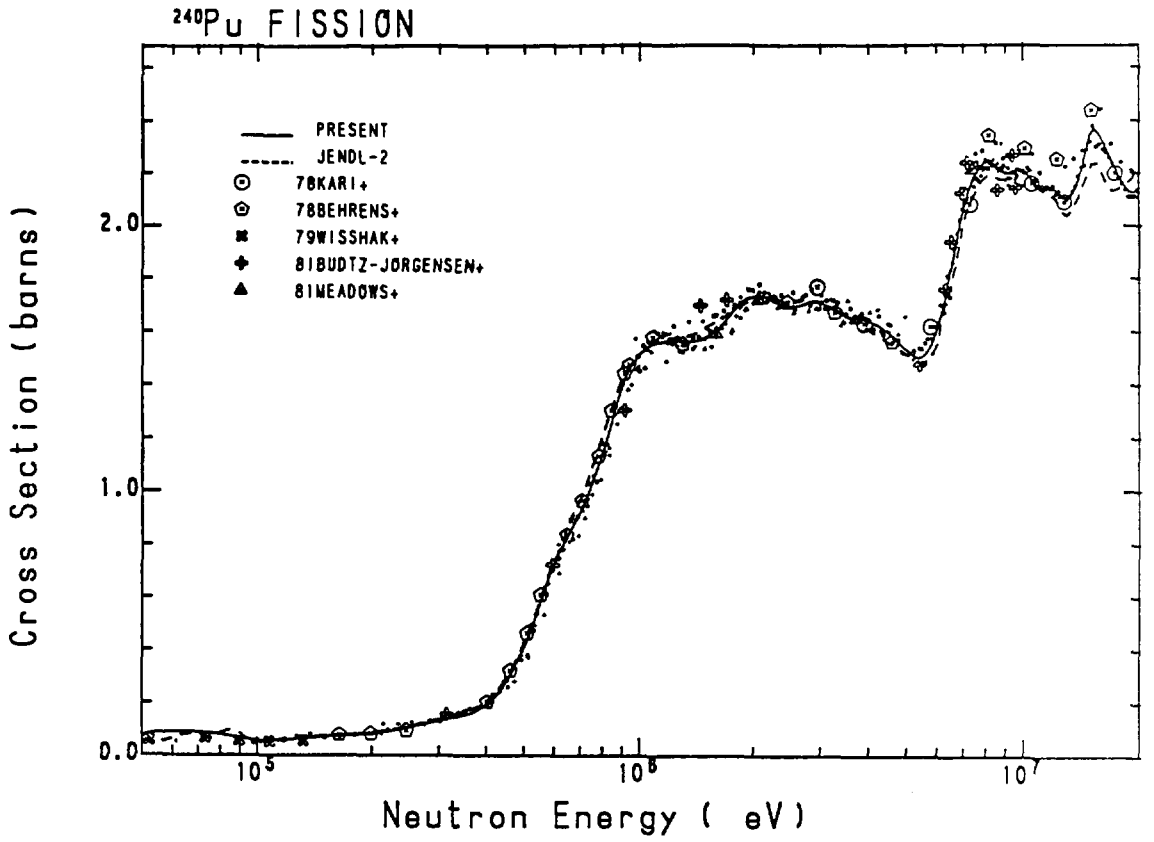

Fig. 10 ^{240}Pu fission cross section.

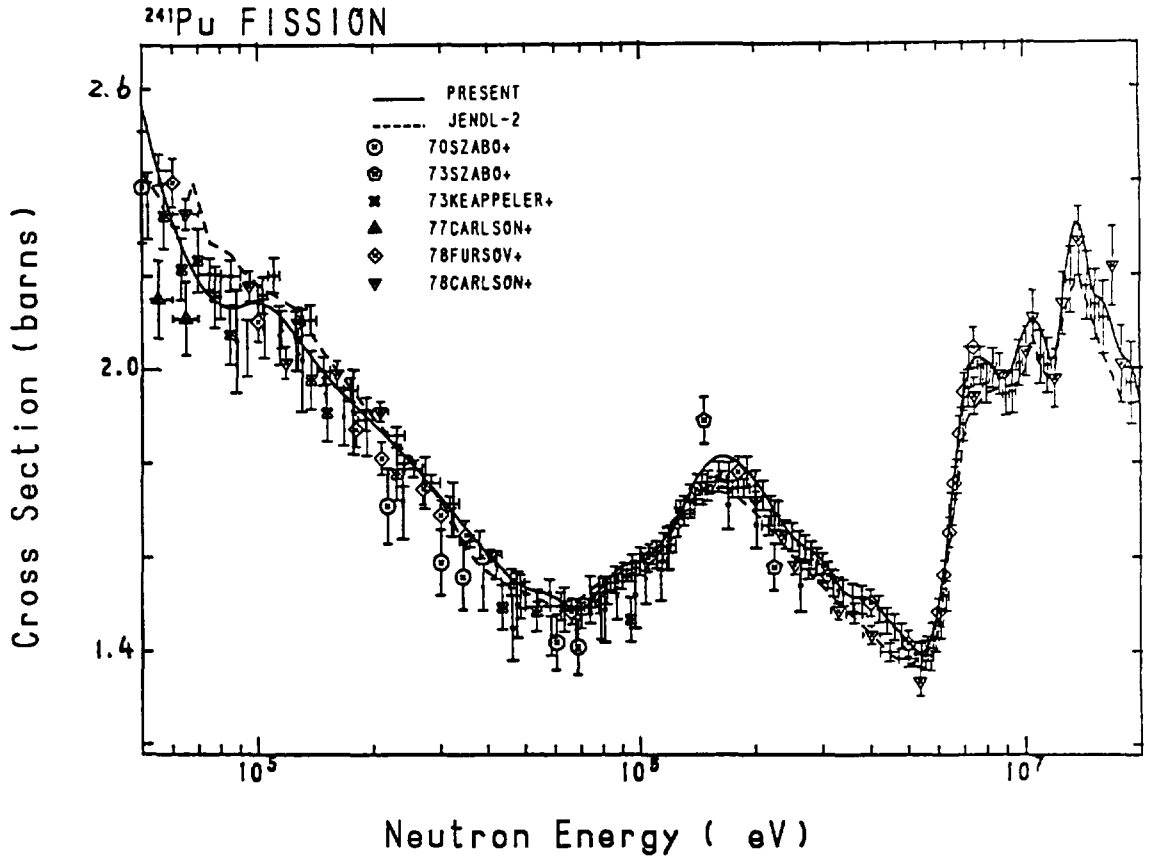

Fig. 11 ^{241}Pu fission cross section.

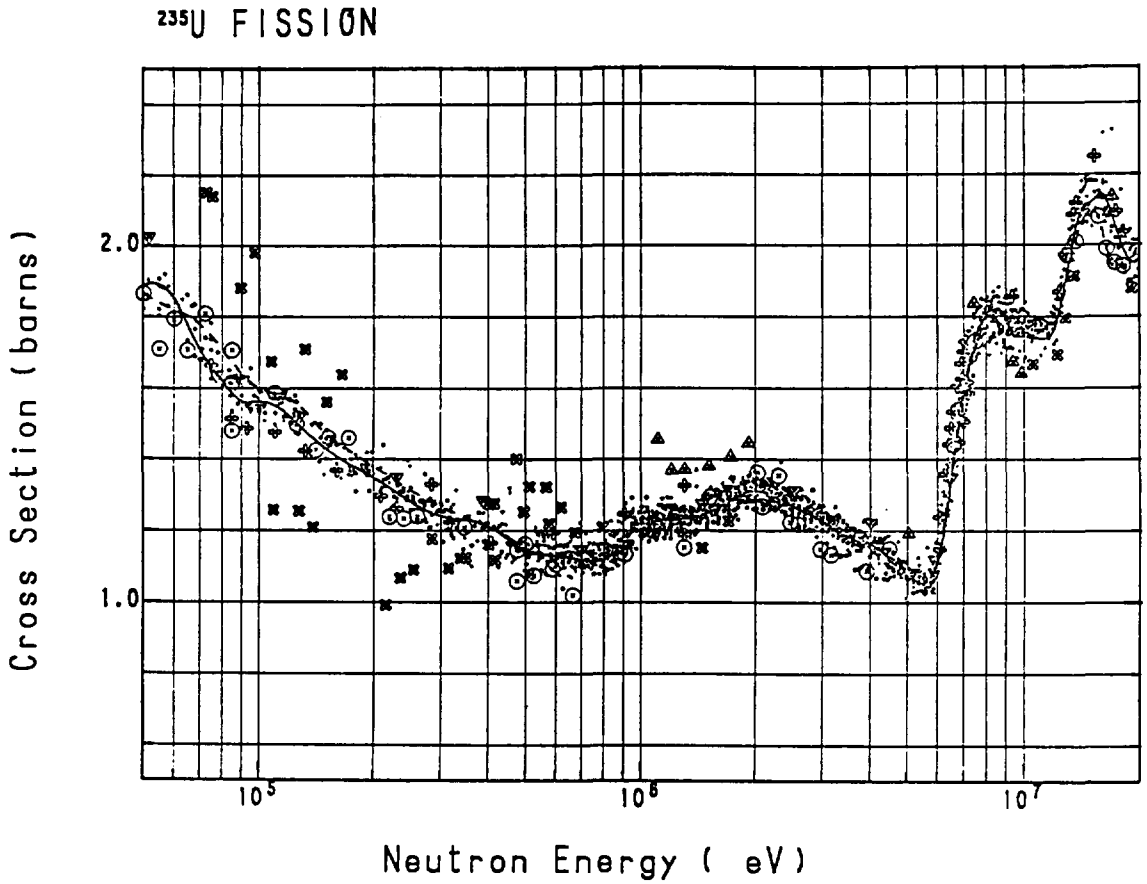

Fig. 12 ^{235}U fission cross section.
Derived cross sections are also shown in this figure.

6.2 Integral Test for Heavy Nuclides

T. TAKEDA, T. NISHIGORI, T. AOYAMA and T. SUZUKI

Department of Nuclear Engineering, Osaka University
Yamadaoka 2-1, Suita, Osaka 565

The characteristic feature of JENDL-2 is discussed through the benchmark test for several fast critical assemblies. It predicts the effective multiplication factors accurately, but overestimates the sodium void worths and the reaction rate ratio ^{238}U capture/^{239}Pu fission. Integral tests are carried out for the fission and capture cross sections of heavy nuclides, SEND-1, which were evaluated recently above 50 keV by Kanda et al. in preparation for JENDL-3. The effective multiplication factors are reduced by about 1.3% Δk from the JENDL-2 results, due mainly to the reduction of the fission cross sections of Pu-239 and U-235. The benchmark test data are applied to adjustment of the JENDL-2 cross sections. The cross section changes are found to be in qualitative agreement with those newly evaluated by Kanda et al. It can thus be anticipated that the tentative unfavourable predictions by the new cross sections will be much improved when JENDL-3 is fully compiled.

1. Introduction

Integral tests of JENDL-2 have been carried out for fast and thermal reactor problems, and for shielding problems.[1] After the benchmark tests for fast critical assemblies were carried out, it was found that there had been a processing error caused by a wrong treatment of the JENDL-2 data in the unresolved resonance region. The correction for this error was made by using sensitivity coefficients calculated by the SAGEP code[2], which is based on generalized perturbation theory. Some of the correc-

ted results are shown in Ref. 3. In order to investigate the applicability of JENDL-2, benchmark tests are necessary for many fast critical assemblies with different neutron spectra. Therefore, we first show the corrected values of calculation to experiment ratios of k_{eff}, reaction rate ratios, control rod worths, sodium void worths, and reaction rate distributions in several assemblies. The applicability of JENDL-2 is investigated in Chap. 2 in terms of the C/E ratios of these core parameters.

In preparation for JENDL-3 Japanese Nuclear Data Committee (JNDC) is now re-evaluating fission and capture cross sections of five primary nuclides, U-235, U-238, Pu-239, Pu-240 and Pu-241 on the basis of the simultaneous evaluation method. Preliminary results are coming out,[4] and we have tried to study the change in C/E values due to the alteration of JENDL-2 to the re-evaluated data SEND-1. Since the SEND-1 data are prepared only above 50 keV for a limited number of nuclides, the change of the C/E values given below are preliminary. The results, however, give information on the evaluation of the cross sections in lower energy ranges and of other nuclides.

In addition to the above-mentioned integral test, we compare the SEND-1 data with those predicted by a cross section adjustment of JENDL-2. In the cross section adjustment, the C/E values obtained in Chap. 2 are used along with the sensitivity coefficients calculated by SAGEP and with cross section covariance data produced from the ORNL 26 group covariance matrix library.[5] The adjustment is performed in 16 groups, and the results are compared with SEND-1.

2. Integral Test of JENDL-2 for Fast Critical Assemblies

Through various thermal and fast fission reactor calculations and shielding calculations, the applicability of JENDL-2 has been investigated in many respects. Here, we show benchmark test results for fast critical assemblies. Benchmark tests [6],[7] were made by Working Group on Integral Tests for JENDL in JNDC with one- and two-dimensional models of various fast critical assemblies such as FCA V-1, V-2, VI-1, VI-2, MZB, ZPPR-2,

ZPR-6-6a, ZPR-6-7, and ZPPR-9. Furthermore, JENDL-2 has been utilized for the analysis of the JUPITER (Japanese-United States Program of Integral Tests and Experimental Researches) experiments. The JUPITER Phase-I experiments were performed using ZPPR-9 and -10 to get information on a large homogeneous fast reactor, and the Phase-II experiments used ZPPR-13 to get information on a radially heterogeneous fast reactor. The group constants used in the integral test were produced by processing JENDL-2 with PROF-GROUCH-G-II and TIMS-1.[8] In the calculation of infinite dilution cross sections by TIMS-1, a processing error was found after the benchmark calculations. Therefore, corrections were made using sensitivity coefficients calculated by SAGEP.

Table 1 lists the C/E values of the effective multiplication factor k_{eff}, with the percent corrections for the above-mentioned error shown in parentheses. In the cell calculation of the heterogeneous core ZPPR-13A a sophisticated multi-drawer model was used to take account of the interference effect between core and blanket drawers. If we take no account of this effect, the C/E ratio reduces to 0.9997. From the Table it is seen that JENDL-2 predicts the k_{eff} values satisfactorily for the homogeneous, as well as the heterogeneous, cores.

Table 2 lists the C/E values of the central reaction rate ratios ^{238}U fission/^{235}U fission, ^{239}Pu fission/^{235}U fission and ^{238}U capture/^{239}Pu fission. The C/E ratios for $^{28}f/^{25}f$ are remarkably different between the two measurements by back-to-back fission chamber and by foil irradiation. For $^{49}f/^{25}f$ the C/E values are underestimated by 4%, and for $^{28}c/^{49}f$ they are overestimated by 6%. The reaction rate ratio $^{28}c/^{49}f$ is closely related to the breeding ratio, and their overestimation should be investigated in detail.

Table 3 gives the C/E values of the Doppler reactivity worths of UO_2, Fe and stainless steel. The calculated Doppler reactivity worths are underestimated for UO_2 by about 14%, and largely overestimated for Fe.

Table 4 lists the C/E ratios of sodium void worth. For a large zone voiding in large fast critical assemblies (e.g., ZPPR-

9, -10A, and -13A) the calculation overestimates the void worth by about 30%.

Tables 5 and 6 show a spatial dependence of the C/E values of the ^{239}Pu fission rate distributions and control rod worths. A significant spatial change is seen in both the results. For the case of ZPPR-10D the C/E values of the control rod worth change by about 12%. This has a large effect on the design accuracy of a large FBR, and a detailed study is further required.

3. Integral Test of SEND-1

In preparation for JENDL-3, much effort is being devoted to a revision work of JENDL-2. Using the fission and capture cross sections of five primary nuclides, U-235, U-238, Pu-239, Pu-240 and Pu-241 in SEND-1, we calculated the C/E changes when going from the JENDL-2 data to the SEND-1 data. We further compared the fission and capture cross sections of the SEND-1 data with those obtained from a cross section adjustment of JENDL-2 carried out by using the integral data of fast critical assemblies.

3.1 Change in Fast Reactor Parameters

Using the sensitivity coefficients calculated by SAGEP we predict the fast reactor parameters based on the SEND-1 data re-evaluated by Kanda et al.[4] Here, it should be mentioned that the evaluation has been carried out only above 50 keV for the five heavy nuclides, and the results are, therefore, tentative. Tables 7(a)-(f) list the contributions from each cross sections to the percent change of C/E values of k_{eff}, central reaction rate ratios, Doppler reactivities and sodium void worths. The k_{eff} values are reduced by about 1.3% for large Pu cores, and much deviated from unity compared with JENDL-2. This is mainly due to the reduction of the fission cross sections of Pu-239 and U-235 between 100 keV and 1 MeV (see Table 9).

3.2 Comparison with Adjusted Cross Sections

Independently of the above-mentioned integral test, we have

carried out an adjustment of JENDL-2 using the C/E values for large fast critical assemblies ZPPR-9, -10 and -13. The adjustment was performed in 16 groups with sensitivity coefficients calculated by SAGEP and with a cross section covariance file produced from the ORNL 26 group fast reactor benchmark covariance matrix library.[5] As the reactor parameters we have used k_{eff}, reaction rate ratios ^{235}U fission/^{239}Pu fission and ^{238}U fission /^{239}Pu fission, reaction rate distribution of ^{239}Pu fission, control rod worths and sodium void worths.

Table 8 lists the C/E values of these parameters before and after the adjustment. The standard deviations (V_E and V_M) of experiments and calculations are shown in the Table in addition to the relative uncertainties due to cross section errors before and after the adjustment (GMG and GM'G). The overestimation of the sodium void worths by JENDL-2 is remarkably improved through the adjustment, and the overestimation of the reaction rate ratio ^{238}U capture/^{239}Pu fission is also improved. Furthermore, the relative uncertainties GM'G for the individual reactor parameter are much smaller than those before the adjustment. The uncertainty for k_{eff} is reduced from 2.3% to 0.3%.

Table 9 presents the percent changes of the Pu-239 fission, U-235 fission, U-238 fission and U-238 capture cross sections. The results given in Table 10 are obtained for the case where the C/E values of sodium void worths are not utilized in the adjustment. Since the C/E values of sodium void worths are almost 1.3 before the adjustment, the exclusion of the sodium void worth data has a large effect on the cross section changes. In these Tables we also show the relative changes of the SEND-1 data from JENDL-2. It is interesting to note that the Pu-239 fission cross section is reduced in both the results. Though this agreement may be accidental, we can do expect by considering the good adjustment results that JENDL-3, when its compilation is finished, will predict the reactor parameters accurately.

4. Concluding Remarks

The results of the benchmark tests of JENDL-2 have been

shown for several fast critical assemblies, and the feature of JENDL-2 has been discussed for individual core parameters; JENDL-2 predicts k_{eff} accurately, and overestimates the sodium void worths and the reaction rate ratio ^{238}U capture/^{239}Pu fission.

With the heavy nuclide data SEND-1, re-evaluated in preparation for JENDL-3, the change of core parameters of fast critical assemblies has been investigated. The k_{eff} values were reduced by about 1.3% Δk. However, since the data are supplied only above 50 keV and only for the five primary nuclides, it is anticipated that this too much reduction will be eliminated by the final version of JENDL-3. A reason for this comes from the comparison between the SEND-1 data and the adjusted ones. The good agreement given by the adjusted data suggests a good applicability of JENDL-3 to fast reactors.

Acknowledgement

We express our deep appreciation to the members of the Working Group on Integral Tests for JENDL in JNDC for their valuable comments and discussions.

References

(1) Y. Kikuchi et al., J. Nucl. Sci. Technol. **22**(8), 593 (1985).
(2) A. Hara, T. Takeda and Y. Kikuchi, JAERI-M 84-027 (1984).
(3) T. Takeda et al., Paper JC31, Nuclear Data Conference, Santa Fe, May 1985.
(4) Y. Kanda et al. Paper IB07, Nuclear Data Conference, Santa Fe, May 1985.
(5) J. D. Drischler and C. R. Weisbin, ORNL-5318 (1977).
(6) Y. Kikuchi et al., J. Nucl. Sci. Technol. **17**(7),567 (1980).
(7) Y. Kikuchi et al., Proc. Int. Conf. on Nuclear Data for Science and Technology, Antwerp 1982, p. 615 (1983).
(8) H. Takano et al., JAERI 1267 (1980).

Table 1 C/E values of k_{eff} for JENDL-2

Assembly	Fuel	Core volume	Fissile to fertile ratio	C/E of k_{eff}
FCA V-1	U+(Pu)	153	2.6	1.0054 (0.16)
V-2	Pu+U	214	2.3	1.0068 (0.20)
VI-1	Pu+(U)	472	3.6	1.0068 (0.28)
VI-2	Pu+U	627	3.2	1.0080 (0.27)
MZB	Pu	1777	5.2	0.9992 (0.40)
ZPPR-2	Pu	2407	5.1	0.9970 (0.51)
ZPR-6-6A	U	3990	5.0	1.0025 (0.28)
ZPR-6-7	Pu	3120	6.5	0.9962 (0.56)
ZPPR-9	Pu	4600	7.8	0.9993 (0.49)
ZPPR-10A	Pu	5127	6.9	0.9972 (0.50)
ZPPR-13A	Pu	4011*	3.5	1.0027 (0.45)
Average				1.0019±0.0042

* excluding internal blanket

Table 2 C/E values of central reaction rate ratios for JENDL-2

Assembly	$^{28}f/^{25}f$	$^{49}f/^{25}f$	$^{28}c/^{49}f$	Others
FCA V-1	1.060 (-0.17)	0.938 (0.02)	- -	
V-2	1.086 (-0.18)	0.973 (0.08)	- -	
VI-1	1.009 (-0.26)	0.960 (0.10)	- -	
VI-2	1.031 (-0.33)	0.953 (0.12)	- -	
MZB	- -	- -	- -	
ZPPR-2	1.103 (-0.51)	0.960 (0.12)	- -	$^{40}f/^{25}f$=1.135
ZPR-6-6A	0.992 (-0.31)	- -	- -	$^{28}c/^{25}f$=0.952
ZPR-6-7	1.016 (-0.55)	0.957 (0.12)	1.056 (-0.56)	
ZPPR-9	1.086*	0.971 (0.13)	1.060 (-0.51)	
	0.961**			
ZPPR-10A	0.950**	0.963 (0.12)	1.062 (-0.55)	
ZPPR-13A	0.947**	0.960 (0.13)	1.058 (-0.53)	
Average		0.959±0.010	1.059±0.002	

*back-to-back fission chamber

**foil irradiation

Table 3 C/E values of Doppler reactivity worth for JENDL-2

Assembly	UO2	Fe	Steel
FCA V-1	0.880 (0.38)	- -	1.573 (-0.35)
V-2	0.760 (0.53)	1.753 (-0.20)	- -
VI-1	0.873 (1.82)	1.298 (0.34)	0.715 (0.37)
VI-2	0.880 (1.80)	1.221 (0.70)	0.999 (0.75)
ZPPR-9	0.903 (1.33)	- -	- -
Average	0.859±0.051	1.424±0.235	1.096±0.357

Table 4 C/E values of sodium void worth for JENDL-2

Assembly	Viod pattern (R cm × Z cm)	C/E
FCA V-1	(3.10×60.96)	0.545 (7.5)
	(9.25×60.96)	0.645 (6.7)
VI-2	(9.34×20.32)	1.213 (-7.5)
	(15.57×30.48)	1.287 (-8.0)
	(21.80×40.64)	1.413 (-8.7)
ZPPR-9	(9.25×40.64)	1.044 (-4.9)
	(30.67×40.64)	1.101 (-4.8)
	(30.67×101.75)	1.278 (-6.1)
ZPPR-10A	(18.96×40.64)	1.307 (-5.3)
	(41.93×40.64)	1.282 (-5.8)
	(41.93×101.75)	1.356 (-6.0)
ZPPR-13A	(54.00×60.96)	1.272 (-8.1)

Table 5 Spatial dependence of C/E values of ^{239}Pu fission rate distribution for JENDL-2

Assembly	Drawer position	C/E
ZPPR-9	149-49	0.991
	144-49	1.010
	137-49	1.022
	129-49	1.022
ZPPR-10A	149-45	0.998
	149-43	1.008
	149-38	1.022
	149-28	1.037
ZPPR-13A	149-48 (CB)	0.942
	147-43 (F1)	0.965
	147-38 (B1)	0.982
	147-34 (F2)	0.996
	147-31 (B2)	1.029
	147-25 (F3)	1.032
	147-21 (RB)	0.992

Table 6 Spatial dependence of C/E values of control rod worth for JENDL-2*

Assembly	CR pattern	C/E**
ZPPR-9	central CR	0.961
	6 mid inner core CRs	0.964
	6 edge inner core CRs	1.000
ZPPR-10A	central CR	0.951
	6 1st ring rods	0.947
	6 2nd ring rods	0.988
ZPPR-10D	central CR	0.943
	6 1st ring rods	0.954
	6 2nd ring rods	1.003
	6 3rd ring rods	1.064

*ANS Topical Meeting, Chicago, Sept. 1984.

**The corrections are small and neglected.

Table 7(a) Change of C/E values of k_{eff} due to cross section change from JENDL-2 to re-evaluated data SEND-1

(%)

	FCA V-1	FCA V-2	FCA VI-1	FCA VI-2
^{235}U (n, γ)	0.046	0.039	0.022	0.045
^{235}U (n, f)	-0.353	-0.297	-0.185	-0.341
^{238}U (n, γ)	-0.097	-0.093	-0.085	-0.092
^{238}U (n, f)	-0.042	-0.039	-0.040	-0.042
^{239}Pu (n, γ)	0.039	0.044	0.059	0.029
^{239}Pu (n, f)	-0.628	-0.702	-1.000	-0.494
^{240}Pu (n, γ)	0.001	0.001	0.001	0.000
^{240}Pu (n, f)	-0.009	-0.010	-0.013	-0.006
^{241}Pu (n, γ)	0.000	0.000	0.000	0.000
^{241}Pu (n, f)	-0.000	-0.000	-0.001	-0.000
total	-1.044	-1.057	-1.241	-0.902
(C/E) JENDL-2	1.0055	1.0068	1.0068	1.0080
(C/E) NEW *	0.9941	0.9953	0.9935	0.9982
(C/E) NEW **	0.9950	0.9961	0.9943	0.9989

	ZPR-6/7	ZPR-6/6A	ZPPR-2	ZPPR-9
^{235}U (n, γ)	0.001	0.063	0.001	0.001
^{235}U (n, f)	-0.007	-0.458	-0.006	-0.007
^{238}U (n, γ)	-0.070	-0.057	-0.064	-0.079
^{238}U (n, f)	-0.037	-0.034	-0.035	-0.043
^{239}Pu (n, γ)	0.067	----	0.071	0.065
^{239}Pu (n, f)	-1.271	----	-1.315	-1.297
^{240}Pu (n, γ)	0.002	----	0.002	0.002
^{240}Pu (n, f)	-0.022	----	-0.024	-0.022
^{241}Pu (n, γ)	0.000	----	0.000	0.000
^{241}Pu (n, f)	-0.002	----	-0.002	-0.002
total	-1.339	-0.486	-1.371	-1.382
(C/E) JENDL-2	0.9962	1.0025	0.9970	1.0000
(C/E) NEW *	0.9822	0.9970	0.9825	0.9855
(C/E) NEW **	0.9829	0.9977	0.9833	0.9862

Average of (C/E) JENDL-2 = 1.00286 ± 0.0044
Average of (C/E) NEW* = 0.99104 ± 0.0061
‡ Re-evaluated 6 cross sections are considered.
‡‡ Re-evaluated 10 cross sections are considered.

Table 7(b) Change of C/E of $^{238}U(n, f)/^{235}U(n, f)$ due to cross section change from JENDL-2 to re-evaluated data

(%)

	FCA V-1	FCA V-2	FCA VI-1	FCA VI-2	ZPPR-2	ZPR-6/6A
$^{235}U(n, \gamma)$	-0.059	-0.049	-0.021	-0.043	-0.001	-0.072
$^{235}U(n, f)$	0.831	0.797	1.091	1.010	0.756	0.528
$^{238}U(n, \gamma)$	0.024	0.029	-0.005	-0.008	-0.032	-0.024
$^{238}U(n, f)$	-0.435	-0.437	-0.436	-0.445	-0.446	-0.455
$^{239}Pu(n, \gamma)$	-0.050	-0.056	-0.097	-0.060	-0.096	----
$^{239}Pu(n, f)$	-0.399	-0.451	-1.226	-1.334	-0.652	----
$^{240}Pu(n, \gamma)$	-0.001	-0.001	-0.000	0.001	-0.001	----
$^{240}Pu(n, f)$	-0.006	-0.006	-0.016	-0.016	-0.011	----
$^{241}Pu(n, \gamma)$	-0.000	-0.000	-0.000	-0.000	-0.000	----
$^{241}Pu(n, f)$	-0.001	-0.001	-0.003	-0.003	-0.003	----
total	-0.096	-0.175	-0.713	-0.898	-0.487	-0.023
$(C/E)_{JENDL-2}$	1.060	1.086	1.009	1.031	1.103	0.992
$(C/E)_{NEW}$*	1.060	1.085	1.003	1.023	1.099	0.992
$(C/E)_{NEW}$**	1.059	1.084	1.002	1.022	1.098	0.992

Average of $(C/E)_{JENDL-2}$ = 1.047 ± 0.0399
Average og $(C/E)_{NEW}$* = 1.044 ± 0.0404
* Re-evaluated 6 cross sections are considered.
** Re-evaluated 10 cross sections are considered.

Table 7(c) Change of C/E of $^{239}Pu(n, f)/^{235}U(n, f)$ due to cross section change from JENDL-2 to re-evaluated data

(%)

	FCA V-1	FCA V-2	FCA VI-1	FCA VI-2	ZPPR-2	ZPPR-9
$^{235}U(n, \gamma)$	-0.011	-0.009	-0.005	-0.008	-0.001	-0.002
$^{235}U(n, f)$	1.050	0.979	0.989	0.804	0.759	0.755
$^{238}U(n, \gamma)$	-0.011	-0.008	-0.017	-0.017	-0.020	-0.025
$^{238}U(n, f)$	0.002	0.003	0.002	0.001	0.003	0.000
$^{239}Pu(n, \gamma)$	-0.009	-0.010	-0.016	-0.009	-0.015	-0.013
$^{239}Pu(n, f)$	-2.805	-2.680	-2.764	-2.418	-2.276	-2.266
$^{240}Pu(n, \gamma)$	0.001	0.001	0.001	0.001	0.001	0.001
$^{240}Pu(n, f)$	-0.000	-0.000	-0.001	-0.001	-0.000	-0.000
$^{241}Pu(n, \gamma)$	-0.000	-0.000	-0.000	-0.000	-0.000	-0.000
$^{241}Pu(n, f)$	-0.000	-0.000	-0.001	-0.000	-0.001	-0.001
total	-1.783	-1.725	-1.812	-1.647	-1.551	-1.549
$(C/E)_{JENDL-2}$	0.938	0.973	0.960	0.953	0.960	0.971
$(C/E)_{NEW}$*	0.921	0.956	0.944	0.938	0.945	0.956
$(C/E)_{NEW}$**	0.921	0.956	0.943	0.937	0.945	0.956

Average of $(C/E)_{JENDL-2}$ = 0.954 ± 0.0120
Average of $(C/E)_{NEW}$* = 0.943 ± 0.0120
* Re-evaluated 6 cross sections are considered.
** Re-evaluated 10 cross sections are considered.

Table 7(d) Change of C/E of Doppler UO_2 due to cross section change from JENDL-2 to re-evaluated data

(%)

	FCA V-1 (300k - 1073k)	FCA V-2 (300k - 1073k)	FCA VI-1 (300k - 823k)	FCA VI-2 (300k - 823k)	ZPPR-9 (298k - 935.4k)
^{235}U (n, γ)	0.003	-0.004	-0.039	-0.103	0.000
^{235}U (n, f)	1.078	0.919	0.714	1.409	0.015
^{238}U (n, γ)	0.224	0.205	0.201	0.214	0.137
^{238}U (n, f)	0.129	0.125	0.122	0.133	0.093
^{239}Pu (n, γ)	0.009	0.003	0.056	0.092	-0.050
^{239}Pu (n, f)	1.710	1.931	2.232	0.256	3.848
^{240}Pu (n, γ)	-0.004	-0.004	-0.007	-0.003	-0.010
^{240}Pu (n, f)	0.021	0.023	0.022	-0.002	0.074
^{241}Pu (n, γ)	0.000	0.000	0.000	0.000	0.000
^{241}Pu (n, f)	0.002	0.002	0.005	0.002	0.004
total	3.172	3.199	3.307	1.998	4.111
(C/E) JENDL-2	0.880	0.760	0.873	0.880	0.903
(C/E) NEW*	0.908	0.784	0.902	0.898	0.941
(C/E) NEW**	0.908	0.784	0.902	0.898	0.940

Average of (C/E) JENDL-2 = 0.859 ± 0.0506
Average of (C/E) NEW* = 0.887 ± 0.0535
* Re-evaluated 6 cross sections are considered.
** Re-evaluated 10 cross sections are considered.

Table 7(e) Change of C/E of Doppler Fe(SS) due to cross section change from JENDL-2 to re-evaluated data

(%)

	FCA V-1 (SS) (300k - 1073k)	FCA V-2 (300k - 1073k)	FCA VI-1 (300k - 823k)	FCA VI-2 (300k - 823k)	FCA VI-2 (SS) (298k - 935.4k)
^{235}U (n, γ)	0.032	0.019	-0.043	-0.105	-0.102
^{235}U (n, f)	0.916	0.778	0.693	1.362	1.354
^{238}U (n, γ)	0.248	0.231	0.237	0.227	0.231
^{238}U (n, f)	0.133	0.127	0.123	0.132	0.135
^{239}Pu (n, γ)	0.035	0.028	0.097	0.111	0.118
^{239}Pu (n, f)	1.400	1.589	1.654	-0.042	-0.083
^{240}Pu (n, γ)	-0.005	-0.004	-0.007	-0.003	-0.004
^{240}Pu (n, f)	0.022	0.024	0.024	-0.001	-0.001
^{241}Pu (n, γ)	0.000	0.000	0.001	0.000	0.000
^{241}Pu (n, f)	-0.000	-0.000	0.001	0.000	0.001
total	2.781	2.793	2.780	1.681	1.649
(C/E) JENDL-2	1.573	1.753	1.298	1.221	0.999
(C/E) NEW*	1.616	1.801	1.333	1.242	1.015
(C/E) NEW**	1.617	1.802	1.334	1.242	1.015

Average of (C/E) JENDL-2 = 1.369 ± 0.266
Average of (C/E) NEW* = 1.401 ± 0.278
* Re-evaluated 6 cross sections are considered.
** Re-evaluated 10 cross sections are considered.

Table 7(f) Change of C/E of Na-void worth due to cross section change from JENDL-2 to re-evaluated data

(%)

	FCA VI-2			ZPPR-9		
	(9.34 X 20.32)	(15.57 X 30.48)	(21.80 X 40.64)	(9.25 X 40.64)	(30.67 X 40.64)	(30.67 X 101.8)
^{235}U (n, γ)	-0.020	0.002	0.036	-0.010	-0.012	-0.016
^{235}U (n, f)	0.559	0.379	0.079	-0.010	-0.012	-0.016
^{238}U (n, γ)	-0.457	-0.504	-0.594	-0.375	-0.428	-0.538
^{238}U (n, f)	-0.074	-0.091	-0.121	-0.068	-0.074	-0.116
^{239}Pu (n, γ)	0.167	0.157	0.143	-0.766	-0.816	-1.487
^{239}Pu (n, f)	-3.217	-3.043	-2.814	-0.766	-0.816	-1.487
^{240}Pu (n, γ)	0.003	0.002	0.002	-0.766	-0.816	-1.487
^{240}Pu (n, f)	-0.067	-0.067	-0.068	-0.029	-0.030	-0.049
^{241}Pu (n, γ)	0.000	0.000	-0.000	-0.766	-0.816	-1.487
^{241}Pu (n, f)	0.002	0.003	0.004	-0.002	-0.003	-0.004
total	-3.103	-3.161	-3.334	-1.250	-1.363	-2.207
(C/E) JENDL-2	1.213	1.287	1.413	1.044	1.101	1.278
(C/E) NEW*	1.174	1.244	1.363	1.033	1.087	1.252
(C/E) NEW**	1.175	1.246	1.366	1.031	1.086	1.250
Average of						
(C/E) JENDL-2	1.304 ± 0.0826			1.141 ± 0.0996		
(C/E) NEW*	1.260 ± 0.0780			1.124 ± 0.0931		

* Re-evaluated 6 cross sections are considered.
\# Re-evaluated 10 cross sections are considered.

Table 8 C/E VALUES BEFORE AND AFTER THE ADJUSTMENT

NO.	REACTOR CHARACTERISTICS			C/E VALUE BEFORE	C/E VALUE AFTER	STANDARD DEVIATION (%) VE	VM	GMG	GM'G
1	ZPPR9	KEFF		0.9984	1.0038	0.04	0.50	2.43	0.28
2	ZPPR10A	KEFF		0.9953	0.9998	0.04	0.50	2.34	0.28
3	ZPPR13A	KEFF		0.9994	1.0020	0.04	0.50	2.18	0.28
4	ZPPR9	NAVOID	1	1.0448	0.9453	0.70	10.00	8.37	3.30
5	ZPPR9	NAVOID	2	1.1012	0.9922	0.70	10.00	8.38	3.33
6	ZPPR9	NAVOID	3	1.2779	1.1107	0.70	10.00	10.29	4.26
7	ZPPR10A	NAVOID	1	1.2951	1.1716	2.00	10.00	6.59	2.71
8	ZPPR10A	NAVOID	2	1.2819	1.0933	1.08	10.00	10.66	4.45
9	ZPPR10A	NAVOID	3	1.3561	1.0788	1.10	10.00	14.26	6.50
10	ZPPR13A	NAVOID	1	1.2721	1.0940	0.20	10.00	13.51	5.66
11	ZPPR9	DOP.UO2	1	0.9047	0.9523	1.00	10.00	5.41	3.40
12	ZPPR9	CR.WORTH	1	0.9606	1.0174	2.00	10.00	3.96	1.61
13	ZPPR9	CR.WORTH	2	0.9637	1.0149	2.00	10.00	3.67	1.55
14	ZPPR9	CR.WORTH	3	1.0000	0.9993	2.00	10.00	2.32	0.82
15	ZPPR9	25F/49F	1	1.0312	1.0094	1.00	2.00	3.36	1.40
16	ZPPR9	28F/49F	1	0.9896	1.0129	2.00	2.00	7.63	1.99
17	ZPPR13A	25F/49F	1	1.0332	1.0155	1.00	2.00	3.20	1.34
18	ZPPR13A	28F/49F	1	0.9670	0.9899	1.50	2.00	4.84	1.45
19	ZPPR13A	28C/49F	1	1.0587	1.0237	1.00	2.00	6.69	1.57
20	ZPPR9	RRD.49F	1	1.0187	1.0174	0.90	2.00	0.10	0.03
21	ZPPR9	RRD.49F	2	1.0313	1.0232	0.90	2.00	0.62	0.19
22	ZPPR9	RRD.49F	3	1.0313	1.0011	0.90	2.00	2.12	0.68
23	ZPPR10A	RRD.49F	1	1.0100	1.0070	0.90	2.00	0.18	0.08
24	ZPPR10A	RRD.49F	2	1.0240	1.0100	0.90	2.00	1.03	0.33
25	ZPPR10A	RRD.49F	3	1.0390	1.0016	0.90	2.00	2.54	0.85
26	ZPPR13A	RRD.49F	3	1.0321	1.0223	0.80	2.00	0.99	0.30
27	ZPPR13A	RRD.49F	5	1.0694	1.0389	0.80	2.00	2.93	0.86

TABLE 9 PERCENT CHANGES OF RE-EVALUATED AND ADJUSTED CROSS SECTIONS

GRP	E-UPPER	PU-239 FISSION		U-235 FISSION		U-238 FISSION		U-238 CAPTURE	
		NEW*	ADJ.**	NEW	ADJ.	NEW	ADJ.	NEW	ADJ.
1	1.000E+7	3.27	-0.66	-0.36	-0.54	-0.58	1.31		14.57
2	6.065E+6	0.08	-0.78	0.86	-0.25	0.10	1.43		11.44
3	3.679E+6	-0.23	-1.18	-0.59	-0.40	-0.79	1.82	14.07	5.69
4	2.231E+6	-0.03	-1.08	-0.05	-0.41	0.72	1.62	25.79	4.03
5	1.353E+6	-1.33	-1.67	-0.49	-0.66	-10.98	1.46	3.53	1.18
6	8.209E+5	-4.31	-2.76	-1.91	-1.23		0.87	4.84	2.54
7	3.877E+5	-4.61	-2.58	-1.79	-1.48		0.47	2.46	3.43
8	1.832E+5	-5.28	-2.12	-2.89	-1.98		0.21	-5.18	1.69
9	8.652E+4	-3.84	-1.72	-1.00	-2.86		0.05		-0.89
10	4.087E+4		-1.43		-3.99		-1.27		-5.38
11	1.931E+4		-1.33		-4.18		-1.28		-8.31
12	9.119E+3		4.93		-5.07		-1.28		-7.04
13	4.307E+3		4.93		-5.34		0.0		-8.54
14	2.035E+3		4.93		-4.84		-1.29		-13.64
15	9.611E+2		4.93		-2.61		-1.29		-10.28
16	4.540E+2		4.93		-1.36		-1.28		-0.42
	3.224E-1								

* SEND-1 **ADJUSTED CROSS SECTIONS

TABLE 10 PERCENT CHANGES OF CROSS SECTIONS ADJUSTED WITHOUT SODIUM VOID WORTH DATA

GRP	E-UPPER	PU-239 FISSION		U-235 FISSION		U-238 FISSION		U-238 CAPTURE	
		NEW*	ADJ.**	NEW	ADJ.	NEW	ADJ.	NEW	ADJ.
1	1.000E+7	3.27	-0.65	-0.36	-0.54	-0.58	0.22		-20.56
2	6.065E+6	0.08	-0.76	0.86	-0.26	0.10	0.26		-3.68
3	3.679E+6	-0.23	-1.10	-0.59	-0.41	-0.79	0.38	14.07	-0.90
4	2.231E+6	-0.03	-1.03	-0.05	-0.42	0.72	0.48	25.79	-3.94
5	1.353E+6	-1.33	-1.47	-0.49	-0.66	-10.98	0.50	3.53	-10.59
6	8.209E+5	-4.31	-2.25	-1.91	-1.22		0.28	4.84	-6.57
7	3.877E+5	-4.61	-2.04	-1.79	-1.45		0.14	2.46	-4.57
8	1.832E+5	-5.28	-1.69	-2.89	-1.92		0.07	-5.18	-3.33
9	8.652E+4	-3.84	-1.31	-1.00	-2.76		0.02		-2.31
10	4.087E+4		-1.16		-3.85		-4.31		-5.70
11	1.931E+4		-1.17		-4.02		-4.38		-8.57
12	9.119E+3		1.59		-4.87		-4.38		-6.82
13	4.307E+3		1.59		-5.14		0.0		-5.24
14	2.035E+3		1.59		-4.65		-4.38		-4.34
15	9.611E+2		1.59		-2.52		-4.38		-2.56
16	4.540E+2		1.59		-1.31		-4.38		-0.10
	3.224E-1								

* SEND-1 **ADJUSTED CROSS SECTIONS

6.3 Reactor Burnup and Heavy Nuclide Nuclear Data

Tadashi Yoshida

NAIG Nuclear Research Laboratory
4-1 Ukishima-cho, Kawasaki-ku
210 Kawasaki, Japan

Present status of the heavy nuclide nuclear data is reviewed. Emphasis is placed on the uncertainty evaluation of the large FBR burnup characteristics in relation to the nuclear data and on the validation of cross sections based on the analysis of fuel irradiation experiment. In addition the nuclear data pertinent to the formation of minor actinides such as U-232, -236, Pu-238, and Am and Cm isotopes are reviewed.

1. Introduction

Reliable calculation of the reactor burnup characteristics is indispensable in design work of power reactors, in handling of spent fuels and in operation of fuel reprocessing facilities. The accuracy of the calculation primarily depends on the quality of nuclear data for actinide

nuclides as well as fission-product nuclides. On the one hand old requirements for these data are being met by world-wide efforts. A recent example is the solution of a puzzle concerning the Np-237(n,2n) branching ratio. On the other hand, however, some long-standing problems including the capture rate discrepancy in U-238 still remain unresolved, and further new requirement will be added along with the realization of very-high burnup of reactor fuels, the introduction of mixed-oxide fuels in thermal reactors, the progress in the fast-reactor fuel reprocessing, and with start of Tight-Lattice LWR studies.

The heavy nuclide nuclear data in need are reviewed and summarized from these aspects. Qualification of these data by analysis of post-irradiation experiments and the assessment of the prediction accuracy of the burnup characteristics carried out at NAIG are featured as examples of the same kind of studies being done over the world.

2. Major Actinide Nuclear Data

2.1 Reactor Burnup and Data Qualification

Many organizations over the world participated in a benchmark study of burnup reactivity based on a LMFBR model prosoped by NEACRP[1]. The results scattered largely depending on the variety in the data-and-methods employed, and revealed problems inherent to nuclear data of actinide and fission-product nuclides (see Table I). Another indication of insufficiency of the cross-section data accuray is given by a study carried out at NAIG[2], in which the prediction uncertainty of a 1000-MWe FBR burnup characteristics

were evaluated from the present accuracy of the nuclear data. A part of the result is shown in Table II. As is seen here, the prediction uncertainties in the burnup reactivity and in the breeding ratio are nearly 30% and 4% on one-sigma basis, respectively. The atomic inventory of Pu-239, for example, becomes uncertain by 1 ~3 % after one-cycle burnup. These uncertainties, which seem to be too large for economic design of large FBRs, originates mainly from the heavy-nuclide nuclear data.

Table III lists the sensitivity coefficients of the influential heavy nuclides, which are extracted from Table VI of Ref. 2. As one readily expects, the sensitivity coefficients are large for U-238(n,γ), Pu-239(n,f) and (n,γ). Among these, the 3rd-group value of U-238(n,γ) is noticably large exceeding unity. This is due to the fact that this reaction influences the burnup-reactivity change in two-hold ways, namely, by reduction of the absorber (U-238 itself) and by production of the fuel (Pu-239). In this respect, solving of the well-known U-238(n,γ) discrepancy[3] has a primary and practical importance. The 3rd group cross-sections of Pu-239(n,γ), -240(n,γ) -241(n,f) and the 2nd-group one of Pu-241(n,f) have large sensitivity both to the burnup reactivity and to the breeding ratio. In addition to this these cross-cections have, in a relative sense, large uncertainty from the point of the microscopic data. In this respect, reduction of the cross-section uncertainty of these reactions will contribute much to improvement of the burnup calculation of large FBRs.

The sensitivity coefficients described above were calculated[2] by use of the genelarized perturbation method improved and applied for reactor burnup by Takeda and his coworkers.[4] It is quite a powerful tool and saves time-and-labor to a tremendous extent in such a sensitivity study as mentioned above and in the cross-section adjustment described in the following section.

It is not exaggerated to say that the sensitivity studies and the cross-section adjustment can not be accomplished effectively without the use of the generalized perturbation method as far as the time-consuming burnup calculation is concerned.

2.2 Utilization of Fuel Irradiation Data

Almost all of the FBRs being operated in the world have their own program of fuel irradiation and post irradiation test (PIE).[5,6,7] These are briefly surveyed in Table IV. Analysis of these data will yield a good basis for validation of the heavy-nuclide nuclear data. As an example of the utilization of fuel irradiation data, we review briefly an analysis of "JOYO" burnup data and their interpretation in terms of the cross-section adjustment performed by Kawashima et al.[8] In this work, the PIE data[5] taken in the Mark I core of the experimental FBR "JOYO" were analyzed by use of the JENDL-2B70 cross-section set and the hexagonal-Z diffusion burnup code. The C/E values thus obtained for the isotope-wise delpetion and generation of the heavy nuclides (U-235, -236, -238, and Pu-239) were used as input of the cross-section adjustment procedure of the heavy nuclides. The sensitivity coefficients were calculated on the basis of the gereralized perturbation theory.[4] A part of the sensitivity table is shown here as Table V. The implications through the study are shown in Table VI. It should be noted that a decrease of U-238(n,γ) cross section is indicated. The same indication is given by another adjustment work based on large FBR mockup criticals.[9]

This work, aimed at effective utilization of the PIE data, has paved a

way to include the result of the burnup analysis into the cross-section adjustment, which had usually been carried out based only on static data taken in zero-power critical experiments. In order to get a more reliable answer, the following items should be cleared: 1) more PIE data to reduce the statistical error, and 2) improvement of reliability of the error covariance matrix. The item 1) seems to be accomplished effectively by some kind of international cooperation.

3. Minor Actinide Nuclear Data

Gererally speaking, the minor actinides such as U-232, -236, Pu-238, and Am and Cm isotopes produced by burnup exert negative influences over reactor performance and handling of the discharged fuel. Hazardous features of important minor actinides are summarized in Table VII. Uranium 232 is an ancestor of Tl-208, a strong emitter of a high-energy gamma-ray, which makes the reprocessing more difficult. Gamma-ray and neutron activity of the trans-plutonium nuclides such as Am and Cm are linked to the need of shielding in the course of the fuel handling after discharge. Alpha-particles from Pu-238 raise the problem of radiolysis of the organic solvent used in reprocessing. The energy release from these nuclides is displayed in Fig. 1 as functions of the cooling time. From the viewpoint of these negative features of the minor heavy-nuclides, it is indispensable to know accurately the accumulation rate of these nuclides.

The main formation routes of these nuclides are displayed in Table VIII after Küsters.[7] As is seen here the (n,2n) reaction play an important role

in the formation of minor actinides as well as the neutron capture. Generally speaking the reliability of the (n,2n) reaction data compare poorly with that of the capture data. In this respect improvement of the (n,2n) data of these nuclides will make a good impact on the formation calculation of minor actinedes. An example is the (n,2n) cross section of Np-237. The dominant formation route of Pu-236, the parent of the unwelcome U-232, is linked by a part of this reaction leading to the 22.5 hour state of Np-236. The portion leading to the ground state is not effective for the Pu-236 formation because of its long life (120000 years). Therefore the branching ratio data to the 22.5 hour state plays a crucial role. This ratio, however, had long been quite ambiguous and on the list of the NEANDC Discrepancy Subcommittee until a new measurement was reported by N.V. Kornilov[10] in 1984.

In fission reactors the (n,2n) reaction is induced by the low energy tail of the cross section curve. Therefore the cross-section shape just above the (n,2n) threshold must be evaluated very carefully.

4. Concluding Remarks

It has been well recognized that the nuclear data of the major actinides such as U-235, -238 and Pu-239 is of primary importance in reactor calculations, and the world-wide efforts have long been concentrated on improvement of these data. From the view point of the burnup calculation, however, the present accuracy is not yet satisfactory. Especially the long-standing discrepancy of the U-238 capture must be cleared up.

The formation calculation of minor actinides such as U-232, -236, Pu-238, and Cm and Am isotopes is performed usually by codes like ORIGEN[11] or COMRAD[12] on the one-group cross-section basis. Reliability of these cross sections deserves further improvement especially for the (n,2n) reaction. The threshold-structure of this reaction makes it difficult to evaluate accurately the reactor-flux averaged value, in which the cross section just above the threshold predominates.

In order to improve and validate these cross sections, the data taken from the analysis of irradiated fuels well supplement the lack of information. In this respect effective utilization of the PIE data should be systematically and comprehensively carried out, if possible, by international cooperation.

Acknowledgement

The author would like to express deep thanks to Dr. H. Küsters of Karlsruhe who kindly permitted to reproduce a table which had been in his publication.

References

1) P. Hammer, "Proposal for Burnup Calculation Applied to the NEACRP Fast Breeder Benchmark," NEACRP-A-439, Nuclear Energy Committee on Reactor Physics (1980): see also M. Nakagawa, "Nuclear Data for Burnup Calculation in FBR," Proc. 1982 Seminar on Nucl. Data, p.82, JAERI-M 83-041 (1983)

2) T. Kamei, T. Yoshida, T. Takeda and T. Umano, Nucl. Sci. Engn., **91**, 11 (1985)

3) for example, Y. Nakajima, "Activities of NEANDC Task Forces on Resonance Parameters of U-238 and Fe-56," Proc. 1984 Seminar on Nucl. Data, p.196, JAERI-M 85-035 (1985)

4) T. Takeda and T. Umano, Nucl. Sci. Engn., **91**, 1 (1985)

5) T. Ikegami, "Burnup experiments of JOYO Fuels," Proc. 1982 Seminar on Nucl. Data, p.91, JAERI-M 83-041 (1983)

6) S. Pickles and H.J. Powell, "Experimental Validation of Irradiated Fuel Inventories Calculated by the FISPIN Code," Proc. Int. Conf. Nucl. Data for Sci. Technol., p.190 (1983)

7) H. Küsters, Nucl. Technol., **71**, 296 (1985)

8) M. Kawashima, et al., Proc. 1984 Fall Mtg of the Atomic Energy Society of Japan.

9) T. Kamei and T. Kato, J. Nucl. Sci. Technol.,**22**, 1025 (1985)

10) N.V. Kornilov, Proc. Mtg. on Transactinium Nucl. Data, Uppsala, (1984) IAEA

11) M. J. Bell, "A Users Manual for the ORIGEN-2 Computer Code", ORNL-4628 (1983)

12) Y. Naito, "Evaluation of Isotopic Compositions in LWR Spent Fuel," Proc. 1984 Seminar on Nucl. Data, p.57, JAERI-M 85-035 (1985)

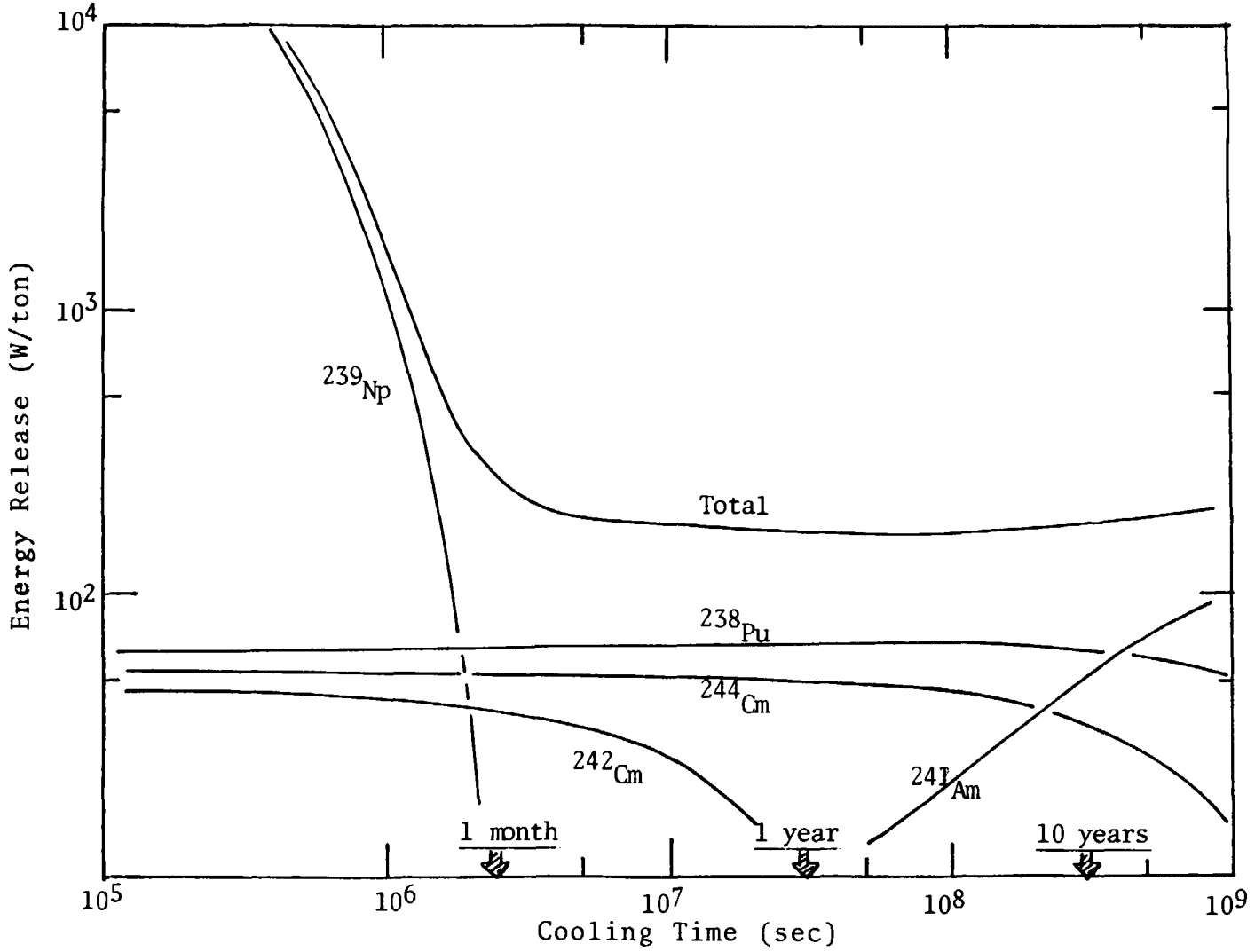

Fig. 1 Energy Release Rate from Heavy Nuclides (BWR Spent Fuel after 30 GWD/T Burnup)

TABLE I

Reactivity Loss of 365-Day Burnup for a 3000-MW(thermal) LMFBR – An International Benchmark for Burnup Calculation

Nuclear Data File	Reactivity Loss	Organization
JENDL-2	1.5% $\Delta k/k$	Japan Atomic Energy Research Institute
ENDF/B-IV	0.5 to 0.7	Swiss Federal Institute for Reactor Research, Comitato Nazionale per l'Energia Nucleare, Australian Atomic Energy Commission
ENDF/B-V	1.0	Argonne National Laboratory
KEDAK-3	1.9	Kernforschungszentrum Karlsruhe
CARNAVAL-IV	1.3	Commissariat à l'Energie Atomique

TABLE II

Prediction Uncertainty of 1000-MW(electric) Core Burnup Characteristics (Nonadjusted Library)– Uncertainty for 292 EFPD Burnup

A. Burnup Reactivity and Breeding Ratio

Burnup Reactivity	$2.557 \times (1 \pm 0.290)\%\ \Delta K/KK'$
Breeding Ratio	$1.204 \times (1 \pm 0.043)$

B. Fissile Number Density [End of Equilibrium Cycle (EOEC)]

Region	^{239}Pu ($\times 10^{20}$ atom/cm^3)	^{241}Pu ($\times 10^{20}$ atom/cm^3)
Inner core	$8.435 \times (1 \pm 0.019)$	$1.271 \times (1 \pm 0.031)$
Outer core	$9.704 \times (1 \pm 0.012)$	$1.733 \times (1 \pm 0.021)$
Radial blanket-1	$1.874 \times (1 \pm 0.031)$	$0.001 \times (1 \pm 0.164)$
Radial blanket-2	$0.636 \times (1 \pm 0.016)$	$\sim 0 \times (1 \pm 0.162)$
Axial blanket-1	$2.286 \times (1 \pm 0.027)$	$0.004 \times (1 \pm 0.142)$
Axial blanket-2	$1.373 \times (1 \pm 0.019)$	$\sim 0 \times (1 \pm 0.146)$

Table III Sensitivity Coefficient of Large FBR Burnup Properties

Reaction	Group	Burnup Reactivity	Breeding Ratio
U-238(n,f)	1	-0.182	-0.011
(n,g)	1	-0.104	0.013
(n,g)	2	-0.612	0.080
(n,g)	3	-2.322	0.306
(n,g)	4	-0.380	0.056
Pu-239(n,f)	1	0.177	-0.060
(n,f)	2	0.390	-0.148
(n,f)	3	0.475	-0.195
(n,g)	2	0.098	-0.012
(n,g)	3	0.561	-0.076
(n,g)	4	0.157	-0.023
Pu-240(n,g)	3	-0.261	0.026
(n,g)	4	-0.084	0.008
Pu-241(n,f)	1	0.134	-0.009
(n,f)	2	0.406	-0.029
(n,f)	3	0.828	-0.059
(n,f)	4	0.135	-0.008

Energy Division : /1/2/3/4/=10MeV-800keV-100keV-1keV-0.025eV

Table IV Postirradiation Experiment Programs

Reactor	Country	Nuclides, Burnup, etc.	Reference
JOYO	Japan	U-234,235,236,238 Pu-238,-239,-240,-241,-242 Pu/(Pu+U)	T.Ikegami Proc. Nucl.Data Seminar (1983)
Phenix	France	PROFIL-I,-II Program	
PFR	U.K.	U-235,-238 Pu-238,-239,-240,241,-242 Am-241,Cm-242, up to 9%	S.Pickles Antwerp Conf (1983)
KNK-II	Germany	Pu-238,-239,240,241,242 KNK-II/2 exp. in plan up to 7%	H.Küsters Nucl. Tech. 71(1985)

Table V Sensitivity Coefficient for Burnup Characteristics of JOYO

(x 10^{-2})

Group	capture				fission			
	1	2	3	4	1	2	3	4
ΔN(Pu)/N_0 in Blanket								
U-235	+0.0	+0.0	+0.0	+0.0	-4.3	-8.0	-18.0	-17.6
U-238	+0.5	+5.5	+25.0	+68.8	-10.8	-0.7	+0.0	+0.0
Pu-239	+0.0	+0.0	+0.0	-0.3	-4.8	-8.4	-13.9	-8.5
ΔN(U-236)/N_0 in Core								
U-235	+3.2	+10.1	+39.2	+46.9	-4.5	-8.2	-18.5	-17.8
U-238	+0.0	+0.0	+0.0	+0.0	-10.5	-0.7	+0.0	+0.0
Pu-239	+0.0	+0.0	+0.0	+0.0	-4.7	-8.1	-13.3	-8.4
ΔN(U-238)/N_0 in Core								
U-235	+0.0	+0.0	+0.0	+0.0	-4.4	-8.0	-18.2	-17.7
U-238	+1.4	+10.2	+26.0	+35.7	+13.9	+0.0	+0.0	+0.0
Pu-239	+0.0	+0.0	+0.0	+0.0	-4.8	-8.4	-13.8	-8.7
ΔN(Pu-239)/N_0 in Core								
U-235	+0.0	+0.0	+0.0	+0.0	-4.3	-7.8	-17.8	-17.3
U-238	-0.8	-0.5	-10.3	-33.2	-4.3	-0.5	+0.0	+0.0
Pu-239	+0.3	+2.1	+10.2	+17.8	+19.7	+33.1	+49.5	+22.6

note: N_0 = U + Pu initial number density

Energy Division: 1) 10 ~ 1.4 MeV, 2) 1.4 MeV ~ 400 keV, 3) 400 ~ 46.5 keV, 3) 46.5 keV ~

(from Kawashima et al., Proc. 1984 Fall Mtg. of AESJ)

Table VI Some Implications from Adjustment

Reaction	Group	Cross-Section Change
U-238 (n,g)	1	0.96
(n,g)	2	0.97
(n,g)	3	0.95
(n,g)	4	0.95
Pu-239(n,f)	1	1.01
(n,f)	2	1.03
(n,f)	3	1.06
(n,f)	4	1.06
Pu-239(n,g)	1	1.02
(n,g)	2	1.03
(n,g)	3	1.05
(n,g)	4	1.04

Energy Division :
/1/2/3/4/=10MeV-1.4MeV-400keV-46.5keV-thrm

Table VII Hazardous Features of Minor Heavy Nuclides

Item	U-232	U-236	Pu-238	Am-241	Am-243	Cm-242	Cm-244
Decay Heat			x	x		x	x
Alpha Emission			x	x	x	x	x
Gamma Emission	x*		x	x			
Neutron (n,alph)			x	x		x	x
Neutron spnt.f.						x	x
Reactivity Loss		x					

*) U-232 → TH-228 → - - - - - - → Tl-208(2.6MeV gamma)

TABLE VIII Formation–Routes of Important MINAC Isotopes

MINAC Isotopes	Approximate Formation Rate		
	PWR	FBR (%)	
		PWR Plutonium	Equilibrium Plutonium
^{236}U, ^{237}Np, ^{236}Pu			
$^{235}U(n,\gamma)^{236}U(n,\gamma)^{237}U(\beta)^{237}Np(n,2n)^{236}Np(\beta)^{236}Pu$	80	10	10
$\uparrow (n,2n)$ ^{238}U	20	90	90
^{241}Am, ^{242}Cm, ^{238}Pu			
$^{241}Pu(\beta)^{241}Am(n,\gamma)^{242g}Am(\beta)^{242}Cm(\alpha)^{238}Pu$	~9	70	55
$^{237}Np(n,\gamma)^{238}Np(\beta)^{238}Pu$	91	15	30
$^{239}Pu(n,2n)^{238}Pu$	<0.1	15	15
^{243}Am			
$^{242}Pu(n,\gamma)^{243}Pu(\beta)^{243}Am$	99.5	95	97
$^{242m}Am(n,\gamma)^{243}Am$	0.5	5	3
^{244}Cm			
$^{243}Am(n,\gamma)^{244}Am(\beta)^{244}Cm$	99.5	99.6	99.8
$^{243}Cm(n,\gamma)^{244}Cm$	0.5	≲0.4	≲0.2

7. CLOSING SESSION

7.1 Summary Talk

Kichinosuke Harada

Radioisotope and Nuclear Engineering School

Japan Atomic Energy Research Institute

Honkomagome 2-28-49, Bunkyo-ku, Tokyo-to

In this summary, I would like to give my general impression for each session as a whole, rather than to comment over specific papers we have heard in this seminar. The latter task would be very difficult - I have not had a time to digest all of the interesting papers.

In the opening session, we have heard nuclear data activities in People's Republic of China and Indonesia. The activity in Indonesia seems to me just in the beginning phase. Dr. Lasijo explained their research plan by making use of the new reactor, and I hope that not only the solid state physics research but also the nuclear data research will grow up steadily.

Dr. Wang Dahai gave us a very impressive talk. We learned that in China both the evaluation and experimental work are carrying on intensively and extensively. Especially, I have noticed their intensive work on nuclear fission. And, also we are very glad to hear that they have completed CENDL-1 this year after hard work done for several years. They are really powerful, indeed. I think we will be able to start some collaboration on for example staff exchange and cooperative researches on some specific subjects, e.g. the fission experiment and the evaluation of the threshold reaction. Of course, the collaboration should proceed in the beneficial form for both side.

In the 2nd session; activities of JNDC working group, some highlights of JNDC work were reported. All these work are related to the evaluation and direct towards the fine fitting to the experimental data. All reported results appeared to be successful in reproducing the experimental data nicely. However, I would like to make two general remarks here concerning

the evaluation work. First, the computer code used for the evaluation work should be made by ourself. Because, one knows everything written in the code if it is the home-made, but not always so for the imported code. To take one example, the GNASH code which is imported from USA has been used frequently at present by many evaluators. I think we should use such an imported code with a thorough knowledge on what is written in it. Secondly, I would say that the current nuclear theory is intrinsically not so precise. So, efforts should be paid not only for getting a nicer agreement with the experimental data by varying parameters, but also for trying to seize the disagreement systematically and to seek after causes physically.

In the 3rd session; topics, we have heard 3 nice talks. An experimental one is related to the traditional subject but very precise. Other two theoretical papers are modern and implicative.

In the 4th session; five papers on the precise and rigorous measurement were presented. I have been a theorist, so I am afraid I couldn't appreciate their worth properly. Though such a kind of work are not luxurious, but are most important. And, I would like to encourage them to continue these elaborate work.

In the 5th session; nuclear data for fusion reactors, one review paper and two experimental reports were presented. Experiments at 14 MeV on both integral and differential are going on quite actively by use of the facilities of FNS and OKTAVIAN. JNDC has made JENDL-3PR1 and 2 which found to be useful for the analysis of the experimental data. However, JENDL-3PR2 includes only the most important nuclide relevant to the fusion. Dr. Kanda stressed that many kinds of neutron cross section data of many kinds of nuclide are needed even to study only the material's characteristics. So, we should strengthen the evaluation work further. Compared with the case of the fission reactor, in the fusion case the number of reaction types one should study is certainly more, but the number of nuclide is less undoubtedly. Therefore, I hope we will be able to complete our fusion data library not in distant future.

In the 6th session; problems on heavy nuclide nuclear data, we have heard 3 reports. All papers pointed out that accurate heavy nuclide nuclear

data are still required with high necessity for the development of the atomic energy. In our JENDL-3 project many improvements are going to be made for heavy nuclide data of JENDL-2, and we wish to complete JENDL-3 just on the schedule. It seems to me that both the experiment and evaluation work concerning heavy nuclide data will meet many difficulties when one try to go a step farther, and I would like to encourage their hard but very important tasks.

I should say a few words about the poster session. I think that the poster session proved very useful. Because, in this seminar plenty of time were devoted to the poster session, and the detailed discussions could be made. It enabled us to make a scientific tour in a very efficient manner. In this sense, the theme of the poster session (facilities of the nuclear data measurement) appeared to be just suitable for chinese nuclear data delegates.

To finish the summary, I would like to say our deep thanks to members of the organising committee of the seminar for their nice arrangement and to beautiful ladies of NDC/JAERI for their careful treatment. Furthermore, I wish to say our congratulations on our success of the first Asian region-international nuclear data seminar. By this seminar, we could deepen the mutual understanding and promote the friendship to a great extent, indeed. In this connection, I would like to appreciate Dr. Wang Dahai for his efforts with which the participation of the four chinese friends has been realized. I hope that a similar interregional nuclear data seminar to the present one will be held in Beijing in the near future.

Thank you and see you again soon.

POSTER SESSION

1) KQCS-2: A Code To Calculate Multigroup Constants For Fast Neutron Reactor

Wang Yaoqing Yu Peihua
(CNDC, Institute of Atomic Energy,
P.O.Box 275-(41), Beijing, China)

ABSTRACT

KQCS-2 code is a new improved version of KQCS code[1], which was designed to calculate multigroup constants for fast neutron reactor. The changes and improvements on KQCS are described in this paper.

I. INTRODUCTION

KQCS-2 code is a new improved version of KQCS, in which the Bondarenko method was used to calculate multigroup constants for fast neutron reactor. The output from KQCS includes infinite dilution group cross sections, resonance self-shielding factors, inelastic scattering transfer matrices and elastic scattering transfer matrices up to P_8. These results can be used in diffusion-, P_N— and S_N— calculations for fast neutron reactor. The details of KQCS have been described in Ref.[1] and its summary has been given in Ref.[2].

However, KQCS code was designed processing the basic nuclear data from Ref.[3], in which the numerical data are expressed in a special format. In order to make KQCS fit for processing ENDF/B format data, besides compiling a special linking code LEK[4] which links ENDF/B-IV with KQCS, it is necessary to make some changes or supplements to KQCS code itself. After these changes or supplements. The new version of KQCS is called KQCS-2.

This paper only describes these changes or supplements as well as the structure of the KQCS-2 system. Other parts which are the same as KQCS code will not be described here.

II. CHANGES OR SUPPLEMENTS IN KQCS CODE

RESOLVED RESONANCE TREATMENT

In KQCS, only single-level Breit-Wigner resonance parameters was taken into account in resolved resonance region calculations owing to no multilevel parameters given in Ref.[3]. However, in the resolved resonance region the ENDF/B format allows parameters from four resonance formalisms:

1. Single-level Breit-Wigner parameters,
2. Multilevel Breit-Wigner parameters,
3. Reich-Moore parameters,
4. Adler-Adler parameters.

In fact, no Reich-Moore parameters are given in ENDF/B-IV and they have been canceled in ENDF/B-V. So except Reich-Moore parameters, other three types of resonance parameters have been taken into account in KQCS-2.

1) Single-level Breit-Wigner Parameters

The treatment method on Single-level Breit-Wigner parameters in KQCS-2 is the same as that in KQCS[1]. The change only occurs in the treatment for negative energy resonance. For negative energy resonance, $\Gamma_n(E)$ was calculated by using the following formula in KQCS:

$$\Gamma_n(E)=\Gamma_n^{o}\sqrt{\frac{E}{1eV}}\left[\frac{(kR')^2}{1+(kR')^2}\right]^{\ell}\quad [5] \qquad \ell=0,1 \ , \tag{1}$$

where Γ_n^{o} is reduced neutron width, R' is the potential scattering radius.

Because no Γ_n^{o} data are given in the resolved resonance region in ENDF/B, the calculation of $\Gamma_n(E)$ in KQCS-2 has been changed using the following formula:

$$\Gamma_n(E)=\frac{P_\ell(E)\Gamma_n(|E_r|)}{P_\ell(|E_r|)}\quad [6] \ , \tag{2}$$

where $P_\ell(E)$ is the penetration factor,

$$P_0=\rho \ , \tag{3}$$

$$P_1=\frac{\rho^3}{1+\rho^2} \ , \tag{4}$$

$$P_2=\frac{\rho^5}{9+3\rho^2+\rho^4} \tag{5}$$

$$\rho=ka \tag{6}$$

$$a=0.123\cdot(AWRI)^{1/3}+0.81\cdot10^{-1} \quad (10^{-12}\ \text{cm}), \tag{7}$$

$$k=2.1916771\frac{AWRI}{AWRI+1.0}\cdot10^{-3}\sqrt{E} \quad (10^{12}\text{cm}^{-1}), \tag{8}$$

2) Multilevel Breit-Wigner Parameters

Doppler broadened multilevel Breit-Wigner resonance cross sections are calculated by using the following formulas[7,8]:

$$\sigma_t(E,T)=\sum_{\ell,\gamma}\sigma^{\ell,\gamma}(E,T) \quad , \tag{9}$$

$$\sigma_x(E,T)=\sum_{\ell,\gamma}\sigma_x^{\ell,\gamma}(E,T) \qquad x=f,c \quad , \tag{10}$$

$$\sigma_e(E,T)=\sigma_t(E,T)-\sigma_f(E,T)-\sigma_c(E,T) \quad , \tag{11}$$

where

$$\sigma_t^{\ell,\gamma}(E,T)=4\pi(2\ell+1)\lambda^2\sin^2\delta_\ell+{}_\gamma\sigma_{oc}(\psi_\gamma\cos2\delta_\ell$$

$$+0.5\cdot\Phi_\gamma\sin2\delta_\ell+\psi_\gamma\alpha_\gamma-0.5\cdot\Phi_\gamma\beta_\gamma) \quad , \tag{12}$$

$$\sigma_x^{\ell,\gamma}(E,T)={}_\gamma\sigma_{ox}\psi_\gamma \quad , \tag{13}$$

$${}_\gamma\sigma_{oc}=4\pi\lambda^2(E_\gamma)g_J\frac{\Gamma_n^\gamma}{\Gamma^\gamma}\left(\frac{E}{E_\gamma}\right)^{\ell-\frac{1}{2}} \quad , \tag{14}$$

$${}_\gamma\sigma_{ox}={}_\gamma\sigma_{oc}\frac{\Gamma_x^\gamma}{\Gamma^\gamma} \quad , \tag{15}$$

ψ and Φ are Doppler broadened line-shape function:

$$\psi_\gamma(\xi_\gamma,X_\gamma)=\frac{\xi_\gamma}{2\sqrt{\pi}}\int_{-\infty}^{\infty}\frac{\exp\left[-\frac{\xi_\gamma^2}{4}(X_\gamma-Y)^2\right]}{1+Y}\,dY \quad , \tag{16}$$

$$\Phi(\xi_\gamma,X_\gamma)=\frac{\xi_\gamma}{\sqrt{\pi}}\int_{-\infty}^{\infty}\frac{Y\exp\left[-\frac{\xi_\gamma^2}{4}(X_\gamma-Y)^2\right]}{1+Y^2}dY \quad , \tag{17}$$

where

$$X_\gamma=\frac{2(E-E_\gamma)}{\Gamma_\gamma} \quad , \tag{18}$$

$$\xi_\gamma=\Gamma^\gamma(E)/\Delta(E,T) \quad , \tag{19}$$

$$\Delta(E,T)=\sqrt{\frac{4EKT}{A}} \quad , \tag{20}$$

$$K=8.6167\cdot10^{-5} \quad (eV/o_K) \quad , \tag{21}$$

$$\delta_\ell=\frac{R}{\lambda\!\!\!^{-}} - \text{arctg}\frac{R}{\lambda\!\!\!^{-}} \cdot \ell \qquad \text{for } \ell=0,1 \quad , \tag{22}$$

$$\alpha_\gamma=\frac{1}{2}\sum_{s\neq\gamma}\Gamma_{sn}(\Gamma_s+\Gamma_\gamma)/D_{s\gamma} \quad , \tag{23}$$

$$\beta_\gamma=\sum_{s\neq\gamma}\Gamma_{sn}(E_s-E_\gamma)/D_{s\gamma} \quad , \tag{24}$$

$$D_{s\gamma}=(E_s-E_\gamma)^2+\frac{1}{4}(\Gamma_s+\Gamma_\gamma)^2 \quad , \tag{25}$$

E_γ — resonance energy,
R — potential scattering radius,
ℓ — orbital angular momentum,
g_J — statistic spin factor,
$\lambda\!\!\!^{-}$ — reduced neutron wavelength.

3) Adler-Adler Multilevel Parameters

Doppler broadened multilevel Adler-Adler resonance cross sections are calculated by using the following formulas:

$$\tilde{\sigma}(E,T)=\frac{C}{\sqrt{E}}\sum_j\frac{1}{\nu_j}\Big[(G_j^x\cos2\delta_\ell+H_j^x\sin2\delta_\ell)\cdot \psi(\xi_j,X_j)+(G_j^x\sin2\delta_\ell-H_j^x\cos2\delta_\ell)\cdot\frac{\phi(\xi_j,X_j)}{2}\Big] \quad , \tag{26}$$

where $x=t,f,c$.

Total, capture, fission and elastic scattering cross sections are respectively given by

$$\sigma_t(E,T)=\tilde{\sigma}_t(E,T)+\sigma_p(E)+\sigma_b{}^t(E) \quad , \tag{27}$$

$$\sigma_f(E,T)=\tilde{\sigma}_f(E,T)+\sigma_b^f(E) \quad , \tag{28}$$

$$\sigma_c(E,T)=\tilde{\sigma}_c(E,T)+\sigma_b{}^c(E) \quad , \tag{29}$$

$$\sigma_e(E,T)=\sigma_t(E,T) \ -\sigma_f(E,T)-\sigma_c(E,T) \quad , \tag{30}$$

where

$$\sigma_p(E)=\frac{2C}{E}(1-\cos 2\delta_\ell) \quad , \tag{31}$$

$$\sigma_b^t(E)=\frac{C}{\sqrt{E}}\ (AT_1+AT_2/E+AT_3/E^2+AT_4/E^3+BT_1*E+BT_2*E^2) \quad , \tag{32}$$

$$\sigma_b{}^f(E)=\frac{C}{\sqrt{E}}(AF_1+AF_2/E+AF_3/E^2+AF_4/E^3+BF_1*E+BF_2*E^2), \tag{33}$$

$$\sigma_b{}^c(E)=\frac{C}{\sqrt{E}}(AC_1+AC_2/E+AC_3/E^2+AC_4/E^3+BC_1*E+BC_2*E^2) \tag{34}$$

G_j^t , G_j^f and G_j^c are the symmetrical total, fission and capture cross section parameters respectively,

H_j^t , H_j^f and H_j^c are the asymmetrical total, fission and capture cross section parameters respectively,

$$\xi_j=\frac{2\nu_j}{\Delta(E,T)} \quad , \tag{35}$$

$$X_j=\frac{E-\mu_j}{\nu_j} \quad , \tag{36}$$

μ_j — the resonance energy,

ν_j — the value of $\Gamma_j/2$

AT_1, AT_2, AT_3, AT_4, BT_1 and BT_2 are the background constants for the total cross section,

AF_1, AF_2, AF_3, AF_4, BF_1 and BF_2 are the background constants for the fission cross section,

AC_1, AC_2, AC_3, AC_4, BC_1 and BC_2 are the background constants for the capture cross section,

$$\frac{C}{E}=\frac{\pi}{k^2} \quad . \tag{37}$$

CALCULATION OF RESONANCE SELF-SHIELDING GROUP AVERAGED CROSS SECTIONS

Following Bonderenko method [91], in the resonance region, the effective group averaged cross sections are expressed as

$$\sigma_x^I(\sigma_o,T)=\int_{E_i}^{E_{i-1}}\frac{\sigma_x(E,T)\,\phi_o(E)dE}{[\sigma_t(E,T)+\sigma_o]}\Big/\int_{E_i}^{E_{i-1}}\frac{\phi_o(E)dE}{[\sigma_t(E,T)+\sigma_o]}\quad , \tag{38}$$

where x=f,c,e.

$$\sigma_t^I(\sigma_o,T)=\frac{\int_{E_i}^{E_{i-1}}\phi_o(E)dE/[\sigma_t(E,T)+\sigma_o]}{\int_{E_i}^{E_{i-1}}\phi_o(E)dE/[\sigma_t(E,T)+\sigma_o]^2}-\sigma_o\quad , \tag{39}$$

where t denotes total.

The resonance self-shilding factors are expressed as

$$f_x^I(\sigma_o,T)=\sigma_x^I(\sigma_o,T)/\langle\sigma_x\rangle^I\quad , \tag{40}$$

$$\langle\sigma_x\rangle^I=\int_{E_i}^{E_{i-1}}\sigma_x(E)\,\phi_o(E)dE\Big/\int_{E_i}^{E_{i-1}}\phi_o(E)dE\quad , \tag{41}$$

x=f,c,e,t

$$\phi_o(E)=\begin{cases}C\sqrt{E}\exp(-E/Q) & E>E_f\\ 1/E & E\leq E_f\end{cases}\quad , \tag{42}$$

where E_f and Q values can be given by users or given as E_f=2.5 MeV, Q=1.35 MeV ,

T is the nuclear temperature of medium,

and

σ_o is the input parameters.

In the KQCS-2 code, values of σ_o and T are inputed as

T=300, 900, 2100 °k

σ_o=1, 10, 10^2, 10^3, 10^4, 10^5.

According to ENDF/B format, in the resolved resonance region parameters from three resonance formalisms are indicated by the LRF flag:

LRF=1: single-level Breit-Wigner Parameters,

LRF=2: Multilevel Breit-Wigner parameters,

LRF=4: Adler-Adler parameters.

KQCS-2 reads parameters in any of these formats and computes the resonance contribution for all resonances.

In order to save computer time and ensure accuracy, in the resolved resonance region the group energy interval (E_i, E_{i-1}) is divided into N_I ultrafine groups, whose group boundaries are generally determined to be $E_\gamma \mp (\Gamma_\gamma(E_\gamma)+\Delta(E_\gamma,T))$ and E_γ. For Adler-Adler parameter, E_γ is substituted by μ_γ and $\Gamma_\gamma(E_\gamma)$ is substituted by $2\nu_\gamma$. For negative energy resonance, $\Delta(E_\gamma,T)$ is taken as 0.0. All integrals in Equation (38)—(41) are calculated for each ultrafine group using the Romberg integration method[11,12]. In each ultrafine group, only those resonances which contribute singnificantly in it are treated exactly. The other resonances which are far away from it's boundaries, i.e. distant resonances, are treated simply, where cross sections are calculated only at two boundary points of each ultrafine group, and at other integral nodes cross sections are determined by linear interpolation.

The results of the energy group integrals in Equation (38)—(41) are obtained by the sum of integral results of N_I ultrafine groups in this energy group.

OTHER CHANGES

In order to fit for ENDF/B formats, the upper limits of some data sets in KQCS-2 code have been extended. For example, the maximal number of Legendre expansion coefficients is extended to 20. In the inelastic secondary neutron spectrum only one Q(E) table function in each reaction channel was allowed in KQCS code. In KQCS-2 code, four Q(E) table functions are allowed for each reaction channel.

Similar changes are not mentioned one by one here.

III. STRUCTURE OF THE KQCS-2 CODE SYSTEM

The structure of the KQCS-2 code system is like the following figure

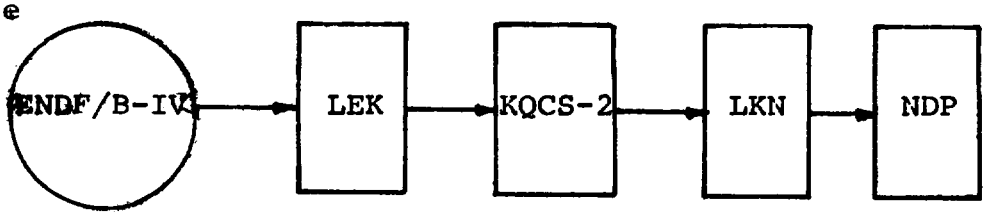

LEK[4] is a linking code which links ENDF/B-IV with KQCS-2 code. It retrieves data from ENDF/B-IV and converts them into the format data required by the input of KQCS-2 code. In addition, it can convert the elastic scattering angular distribution expressed with two-dimensions tabulated function $p(\mu_c,E)$ or $p(\mu,E)$ into the coefficients of Legendre polynomial expansion, which can make the calculations of elastic scattering transfer matrics speed up[12].

LKN[13] is also a linking code which links KQCS-2 code with the code for reactor calculation, such as one-dimensional diffusion code NDP[14]. LKN code can convert the output results from KQCS-2 code into the format data required by the input of NDP code.

REFERENCES

1. Wang Yaoqing, Cai chonghai, Liu Zhaokun, KQCS: A Code to Calculate Multigroup Constants for Fast Neutron Reactor, Chinese Journal of Nuclear Science and Engineering 4, 321(1984).
2. Wang Yaoqing, Codes to Calculate Multigroup Constants for Nuclear Reactor Calculations, JAERI-M 85-035, 118(1985).
3. Nuclear Reactor Data Working Group of CNDC, Nuclear Data Compilation for Reactors, CNDC (1978).
4. Yu Peihua, LEK: A Code to Link ENDF/B-IV with KQCS-2 Code, to be published (1985).
5. I. Broedes, B. Krieg, KFK-2388 (1977).
6. D. Garber, C. Dunford, and S. Pearlstein, "Data Formats and Procedures for the Evaluated Nuclear Data File, ENDF, "Brookhaven National Laboratory Report BNL-NCS-50496 (ENDF 102) (1975).
7. P. Vertes, INDC(HUN)-13/L+Sp (1976).
8. M. F. James, Recommended Formulas and Formats for a Resonance Parameter Library.
9. I. I. Bondarenko et al., Group Constants for Nuclear Reactor Calculations (1964).
10. R. B. Kidman, R. B. Schenter, HEDL-TME-71-35 (1971).
11. W. Romberg, "Vereinfackte Numerische Integration, "Det. Kong. Norske Videnskaber Selskab Forhandlinger, Band 28, Nr.7, 1955.

12. Xu Hanming, Wang Yaoqing et al., RQCS: A Code for Generation of Multigroup constants for Thermal Neutron Reactors, Chinese Journal of Nuclear Science and Engineering 3, 203(1982).
13. Wang Yaoqing, Liu Zhaokun, LKN: A Code to Link KQCS with NDP Code, CNDC (1982).
14. Liu Quisheng et al., One-Dimensional Diffusion Code NDP and Its Application in Fast Critical Benchmark Assemblies, Chinese Journal of Nuclear Science and Technology (5), 587, 1984.

2) Tohoku University Dynamitron Facility

M.Baba
Dapartment of Nuclear Engineering, Tohoku University

The Dynamitron neutron cross section facility at Tohoku University is introduced briefly. The Accelerator, data acquisition system and experimmental apparatus for neutron cross section measurements are described.

1. Introduction

The Dynamitron facility of Tohoku University was installed as a fast neutron cross section facility, and is composed of 1) 4.5MV Dynamitron accelerator equipped with a nano-second pulser, 2) Data acquisition and processing system and 3) experimental apparatuses for fast neutron cross section studies and material science.

At present, main emphases are put on the study of 1) fission cross section, 2) neutron scattering and emission spectra and 3) gamma-ray production cross sections. Neutron transmission experiments, reactor physics experiments using a bulk media of structual material, and development of neutron and gamma-ray detector are carried out as well.

The layout of the facility is shown in Fig.1. The ion beam leaving the Dynamitron is transported to one of the four targets. The beam lines at +-30-deg. and 45-deg. are employed for neutron cross section work. The 60-deg. line is used for ion beam analyses of reactor materials. The experimenntal room has an area of 25m x 20m, wide enough to permit various neutron time-of-flight works using flight path length up to 8m or longer. The shielded room is separated from the main experimental area by a 1m thick concrete wall and is useful for experiments that require lower backgrounds and longer flight path.

2. Dynamitron Accelerator

The pricipal features of the Dynamitron accelerator is summarized in table 1. The Dynamitron is a paralell-coupled cascade generator and is characterized by fully-electronic high voltage generation and

high current capability. The accelerator tube has re-entrant type electrodes for high current operation. A duoplasmatron ion source and a nano-second terminal pulser are equipped to deliver high current pulsed beam of proton and deuteron for neutron generation.

The accelerator has been upgraded in several respects to improve the reliability and flexibility. In 1982, original vacuum tube high voltage rectifiers were replaced completely with new type solid state modules[1]. The replacement was very valuable resulting in extension of the high voltage range, and in dramatic reduction in electric power comsumption and down time due to rectifier failure. Extension of beam transport system and updating of vacuum system were also undertaken[2]. Recently, the terminal mass analyzer was modified to a crossed-field velocity selector from the original permanent magnet for optimum beam transmission and time bunching of heavier ions of $_2D^+$, $_3D^+$ and He^+.

3. Neutron Source

In the facility, various neutron production targets are employed including tritium solid targets. As shown in Fig.2, mono-energetic neutrons are obtained in the energy range from 0.1 to 20 MeV except for 7-14 MeV. The $(d+^7Li)$ reaction on thick lithium target provides continuous neutrons up to 20 MeV covering 7-14 MeV region. The $(d+^{15}N)$ reaction provides quasi-mono-energetic neutrons but has deficiency of smaller neutron yields and larger energy spread. The target assemblies are designed to be of low-mass construction to minimize the energy degradation of primary neutrons. A tritium target is mounted in a differentially-pumped assembly with many baffles and a closed vacuum system consisting of getter and sputter-ion pumps to avoid contamination in extension tubes[3].

4. Data Acquisition and Processing System

In Fig.3 is shown the schematic diagram of the data acquisition system. This consists of the Canberra model-88 multi-parameter pulse height analyzer (16kw,20bit data memory) and NDG model S/140 mini-computer with a multi-user operating system. At present, four ADCs are available for data acquisition. The system enables various data acquisition modes of multiple single-PHAs, dual-parameter and/or list mode[4]. The multi-dimentional list mode data are used effectively for

dynamic-biasing technique in scattering experiments[4].

5. Experimental Apparatuses

Fission cross section measurements[5] are carried out at 30-deg. port using a paralell-plate ionization chamber (Fig.4) for fission event detection. For relative measurements to ^{235}U, a back-to-back type chamber is employed. Neutron fluence is measured using a proton-recoil counter telescope and foil activation technique.

At (-30)-deg. port, a large shield collimator has been installed on a mechanical goniometer for neutron scattering experiment[6]. (Fig.5) A conventional 5" dia. neutron detector or a large Munich type scitillation counter is employed. The measurements can be performed at laboratory angles ranging -20 to 155 deg. at flight path of 3.5 to 7m. Typical experimental results are shown in Fig.6.

A gamma-ray spectrometer is set up in a shield at 45-deg. port. A high pure Ge detector has been used at 1.5m flight path to detect discrete and continuous gamma-rays emitted through the neutron interction with a sample. The detector system can be rotated to measure the gamma-ray angular distribution[7]. In Fig. 1, the experimental set up and sample data are shown.

A summary of recent activities is found in ref.8.

References

1. M.Baba et al., NETU 38, 1 (1981 Annual Report, Fast Neutron Laboratory, Tohoku University)
   M.Baba et al., ibid., 40, 2 (1982)
2. M.Baba et al.,ibid., 41, 3 (1982)
3. K.Kanda et al., ibid, 41, 11 (1982)
4. K.Kanda and S.Iwasaki, ibid., 41, 13 (1982)
5. K.Kanda et al., Int.Conf."Nuc. Data for Sci." Santa Fe (1985)
   K.Kanda et al., JAERI-M-85-035 p.220 (1984)
6. S.Chiba et al., J.Nucl.Sci.Technol. 22, 771 (1985)
   S.Iwasaki et al., Int Conf."Nucl. Data for Sci." Santa Fe (1985)
7. Y.Hino et al., J.Nucl.Sci.Technol. 15, 85 (1978)
   S.Itagaki et al., NETU 46, 23 (1985)
8. K.Sugiyama et al., NETU 43 (1984)

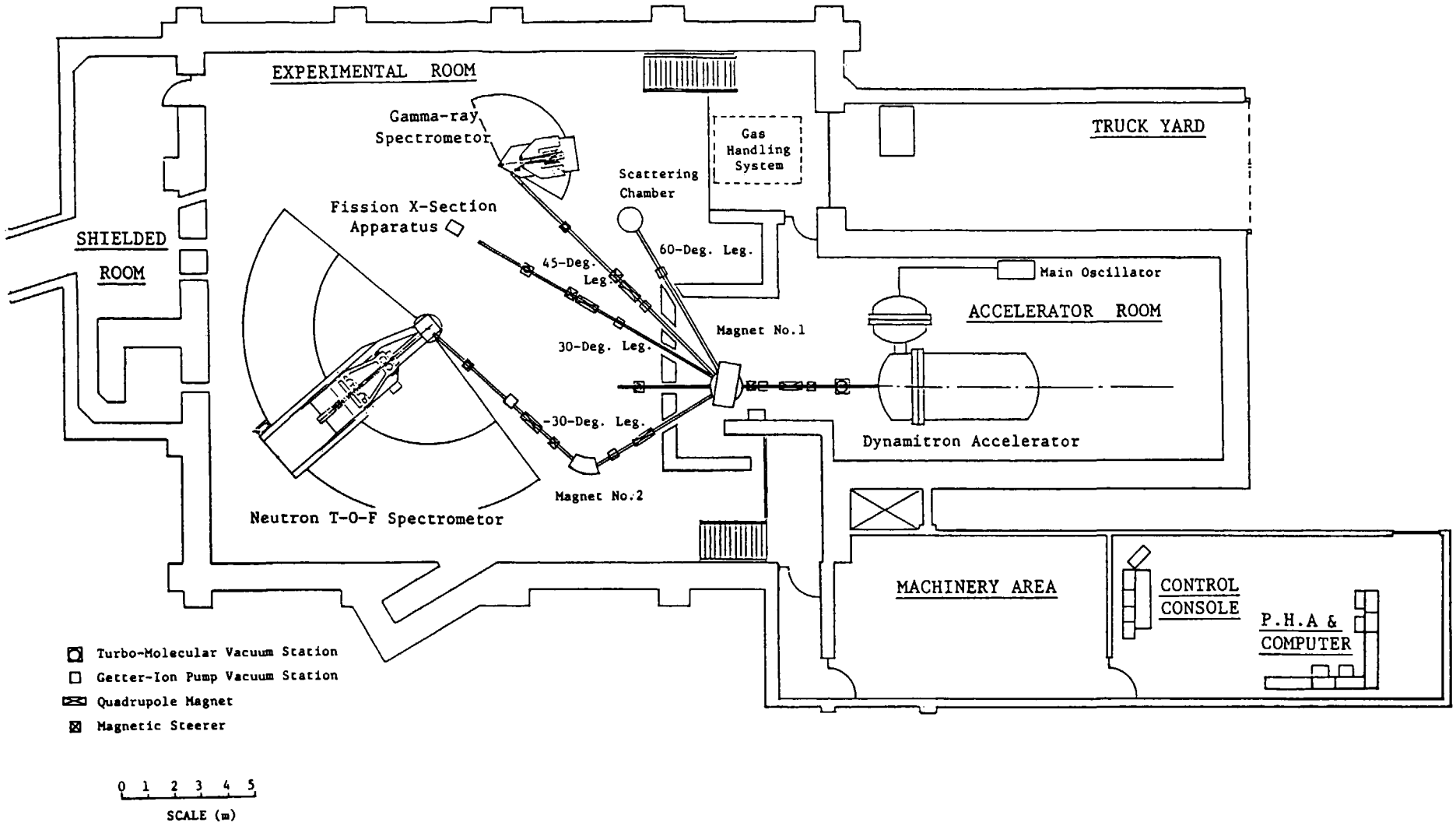

Fig.1 Plan view of Tohoku University Dynamitron facility.

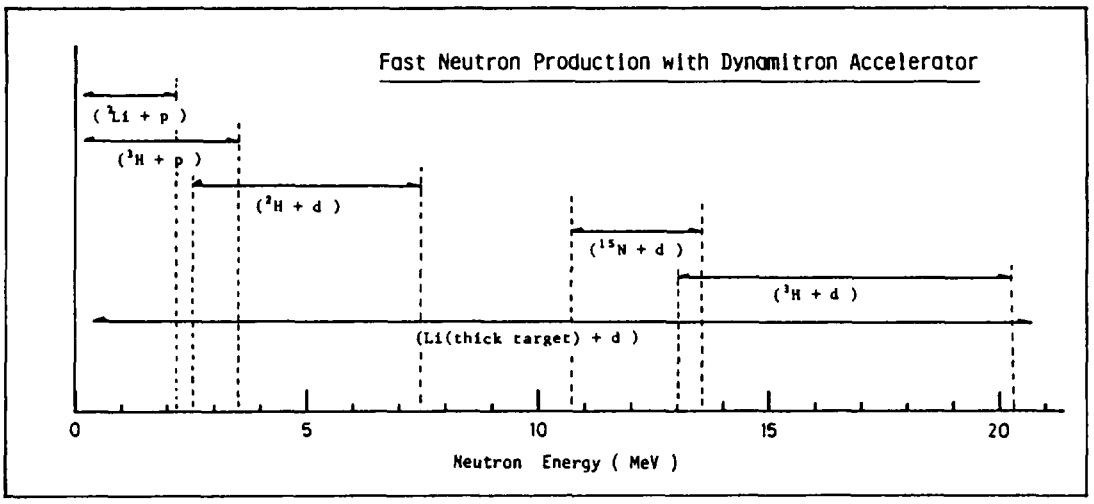

Fig.2 Energy range of fast neutrons produced by 4.5MV Dynamitron accelerator.

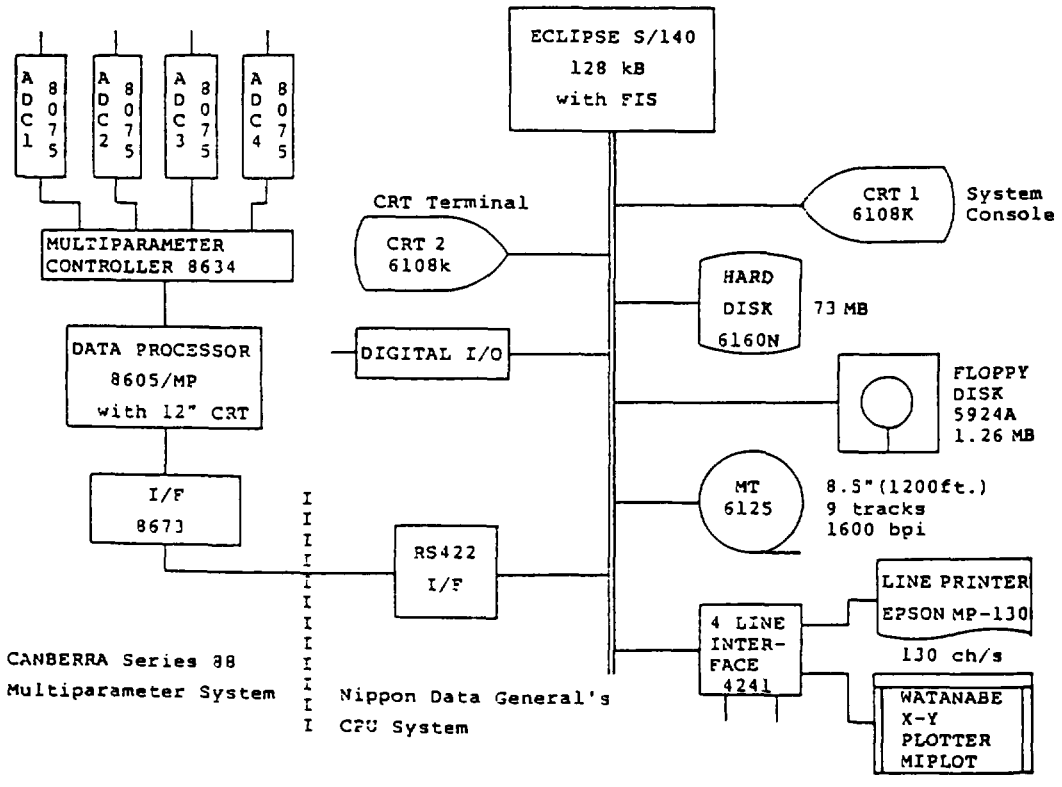

Fig.3 Schematic diagram of data acquisition system.

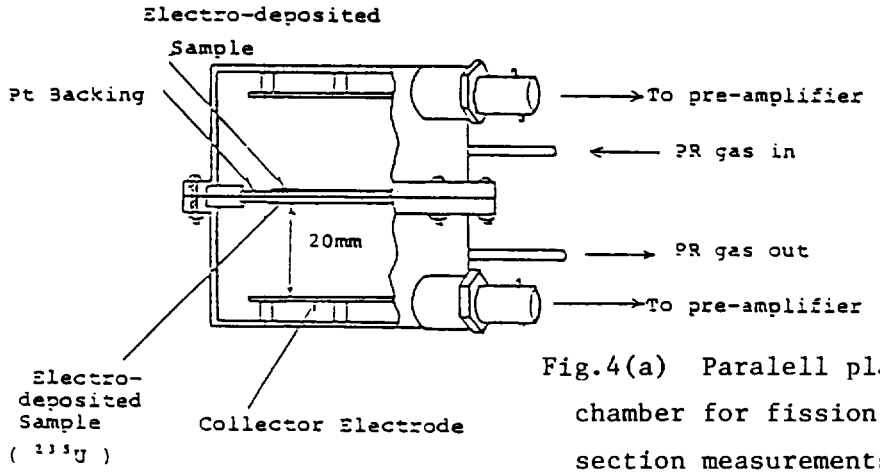

Fig.4(a) Paralell plate fission chamber for fission cross section section measurements.

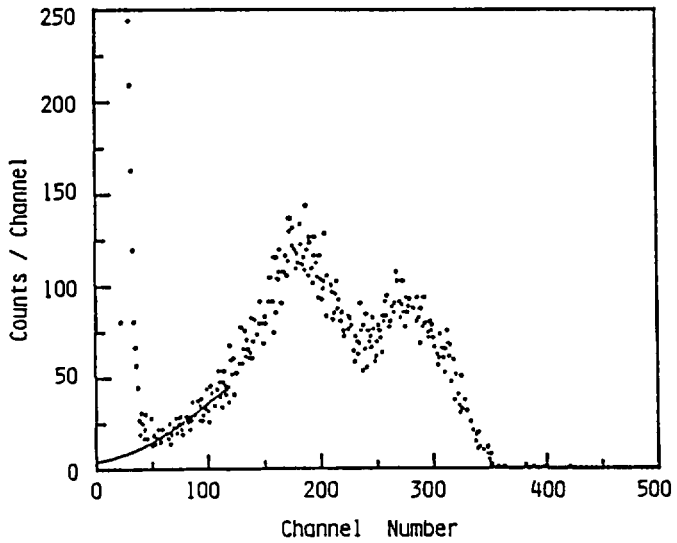

Fig.4(b) Fission fragments pulse height distribution of ionization chamber.

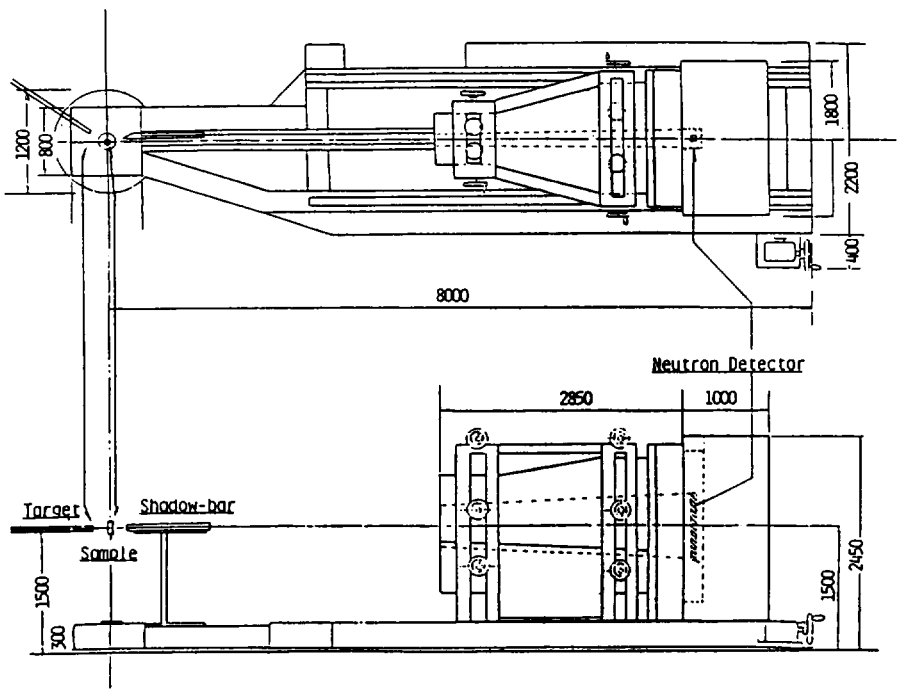

Fig.5 Neutron T-O-F spectrometor for scattering experiments.

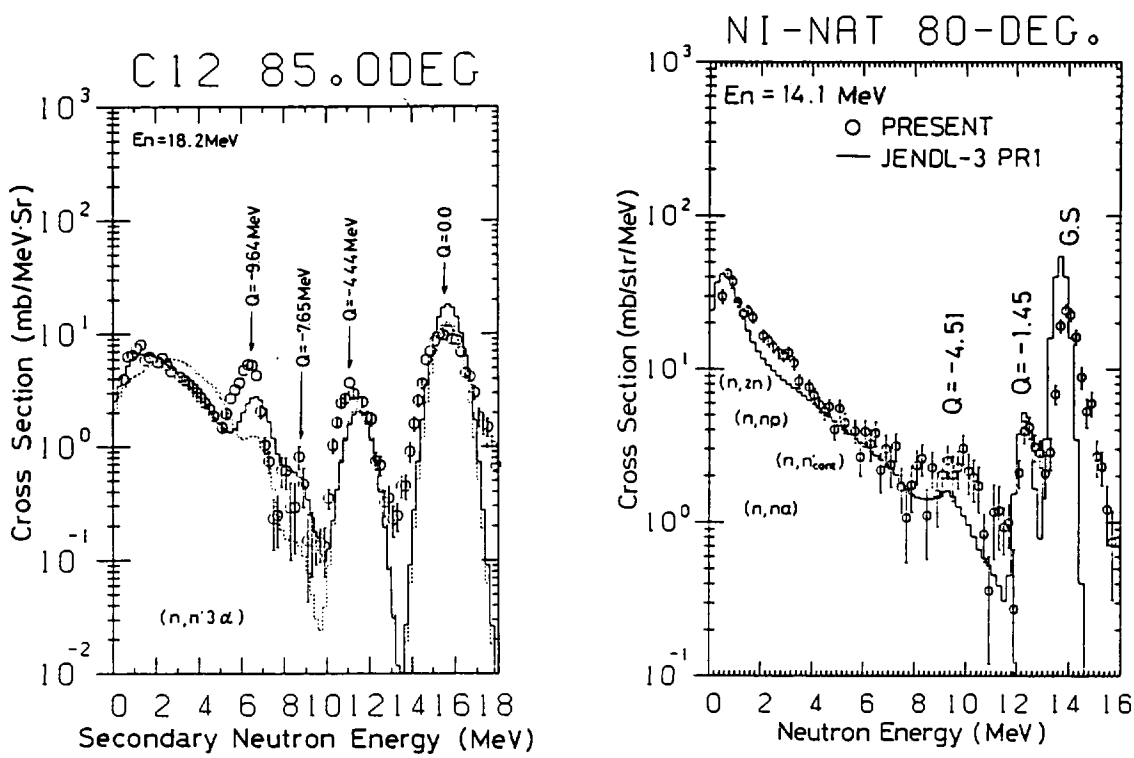

Fig.6 Typical examples of measured emission spectra.

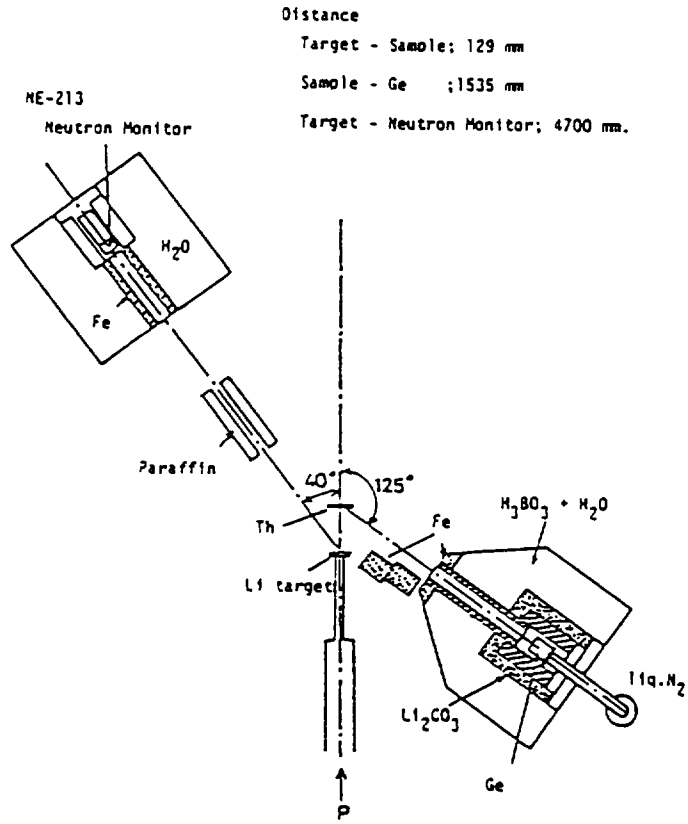

Fig.7(a) Experimental setup for neutron induced gamma-ray measurements.

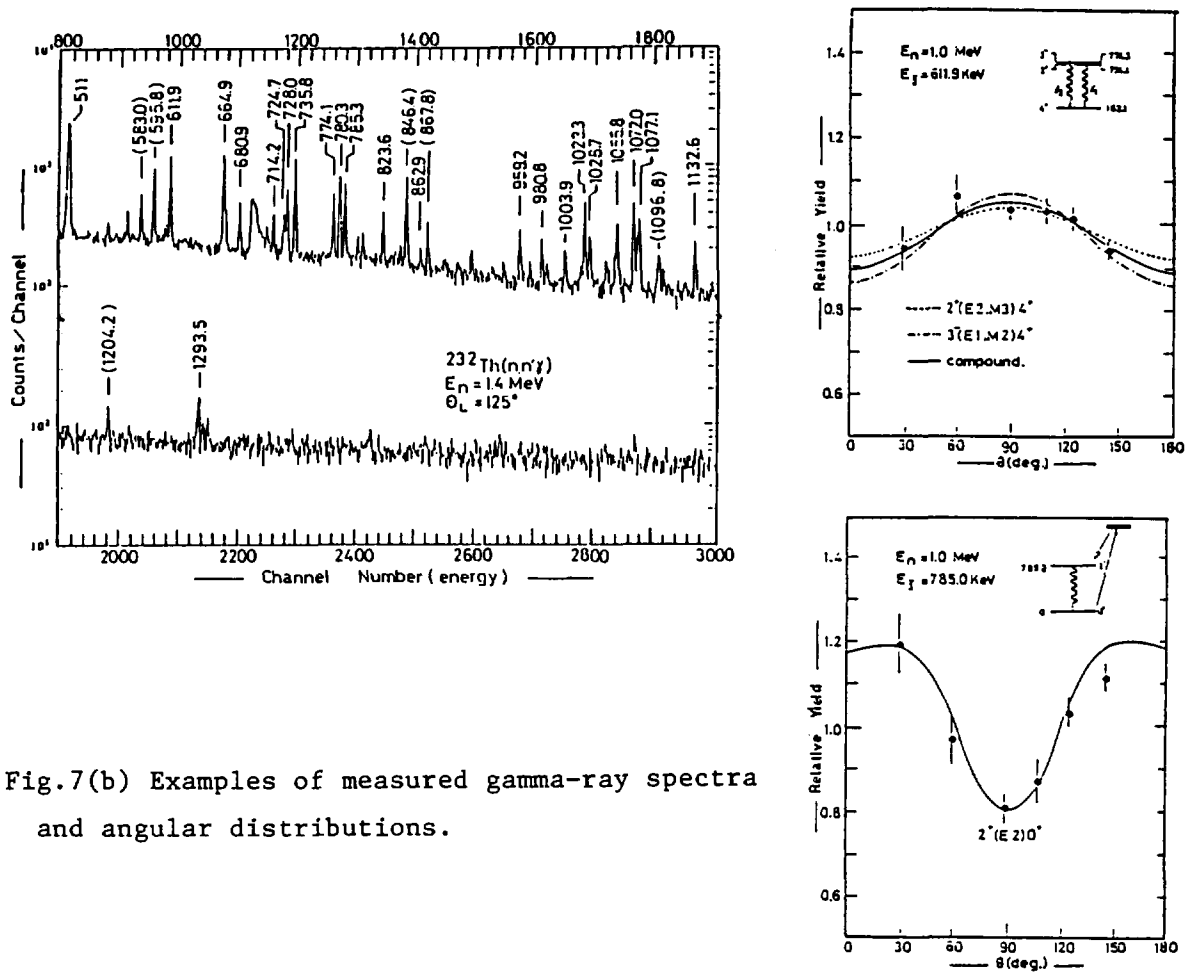

Fig.7(b) Examples of measured gamma-ray spectra and angular distributions.

Table 1 Principal features of Tohoku University Dynamitron accelerator.

1. Parallel-Coupled High Voltage Generator
   - 96 High Voltage Solid State Rectifiers: $300kv_{p-p}$ / Module
   - High Current Capability: 3mA H^+ at 3MV recorded
2. Dynamag type Duoplasmatron Ion Source
   - Nano-Second Terminal Pulser
   - Terminal Mass-Analysis and Pumping
3. 5 Beam Lines with Oil-Free Vacuum Stations;
   Turbo-Molecular / Getter-Ion Pumps

---

a. High-Voltage Range: 0.7 - 4.5 MV (±1 kV)

b. Ion Beam: H^+, D^+, $_2D^+$, $_3D^+$, $^3He^+$, $^4He^+$

c. Pulsed Beam: Duration $\lesssim$ 2 nano-second
   Frequency: 2M $\sim$ 7.8kHz in binary step
   Peak Current: 1 $\sim$ 3 mA

---

3) JAERI Linac TOF Facility

Makio OHKUBO
Linac Laboratory, Japan Atomic Energy Research Institute
Tokai-mura, Ibaraki-ken

Abstract

A brief explanation is made on the neutron Time-of-Flight facility of the JAERI Linac. A raw data on the capture measurements on ^{121}Sb, the total cross sections of ^{142}Ce, O, ^{nat}Ge and ^{nat}Nd measured this system are shown.

Since the construction of the TOF facility based on JAERI 120 MeV electron linac(2nd generation machine) in 1970- 1972,[1] the system has been improved many times in many parts, so we have now the most excellent system since then for the neutron cross section measurements from eV region to several MeV neutron energy. A brief description of this facility is in the following.

A bird's-eye view of the JAERI linac TOF facility is shown in Fig.1. The s-band electron linac produces a pulsed electron beam of energy 120 MeV, the minimum pulse width ~25 nsec, the peak current ~3 A, with a repetition rate 50-600 pps. Neutrons are produced on a tantalum target bombarded by the electron beam, and are emitted from a surrounding moderator to 4-pai direction. A boron loaded polyethylene moderator has been used to eliminate the 2.2 MeV gamma rays from H(n, γ)D reactions in the moderator. The construction of the neutron source is shown in Fig.2. Replacement of the boron-polyethylene moderator to a boron-loaded water circulation system is now going.

There are six neutron flight paths; to a 190-m flight station(mid station at 100 m), to a 15-m flight station, to a 55-m station(capture tank), two flight paths to a 47-m station, and to a 20-m station. These flight tubes are evacuated to reduce neutron scattering loss by the air, which amounts to ~6% per meter of 1 atm air for slow neutrons. The windows of the tubes are 0.1 mm mylar sheets or 0.5~2 mm aluminum sheets. In order to prevent the TOF detector electronics from the paralysis by the gamma flush, the lead and the copper shadow bars(300 mmL x 60 mmW x40 mmH) are settled in every flight tubes, which shield the extremely strong gamma rays and fast neutrons from the target. Hence the TOF detectors view only the neutron moderator surrounding the target.

At the 190-m station, where the maximum available neutron beam cross section is 500 mm X 500 mm, high resolution transmission measurements are made by using a detector bank with seven sets of 5" x 1/2" ^{6}Li-glass(NE908) + EMI-9530 photomultiplier tubes.

At the 100-m midstation, either a neutron detector or the samples for the 190-m station transmission measurements are

placed in the beam, depending on the kind of measurements to be made. On this flight path and the 55-m flight path below, the beam handling booths(for transmission samples) are settled at about 8 m from the neutron source.

At the 55-m station, a 500-l liquid scintillator tank(~1 m dia meter), shown in Fig.3, is placed.[2] The neutron beam passes through the center of the tank with a diameter 60 mm, the beam hole is lined with B_4C layer of 1 cm thickness. A sample is placed at the center of the tank, where the cascade capture gamma rays are effectively stopped in the liquid scintillator. In the tank, the scintillator(NE 224)is optically divided into equal two parts by a foil mirror, each of which is viewed by four 5" dia. photo-multipliers(HAMAMATSU, R1250x). By the coincidence use between the two parts, natural background counts are effectively reduced; the ratio of neutron capture gamma ray signals to the natural background is increased about 10 times. The efficiency for the capture event detection is about ~70 %, which depends on the capture gamma ray spectrum, and the discrimination levels of the electronics. Neutron flux pass through the capture samples is detected by a 5" dia. ^{6}Li-glass detector behind the capture tank.

At the 47-m station now, the transmission measurements are continued. A ^{6}Li-glass (1 1/2" x 1/2" NE912 + RCA-8850) detector is placed in a boron-paraffine shielding of which inner surface is lined with B_4C layer of 1 cm thickness. The samples are placed in a 35 mm dia. collimated beam, ~1.5 m upstream the detector. Between the sample and the detector, an evacuated flight tube of 1 m length is placed to reduce neutron scattering loss. The neutron flux is monitored by a thin ^{6}Li-glass flux monitor upstream the sample and the detectors.

We have several data acquisition systems, USC-3(16K, 25ns), TMC(4K, 31ns), CAMAC system(4K, 50ns), and a new CAMAC system(64K, 1ns) supported by a PC-9801E and a FACOM-S-3300 computers. Data in these acquisition systems are read out onto magnetic tapes, and raw data processing are made by FACOM U-200 computer in the Linac laboratory. Further analyses are made by a central computer FACOM M-380 at the JAERI computing center, through remote operation terminal based on the U-200 or the S-3300 computer.

An example of neutron resonance capture counts vs. time-of-flight channel measured by the liquid scintillator tank are shown in Fig.4, where capture sample was a separated isotope of ^{121}Sb. In Fig.5 is shown the neutron total cross section of ^{142}Ce measured at the 47 m station. As the cerium is included in the ^{6}Li-glass scintillator as an activator, the cross section of cerium is important for the accurate calculation of the neutron detection efficiency. In fact, an effect of scattered neutrons from the lowest 1.27 keV resonance of ^{142}Ce can be seen in the neutron TOF spectrum as a small bump.(The effective neutron path length in the scintillator increases by the resonance scattering

from ^{142}Ce nuclei in the scintillator.)

The cross section of oxygen is practically important to determine cross sections of some elements of which available samples are only oxides. We have made transmission measurements on Al and Al_2O_3, and obtained the total cross section of oxygen from 1 keV to 1.2 MeV by the subtraction method. Total cross section of oxygen we obtained is approximately 3.85 - 0.002 E_n (barn) below 100 keV, as shown in Fig.6, where E_n is neutron energy in keV.

In the similar way the total cross sections of ^{nat}Ga, ^{nat}Ge, ^{nat}Nd, ^{140}Ce, ^{nat}Ce, ^{121}Sb, ^{123}Sb were measured from 0.1 keV to several hundred keV. For the natural germanium, total cross section are shown in Fig.7 from 0.7 to 10 keV, where the germanium oxide are used for the transmission sample. Many fine resonances are observed, and the large resonances are due to that of even isotopes. In Fig.8, total cross section of natural neodymium (Z=60) is shown up to 1 keV, where many fine resonances are observed. Very large resonances are due to even isotopes.

Observed transmission and capture data are analyzed to obtain resonance parameters; E_n, $g\Gamma_n$, Γ_γ, L and J. Statistical properties of these resonances agree quite well with the predictions of the random matrix theory; the Porter-Thomas and the Wigner distributions and further long range correlations. However it is stressed that these facts not always support the random hypothesis which is usually accepted as the nature of highly excited states of the nucleus. Deviations from the statistical theories are reported on many nuclei for many years. To deepen the understanding of the neutron resonance region , further analyses and experiments are needed.

References

1) Takekoshi,H.(ed) JAERI-Report-1238(1975)
2) Mizumoto,M., Sugimoto,M. and Shoji,T.; JAERI-M-84-211(1984)

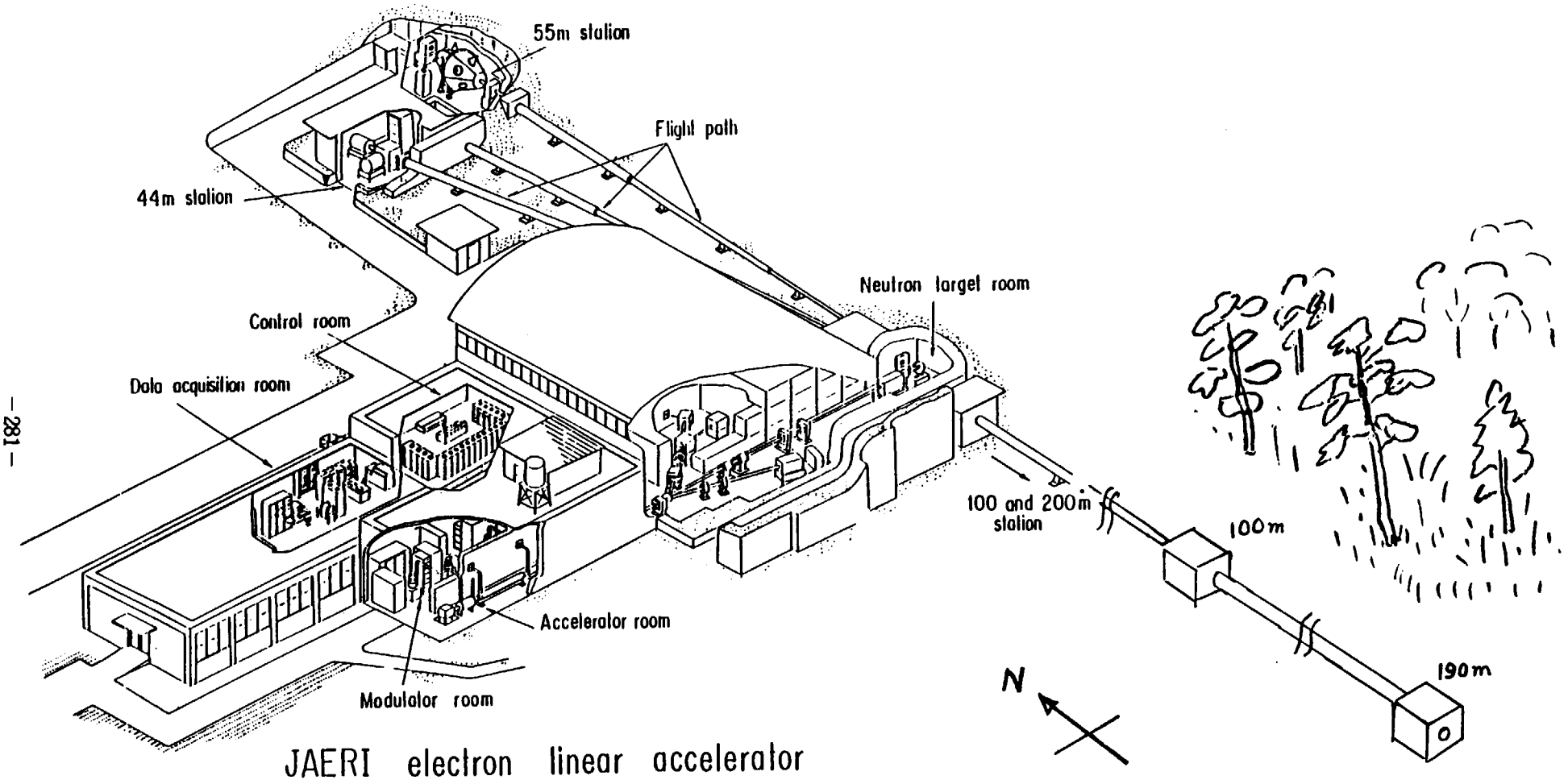

Fig.1 A bird's-eye view of the JAERI Linac TOF facility.

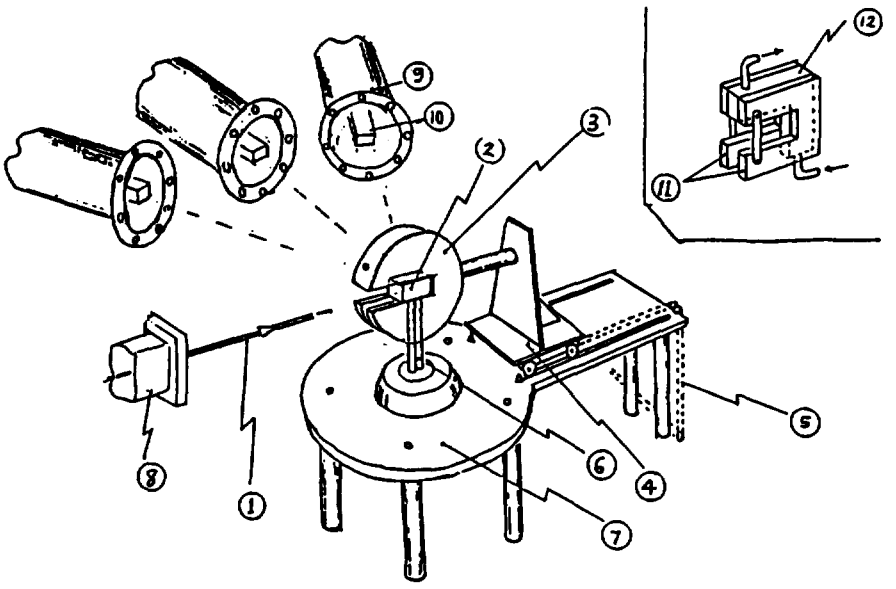

Fig.2 The target and the moderator assembly for the pulsed neutron source. 1) electron beam, 2) water-cooled laminated tantalum target packed in a stainless-steel can. 3) boron-polyethylene moderator, 9) neutron flight tubes. 10) shadow-bars to shield the gamma flush from the target.

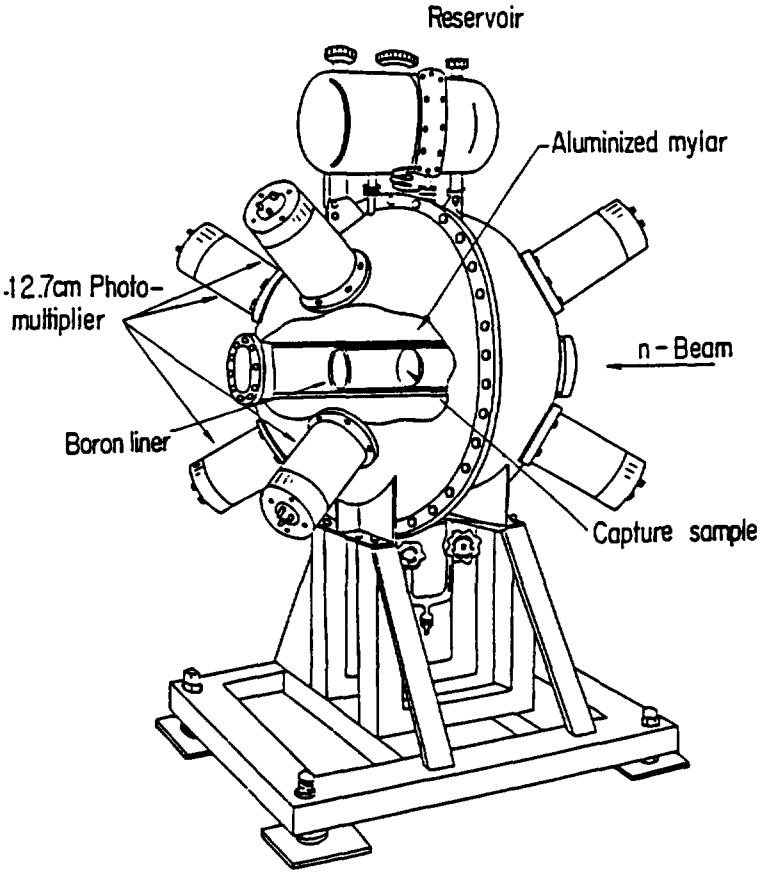

Fig.3 The 500-l liquid scintillation detector. A mirror foil is placed in the central plane perpendicular to the neutron beam.

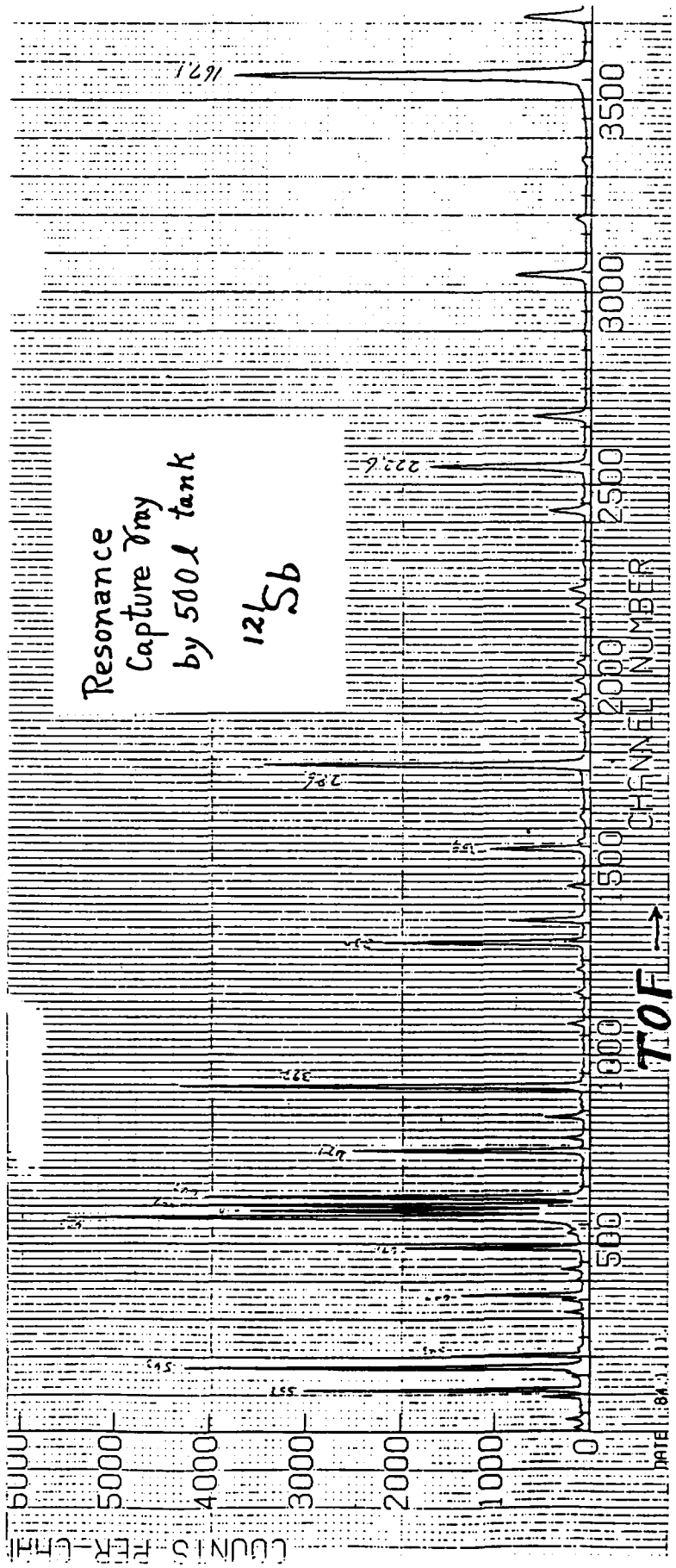

Fig.4 The gamma ray yields vs. time of flight measured by the capture tank. The sample is a separated isotope ^{121}Sb. Neutron energy region from 160 to 570 eV is shown.

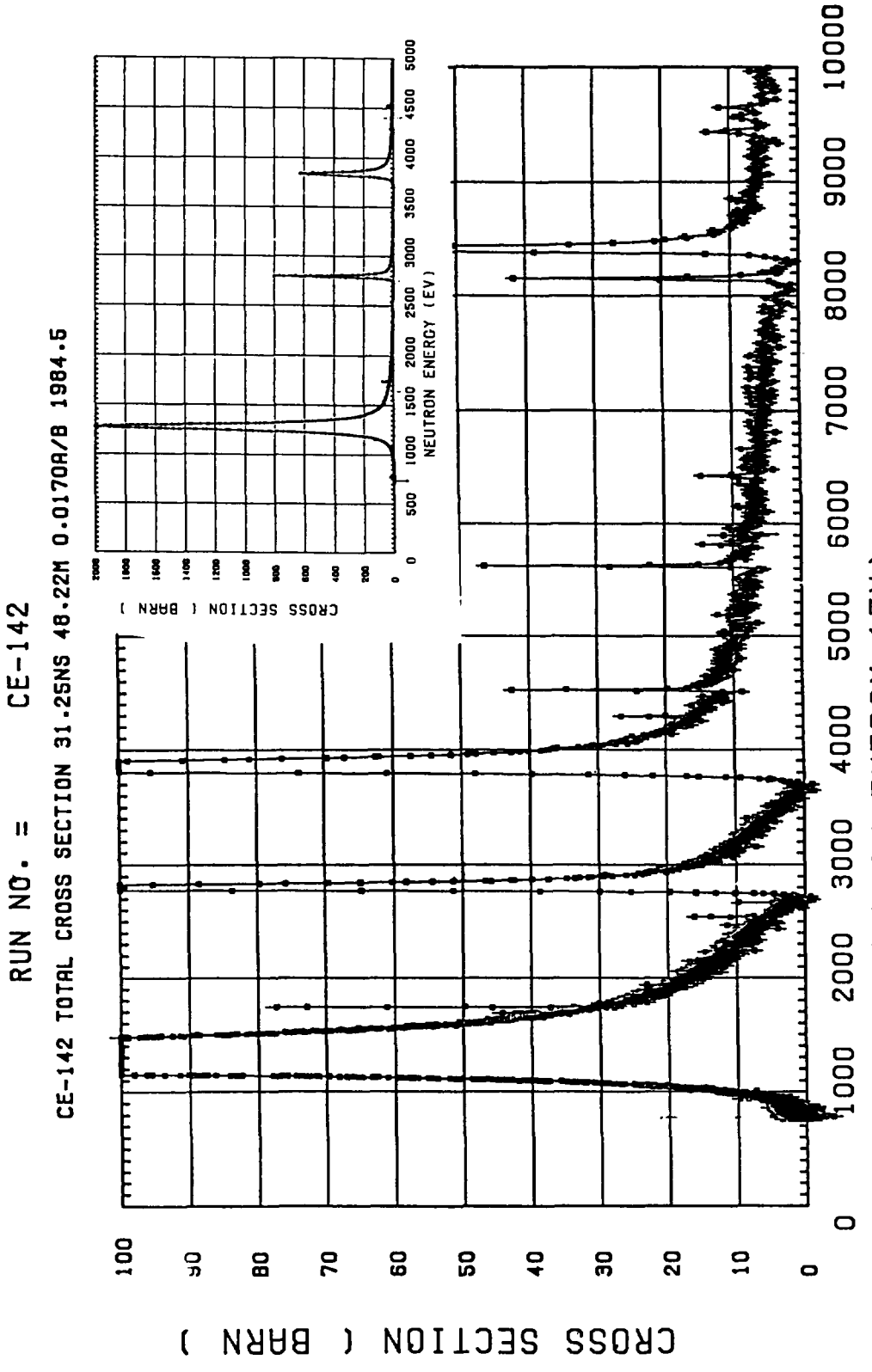

Fig.5 Total cross section of ^{142}Ce from 0.7 to 5 keV. The peak cross section of the lowest resonance at 1.27 keV is 2000 barn.

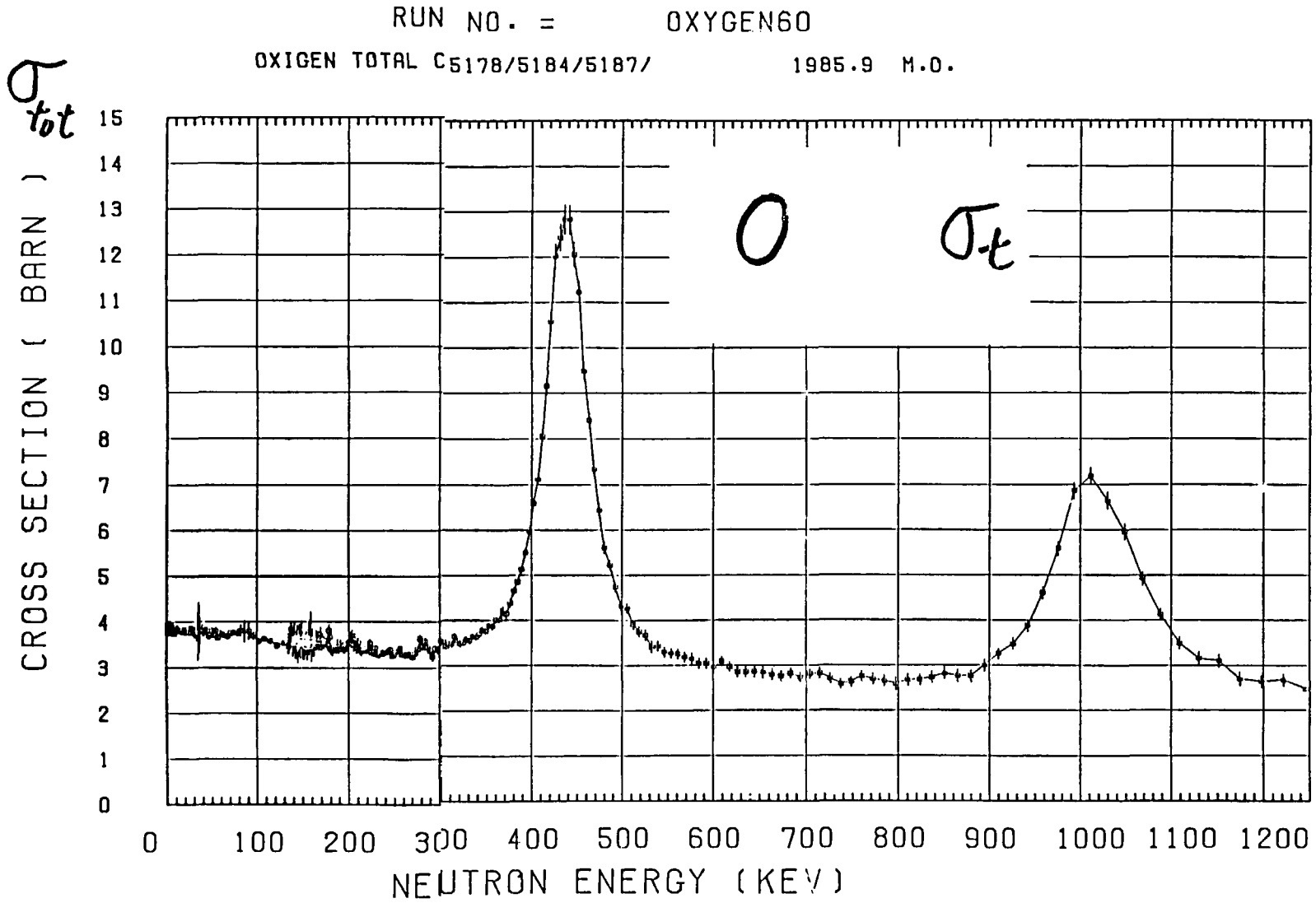

Fig.6 Observed total cross section of oxygen up to 1.2 MeV, where structures at 35keV, 130-180 keV are due to aluminum resonances.

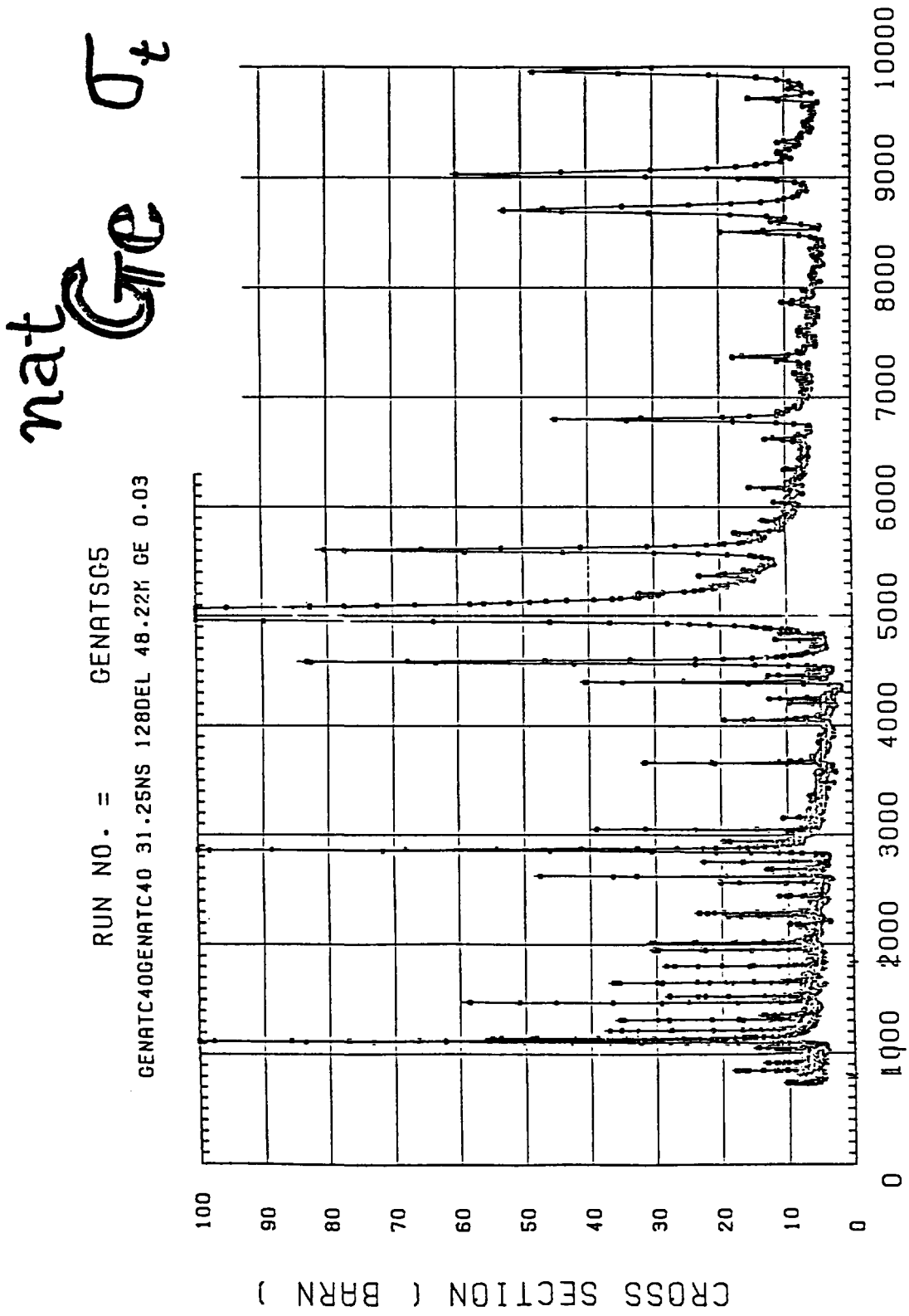

Fig.7 Total cross section of natural germanium from 0.7 to 10 keV.

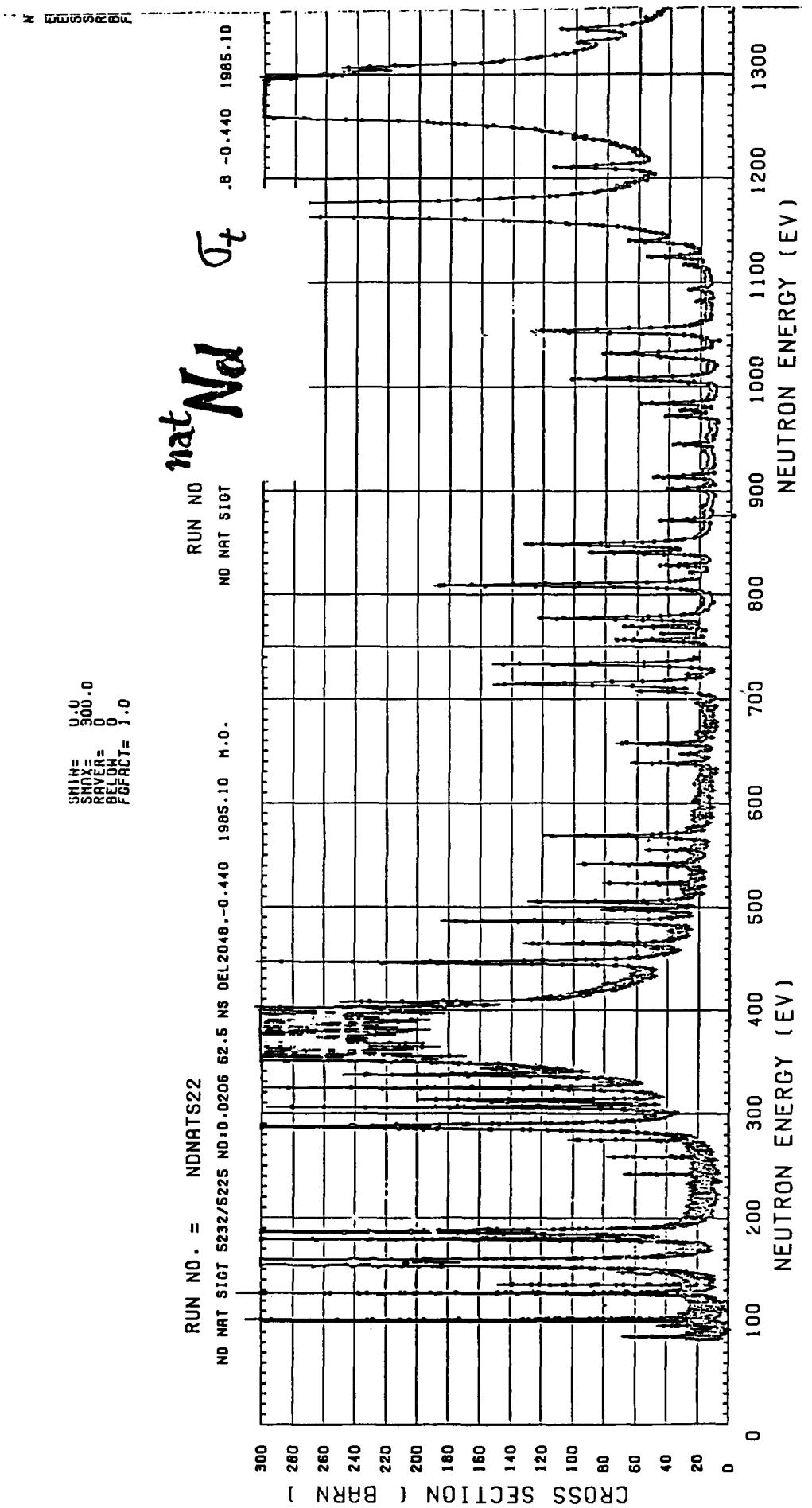

Fig.8 Total cross section of natural neodymium(Z=60) from 0.1 to 1.3 keV. The large resonances are that of even isotopes.

4) Tandem Fast Neutron TOF Facility

M. Sugimoto, Y. Yamanouti, S. Chiba,

M. Mizumoto, Y.Furuta, and M. Hyakutake*

The tandem fast neutron time-of-flight(t-o-f) spectrometer was used to measure the elastic and inelastic scattering cross sections of the neutrons in the energy rage from 13 to 18 MeV. The large volume detector system can make possible the efficient measurements of the low yield levels. The improvement of the time resolution of the detectors was tried by using the two techniques.

We have measured the neutron elastic and inelastic scattering cross sections from ^{27}Al and ^{28}Si at 13 MeV, and from ^{118}Sn at 15 and 18 MeV using the tandem fast neutron t-o-f spectrometer shown in Figure 1. The spectrometer consisted of the 8 meter long goniometer on which the massive shield-collimator system was placed for the main neutron detectors: 2 by 2 array of the 10 liter volume NE213 scintillators. The measured angular range was 15 - 140 deg in the normal setup and the modified setup[1] was used in the measurements at the larger scattering angles (140 - 160 deg). The neutron source reaction was the D(d,n)^{3}He and the neutron intensity was 9 x 10^{7} n/sr/sec, by using the 3cm long gas call filled with 2 atm deuterium. The overall timing resolution was 3 nsec fwhm measured from the gamma ray peak in the t-o-f spectrum. To improve the time resolution of the large detectors we employed the two time-compensation techniques: (1) the hardware method that was developed at Ohio[2] and (2) the software method that was the off-line processing of the list mode event data to obtain the best time compensated spectrum empirically with the help of the interactive graphics system. The latter was superior to separate the inelastic peak close to the elastic peak and to obtain the well-resolved time spectrum over the wide energy range.

In the above measurements we used the in-terminal ion source to get the higher beam intensity, so that the accelerator was operated as the single mode Van de Graaff, but at the expense of the intensity the tandem

* Kyushu University

acceleration mode may be used to produce the 30 MeV neutrons by the $^{7}Li(p,n)^{7}Be$ reaction. The t-o-f spectrometer was designed to be able to measure at such an energy region.

References

1) E. Ramstrom and P. A. Goransson, Nucl. Phys. A284, 461 (1977).

2) J. D. Carlson, R. W. Finlay and D. E. Bainum, Nucl. Instr. Methods 147, 353 (1977).

Fig.1 The picture of the tandem fast neutron t-o-f spectrometer installed at the neutron target room.

5) Fusion Neutronics Source (FNS) Facility

Tomoo Nakamura

Abstract

The Fusion Neutronics Source Facility is an intense D-T neutron source devoted solely to fusion neutronics research in JAERI. It has a capability to produce 14 MeV neutrons in various operation modes to satisfy diverse experimental requirements. The activities on nuclear data at FNS include both differential cross section measurements and examination of nuclear data by integral experiments.

The objectives of the Fusion Neutronics Source Facility (FNS) are to provide experimental data on neutronic parameters in supporting the nuclear design of components in a D-T fusion reactor.[1] The FNS was completed in April, 1981 and has been successfully operated for a variety of experiments since then.

The FNS consists basically of a 400 kev electrostatic deuteron accelerator of high beam current and heavy-duty type tritium metal targets.[2] In Fig. 1 is shown the artist's sketch of the main part of the FNS facility, and detailed component layout in Fig. 2. Various neutron source conditions can be realized by suitable combinations out of

a) two Duoplasmatron-type ion sources - high current(GIC 740A) and low current(GIC 820) -
b) two operation modes - direct current and pulsed beam -
c) two beam lines - 0 degree and 80 degree directions leading to separate target rooms #1 and #2,respectively -
d) various target assembly types - rotating target with swing motion for 0 degree beam line, and air-cooled, water-cooled fixed-type targets and small rotating target for 80 degree beam line -

The neutron source performances for typical cases are summarized in Table 1. Photographs 1-4 shows FNS accelerator, beam lines and target assemblies.

The experimental program at FNS is typically categorized into following four items:

a) integral clean benchmark experiment to examine nuclear data and/or calculational methods of radiation transport in blanket or shielding materials in the system of simple geometry and composition

b) design-oriented benchmark experiment to examine the accuracy of nuclear calculation of breeder blanket design by using model modules that incorporate the complexity of radial structure

c) shielding experiment to examine the accuracy of calculation technique by making use of experimental ports, shielding doors and personnel access maze prepared in the building

d) experiments on fast neutron induced nuclear effects to provide the nuclear data for D-T neutrons such as activation, transmutation and gamma-ray production by irradiating various samples with the related development of dosimetry technique in D-T field

The activities related to nuclear data so far conducted at the FNS are:

1) Integral experiments reaction rates and spectra measurements in bulk media, and angle-wise measurements of neutrons emerging from slab assemblies by TOF method[3)]

2) Cross section measurements near 14 Mev neutron energy Activation cross sections of various structural materials[4)] and tritium production cross section[5)]

Reference

1) T. Nakamura and H. Maekawa, " Blanket and Shield Experiments in Fusion Neutronics Source(FNS)" IAEA-CN-41/04 (1983)
2) T. Nakamura et al., " A D-T Neutron Source for Fusion Neutronics Experiments at the JAERI", Proc. 7th symposium on ion sources and ion assisted technology -ISIAT'83 - & 4th Intn'l conf. on ion and plasma assisted techniques - IPAT'83 - (1983)
3) Y. Oyama private communication
4) Y. Ikeda et al., "Measurement of Some (n,2n) Activation Cross Sections for 13.5 - 15.0 MeV Neutrons", Proc Int.Conf. on Nuclear Data for Basic and Applied Science (1985)
5) K. Tsuda, private communication

Table 1 Performance characteristics of the FNS

Acceleration voltage : 400 kV					
Beam characteristics :			80° beam line		
DC Mode	0° beam line	80°beam line	Pulse Mode	Bunching	Sweeping
Max. Beam current	23 mA	3.0 mA	Pulse Width	1.6 ns	20ns-8μs
Target type	23 cmϕ RT*	HSWCST**	Interval	0.5-256μs	2-512μs
^{3}T amount	1,000 C_i	25 C_i	Peak Current	45 mA	3.0 mA
Max. neutron Yield	5×10^{12} n/s	5×10^{11} n/s	On/Off Ratio	4×10^5	2×10^5

* : Rotating Target, ** : High Speed Water Cooled Stationary Target

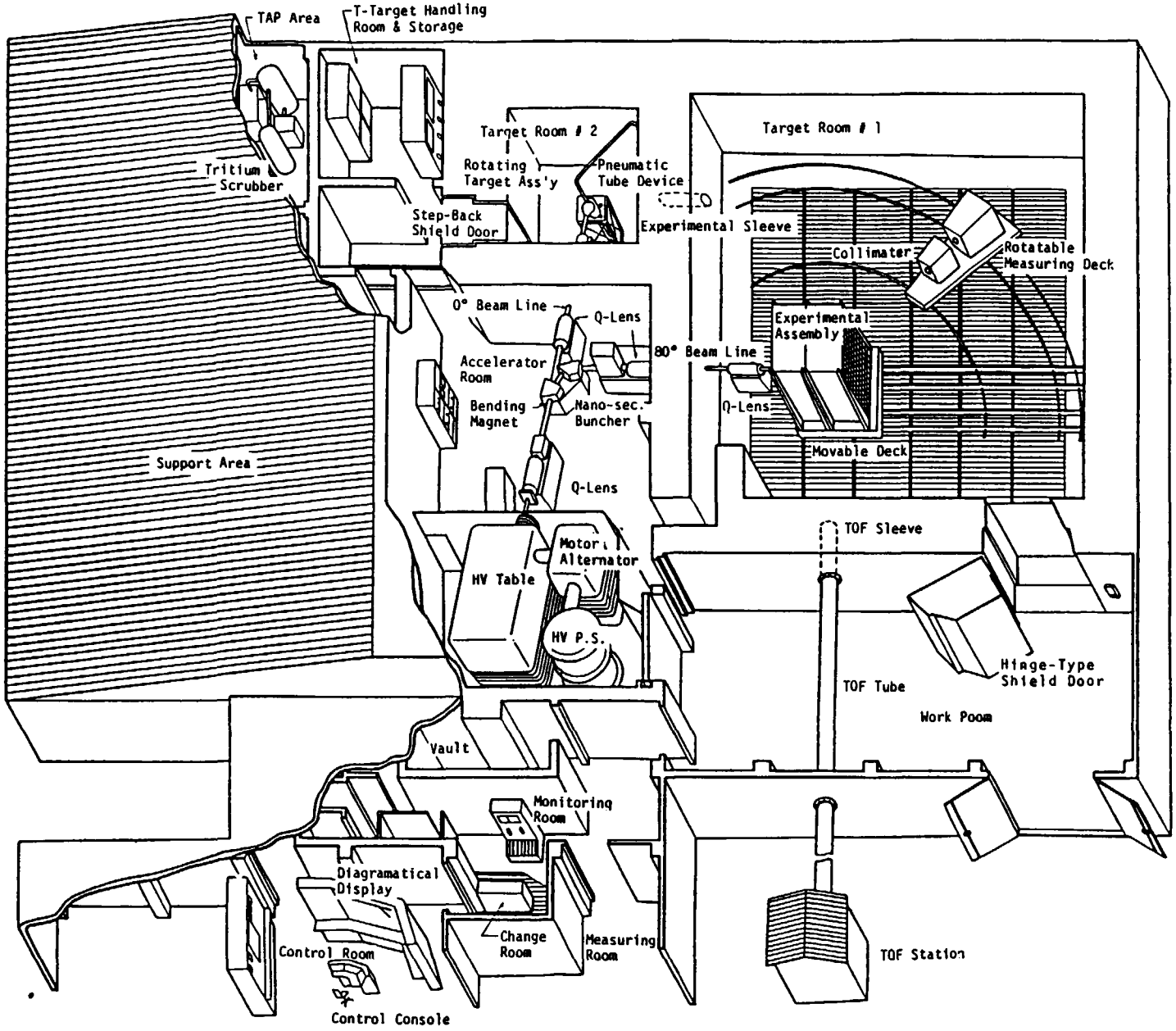

Fig. 1 Artist's sketch of the Fusion Neutronics Source (FNS) facility

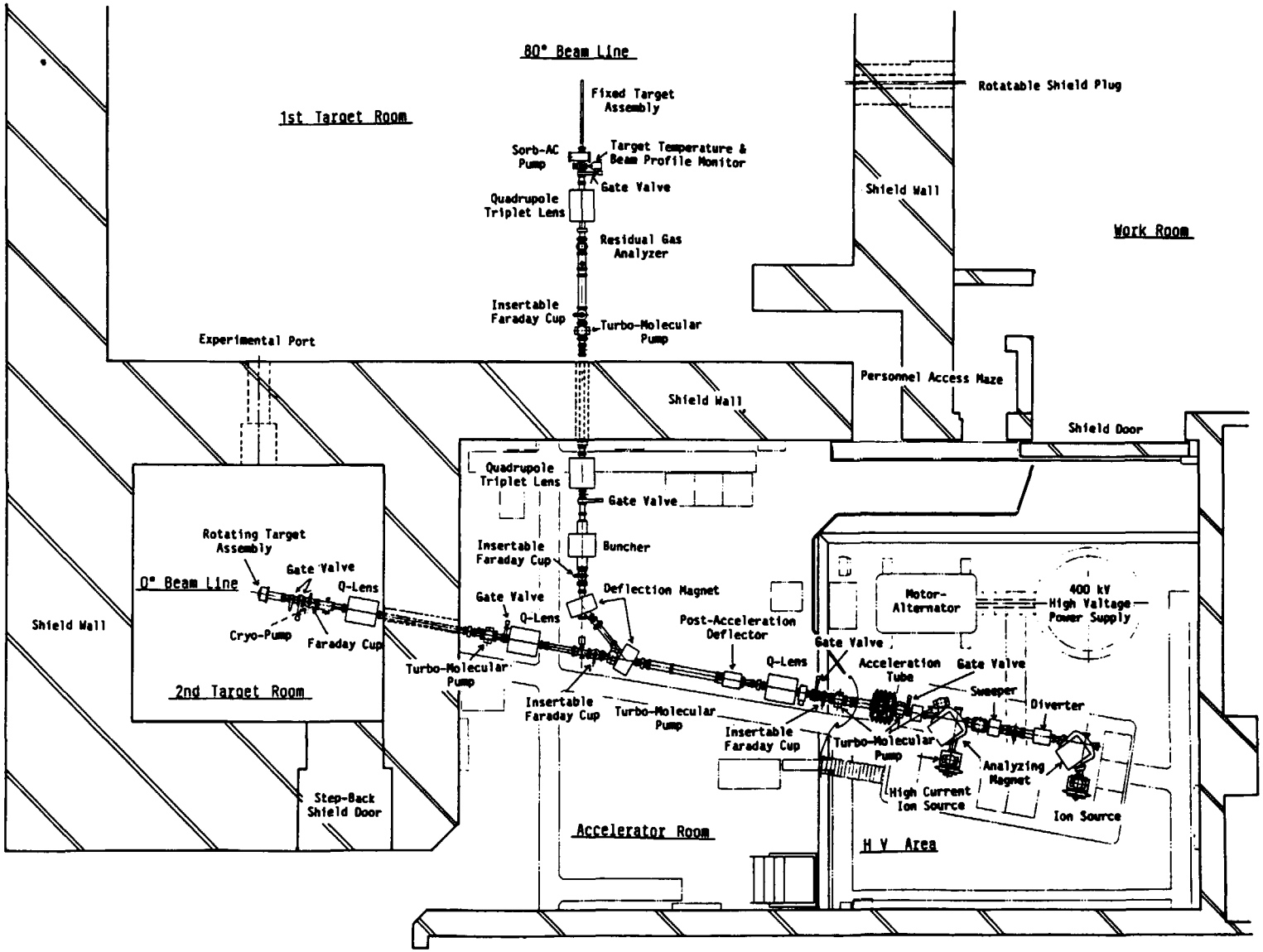

Fig. 2 Layout of FNS accelerator components

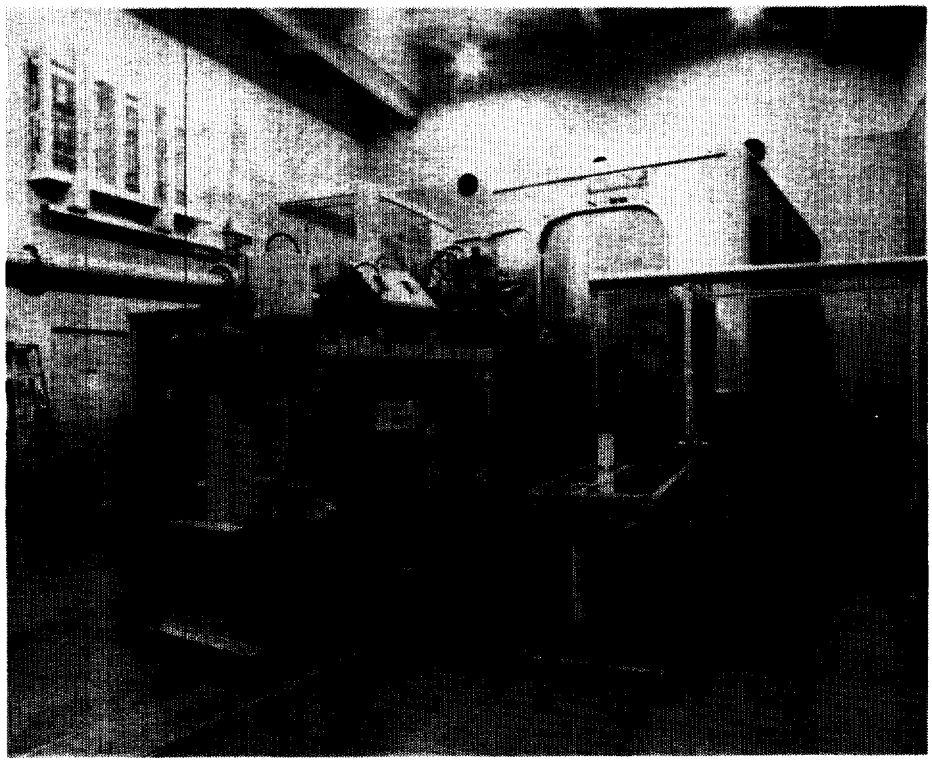

Photo. 1 FNS 400kV DEUTERON ACCELERATOR

Photo. 2 FNS BEAM LINES IN THE ACCELERATOR ROOM

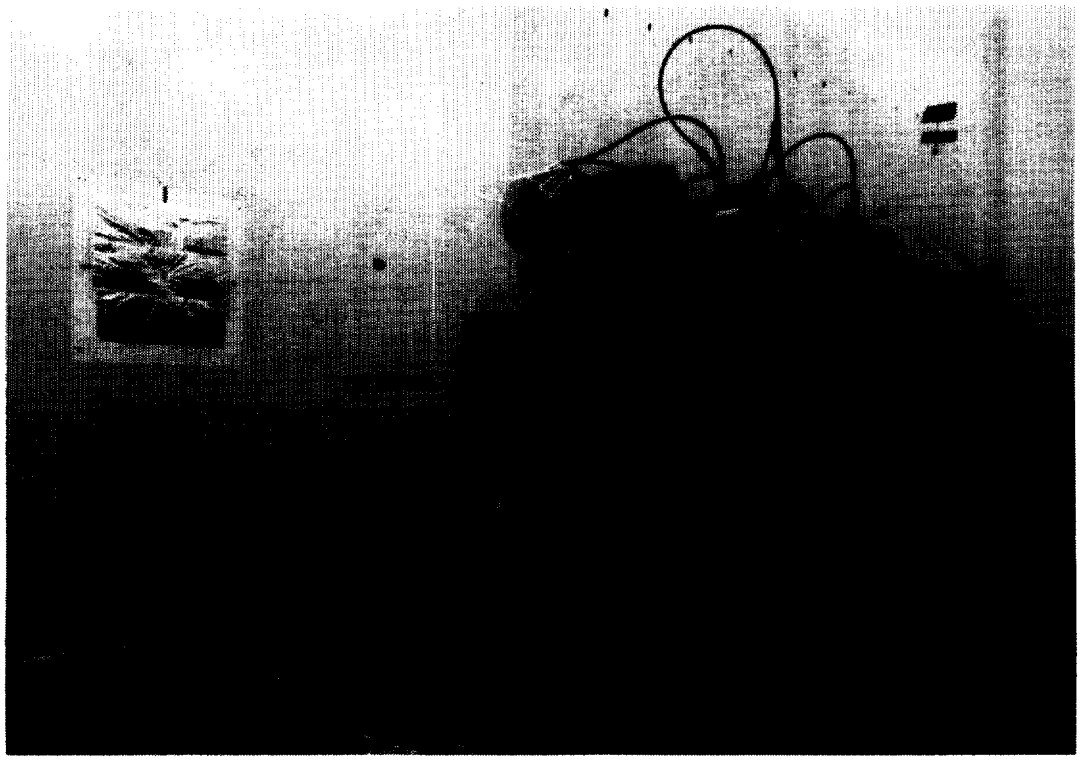

Photo. 3 0 DIRECTION BEAM LINE IN THE 2ND TARGET ROOM

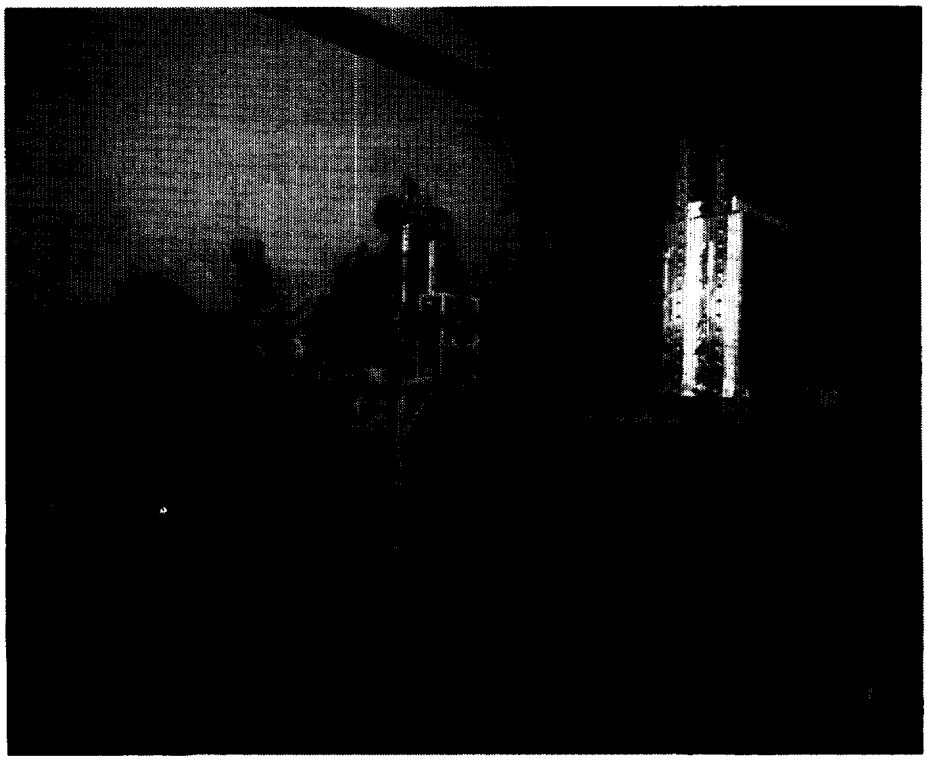

Photo. 4 80 DIRECTION BEAM LINE IN THE 1ST TARGET ROOM

6) Rikkyo University Fast-Neutron Facility

Y. Ando, T. Motobayashi and S. Shirato

Department of Physics, Rikkyo University, Nishi-Ikebukuro, Tokyo 171

Abstract: The fast-neutron facility of Rikkyo University is briefly reviewed. A 200 kV Cockcroft-Walton accelerator constructed in 1955 was continued to produce ^{3}H-d neutrons until it was shut down at the beginning of 1985, and a new one of 300 kV was installed at present. The recent experimental activities made by using the old accelerator have been summarized.

1. Old Apparatus (1955 ∿ January 1985)

A 200 kV Cockcroft-Walton type accelerator with a 21 MHz RF ion source provided a d^{+} beam current less than 500 μA focussing to a beam spot of 2 mmΦ on a target. This facility shown in Fig. 1 has been shut down at present.

^{3}H-d (or ^{2}H-d) neutrons were produced with a ^{3}H-Ti-Cu (TRT-31) target (or ^{2}H-Ti-Cu), which was mounted on an apparatus as shown in Fig. 2.[1] The neutron flux was determined with an accuracy of 1 ∿ 3% by counting the associated α-particles from the ^{3}H(d,n)^{4}He reaction with a silicon p-n junction detector[1,2] or a NE102A plastic scintillator of 10 μm[3] ("the α-monitor"). A typical spectrum of the associated α-particles is seen in Ref. 2 for the former case, and also is shown in Fig. 3 for the latter one.

Charged particles produced by fast-neutron induced reactions were detected with mostly two counter-telescopes in the close geometry[1], in which a geometrical uncertainty of the order of ±3% was obtained. Each telescope consists of two gas proportional counters and the ΔE- and E-silicon surface-barrier detectors. In this laboratory, the most efforts have been made at detecting charged particles in the neutron field rather

than detecting neutrons, but in recent experiments the TOF system consisting of a NE213 liquid scintillation counter of 2"Φ x 2" in coincidence with signals of the α-monitor was often used simultaneously. The experimental arrangement of the TOF system is shown in Fig. 4 and can be also seen in Fig. 1. Since in our arrangement the neutron counter was fixed at some place in a cave of the accelerator room, the α-monitor was rotated around the neutron source point in order to measure the angular distribution, as was illustrated in Fig. 4.

A typical electronic system used in our recent n-Li experiments[3,4] is schematically shown in Fig. 5. A CAMAC data-handling system based on the NOVA01-NOVA3 computers[1,5] was currently used in these experiments. The overall time resolution in the present TOF system was determined to be 1.35 ns in FWHM by measuring directly the time of flight of the incident neutrons of 14.1 (± 0.4) MeV, as is shown in Fig. 6.

The following reaction products were measured in our recent works:

1) Charged particles from (n,p), (n,d), (n,t) and (n,α) on ^{1}H[6], ^{2}H[2], ^{3}H[7], ^{6}Li[8,3], ^{7}Li[4] and ^{9}Be[9];

2) Elastic and inelastic neutrons from (n,n) and (n,n') on ^{12}C, ^{1}H, Al, Fe, Cu and Pb.[10]

The absolute measurements of reaction cross sections larger than about 1 mb/sr were found to be feasible in the close geometry with overall accuracies of about ±5%.[8] The TOF neutron work was preliminary, and the experiment will be continued as soon as fast neutrons can be produced by a new accelerator being in preparation.

2. New Apparatus (October 1985 ∿)

A 300 kV Cockcroft-Walton type accelerator with a duoplasmatron ion source was constructed as shown in Fig. 7, and now is in preparation to

produce fast neutrons. We have a plan of using the RF ion source and a heavy ion source to study low-energy ion physics as well as fast-neutron physics.

A d^+ beam of about 500 μA from the duoplasmatron has been provided on the ^{3}H-Ti-Cu target for the fast-neutron production. Because of high vacuum of oil free which was obtained by using all turbo molecular pumps in this accelerator, the neutron yield degradation due to the carbonized target surface as occured in the old accelerator should be avoided.

Improved detection and data-handling systems such as a large liquid scintillator (10cmΦ x 30cm) for TOF, multiwire proportional counters for multi-telescopes and a CAMAC system based on the NOVA3-MV4000 computers as shown in Fig. 8 are now in construction.

References :

1) S. Shirato, K. Shibata, M. Saito and S. Higuchi, Nucl. Instr. Meth. 199 (1982) 469.

2) S. Shirato, K. Saitoh, N. Koori and R. T. Cahill, Nucl. Phys. A215 (1973) 277.

3) Y. Ando, S. Shirato and H. Yamada, NEANDC(J)-106/U, INDC(JPN)-92/U, (JAERI Report 1984, unpublished) p.58.

4) I. Furutate, T. Kokubu, Y. Ando, T. Motobayashi and S. Shirato, NEANDC(J)-116/U, INDC(JPN)-102/U, (JAERI Report 1985, unpublished) p.81.

5) M. Saito, K. Shibata and S. Shirato, Genshikaku Kenkyu (Japanese circular) 25 (1980) 49; M. Saito and S. Shirato, Rikkyo University Report RUP-83-2 (1983, unpublished).

6) S. Shirato and K. Saitoh, J. Phys. Soc. Japan 36 (1974) 331.

7) S. Shirato, Y. Suda, S. Tsuruta and S. Oryu, Nucl. Phys. A267 (1976) 157.

8) S. Higuchi, K. Shibata, S. Shirato and H. Yamada, Nucl. Phys. A384 (1982) 51.

9) K. Shibata and S. Shirato, J. Phys. Soc. Japan 52 (1983) 3748.

10) T. Kokubu, to be presented.

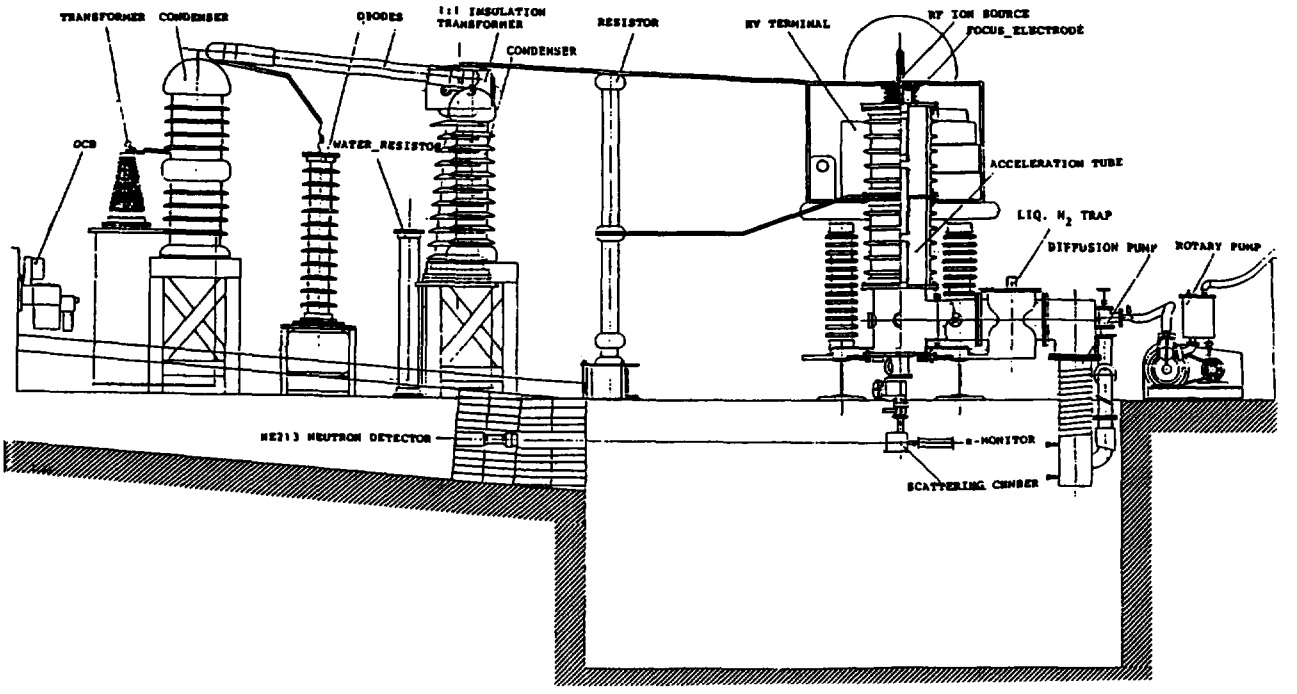

Fig. 1 The old Cockcroft-Walton accelerator of Rikkyo University.

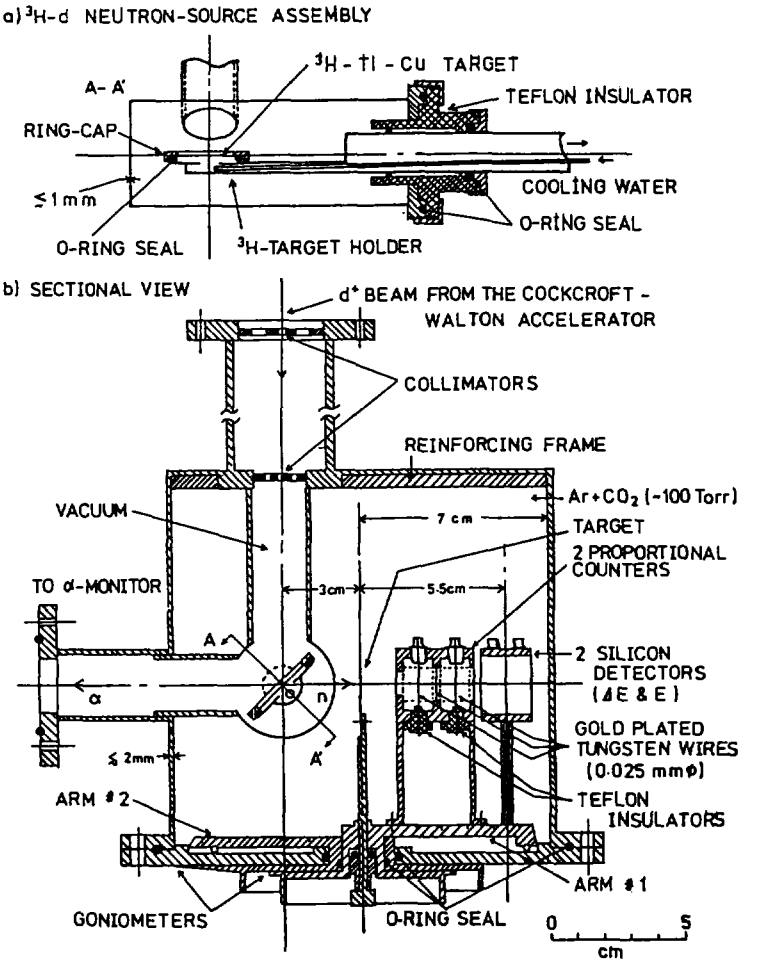

Fig. 2 A ^{3}H-d neutron source in which only the ^{3}H-target holder is movable without changing the position of neutron production.

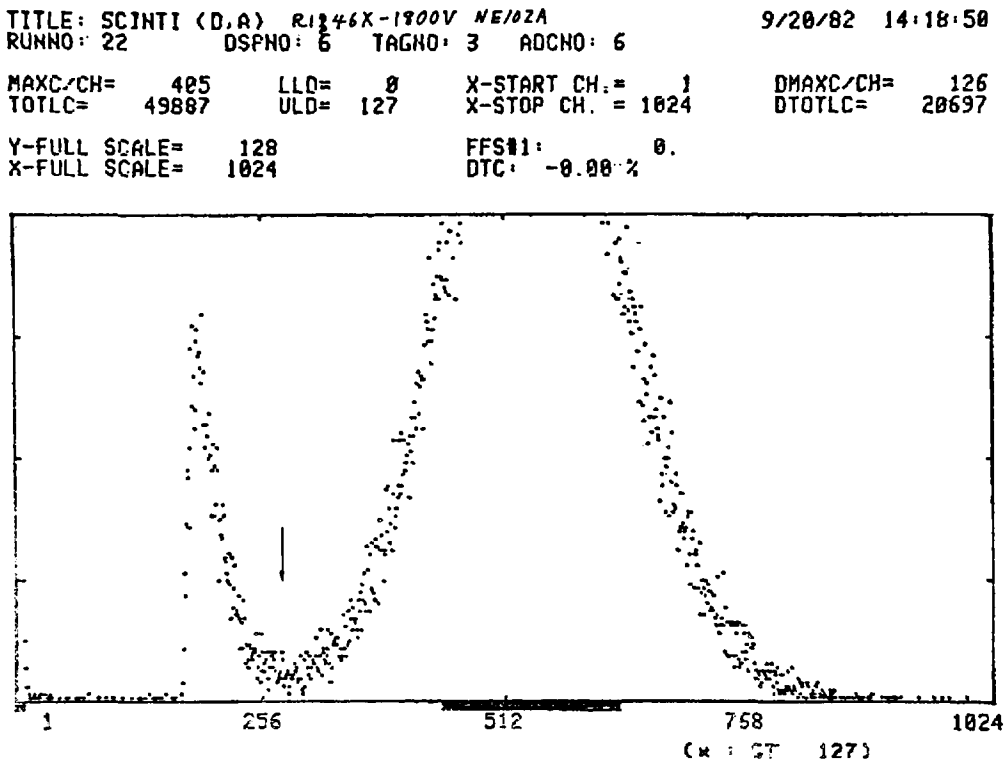

Fig. 3 A typical spectrum of the associated α-particles measured with a thin plastic scintillator of the α-monitor.

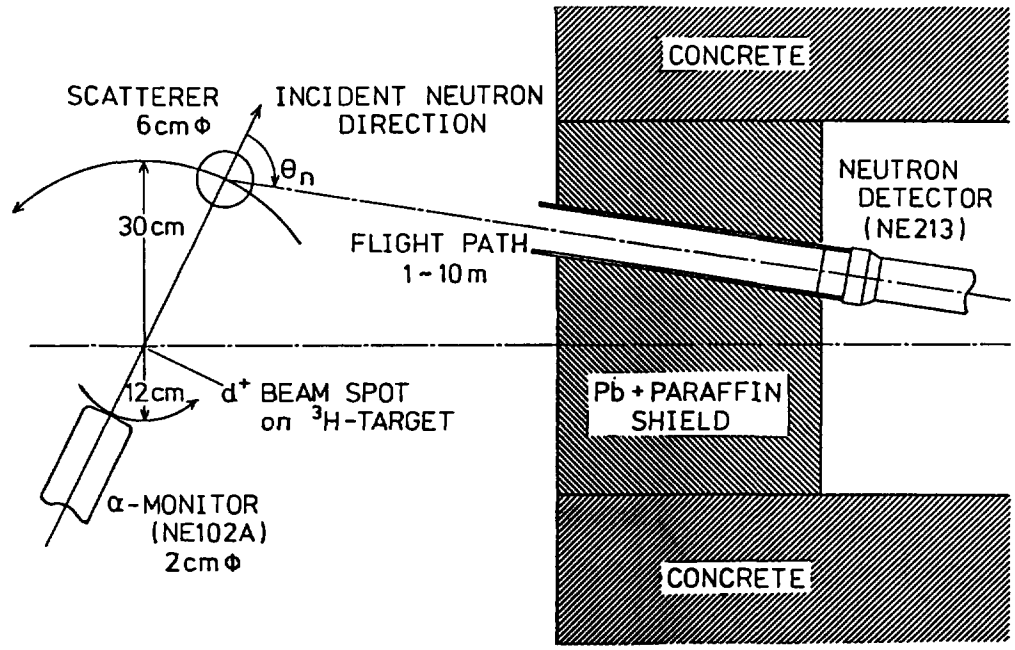

Fig. 4 The experimental arrangement of the TOF system.

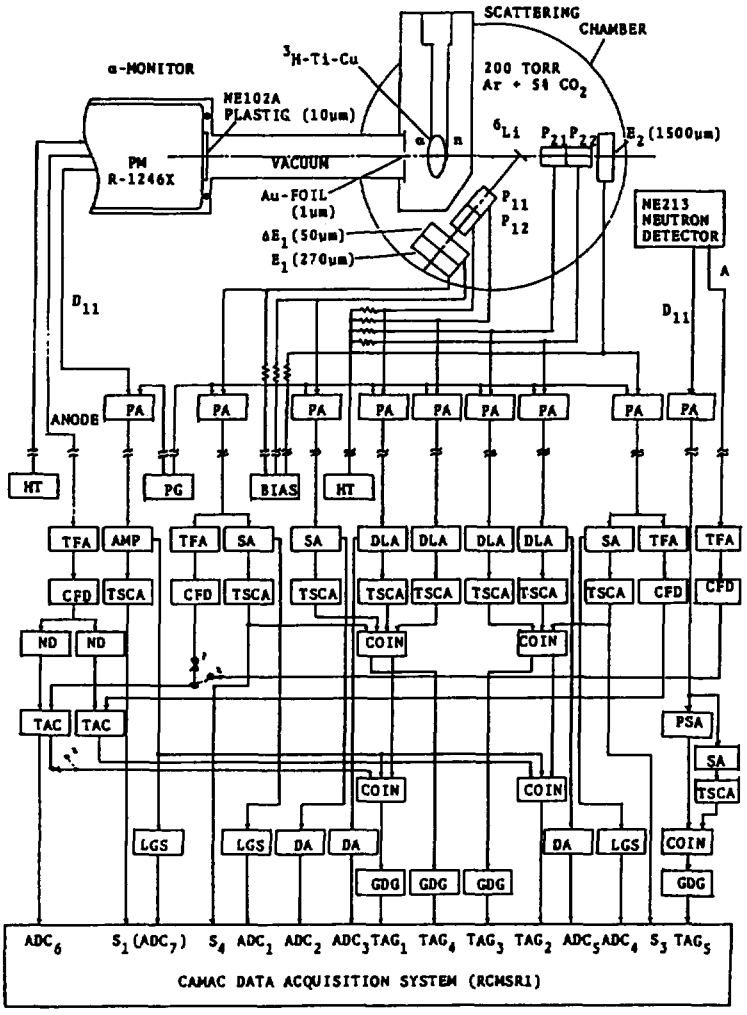

Fig. 5 A typical electronic system used in the backward measurement of the n-^{6}Li work using the old CAMAC data acquisition system[1].

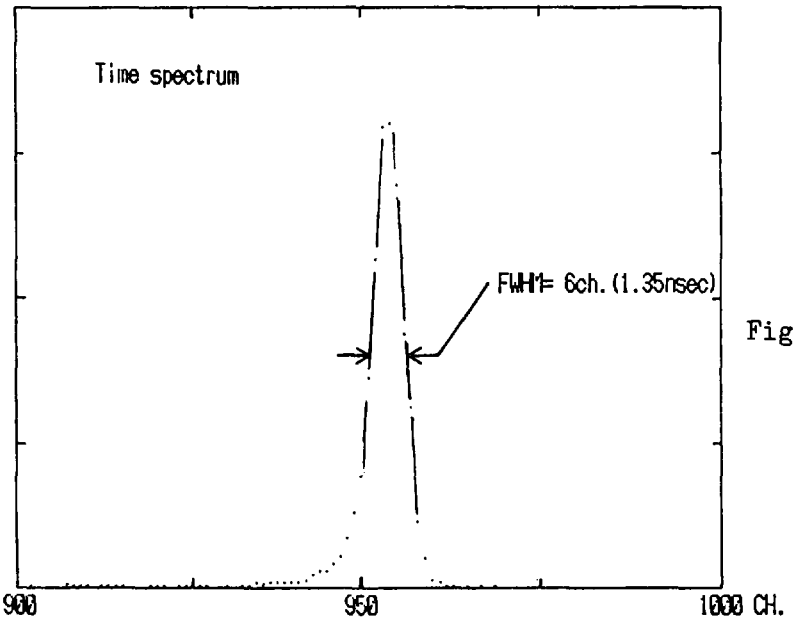

Fig. 6 Measured time spectrum of incident neutrons of 14.1 MeV.

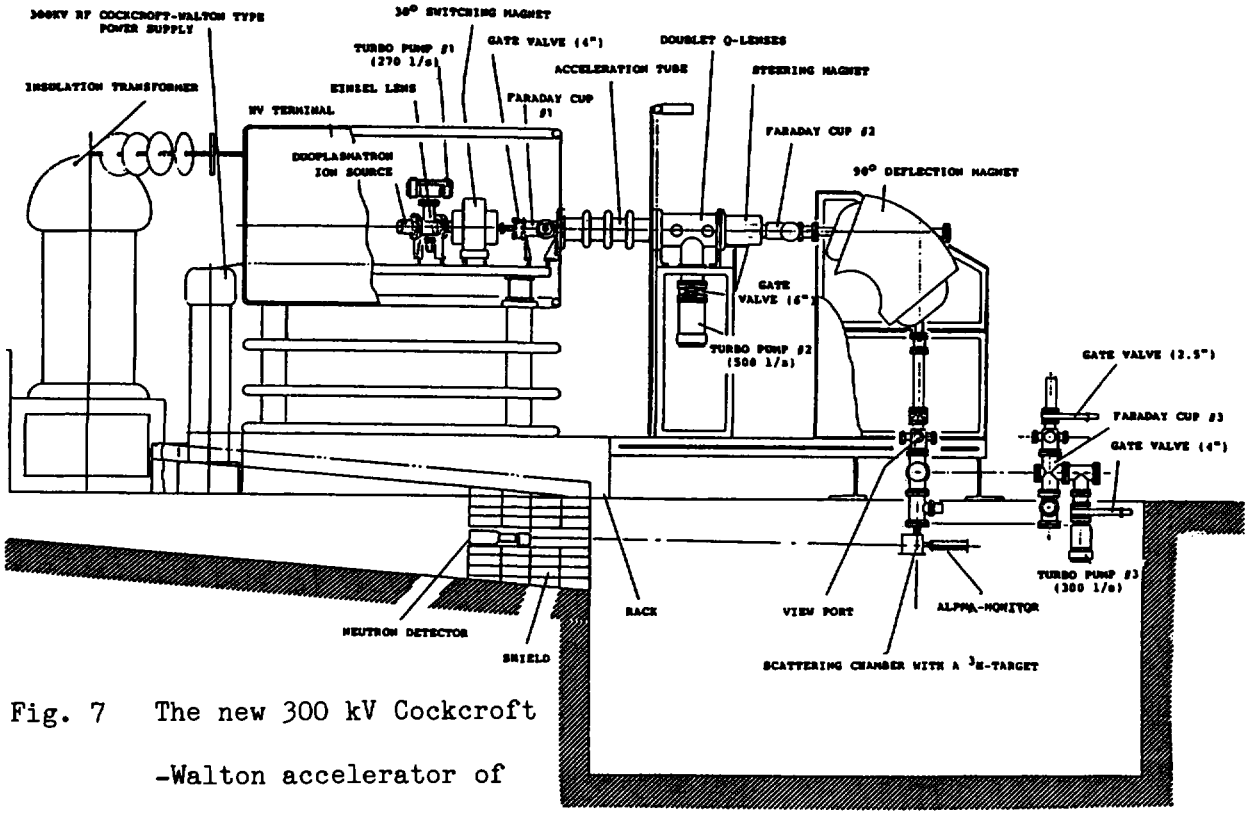

Fig. 7 The new 300 kV Cockcroft -Walton accelerator of Rikkyo University.

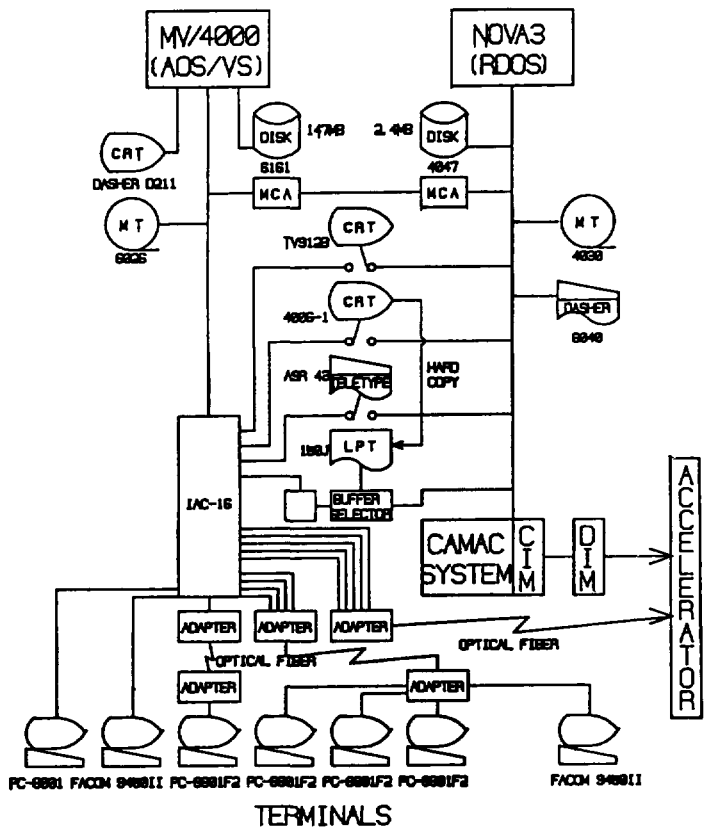

Fig. 8 The present hardware of the data handling system.

7) Pseudo-Monoenergetic Neutron Beam Course from 15 to 40 MeV for Activation Cross Section Measurements

T. Nakamura, Y. Uwamino
Institute for Nuclear Study, University of Tokyo
and A. Torii
Department of Nuclear Engineering, Kyoto University

A pseudo-monoenergetic neutron beam course in the energy range from 15 to 40 MeV by using the Be(p,n) reaction, has been installed in the SF cyclotron of Institute for Nuclear Study, University of Tokyo. It was confirmed by the measurements of the NE-213 scintillator and the Al(n,α) activation that the neutron spectra have pretty good pseudo-monoenergies, whose peak energies change with the proton energy, as expected, and the absolute values of the neutron fluxes have been characterized in good accuracy. This neutron beam can be used for activation cross section measurements, induced radioactivity study, activation analysis and so on.

1. Introduction

The neutron cross sections of energy above 15 MeV are quite insufficient and no evaluated data files exist in the present. The importance of these cross section data is of rapid increase for cosmic physics, neutron damage study, induced activity evaluation, accelerator shielding and so on. Then, we started to build two neutron beam courses of energy from 15 MeV to 40 MeV

in the SF cyclotron of the Institute for Nuclear Study, University of Tokyo; one is a pseudo-monoenergetic neutron beam course of high fluxes, mainly for activation cross section measurements and the other is a monoenergetic neutron beam course of high energy resolution, mainly for neutron cross section measurements using the counter. The later course is now in the design and can also be used as the neutron reference field for neutron detector calibration in high energy region.

2. Installation of neutron beam course

A neutron beam course of pseudo-monoenergy from 15 MeV to 40 MeV was installed by the Be(p,n) reaction, with changing the proton energy up to 40 MeV. The beryllium target backed by the cooling water is bombarded through a 20-mm diam carbon collimator by a proton beam of 5 mm x 5 mm from the cyclotron. The water backing for target cooling has a great advantage of very low neutron production yield by proton bombardment, because of low neutron production cross section and high threshold energy of oxygen. The target thickness is selected to be 2 mm for 40 and 35 MeV protons and 1 mm for proton energy lower than 30 MeV. The energy loss, ΔE_p, in the target is shown in Table 1, together with the proton energy E_p. Figure 1 shows the schematic cross-sectional view of the target. The angular distribution of produced neutrons was measured by gold foils of 10 mm x 10 mm size and 0.05 mm thickness which were placed in a line normal to the beam axis, 20 cm away from the target. Figure 2 exemplifies the gamma-ray activities of radioisotopes produced by $^{197}Au(n,\gamma)$, (n,2n), (n,3n) and (n,4n) reactions in the case of 35 MeV proton bombardment, which correspond to the relative values of neutron

angular distributions, together with the Q values of reactions. This figure clearly reveals that thermal neutrons, that is Au(n, γ) reaction, are emitted isotropically and the higher energy neutrons in the order of Au(n,2n), (n,3n) and (n,4n) reactions, are emitted in more forward direction.

The neutron energy spectra at 0 degree to the proton beam axis for 40, 35, 30 and 25 MeV proton energy were measured with a 2-in. diam by 2-in. long NE-213 scintillator placed about 150 cm away from the target. The unfolded spectra are shown in Fig. 3 (a) - (d), in units of neutron flux density per incident proton. The proton current was measured by the current integrator connected to the target chamber. These neutron energy spectra indicate pretty good pseudo-monoenergetic spectra, although they are contaminated with low energy neutron components. For above four proton energies, the peak neutron energies $\bar{E}_n$ and their energy resolutions ΔE_n are listed in Table 1, with the peak and the total (neutron energy above 4 MeV) neutron fluxes. The $\bar{E}_n$ value moves upward with increasing the proton energy and the monoenergetic neutrons in the peak area are about a half of all neutrons produced in the beam course as shown in Table 1. For 20 MeV protons, the experiment will be done in the near future.

The absolute values of neutron fluxes were also checked by the activation of gold and aluminum foils. The measured saturated activities, A^{meas}, were compared with the calculated activities, A^{calc}, as follows,

$$A^{calc} = \int_{E_{th}}^{E_p} \sigma(E)\, \phi(E)\, dE$$

where E_{th} = threshold energy

$\sigma(E)$ = activation cross section data given by Ref. (1)

$\phi(E)$ = neutron fluxes given in Fig. 3.

Table 2 shows this comparison. The activity comparison due to Al(n,α) reaction shows surprizingly good agreement between experiment and calculation only within about several % difference, but the calculated activities of Au(n,2n) and Au(n,4n) reactions are several tenth % larger than the measured results. This fact suggests the accurate absolute values of neutron fluxes obtained by NE-213 and the possibility of the poor accuracy of Au(n,2n) and Au(n,4n) cross section data in Ref. (1), when the Al(n,α) cross section data have good accuracy.

3. Application of neutron beam course

This pseudo-monoenergetic neutron beam course of variable energy between 15 MeV and 40 MeV can be used for induced radioactivity studies of materials, activation analysis of trace elements, activation cross section measurements, study on neutron-rich short-lived nuclei, neutron damage study and so on.

We are now doing the following three studies,

1) measurements of activation cross section data of carbon, aluminum, cobalt, gold and niobium above 15 MeV neutron energy,
2) studies on induced radioactivities of fusion reactor materials of titanium, zirconium, niobium and molybdenum,
3) activation analysis of trace elements in concrete.

Here in this report, as an example, the measured results of radioisotopes produced in niobium metal of 20 x 20 mm^2 size and 1 mm thickness are shown in Table 3. The niobium metal was irradiated by neutrons produced from the beryllium target, in the direction

of 0 deg to the proton beam axis, at a point 20 cm away from the target. The measured reaction rates are normalized to the total neutron flux above 4 MeV energy incident to niobium. The neutron energy dependence of the reaction rates in Table 3 reasonably corresponds to the Q value of the production reaction as also shown in the table.

We are now performing the data analysis to get the activation cross section values of several materials.

This research is being performed under the financial support of the Grant-in-Aid for Cooperative Research of Japanese Ministry of Education.

Reference

1) L. R. Greenwood: Extrapolated Neutron Activation Cross Sections for Dosimetry to 44 MeV, ANL/FPP/TM-115, Fusion Power Program, Argonne National Laboratory, Sept. 1978.

Table 1 Characteristics of Pseudo-Monoenergetic Neutron Field

Proton Energy E_p (MeV)	Energy Loss ΔE_p (MeV)	Target Thickness (mm)	Mean Neutron Energy $\bar{E}_n$ (MeV)	Energy Spread ΔE_n (MeV)	Total Flux ($\geq$4 MeV) ϕ_t	Peak Flux ϕ_p	Ratio ϕ_p/ϕ_t
40	4.4	2	34.0	$\pm$ 3.0	5.99 + 11*	2.54 + 11	0.42
35	4.9	2	30.0	$\pm$ 3.5	5.11 + 11	2.31 + 11	0.45
30	2.8	1	26.5	$\pm$ 3.2	3.28 + 11	1.76 + 11	0.53
25	3.2	1	21.0	$\pm$ 3.0	2.53 + 11	1.49 + 11	0.59
20	3.9	1	Experiment will be done soon.				

* 5.99 + 11 means 5.99×10^{11} in units of $n \cdot cm^{-2} \cdot Coulomb^{-1}$.

Table 2 Comparison of measured and calculated activities

Proton Energy (MeV)	Reaction	Activity ($n \cdot g^{-1} \cdot Coulomb^{-1}$) Calculated	Experimental	Ratio Calc/Exp
40	$^{197}Au(n,4n)$	7.08 + 10	5.21 + 10*	1.36
	$^{197}Au(n,2n)$	6.23 + 10	5.24 + 10	1.19
	$^{27}Al(n,\alpha)$	2.07 + 10	2.03 + 10	1.02
35	$^{27}Al(n,\alpha)$	1.91 + 10	1.77 + 10	1.08

* 5.21 + 10 means 5.21×10^{10}.

Table 3 Induced radioactivity in natural niobium (^{93}Nb 100%)

Radio Isotope	Half Life	Reaction Rate ($n \cdot g^{-1} \cdot Neutron^{-1}$) p 40 MeV	p 35 MeV	Produced Reaction	Q-value (MeV)
^{87m}Y	13.0 h	2.57 - 7*	-----	$^{93}Nb(n,3n\alpha)$	-23.2
^{87}Y	80.3 h	1.10 - 7	-----	$^{93}Nb(n,3n\alpha)$	-22.8
^{88}Y	106.6 d	2.72 - 5	1.23 - 5	$^{93}Nb(n,2n\alpha)$	-13.4
^{90}Nb	14.6 h	5.51 - 5	2.22 - 6	$^{93}Nb(n,4n)$	-28.8
^{90m}Y	3.19 h	3.44 - 6	3.69 - 6	$^{93}Nb(n,\alpha)$	+ 4.24
^{91m}Y	49.7 m	8.56 - 7	4.02 - 7	$^{93}Nb(n,n2p)$	-16.0
^{92m}Nb	10.15 d	1.97 - 4	2.07 - 4	$^{93}Nb(n,2n)$	- 8.97
^{94m}Nb	6.26 m	5.24 - 5	4.89 - 5	$^{93}Nb(n,\gamma)$	+ 7.19

* 2.57 - 7 means 2.57×10^{-7}.

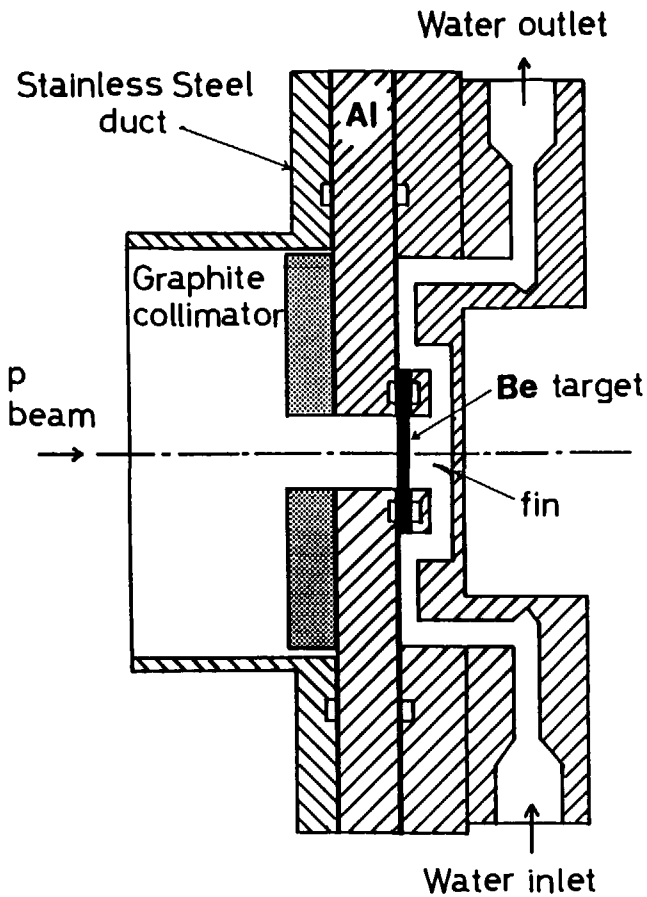

Fig. 1 Cross sectional view of the target chamber

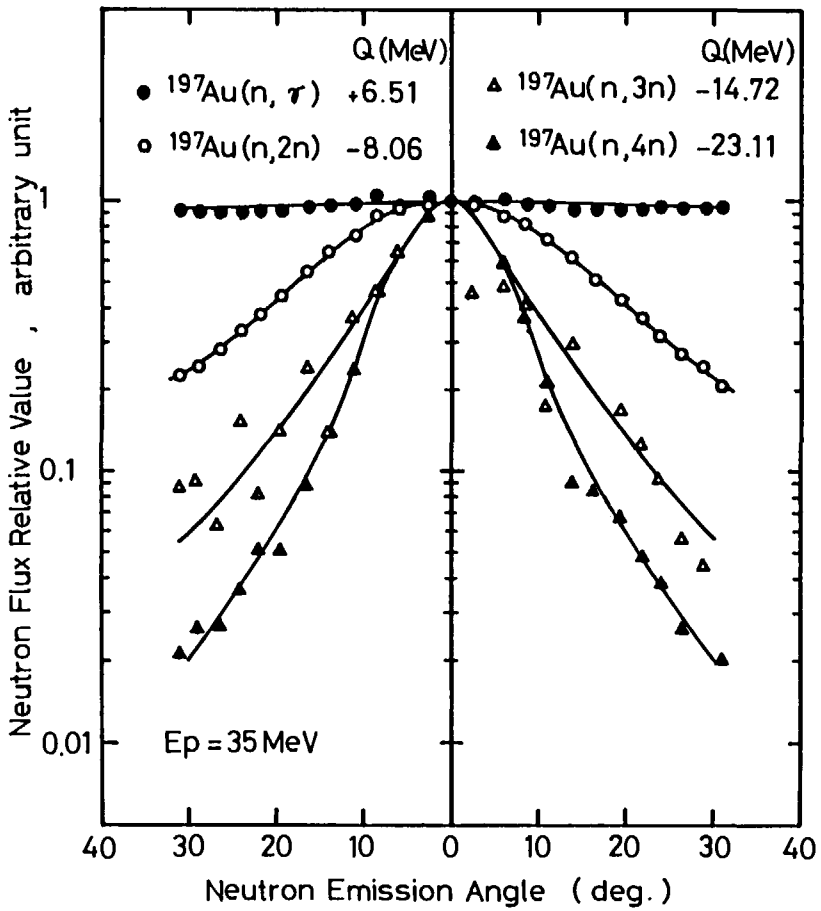

Fig. 2 Angular distribution of neutrons produced from the beryllium target in relative values which are radioactivities induced in gold

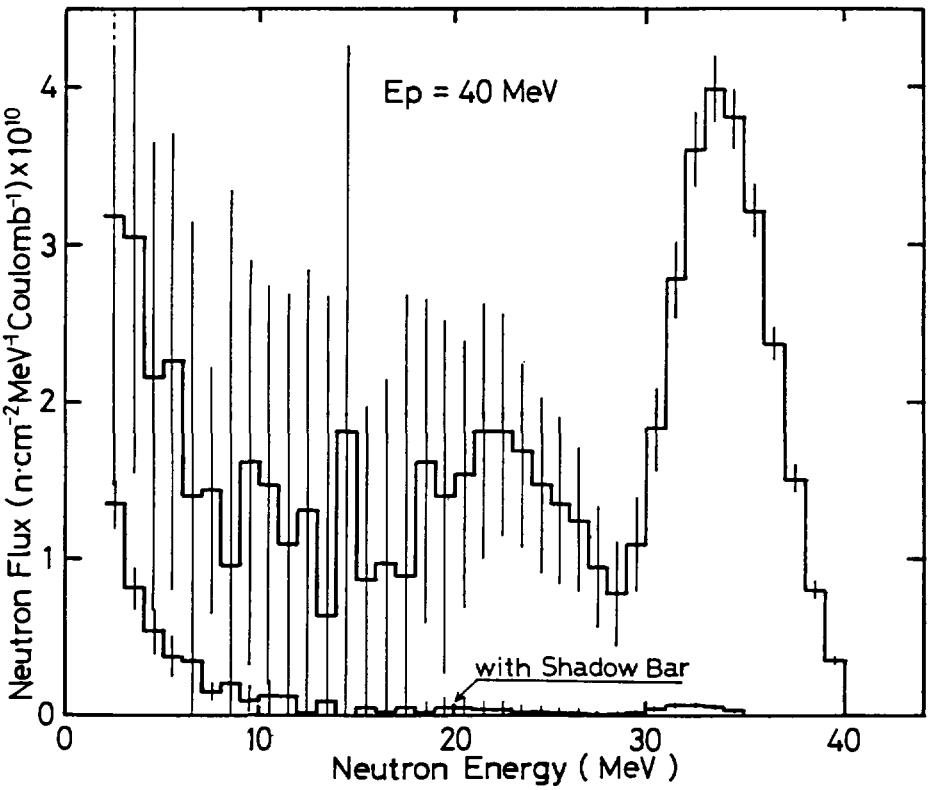

(a) 40 MeV proton,

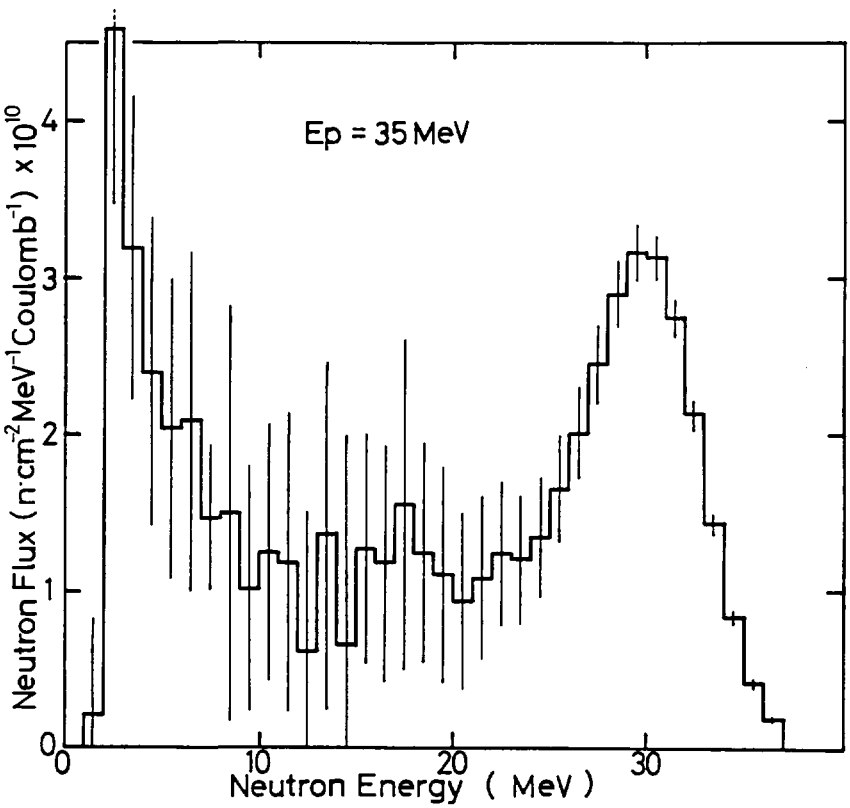

(b) 35 MeV proton,

Fig. 3 Neutron energy spectra at 0 deg to the proton beam axis measured with the NE-213 scintillator

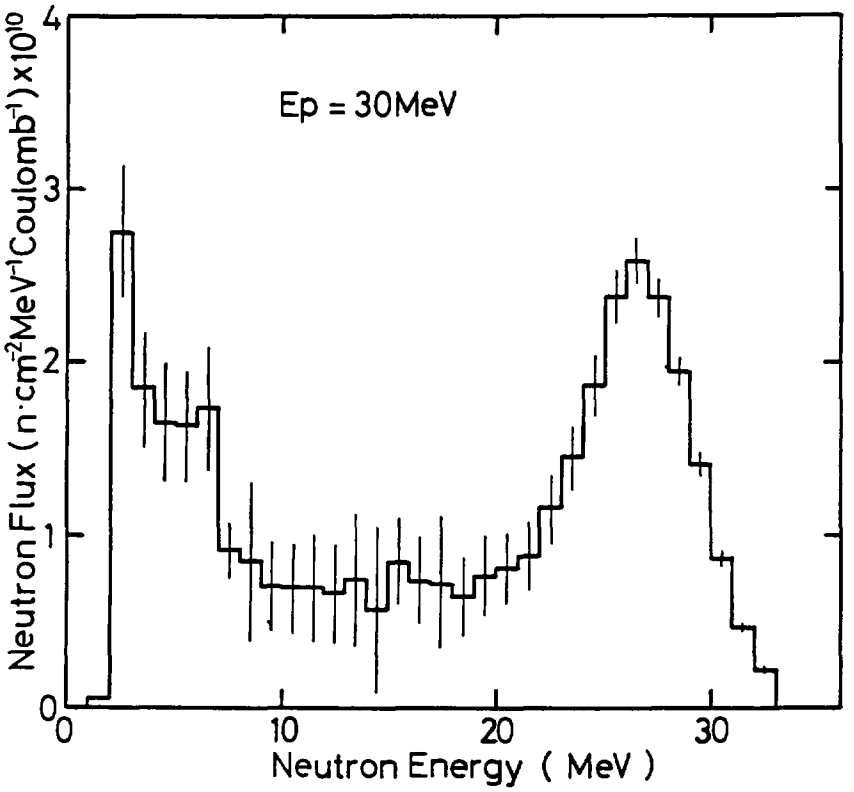

(c) 30 MeV proton,

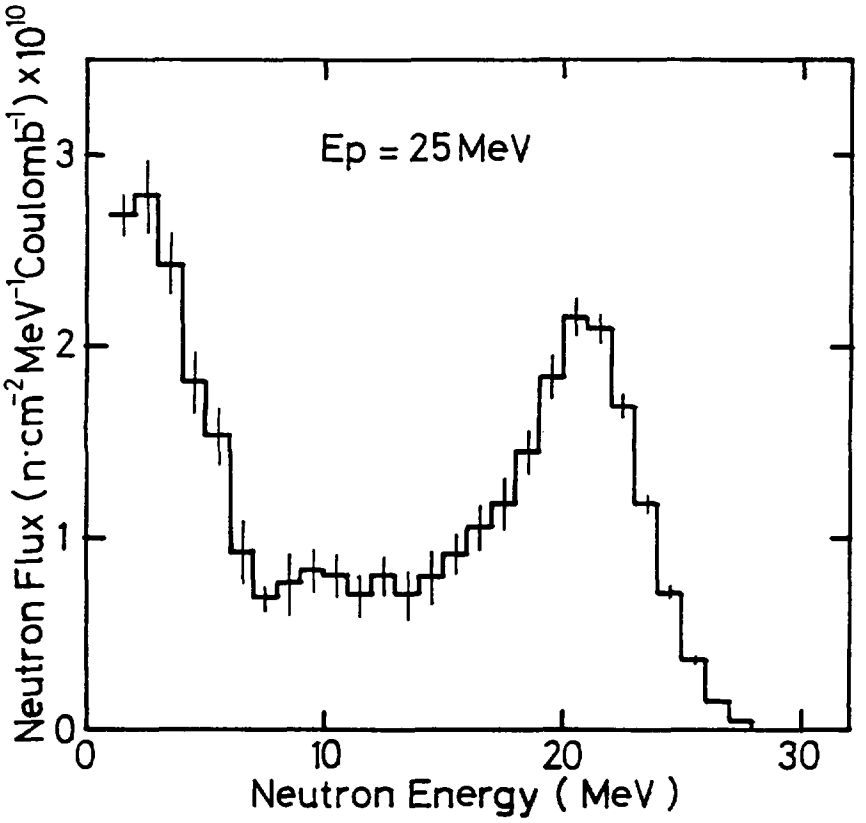

(d) 25 MeV proton.

Fig. 3 Neutron energy spectra at 0 deg to the proton beam axis measured with the NE-213 scintillator

8) Time-of-Flight Facility and Filtered Beam Facility for Total Neutron Cross Section Measurements at the Musashi Reactor

O. Aizawa

Atomic Energy Research Laboratory
Musashi Institute of Technology

Ozenji 971, Asao-ku, Kawasaki-shi, Kanagawa-ken

Two kinds of facilities for total neutron cross section measurements have been installed at the Musashi reactor (TRIGA-II, 100 kW). The one is a time-of-flight facility for the total neutron cross section measurements at the energy range from 0.001 to 0.1 eV. The other is a filtered beam facility for the monochromatic neutrons of 24, 54 and 144 keV. The temperature dependence of the total neutron cross sections can be measured both at these facilities.

1. Introduction

A chopper-TOF facility for thermal neutrons was installed at the one of the horizontal hole of the Musashi reactor in 1977. Figure 1 shows the cross-sectional arrangement of the Musashi reactor. Total cross sections of Mg, Al, Si, Zr, Nb and Mo have been measured in the energy range of 0.001~0.3 eV by using this facility.[1] An Fe-filter for 24-keV neutrons was also constructed in 1981, and a Si-filter for 54-keV and 144-keV neutrons in 1982. Precise measurements of total neutron cross sections have been made by using these filtered beams.[2),3)]

2. Chopper-TOF Facility for Total Neutron Cross Section Measurements in Thermal Region

The cross-sectional view of the chopper is shown in Fig. 2. The BN(boron-nitride) rotor is 12 cm in diameter and 12 cm in height.

The rotor has nine slits (0.4 x 7.0 cm^2), and the separation distance of each slit is 0.4 cm. The neutron burst shape is shown in Fig. 3. It can be seen from this figure that the neutron burst width becomes small with an increase of the rotaing speed. The full-width at half-maximum (FWHM) of the shape is plotted in Fig. 4 as a function of a rotating speed. An example of the Be-transmission spectrum is also shown in Fig. 5 as a function of a rotating speed. It is clear from this figure that the resolution becomes better with an increase of the rotating speed. Two kinds of filtered beams are available. The one is a beam filtered by a large nearly-perfect single-crystal Si-rod, 52.2 cm in length. Silicon acts as a very effective thermal neutron filter, reducing fast-neutron background. The other is a cold neutron beam below 5 meV, which is transmitted through a 15-cm-thick polycrystalline Be-block. The filters were inserted at the collimator position shown in Fig. 1. They are called the "Si-beam" and the "Be-beam", respectively. These time spectra are shown in Fig. 6. It can be seen from this figure that the background neutrons are decreased by a factor of about 1/100 in the cases of the "Si-beam" and the "Be-beam" in comparison with the case of the "complete open" beam, in which no filter was inserted into the experimental hole.

3. Filtered Beam Facility for Total Neutron Cross Section Measurements in keV-Region

Three kinds of filter arrangements have been investigated at the Musashi reactor. The first is an Fe-filter for 24-keV neutrons, which consists of 40-cm-thick iron, 20-cm-thick aluminum, and 10-cm-thick sulfur as shown in Fig. 7. The second is a Si-filter for 54-keV neutrons, which consists of 90-cm-thick silicon and 40-cm-thick sulfur as shown in Fig. 8. The third is also a Si-filter for 144-keV neutrons, which consists of 74-cm-thick silicon and 4-cm-thick titanium as shown in Fig. 9. In all these filter-arrangements a thin Cd-filter is added for removing thermal neutrons.

A proton recoil counter of 1 atm or 3 atm hydrogen gas pressure was used as a neutron detector. The electronics diagram is shown in Fig. 10. Figure 11 shows an example of pulse-height spectra for the cross section

measurements of 24-keV neutrons. Figure 12 shows an example of pulse-height spectra for silicon-filter beam as a function of sulfur-thickness. It can be seen from this figure that the 144-keV neutrons of the higher pulse-height plateau are supressed with the increase of sulfur thickness.

4. Examples of Total Cross Section Measurements

(1) Total Cross Sections in Thermal Neutron Energy Region

Some examples are shown in Fig. 13. In the Si-case of the upper figure, the open triangles show the experimental results measured with a single-crystal rod. The triangular dots show the present results measured with the polycrystalline samples in powder form. The open circles show the BNL-325 data. We note that the agreement between the experiments and the calculations is fairly good. The total cross sections between 0.0033 and 0.013 eV have been newly measured in the present experiment.

In the Zr-case of the center figure, the experimental data plotted as open triangles were measured with the metallic rod. The data plotted as triangular dots were measured with the slugs in sponge form. The BNL-325 data are also shown in this figure with open circles. The total cross sections between 0.003 and 0.02 eV are new data for Zr.

In the Mo-case of the lower figure, the open triangles show the present results measured with a solid rod. The triangular dots show the experimental results measured with the powder in polycrystalline state. The agreement between the experiments and the calculations is very good.

(2) Total Cross Sections in keV Energy Region

Figure 14 shows an example of the measured cross sections for Nb. The present experimental cross sections show good agreement with the existing data.

REFERENCES

(1) AIZAWA, O., et al.: J. Nucl. Sci. Tech., 20, 713～721 (1983)
(2) AIZAWA, O., et al.: J. Nucl. Sci. Tech., 20, 354～356 (1983)
(3) AIZAWA, O., et al.: to be published in J. Nucl. Sci. Tech.

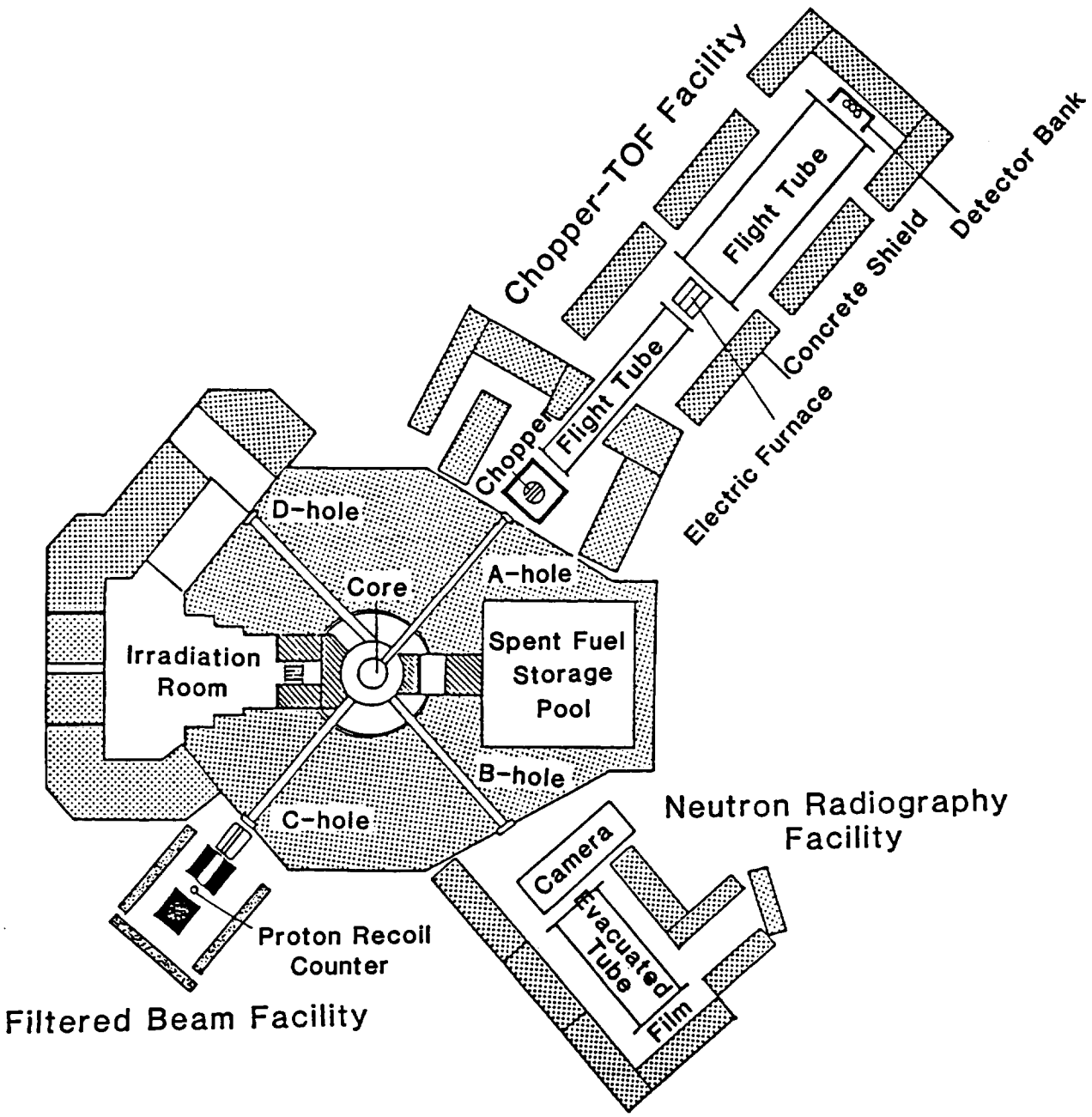

Fig. 1 Cross-sectional arrangements of the Musashi reactor

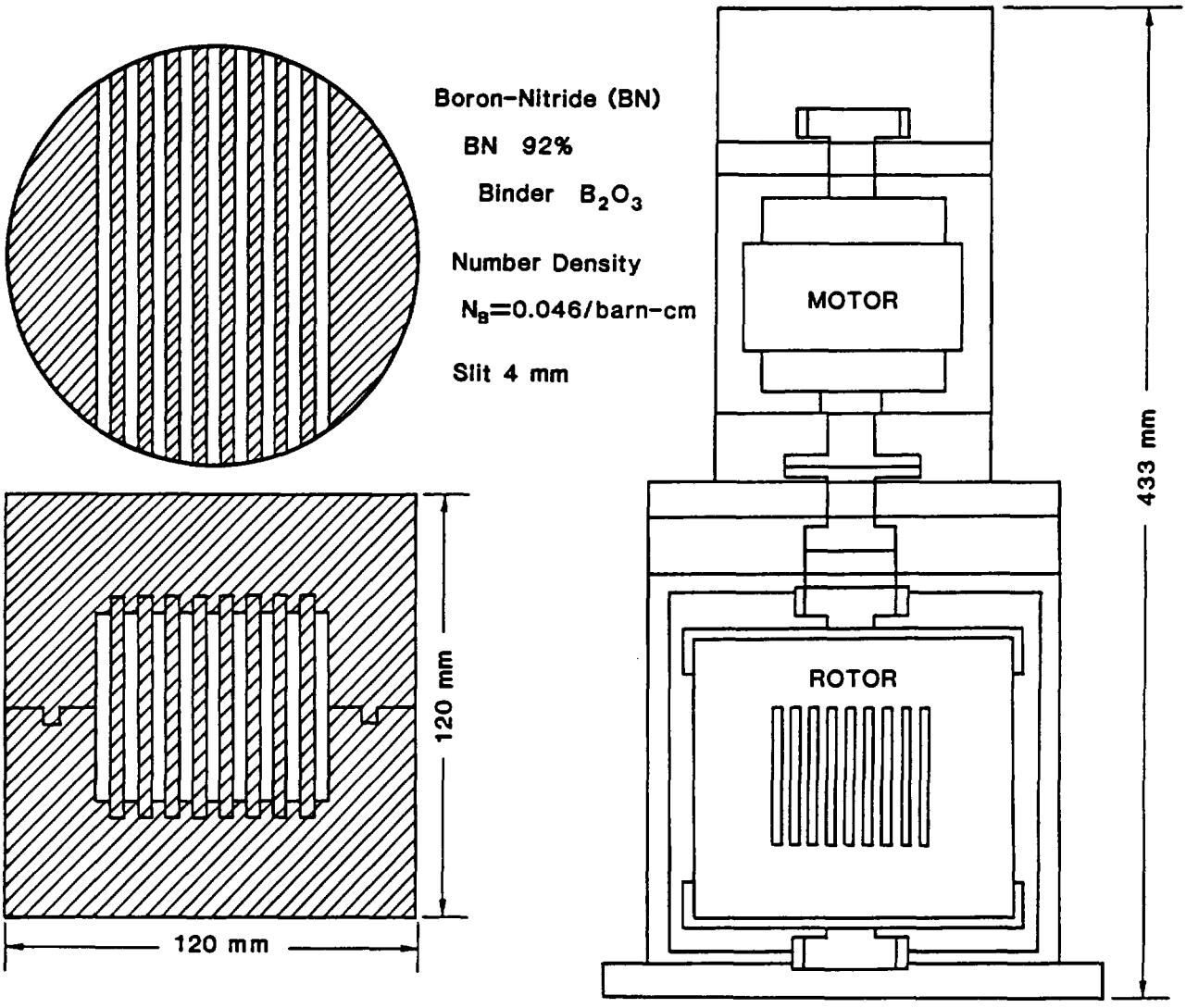

Fig. 2 Cross-sectional view of chopper

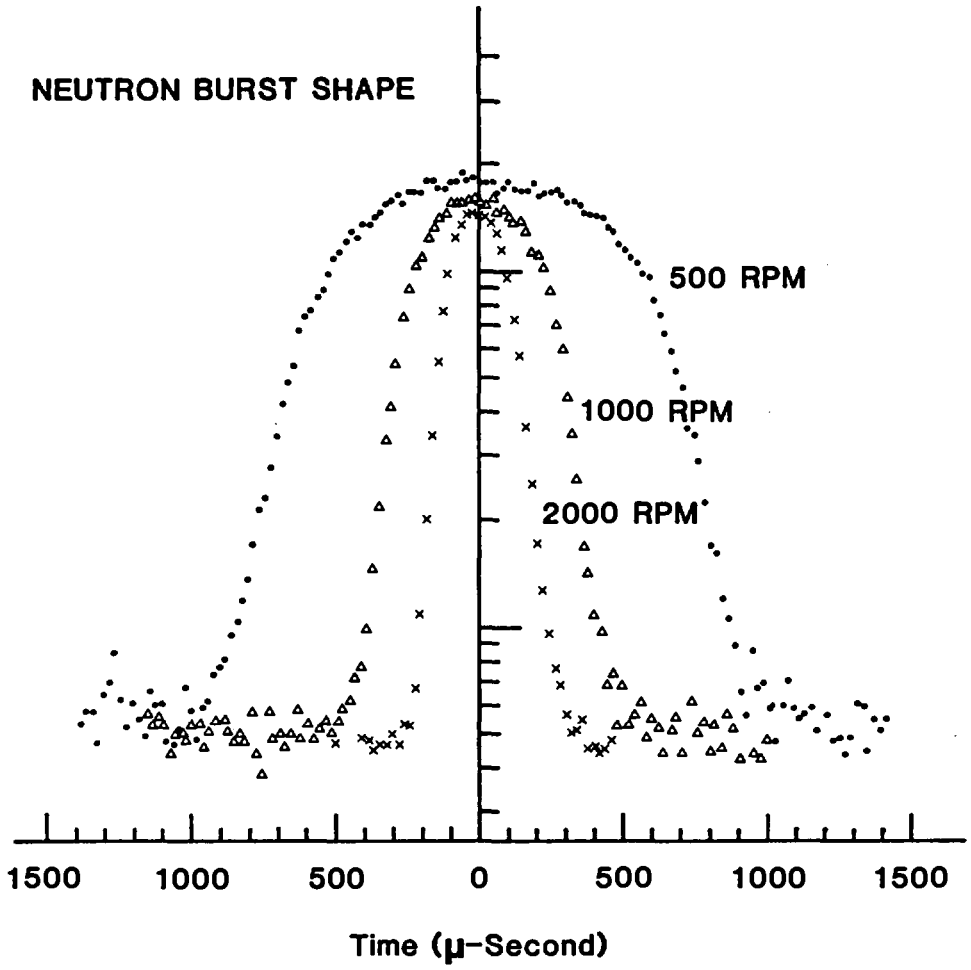

Fig. 3 Change of neutron burst shape

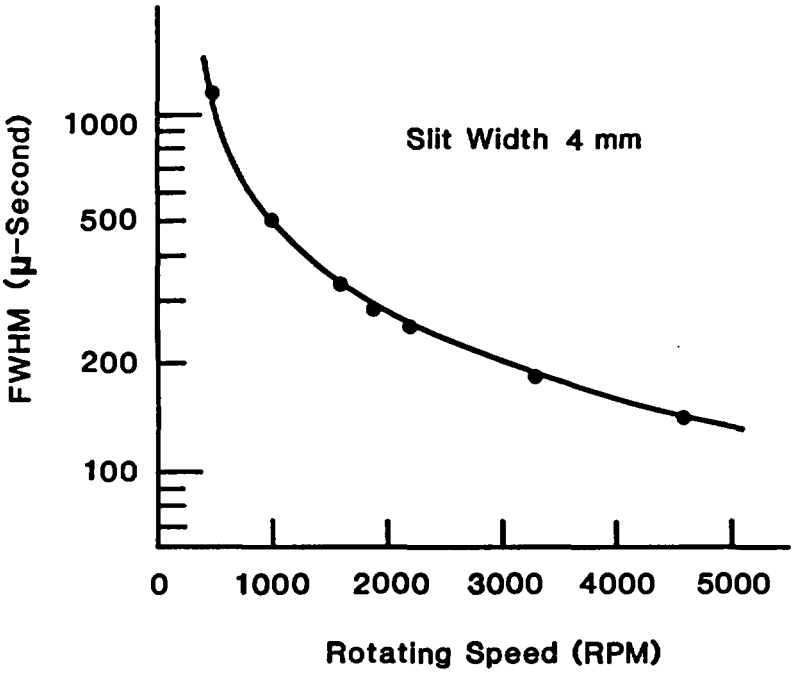

Fig. 4 Full-width at half-maximum as a function of rotating speed

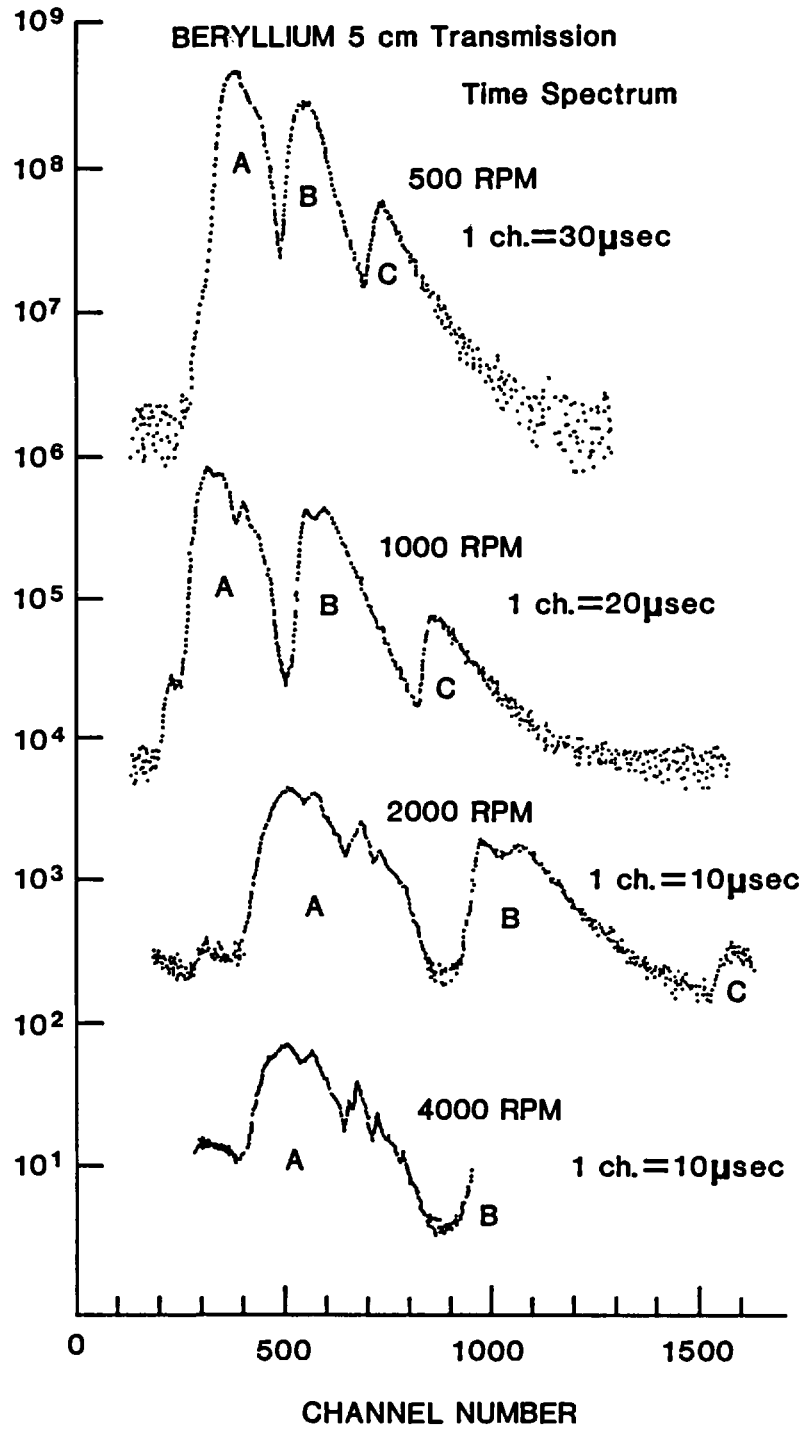

Fig. 5 Example of the Be-transmission spectra as a function of rotating speed

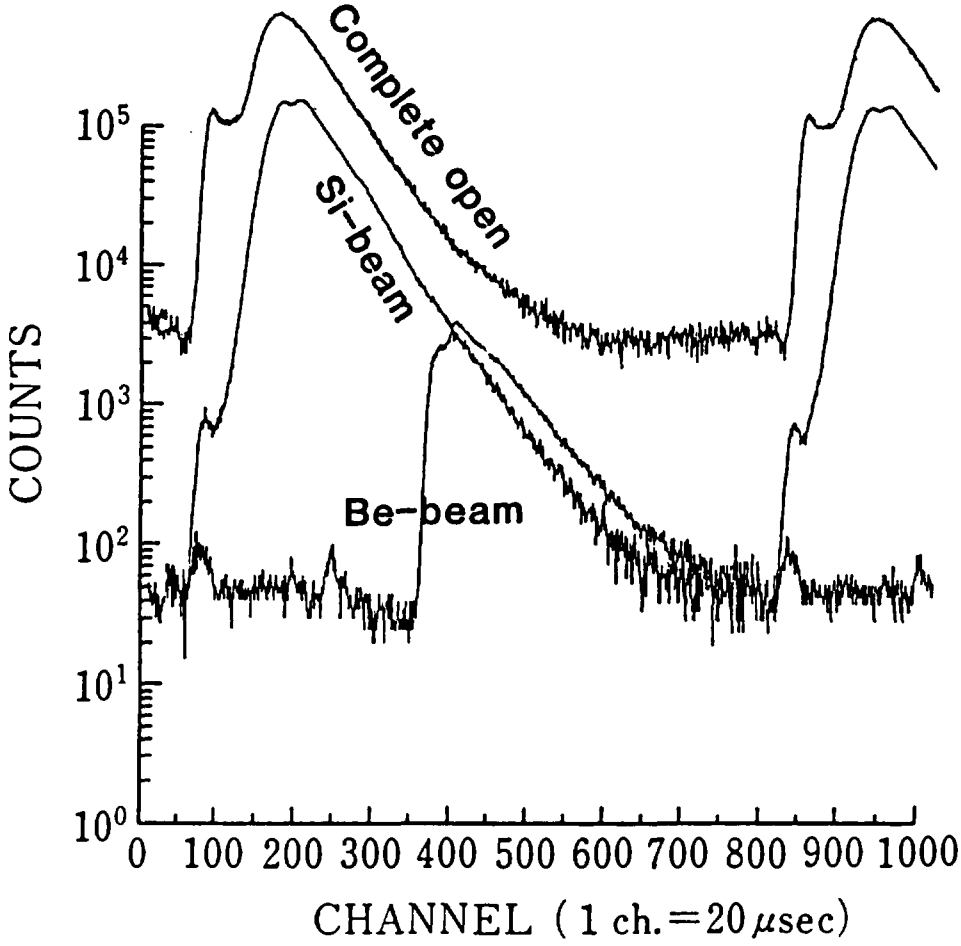

Fig. 6 Time spectra of the "Si-beam" and the "Be-beam" in comparison with the "complete open" beam

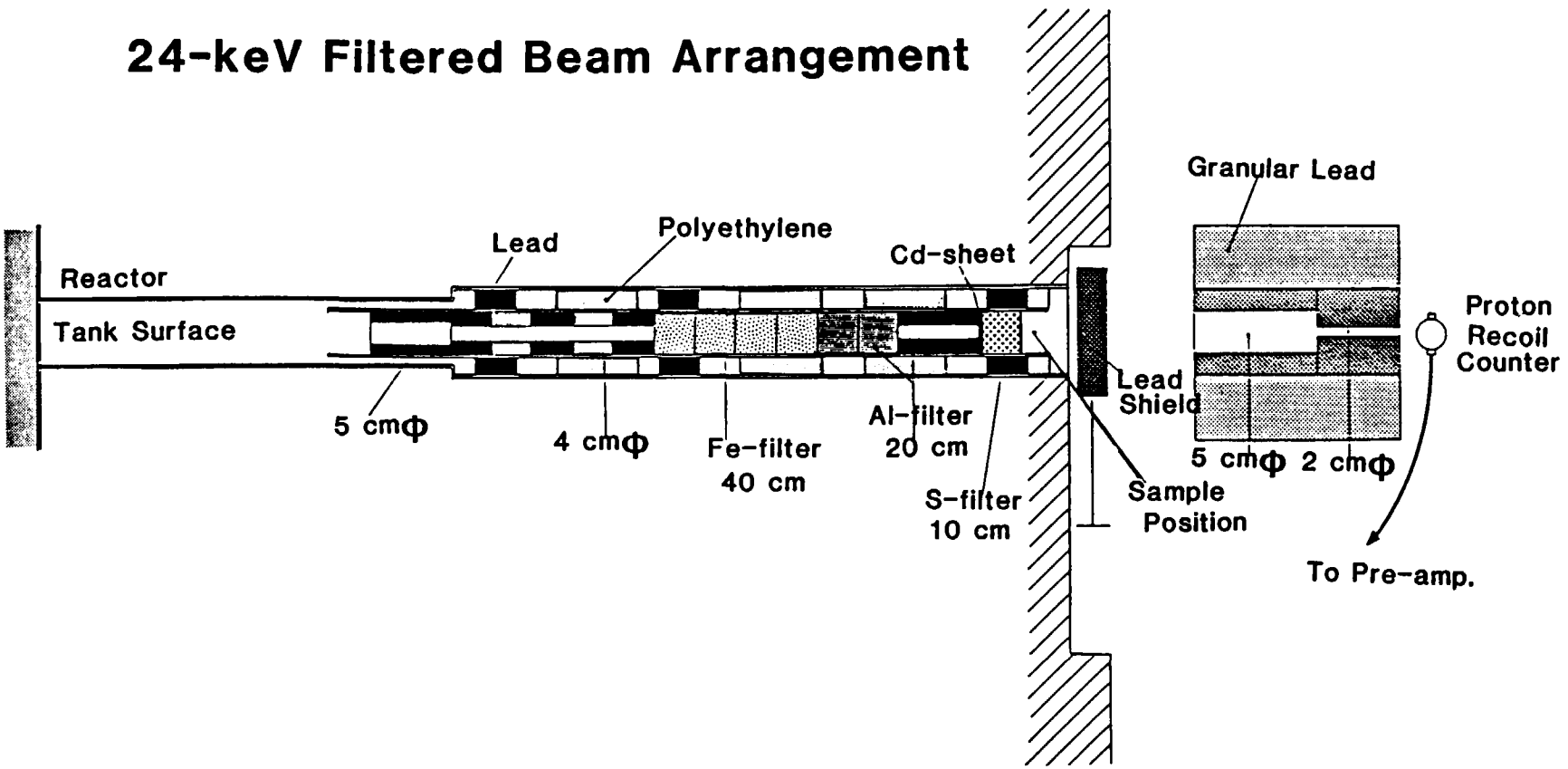

Fig. 7 24-keV filtered beam arrangement

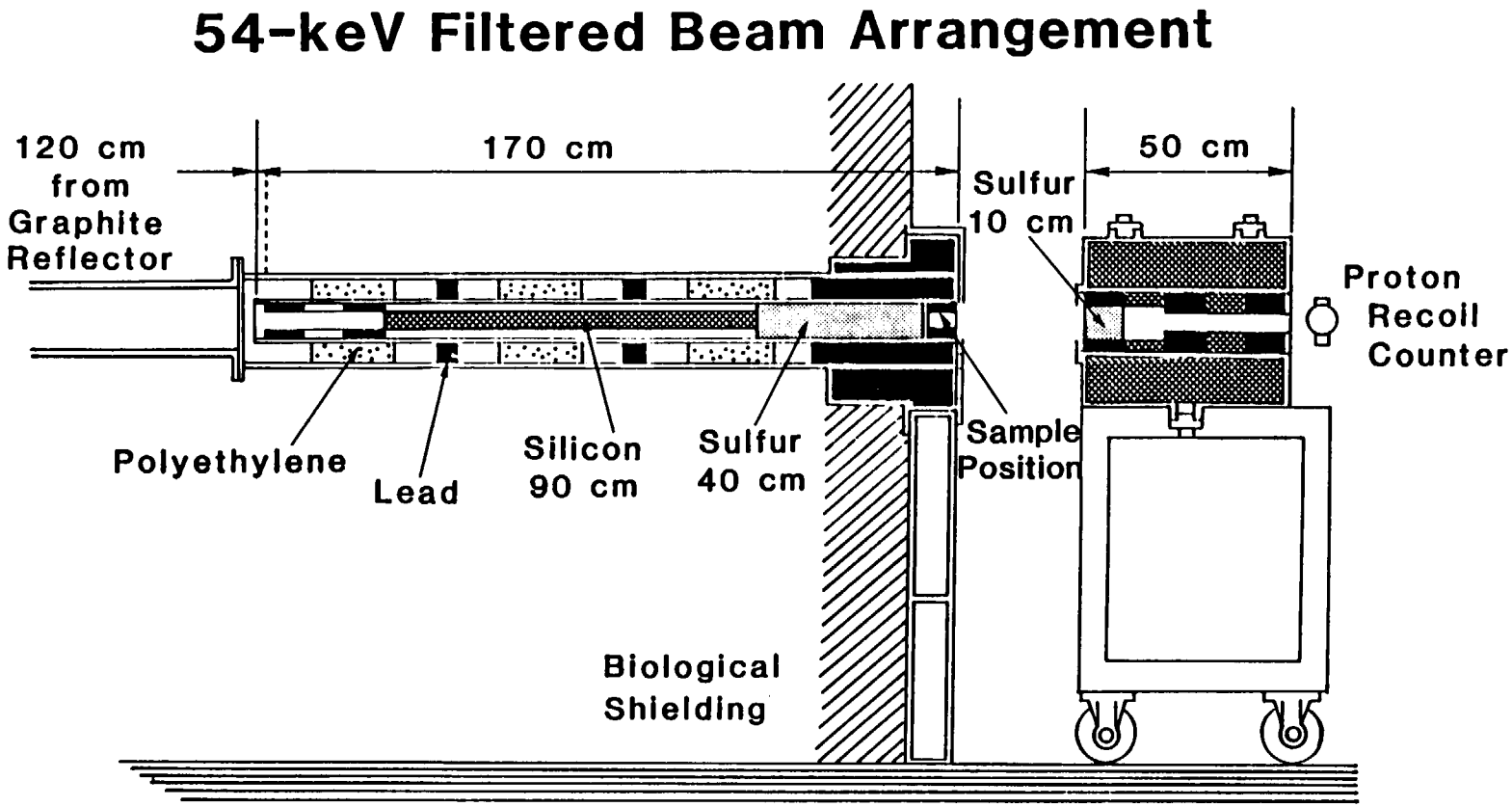

Fig. 8 54-keV filtered beam arrangement

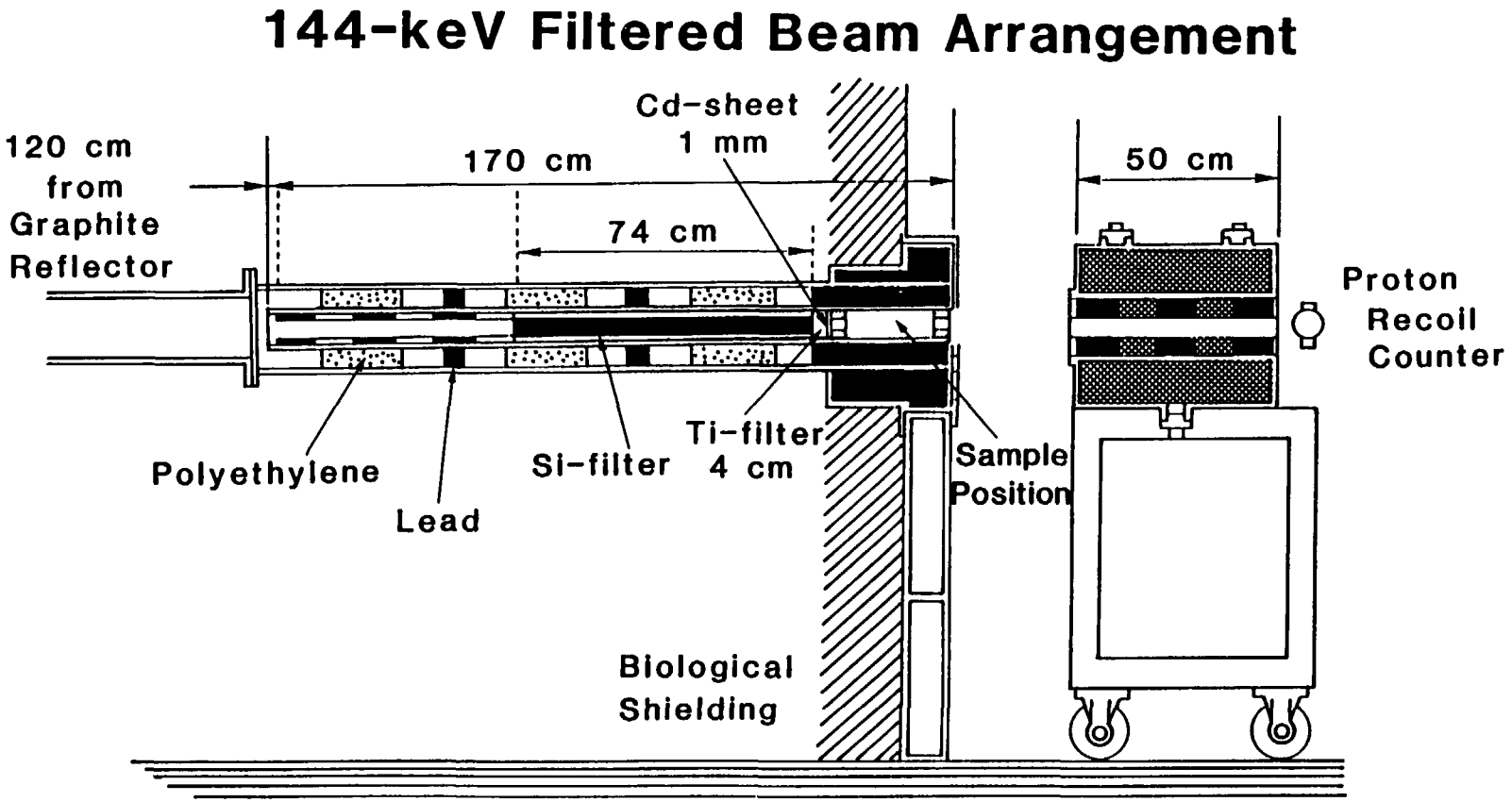

Fig. 9 144-keV filtered beam arrangement

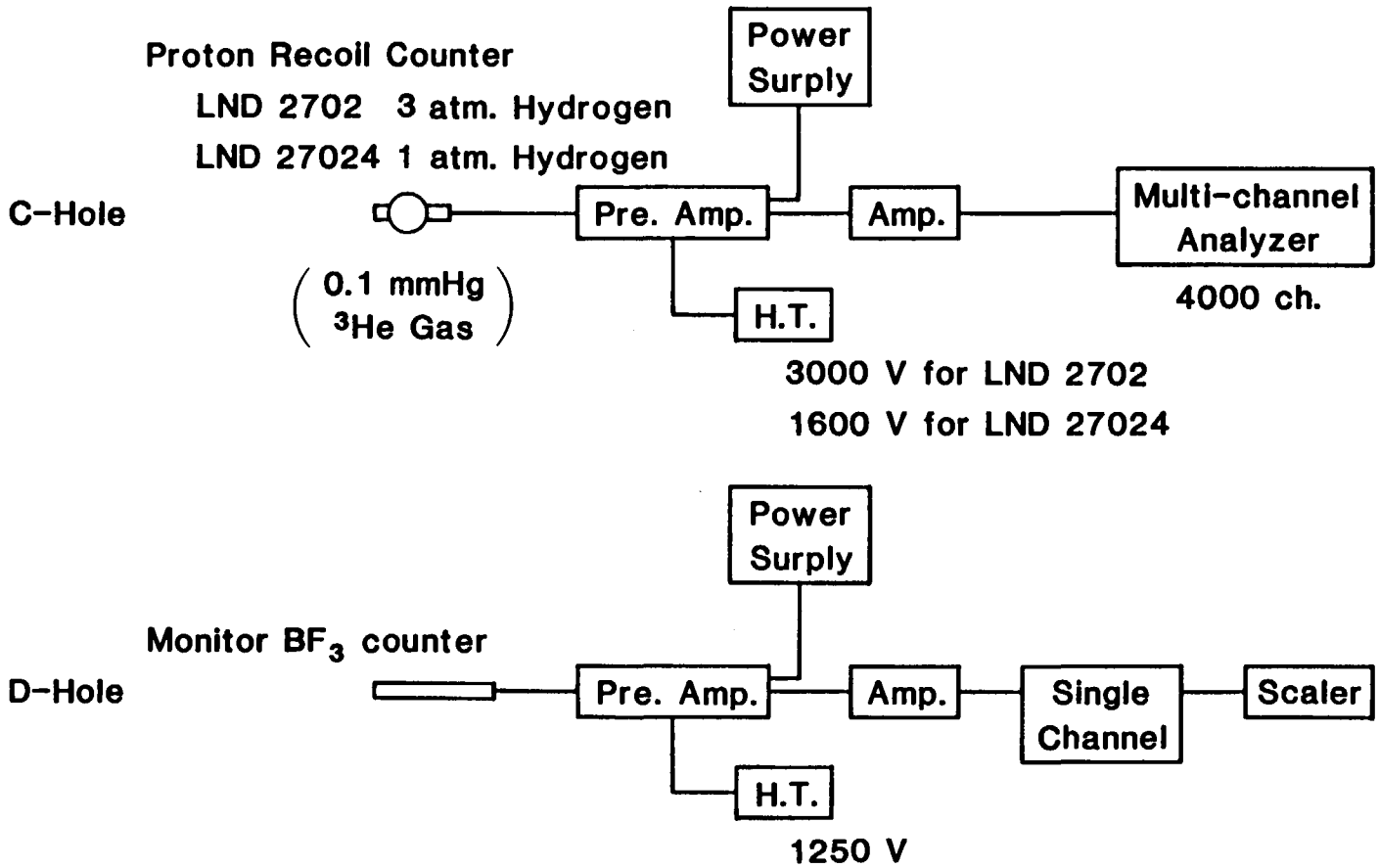

Fig. 10 Block-diagram of electronics

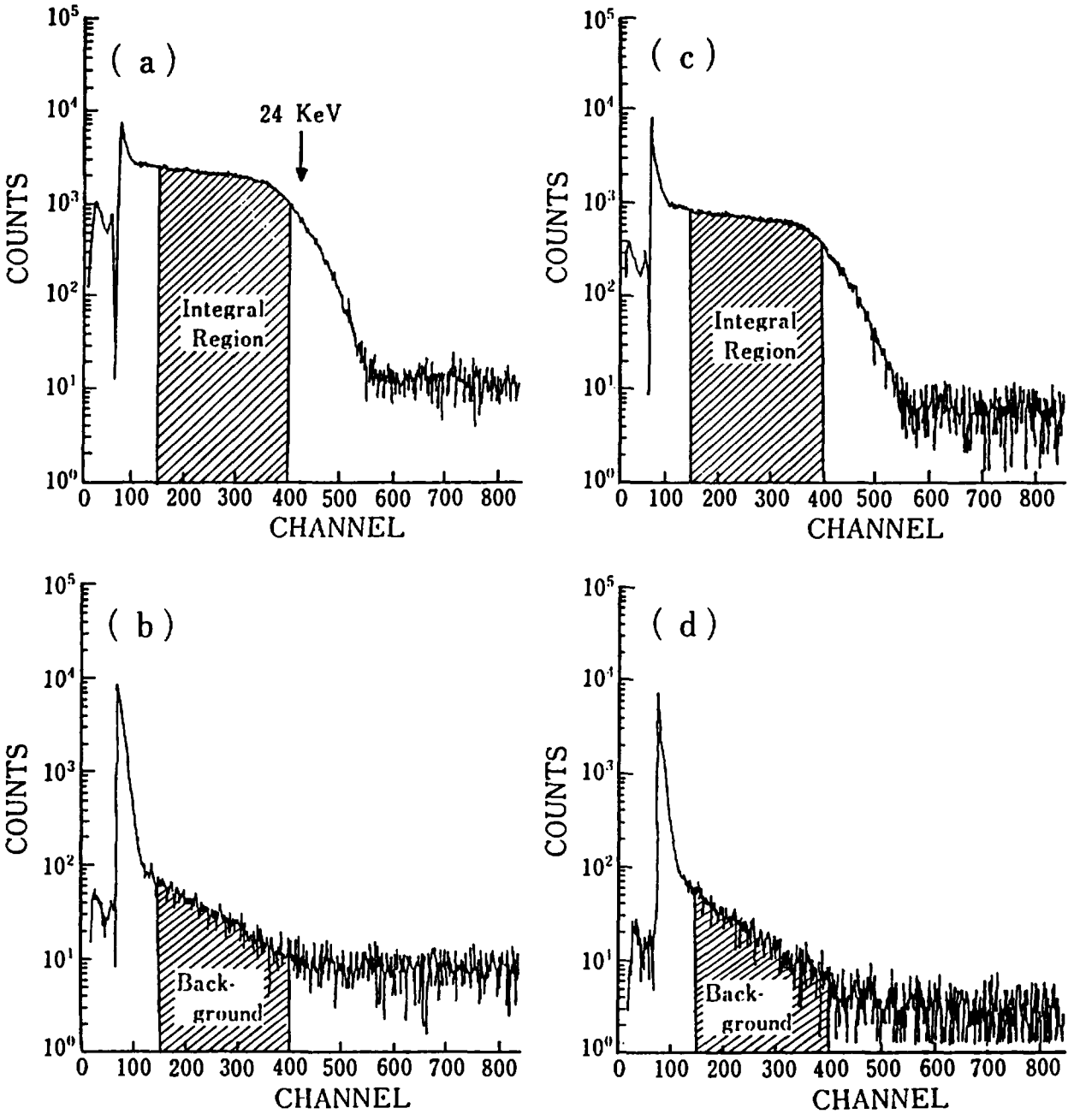

Fig. 11 Example of pulse-height spectra for cross section measurement
(a) without sample (b) with only Ti-filter
(c) with sample (d) with sample and Ti-filter

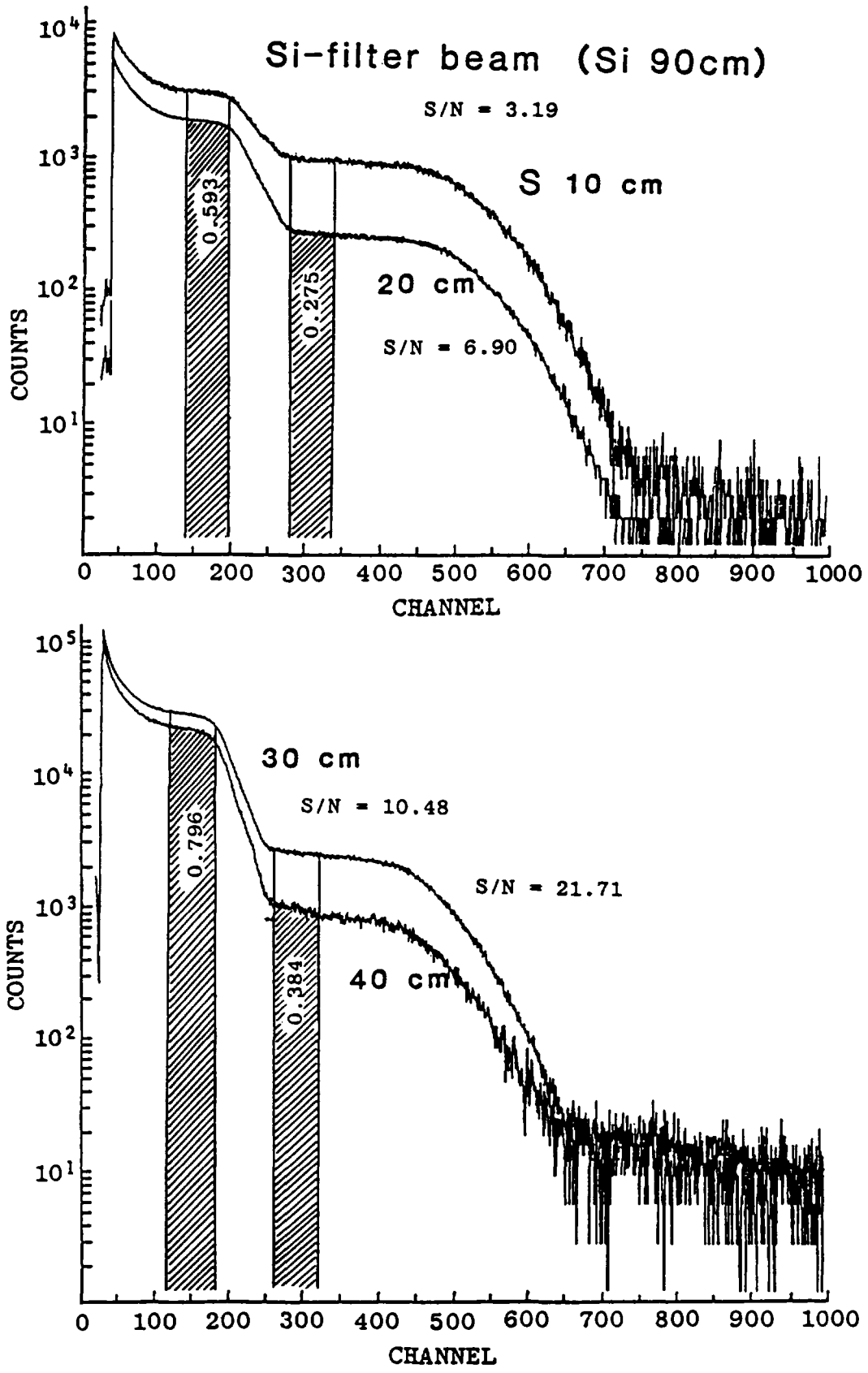

Fig. 12 Example of pulse-height spectra for silicon-filter beam as a function of sulfur thickness

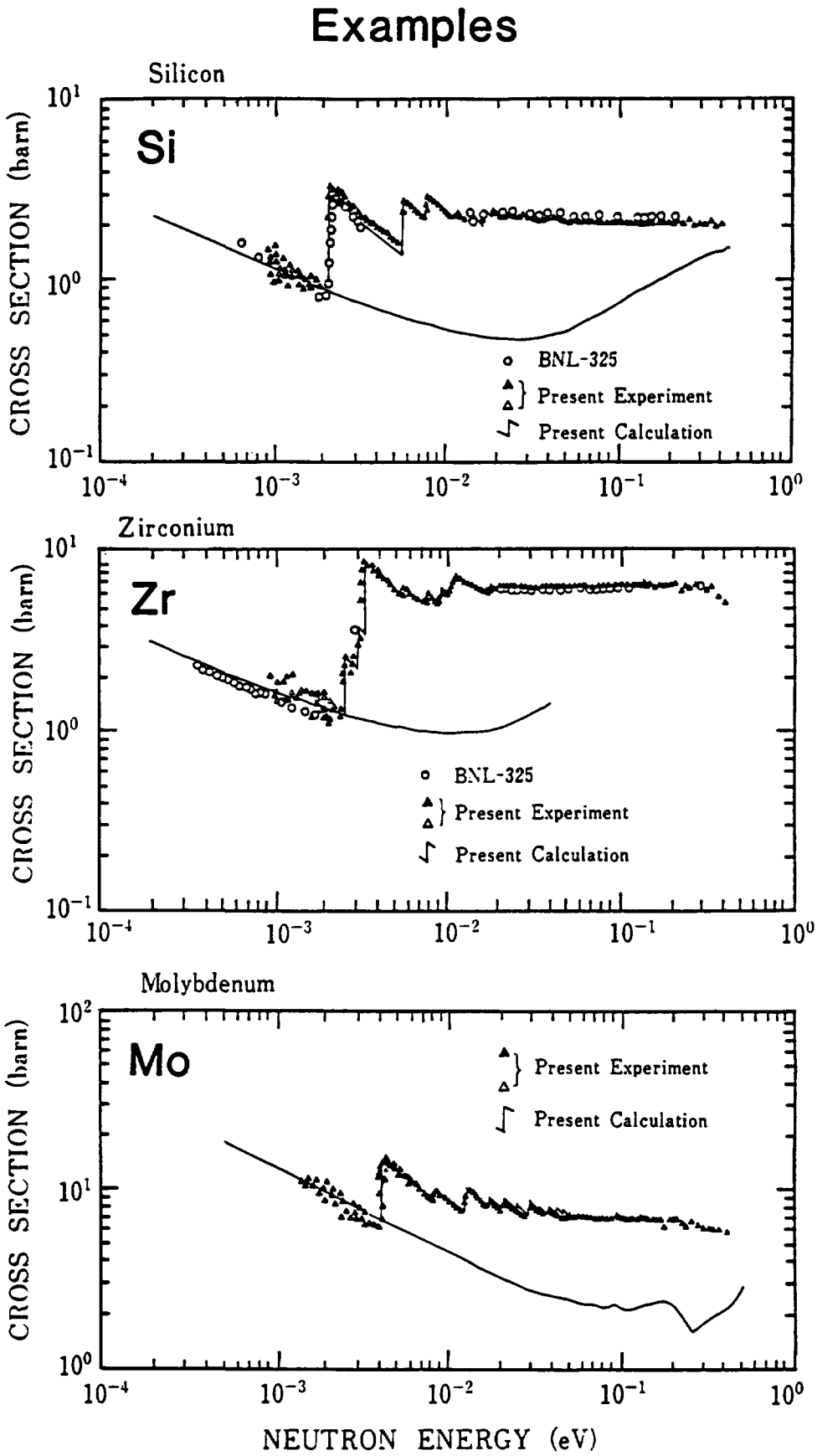

Fig. 13 Example of total cross section of thermal neutrons

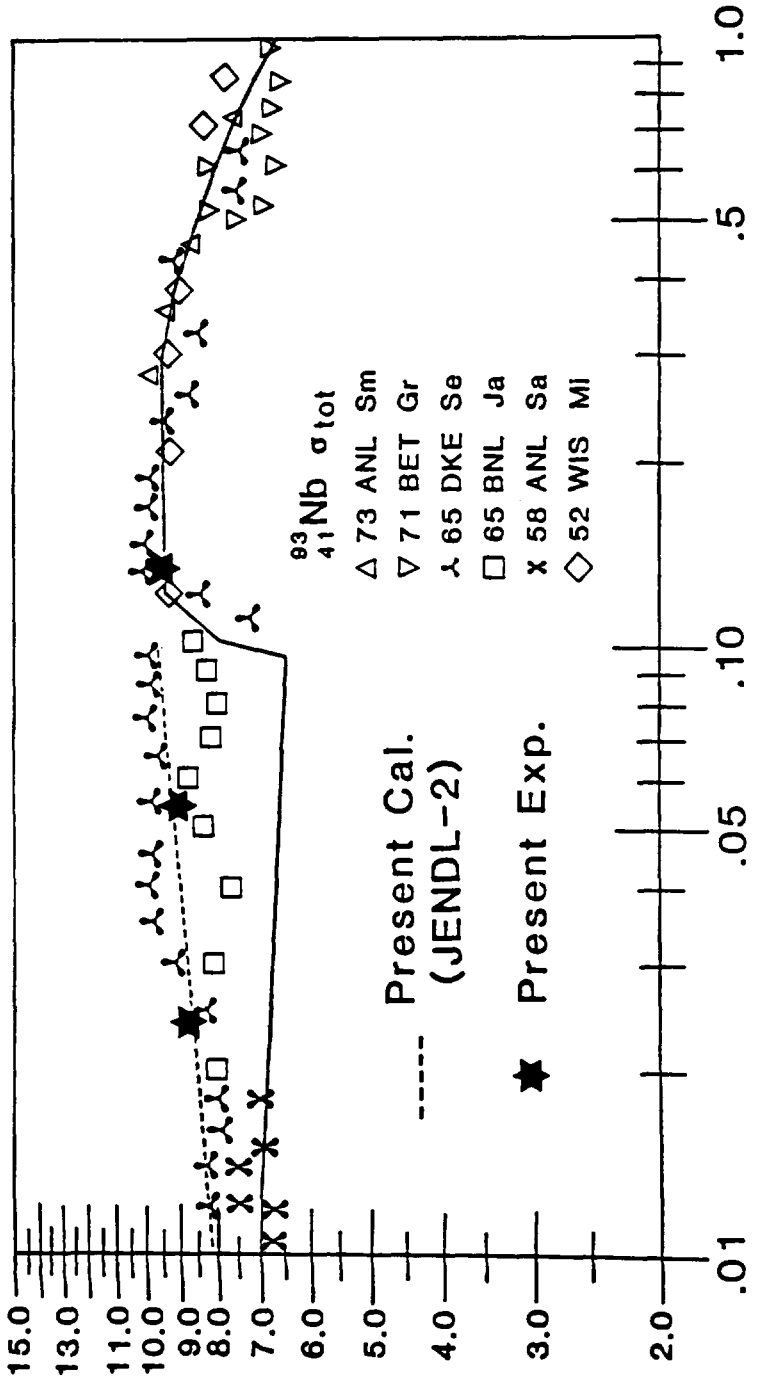

Fig. 14 Example of total cross section for Nb in keV energy region

9) 3.2-MV Pelletron Accelerator for Neutron Cross Section Measurements

H. Kitazawa and M. Igashira
Research Laboratory for Nuclear Reactors,
Tokyo Institute of Technology,
2-12-1 O-okayama, Meguro-ku, Tokyo 152, Japan

A Pelletron accelerator for neutron cross section measurements is briefly presented. The paper also reports on recent research activities of the neutron cross section group in our laboratory.

1. Accelerator specifications

The accelerator is a single-ended electrostatic Pelletron accelerator of high current type(Model 3UH-HC), which was built by National Electrostatic Corporation in 1976-1978. It includes the four charging chains installed in the column to provide four times as much current as in the standard 3UH accelerator. A characteristic feature of the accelerator is that the high voltage terminal permits an easy exchange of either the duoplasmatron nanosecond pulsed ion source or heavy ion source, according to research programs concerning neutron and atomic physics.

Max. voltage rating	3.2 MV
Voltage stability	± 2 keV
Proton energy range	0.4-3.0 MeV
DC proton beam	30 μA at 0.4 MeV
	45 μA at 1.5 MeV
	45 μA at 3.0 MeV
DC heavy ion beam	1 particle- μA krypton at 3 MV terminal voltage
Peak pulsed proton beam	1 mA at 2 nsec full width at half maximum and 2 MHz repetition rate and 3 MV terminal voltage
Analyzing switching magnet	ME/Z^2 = 120 at 45°

2. Measuring apparatus

Pure Ge gamma-ray detector(relative efficiency 10 %)

Ge(Li) gamma-ray detector with a long cold finger(relative efficiency 20 %)

Large anti-Compton NaI(Tl) gamma-ray detector with a heavy shield(see the figure)

Neutron goniometer

Charged particle scattering chamber

Data acquisition system(minicomputer + CAMAC system)

Personal computer terminals

Electric circuit modules

3. Research activities

We have continued to make a study of unpolarized and polarized neutron radiative capture reactions. Recently, several noteworthy experimental results were obtained for keV-neutron radiative capture reactions, using the 3.2-MV Pelletron accelerator.

On the $^{56}Fe(n,\gamma)^{57}Fe$ reaction, we have measured gamma rays for the transition to the ground state and to the first excited state following 27.7-keV s-wave neutron resonance capture by ^{56}Fe with a good signal-to-noise ratio, using a 60-cm^3 pure Ge detector. The results show that the partial radiation widths are not comprehensible in the valence capture model.[1] Moreover, strong anomalous M1 transitions from p-wave neutron resonances to either ground or first excited state have been observed at the neutron energies of 30-100 keV. These transitions can be explained in the framework of the semidirect model, assuming excitation of isovector M1 states in the target nucleus and using a reasonable spin-isospin dependent force in the two-body nucleon interaction.[2]

In the case of ^{28}Si, experimental observations have been made for gamma rays from the 565- and 806-keV $p_{3/2}$-wave neutron resonance states, using an anti-Compton NaI(Tl) detector. The partial radiative widths of both p-wave resonances cannot be reproduced by the Lane-Mughabghab optical model formulation of the valence model,[3],[4] but are in excellent agreement with the core-particle coupling model calculations taking account of the 2^+ and 3^- one-phonon excitations of the ^{28}Si core.

In the unresolved region, we have measured capture gamma-ray spectra of Pr, Tb, Ho, Lu, Ta, and Au at the neutron energies of 10-800 keV. An anomalous bump, so-called the pygmy resonance, was observed in all these spectra. Remarkable features of the pygmy resonance were found to be that the resonance energy and the electric dipole strength exhausted in the resonance increase with neutron number and decrease catastrophically around the neutron magic number of N = 82.[5]

An additional experiment has been initiated using the Pelletron accelerator. A detector system has been developed to measure the right-left asymmetry for the scattering of polarized neutrons from the $^{7}Li(p,n)\ ^{7}Be$ reaction. We aim at introducing these polarized neutrons to the studies of polarized neutron capture reactions.

A study of polarized neutron capture on ^{13}C in cooperation with the TUNL capture group has been completed. Striking evidence is given for the presence of isovector M1 resonances at E_x = 16.5 and 17.5 MeV.[6]

Several other projects are simultaneously carried on with neutron capture programs. Gamma-ray production cross sections at the neutron energies of 1-20 MeV have been evaluated for 10 nuclei from light to heavy nuclei.[7] The evaluated data for gamma-ray production will be filed in the 3rd version of Japanese Evaluated Neutron Data Library(JENDL). Furthermore, new experiments are being planned to measure the gamma-ray production data for D-D neutrons and to measure the neutron production from (α,n) reactions on light nuclei.

References

(1) H. Komano, M. Igashira, M. Shimizu and H. Kitazawa: Phys. Rev. C29, 345(1984)

(2) H. Kitazawa, H. Komano, M. Igashira and M. Shimizu: Proc. 5th Int. Symp. on Capture Gamma-Ray Spectroscopy and Related Topics, Knoxville, (1984) p.520

(3) M. Shimizu, M. Igashira, H. Komano and H. Kitazawa: idem p.517

(4) M. Shimizu, M. Igashira, K. Terazu and H. Kitazawa: to be published in Nuclear Physics A

(5) M. Igashira, M. Shimizu, H. Komano, H. Kitazawa and N. Yamamuro: Proc. 5th Int. Symp. on Capture Gamma-Ray Spectroscopy and Related Topics, Knoxville, (1984)p.523

(6) M. C. Wright, H. Kitazawa, N. R. Roberson, H. R. Weller, M. Jensen and D.R. Tilly: Phys. Rev. C31, 1125(1985)

(7) H. Kitazawa, Y. Harima, M. Kawai, H. Yamakoshi, Y. Sano and T. Kobayashi: J. Nucl. Sci. Technol., 20, 273(1983)

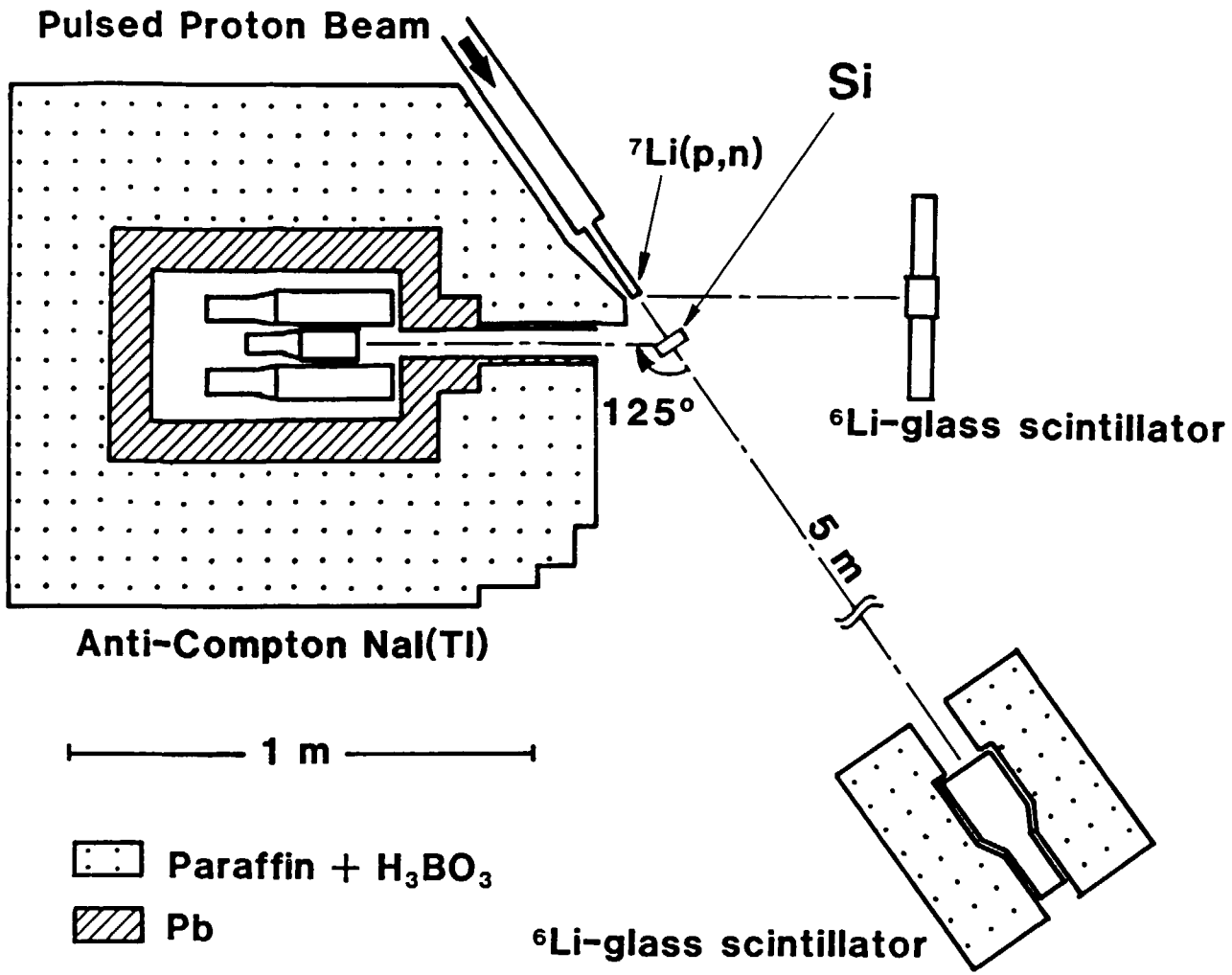

Fig.1 Experimental arrangement using a large anti-Compton NaI(Tl) gamma-ray detector.

10) Neutron TOF Spectrometer at KURRI Electron Linac

Y. Fujita

Research Reactor Institute, Kyoto University
Kumatori-cho, Sennan-gun, Osaka

This is a short report on the neutron time-of-flight spectrometer at the electron linac facility of Kyoto University Research Reactor Institute, including the accelerator specifications and detectors used for measurements of neutron crosss sections and of the energy spectrum in reactor structural materials.

1. Electron Linac at KURRI

The electron linear accelerator was installed in 1966 as a common facility for the visiting researchers from the universities and public research organizations in Japan. During the first four years, it was a one-section, L-band machine with 23 MeV in the maximum energy and 5 kW in the average beam power. In 1971, it was graded-up to a two-section, 46 MeV-, 10 kw-machine. Since then, it has been used mainly as a neutron generator. Current research works are as follows:

(1) Measurements of neutron energy spectra in reactor structural materials using the time of flight method with the purpose of experimental assessments of neutron transport calculations and neutron cross sections.
(2) Measurements of neutron total and capture cross sections in keV range of several reactor materials.
(3) Radiation damage studies of reactor materials with electron irradiation.
(4) Radio-isotope production with (gamma,n) and (gamma,p) reactions for uses in nuclear physics.

The specifications of the machine are shown in Table-1. The installation is shown in Fig.1.

2. TOF Spectrometer

There are four flight tubes, 12,20,20,45 meters in length, which are also shown in Fig.1. Neutrons are collimated with such materials as Pb, B_4C and $LiCO_3$. A systematic study has been carried out on the characteristics of photo-neutron targets[1]. A water-cooled Ta target is usually used in neutron cross section measurements in keV region. In neutron spectrum measurements in reactor materials, an air-cooled Ta- or Pb-target is used so as to escape from the neutron moderation with the cooling water. Typical energy spectra of photo-neutron targets are shown in Fig.2.

As for neutron detectors, a ^{6}Li-glass scintillator, an NaI(Tl) scintillator with ^{10}B-vaseline, and an NE-213 liquid scintillator are used depending on the energy region relevant to experiments. The ^{6}Li-glass scintillator(95% enriched ^{6}Li, NE-912),12.7 cm in diam., 1.27 cm thick, is used from thermal neutron energy up to a few MeV. The NaI(Tl) with ^{10}B -vaseline consists of a 13x13x8.5 cm^3 volume case filled with ^{10}B (884 g of 90.4% enriched ^{10}B) and vaseline (972 g) surrounded with four NaI (Tl) scintillators of 12.7 cm diam. and 5.08 cm thickness. This detector has an efficiency almost indenpendent of neutron energies from keV to MeV and is used parallely with the ^{6}Li-glass scintillator in neutron spectrum measurements in reactor structural materials. The efficiencies of the detectors were caliblated by experiment employing a borated graphite standard assembly[2] in which the neutron energy spectrum can be reliably estimated by calculation in low keV to high keV region. The calibrated efficiency curves are shown in Figs.2 and 3 to illustlate typical examples of detectors of this kind. The NE-213 detectors(12.7 cm diam. and 12.7 cm thick, 5 cm diam. and 5 cm thick) are used mainly in the measurements of photo-neutron energy spectrum of MeV neutrons produced in the target.

The gamma-ray detectors used for capture cross section measurements in this facility are a total energy detector used with the pulse height weighting technique and a total absorption detector made with BGO(Bismuth Germanium Oxide) scintillator. The detector of the first kind is made of liquid scintillator of C_6F_6(hexafluorobenzene) or C_6D_6(deuterated benzene). To deduce the number of capture events occured in a sample from the counts of the detector, the counts are summed-up by weighting with a

function of their respective pulse heights. The detector consists of a pair of cylindrical scintillators; 10 cm diam. and 4 cm thick for C_6F_6 (NE-226)[3], and 11 cm diam. and 4 cm thick for C_6D_6(NE-230)[4]. The detector has a low efficiency to scattered neutrons and is suited to a sample whose capture cross section is much smaller than the scattering cross section. As for the second type, the total absorption detector which has a simple characteristic to count the number of capture events has been developed using BGO scintillator[5] instead of usually employed organic liquid scintillator. The BGO assembly is shown in Fig.4. The volume of BGO is only 1.5 liter. A typical response to neutron capture is shown in Fig.5 taking Au as an example. The response is almost equivalent to that of organic liquid scintillator of about 1500 liters in volume.

Neutron production rate is monitored during measurements in the target room or in the neutron beam inside the flight tube. The detector is selected from proportional counters of BF_3 and ^3He,and a thin ^6Li glass scintillator. For the use in the flight tube, the detector is placed fully or partialy in the neutron beam.

3. Accelerator-Based Filtered Neutrons

Monoenergetic neutrons in keV range can be obtained with placing a thick filter material (commonly used materials are shown in Table 2) in the flight path of neutrons leaking out from a source having a continuous energy spectrum. Filtered neutrons are intense and clean; they are monochromatized with little loss of intensity and the contamination of background neutrons and gamma-rays is very low. The (pulsed) accelerator-based filtered neutron source has another excellent characteristic, if it is used with the neutron time-of-flight technique. The filtered neutrons can be seperated by their flight time from background neutrons and gamma-rays. The background is reduced to an extremely low level and is reliably estimated in the amount. This is one of the reasons for the accelerator-based filtered neutrons to be effectively used to precise point cross section measurements.

A systematic study of filtered neutrons has been carried out at this facility. The study includes refined measurements of the cross section

minima of filter materials, Sc[6], Fe[7] and Si[8], and the utilization of the neutrons to precise measurements of total[9] and capture[10] cross sections.

References:

1) S.A.Hayashi; Desertation of Doctor's Degree at Kyoto University (1985).
2) I.Kimura et al.; Nucl. Instr. Meth., 137, 85 (1976).
3) N.Yamamuro et al.; Nucl. Instr. Meth., 133, 531 (1976).
4) H.Shirayanagi ; Desertation of Master's Degree at Tokyo Institute of Technology (1981).
5) S.Yamamoto et al.; submitted to Nucl. Instr. Meth.
6) Y.Fujita; J. of Nucl. Sci. Technol., 20(3), 191 (1983).
7) K.Kobayashi et al.; Annals of Nucl. Energy, 4, 499 (1977).
8) Y.Fujita et al.; J. of Nucl. Sci. Technol., 21(11), 879 (1984).
9) R.C.Block et al.; J. of Nucl. Sci. Technol., 12(1), 1 (1975).
10) N Yamamuro et al.; J. of Nucl. Sci. Technol.; 15(9), 637 (1978).

Table 1 Specifications of KURRI-Linac

1) Beam energy	unloaded	: 46 MeV	
	loaded (max. power)	: 28 MeV at 500 mA	
2) Beam current	4 microsec pulse	: 500 mA	
	short pulse	: ~6 A at 22 nS	
3) Beam power	max.	: 10 kW	
4) Beam width		: 0.01~4 μsec	
5) Repetition	short pulse	: single ~ 400 Hz	
	long pulse	: single ~ 180 Hz	

6) Accelerating tubes	1st section	2nd section
a) type	constant impedance	constant gradient
b) mode	2/3 π	2/3 π
c) frequency	1300.7 MHz	1300.7 MHz
d) length	2.38 m	1.845 m
e) loading factor	-20.8 MeV/A	-12.2 MeV/A

7) Injector	
a) type	: Cockcroft-Walton
b) injection voltage	: ~100 kV
c) electron gun	: Applied Radiation-Model 12

8) Rf-driver	
a) out-put power	: 3 kW (pulsed)
b) frequency	: 1300.7 MHz
c) stability	: 5×10^{-9}

9) Modulator	1st section	2nd section
a) peak Rf-power	: 10 MW	: 20 MW
b) klystron	: Litton-3661	: TV2022B(THOMSON-CSF)
c) pulse transformer	: 1 : 18	: 1 : 14
d) PFN stages	: 14	: 16

Table 2 Commonly used filter materials

Filter Materials	Main Isotope in Natural Element (%)	Spin Parity	Average Energy* (keV)	Energy Spread* (keV)	Auxiliary Filter Materials
U	^{238}U : 99.27	0^+	0.186	0.00145	Se, Mn, Ge
Sc	^{45}Sc: 100	$7/2^-$	2.0	0.8	Ti, ^{60}Ni, ^{64}Zn
Fe	^{56}Fe: 91.66	0^+	24	2	Al, S
Si	^{28}Si: 92.21	0^+	144 54	24 1	Ti S
O	^{16}O : 99.759	0^+	2350	100	Bi

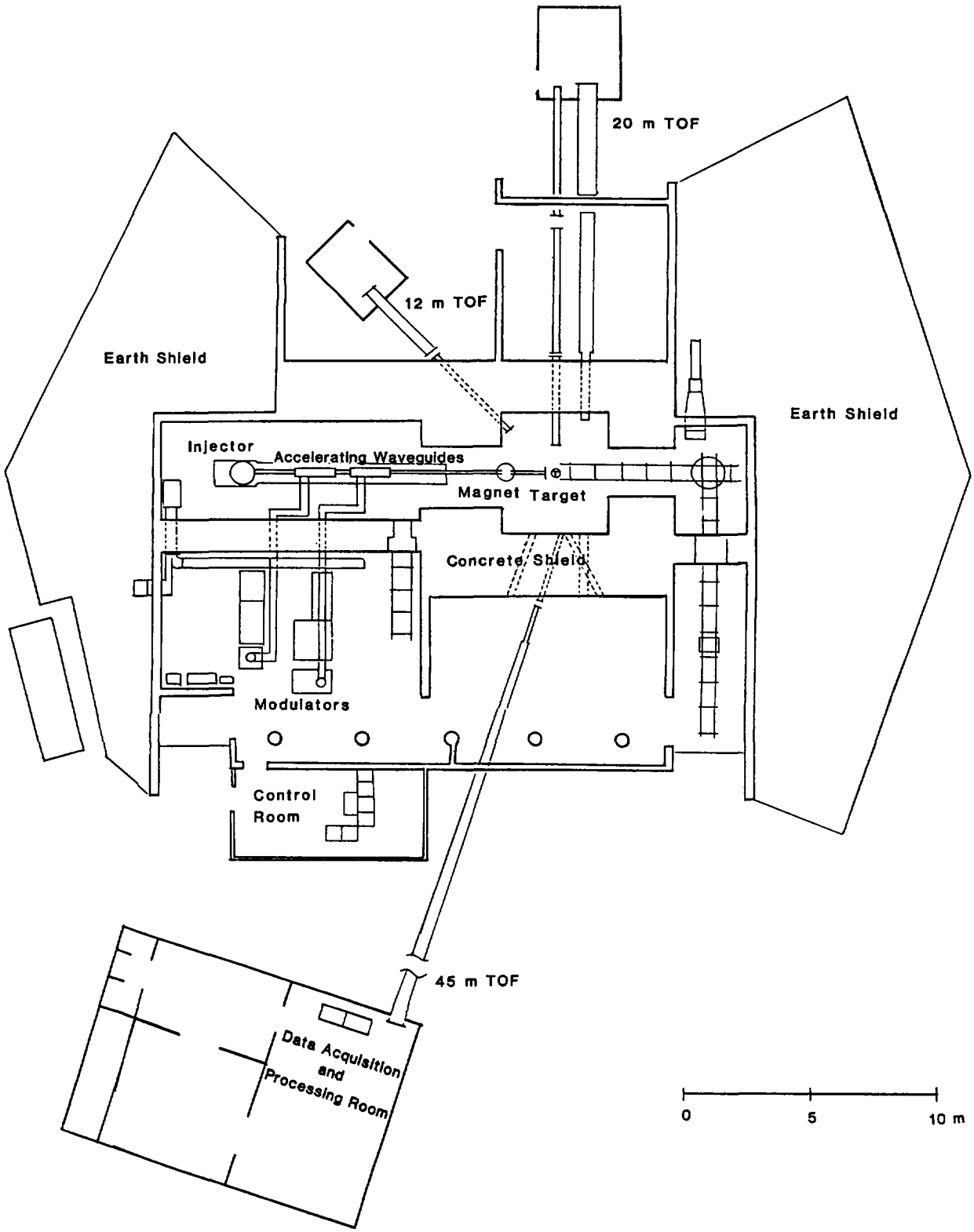

Fig.1: Installation of neutron flight tubes at KURRI-Linac.

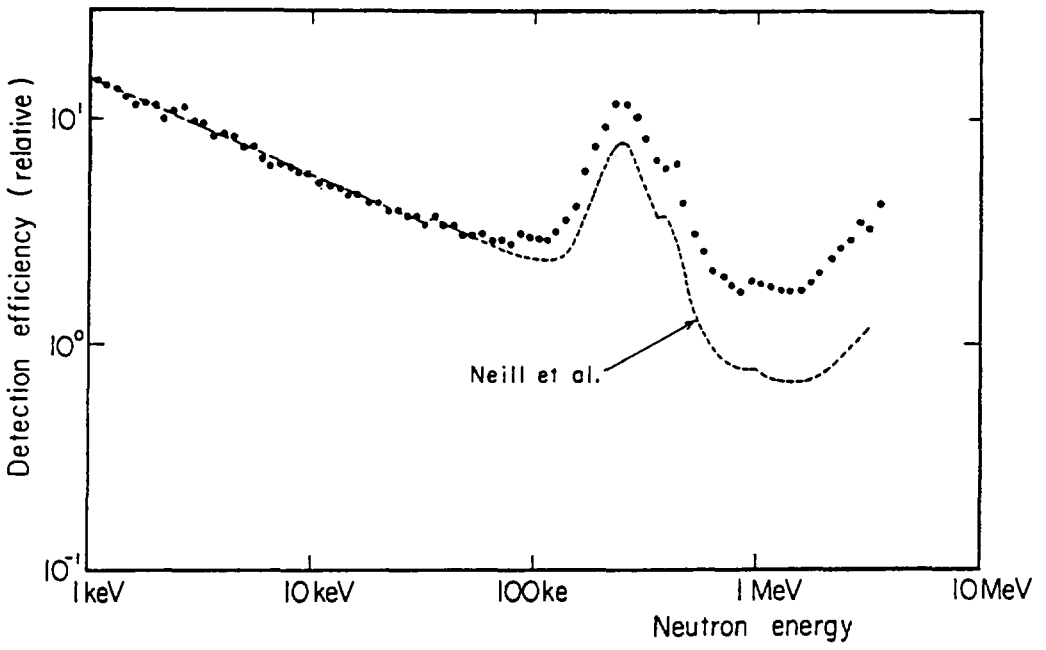

Fig.2: Efficiency of the ^{6}Li glass scintillator experimentally calibrated using a standard pile of barated graphite.

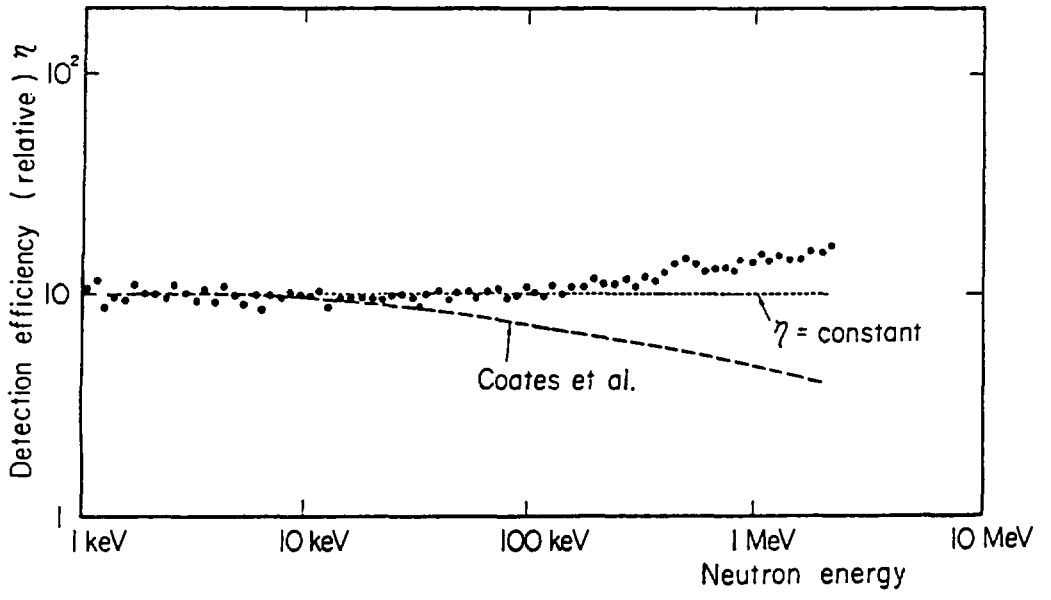

Fig.3: Efficiency of the NaI(Tl) with ^{10}B-vaseline neutron detector experimentally calibrated using a standard pile of borated graphite.

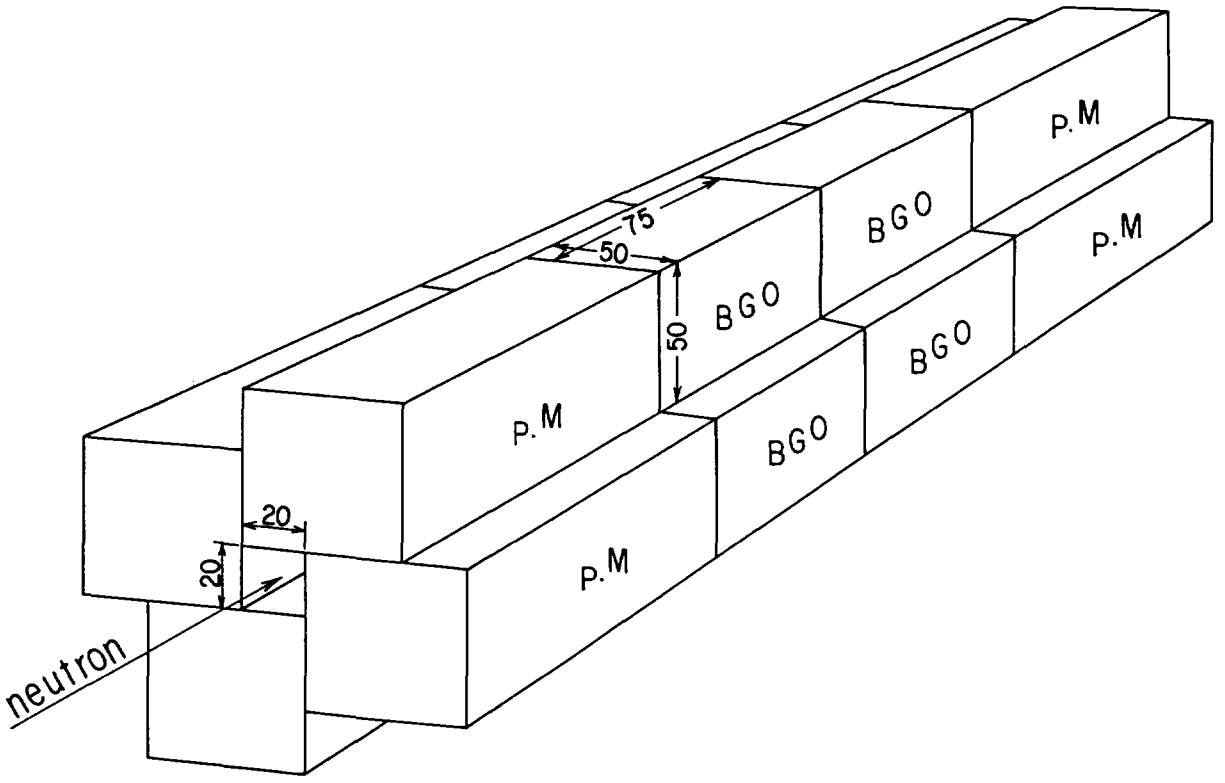

Fig.4: Arrangement of the total absorption detector of BGO scintillator designed for the use in neutron capture cross section measurements.

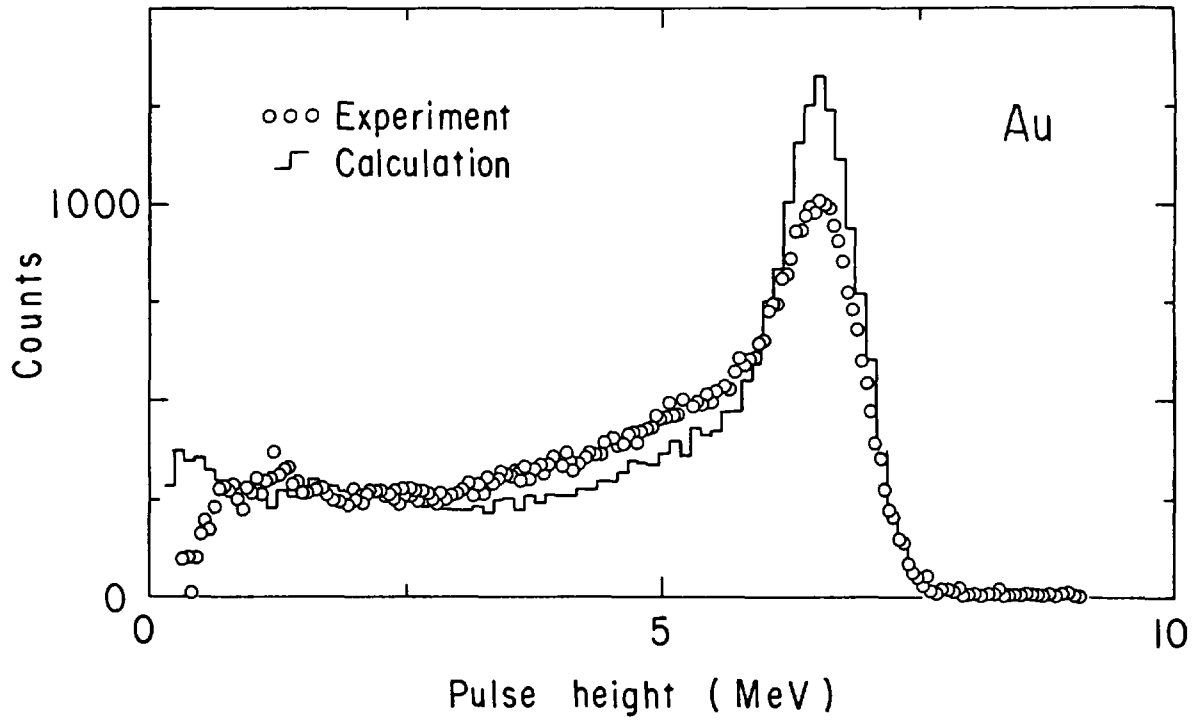

Fig.5: Pulse-height response of the BGO detector to the gamma-ray cascade following neutron-capture with Au.
The solid line is a calculation with a Monte Carlo code using an experimental gamma-ray spectrum.

11) The He-jet Fed ISOL Facility KUR-ISOL at the Kyoto University Reactor

K. Okano and Y. Kawase

Research Reactor Institute, Kyoto University,
Kumatori-cho, Sennan-gun, Osaka 590-04

The He-jet fed isotope separator on-line(ISOL) facility, KUR-ISOL, is used for the studies of nuclear data and structure of fission produced short-lived nuclei. The characteristics of the He-jet transport and ion source systems and the main parameters of the facility are presented. The researches so far performed on the nuclear data of FP nuclei are also described.

1. Introduction

In order to investigate systematically the nuclear data and structure on nuclei far from the stability line, the availability of an ISOL facility which separates the fission products continuously according to the mass and charge is of importance. It was proposed[1,2] to install an ISOL facility to a planned high-flux reactor(HFR).[3] A He-jet transport system was employed in order to minimize the activation of the material around an ion source. This type of ISOL allows the use of a small ionization chamber that may easily be heated to high temperature and allows the efficient ionization of rare-earth elements which can not efficiently be mass-separated by other means. A model machine was installed at the through-tube facility of the KUR and the performance of a He-jet fed ISOL was examined.[4-7] This machine

is now in use for nuclear spectroscopic studies of fission-produced short-lived nuclei. The details of the apparatus,especially the target and the He-jet transport system and the high-temperature thermal ion source, and the researches on the nuclear data of short-lived fission-product nuclei so far performed by using this apparatus will be described.

2. Basic layout

A schematic diagram of the apparatus is shown in Fig. 1. The target material of 93% enriched ^{235}U is irradiated by the neutron flux of maximum 3 x 10^{12} n/cm^2·s at the through-tube facility of the KUR. The recoiled fission products are slowed down to thermal velocity in the He gas atmosphere(1~3 atm) and are attached to DOP aerosols. After transported through a capillary of 1.0 mm in inner diameter to a two-stage flat-skimmer chamber in a few seconds, the fission products are ionized by an ion source.[7,8] The ionized activities are extracted from the ion source and focused in a parallel beam by accelerating and focusing electrodes. The activities mass-separated by an analyzer magnet are collected on an Al-coated Mylar tape to perform the nuclear spectroscopic studies on neutron-rich nuclei as will be described below. The available intensity of the individual isotope depends on the independent or cumulative fission yield, the half-life and the ionization efficiency of the relevant isotope. Typical parameters of the apparatus are listed in Table 1 and an example of the mass spectrum measured for rare-earth isotopes is shown in Fig. 2.

The overall efficiency of KUR-ISOL has been measured to be about 2 x 10^{-3} at 1.85 atm of He gas by using the fission yield

of 65 s ^{140}Cs and measuring the yield of its 602 keV γ ray. The actual efficiencies of various processes involved may then be approximately evaluated as follows: recoil into gas 0.2 ; range effect 0.5 ; capillary transportation 0.35 ; skimmer-ion source coupling 0.4 ; ionization 0.3 ; extraction and ion optics 0.5. These values are somewhat smaller than the values calculated using the results of the test experiments on the efficiency of individual process, although the overall efficiency of He-jet fed ISOL is reported to be generally $10^{-3} \sim 10^{-5}$. [9,10] We are now trying to increase the overall efficiency by improving the target-capillary-skimmer and ion source systems.

As shown in Fig. 1, special care is paid for the rare gas activities produced and pumped out together with He gas used for transportation. The Kr, Xe and I activities in the He gas are caught by a cold trap and different kinds of filters(F1, F2 and F3). As most of the He gas is pumped out by a Roots pump at the 1st stage skimmer, the activities in the pumped-out gas of the Roots pump decay out at the F1 chamber (60 l) and F2 chamber (260 l) during the residence time of more than 4 hours. The final activity level is negligible compared with that of ^{41}Ar produced by the reactor operation. This level is monitored by a NaI(Tl) counter. For an unexpected leakage of the radioactive gas from the target chamber, another NaI(Tl) monitor always records the radioactive level between the middle and outer target chamber(Fig. 3). If the abnormally high level of either of the monitor counters is recorded, magnetic valves for He flow are closed and whole ISOL systems are shut down automatically. This operates also in the cases of abnormally high He pressure and vacuum failure of ISOL.

3. Target and He-jet transport system

It was verified experimentally that the time duration τ necessary to sweep out the recoiled products from the target chamber is equal to the exchange over time of the gas through the chamber, PV/Q, where P is the pressure of the gas, V is the volume of the chamber and Q is the flow rate of the gas($cm^3 \cdot atm/s$).[6] It was found, however, that no turbulence nor standing space should exist to ensure the above relation to hold. As the recoiled particle must stop inside the gas, the range of the particle R must nearly be proportional to $PV^{1/3}$ and τ to $RV^{2/3}/Q$. Although it is clear that the value of Q is larger the better to get short sweep-out time, it is limited to about 20 $cm^3 \cdot atm/s$ in our case by the pumping speed of the Roots pump used. The value of P is also limited to about 3 atm by the security consideration and also by the upper limit of Q mentioned because too small a diameter of the capillary is liable to lead to blocking of He flow by aerosol materials. The target chamber now in use consists of three aluminium chambers as shown in Fig. 3 and the volume of its inner chamber(V) is 50 cm^3. Using a capillary tube 0.1 cm in inner diameter and 11.5 m in length, Q becomes 14 $cm^3 \cdot atm/s$ and τ is then about 6.8 s at the pressure of 1.9 atm. At the He pressure of 2.0 atm, the range of heavy fission products is about 3 cm.

A 93% enriched ^{235}U target material in the form of U_3O_8 was electrodeposited on an inner aluminium cylinder. The weight and thickness of ^{235}U is 10 mg and 0.5 mg/cm^2, respectively. The top lid of the middle chamber is welded in order to secure tight sealing. The middle chamber is encased in an outer chamber

to detect the leakage of pressurized radioactive gas as mentioned before. Some modifications of the target chamber are now planned to facilitate the exchange of the capillary tube which tends to be blocked by aerosol material after prolonged periods of use.

It was experimentally ascertained[6] that the transit time Δt of fission products through a capillary is approximately given by the theoretical relation

$$\Delta t = \frac{128 \eta L^2}{3PD^2} ,$$

where η is the coefficient of viscosity of the gas and L and D the length and inner diameter of the capillary, respectively. The value of Δt is about 0.6 sec under the conditions mentioned before for τ of 6.8 s.

The transport efficiency through the capillary was also experimentally measured to be (60 $\pm$ 15)% at the He pressure of 1.08 atm, at the neutron flux of 2.4 x 10^{12} n/cm^2·s and for the capillary 11.5 m in length and 0.1 cm in inner diameter.

4. High-temperature thermal ion source and the ionization of rare-earth elements

It is the most characteristic merit of the He-jet fed ISOL that the time delay due to the desorption at the surface or to the diffusion in the target matrix does not occur even for high melting-point elements. In order to obtain high ionization efficiencies for rare-earth elements, a high-temperature thermal ion source has been constructed. Its cross-sectional view is shown in Fig. 4. The ionization chamber consists of a tungsten cylinder 6.0 mm in inner diameter and 52 mm in length. The

cylinder has an outlet hole of 0.8 mm in diameter at the front end. A cylindrically wound rhenium foil of 0.05 mm in thickness and 20 mm in length is placed inside the front half of the inner capsule made of tungsten. This inner capsule is tightly fitted to the cylinder at the front half and ensures holding high temperature at the rear half where the tungsten cylinder is thin (0.4 mm) in order to maintain the temperature gradient between the front half of the cylinder and the molybdenum base plate. The front half of the cylinder is heated by the radiation from a tungsten filament of 1.5 mm in diameter situated outside the cylinder as well as by the bombardment of electrons. The cylinder and the filament are covered by a threefold thermal shield made of tantalum and molibdenum. The potential of the filament and the shield is kept at about -400V with respect to the cylinder, with the bombardment current variable up to 1.0 A. Fig. 5 shows the temperature inside the cylinder measured by an optical pyrometer as a function of the input power. The high performance of temperature versus input power observed is the result of the compact design of the He-jet coupled ion source.

Aerosols with fission products come from the rear side of the cylinder through a two-stage flat-skimmer system with holes of 1.5 and 3.5 mm in diameter for the 1st and 2nd stage,respectively. As the full diverging angle of the aerosol jet from the skimmer has been measured to be about 12°, the geometry of the present skimmer-ion source coupling allows about a half of the aerosols to impinge on the high temperature region of the tungsten cylinder.

The ionization characteristics were studied for alkali, alkaline earth and rare-earth elements.[7,12] The alkali elements, Rb and Cs,are ionized with high efficiency(max. 45～50%) at the temperature

below 1500 °C, while alkaline-earth elements, Sr and Ba, are ionized at the temperature above 2300 °C with reasonable efficiencies(10～20%). The temperature dependence of ionization efficiencies for these elements is shown in Fig. 6. Rare-earth elements are also ionized at the temperature above 2200 °C, the efficiency increasing rapidly with temperature. The temperature dependence of the efficiencies was measured for Ce, Pr and Nd using the following nuclides: $^{148}Ce(T_{1/2}$ = 48 s, E_γ = 292.6 keV), $^{149}Ce(T_{1/2}$ = 5 s, E_γ = 57.7 keV), $^{152}Ce(T_{1/2}$ = 3.1 s, E_γ = 285.0 keV), $^{152}Pr(T_{1/2}$ = 3.24 s, E_γ = 164.0 keV), $^{152}Nd(T_{1/2}$ = 11.4 m, E_γ = 278.5 keV), $^{153}Nd(T_{1/2}$ = 29 s, E_γ = 105.4, 418.3 keV). The results are shown in Figs. 7-8. The efficiencies shown in Figs. 6-8 were normalized assuming the ionization efficiency for Cs as 1.0. The efficiencies for Nd were normalized to the values of Ce and Pr which were measured by using a tungsten ionizer(no Re foil). It may be seen that the efficiency near 10% can be obtained for rare-earth elements at the operating temperature of 3000 °C.

One advantage of the use of an ion source for isotope separation on-line is the capability of Z separation utilizing the temperature dependence of the ionization efficiency. It is clear that the alkali, alkaline-earth and rare-earth elements can be well separated each other as can be seen from Fig. 6. It may be seen from Fig. 7 that the temperature dependence of ionization efficiency for Nd is different from that of Ce or Pr. Recently it was also found that the temperature dependence for Pm is clearly different from that of Nd. These characteristics can conveniently be utilized for Z assignment of γ rays in the rare-earth region when other relations are hard to apply.

It should be mentioned here that the experimental results presented in Figs.6-8 were obtained by a high-temperature thermal ion source with a tungsten cylinder of 4.0 mm in inner diameter and without an inner capsule described before. The present version with an inner capsule clearly shows better performance, but the quantitative behaviour may be somewhat different from that shown.

One difficulty encountered in the use of the high-temperature thermal ion source is the occasional instability of the beam position which occurs when the temperature of the source is very high. Improvements on the constructional details of the ionization chamber and its subsequent performance tests are now in progress.

5. Researches on nuclear data of short-lived fission-product nuclei

The investigation of the phenomena associated with the decays of short-lived fission products provides the basic nuclear data for reactor design, especially for the developments of a new reactor using Th as fuel. It also provides interesting quantities to compare with theoretical predictions based on the theory of nuclear structure. Following investigations have been performed or now in progress using KUR-ISOL. Some of these investigations were performed mainly by the visiting researchers from Nagoya University* and from Himeji Institute of Technology**.

---

*T. Katoh, K. Kawade, H. Yamamoto et al.

**H. Matsui, K. Hiromura, T. Mitamura, K. Aoki and T. Sekioka.

(i) Decay scheme studies of short-lived nuclei

The β^- decays of $^{90-95}$Rb, ^{92,94,96}Sr and ^{96}Y have been studied by measurements of γ-ray singles and coincidence spectra, of conversion electron and X-ray spectra and of time delay between γ rays, using large volume Ge(Li) and high resolution HPGe detectors.[13-19] The studies on the decays of ^{91}Rb, ^{92}Y, ^{93}Rb, ^{96}Sr and ^{96}Y are now in progress. Newly established decay scheme of ^{94}Y is shown in Fig. 9.

(ii) Measurements of delayed neutron emission probability by a β-γ spectroscopic method

It has been shown that the delayed neutron emission probability (P_n) of the individual precursor can be determined by the precise γ-ray measurements on mass-separated activities from ISOL provided that the decay schemes of nuclides concerned are well established.[20] The P_n values of ^{94}Rb and ^{95}Rb have been determined as 9.73 ± 0.62 and 8.60 ± 0.57, respectively.[20-22] This method can be applied to other Z-separated precursors obtained by ISOL if the decay schemes of nuclides concerned are well established.

(iii) Q_β-value measurements

The Q_β-values of neutron-rich nuclei ^{143}La and ^{145}La have been measured by using a HPGe detector. Its response function for monoenergetic electrons has been determined by using a sector type double focusing β-ray spectrometer.[23] The investigations in this direction are now in progress.

(iv) Measurements of absolute γ-ray emission probability

In the case of a fission-product nuclei, the absolute γ-ray emission probability per decay(P_a) can be determined rather precisely by a filiation method. As an example, we have determined

the P_a values of the 352.0, 685.9 and 954.2 keV γ rays following the decays of ^{95}Rb, ^{95}Sr and ^{95}Y as 49.2 ± 3.1, 21.8 ± 1.8 and 15.9 ± 0.7 per 100 decays, respectively,[24] utilizing the known P_a values of the 724.2 and 756.7 kev γ rays following the decay of 64 d ^{95}Zr.[25,26]

(V) Half-life measurements of short-lived isotopes

Although the precise measurements of half-lives are important to establish fundamental nuclear data, it is not rare that the considerable discrepancies are found among a few reported values of half-lives.[27,28] We have determined precisely[29,30] the half-lives of ^{93}Sr, ^{94}Sr, ^{95}Sr, ^{139}Cs, ^{141}Cs and ^{143}Ba whose reported half-lives are not in agreement with each other. Further measurements on rare-earth nuclides are now in progress. In Fig. 10, the decay curves observed for X-rays and γ rays following the decay of the newly identified isotope ^{156}Pm are shown.

(VI) Search for new isotopes and isomers

The possible existence[31] of an isomeric state in ^{94}Rb has been examined, but no indication of its existence has been found.[32]

As the rare-earth elements are ionized with high efficiency by a high-temperature thermal ion source, it is expected that the short-lived rare-earth nuclides with low fission yields can be identified by using KUR-ISOL. The candidates are, for example, ^{150}La, $^{153,154}Pr$, $^{155,156}Nd$ and $^{156-158}Pm$. At the mass 156, γ-ray spectrum following the decay of ^{156}Pm has been obtained as shown in Fig.11, and the ^{156}Pm has newly been identified to decay with the half-life of 29 ± 2 s.[33] Searches for other new isotopes are now in progress.

6. Remarks

The ISOL facility KUR-ISOL described here has originally been constructed as a model machine for ISOL which is to be installed at the planned HFR. The apparatus now in use, therefore, is far from satisfactory for various kinds of works. Improvements on the safety-interlock, vacuum exhausting and mass-analyzing systems as well as on the target-capillary and ion source systems are keenly requested to ensure safe operation of the apparatus, to stabilize the operation at extreme conditions, to increase the ionization efficiencies, to extend the region of elements available and to increase the mass-resolving power. In order to extend the experiments to a new field of research,provision of ingenious detection systems such as a large crystal total γ absorption spectrometer or a HPGe multicounter goniometer is also necessary.

Acknowledgement

The authors are grateful to Prof. T. Shibata and Emeritus Prof. T. Hayashi for their continuous supports and interests to this work. They are also indebted to Prof. I. Fujiwara for his kind supports. This work was supported by a Grant-in-Aid of the Ministry of Education, Science and Culture.

REFERENCES

(1) OKANO, K., et al. : KURRI-TR-93, 41 (1971).
(2) OKANO, K.: KURRI-TR-110, 33 (1972).
(3) SHIBATA, T.: KURRI-TR-93 5 (1971).
(4) OKANO, K., KAWASE, Y.: KURRI-TR-146, 4 (1976).
(5) OKANO, K., et al.: Nucl. Instrum. Methods, 186, 115 (1981).
(6) KAWADE, K., et al.: Nucl. Instrum. Methods, 200, 417 (1982).

(7) KAWASE, Y., et al.: Nucl. Instrum. Methods, 241, 305 (1985).
(8) KAWASE, Y., et al.: Annu. Rep. Res. Reactor Inst. Kyoto Univ., 14, 181 (1981).
(9) MAZUMDAR, A. K., et al.: Nucl. Instrum. Methods, 174, 183 (1980).
(10) ZIRNHELD, J. P., et al.: Nucl. Instrum. Methods, 158, 409 (1979).
(11) MÜNZEL, J., et al.: Nucl. Instrum. Methods, 186, 343 (1981).
(12) OKANO, K., et al.: KURRI-TR-266, 42 (1985).
(13) FUNAKOSHI, Y.: Master thesis, Kyoto Univ. (1981), (unpublished), in Japanese.
(14) KAWADE, K., et al.:Annu. Rep. Res. Reactor Inst. Kyoto Univ., 16, 125 (1983).
(15) FUNAKOSHI, Y., et al.: Nucl. Phys., A431, 461 (1984).
(16) MITAMURA, T., et al.: KURRI-TR-266, 37 (1985).
(17) OKANO, K., et al.: Thorium Fuel Reactors, (SHIBATA, T., ed.), p. 112 (1985), The Atomic Energy Society of Japan.
(18) ISHII, T., et al.: Annu. Rep. Res. Reactor Inst. Kyoto Univ., 17, 122 (1984).
(19) KAWADE, K., et al., to be published.
(20) OKANO, K., et al.: Annu. Rep. Res. Reactor Inst. Kyoto Univ., 16, 47 (1983).
(21) OKANO, K., et al.: Annu. Rep. Res. Reactor Inst. Kyoto Univ., 17 110 (1984).
(22) OKANO, K., et al., to be published in Ann. Nucl. Energy.
(23) ISHII, T., et al.: Annu. Rep. Res. Reactor Inst. Kyoto Univ., 17 132 (1984).
(24) OKANO, K., et al.: to be published in J. Phys., G (London).
(25) DEBERTIN, U., et al.: Ann. Nucl. Energy, 2, 37 (1975).
(26) HOPKE, P. K., MEYER, R. A.: Phys. Rev. C13, 434 (1976).
(27) "Table of Isotopes", 7th Edition, (LEDERER, C. M., ed.), (1978), John Wiley & Sons, New York.
(28) "Nuclear Data Sheets", (National Nuclear Data Center), Academic Press, New York.
(29) OKANO, K., et al.: Annu. Rep. Res. Reactor Inst. Kyoto Univ. 16, 108 (1983).
(30) OKANO, K., et al., to be published in Int. J. Appl. Radiat. Isotop.
(31) PAHLMANN, B., et al.: Z. Phys. A-Atoms and Nuclei, 308, 345 (1982).
(32) KAWASE, Y., et al.: Z. Phys. A-Atoms and Nuclei, 318, 191 (1984).
(33) OKANO, K., et al.: to be published in J. Phys. Soc. Jap.

Table 1 Typical parameters of KUR-ISOL

Target	93% enriched ^{235}U 10mg (0.5mg/cm^2)
Neutron flux	3×10^{12} n/cm^2.s (max.)
He-jet system	
Capillary	0.1cm(inner dia.)x11.5m
He pressure	1~2atm, max. 3.0atm
He flow rate	5~15cm^3·atm/s
Aerosol generator	Sinclair-LaMer type: DOP(100~120°C) with NaCl nuclei(550~600°C) and reheater(≈150°C)
Skimmer	Two-stage flat type: 1st stage;1.5mmφ, 2nd stage;3.5mmφ
Ion source	High-temperature thermal type:
	Temperature;1500~3000°C
	Ionized elements;Rb, Sr, Cs, Ba, rare-earth
	Nielsen type:
	Temperature; ≈1500°C
	Ionized elements;Kr, Rb, Sr, Sn, Sb, Te, I, Xe, Cs, Ba
Accelerating and focusing system	
Type	Electrostatic focusing by an einzel lens
Voltage	Acceleration;26~30kV, extraction;13~14kV, focusing;10~13kV
Vacuum	≤ 1×10^{-5}mmHg(acceleration chamber) $2\sim4\times10^{-6}$mmHg(focusing chamber)
Mass analyzing system	
Type	Double focusing by a fringing field
Deflection radius	60cm
Deflection angle	45°
Measured mass resolution(FWHM)	600(Xe), 280(rare-earth)
Overall efficiency	2×10^{-3} (^{140}Cs)

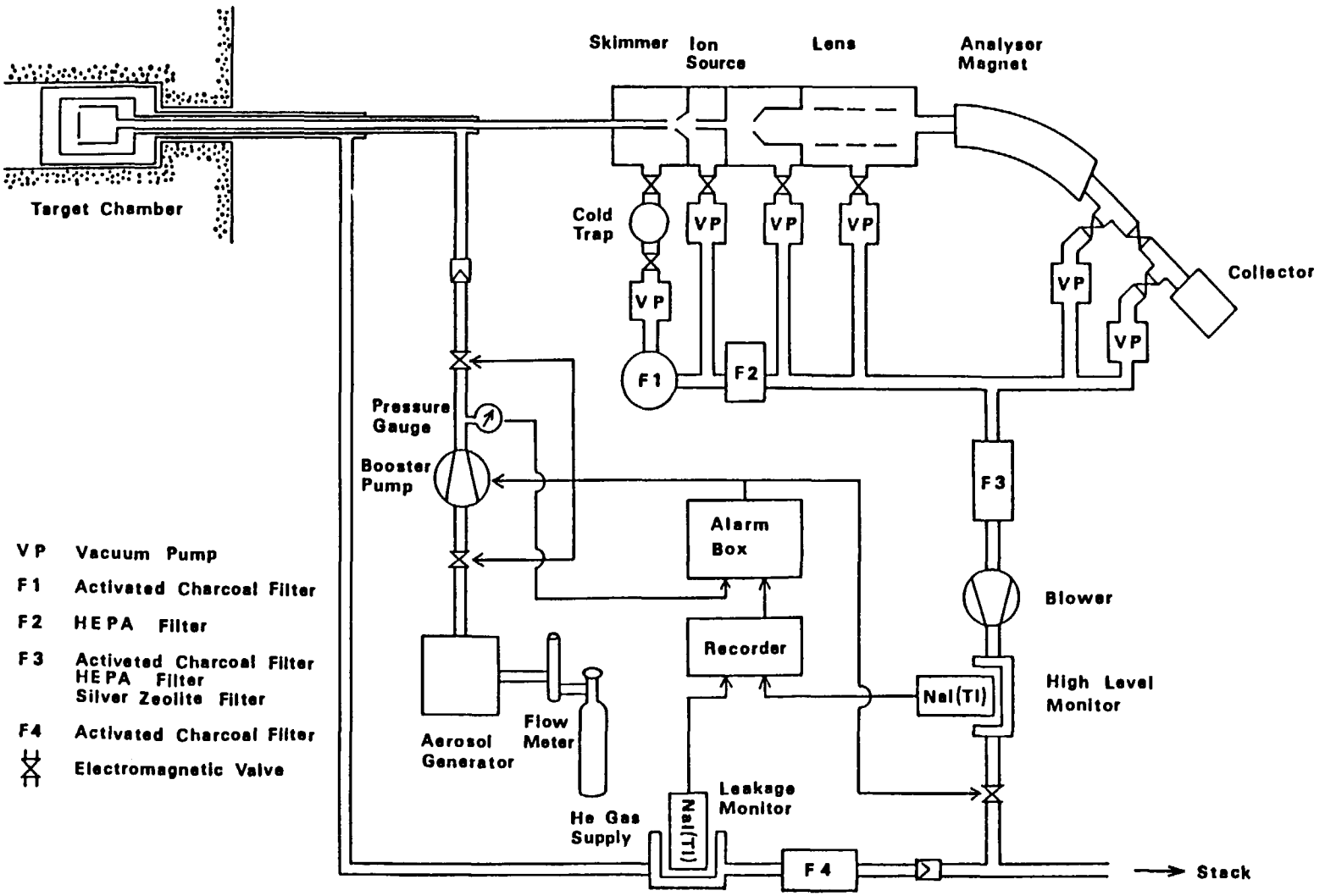

Fig. 1 Schematic diagram of KUR-ISOL showing the He-gas flow path.

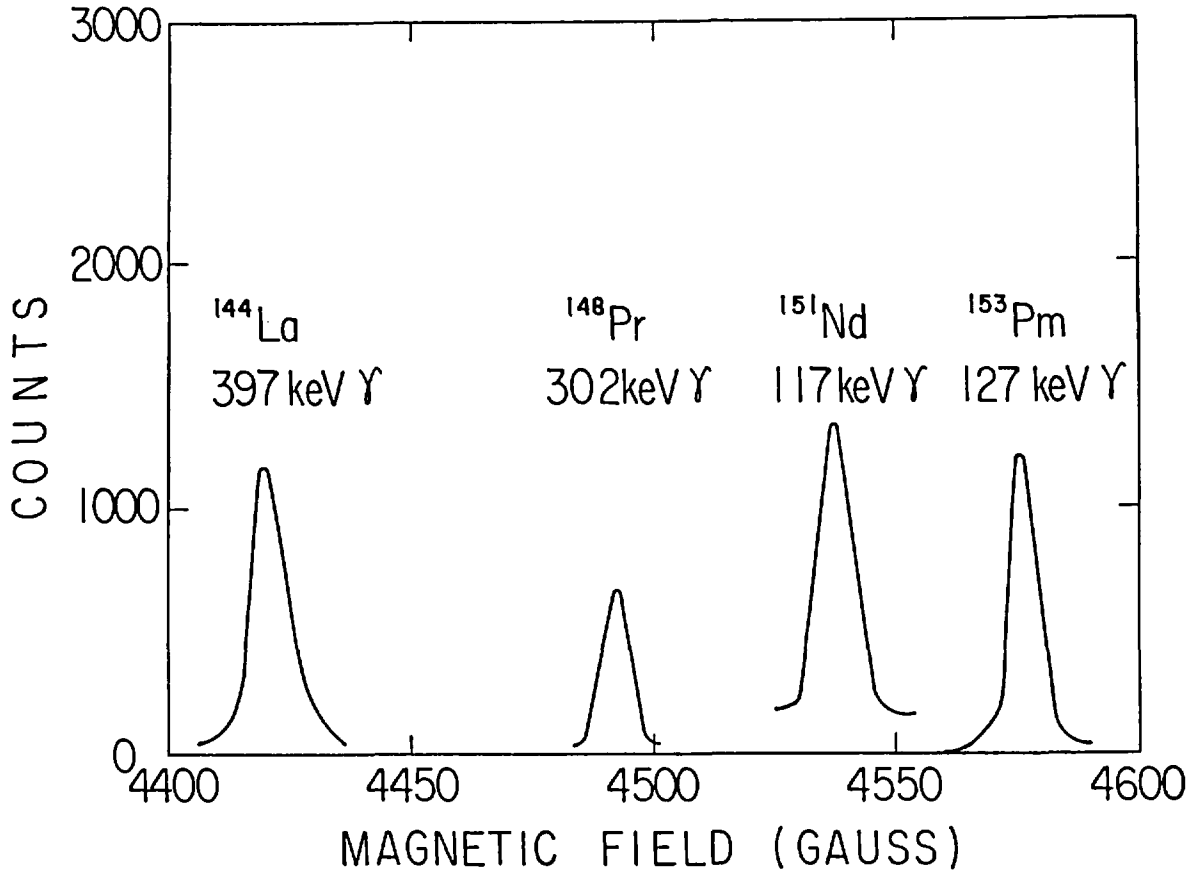

Fig. 2 Mass spectrum of rare-earth elements separated by KUR-ISOL.

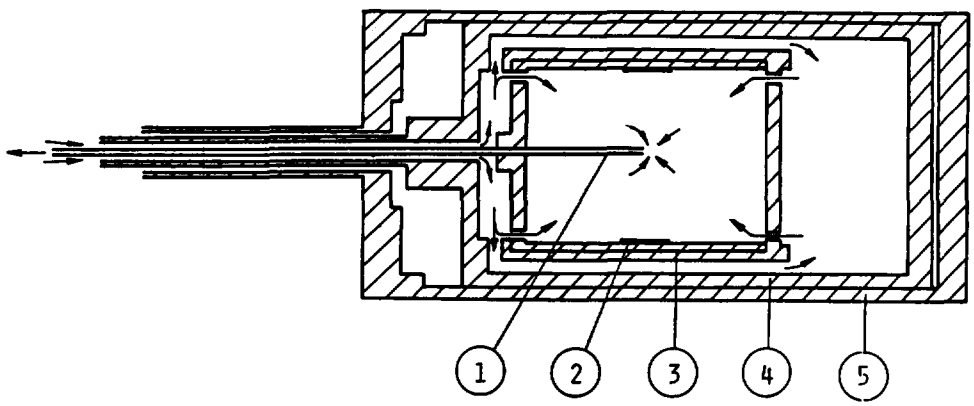

Fig. 3 Target chamber for fission products. The He gas flows as shown by arrows. 1. Capillary(1.0mm in inner diameter), 2. ^{235}U target(0.5mg/cm^2 in thickness), 3. inner chamber, 4. middle chamber, 5. outer chamber.

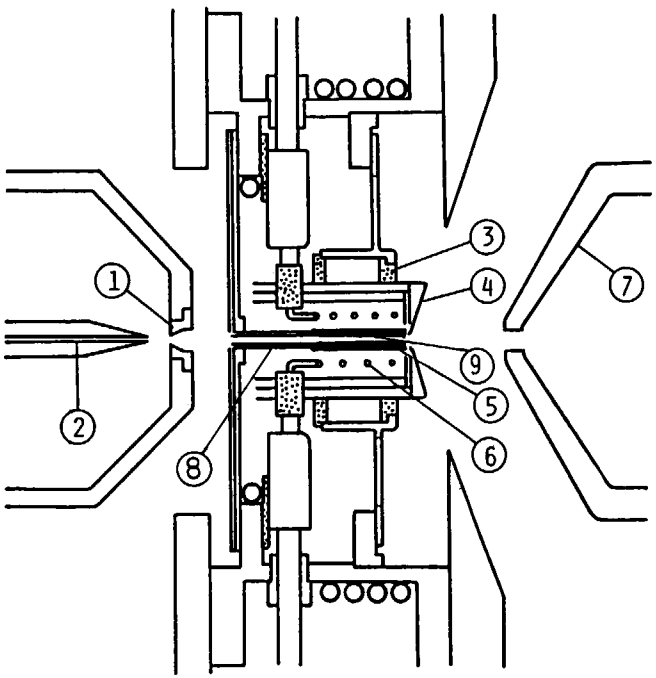

Fig. 4 High-temperature thermal ion source for He-jet type
ISOL. 1. Skimmer, 2. capillary,
3. insulator(BN), 4. thermal shield(Ta and Mo),
5. ionization chamber(W), 6. filament(W),
7. extractor(C), 8. inner capsule(W),
9. rhenium foil.

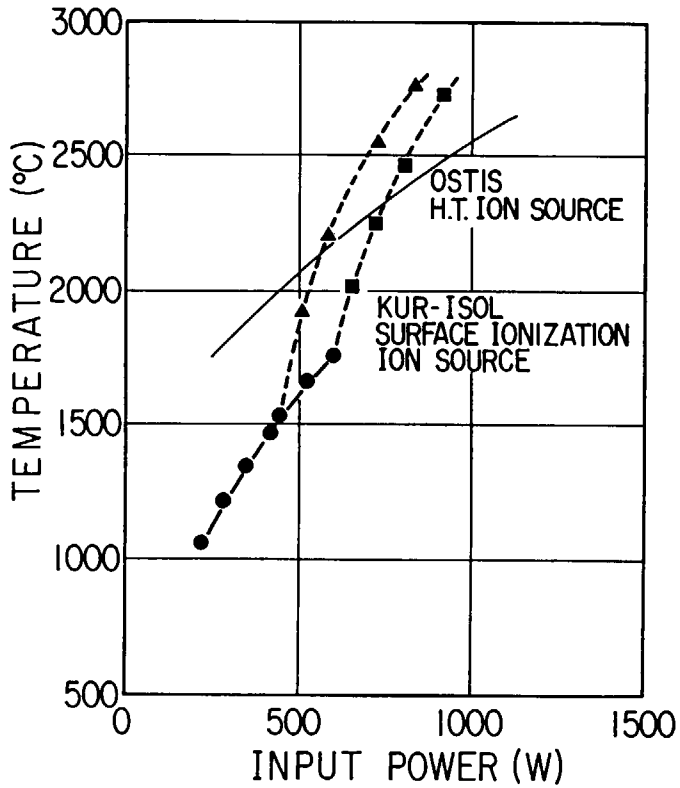

Fig. 5 Temperature of the tungsten ionizer of the high-tempe- rature thermal ion source heated by the radiation from the filament(solid circles)and by the bombardment of electrons (solid triangles and squares). For reference, temperature of the similar ion source of OSTIS(ISOL at Grenoble) is also shown. The data shown were taken without the inner capsule(see Fig. 4.).

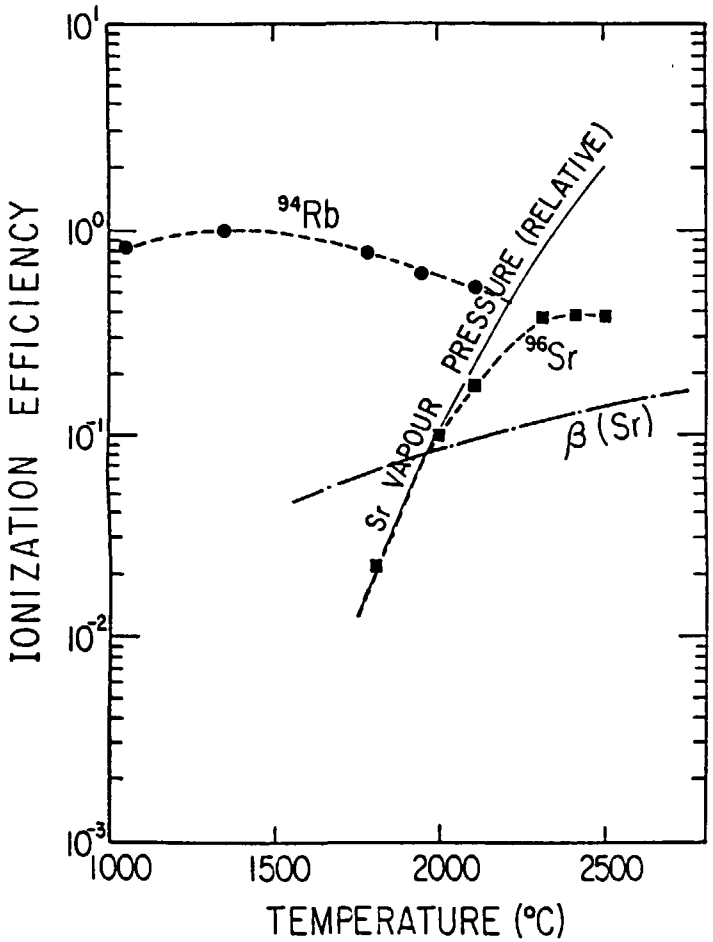

Fig. 6 (a) Ionization efficiencies for Rb and Sr assuming $\eta_{Rb}^{max}=1$. A solid line shows a vapour pressure curve for Sr normalized to the relative efficiency curve at lower temperature. Calculated values by a Langmuir equation for a rhenium ionizer, β (Sr), are given by a dot-and-dash line. Dashed lines are drawn to guide the eye.

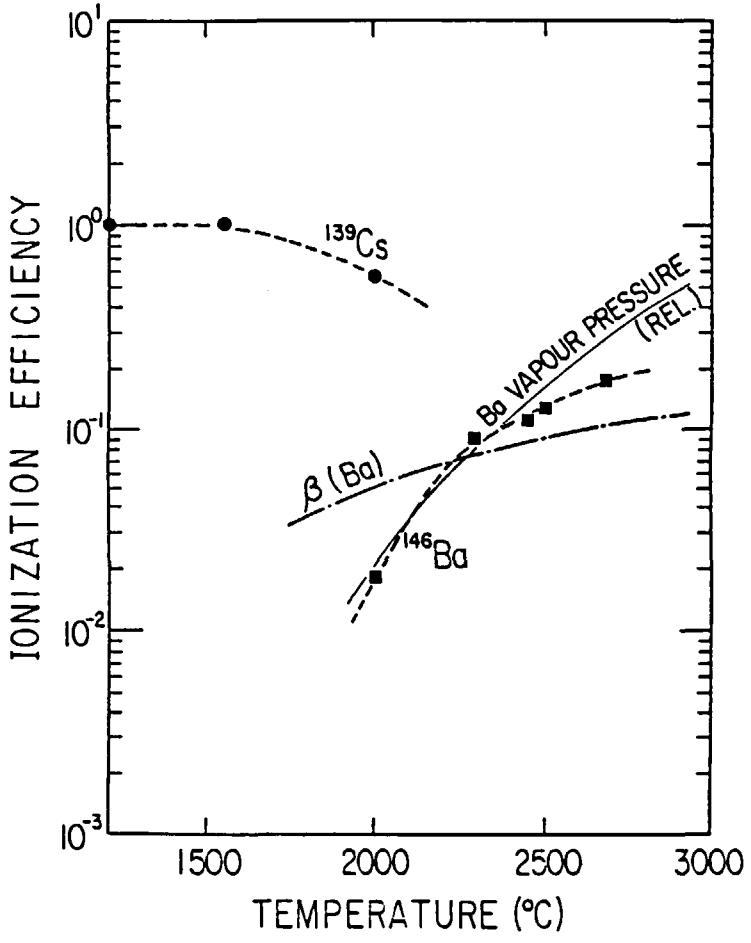

Fig. 6 (b) Same as Fig.7 (a) but for Cs and Ba assuming $\eta_{Cs}^{max}=1$. Langmuir estimates for a tungsten ionizer, β (Ba), are given by a dot-and-dash line, as this measurement was performed without a rhenium foil.

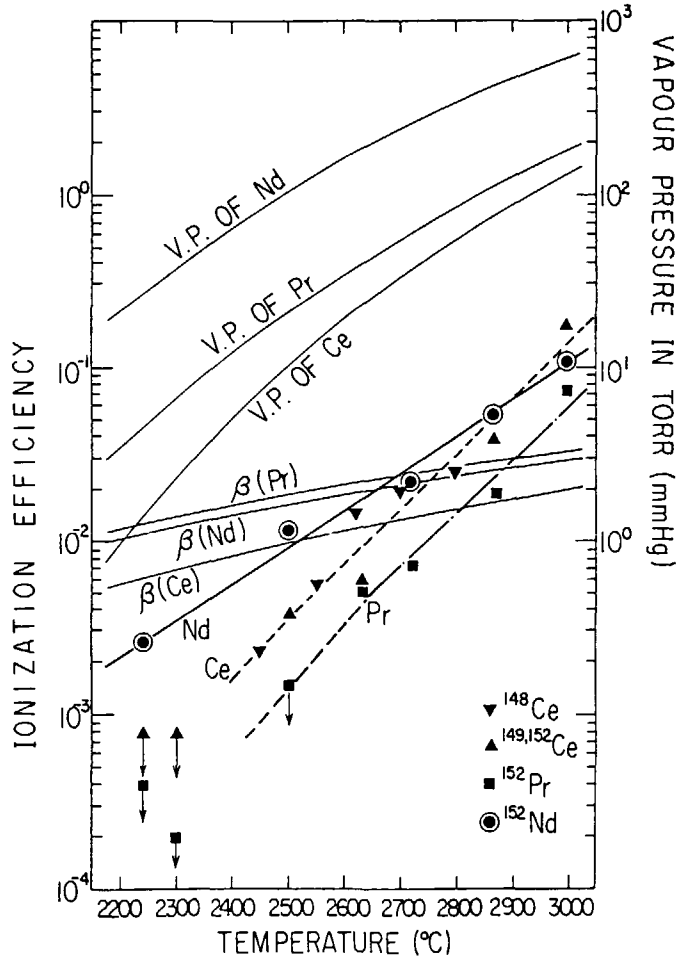

Fig. 7

Ionization efficiencies for Ce, Pr and Nd as a function of the ionizer temperature. Vapour pressure curves for these elements are given in the upper part of the figure. Calculated values of β for a tungsten ionizer are also shown.

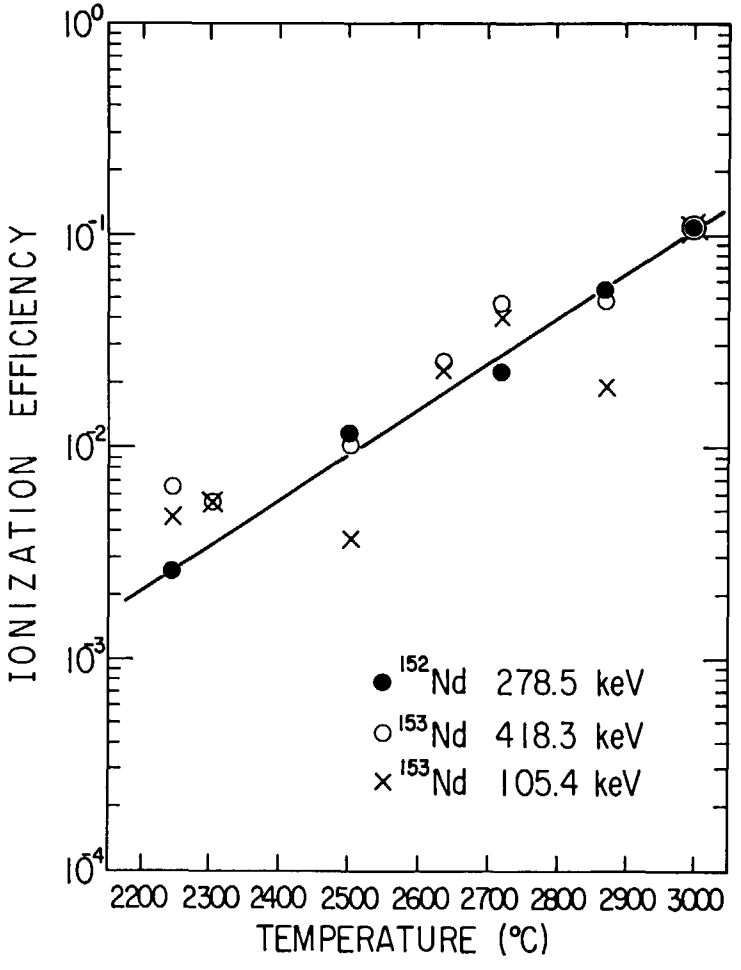

Fig. 8

Ionization efficiencies of Nd isotopes as a function of the ionizer temperature, measured by the yields of the 278.5 keV (^{152}Nd), 105.4 keV(^{153}Nd) and 418.3 keV (^{153}Nd) γ-rays. The yields are normalized at 3000 °C.

12) Kyoto University Reactor Fission Plate (Energy Converter)

Hiroshi Chatani, Keiji Kanda, Keiji Kobayashi
Tooru Kobayashi

Research Reactor Institute, Kyoto University
Kumatori-cho, Sennan-gun, Osaka 590-04, Japan

Abstract

For the estimation of the nuclear data, it is required a number of experimental results of cross section values with various neutron sources. As one of the fast neutron sources, we report the Kyoto University Reactor(KUR) fission plate which have a many advantages in measurement of cross sections; (1) well known fission neutron spectrum (2) high fast neutron flux as 10^9 n/sec/cm^2, extremely low thermal neutron back ground etc. These characteristics and the specifications of the plate are refered in this report. Furthermore, we explain some results of the cross section measurements for the several nuclides by making use of the fission plate.[1]-[4]

The energy spectrum of the fission plate has not been directly measured, however, it is confirmed to be a fission spectrm by means that the neutron fluxes measured with several fission neutron spectrum averaged cross sections are in good agreement with each other.[3][4]

Introduction

The objective of the KUR fission plate is to obtain the standard neutron field with fission spectrum, which is provided in the heavy water thermal neutron facility of KUR.

The field of applications of the fission plate is very wide; such as, measurements of the averaged cross sections, calibrations of fast neutron detectors, slowing-down experiments of fission neutrons [5]. In the measurement of the cross sections, the characteristics of the plate have various advantages. We report that the characteristics and specifications of the fission plate and also the applied studies with the fission plate.

Specification of the Fission Plate and the Characteristics of the Irradiation Facility

Neutron flux

The principal items of the specifications and the characteristics are tabulated in Table 2. Figures 2 and 3 show the neutron flux distributions, along the axis and the surface of the fission plate, respectively.[6] In the figures, the cadmium collimaters keep down the surplus neutrons, which leak out from the experimental facility.

Thermal neutron fluxes were measured using gold foils with and without cadmium covers, and fast neutron fluxes were also measured using the reaction of $^{103}Rh(n,n')^{103m}Rh$, whose averaged cross section is 558mb [7] and the effective threshold energy is 1.28MeV.

Irradiation

The samples were irradiated at the center on the surface of the fission plate. Fission neutron flux at the irradiation position is high: 10^9n/sec/cm^2, whereas the thermal neutron flux is 2 decards lower than the fast one as

shown in Table 3[3] and Fig.s 2 and 3[6]. A surface areas of the plate is extent and the incident neutrons to the surface is of uniformity at the varied places. These aspects mean that the measurement of γ-rays from the product nuclides induced from the threshold reactions is precisely performed, because that the activity induced by thermal neutrons is extremely low, and that the simultanious irradiation of several activation foils under the same condition is possible.

The details of the heavy water facility are discribed in reference [8]

Manipulation

A well devised remote control system is attached, which makes it possible to perform the experiments during the continuous reactor operation. The functions of the system are (1) putting the fission plate back in its lead container, and vice versa, and (2) continuance and discontinuance of irradiation by making use of a 0.7 mm thick cadmium shutter.

Pulling out the samples outside of the irradiation room is easily done by using a string fastened the samples, which makes the irradiation time to be estimated exactly.

Circumstance of the Utilization of the Fission Plate on Nuclear Data

A number of experimental nuclear data are indispensable for the sake of the good estimation of nuclear data. So far, some threshold reaction cross sections using the fission plate have been reported by Kobayashi, Kimura et al.[1]. and Kanda, Chatani et al.[2]. No report on the experimental cross section value of the $^{232}Th(n,2n)^{231}Th$ for fission neutrons using the fission plate has been published,

except the one which has been reported by one of the authors.[3] O.Horibe[9] has proposed "a new empirical rule for the estimation of fission neutron spectrum averaged cross section of (n,p) and (n,α) reactions", through the new measurement of the cross sections, using the fission plate, [4] in the Visiting Researcher's Program of Research Reactor Institute of Kyoto University.

1.] Kobayashi,K. and Kimura,I.: Proc. of the 3rd ASTM -EURATOM Symp. on the Reactor Dosimetry, EUR-6813, Vol.11, pp.1004-1015,(1980).

2.] Kanda,K.,Chatani,H., et al. Annu. Rep. Res. Reactor Inst. Kyoto Univ., 4, pp.94-98,(1971).

3.] Chatani,H.: Nucl. Inst. Meth., 203, pp.501-504, (1983).

4.] Horibe,O.: Int. Con. on Nucl. Data for Basic and Applied Sci., Santa Fe, New Mexico, U.S.A., May 13th-17th,(1985).

5.] Kanda,K.,Kobayashi,K.,Chatani,H. et al.: "Neutron Energy Converter of Fission Pate Type": KURRI-TR-96,(in Japanese),(1972).

6.] Kobayashi,T.,Kozuka,T.,Chatani,H.,Kanda,K., et al.: Annu. Rep. Res. Reactor Inst. Kyoto Univ., 18,pp.133 -138,(1985).

7.] Kimura,I.,Kobayashi,K., et al.: J. Nucl. Sci. Technology, 6, pp.485-493.(1986).

8.] Kanda,K., Kobayashi,K., et al.: Nucl. Inst. Meth.,148, p.p.535-541,(1987).

9.] Horibe,O.: Ann. Nucl. Energy, 10, pp.359-373,(1983).

Table 1 Specification of Fission Plate

shape:	disk
geometrical diameter:	31 cm
effective diameter:	27 cm
equivalent thickness of uranium:	1.95 g/cm
uranium enrichiment:	99 %
total uranium:	1114.19 g
total uranium-235:	1002.00 g
chemical form:	UO_2-Al cermet

Table 2 Characteristics of Irradiation Facility

High intensity neutron flux,(see Fig.3).
Pure fission neutrons.
* Thermal neutrons incident to the plate have a Maxwellian distribution.
* Fast neutron background in incident neutrons is negligible.
* Fast neutron fluxes obtained by several investigators from the fission spectrum averaged cross sections are in good agreement with each other,(see Table 3).

Large irradiation room,(see Fig.1).
* Return neutrons from the wall of the exposure room is negligible.

Remote control irradiation,(see Photo.1).

Table 3 Measured fast neutron flux and nuclear data used, (KUR:5MW). (from Ref.3)

Reaction	Isotope abundance (%)	Cross section (mb)	Half-life	Measured γ-ray (keV) and its intensity (%)	Fast neutron flux ($\times 10^9$ cm^{-2} s^{-1})
^{24}Mg(n, p)^{24}Na	79	1.62 [15]	15.0 h	1369 (100)	1.53 ± 0.03
^{46}Ti(n, p)^{46}Sc	8.2	11.2 [16]	83.8 d	889 (100)	1.56 ± 0.03
				1120 (100)	1.56 ± 0.04
^{47}Ti(n, p)^{47}Sc	7.4	19 [16]	3.43 d	160 (68.5)	1.58 ± 0.03
^{58}Ni(n, p)^{58}Co	68.3	112 [17,18]	70.3 d	511 (30)	1.53 ± 0.03
				811 (99.4)	1.57 ± 0.03
				Weigted mean:	1.56 ± 0.08

Table 4 Comparison of measured averaged cross section and the previous results, (in mb). (from Ref.1)

Reaction	Present work ^{235}U plate	Present work YAYOI core	Previous data YAYOI core 3)	Zijp (calc.)[15]	Calamand[16]
^{24}Mg(n,p)^{24}Na	1.38 ± 0.07	1.35 ± 0.07	1.36 ± 0.065	1.451	1.53 ± 0.09
^{27}Al(n,p)^{27}Mg	3.65 ± 0.20	3.64 ± 0.21	3.64 ± 0.17	4.059	4.0 ± 0.45
^{31}P(n,p)^{31}Si	33.5 ± 2.0	34.0 ± 2.5		32.81	36 ± 3
^{32}S(n,p)^{32}P	64.7 ± 3.8			65.42	69 ± 4
^{51}V(n,p)^{51}Ti			0.456±0.023		0.87 ± 0.11
^{52}Cr(n,p)^{52}V	1.06 ± 0.11	1.07 ± 0.07			1.09 ± 0.08
^{53}Cr(n,p)^{53}V		0.306±0.027			0.44 ± 0.04
^{54}Fe(n,p)^{54}Mn	78.1 ± 3.7	76.7 ± 4.6		77.96	82.5 ± 5
^{56}Fe(n,p)^{56}Mn	1.02 ± 0.05	0.997±0.06		1.019	1.07 ± 0.08
^{59}Co(n,α)^{56}Mn		0.143±0.008	0.131±0.0061	0.1421	0.156±0.009
^{64}Zn(n,p)^{64}Cu			30.9 ± 2.1	42.81	31 ± 2.3
^{93}Nb(n,n')^{93m}Nb	122 ± 9 *				87 ± 14
^{113}In(n,n')^{113m}In		155 ± 13			
^{197}Au(n,2n)^{196}Au	3.00 ± 0.16	3.09 ± 0.17			3.0 ± 3

* Uncertainties of the half life and the branching ratio of ^{93m}Nb are not included.

Table 5 Comparison of averaged cross section for the $^{232}Th(n,2n)^{231}Th$ reaction, (from Ref.3).

Cross section (mb)	Ref.
15.5 ± 1.2	Present value, measured with a fission plate
16	Pearlstein [12], predicted value
15	Zijp and Nolthenius [13], calc. value
12.5 ± 0.84	Kobayashi et al. [4], measured in the KUR core
12.4 ± 0.6	Phillips [8], measured in the BEPO core

Table 6 Value of the cross sections measured and estimated, deviation factors and nuclear data used, (from Ref.4).

Reaction	Isotope abundance (%)	Half-life	Measured γ-ray (keV) and intensity (%)	[a] Cross-section Measured (mb)	[b] Estimated (mb)	Deviation Factor (a/b)*
$^{27}Al(n,p)^{27}Mg$	100	9.46 m	843.8 (73.0)	4.4±0.3	9.37	2.34
$^{42}Ca(n,p)^{42}K$	0.647	12.36 h	1524.6 (18.8)	3.4±0.3	1.96	1.73
$^{43}Ca(n,p)^{43}K$	0.135	22.3 h	617.8 (80)	2.7±0.2	2.03	1.34
$^{47}Ti(n,p)^{47}Sc$	7.4	3.42 d	159.4 (68.5)	21.2±0.9	8.73	2.43
$^{48}Ti(n,p)^{48}Sc$	73.7	43.7 h	983.5 (100)	0.29±0.02	0.595	2.05
$^{56}Fe(n,p)^{56}Mn$	91.8	2.579 h	846.8 (98.87)	1.13±0.06	0.411	2.75
$^{59}Co(n,p)^{59}Fe$	100	44.6 h	1099.2 (56.5)	1.54±0.09	0.874	1.75
$^{60}Ni(n,p)^{60}Co$	26.1	5.271 y	1173.2 (100)	2.4±0.3	1.30	1.85
$^{61}Ni(n,p)^{61}Co$	1.13	1.65 h	67.4 (86)	1.43±0.08	1.10	1.3
$^{64}Zn(n,p)^{64}Cu$	48.6	12.70 h	1345.6 (0.6)	32±2	48.3	1.52
$^{67}Zn(n,p)^{67}Cu$	4.10	61.9 h	184.5 (47)	1.17±0.07	2.51	2.15
$^{84}Sr(n,p)^{84}Rb$	0.56	32.9 d	881.6 (74)	5.7±0.5	6.29	1.1
$^{86}Sr(n,p)^{86}Rb$	9.8	18.8 d	1076.6 (8.79)	0.70±0.08	1.40	2
$^{92}Mo(n,p)^{92m}Nb$	14.8	10.15 d	934.7 (99.2)	7.3±0.4	7.19	1.02
$^{95}Mo(n,p)^{95}Nb$	15.9	35.0 d	765.2 (99.82)	0.20±0.02	0.208	1.04
$^{96}Mo(n,p)^{96}Nb$	16.7	23.4 h	1091.3 (49.4)	0.027±0.003	0.0524	1.94
$^{103}Rh(n,p)^{103}Ru$	100	39.4 d	497.1 (86.4)	0.125±0.007	0.171	1.37
$^{115}In(n,p)^{115}Cd$	95.7	53.58 h	527.7 (33.8)	0.009±0.001		
$^{115}In(n,p)^{115m}Cd$	95.7	44.8 d	933.6 (2.0)	0.05±0.01	0.0342	1.73
$^{132}Ba(n,p)^{132}Cs$	0.101	6.47 d	667.5 (97.5)	(0.5±0.3)	0.147	(3)§
$^{140}Ce(n,p)^{140}La$	88.5	40.3 h	1596.5 (95.5)	0.006±0.002	0.00122	5.56
$^{45}Sc(n,\alpha)^{42}K$	100	12.36 h	1524.6 (18.8)	0.27±0.02	0.333	1.23
$^{50}Ti(n,\alpha)^{47}Ca$	5.2	4.536 d	1297.1 (77)	0.021±0.004	0.0102	2.06
$^{54}Fe(n,\alpha)^{51}Cr$	5.8	27.70 d	320.1 (10.2)	1.0±0.2	0.992	1.01
$^{59}Co(n,\alpha)^{56}Mn$	100	2.579 h	846.8 (98.87)	0.18±0.01	0.136	1.32
$^{68}Zn(n,\alpha)^{65}Ni$	18.8	2.52 h	1481.8 (23.5)	0.08±0.03	0.11	1.38

* If a is larger than b, then the ratio is given by a/b, otherwise, b/a.

§ Values in parenthises are not yet definite ones, because of interference with the 665 keV γ peak of the natural background.

The above nuclear data were quoted from the same reference used in TABLE II.

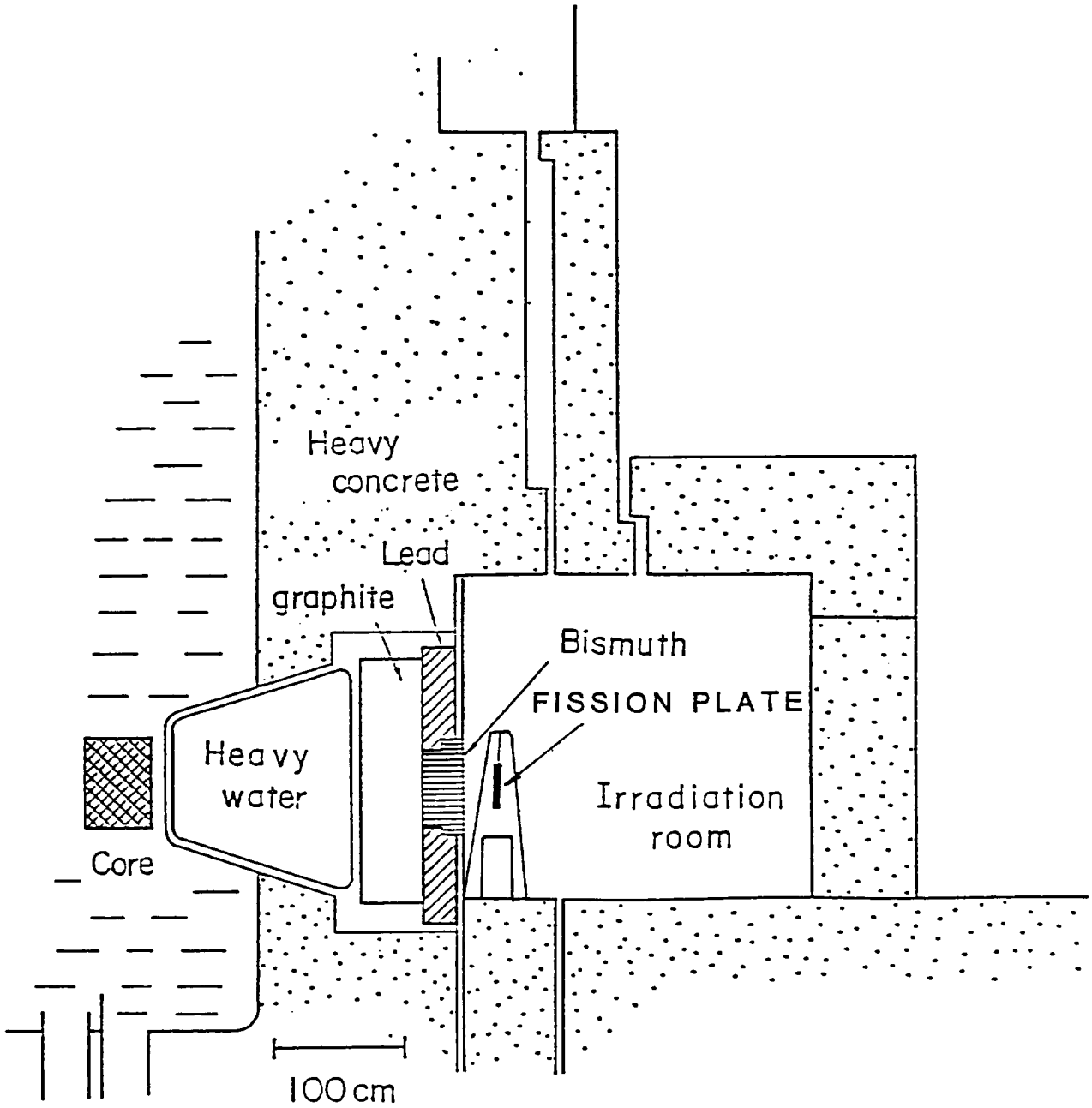

Fig.1 Schematic drawing of the experimental facility provided with the fission plate.

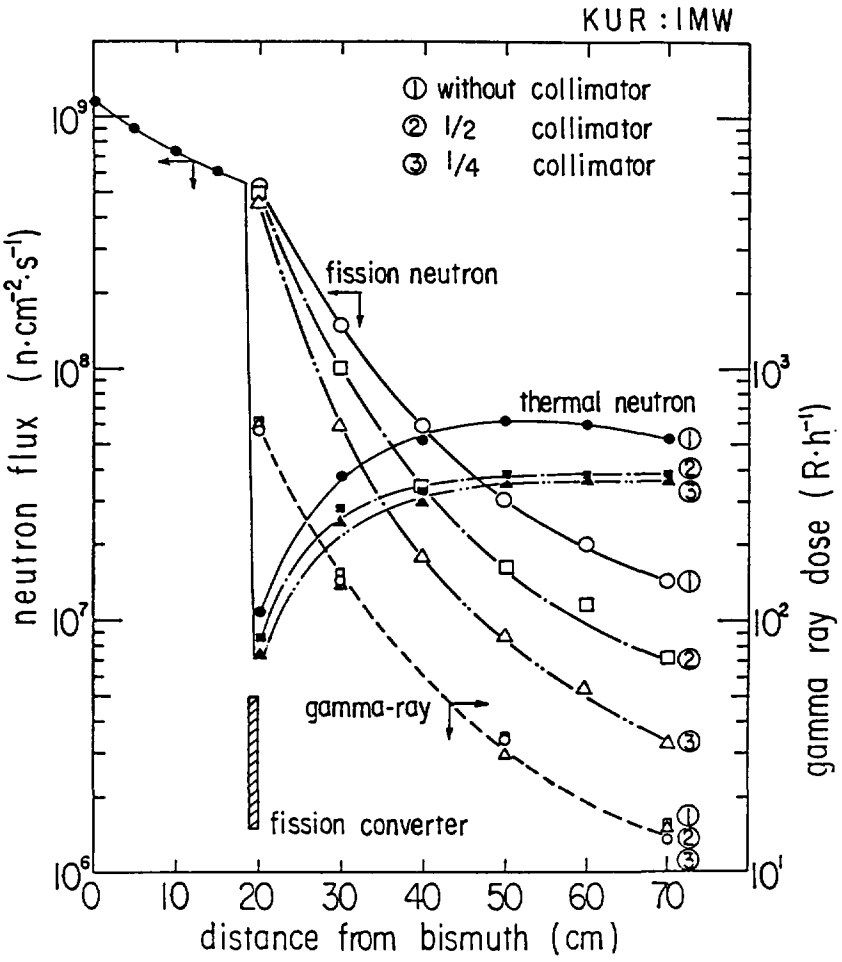

Fig.2 Distribution of neutron flux along the axis of the fission plate with and without cadmium collimator.

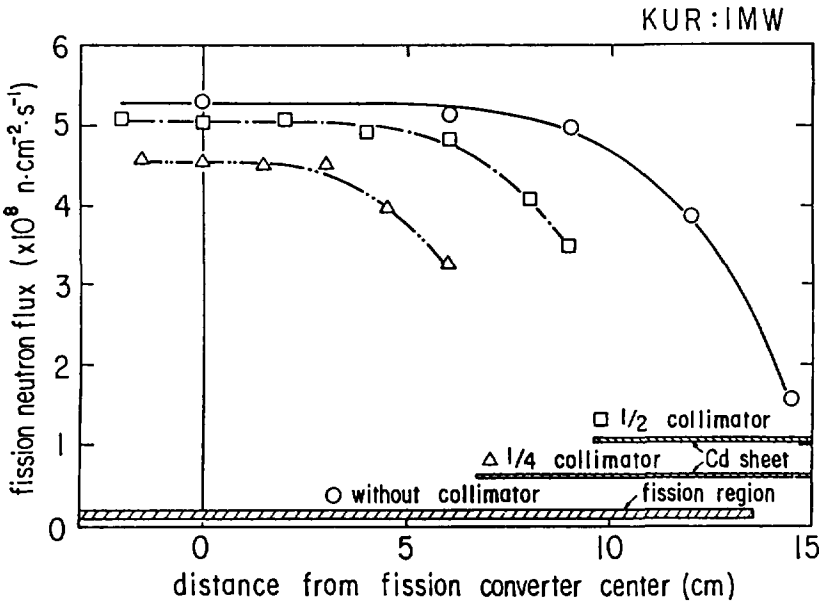

Fig.3 Fission neutron flux on the surface of the fission plate.

Photo.1 The U-235 fission plate with the remote control system and the threshold detectors.

13) THERMAL NEUTRON STANDARD FIELD USING THE KUR HEAVY WATER FACILITY

Keiji Kanda, Keiji Kobayashi

Research Reactor Institute, Kyoto University,
Kumatori-cho, Sennan-gun, Osaka, Japan

ABSTRACT

A heavy water facility attached to the KUR (Kyoto University Reactor, swimming pool type, 5MW) yields pure thermal neutrons with a Maxwellian distribution.

The facility is placed next to the core of KUR and contains about 2t of heavy water. The width of the heavy water layer is about 140cm.

The neutron spectrum was measured with the time-of-flight technique using a fast chopper. The measured spectrum was in good agreement with a Maxwellian distribution in the whole energy region for thermal neutrons. The neutron temperature was slightly higher than the heavy water temperature.

The contamination of epithermal and fast neutrons caused by photo-neutrons from the γ-n reaction in heavy water is very small. The maximum intensity of thermal neutrons is 3×10^{11}n/cm.s. When a bismuth scatterer is attached, the gamma ray contaminations is decreased to a ratio of 0.05 of gamma rays to neutron in Rem.

This standard neutron field has been used for such experiments as thermal neutron cross section measurement, diffusion length measurement, detector calibration, activation analysis and for biomedical purposes.

INTRODUCTION

In order to offer a universal means of comparison between one experiment and others, or between calculation and experiment, a thermal neutron standard field should satisfy the following conditions:

a) the neutron source should produce mainly thermal neutrons,
b) the neutron spectrum must be known,
c) the spectrum does not depend on a certain facility itself, that is, it must be common, universal and reproducible,

d) the spectrum can be expressed in analytical form, if possible,
e) the absolute value of neutron fluence should be known,
f) the intensity of neutron fluence is variable in a wide range,
g) the direction of neutron current is known, e.g. beam or isotropic field etc.,
h) the contamination with other radiation, i.e. gamma radiation, fast neutrons etc., is reduced as low as possible to eliminate unwanted nuclear reactions.

The thermal neutron fields obtained in our institute are shown in table 1, which shows the advantages of the heavy water facility. This is due mainly to the characteristics of different moderators, as shown in table 2. Since such solid moderators as graphite and beryllium have crystalline structure in the neutron cross section, the spectrum of neutrons from these moderators has a discontinuous structure on the low energy side.

In the present paper, the characteristics of the KUR heavy water facility[1]) are described; this facility has served as the standard neutron field for such experiments as thermal neutron cross section measurement, diffusion length measurement, detector calibration, activation analysis, and biomedical purposes.

FACILITY

The heavy water tank containing 2t of heavy water is placed next to the core of KUR (Fig. 1). The thickness of the heavy water layer is about 1.4m. The tank has the shape of a trapezoid cone and is made of aluminum, of which the thickness on the neutron outlet side is 10mm.

The purity of the heavy water is 99.75%. The temperature is continuously measured by a thermocouple, and is usually kept at about 40°C.

Outside the heavy water layer, a removable graphite layer 48cm thick and a removable bismuth layer 15cm thick are placed. For irradiation purposes, there is an irradiation room of 2.4m × 2.4m × 2.4m, surrounded by 90cm thick heavy concrete.

In the graphite layer, the bismuth scatterer[2]) can be attached; this reduces the gamma ray contamination to the ratio of 0.05 of gamma-rays to neutrons in Rem (0.96×10^9 neutrons = 1 Rem).

A fission plate of 90% enriched uranium of 29cm in diameter is attachable to offer a fission neutron field[3]).

The advantage of the facility is that Maxwellian neutrons are available for various kind of experiments; the leakage neutrons in a large space can be used as the neutron source of beam or plane type, while by using neutrons inside the moderator the application for the standard neutron field is restricted.

EXPERIMENT

Neutron Spectrum Measurement

The experimental arrangement is shown in Fig.2. The detail of the neutron collimator is shown in Fig.3. The neutron spectra obtained from the facility and heavy water samples were measured with the time-of-flight technique using a fast chopper with a perpendicular rotor of K-monel as shown in Fig.4. The block diagram of the electronic circuit is shown in Fig.5. The length and diameter of the flight tube were 5m and 10cm respectively. A BF_3 counter shielded with boric anhydride and cadmium sheet was used as a neutron detector.

The measured spectra were on neutron(1) from the surface of the heavy water tank, (2) from the graphite layer, (3) from the heavy water can of 60cm in diameter and 100cm in height and (4) from the can of 15 × 15 × 10cm^3, both placed in the irradiation room.

Neutron Flux and Gamma Ray Dose Rate Measurement

The intensity of neutron flux was measured with gold foils of 3mm in diameter and 0.05mm thick. The induced activity was counted by a $4\pi\beta$-γ coincidence equipment and a well-type NaI(Tl) scintillator. The gamma ray dose was measured with thermoluminescence detectors of $CaSO_4$ encased in polyethylene pipes 1mm in diameter and 10mm long, which were insensitive to thermal neutrons.

RESULTS AND DISCUSSION

Neutron Spectrum

The obtained time spectrum was converted to an energy spectrum after several corrections: (1) chopper transmission, (2) neutron arrival probability to the detector, (3) detector efficiency, (4) background and (5) dead time of the multichannel analyzer.

Fig.6 shows the neutron spectra from the heavy water tank (a) and the graphite layer (b). The former is in good agreement with a Maxwellian distribution of 60°c, which is slightly higher than the heavy water temperature of 40°c, while the latter shows several structures due to the crystal fine properties of graphite. In neither case were epithermal neutrons observed. This was supported by the fact that the cadmium ratios of a gold foil for (a) and (b) were 5 × 10^3 and 10^4 respectively. In the case of the heavy water (a), however, a very small contamination of fast neutrons was observed, which may be due to photo-neutrons from deuterium.

CONCLUDING REMARKS

The characteristics of the KUR heavy water facility are as follows:

1) The layer of heavy water is so thick that pure Maxwellian neutrons are obtained.
2) As the heavy water tank is placed adjacent to the KUR core, a high neutron fluence rate is available.
3) The irradiation room is so wide that a large sample (e.g. a cow) can be irradiated.
4) When the removable neutron collimator is used, experiments using beam neutrons can be carried out.
5) By means of the time-of-flight technique using the chopper, neutron spectrum measurements and neutron cross section measurements can be made.
6) A standard field of fission neutrons is also offered, making use of the fission plate.
7) Using the bismuth scatterer, high quality thermal neutrons with low gamma ray contamination are available.

The standard neutron field has been used for such experiments as thermal neutron cross section measurement[5,6], diffusion length measurement[7], detector calibration[8], activation analysis[9], and for biomedical purposes[10] including neutron capture therapy[11] etc. The fission plate has been used for such experiments as fission neutron cross section[12,13], neutron slowing down[14], etc.

The authors wish to acknowledge Prof. T. Shibata, Prof. S. Okamoto and Prof. I. Kimura of Kyoto University for his valuable suggestions and discussion, and they are also indebted to Mr. T. Kozuka of Kyoto University, Mr. T. Kawamoto of Hitachi Ltd. and Dr. T. Mizuno of Hokkaido University for their assistance in carrying out the experiments.

They also thank Mr. Kadotani of Century Research Center for calculating the neutron spectra.

REFERENCE

1) T. Shibata et al., KURRI-TR-28 (1967) (in Japanese).
2) K. Kanda et al., Biomedical dosimetry (IAEA, Vienna, 1975) p.205
3) K. Kanda, KURRI-TR-96 (1972) (in Japanese).
4) R. Ramanna et al., 2nd Geneva Conf. P/1636 (1958).
5) K. Kanda et al., J. Nucl. Sci. Technol. 12 (1975) 601.
6) K. Kanda and O. Aizawa, Nucl. Sci. Eng. 60 (1976) 230.
7) K. Kanda et al., Ann. Symp. Res. Reactor Inst. Kyoto Univ. 7 (1973) 11 (in Japanese)

8) N. Hirakawa et al., Technol. Rep. Tohoku Univ. 41 (1976) 447.
9) T. Takeuchi and T. Hayashi, Ann. Rep. Res. Reactor Inst. Kyoto Univ. 6 (1972) 68.
10) Y. Mishima, Pigment Cell 1 (1973) 215.
11) H. Hatanaka et al., Biomedical dosimetry (IAEA, Vienna, 1975) p.147
12) I. Kimura et al., Prompt fission neutron spectra (IAEA, Vienna, 1972) p.113
13) K. Kanda et al., Ann. Rep. Res. Reactor Inst. Kyoto Univ. 4 (1971) 94.
14) K. Kanda et al., ibid. 3 (1970) 93.
15) K. Kanda et al., Nucl. Inst. Meth., 148 (1978) 535.

Table. 1 Comparison of thermal neutron field (in the case of our institute).*

Facility \ Condition	a	b	c	d	e	f	g	h
Heavy water facility	○	◎	◎	◎	○	○	○	○
Graphite thermal column	○	○	○	△	○	○	○	○
Thermal assembly using Linac etc.	×	○	○	○	△	○	○	×
Thermal assembly using converter	×	○	○	○	△	○	○	△
Thermal assembly using Pu-Be source	×	△	○	○	○	×	○	△

* ◎ Excellent, ○ good, △ fairly well, × unsatisfactory.

Table. 2 Characteristics of moderators.

Moderator	Diffusion length (L, cm)	Moderating power ($\xi\Sigma_s$, cm^{-1})	Moderating ratio ($\xi\Sigma_s/\Sigma_a$)	Neutron cross section
Light water	2.7	1.35	71	no structure
Heavy water (99.8 mol %)	110	0.178	2540	no structure
Graphite	53	0.060	192	crystalline structure
Beryllium	21	0.158	143	crystalline structure

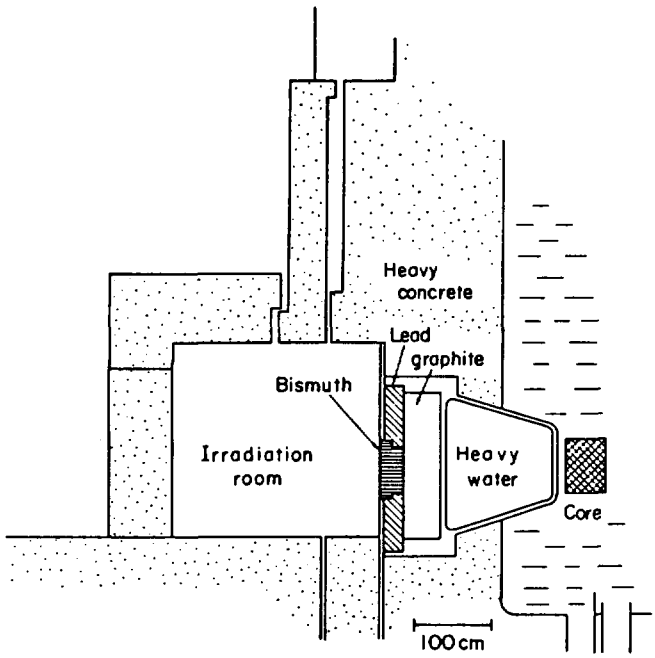

Fig. 1 Kyoto University reactor (KUR) heavy water facility.

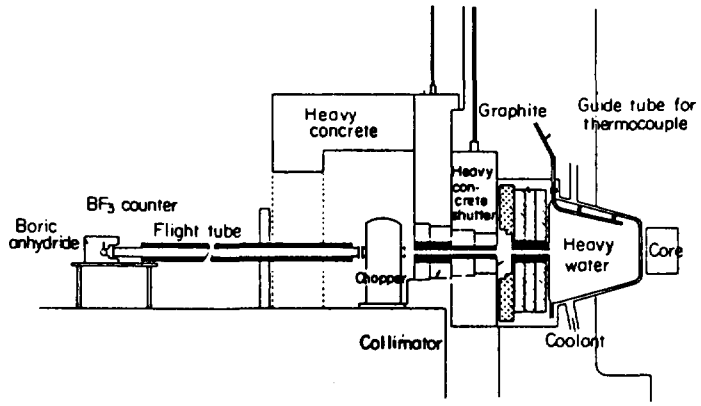

Fig. 2 Experimental arrangement of time-of-flight measurement.

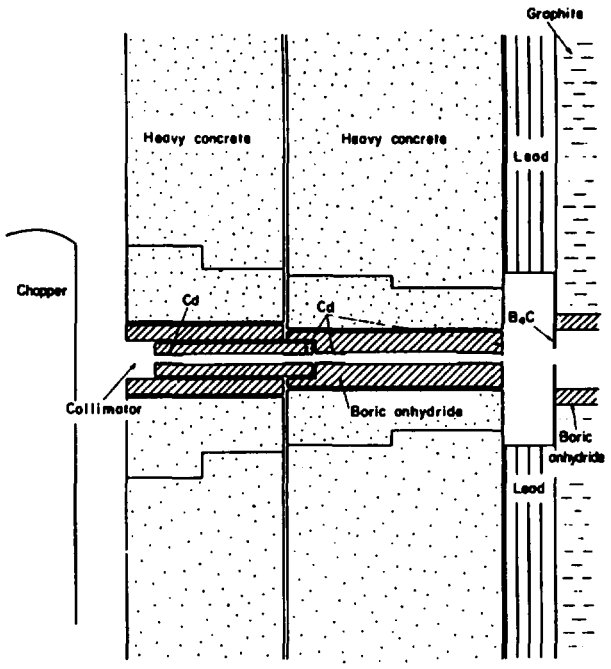

Fig. 3 Collimator system.

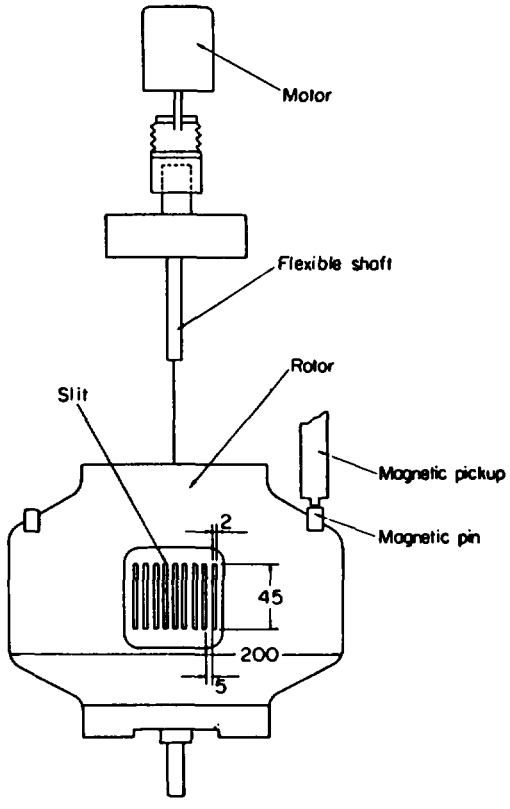

Fig. 4 Fast chopper.

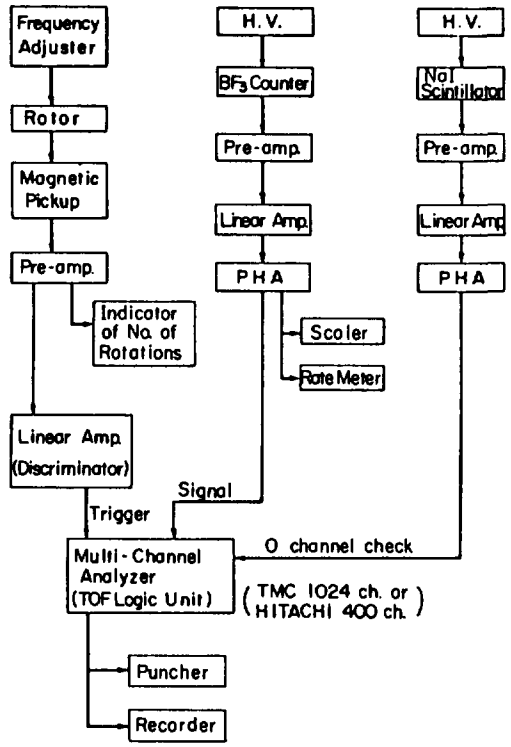

Fig. 5 Block diagram of time-of-flight measurement.

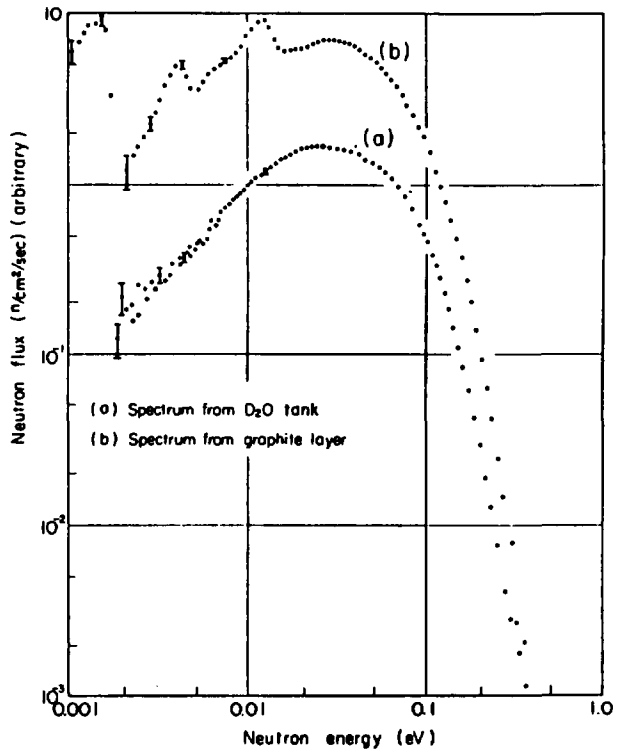

Fig. 6 Neutron spectra from KUR D_2O tank and graphite layer.

14) KUR Neutron Guide Tubes

T.Akiyoshi, T.Ebisawa, T.Kawai, F.Yoshida,
M.Ono, S.Mitani, T.Kobayashi
and
S.Okamoto

Research Reactor Institute of Kyoto University,
Kumatori-Cho, Sennan-Gun, Ohsaka

The outlines for two kinds of neutron guide tubes(NGTs) in KUR are described briefly. Available neutron sectional size for each of them is 10x74 mm^2. The values of total neutron flux of nickel mirror and supermirror NGTs are about $2x10^6$ and $5x10^7$ n/cm^2 sec. The contamination of gamma rays, epithermal neutrons and fast neutrons is very low and they are being used for the research works of material physics, biological physics, nuclear physics and so on.

1. Introduction

A neutron guide tube (NGT) is an apparatus which guides slow neutrons effectively to a distant experimental area from a neutron source. NGT has two main merits, that is, one is to supply slow neutron beam with very low contamination of gamma-rays, epithermal neutrons and fast neutrons, and the other is to make us possible to get a large experimental space. Nowadays it is, then, recognized to be indispensable to slow neutron experiments.

The NGTs of Kyoto University Research Reactor Institute are the nickel mirror-NGT(NMNGT)[1] and the supermirror-NGT(SMNGT), which have been installed in the reactor room. Outside of the reactor room experimental rooms have been built, where intense slow neutron beams and low background environment are available (see Fig.1). They are being used for co-operative research works

of material physics, biological physics, nuclear physics and so on.

2. KUR Nickel Mirror Neutron Guide Tube

KUR-NMNGT which may be called as cold neutron guide was installed at KUR(Kyoto University Reactor) E-3 beam-hole in 1973. The nickel mirrors of KUR-NMNGT are nickel films of 3000 A in thickness sputtered on float glass plates of 6 mm in thickness. The reflectivity is more than 0.98 for neutrons of wavelength larger than critical wavelength($(\lambda/\theta)_{crit}$= 580 A).[1] The KUR-NMNGT is composed of 12 guide tube elements and its total length is 10.8 m. The sectional size of the neutron beam is 10 mm x 74 mm and the characteristic wavelength is 2.8 A. The specifications are shown in Table 1. The total neutron flux is about 2×10^6 n/cm^2•sec.

Fig. 2 shows the wavelength distributions of neutrons emitted from KUR-NMNGT. Because of the contribution of "garland transmission", reflected by outer side-mirrors only, the neutron flux and the mean energy of neutrons are higher at the outer side than at the inner where most of neutrons is guided by the "zigzag transmission" reflected by the mirrors of both sides.

The contaminations of gamma-ray and epithermal neutron are about 1mr/hr and 0.5 n/cm^2•sec, respectively. KUR-NMNGT is, then, seems to be useful for the elastic and inelastic scattering experiments of slow neutrons, and also neutron optics experiments etc..

3. KUR Supermirror Neutron Guide Tube

KUR SMNGT is the thermal neutron guide and has been installed at KUR B-4 beam hole in 1984. Its basic dimensions are almost the same as those of NMNGT. The supermirrors of KUR-SMNGT are alternate multi-layer films of two kinds of metals with different scattering lengths(Ni and Ti) deposited onto float glass plates[2]-[4]. Fig. 3 shows the reflectivity of neutrons averaged

over all supermirrors employed for SMNGT((λ/θ)crit = 250 A). The basic specifications are given in Table 1. KUR- SMNGT is composed of 13 elements and the total length is 11.7 m.

Fig. 4 shows the wavelength spectrum of the neutrons emitted from SMNGT. It is appears that it covers almost the total region of the reactor core spectrum. The effect of Garland transmission is somewhat found like in NMNGT. The total neutron flux obtained is about 5 x 10^7 n/cm^2•sec and is about 20 times higher than that of NMNGT. The additional neutron flux is due to neutrons of shorter wavelength and larger divergence angle .

Gamma ray contamination is about 3 mr/hr and values of gamma-ray background are about 0.4 and 0.1 mr/hr at the places of 100 and 200 cm apart from the beam center of the exit,respectively. KUR-SMNGT is, then, seems to be useful for thermal neutron experiments requiring the high flux beam.

4. Slow Neutron Experiments

NMNGT is profitable for cold neutron experiments with the very low divergence angle, while SMNGT for thermal neutron experiments with high flux.

The main experiments, under going and planning, are following;

for NMNGT:

(1) Small angle neutron scattering;
metals, polymers, biological substance.

(2) Neutron optics;
neutron mirror, neutron interferometer.

(3) Development of experimental apparatus;
neutron spin echo, position sensitive detector, neutron mirror monochrometer.

for SMNGT;

(1) Nuclear physics:
nuclear fission, neutron capture gamma-ray spectroscopy.

(2) Inelastic scattering of slow neutron:
polymer, liquid material.

References

(1) OKAMOTO,S., et al.:KUR Neutron Guide Tube (in Japanese), R.A.Div. of Res. Reactor Inst. Kyoto Univ. (1978)

(2) YAMADA,S., et al.: Ann. Res. Reactor Inst. Kyoto Univ., vol. 11 (1978)8

(3) EBISAWA,T., et al.: J. Nuclear Sci. Technol., vol.16(1979)647

(4) EBISAWA,T., et al.: Ann. Rep. Res. Reactor Inst. Kyoto Univ. vol. 14(1981)10

Table 1 Basic Parameters of KUR-NGT

		NMNGT	SMNGT
Sectional Size (mm^2)		10 x 74	10 x 74
Radius of Curvature (m)		833	978
Total Length	L (m)	10.8	11.7
	L1(m)	8.2	8.8
Characteristic Wavelength (A)		2.85	1.17
Element-Length l (mm)		900	900
Total Flux n/cm^2 sec		2×10^6	5×10^7

NMNGT:Nickel Mirror Neutron Guide Tube
SMNGT:Supermirror Neutron Guide Tube

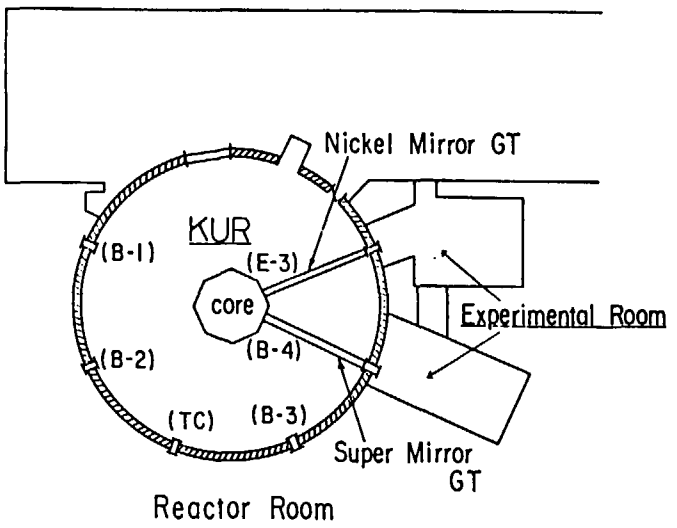

Fig. 1. KUR reactor room, neutron guide tubes and experimental rooms.

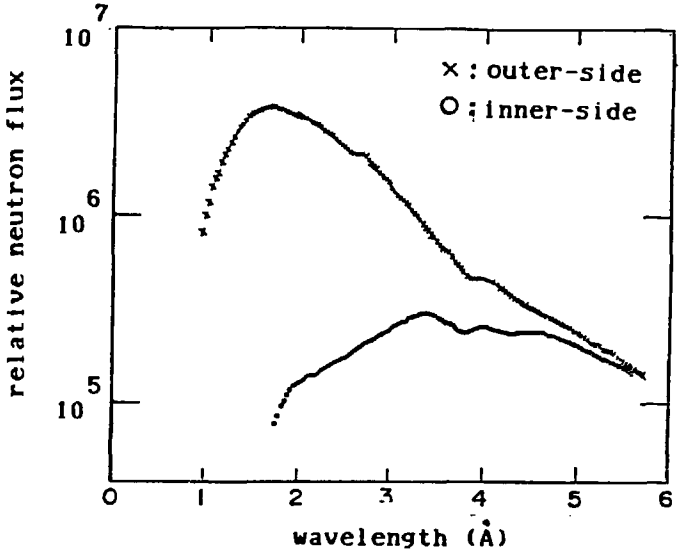

Fig. 2. Wavelength distributions of neutrons emitted from KUR nickel mirror neutron guide tube.

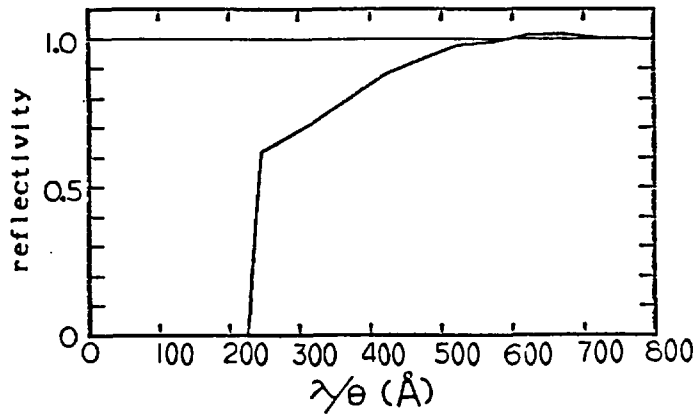

Fig. 3. Neutron-reflectivity averaged over all supermirrors employed for KUR supermirror neutron guide tube.

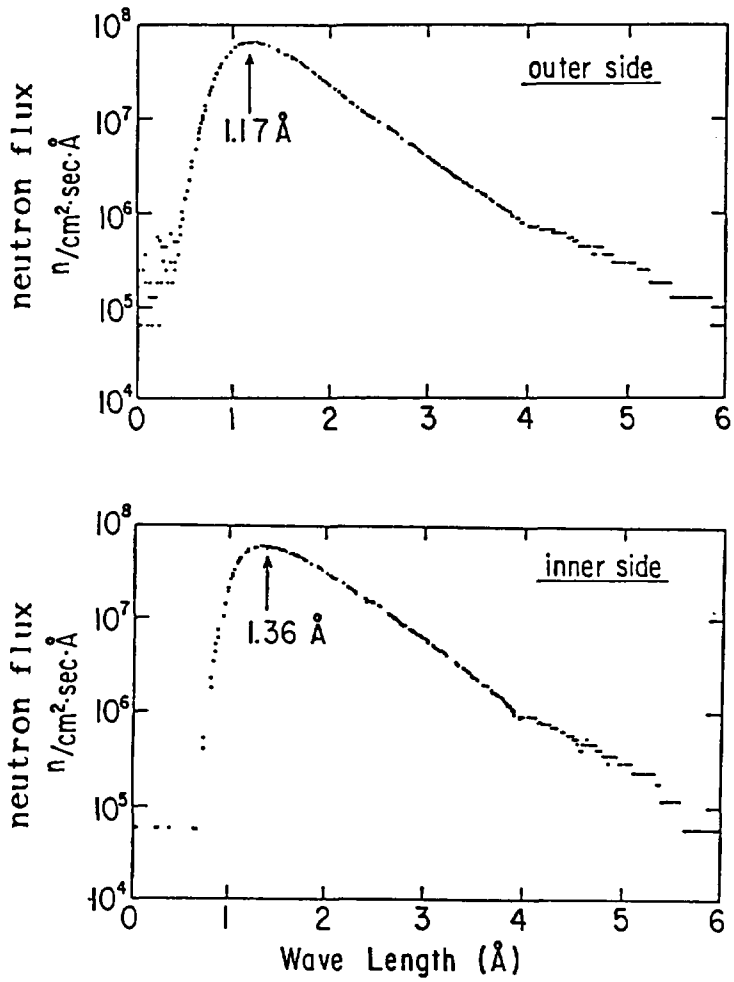

Fig. 4. Wavelength distributions of neutrons emitted from KUR supermirror neutron guide tube.

15) Standard 1/E Spectrum Neutron Field installed in UTR-KINKI

R. MIKI, T. ITOH, K. KOBAYASHI*, I. KIMURA*,
S. YAMAMOTO* and K. TSUCHIHASHI**

Kinki University Atomic Energy Research Institute
3-4-1 Kowakae, Higashi-Osaka, Osaka 577, Japan

An experimental hole installed in the center of internal graphite reflector between the two separate cores of Kinki University Reactor, UTR-KINKI, has been proved experimentally and analytically to have excellent 1/E characteristic. The measured resonance integrals for several nuclides relative to that of $^{197}Au(n,\gamma)^{198}Au$ reaction agree very well with the evaluated data. Analytical calculations on the neutron spectrum in this void region was carried out by JAERI Thermal Reactor Standard Code System (SRAC Code)[1].

1. Introduction

UTR-KINKI is a light-water moderated and cooled, graphite reflected, heterogeneous highly enriched uranium thermal reactor with 46cm-separated two-slab core arrangement. There are 12 fuel elements, each consists of 12 Al-clad, flat MTR-type fuel plates. It is a modified ARGONAUT research reactor with output power of 1W. The maximum thermal neutron flux in the core is about 1.5×10^7 n/cm^2-sec.

Between the two separate cores of UTR-KINKI, there exists a wide internal graphite reflector of 46cm thick and a vertical stringer, 9.6cm or 16.4cm square and 122 cm long, at the center of internal reflector can be withdrawn to provide an

---

* Kyoto University Research Reactor Institute
** Japan Atomic Energy Research Institute

experimental hole. The reactor cross section and core plan of UTR-KINKI are shown in Figs. 1 and 2 and the details of the enlarged central stringer are also shown in Fig. 3.

2. Main specifications of UTR-KINKI

Power	1W
Critical mass	3,018g
Excess reactivity	0.5% dk/k (max.)
Geometry	Two 15 x 51cm fuel slabs separated by 46cm of graphite and reflected by 30cm of graphite
Moderator	Light water
Neutron life time	1.35×10^{-4} sec
Fuel element/fuel plate	
Number of fuel elements	12, each consists of 12 plates
Fuel plate dimension	77 x 7.6 x.0.2cm
Enrichment	90% U-235
U-235 per plate	22.3g (average)
Water gap	1.0cm
Cladding	0.5mm of aluminum
Fuel-containing matrix	UAl_4 + Al
Reflector	
Material	Graphite
Dimension	112 x 142 x 122cm (high)
Control rods and rod worths	
Regulating rod	1 / 0.1% dk/k (min.)
Shim-safety rod	1 / 0.54% dk/k (min.)
Safety rods	2 / 0.54% dk/k (min.)
Control element	Cadmium
Reactivity effects	
Temperature coefficient	-0.00796% dk/k/°C
1% change of fuel loading	± 0.336% dk/k

3. Standard 1/E spectrum neutron field in UTR-KINKI

Since the two cores of UTR-KINKI are widely separated by internal graphite reflector and the neutron flux distribution between two cores is almost flat, the central region of this graphite reflector is supposed to have an excellent, non-directional 1/E spectrum neutron field. A vertical stringer 9.6cm or 16.4cm square and 122cm long at the center of internal reflector can be withdrawn to provide an experimental hole for standard 1/E spectrum neutron field facility.

Analytical calculation on the neutron spectrum in this void region was carried out by SRAC Code , 2-D diffusion (CITATION) and 2-D SN transport codes, on X-Y and R-Z geometries.

The calculated neutron spectrum of this region is shown Fig. 4. Between few eV and 100 keV, the calculated spectrum shows an excellent 1/E characteristic.

The thermal and epi-thermal neutron flux distributions in this region were measured by Au foil activation. The results show that the distributions are almost flat, with thermal flux, about 1.5×10^7 n/cm^2-sec, epi-thermal flux, about 9×10^5 n/cm^2-sec/unit lethargy and fast flux, about 1.3×10^7 n/cm^2-sec, respectively.

So far, we have measured the several resonance integrals for $^{55}Mn(n,\gamma)^{56}Mn$, $^{232}Th(n,\gamma)^{233}Th$ and $^{238}U(n,\gamma)^{239}U$ reactions relative to that of $^{197}Au(n,\gamma)^{196}Au$ reaction. Each sample foils was covered with cadmium case, 0.5mm thick, and irradiated at the center of void region for 2.5 hours at 1W. After irradiation, induced activities were measured with Ge gamma-ray spectrometer.

In the data processing to obtain the resonance integrals, we have considered data correlations due to the uncertainties from each error element, such as counting statistics, detector efficiency, neutron self-shielding correction and so on, as we did before[2].

Table 1 summarizes the result of the resonance integral

measurements and the correlation matrix. In the last two columns, evaluated data are given to compare with our measured values. The data agree very well with our measured values and show that the void region has an excellent 1/E neutron spectrum.

4. Future plan

Upgrade of UTR-KINKI to 10W is under contemplation. It will make our standard 1/E neutron spectrum field more useful and versatile. Also, by introducing the spare 16 fuel plates in ring geometry into the central void region, we are planning to establish a "non-directional" standard fission neutron field. Preliminary design calculation on this experimental facility by SRAC Code System has already been done. The results show that the incorporation of 2mm thick inner boron layer with fission plates to compensate the increased reactivity and to cut the thermal neutron will give rise to a modified fission spectrum of relatively simple form. Some of the results of analytical calculation are shown in Figs. 5 and 6.

---

[1] K.Tsuchihashi, SRAC Thermal Reactor Standard Code System for Reactor Design and Analysis, JAERI 1285 (1983)

[2] K.Kobayashi. et al., J.Nucl. Sci. Tech.,19.341 (1982)

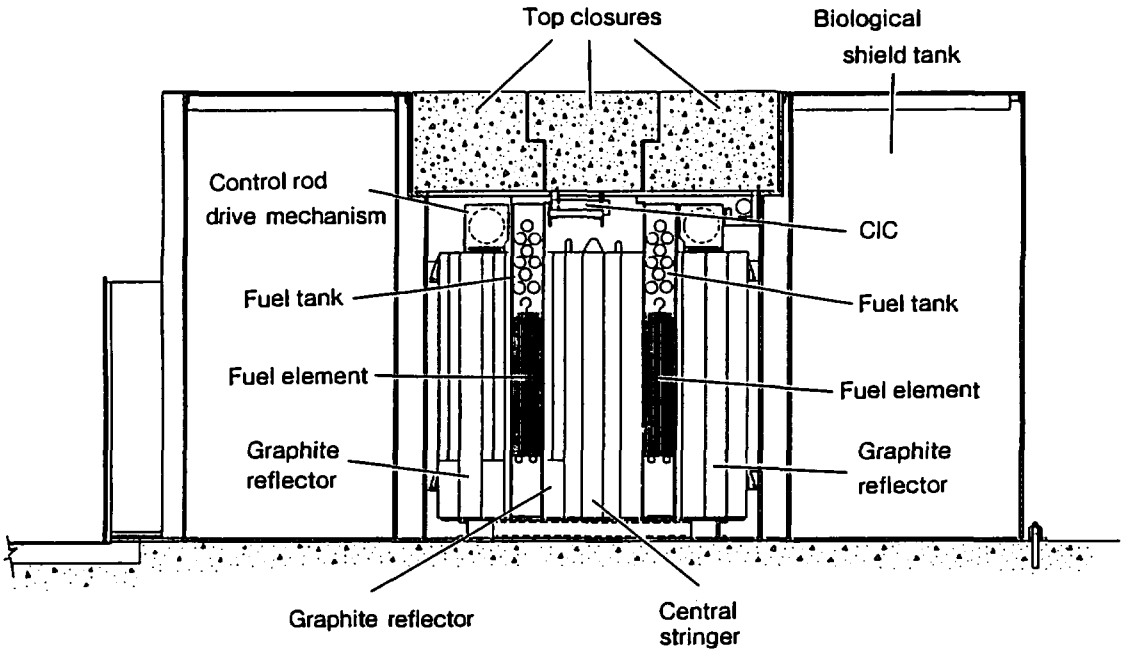

Fig. 1 REACTOR CROSS SECTION (N-S) (unit : mm)

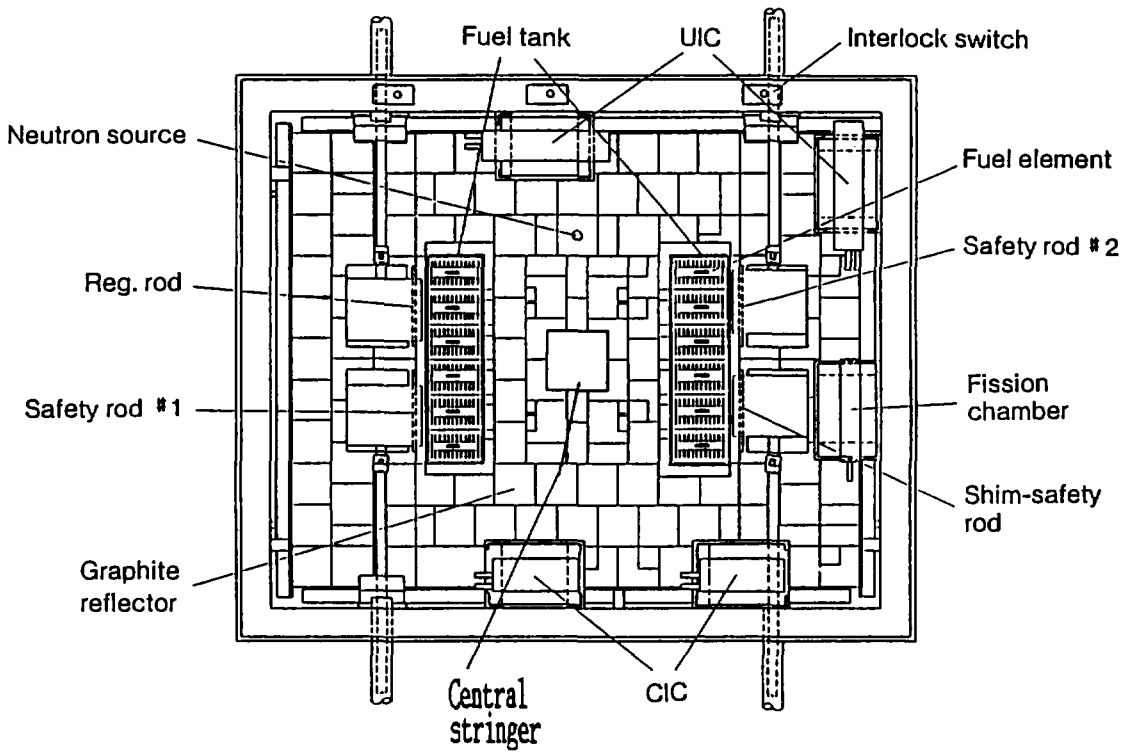

Fig. 2 REACTOR CORE PLAN (unit : mm)

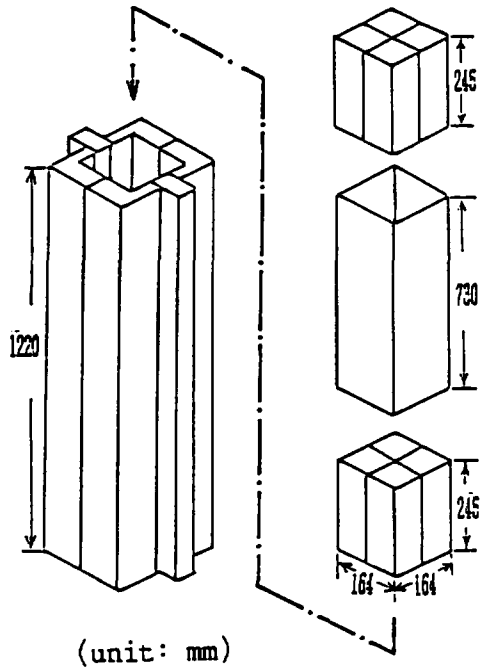

Fig. 3 DETAILS OF ENLARGED VERTICAL SIRINGER AND VOID REGION

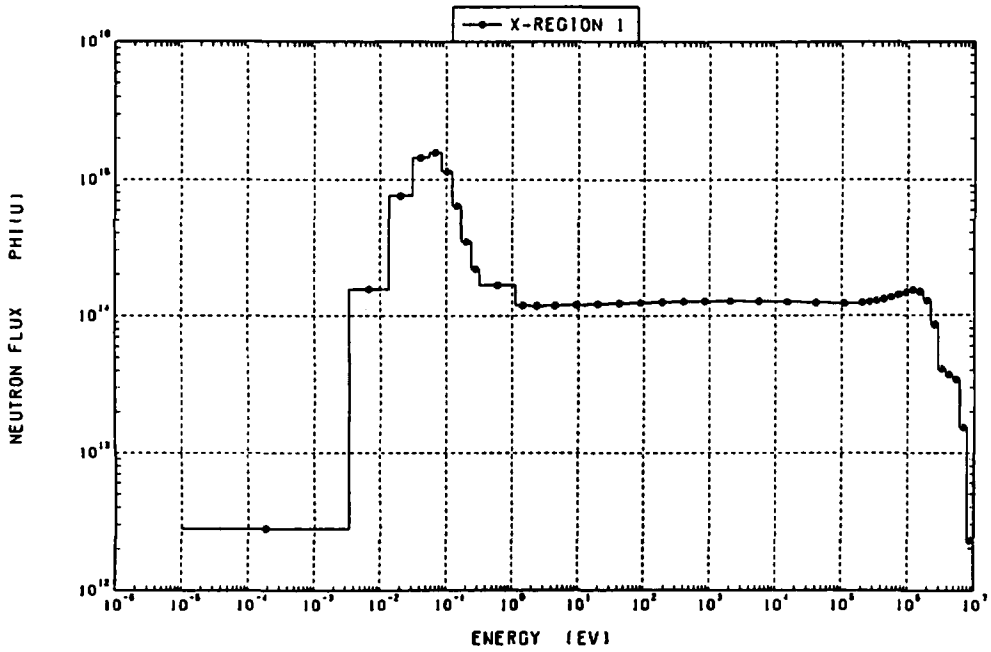

Fig. 4 NEUTRON SPECIRUM IN THE CENTRAL VOID REGION
(CENTRAL SIRINGER WITHDRAWN)

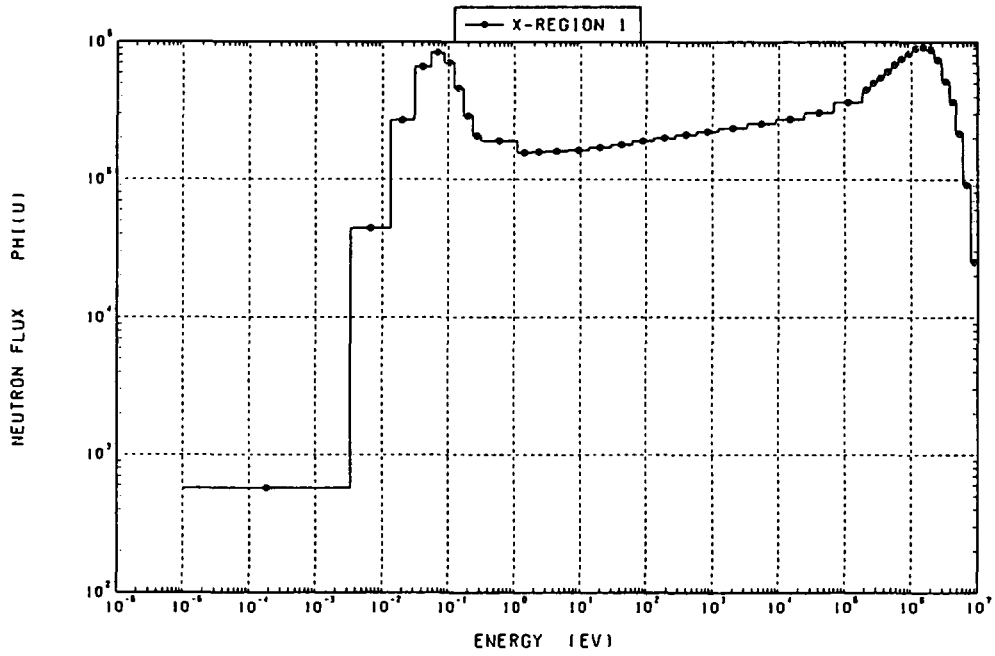

Fig. 5 NEUTRON SPECTRUM IN THE CENTRAL VOID REGION
(FISSION PLATES INSTALLED)

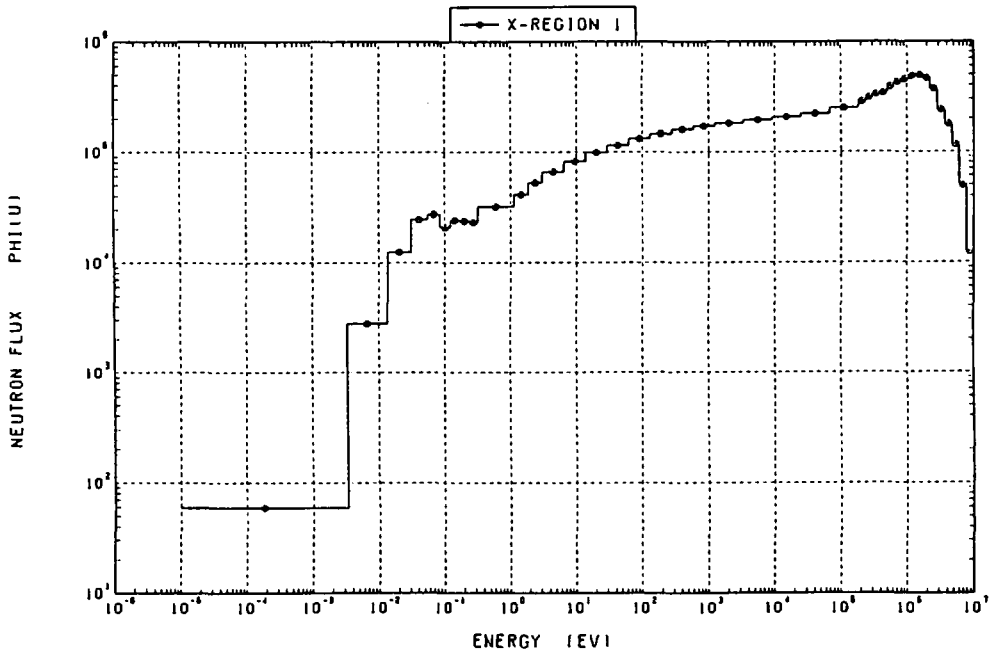

Fig. 6 NEUTRON SPECTRUM IN THE CENTRAL VOID REGION
(FISSION PLATES AND BORON LAYER INSTALLED)

16) The OKTAVIAN neutron TOF and irradiation facility

A. Takahashi, E. Ichimura, H. Sugimoto and T. Katoh*

Department of Nuclear Engineering, Osaka University

Yamadaoka 2-1, Suita, Osaka, Japan

There are introduced neutron time-of-flight facilities and an irradiation facility at OKTAVIAN. Especially, somewhat detailed description is given for a new TOF facility of double differential neutron emission cross section measurement at 14.1 MeV, and for irradiation experiment using a rotating target neutron source.

1. The OKTAVIAN facility

The Osaka University Intense 14 MeV Neutron Source (OKTAVIAN) facility was constructed in the period 1978 - 1983, aiming at utilizations for fusion neutronics experiments and material irradiation experiments[1]. The main machine is a 300 keV deuteron accelerator which has two beam lines ; One is the pulse operation line providing D-T neutron bursts with 1.5 - 3 ns width and 1 kHz - 2 MHz repetition, by a post-acceleration pulsing system of X-Y deflection and klystron-bunching. In usual operation, 3 - 4 mA continuous deuteron beam is chopped and then bunched, so that time-averaged current at the final tritium target is ranging from 10 to 20 μA for 1 MHz operation. The maximum neutron yield ever observed is 5×10^3 n/pulse. This pulse line has been used for neutron TOF spectrometry such as the double differential neutron emission cross section measurement based on a ring geometry[2,3] and the leakage or emitted spectrum measurements from bulk media[4-7]. A schematic view of the facility is shown in Fig.1. Two new TOF lines (85-deg and 55-deg) have been constructed recently. A detailed description for the 85-deg line experiment is given in the next section.

The other operation line is provided for 14 MeV neutron irradiation experiments[8-10] by using continuous deuteron beam (20 mA Max.) and a rotating target. This line has been operated with 5-15 mA, mostly, and utilized for breeder neutronics experiments[8], material damage studies[9] and

* Nagoya University

activation cross section measurements[8, 10]. The characteristics of the irradiation field are shown in Section 3.

2. 85 deg TOF facility

This TOF line was designed for the proper use of neutron scattering experiments at 14.1 MeV incident energy, e. g., differential neutron emission cross section measurements. In ideal sense, 90 deg to the pulse beam should be selected, but a little bit bent line of 85 deg was chosen to avoid the direct effect of source neutron scattering by the support flange (SS) of a 2 cm diam 10 Ci TiT target. The total system was designed to realize energy-resolution and counting statistics as good as those of the ring-geometry experiment at 0 deg line[3], namely to obtain an emission spectrum by an hour run.

As shown in Fig.2, a sample of 3 cm in diameter and 5-7 cm in length is rotated with 17 cm radius around the target (PNS) to change scattering angle. Special shadow bar, collimator and heavy detector shield are installed. Background by room-scattered neutrons is almost completely eliminated by this shielding set-up, so that air-scattered neutrons within a cylindrical region drawn with two broken lines in the vicinity of PNS are coming into the neutron detector to become background. As the neutron detector, a 10" diam 10 cm long NE213 scintillator in an aluminum capsule is mounted on a R1250 photomultiplier via a conical light-pipe in between. This detector shows excellent n-γ separability in a dynamic range of 0.3 - 14 MeV, by applying an usual pulse shape discrimation circuit as shown in Fig.3. Neutron flight path changes a little bit around 8.25 m, with the change of sample position.

The measuring electronics is the same one with that of 0 deg line[3], and is shown in Fig.3. The efficiency curve of the neutron detector was determined by TOF runs with a polyethylene cylindrical sample of 1 cm in diameter and 5 cm in length for 5-14 MeV range, and with a Cf-252 source for 0.3-7 MeV range, as is the case of the ring-geometry experiment[3]. The efficiency curve is shown in Fig.4.

By the same measuring system, source neutron spectrum was observed by removing the shadow bar, as shown in Fig.5 where are seen low energy component by 14 MeV neutron scattering with the target assembly. The effect of this contamination (low energy component) of source spectrum should be eliminated from measured sample-emission spectra by correction calculation in addition to the multiple scattering correction. For another correction,

the dependence of source neutron yield on scattering angle shown in Fig.6 should be taken into account. Figure 6 was obtained by measuring activations of $^{27}Al(n,\alpha)^{24}Na$ in 1cmx5cm Al plates surrounded the target with 17 cm radius. Somewhat higher yield in backward angles can be explained by thinner support material (SS) in those directions.

Examples of TOF spectra are shown in Fig.7 (carbon) and Fig.8 (lead), in comparison with background runs which were taken by removing sample. For each run, data accumulation time was about an hour. Further improvement of foreground/background ratio requires the evacuation of air in the vicinity of the target. Examples of double differential neutron emission cross sections after corrections are shown in Fig.9 (carbon) and Fig.10 (lead), in comparison with evaluated data. Energy-resolution at 14 MeV is about 0.2 MeV. Counting statistics as well as energy-resolution are comparable with those of the ring-geometry experiment[2,3], and sufficient enough to separate partial differential cross sections such as elastic, level-inelastic scattering and (n,2n) reaction. Results of this kind of experiment are presented in a separate report[11] of this seminar.

3. Rotating target neutron source for irradiation

A 400 Ci TiT rotating target with 20 cm in diameter is now in operation. Characteristics of source neutron field should be known for irradiation experiments. Due to the TiT layer thichness of about 4 μm, this target is so-to-say a thick target which produces most neutrons during the slowing-down of 300 keV incident deuterons. The energy-angle correlation of emitted neutrons has been determined by the reaction rate ratio of $^{90}Zr(n,2n)/^{93}Nb(n,2n)$. The result[10] is shown in Fig.11. Calculation by the D-T reaction kinematics with a deuteron energy of 120 keV that is near to the resonance energy 110 keV of that reaction fits well the experiment.

Since the structure of target, support, cooling and housing assembly is very complicated, as shown in Fig.12, emitted D-T neutron yields are strongly angle-dependent and source spectra have lower-energy tails. Angular distributions of source neutron yields have been measured by $^{27}Al(n,\alpha)^{24}Na$ and $^{93}Nb(n,2n)^{92m}Nb$ reaction, i.e., by irradiating Al and Nb foils surrounding the rotating target in circle. A 60 cc high purity Ge detector is available for measuring induced γ-ray spectra. The result is shown in Fig.13, where dips of yields are easily explained by the structure of the rotating target assembly. Integrated D-T neutron yield

is 2×10^{12} neutrons/10 mA.

The measurement of source neutron spectrum including low-energy tail of scattered neutrons is rather difficult, since the OKTAVIAN DC line has no ns-pulsing system. Instead, a double-scintillator-TOF measurement was tried to measure source spectrum through a collimator hole of room wall. The first scintillator (scatterer) of 1.5" diam NE213 was placed just at the out-let of the wall-hole, and the second one of 5" diam. NE213 at about 4 m from the first. Using a measuring system similar to Fig.3, TOF spectrum was obtained. The result is shown in Fig.14, where we find a parasitic peak by $^{12}C(n,n'3\alpha)$ reaction in the first scintillator. This parasitic peak must be eliminated and the spectrum in this energy region should be replaced with a flat curve of interpolation from both sides. Consequently, the contamination, i. e., low energy component is about 15 % of direct D-T neutrons. The effect of this low energy component has been corrected in irradiation experiments, especially for measuring activation and/or reaction cross sections around 14 MeV[8,10].

Application of this rotating target neutron source to a breeder neutronics experiment is also shown in a separate report[11] of this seminar.

4. Closing remarks

The 85 deg neutron TOF facility will be the main tool of double differential neutron emission cross section measurements for fusion applications in coming days. The 55 deg line which is not mentioned in this report is being used for neutron TOF measurements of bulk assemblies, and this line can be extended upto about 16 m in flight path. Some of other TOF lines are now in preparation for the spectroscopy of 14-MeV-neutron-induced γ-rays. These works will be reported elsewhere.

With respect to the rotating target section, the original design of tritum amount claims a 800 Ci one. However, we started from a 200 Ci and are now using a 400 Ci target so as to observe target-lives. A 400 Ci one has shown longer life (about 1000 mAxhour half life) than a 200 Ci, but the increment is not doubled, i. e., smaller.

The authors wish to thank the operating crew of OKTAVIAN for their assistances in constructing TOF lines and natuarally for their operations of the machine.

References

1) K. Sumita, A. Takahashi, T. Iida, J. Yamamoto, S. Imoto and K. Matsuda : Proc. 12th Symp. Fusion Technology, Sept. 1982, Juelich FRG, Vol.1, 675-680, Pergamon Press (1982)
2) A. Takahashi, J. Yamamoto, T. Murakami, K. Oshima, H. Oda K. Fujimoto and K. Sumita : Proc. Conf. Nuclear Data for Science and Technology, Sept. 1982, Antwerp Belgium, 360-367, D. Reidel Pub. (1983)
3) A. Takahashi, J. Yamamoto, K. Oshima, M. Ueda, M. Fukazawa, Y. Yanagi, J. Miyaguchi and K. Sumita : J. Nucl. Sci. Technol., 21[8], 577-598 (1984)
4) A. Takahashi, J. Yamamoto, T. Murakami, K. Oshima, H. Oda, K. Fujimoto and K. Sumita : Proc. 12th Symp. Fusion Technology, Sept. 1982, Juelich FRG, Vol.1, 687-692, Pergamon Press (1982)
5) J. Yamamoto, A. Takahashi, K. Sumita, K. Shin, T. Hyodo, S. Itoh, K. Sekimoto and K. Kanda : Proc. 6th Conf. Rad. Shield., May 1983, Japan
6) K. Sugiyama, K. Kanda, S. Iwasaki, M. Nakazawa, H. Hashikura, T. Iguchi, H. Sekimoto, S. Itoh, K. Sumita, A. Takahashi and J. Yamamoto : Proc. 13th Symp. Fusion Technology, Sept. 1984, Varese Italy, Vol.2, 1375-1381, Pergamon Press (1984)
7) H. Hashikura, T. Kasahara, Y. Oka, M. Akiyama, S. Kondo, A. Takahashi and J. Yamamoto : "Measurements and Calculations of the Neutron Leakage Spectrum from a Nickel Sphere for a D-T Neutron Source", to be pub. in J. Nucl. Sci. Technol.
8) A. Takahashi, K. Yanagi, S. Kohno, N. Ishigaki, J. Yamamoto and K. Sumita : Proc. 13th Symp. Fusion Technol.,Sept. 1984, Varese Italy, Vol.2, 1235-1241, Pergamon Press (1984)
9) T. Iida, T. Maekawa, K. Sumita, C.M. Logan and D.W. Heikkinen : J. Nucl. Sci. Technol., 21[8], 634-641 (1984)
10) K. Kawade, H. Yamamoto, H. Atsumi, H. Miyade, T. Katoh, Y. Ikeda, T. Nakamura, A. Takahashi and T. Iida : J. Nucl. Sci. Technol., 22[10], 851-852 (1985)
11) A. Takahashi : "Nuclear Data for Fusion Blanket Neutronics", Proc. JNDC 1985 Seminar on Nuclear Data, Nov. 1985, Tokai Japan (this Conf.)

OSAKA UNIVERSITY INTENSE 14 MeV NEUTRON SOURCE FACILITY (OKTAVIAN)

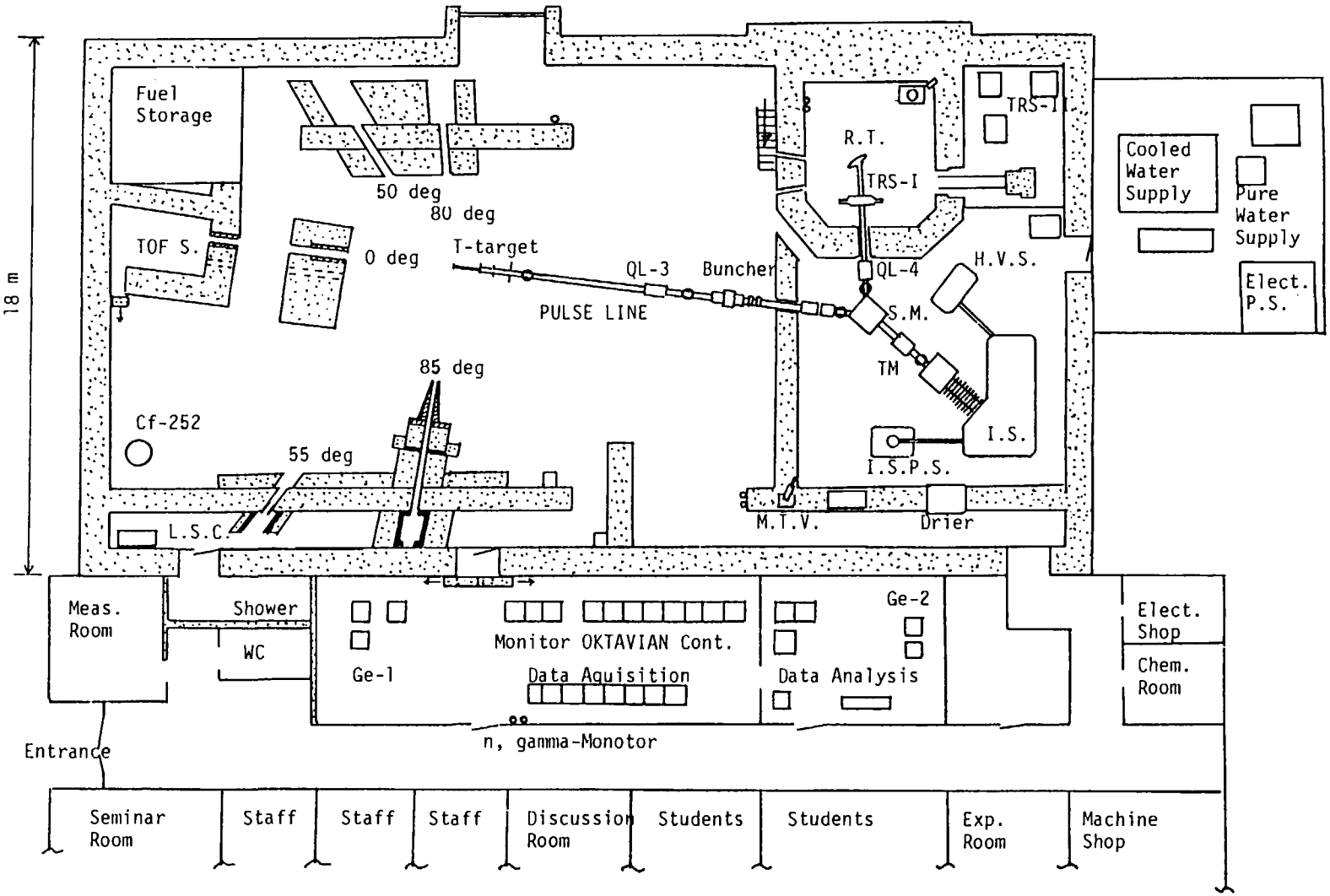

Fig.1 Schematic view of the OKTAVIAN facility

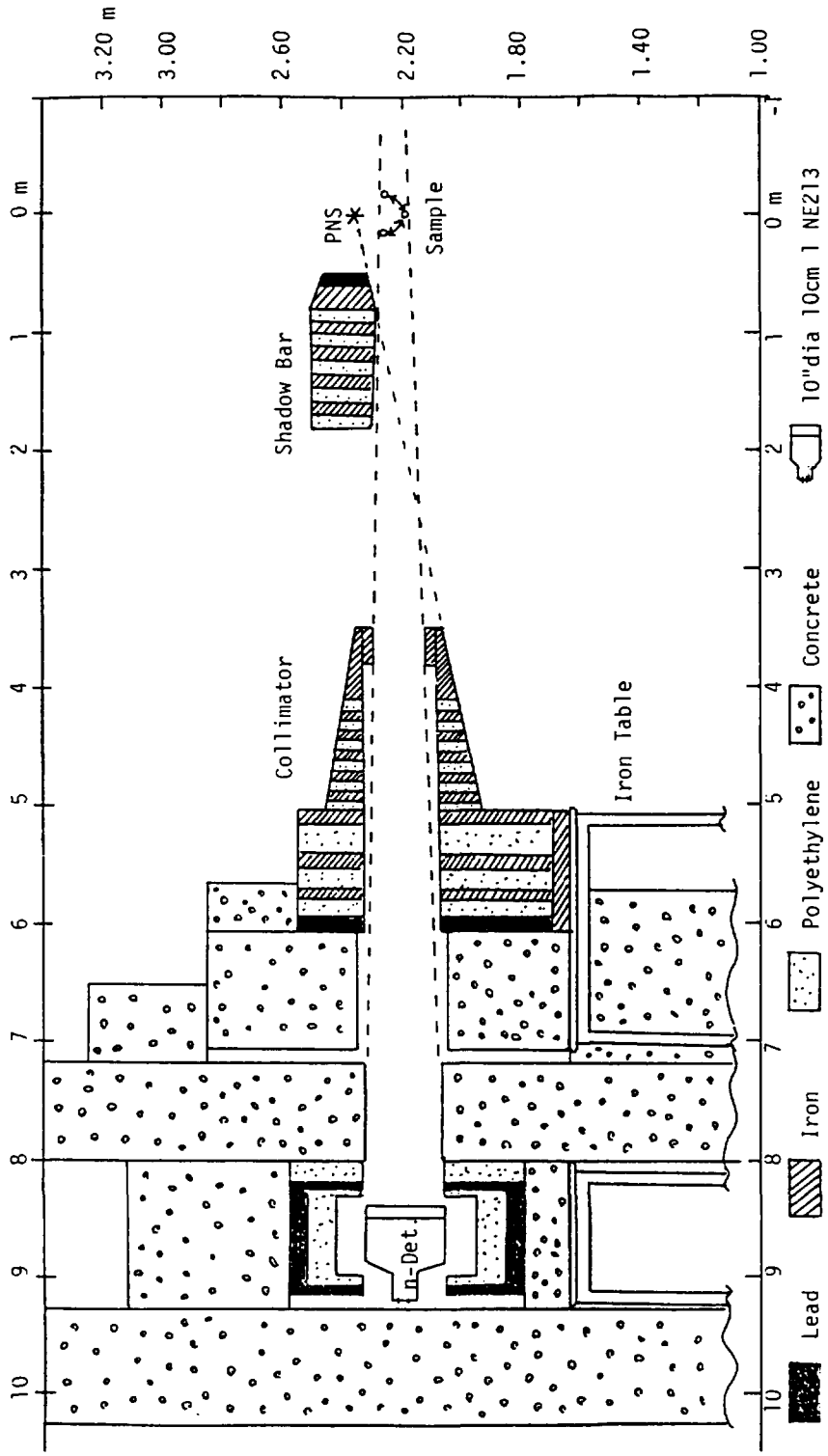

Fig.2 Shielding setup for the 85 deg TOF experiment at OKTAVIAN

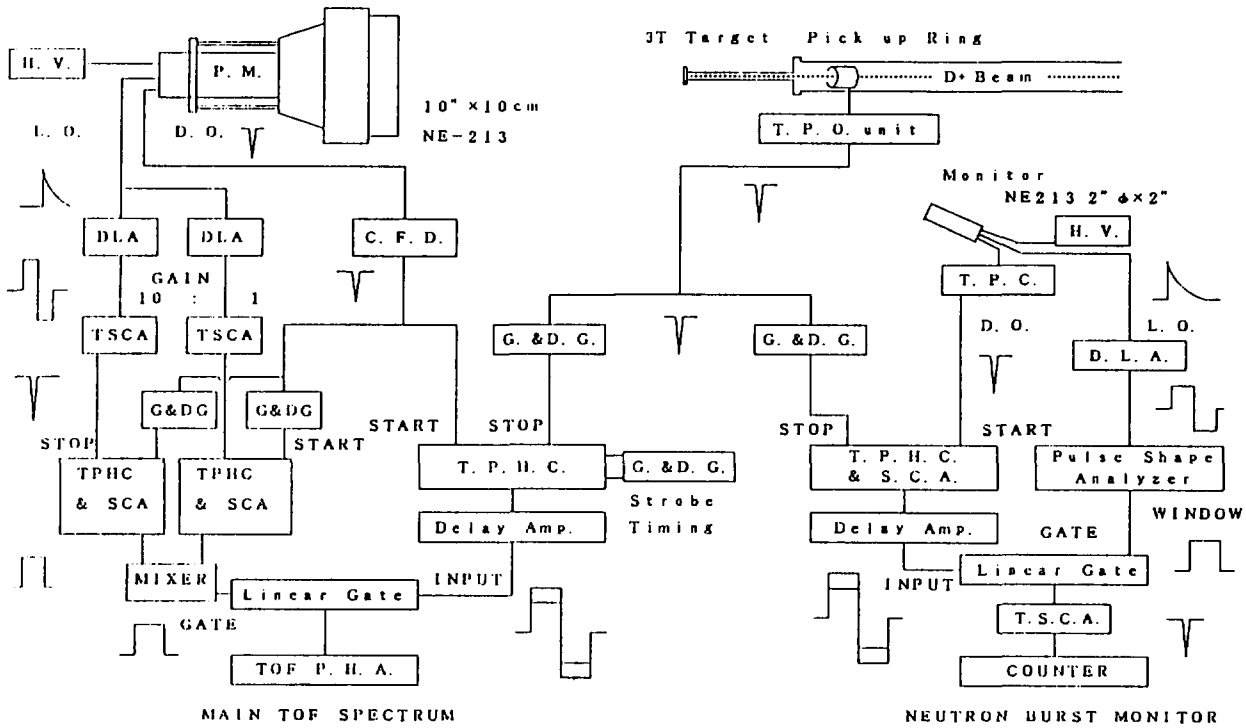

Fig.3 Block-diagram of the measuring system for TOF experiment

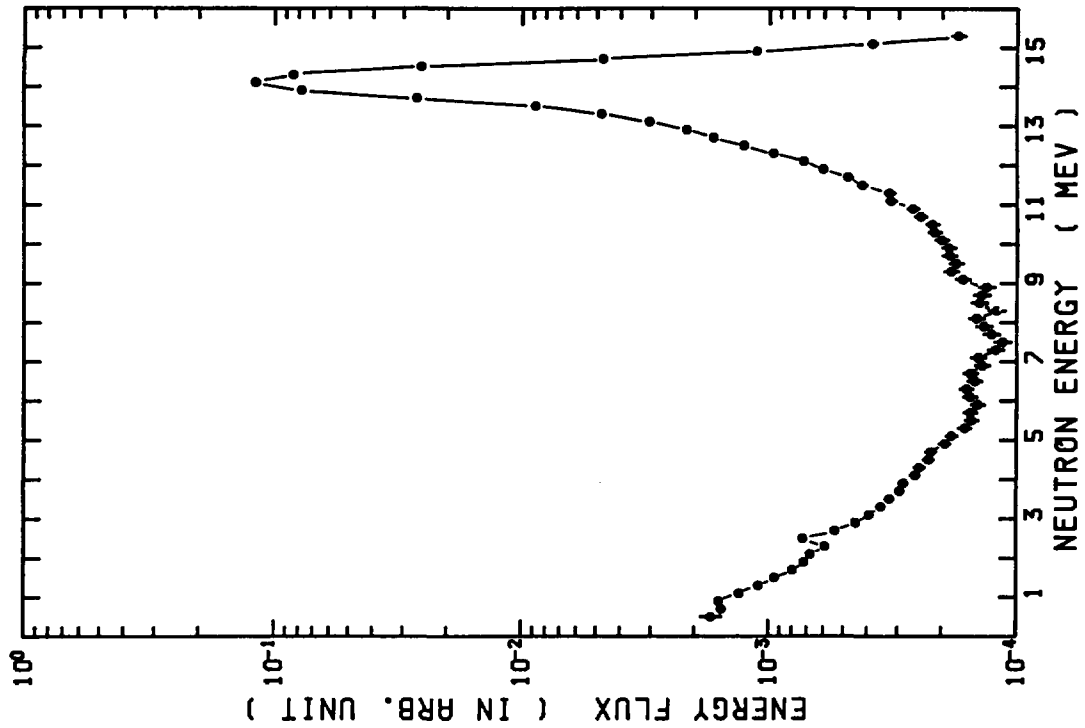

Fig.5 Measured source neutron spectrum at 85 deg

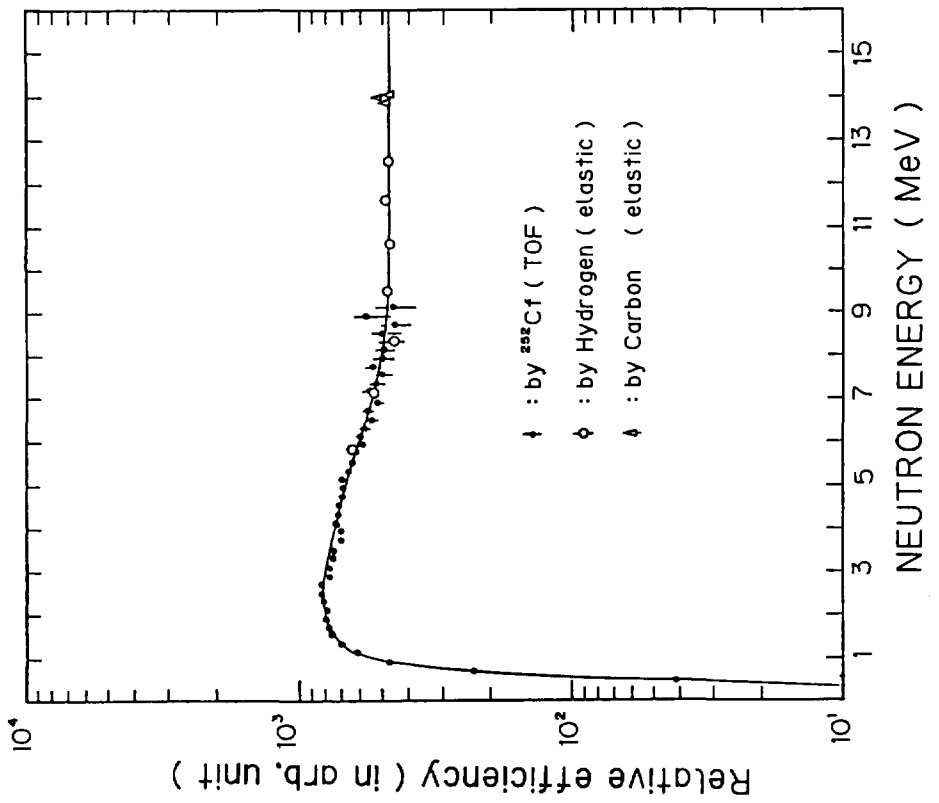

Fig.4 Measured efficiency curve for a 10" diam. 10 cm long NE213 detector

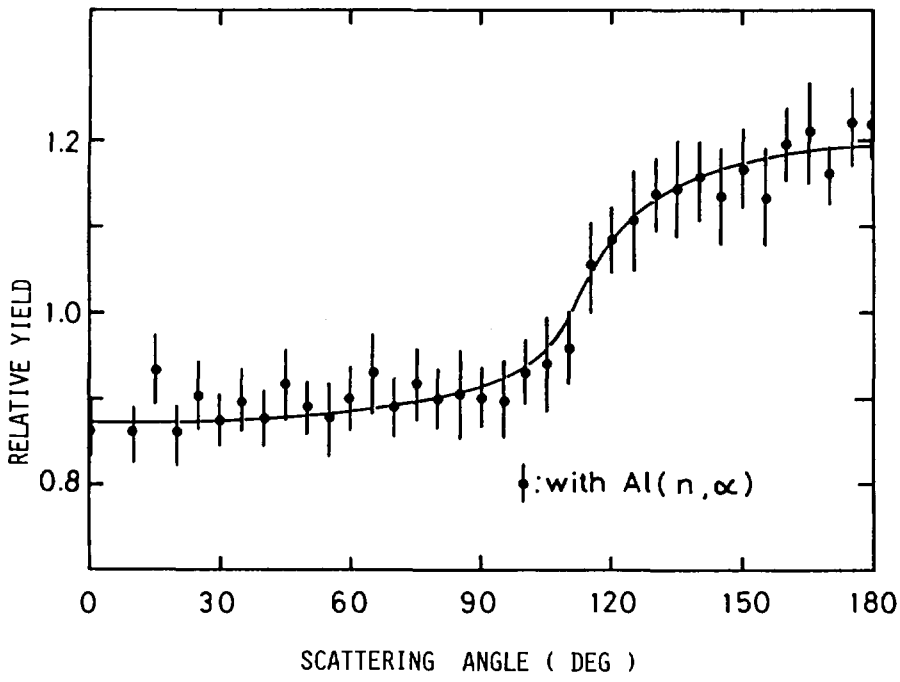

Fig.6 Scattering-angle-dependence of source (14.1 MeV neutron) yield, measured by Al(n,α) reaction

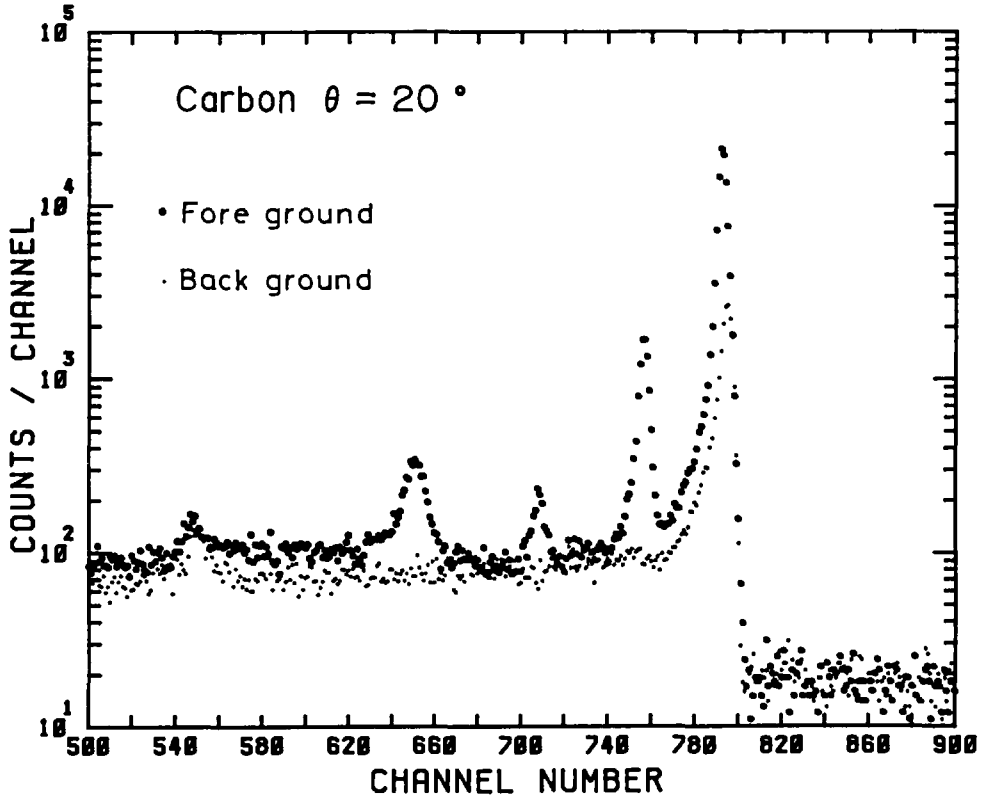

Fig.7 Time-of-flight data with carbon sample (upper) and without sample (lower)

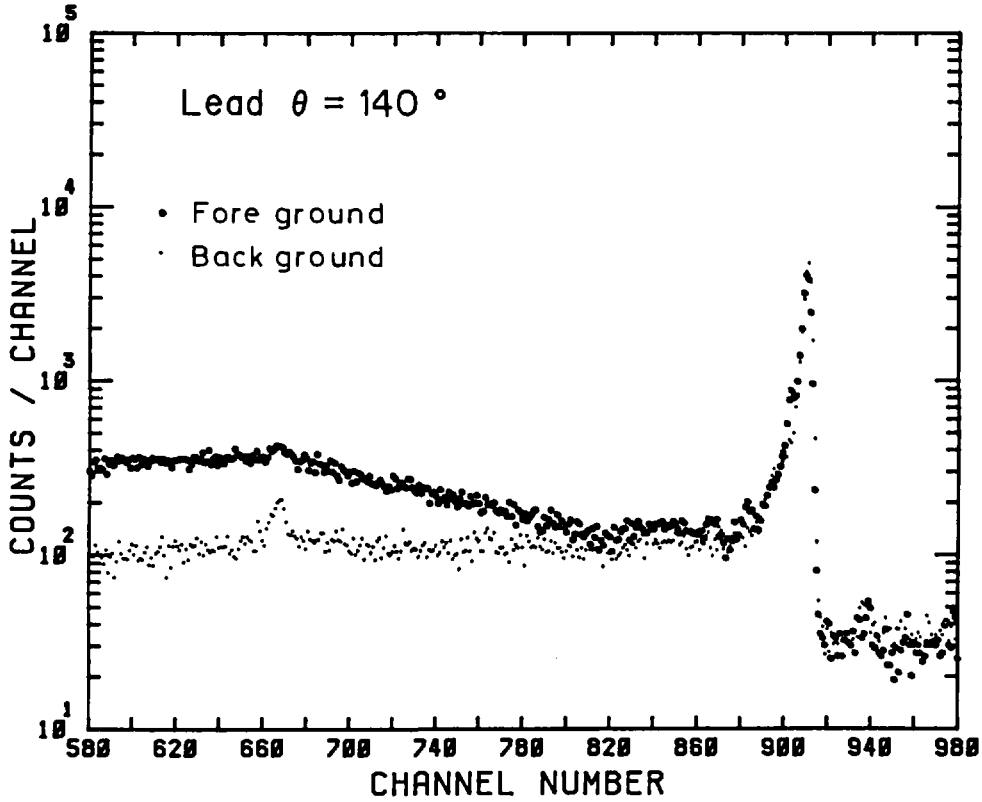

Fig.8 Time-of-flight data with lead sample (upper) and without sample (lower)

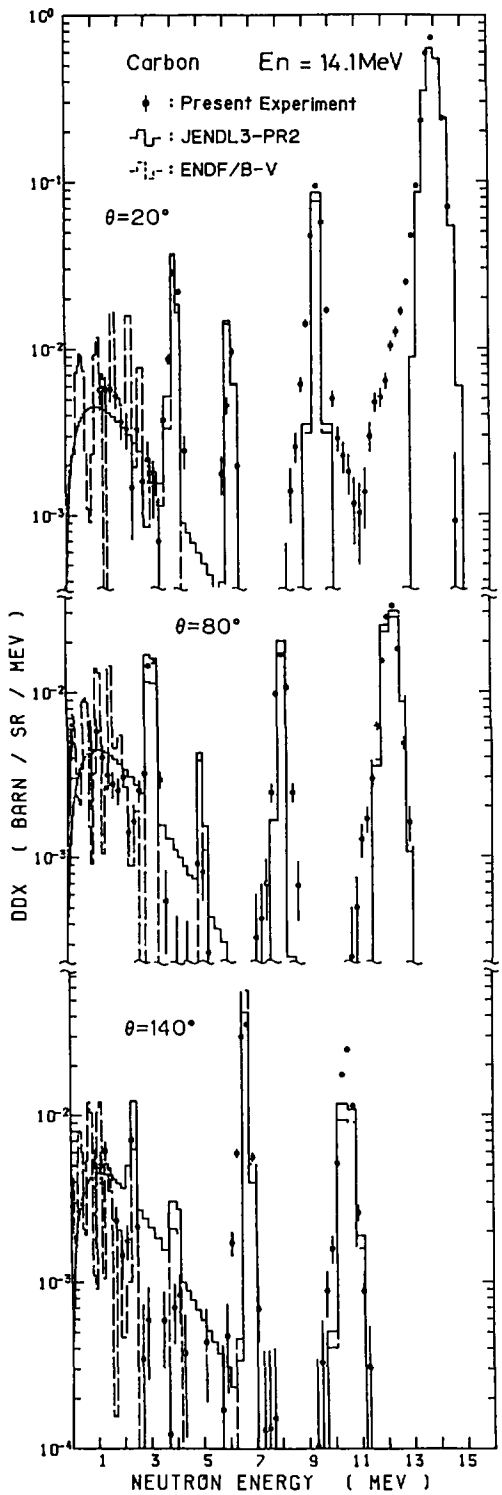

Fig.9 Double differential cross sections for carbon

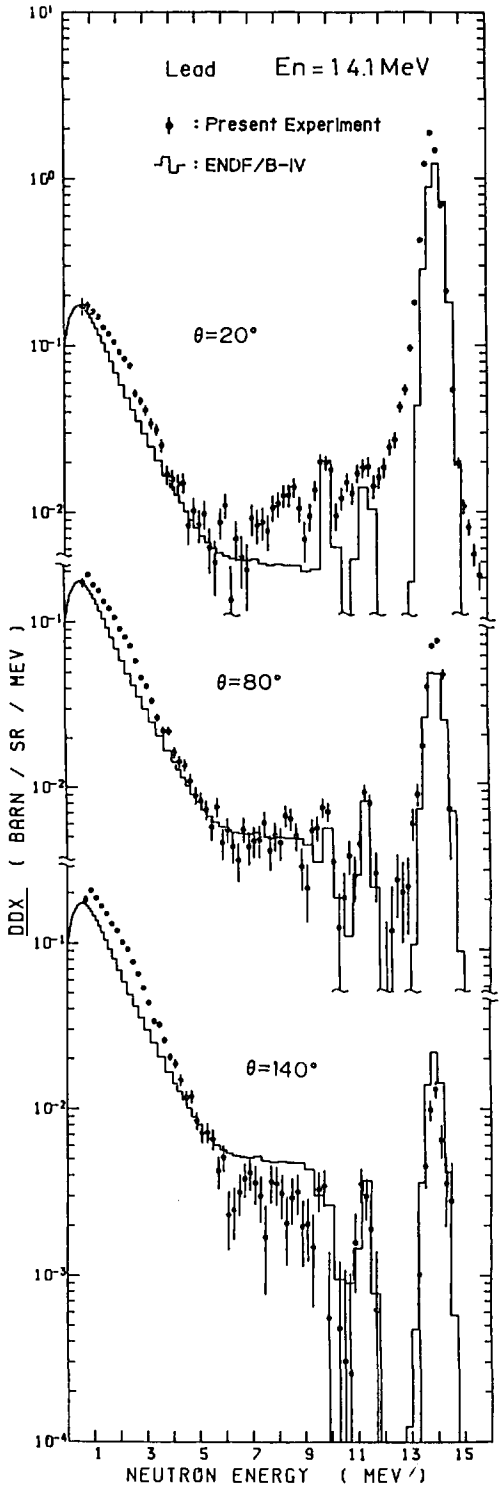

Fig.10 Double differential cross sections for lead

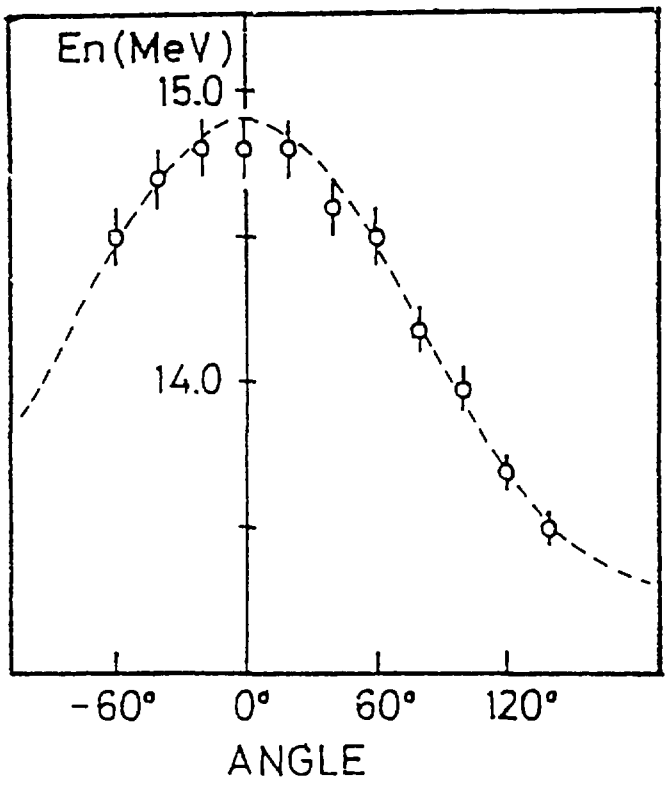

Fig.11 Energy-angle correlation of emitted neutrons from rotating target

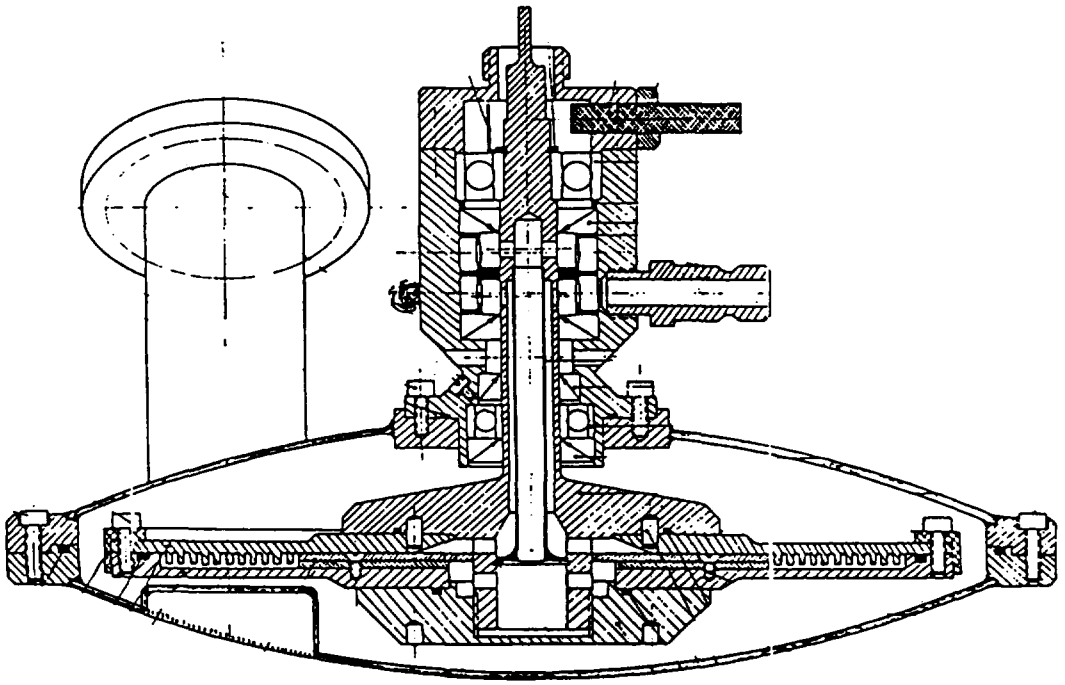

Fig.12 A rotating target being used in OKTAVIAN

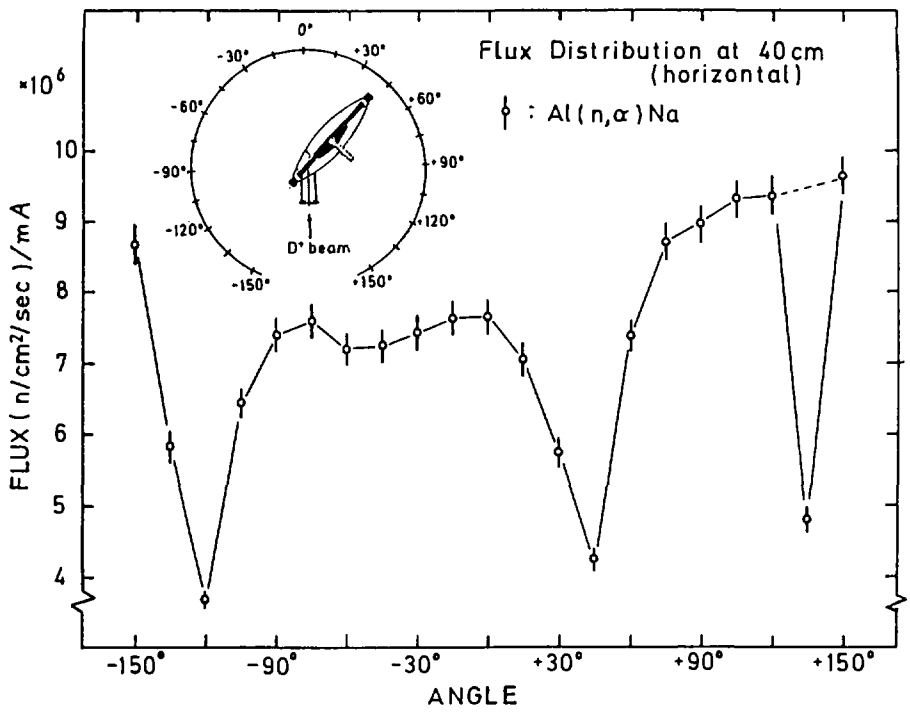

Fig.13 Angular dependence of D-T neutron yields from rotating target

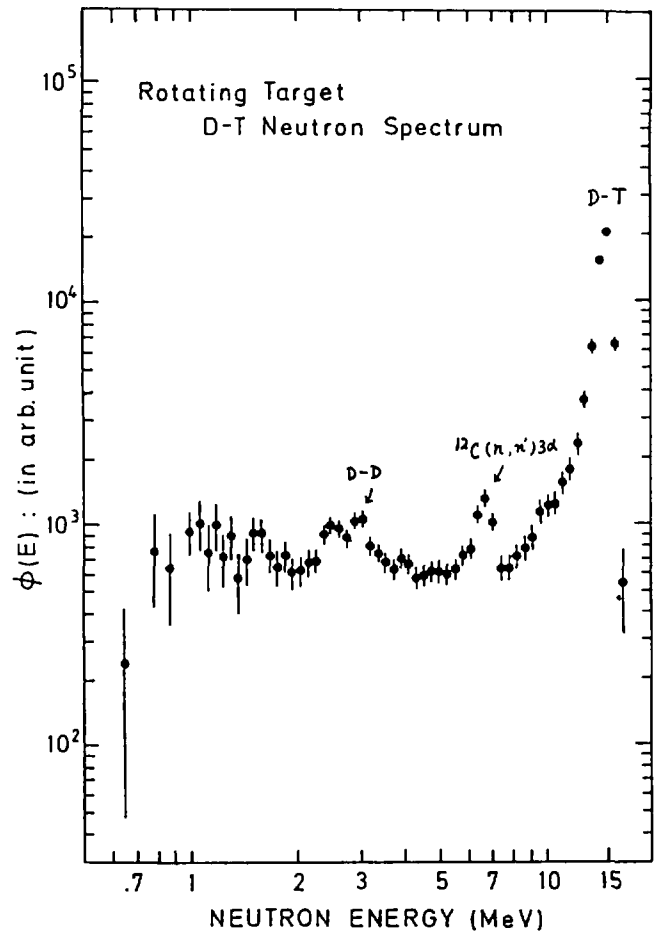

Fig.14 Source neutron spectrum from rotating target, measured by double scintillator technique

17) A Helium Atom Measurement System for a Helium Accumulation Method Applied to Measure Helium Production Cross Section

Tokio FUKAHORI, Yukinori KANDA, Hiroki TOBIMATSU,
Yoshifumi MAEDA, and Koji YAMADA

Department of Energy Conversion Engineering, Kyushu University,
Kasuga, Fukuoka, 816 Japan

A helium accumulation method is a useful means to measure helium production cross section. The number of helium atoms produced by (n, xα) reactions should be absolutely and directly measured in this method. An apparatus with high sensitivity to helium atom is required in the usage of the helium accumulation method. A helium atom measurement system for this method has been constructed in our laboratory. A helium-ion-implanted sample method has been developed as a new method for the calibration of the system. For an example experiment, the helium production cross section of Al at 14.8 MeV has been measured with the helium accumulation method referring the cross section of ^{27}Al(n, α) reaction.

A helium production cross section is an important nuclear data on neutron-induced damage in structural materials of fusion

and fast reactors. An helium accumulation method recently developed is very useful for measurement of the cross section. In the method, the number of α-particles produced, stopped, and held in the sample is directly counted as helium atoms by a mass spectrometer after the neutron irradiation. It is rightly proportional to the helium production cross section differing with an activation method.

A block diagram of a helium atom measurement system is shown in Fig.1. The sample is evaporated to be released helium gas on a tungsten boat heated electrically in a furnace. Undesirable background gases are also emitted from the sample as well as the inner surface of the furnace. It was found by analyzing the gases with a quadrupole mass spectrometer (QMS) that the major components of the background are compounds of hydrogen. A trap consisting of molecular sheaves and a getter pump is applied to reduce the background gases before mass analysis. The QMS is used to measure the number of helium atoms. The outputs from it and other sensers are fed to a microcomputer to calculate the number of helium atoms in the sample.

A cut-away view of the furnace is shown in Fig.2. The tungusten boat is connected to Cu-terminals through Ta-adapters. Temperature of the boat is reached to 2200 ℃ with the electrical current of 350 A. Therefore, the metals which have high melting points can be melted down and Al, Ag, Cu etc. can be evaporated.

The standard gas which is helium-3 or helium-4 selected for an option of experiments is prepared in the standard gas supply whose schematic diagram is shown in Fig.3. The standard, storage, and inlet vessels, cocks, and connecting pipes are made of pylex glass, because reproducibillity of volumes on handling of glass cocks is more reliable comparing with metal ones. This is similar to the device used by Kneff et al.[1]. The number of helium atoms in the primary standard gas is determined by measuring absolutely the pressure of the helium gas contained in the known-volume vessel and the temperature of the gas. Chemical purities of the primary gases are 99.9 % for helium-3 and 99.99 % for helium-4. The appropriate standard helium gas containing helium atoms in nearly equal to the number with that of the sample can be obtained by diluting the primary standard gas with a pair of vessels chosen from the known-volume vessels whose volumes range from 2 to 500 cm^3. The uncertainties of the volumes are about 2 % each.

The QMS and sensers are connected to a personal computer. The block diagram of control and signal lines is shown in Fig.4. The personal computer feeds a mass-sweep voltage to QMS. The output signals from QMS are analyzed by the personal computer and mass data are obtained automatically.

A helium-ion-implanted sample method has been developed for the calibration of the helium atom measurement system. The uncertainties in the calibration with this method can be expected

to be smaller than those with the standard gas prepared by the apparatus shown in Fig.3, since the number of helium atoms implanted in the sample is obtained only by measurement of ion current. An apparatus for implanting helium ions into samples consists of an ion source, analyzing magnet, and irradiation chamber equipped with a sample holder. A schematic diagram is shown in Fig.5. Helium-4 ions are implanted into the samples after being accelerated to 20 keV and then being bent by 10° with the analyzing magnet to select helium-4 ions. The number of helium-4 ions implanted into the sample can be estimated from the ion current measured by a current integrator connected to the sample. A sample disk is placed in a Faraday-cup in order to exclude contribution of the secondary electrons emitted from the helium-irradiated sample surface in measuring the ion current. It is confirmed by carefully checking of secondary electron effects that the experimental arrangement can be allowed the correct ion current measurement.

For an example experiment of the helium atom measurement system, the helium production cross section of Al at 14.8 MeV has been measured[2]. Aluminium samples were irradiated with FNS (Fusion Neutronics Source) which is a D-T neutron generator at JAERI (Japan Atomic Energy Research Institute). The number of helium atoms produced in the Al sample by (n, xα) was measured with the helium accumulation method using the helium atom

measurement system. The absolutely measured activity of the Al sample can be converted into the number of helium atoms produced by $^{27}Al(n, \alpha)^{24}Na$ reaction. The helium production cross section is estimated from the ratio of this number to the number of helium atoms produced by (n, xα) reaction, and the cross section for $^{27}Al(n, \alpha)$ reaction which is evaluated by Vonach[3]. The present result of the helium production cross section of Al at 14.8 MeV is 141 ± 8 mb.

The authors wish to thank Dr. Tomoo Nakamura and Dr. Yujiro Ikeda in FNS at JAERI for their kindly support about the neutron irradiation and the activity measurement.

References

1) D.W. Kneff et al.; J. Nucl. Mater., 103&104 (1981) 1451

2) T. Fukahori et al.; submitted to J. Nucl. Sci. Technol.

3) H. Vonach; "Nuclear Data Standards for Nuclear Measurements", INTERNATIONAL ATOMIC ENERGY AGENCY (1983, VIENNA) p59

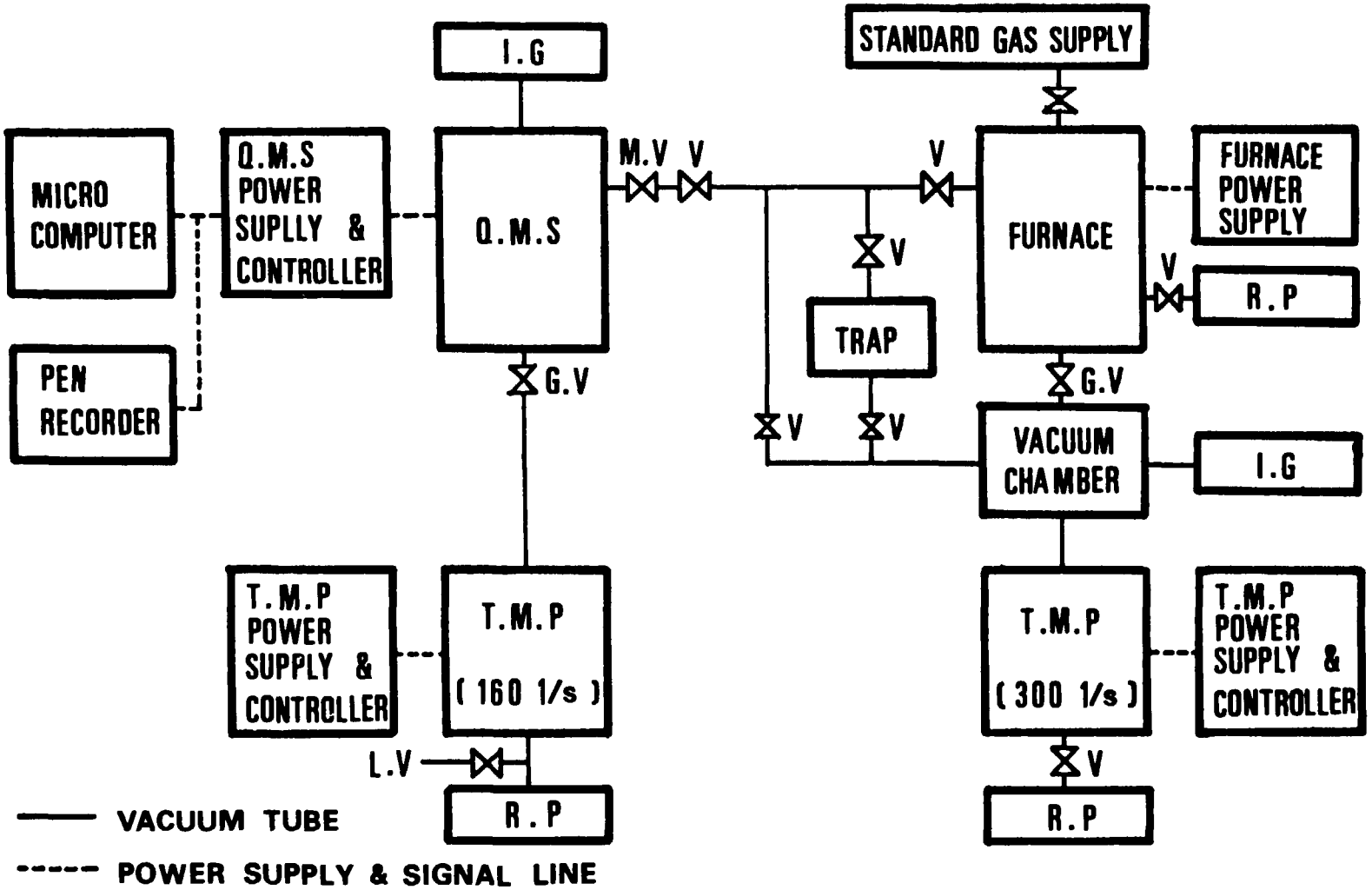

Fig.1 A block diagram of the helium atom measurement system.

Q.M.S; Quadrupole Mass Spectrometer, T.M.P; Turbo Molecular Pump,

R.P; Rotary Pump, I.G; Ionization Gauge, V; Valve,

M.V; Micro Valve, G.V; Gate Valve, L.V; Leak Valve.

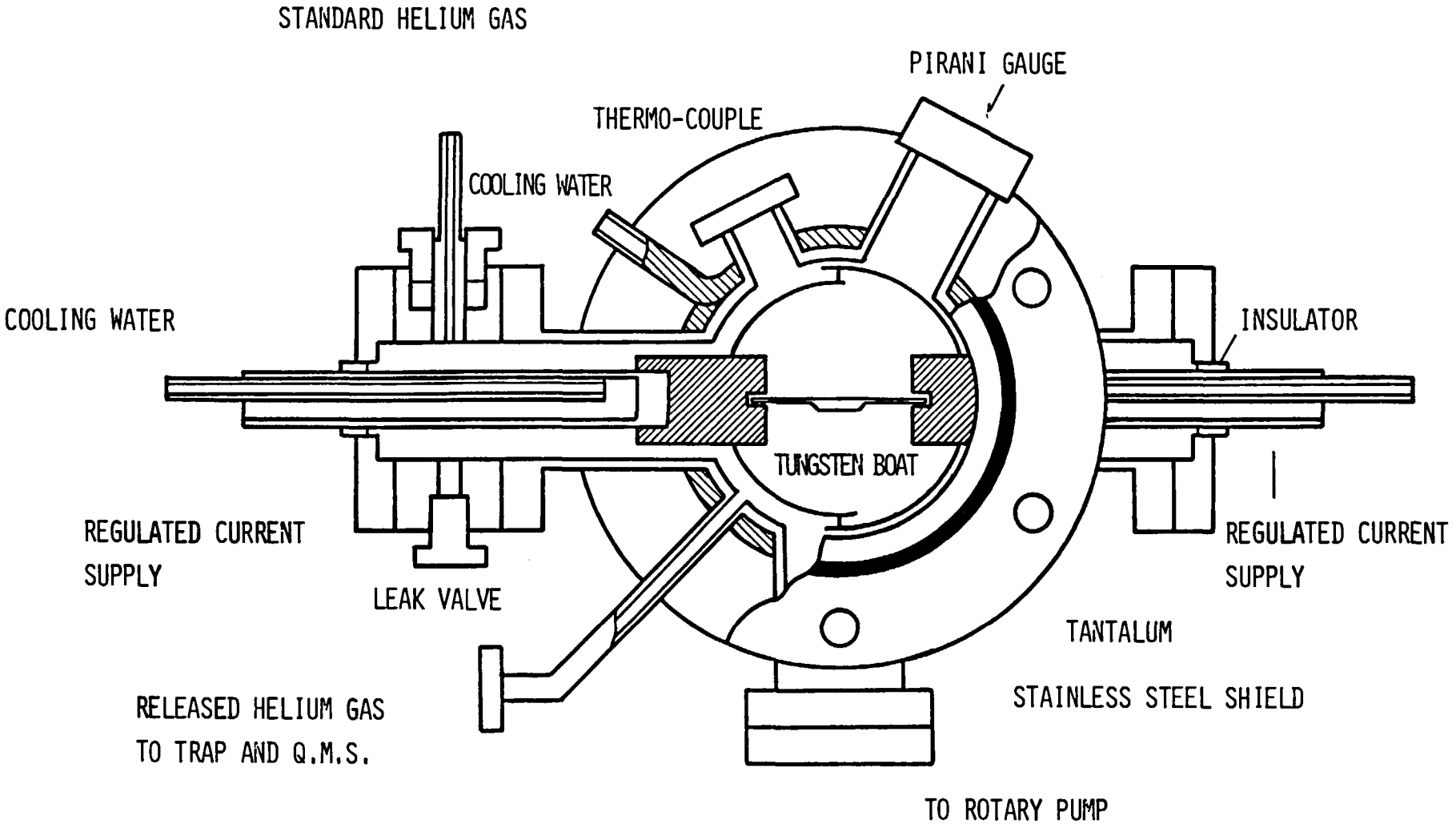

Fig.2 A cut-away view of the furnace.

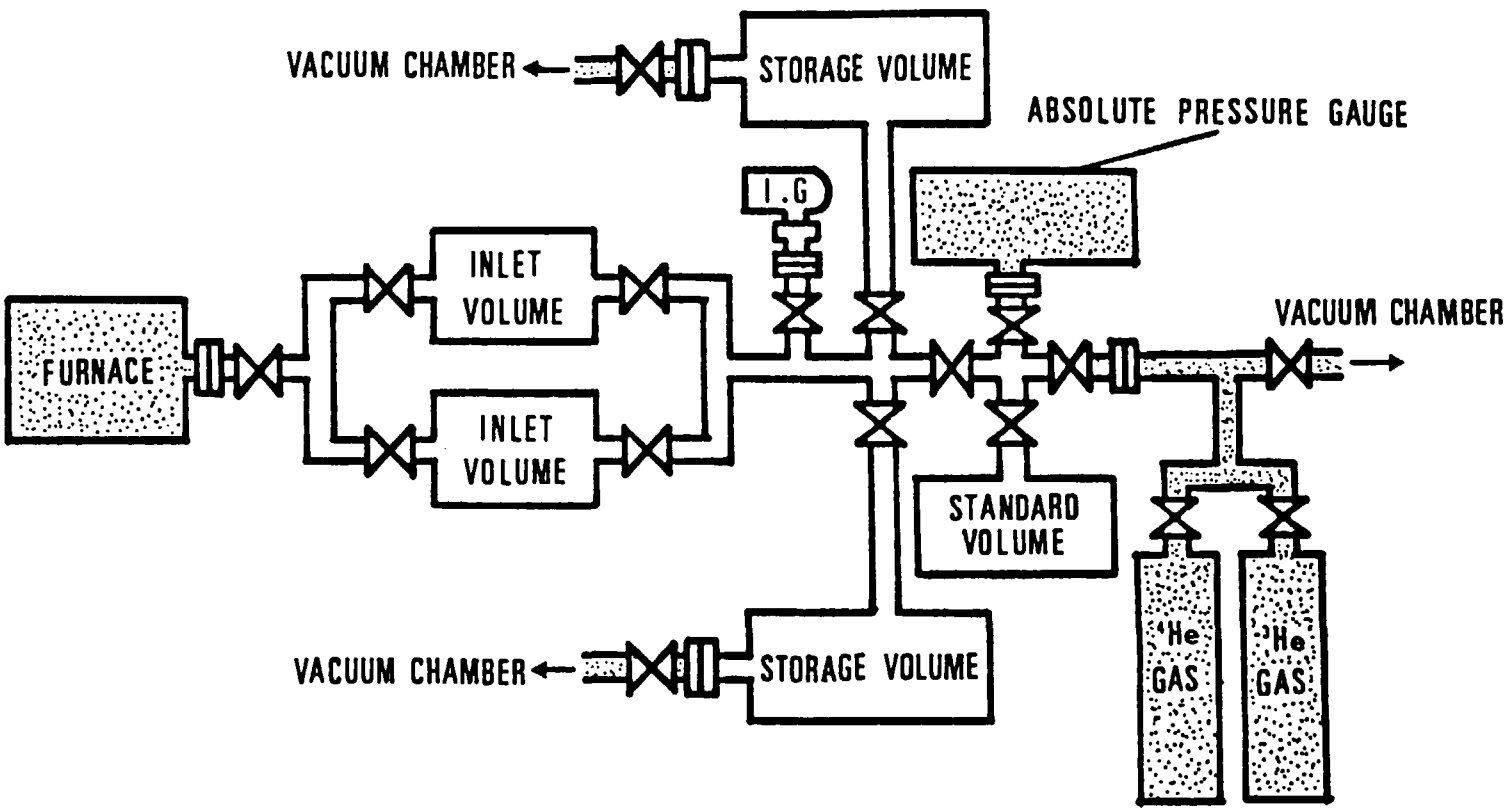

Fig.3 A schematic diagram of the standard gas supply.

I.G; Ionization Gauge.

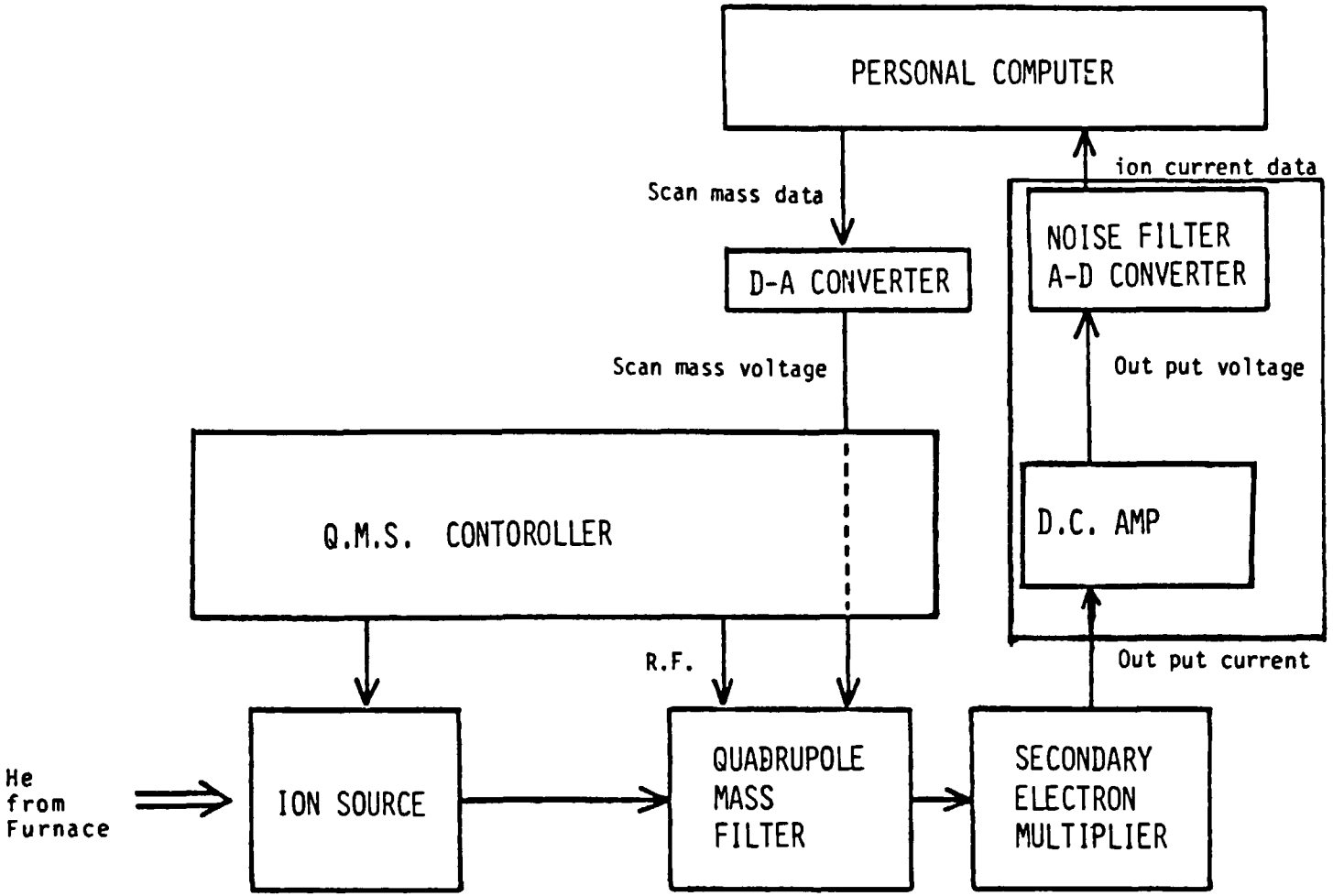

Fig.4 A block diagram of the gas analysis system (QMS and the controller).

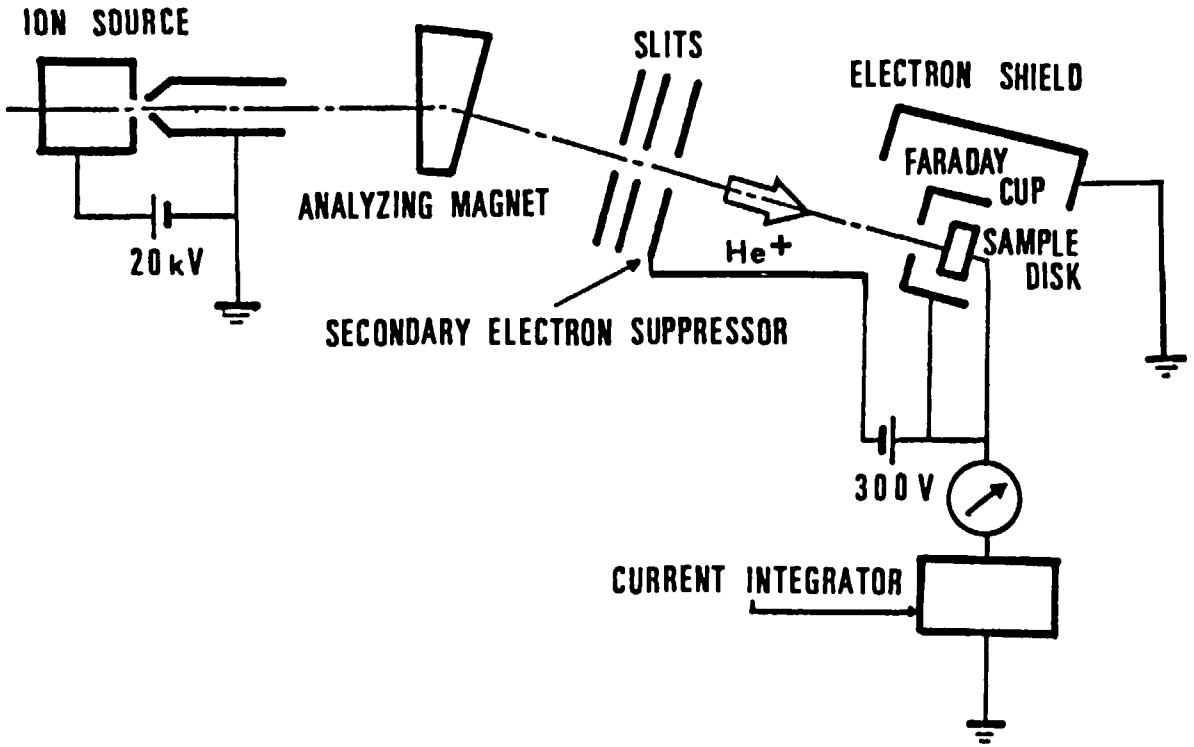

Fig.5 A schematic diagram of the apparatus for the helium-ion-implantation.

18) Research with Cockcroft-Walton Neutron Generator in Kyushu University

Mikio HYAKUTAKE

Department of Nuclear Engineering, Faculty of Engineering,
Kyushu University, Fukuoka, 812 Japan

Since a 500-kV Cockcroft-Walton generator was constructed in 1961, measurements on the neutron-induced reaction cross-sections(scattering, fission, activation and proton emission) were started. A brief description of experimental results obtained recently in our laboratory is presented.

1. Introduction

In 1961 the 500-kV Cockcroft-Walton (CW) accelerator(maximum beam current 1mA) was constructed in Kyushu University[1]. This machine with a multiplying circuit of 12 stages was driven by a frequency of about 40 KHz. An ion source of high frequency discharge type was used because of its high atomic concentration[2]. The neutron yield of about 10^8 n/sec/μA was obtained when a thick tritium-titanium target was bomberded with 170 keV deuterons and the ion current of about 100 μA. The ripple was about 20 V at such a condition.

In 1974 this neutron generator was modified temporarily to

one with the driving frequency of 60 Hz and the multiplying circuit of 6 stages because of a trouble in the circuit of the driving frequency. At the operating condition of acceleration of 150 kV and the beam current of 100 μA, ripple and neutron intensity are 3500 V and 0.8 10^8 n/sec, respectively, using the thick target.

Since the construction of the CW generator, the experiments of neutron scattering, fission, activation and proton emission have been achieved. This paper reports the typical results obtained in relatively recent experiments.

2. Scattering Experiments

Since a time-of-flight (TOF) spectrometer has been developed in Kyushu University in 1964[3], several experiments have been achieved to obtain the elastic and inelastic scattering cross sections[4,5,7-11].

2.1 Elastic and inelastic scattering to discrete levels

A new TOF spectrometer with the time resolution of 1.4 nsec and 7.6 m flight path was constructed to achieve the experiment of good resolution (Fig. 1)[6]. This corresponds to an energy resolution of 260 keV for 14 MeV neutrons. The experiment of scattering from Fe by using this spectrometer was done, which is enough to separate clearly the first excited state from the ground state in ^{56}Fe (natural abundance 91.7%)[7].

An optimum fit to the elastic scattering data was obtained by using an automatic search routine. The results are shown by solid lines in Fig. 2. Fits are quite good for both parameter sets (ST1 and BG1).

The inelastic scattering was compared with the prediction of DWBA calculations. The results are shown by the solid lines in Fig. 3. The angular distribution was also analyzed by the coupled channel (CC) method. The good fits to both channels were obtained when the strength of surface imaginary potential was set equal to 0.8 of the values used DWBA calculations. The calculated angular distributions for the elastic scattering and the first excited state are shown by dashed lines in Fig. 2 and 3, respectively. The CC calculations give reasonably good agreement with the experimental data.

2.2 Inelastic scattering to continuum region

Several experiments were carried out in order to obtain systematic information on the nuclear level density for heavy and medium mass nuclei[8,9].

In order to investigate the pre-equilibrium process of neutron inelastic scattering, energy and angular distributions of 14.1 MeV neutrons by several nuclei were measured[10,11]. The TOF spectrometer with the time resolution of about 2 nsec and flight path of 1.5 to 3 m was used. Typical energy spectrum for Nb was shown in Fig. 4. Angle-integrated energy spectra were analyzed by both the evaporation and pre-equilibrium models and best-fit values were obtained for the model parameters related to the absolute inelastic scattering cross section. The exciton and the geometry dependent hybrid models were used for the pre-equilibrium model calculations. It was found that the geometry dependent hybrid model can reproduce well the experimental cross sections when the average values of the best-fit parameters are used.

Angular distributions of neutrons from the pre-equilibrium decay were calculated by the simple analytical method in terms of surface interaction (Fig. 5)[11,12]. A general trend of the experimental results were reasonably well reproduced.

3. Fission

Recently a study on 14.5 MeV neutron induced fission of ^{235}U was performed by means of three-parameter experiment[13,14]. The energies of both fragments and the TOF of one fragment were measured. A mosaic-arrayed surface barrier detector of large sensitive area was used at the remote end of a flight tube. In Fig. 6 are shown the cross section of flight-tube for fission fragment measurement. The pre- and post-neutron emission fragment mass distributions were obtained, together with the average total kinetic energy of fragment as a function of its mass. The average number of neutrons from an individual fragment and the average total number of emitted neutrons are also derived as a function of fragment mass (Fig. 7). The results agree well with those calculated by the method developed in our laboratory for medium-excited fission[15]. The average number of emitted neutrons and the mass distribution of fission fragment are derived for the respective reactions of first-, second- and third-chance fission.

4. Activation method

Activation cross sections for (n,p), (n,α) and (n,2n) reactions of a large variety of elements have been at 14.6 MeV by using a Ge(Li) γ-ray detector[16,17]. These results were compared with the predictions based on the pre-equilibrium model,

evaporation model and other model.

5. (n,p) reactions

In order to obtain more reliable and precise results, and to compare the results with the pre-equilibrium model and the evaporation model, the energy and angular distributions of protons from the interaction of 14.1 MeV neutrons with indium were measured using a counter telescope. The energy spectrum obtained by integrating the measured differential energy spectra and solid angle was compared with the results predicted by the pre-equilibrium and evaporation model[18]. The agreement between experiment and calculation is good.

More recently both energy and angular distributions of proton emitted from the ^{93}Nb(n,p) reaction were measured by using a position-sensitive counter-telescope (PSCT) with large angular acceptance[19,20]. As shown in Fig. 8, the PSCT consists of two ΔE proportional counters, a large rectangular Si(Li) detector, and two position sensitive proportional counters (PSPCs). Energy spectrum integrated over the solid angle and angular distributions are shown in Fig. 9 and Fig. 10, respectively. The multi-step direct reaction (MSDR) model calculation satisfactorily explains the shape of the experimental angular distribution but indicates a little discrepancy in the absolute cross section. However, the energy spectrum calculated on the basis of the MSDR model is in fairly good agreement with that calculated for the pre-equilibrium emission from the three-exciton states.

Acknowledgement

The author would like to express his appreciation to the members of Cockcroft-Walton accelerator laboratory.

References

1) SONODA, M., KATASE, A., SEKI, M., and WAKUTA, Y.: Memo. Fac. Eng., Kyushu Univ., XX, 367(1961).

2) SEKI, M., KATASE, A., WAKUTA, Y. and SONODA, M.: Memo. Fac. Eng., Kyushu Univ., 3, 9(1960).

3) YOSHIMURA, A., SONODA, M., KATASE, A., WAKUTA, Y. SEKI, M., AKIYOSHI, T., FUJITA, I. and HYAKUTAKE, M.: Genshikaku Kenkyu (in Japanese), 9, 409(1964).

4) MATOBA, M., HYKUTAKE, M., TAWARA, H., TSUJI, K., HASUYAMA, H., 180 'MATSUKI, S., KATASE. A. and SONODA, M.: Nucl. Physics, A204, 129(1973).

5) HYAKUTAKE, M., SONODA, M., KATASE, A., WAKUTA, Y., MATOBA, M., TAWARA, H. and FUJITA, I.: J. Nucl. Sci. and Technol., 11, 407(1974).

6) MATOBA, M., HYAKUTAKE, M., TONAI, T., NIIDOME, J., MATSUMOTO, Y. and KIMURA, N. : Nucl. Instr. & Meth., 116, 405(1974).

7) HYAKUTAKE, M., MATOBA, M., TONAI, T., NIIDOME, J. and NAKAMURA, S.: J. Phys. Soc. Japan, 38, 606(1975).

8) AKIYOSHI, T., KATASE, A. and SONODA, M. :J. Nucl. Sci. and Technol., 11, 523(1974).

9) FUJITA, I., SONODA, M., KATASE, A. WAKUTA, Y., TAWARA, H., HYAKUTAKE, M. and IWATANI, K.: J. Nucl. Sci. and Technol., 9, 301(1972).

10) IRIE, Y., TSUJI, M., HYAKUTAKE, M., KOORI, N., MATOBA, M. and KUMABE, I.: J. Nucl. Sci. and Technol., 13, 334(1976).

11) IRIE, Y., HYAKUTAKE, M., MATOBA, M., KUMABE, I. and SONODA, M.: Memo. Fac. Eng., Kyushu Univ., 37, 19(1977).

12) IRIE, Y., HYAKUTAKE, M., MATOBA, M. and SONODA, M.: Phys. Lett., 62B, 9(1976).

13) YAMAMOTO, H., MORI, Y., WAKUTA, Y. and SONODA, M.: Nucl. Instr. & Meth., 134, 119(1976).

14) YAMAMOTO, H., MORI, Y., WAKUTA, Y., KATASE, A. and SONODA, M.: J. Nucl. Sci. and Technol., 16, 779(1979).

15) YAMAMOTO, H., MORI, Y., WAKUTA, Y., KATASE, A. and SONODA, M.: J. Nucl. Sci. and Technol., 16, 466(1979).

16) SATO, T., KANDA, Y. and KUMABE, I.: J. Nucl. Sci. and Technol., 12, 681(1975).

17) FUJINO, Y., HYAKUTAKE, M. and KUMABE, I.: Bul. Inst. Chem. Research (Kyoto univ.), 60, 205(1982).

18) NIIDOME, J., HYAKUTAKE, M., KOORI, N., KUMABE, I. and MATOBA, M.: Nucl. Physics, A245, 509(1975).

19) KOORI, N., GOTO, T., KONISHI, H. and KUMABE, I.: Nucl. Instr. & Meth., 206, 413(1983).

20) KOORI, N., OHSAWA, Y. and KUMABE, I.: Nucl. Sci. Eng., 87, 34(1984).

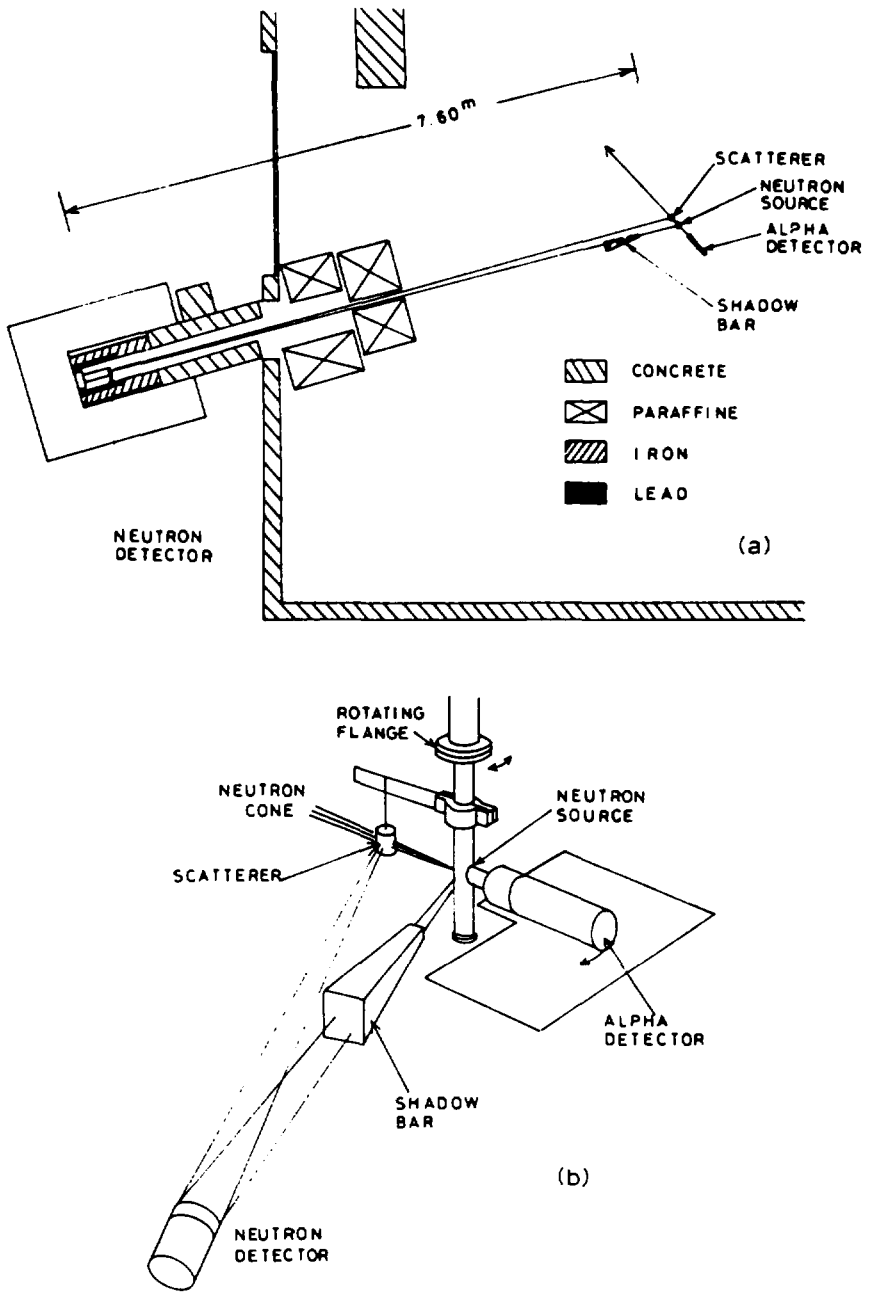

Fig. 1 a) The experimental arrangement. b) Schematic drawing of the system of the neutron source, the scatterer and the alpha detector(from ref. 5).

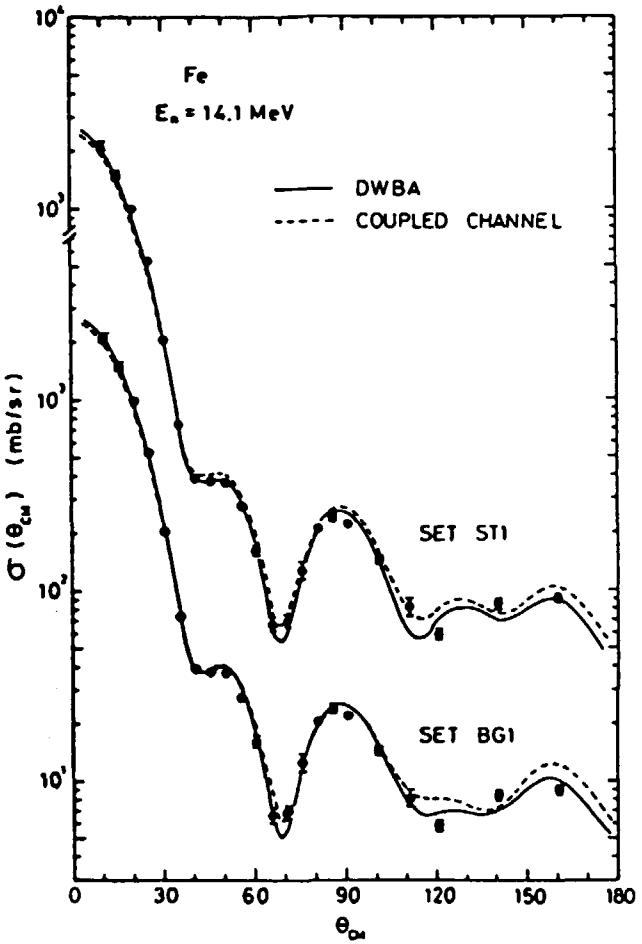

Fig. 2 Differential cross sections for the elastic scattering from Fe. The solid lines are fits obtained from the optical model calculations, while the dashed lines from the coupled channel caculations (from ref. 7)

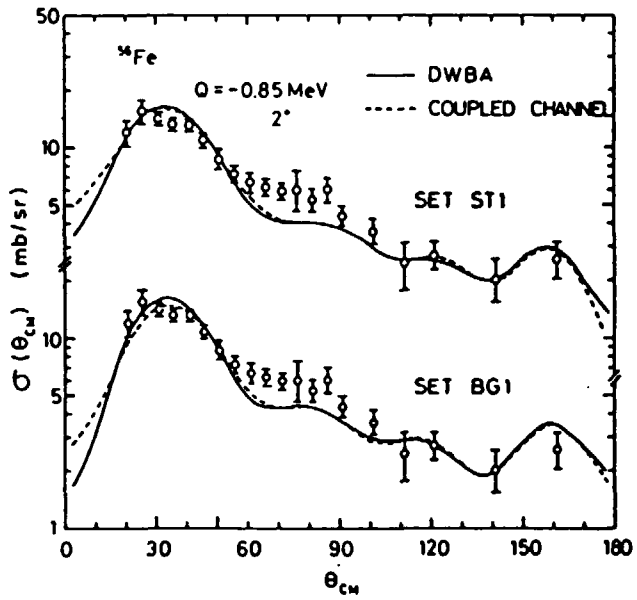

Fig. 3 Differential cross sections for the inelastic scattering to 0.85 MeV in 56Fe. The solid lines are the DWBA prediction and the dashed lines the coupled channel prediction (from ref. 7).

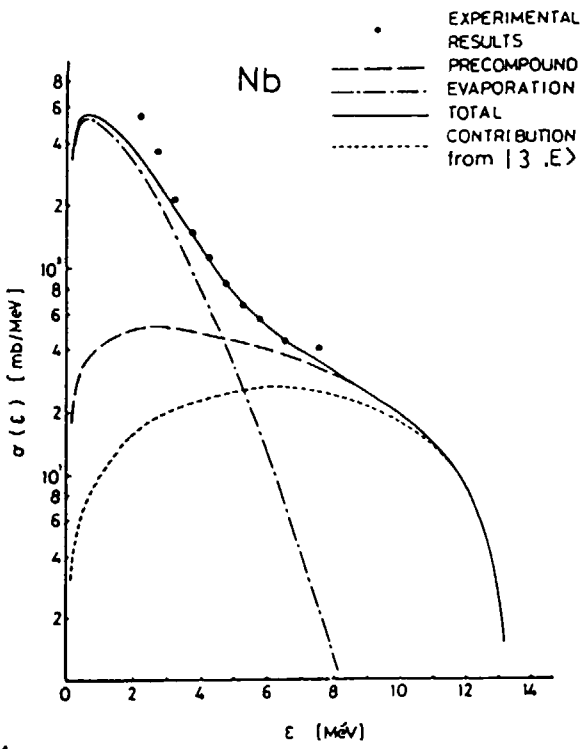

Fig. 4

Comparison of experimental energy spectrum and results calculated by the exciton model in inelastic scatterig of neutrons by Nb. The closed circles show the experimental results, the solid curves are the calculated total energy spectrum, the dot-dashed curves the evaporation spectrum, the dashed curve the pre-equilibrium spectra and the dotted curve the contributions from initial exciton state(n=3) (from ref. 11).

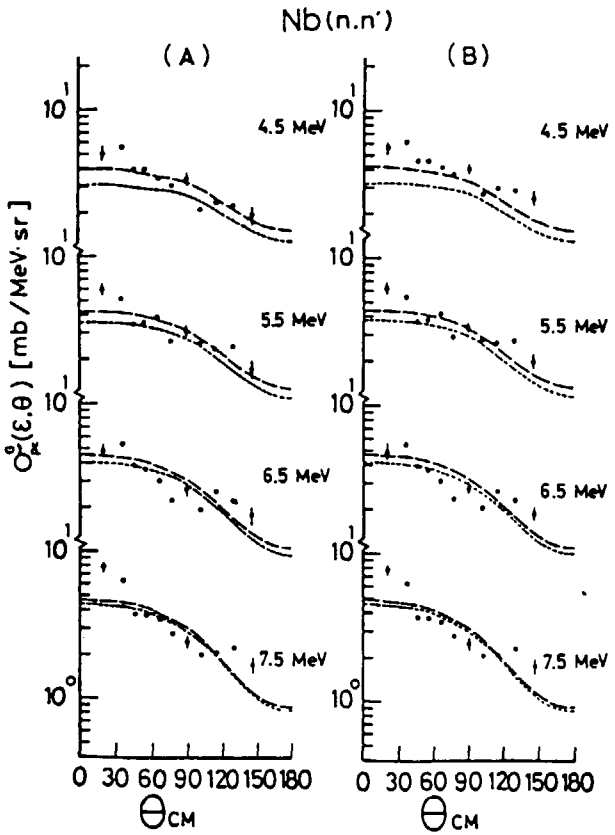

Fig. 5

Comparison of experimental and calculated angular distributions of neutrons inelastically scattered through pre-equilibrium decay from Nb. The dashed curves are the calculated total angular distributions and the dotted curves the distributions from initial exciton state.

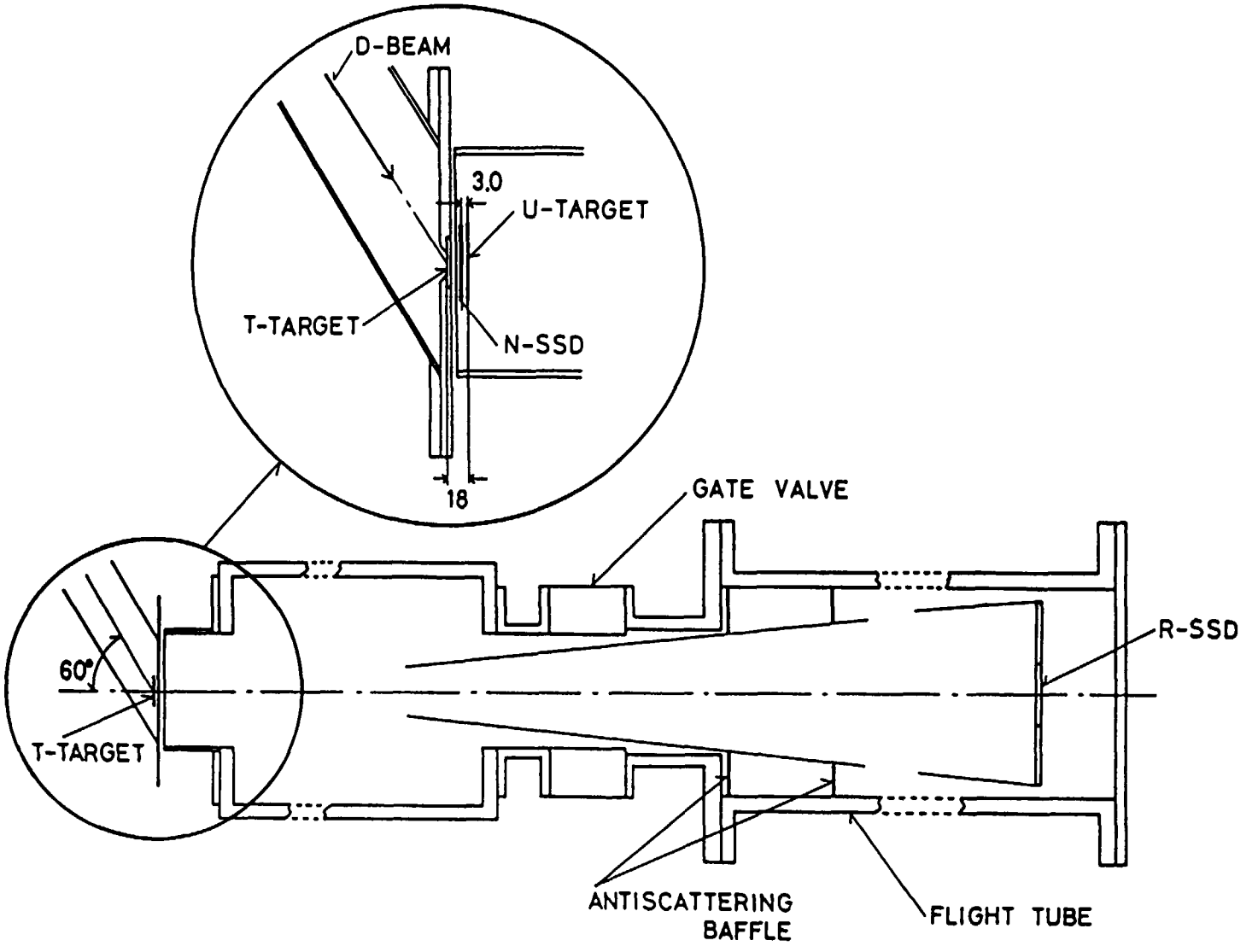

Fig. 6 Cross section of flight-tube of fission fragments. N-SSD: silicon surface-barrier detector, R-SSD: large-area detector located at end of the 101.8 cm evacuated flight-tube.

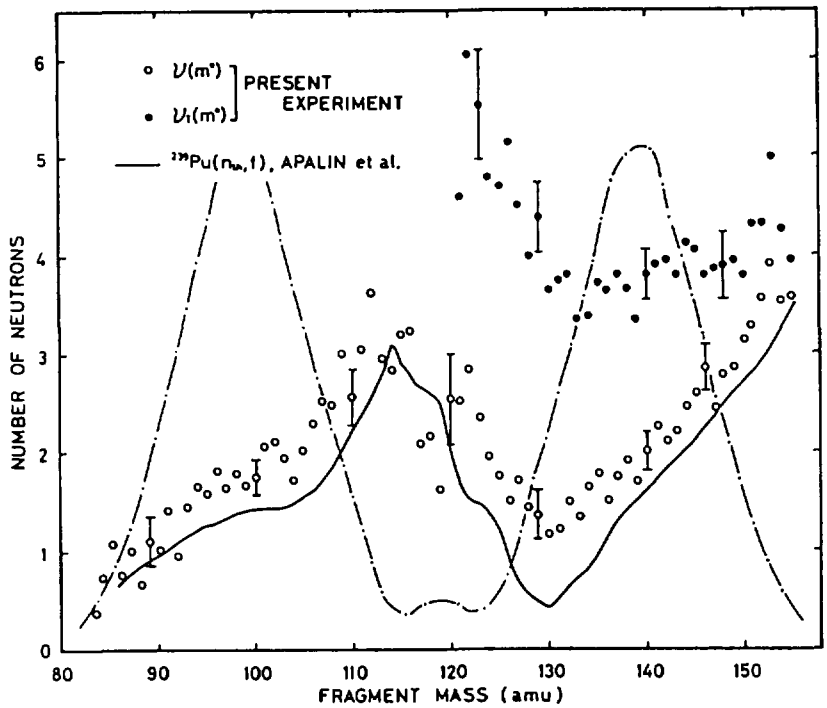

Fig. 7 Average number of emitted neutrons as function of pre-neutron- emission fragment mass(from ref. 14).

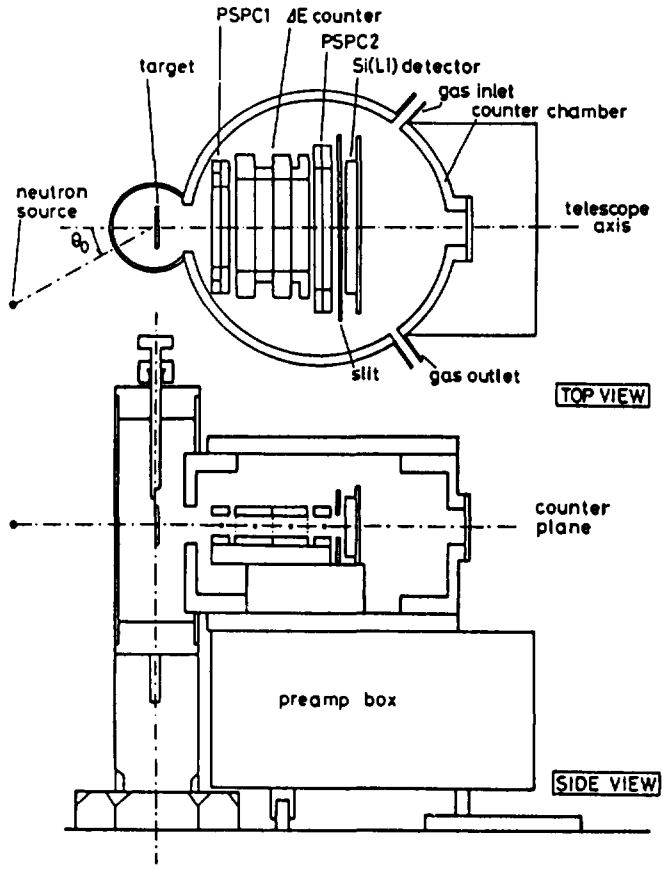

Fig. 8 Schematic views of the position sensitive counter-telescope(from ref. 19).

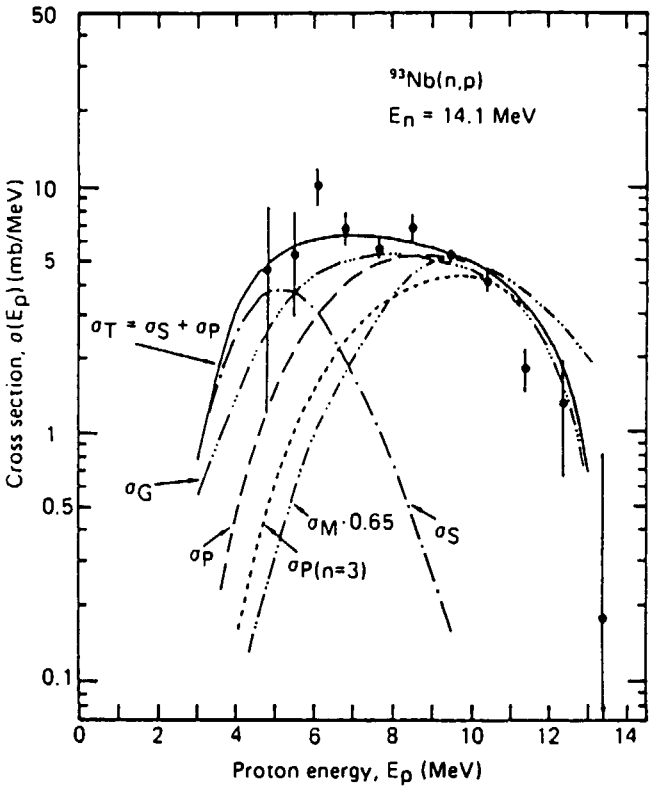

Fig. 9

Energy spectrum integrated over the solid angle for the ^{93}Nb(n,p) reaction at 14.1 MeV. The calculated spectrum σ_S is obtained by the statistical evaporation model, $\sigma_{P(n=3)}$ by the pre-equilibrium model(n=3), σ_P by the pre-equilibrium model(total), σ_G by the generalized exciton model, and σ_M by the MSDR model(one-step case). The spectrum σ_T is obtained as the sum of spectra σ_S and σ_P (from ref. 20).

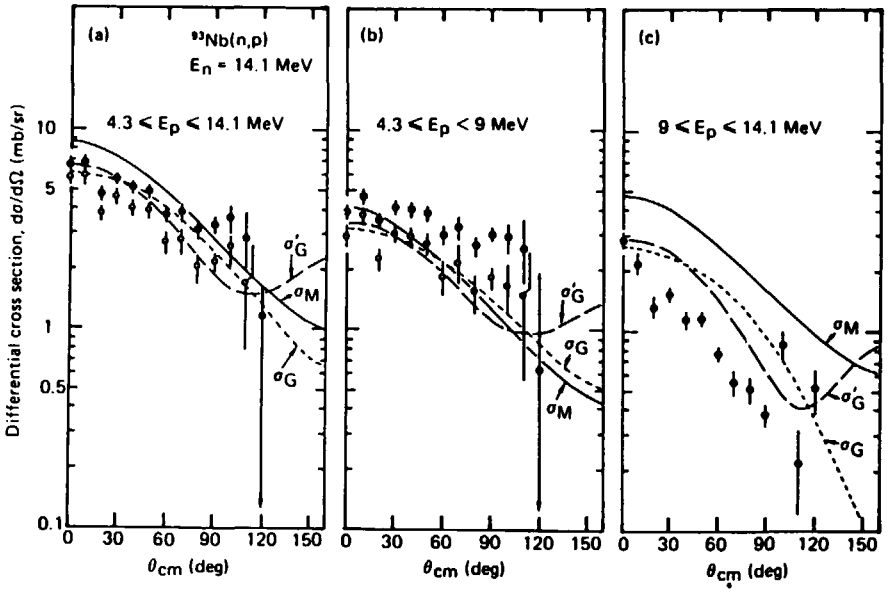

Fig. 10

Angular distributions for the ^{93}Nb(n,p) reaction at 14.1 MeV. Solid circles=measured differential cross sections. Open circles= differential cross sections after the subtraction of the isotropic contribution from the statistical evaporeation process. Dotted curves are calculated by means of of the generalized exciton model with the theoretical eigenvalues of Legendre polynomial series , and long dashed curves with the adjusted eigenvalues. Solid curves indicate the angular distributions for the one-step case within the framework of the MSDR theory(from ref. 20).